DANIEL KINGSLEY CUDJOE

PHENOTYPING THE NUTRITIONAL STATUS OF CROPS USING PROXIMAL AND REMOTE SENSING TECHNIQUES

SCHOOL OF WATER, ENERGY AND ENVIRONMENT
Environment and Agrifood

DOCTOR OF PHILOSOPHY (PHD) THESIS
Academic Year: 2019-2024

Supervisor: Prof. Fady Mohareb
Associate Supervisors: Dr. Toby W. Waine
Prof. Malcolm J. Hawkesford

May 2024

SCHOOL OF WATER, ENERGY AND ENVIRONMENT
Environment and Agrifood

DOCTOR OF PHILOSOPHY (PHD) THESIS

Academic Year 2019-2024

DANIEL KINGSLEY CUDJOE

PHENOTYPING THE NUTRITIONAL STATUS OF CROPS USING PROXIMAL AND REMOTE SENSING TECHNIQUES

Supervisor: Prof. Fady Mohareb
Associate Supervisors: Dr. Toby W. Waine
Prof. Malcolm J. Hawkesford

May 2024

ACADEMIC INTEGRITY DECLARATION

I declare that:

- the thesis submitted has been written by me alone.
- the thesis submitted has not been previously submitted to this university or any other.
- that all content, including primary and/or secondary data, is true to the best of my knowledge.
- that all quotations and references have been duly acknowledged according to the requirements of academic research.

I understand that to knowingly submit work in violation of the above statement will be considered by examiners as academic misconduct.

EXECUTIVE SUMMARY

This PhD thesis project was conducted within the framework of a collaborative programme involving Cranfield University, Rothamsted Research and Mohammed VI Polytechnic University (UM6P), supported by funding from OCP Africa. The project aimed to pioneer novel techniques in remote sensing (RS) and automated crop phenotyping technologies tailored specifically for agricultural contexts in Africa.

Efficient production of crops along with the optimal use of fertilisers is fundamental for ensuring sustainable, secure and healthy crop production. Currently, efforts in developing and utilising high-throughput tools for crop phenotyping is predominantly directed towards the crop portfolio characterised by high input and high yield in developed countries. The complexity and cost of existing plant phenotyping equipment have hindered their widespread use in Africa. Moreover, inadequate technical expertise, operational know-how, regulatory constraints and conceptual capacity within the plant science community have compounded the challenges, further impeding adoption. The literature review of this PhD thesis (Chapter 2, section 2.2) which is a published paper extensively discusses and addresses these challenges.

This project exploited phenotyping technologies from Cranfield University and Rothamsted Research with a specific goal of implementation of low-cost portable tools to acquire, analyse and interpret high-throughput plant phenotyping data in Africa/Morocco, for locally important crops and cropping systems with particular emphasis on optimising the use of fertilisers. This PhD thesis focused on the use of ground-based proximal sensors and drone-based imagery to assess the nutritional status of African crops. Low-cost hand-held sensors and drone were used to collect spectral reflectance data in tandem with agro-morpho-physiological metrics for nutrient and drought status evaluation in quinoa, cowpea and wheat. Datasets were collected and analysed at multiple scales: aerial, ground-based in the field and in glasshouse-controlled environment experiments.

In the glasshouse at Cranfield, experiments were conducted examining nitrogen (N) and phosphorus (P) stress on quinoa and cowpea (Chapter 3). Additionally, a drought and N stress experiment on spring wheat was conducted in the glasshouse (Chapter 4). These experiments were used to collect time series of spectral data to test an extensive range of known existing canopy spectral reflectance indices (SRIs) for effectiveness and specificity for the various stresses, and to search for novel indices using the spectral information. These experiments

yielded a high-quality dataset for investigating the interaction between these two nutrients and identifying nutrient specific characteristics for diagnostic protocols.

Specific spectral indices that could distinguish between N and P stress at the early growth stage of quinoa were found. However, identifying SRIs for P stress was challenging particularly in cowpea. Specific spectral reflectance canopy indices have been shown to be more sensitive to either water or N stress. Amongst 39 SRIs tested, the Renormalised Difference Vegetation Index (RDVI) and Red Difference Vegetation Index (rDVI_790) demonstrated best sensitivity for detecting drought stress. Chlorophyll-sensitive indices such as the chlorophyll Index (mNDblue_730), Greenness Index (G), Lichtenthaler Index (Lic2), as well as red-edge indices including Modified Red-Edge Simple Ratio (MRESR), chlorophyll Index Red-Edge (CIrededge) and Normalised Difference Red-Edge (NDRE) exhibited best specificity for detecting N stress. In the field at Rothamsted, a multiscale approach employing aerial drone imagery and ground-based handheld sensors at the aerial, canopy and leaf scales was utilised to assess the nutritional status of winter wheat (Chapter 5). The Normalised Difference Vegetation Index (NDVI) measured on the ground with a handheld sensor at the leaf level indicated the best sensitivity for assessing the N status of winter wheat compared to the drone and canopy sensor.

Four (4) publications were produced in addition to one manuscript under review. Aspects of the PhD project have been presented at 5 international scientific conferences and workshops earning recognition with an award. Significant progress was consistently made during the 4-year PhD programme in Environment and Agrifood at Cranfield University, successfully accomplishing the project’s objectives.

GENERAL AUDIENCE ABSTRACT

Understanding the nutritional needs of crops is crucial for ensuring their health and maximising yield. However, the capability to accurately measure relevant physical characteristics (phenotypes) of important crops in response to complex nutrient stresses is limited. For crop breeders and researchers, the existing capacity to characterise crops with adequate precision, detail and efficiency is hindering significant progress in crop development. In this PhD thesis, the use of advanced sensing techniques to assess the nutritional status of African crops was explored, focusing on three main objectives.

First, the use of a handheld proximal sensor was investigated to evaluate the spectral properties of quinoa and cowpea crops grown under different N and P supplies in controlled glasshouse conditions (Chapter 3). By analysing these spectral properties, the aim was to identify spectral indices that could show early signs of N and P stress separately in the plants. These stress indicators were related to the overall performance of the crops. Spectral indices were found that could distinguish between N and P stress at the early growth stage of the crops. However, identifying spectral indices for P stress was limited, particularly in cowpea due to the shorter wavelength range of the handheld device. The results showed significant relationships between the spectral indices and traits related to the morphology, physiology and agronomy of the crops.

Second, it was demonstrated that different levels of N impact the drought responses of spring wheat (Chapter 4). By evaluating morpho-physiological changes in the plants under high N and low N conditions, an understanding of how spectral reflectance measured at the leaf level could help distinguish between combined and complex stresses such as drought and nutrient deficiency was investigated. The results showed a greater amplitude of drought response in plants that were supplied with high N compared to low N levels, with interactive effects on many morphological and physiological traits. Out of a group of 39 different SRIs, only the Renormalised Difference Vegetation Index (RDVI) and the Red Difference Vegetation Index (rDVI_790) showed better accuracy in detecting drought stress. The results also revealed that indices sensitive to chlorophyll levels, such as the chlorophyll Index (mNDblue_730), Greenness Index (G) and Lichtenthaler Index (Lic2), as well as red-edge indices like Modified Red-Edge Simple Ratio (MRESR), chlorophyll Index Red-Edge (CIrededge) and Normalised Difference Red-Edge (NDRE), were more accurate in detecting N stress.

Lastly, the effectiveness of using spectral information from images collected from a drone and spectral reflectance measured with proximal sensors on the ground were compared for detecting N stress in winter wheat under field conditions (Chapter 5). By comparing these two sensing methods, it was assessed which approach is more accurate, reliable and cost-effective for assessing the N nutritional needs of the crop in real-world agricultural settings. The results indicated that the NDVI measured on the ground at the leaf level could accurately detect the small changes in N levels earlier compared to the drone NDVI and canopy level NDVI and for assessing the agronomic performance of winter wheat. Overall, this PhD research sheds new light on the potential of advanced sensing techniques to improve crop management practices and enhance agricultural productivity by providing timely and accurate information about the nutritional status of the studied crops.

Keywords:

Phenotypes, sensing techniques, spectral properties, drought stress, nutrient deficiency, quinoa, cowpea, wheat

ACKNOWLEDGEMENTS

First and foremost, I would like to extend my heartfelt gratitude to my supervisors, Prof. Fady Mohareb, Dr. Toby W. Waine and Prof. Malcolm J. Hawkesford for their outstanding guidance, motivation, constructive criticism and unwavering support throughout my Doctoral research. I am grateful for the opportunity to engage in innovative research under their supervision in an environment that fosters both rigorous scientific inquiry and deep understanding. I would like to thank Frank Gyan Okyere, my PhD project partner, for his great collaborative work, research ideas and significant contribution to this Doctoral work.

Special thanks to the 'Malcolm Research Group' at Rothamsted Research particularly, Dr. Nicolas Virlet for offering technical support, fruitful scientific discussions and for reading and providing critical comments on my thesis, Sue Steele for her excellent administrative support, Andrew Riche for his technical support on UAV imagery and meaningful scientific discussions, Dr. Parul Sehrawat for her data analysis support. My sincere appreciation and a big round of applause go to March Castle for collecting and processing the UAV data and training me in UAV data extraction. I am also thankful to him for driving me to Cranfield and supporting me in data collection most especially during the Covid-19 pandemic. I would like to thank Dr. Petros Sigalas for his guidance in nutrient solution preparation and for reading and providing constructive comments on my thesis. My sincere thanks also go to Saroj Parmar for her timely analyses of the plant nutritional contents.

Again, I express my gratitude to the various individuals at Rothamsted Research whose contributions have been indispensable throughout my PhD journey. In particular, Nicola Yates (International Programmes Manager) for her administrative support. Thank you so much, Donna Fellows (Studentship Officer) for your cordial relationship with me and the Fellows award to me as the most interesting student to work with. Many thanks to Suzanne Clark (Senior Statistician) for her fruitful scientific discussion on experimental designs and for providing statistical and data analysis support. Much appreciation to Chris Hall for his technical assistance and guidance during post-harvest sample processing at the Jenkinson experimental facility.

I want to thank the Environment and Agrifood Programme at Cranfield University for the opportunity to develop new skills and experiences throughout the Doctoral programme. I give much thanks to Lynne Roxbee Cox and Ian Truckell (Cranfield University) for their support

in running the experiment at the Plant Growth Facility at Cranfield University. Additionally, I thank the UK Agri-Tech Centres–Crop Health and Protection (CHAP) and Agri-EPI Centre, funded by Innovate UK, for the use of their facilities to conduct part of this research at Cranfield University. I would also take this opportunity to thank OCP SA for funding this Doctoral research under the UM6P, Rothamsted Research and Cranfield University programme. Rothamsted Research receives grant-aided support from the Biotechnology and Biological Sciences Research Council (BBSRC) through the Delivering Sustainable Wheat programme (BB/X011003/1). I would like to acknowledge the Sustainable Agriculture for Africa (SAFA) for its significant contribution to the PhD project. I am grateful to colleagues and PIs of the FP04 project for fruitful discussions and for sharing research ideas during progress meetings.

My heartily gratitude goes to Dr. Manal Mhada, Prof. Bruno Gerard, Dr. Manal EL Akrouchi and Kamal Hejjaoui all at the UM6P, for hosting me and providing all support for a successful research stay in Benguerir, Morocco. I am thankful to all co-authors for their critical comments and for offering valuable contributions during manuscript preparations for publication. Huge shout out to the 'UROC cohort' and Rothamsted Research and Cranfield University student community for making the Doctoral studies a great experience. The academic and social atmosphere was instrumental to destress and relax the mind. I would like to express my deep gratitude to Dr. Tobias Wojciechowski (Forschungszentrum, Jülich, IBG-2) and Dr. Beloved Mensah Dzomeku (CSIR-Crops Research Institute, Kumasi) for their valuable contribution to my professional and academic growth. I would also send my sincere appreciation to my lovely friends including Sarah Ansah, Efua Yeboah, Nana Akua, Linda Tetteh, Loretta Gidi, Dr. Sally Nyarko, Paul Opoku, Raphael Acquah, William Kota and Dr. Felix Frimpong for their encouragement and for providing 'morale'.

A remarkable depth of gratitude is extended to my family, especially my parents; Mr. Daniel Kingsley Cudjoe and Juliana Cudjoe, and siblings; Gifty, Haggar, Ruth, Alphonsar, Enock and my nephew, Jerfnick for being the beacon of my emotional and spiritual stability. Finally, I am greatly indebted to everyone who sacrificed the most throughout my Doctoral research. Indeed, your support, love, patience, understanding and commitment have helped me walk this far. Thank you all.

To God be the Glory for the great things he has done!

TABLE OF CONTENTS

LIST OF FIGURES

LIST OF TABLES

LIST OF EQUATIONS

LIST OF ABBREVIATIONS

A_n	Net CO_2 Assimilation Rate
3D	3 Dimensional
AAPA	Association for Precision Agriculture (AAPA)
AGRA	Alliance for a Green Revolution in Africa
AI	Artificial Intelligence
ANOVA	Analysis of Variance
APNI	African Plant Nutrition Institute
ARC	Agricultural Research Council
ARI1	Anthocyanin Reflectance Index 1
ARI2	Anthocyanin Reflectance Index 2
CERAAS	Centre for the Improvement of Drought Adaptation
CGIAR	Consultative Group on International Agricultural Research
CIAT	International Centre for Tropical Agriculture
CI_{green}	Green Chlorophyll Index
CIgreen	Chlorophyll Index Green
$CI_{rededge}$	Red Edge Chlorophyll Index

CIrededge	Chlorophyll Index Red Edge
CRI1	Carotenoid Reflectance Index 1
CRI2	Carotenoid Reflectance Index 2
Ctr1	Carter Index 1
Ctr2	Carter Index 2
DAS	Days After Sowing
DAWS	Days After Water Stress
DEM	Digital Elevation Model
df	Degrees of Freedom
DM	Dry Matter
DSS	Decision Support System
DW	Dry Weight
E	Transpiration Rate
EMPHASIS	Multi-Scale Plant Phenomics and Simulation
FABI	Forestry and Agricultural Biotechnology Institute
FAOSTAT	Food and Agriculture Organisation Statistics
FLIR	Forward-Looking Infrared
G	Greenness Index
G×E	Genotype-Environment Interaction
G×E×M	Genotype, Environment, and Management
GCPs	Ground Control Points
GDP	Gross Domestic Product
GIS	Geographic Information System
GLAI	Green Leaf Area Index
GM1	Gitelson and Merzlyak Index 1
GM2	Gitelson and Merzlyak Index 2
GNDVI	Green Normalised Difference Vegetation Index
GNDVI_780	Green Normalised Difference Vegetation Index (780 nm)
GPS	Global Positioning System
G*s*	Stomatal Conductance
GSD	Ground Sampling Distance
gSRa_790	Green Simple Ratio (790 nm)
GVI	Green Vegetation Index
GY	Grain Yield
HIPC	Highly Indebted Poor Countries
HN	High Nitrogen
HNHP	High Nitrogen, High Phosphorus
HNLP	High Nitrogen, Low Phosphorus
HN-WS	High Nitrogen-Water Stressed
HN-WW	High Nitrogen-Well Watered
HSW	Hundred Seed Weight
HTPPs	High Throughput Phenotyping Platforms
ICARDA	International Centre for Agricultural Research in the Dry Areas

ICP-OES	Inductively Coupled Plasma Optical Emission Spectroscopy
IER	Institute of Rural Economy
IITA	Institute of Tropical Agriculture
INERA	Environment and Agricultural Research Institute
IoT	Internet-of-Things
IPPN	International Plant Phenotyping Network
ISRA	Senegalese Agricultural Research Institute
LA	Leaf Area
LAI	leaf Area Index
Lic1	Lichtenthaler Indices 1
Lic2	Lichtenthaler Indices 2
LiDAR	Light detection and ranging
LIFT	light-induced fluorescence transient
LMMs	Linear Mixed Models
LN	Low Nitrogen
LNA	Leaf Nitrogen Accumulation
LNC	leaf Nitrogen Content
LNHP	Low Nitrogen, High Phosphorus
LNLP	Low Nitrogen, Low Phosphorus
LN-WS	Low Nitrogen-Water Stressed
LN-WW	Low Nitrogen-Well Watered
LPC	Leaf Phosphorus Concentration
LSD	Least Significant Difference
MCARI	Modified Chlorophyll Absorption in Reflectance Index
MCARI1	Modified Chlorophyll Absorption in Reflectance Index 1
MENA	Middle East and North Africa
ML	Machine Learning
mNDblue_530	Chlorophyll Index (530 nm)
mNDblue_730	Chlorophyll Index (730 nm)
MRESR	Modified Red Edge Simple Ratio
MSV	Maize Streak Virus
N	Nitrogen
NDRE	Normalised Difference Red Edge
NDVI	Normalised Difference Vegetation Index
$NDVI_{rededge}$	Red Edge Normalised Difference Vegetation Index
NIR	Near Infrared
NPCI	Normalised Pigment Chlorophyll Index
NPQI	Normalised Phaeophytinisation Index
NUE	Nitrogen Use Efficiency
OSAVI	Optimised Soil-Adjusted Vegetation Index
P	Phosphorus
PA	Precision Agriculture

PAR	Photosynthetically Active Radiation
PH	Plant Height
PRI	Photochemical Reflectance Index
PRI/NDVI	Photochemical Reflectance Index/Normalised Difference Vegetation Index
PRI_550	Photochemical Reflectance Index (550 nm)
PRI_norm	Normalised Photochemical Reflectance Index
PRS	Proximal and Remote Sensing
PS	Proximal Sensing
RCBD	Randomized Complete Block Design
RDVI	Renormalised Difference Vegetation Index
rDVI_790	Red Difference Vegetation Index (790 nm)
REIP	Red Edge Inflection Point
REML	Residual Maximum Likelihood
RENDVI	Red Edge Normalised Difference Vegetation Index
REP	Red Edge Position
ReVI	Red Vegetation Index
RGB	Red-Green-Blue
RH	Relative Humidity
RMA	Repeated Measures ANOVA
RMSE	Root Means Square Error
RS	Remote Sensing
RVI	Ratio Vegetation Index
RWC	Relative Water Content
SADC	Southern African Development Community
SAVI	Soil Adjusted Vegetation Index
SfM	Structure-from-Motion
SFW	Shoot Fresh Weight
SGCI	Science Granting Councils Initiative
SGCs	Science Granting Councils
SIPI	Structure Intensive Pigment Index
SMC	Soil Moisture Content
SPAD	Soil Plant Analysis Development
SPRI	Simple Ratio Pigment Index
SR	Simple Ratio
SRa_790	Red Simple Ratio (790 nm)
SRIs	Spectral Reflectance Indices
$SR_{rededge}$	Red Edge Simple Ratio
SRVIs	Simple Ratio Vegetation Indices
SSA	Sub-Saharan Africa
STI	Science, Technology and Innovation
SWIR	Short Wave Infrared
SY	Seed Yield
TCARI	Transformed Chlorophyll Absorption in Reflectance Index

TGW	Thousand Grain Weight
TPB	Total Plant Biomass
TVI	Triangular Vegetation Index
TW	Turgid Weight
UAV	Unmanned Aerial Vehicle
VB	Vegetative Biomass
VCs	Variance Components
VIs	Vegetation Indices
VNIR	Visible Near Infrared
WGIN	Wheat Genetic Improvement Network
WS	Water-Stressed
WSN	Wireless Sensor Network
WUEi	Intrinsic water use efficiency
WW	Well-Watered
ZMI	Zarco-Tejada and Miller Index

LIST OF PUBLICATIONS

1. **Cudjoe, D. K**., Virlet, N., Castle, M., Riche, A. B., Mhada, M., Waine, T. W., Mohareb, F., and Hawkesford, M. J. (2023a). Field phenotyping for African crops: overview and perspectives. *Frontiers in Plant Science*, 14. https://doi.org/10.3389/fpls.2023.1219673

2. **Cudjoe, D. K**., Okyere, F. G., Virlet, N., Castle, M., Buchner, P., Parmar, S., Sadeghi-Tehran, P., Riche, A. B., Sohail, Q., Mhada, M., Ghanem, M., Waine, T. W., Mohareb, F., and Hawkesford, M. J. (2023b). Using proximal sensing parameters linked to the photosynthetic capacity to assess the nutritional status and yield potential in quinoa. *Acta Horticulturae*, 1360, 373-379. https://doi.org/10.17660/ActaHortic.2023.1360.45

3. **Cudjoe, D. K**., Okyere, F. G., Clark, S. J, Virlet, N., Sehrawat, P., Castle, M., Riche, A. B., Waine, T. W., Mohareb, F., and Hawkesford, M. J. Interaction of water and nitrogen stress in wheat and the potential for independent detection using a handheld proximal sensor. *Manuscript has been submitted to the Plant Phenomics Journal with manuscript number: PlantPhenomics-D-24-00072 and it is under review.*

4. Okyere, F. G., **Cudjoe, D**., Sadeghi-Tehran, P., Virlet, N., Riche, A. B., Castle, M., Greche, L., Simms, D., Mhada, M., Mohareb, F., and Hawkesford, M. J. (2023). Modeling the spatial-spectral characteristics of plants for nutrient status identification using hyperspectral data and deep learning methods. *Frontiers in Plant Science*, 14, https://doi.org/10.3389/fpls.2023.1209500

5. Okyere, F. G., **Cudjoe, D**., Sadeghi-Tehran, P., Virlet, N., Riche, A. B., Castle, M., Greche, L., Mohareb, F., Simms, D., Mhada, M., and Hawkesford, M. J. (2023). Machine Learning Methods for Automatic Segmentation of Images of Field-and Glasshouse-Based Plants for High-Throughput Phenotyping. *Plants*, 12 (10), 2035. https://doi.org/10.3390/plants12102035

LIST OF CONFERENCES

1. The 31st International Horticultural Congress at the Congress Centre in Angers, France from 14 to 20 August 2022. Conference paper (https://doi.org/10.17660/ActaHortic.2023.1360.45) and poster presentation.

2. The 7th International Plant Phenotyping Symposium 2022 (IPPS7) held in Wageningen, the Netherlands between 27 to 30 September 2022. Poster presentation.

3. The 75th Anniversary Conference of the International Fertiliser Society on plant nutrition and fertiliser production from 6 to 9 December 2022, Cambridge University, United Kingdom. Poster presentation.

4. The North American Plant Phenotyping Network Annual Conference, held from 13 to 17 February 2023 in St. Louis, Missouri, USA. Online poster presentation.

5. The Botany 2023 – One World conference was held from 22 to 26 July 2023, in Boise, Idaho USA. Online poster presentation.

LIST OF AWARDS

1. Best poster presentation Award at the Sustainable Agriculture for Africa (SAFA) workshop held on May 2022 in Benguerir, Morocco.

2. Fellows Award for being the most interesting student to work with at Rothamsted Research in 2023, Harpenden, England, United Kingdom.

The greatest challenge to any thinker is stating the problem in a way that will allow a solution - Bertrand Russell

CHAPTER 1

1 GENERAL INTRODUCTION

1.1 Research background and context

Nutritional status is a useful indicator of crop growth for optimising fertilisation management. In addition, accurate, real-time and non-destructive monitoring of crop nutritional status is crucial for agricultural management decisions and helps guide efficient fertiliser applications as well as enabling the prediction of yields (Silva et al., 2023). Nitrogen (N) and phosphorus (P) are among the most essential nutrients and play critical roles in the optimal growth and development of plants as it is the main driver for yield and quality (Leghari et al., 2016; Lambers, 2022; Hawkesford et al., 2023).

However, the conventional approaches to monitoring these essential nutrients in plants require extensive sampling, time and expensive laboratory chemical analysis, which are neither economically feasible nor environmentally acceptable on a broad scale. These measurements are destructive and affected by spatial heterogeneity of soil and crop parameters. Therefore, reliable and efficient methods for detecting nutrient stresses in crops are needed by farmers to advance current farming practices, particularly in developing countries where conventional agricultural systems are unable to keep up with the needs of rapid population expansion.

Proximal and remote sensing (PRS) has emerged in recent decades as important methodologies for the application of crop status monitoring to improve precision and throughput in phenotyping (Mezera et al., 2021; Tao et al., 2022). The principle behind using PRS techniques to identify crop nutrient status is the changes caused in pigment content, photosynthetic activity, cell structure and other physiological processes that alter the spectral reflectance of plants. The reflectance data is frequently used to generate spectral reflectance indices (SRIs), which are a mathematical computation of multiple wavebands. It has been demonstrated that using SRIs is an effective approach to estimating plant biophysical parameters and quantifying stresses using PRS techniques (Kamenova et al., 2017; Hatfield et al., 2019; Zhang and Zhou, 2019; Galieni et al., 2021).

Recent developments in the fields of spectroscopy using PRS (e.g., handheld spectrometers, drone imagery) provide many opportunities to integrate sensors at leaf,

canopy and aerial scales for efficient data acquisition, enhance crop management, with a focus on nutritional monitoring in various crops (Gabriel et al., 2017; Frels et al., 2018; Aracena Santos et al., 2021; Gordillo-Salinas et al., 2021; Zheng et al., 2022; Amaral et al., 2022).

Whilst nutrient status has been thoroughly investigated as single nutrient stresses (e.g., either N or P), a gap exists when stresses occur concurrently. For instance, P and water stresses could be confounding factors during N stress that can trigger or alter a wide range of physiological, morphological and metabolic stress responses in plants that are more complex than individual stresses (Krouk and Kiba, 2020). These responses are influenced by interactions between the different stresses, which can act as additive, synergistic or antagonistic factors (Crain et al., 2008; Jiang et al., 2019; Tan et al., 2021). However, from a practical standpoint, research needs to focus on the complicated interactions between many environmental stresses. Since most farmers especially in Africa are challenged with the management of multiple stresses, there is a need to assess novel and existing SRIs for specificity to these stresses to support precision agriculture (PA).

Recently, increased attention has been devoted to the use of handheld sensors for monitoring the nutritional status of crops in developing countries because of their ease of operation, non-destructive data collection and low cost (Cudjoe et al., 2023a). This PhD thesis focuses on three (3) crops (quinoa, cowpea and wheat) that are significant to African agriculture and many subtropical regions. Quinoa, cowpea and wheat are all valuable resources of protein, but they have distinct characteristics and uses. Quinoa is a complete protein, containing all nine essential amino acids and gluten-free (Pathan and Siddiqui, 2022). It is used as a grain substitute in salads, bowls and as a side dish. Cowpea is rich in lysine, which is often limited in other grains (Abebe and Alemayehu, 2022). It is commonly used in soups, stews, and as a side dish. It can also be dried and ground into flour for various recipes. Additionally, cowpea grows well in arid conditions and enriches the soil with N, making it beneficial for crop rotation. Wheat offers good protein content, though the protein quality is lower than that of quinoa and cowpea as it is deficient in lysine. It is the primary ingredient in bread, pasta, pastries and other baked products. Wheat is often used as animal feed, particularly in livestock

production. Presently, the use of PRS techniques to assess the complex nutrient stress effects and their interactions in these crops has not been widely investigated.

Therefore, the overall aim of this thesis is to assess the potential of using handheld proximal sensors and drone-based imagery to detect single-nutrient stress and differentiate between combined nutrient stresses, as well as their interactions in quinoa, cowpea and wheat. This assessment aimed to establish their appropriateness for field phenotyping in Africa by employing rapid and non-destructive phenotyping techniques. The objectives of this PhD research were implemented after ethical approval from the Cranfield University Research Ethics System (CURES) (Appendix A).

1.2 Research objectives

The study concentrated on using SRIs derived at leaf, canopy and aerial scales to provide a better estimation of crop nutritional status for improving agricultural fertilisation and water management. The overall aim was achieved by the following three (3) broad objectives:

1. Evaluation of spectral properties from handheld proximal sensors as indicators of individual and combined N and P stress in quinoa and cowpea and how they reflect crop performance. These crops are under-studied when it comes to their response to nutritional stresses and more importantly, using proximal sensors to detect these responses and the inherent interactions. The focus is to identify effective SRIs capable of detecting early N and P nutritional stresses, distinguishing between the two stresses and relating the spectral response to the morphology, physiology and agronomy of the crops. The specific objectives were (1) to identify optimal SRIs indicative of N and P status separately or the combined effect and their interactions, (2) to assess the time-course response of optimal SRIs to identify early nutritional variations, (3) to assess the agro-morpho-physiological responses under the different N and P availabilities and (4) to examine the relationships between optimal SRIs and agro-morpho-physiological parameters. This objective was implemented in 2020 by growing quinoa and cowpea in pots under different N and P supplies in the glasshouse at the Plant Growth Facility at Cranfield University. Spectral reflectance data were collected using the PolyPen RP410 contact spectrometer throughout the crop cycle in tandem with the measurement of agro-morpho-physiological parameters at specific growth stages. Objective 1 is linked

to chapter 3 of the thesis. These objectives connect with the joint PhD thesis in terms of the crops used, experimental design and treatment conditions. However, while this thesis explores proximal contact sensing, the other uses hyperspectral imagery and machine learning approaches to assess the nutritional status.

2. Evaluate the morpho-physiological drought responses at high and low N and examine if SRIs derived at the leaf level could discriminate between the combined stresses in spring wheat. This will allow the identification of indicative spectral signatures and SRIs that are responsive to the combined stresses and specific to either drought or N stress. The specific objectives were to (1) assess the morpho-physiological drought responses at high and low N conditions, (2) assess the time-course response of SRIs to identify early drought responses under high and low N conditions, (3) identify effective SRIs specific for discriminating between drought and N stress and (4) to examine the relationships between spectral response and morpho-physiological status. Experimental work to implement this objective was initiated and completed in 2022. Wheat plants were grown in pots exposed to drought and N stress conditions in the glasshouse at the Plant Growth Facility at Cranfield University. Spectral reflectance data was acquired using the PolyPen RP410 contact spectrometer along with the measurement of morpho-physiological parameters indicative of water and N stress. Objective 2 is linked to Chapter 4 of the thesis. Objective 2 has links with other PhD thesis in terms of the experimental design and treatment application. The difference is that while this thesis employs contact proximal sensing to collect spectral and morpho-physiological data, the other uses hyperspectral and RGB together with deep learning approaches.

3. Compare the effectiveness of proximal sensors and unmanned aerial vehicle (UAV) drone imagery for monitoring N stress responses in winter wheat under field conditions. The emphasis was on detecting the effects of N inputs on wheat performance and quantifying spectral attributes of the leaf, canopy and aerial scales as potential indicators of insufficient N-supply using a multiscale sensing approach. Experimental work on this objective was initiated and completed in 2021 at the experimental farm in Rothamsted Research using data collected from the Wheat Genetic Improvement Network (WGIN) diversity field trial. Spectral reflectance was measured using the PolyPen RP410 spectrometer, Tec5 spectroradiometer and UAV (drone) at leaf, canopy

and aerial scales respectively. In parallel, agro-morphological parameters were measured including the leaf N content (LNC), leaf area (LA), SPAD and yield and yield components. Objective 3 is linked to Chapter 5 of the thesis. This objective does not overlap with the sister PhD thesis.

1.3 Thesis structure and contributions

- This PhD thesis consists of six (6) chapters. My contribution to this thesis is highlighted in each chapter. **Chapter 1** starts with a general introduction that indicates the scope of the study, the problem statement, the significance of the study, the aims and objectives and an outline of the thesis. My contribution involved establishing the research scope and context of the thesis and deciding the aims and objectives. I was responsible for writing the entire text of this chapter.

- **Chapter 2** which is the literature review gives a theoretical perspective of PRS applications in phenotyping for plant nutritional status with a special focus on quinoa, cowpea and wheat. It also highlights field phenotyping for African crops based on (Cudjoe et al., 2023a, published in *Frontiers in Plant Science*: https://doi.org/10.3389/fpls.2023.1219673). In this chapter, I conducted a comprehensive review of the literature surrounding plant phenotyping, with a specific focus on PRS techniques used for crop nutritional status assessment. My contribution involved the selection and critical analysis of key research papers, the synthesis of relevant findings and the framing of these within the context of African agriculture. I was solely responsible for writing the entire text of this chapter and ensuring its alignment with the overall thesis objectives.

- Each experimental study/research chapter focuses on specific aims and objectives stated under section 1.2. These three research studies (Chapters 3, 4 and 5) form the most important parts of this thesis and translate to the main outcomes of the work produced. Therefore, these chapters have distinct abstracts, introductions, materials and methods, results, discussions, conclusions and references sub-sections. Chapters 3, 4 and 5 are formatted versions of peer-

reviewed journal articles and manuscripts submitted for publication or in preparation.

- **Chapter 3** is based on the paper (Cudjoe et al., 2023b; *Acta Horticulturae*: https://doi.org/10.17660/ActaHortic.2023.1360.45 and a manuscript to be submitted to the *MDPI Agronomy Journal*). This is focused on the determination of optimal SRIs for monitoring the nutritional status and agro-morpho-physiological responses in quinoa and cowpea under varying N and P availability using proximal sensing at the leaf level. It is also to identify SRIs specific to N or P stress. I designed and conducted the experiments detailed in this chapter, which involved the use of proximal sensors to monitor quinoa and cowpea under varying N and P conditions. I was directly involved in collecting the spectral data, analysing the agro-morpho-physiological parameters and deriving insights into the nutritional status of the crops. This chapter including the manuscript and published paper was written entirely by me, incorporating both the experimental data I generated and my interpretation of the results. Chapter 3 of the thesis is linked to objective 1.

- **Chapter 4** is based on a manuscript under review in the *Plant Phenomics Journal with manuscript number: PlantPhenomics-D-24-00072*. Chapter 4 is about the interaction of water and N stress in spring wheat and the potential for independent detection using a handheld proximal sensor. The focus of Chapter 4 is to assess the morpho-physiological drought responses at high and low N conditions and examine the potential of SRIs measured at the leaf scale to discriminate the combined drought and N stress effects in spring wheat. The experiments in this chapter were designed and carried out by me. I personally collected and analysed all spectral reflectance and morpho-physiological data, which were used to explore the potential for using handheld sensors to differentiate between these stresses. I authored the texts for this chapter, integrating both the data analysis and scientific discussion to highlight the significance of the findings. Chapter 4 is linked to objective 2 of the thesis.

- **Chapter 5** is focused on a multiscale assessment, employing a comprehensive approach that combines aerial drone imagery and ground-based proximal

sensors at the leaf and canopy scales. This integrated approach aims to evaluate their capabilities in assessing the N status and how the spectral response reflects the agronomic performance of winter wheat. For this chapter, I conducted a field study that utilised both proximal sensors and unmanned aerial vehicle (UAV) imagery to monitor N stress in winter wheat. My involvement extended to the collection of leaf and canopy scale spectral data. The aerial drone data was collected by a licensed technician. I collected data to compare the effectiveness of the different sensing scales in reflecting the N status and agronomic performance of winter wheat. This study was particularly relevant to high-throughput phenotyping and PA. Chapter 5 is linked to objective 3.

- **Chapter 6** gives a general discussion of the findings and provides a synthesis of the main findings of each chapter and research implications. Thus, it summarises the overall outcomes and contributions of the thesis in the context of the objectives, provides an overview of limitations and discusses ideas for future work worthy of further investigation. Future opportunities and practical implications for technology transfer to potential end-users are also discussed. In this final chapter, I synthesised the results from the previous chapters and highlighted the major findings of the research. I also identified potential limitations and provided recommendations for future research directions. This chapter was crucial in integrating the thesis' contributions to both the scientific community and practical applications in agriculture. All the written texts were done by me.

References

Abebe, B. K and Alemayehu, M. T. (2022). A review of the nutritional use of cowpea (*Vigna unguiculata* L. Walp) for human and animal diets. *Journal of Agriculture and Food Research*, 10, 100383

Amaral, J. B. C., Lopes, F. B., Magalhães, A. C. M. D., Kujawa, S., Taniguchi, C. A. K., Teixeira, A. D. S., and Niedbała, G. (2022). Quantifying nutrient content in the leaves of cowpea using remote sensing. *Applied Sciences*, 12 (1), 458. https://doi.org/10.3390/app12010458

Aracena Santos, P., Hakki, E. E., Gezgin, S., Topal, A., and Dedeoglu, M. (2021). Determination of phosphorus status in bread wheat leaves by visible and near-infrared spectral discriminant analysis. *Journal of Applied Remote Sensing*, 15 (1), 014503-014503. https://doi.org/10.1117/1.JRS.15.014503

Crain, C. M., Kroeker, K., and Halpern, B. S. (2008). Interactive and cumulative effects of multiple human stressors in marine systems. *Ecology Letters*, 11 (12), 1304-1315. https://doi.org/10.1111/j.1461-0248.2008.01253.x

Cudjoe, D. K., Virlet, N., Castle, M., Riche, A. B., Mhada, M., Waine, T. W., Mohareb, F., and Hawkesford, M. J. (2023a). Field phenotyping for African crops: overview and perspectives. *Frontiers in Plant Science*, 14. https://doi.org/10.3389/fpls.2023.1219673

Frels, K., Guttieri, M., Joyce, B., Leavitt, B., and Baenziger, P. S. (2018). Evaluating canopy spectral reflectance vegetation indices to estimate nitrogen use traits in hard winter wheat. *Field Crops Research*, 217, 82-92. https://doi.org/10.1016/j.fcr.2017.12.004

Gabriel, J. L., Zarco-Tejada, P. J., López-Herrera, P. J., Pérez-Martín, E., Alonso-Ayuso, M., and Quemada, M. (2017). Airborne and ground level sensors for monitoring nitrogen status in a maize crop. *Biosystems Engineering*, 160, 124-133. https://doi.org/10.1016/j.biosystemseng.2017.06.003

Galieni, A., D'Ascenzo, N., Stagnari, F., Pagnani, G., Xie, Q., and Pisante, M. (2021). Past and Future of Plant Stress Detection: An Overview from Remote Sensing to Positron Emission Tomography. *Frontiers in Plant Science*, 11, 609155. https://doi.org/10.3389/fpls.2020.609155

Gordillo-Salinas, V. M., Flores-Magdaleno, H., Ortiz-Solorio, C. A., and Arteaga-Ramírez, R. (2021). Evaluation of nitrogen status in a wheat crop using unmanned aerial vehicle images. *Chilean Journal of Agricultural Research*, 81 (3), 408-419. http://dx.doi.org/10.4067/S0718-58392021000300408

Hatfield, J. L., Prueger, J. H., Sauer, T. J., Dold, C., O'Brien, P., and Wacha, K. (2019). Applications of Vegetative Indices from Remote Sensing to Agriculture: Past and Future. *Inventions*, 4 (4), 71. http://dx.doi.org/10.3390/inventions4040071

Hawkesford, M. J., Cakmak, I., Coskun, D., De Kok, L. J., Lambers, H., Schjoerring, J. K., and White, P. J. (2023). Functions of macronutrients. in: Rengel, Z., Cakmak, I., and White, P. J. (ed.) Marschner's Mineral Nutrition of Plants 4th edition London Elsevier. pp. 201-281.

Jiang, J., Wang, Y. P., Yang, Y., Yu, M., Wang, C., and Yan, J. (2019). Interactive effects of nitrogen and phosphorus additions on plant growth vary with ecosystem type. *Plant and Soil*, 440, 523-537. https://doi.org/10.1007/s11104-019-04119-5

Kamenova, I., Filchev, L., and Ilieva, I. (2017). Review of spectral vegetation indices and methods for estimation of crop biophysical variables. *Aerospace Research in Bulgaria*, 29, 72-82.

Krouk, G and Kiba, T. (2020). Nitrogen and Phosphorus interactions in plants: from agronomic to physiological and molecular insights. *Current Opinion in Plant Biology*, 57, 104-109. https://doi.org/10.1016/j.pbi.2020.07.002

Lambers, H. (2022). Phosphorus acquisition and utilisation in plants. *Annual Review of Plant Biology*, 73, 17-42. https://doi.org/10.1146/annurev-arplant-102720-125738

Leghari, S. J., Wahocho, N. A., Laghari, G. M., HafeezLaghari, A., MustafaBhabhan, G., HussainTalpur, K., and Lashari, A. A. (2016). Role of nitrogen for plant growth and development: A review. *Advances in Environmental Biology*, 10 (9), 209-219

Mezera, J., Lukas, V., Horniaček, I., Smutný, V., and Elbl, J. (2021). Comparison of proximal and remote sensing for the diagnosis of crop status in site-specific crop management. *Sensors*, 22 (1), 19. https://doi.org/10.3390/s22010019

Pathan, S and Siddiqui, R. A. (2022). Nutritional composition and bioactive components in quinoa (*Chenopodium quinoa* Willd.) greens: A review. *Nutrients*, 14 (3), 558.

Silva, L., Conceição, L. A., Lidon, F. C., and Maçãs, B. (2023). Remote Monitoring of Crop Nitrogen Nutrition to Adjust Crop Models: A Review. *Agriculture*, 13 (4), 835. http://dx.doi.org/10.3390/agriculture13040835

Tan, Y., Chai, Q., Li, G., Zhao, C., Yu, A., Fan, Z., and Tian, X. (2021). Improving wheat grain yield via promotion of water and nitrogen utilisation in arid areas. *Scientific Reports*, 11 (1), 13821. https://doi.org/10.1038/s41598-021-92894-6

Tao, H., Xu, S., Tian, Y., Li, Z., Ge, Y., Zhang, J., and Jin, S. (2022). Proximal and remote sensing in plant phenomics: 20 years of progress, challenges, and perspectives. *Plant Communications*, 3 (6).

Zhang, F and Zhou, G. (2019). Estimation of vegetation water content using hyperspectral vegetation indices: a comparison of crop water indicators in

response to water stress treatments for summer maize. *BMC Ecol*ogy, 19, 18. https://doi.org/10.1186/s12898-019-0233-0

Zheng, J., Song, X., Yang, G., Du, X., Mei, X., and Yang, X. (2022). Remote sensing monitoring of rice and wheat canopy nitrogen: A review. *Remote Sensing*, 14 (22), 5712. https://doi.org/10.3390/rs14225712

CHAPTER 2

2 LITERATURE REVIEW

The literature review gives a general overview of plant phenotyping, the application of PRS techniques in plant phenotyping and its application for the nutritional status assessment in quinoa, cowpea and wheat (section 2.1). Another section (2.2) of the literature review is dedicated to field phenotyping for African crops which is a review paper published in *Frontiers in Plant Science* (Cudjoe et al., 2023a; https://doi.org/10.3389/fpls.2023.1219673).

2.1 Plant phenotyping

The concept of the plant 'phenotype' was first introduced by the Danish botanist Wilhelm Johannsen (Johannsen 1911). The plant phenotype refers to the observable characteristics of the plant that are expressed and measurable as influenced by the dynamic interaction between the genotype and the physical world (environment) in which the plant develops (Pieruschka and Lawson, 2015; Hickey et al., 2019). These interactions underpin crop performance quantified as growth, biomass, abiotic stress tolerance, photosynthetic capacity, resource use efficiency, yield and yield components.

For decades, farmers and plant breeders have made selections based on phenotypes to identify superior candidates or traits of agronomic value (Araus and Cairns, 2014). The conventional methods used for phenotyping were based on the appearance and touch of the crop, requiring experts to visually score plant samples and measure plant features manually, which often was destructive to plants. This method is also tedious, labour-intensive and time-consuming and therefore, limited by its throughput (Dhondt et al., 2013). Robust phenotyping is essential to plant breeding since it serves as the foundation for selecting lines for the development of new varieties. A new era in plant phenotyping measures complex traits linked to growth, yield and stress responses and adaptations with speed, improved accuracy and precision at different levels of organisation, including cells, tissues, organs, canopy, whole plants and populations non-destructively (Fiorani and Schurr 2013).

In recent years, many definitions have been used for plant phenotyping (Fiorani and Schurr 2013; Hickey et al., 2019; Watt et al., 2020; Li et al., 2021). For this PhD thesis, plant phenotyping refers to using a suite of methodologies and protocols developed

through PRS techniques for quantifying plant growth, development, morphology, physiology and biophysical responses to stresses. Delivering quantitative data on the dynamic responses of plants to their environment is one of the targets of contemporary plant phenotyping. To decipher genotype-environment (G×E) interactions and model phenotypic responses, Li et al. (2014) have proposed a scheme for plant phenotyping (Figure 2.1) utilising proximal sensing (PS) for developing cultivars with improved traits which includes the selection of plant germplasm, designing the experiment, measuring phenotypic parameters and interpreting results. Many of the recent advancements in plant phenotyping are driven by innovations in sensor technologies to measure plant growth and physiological status non-destructively in a high-throughput manner (Großkinsky et al., 2015; Li et al., 2021).

Presently, most plant phenotyping is conducted indoors (i.e., in growth chambers or glasshouses), semi-controlled environment and in the natural field environment using a variety of high-throughput phenotyping platforms (HTPPs) (Araus and Cairns, 2014; Virlet et al., 2017; Kirchgessner et al., 2017; Shakoor et al., 2017; Pieruschka and Schurr, 2022). These platforms use robotics, automation, sensors, imaging techniques and precise environmental control for fast, accurate and non-destructive phenotyping based on PRS techniques (Tao et al., 2022; Thakur et al., 2023).

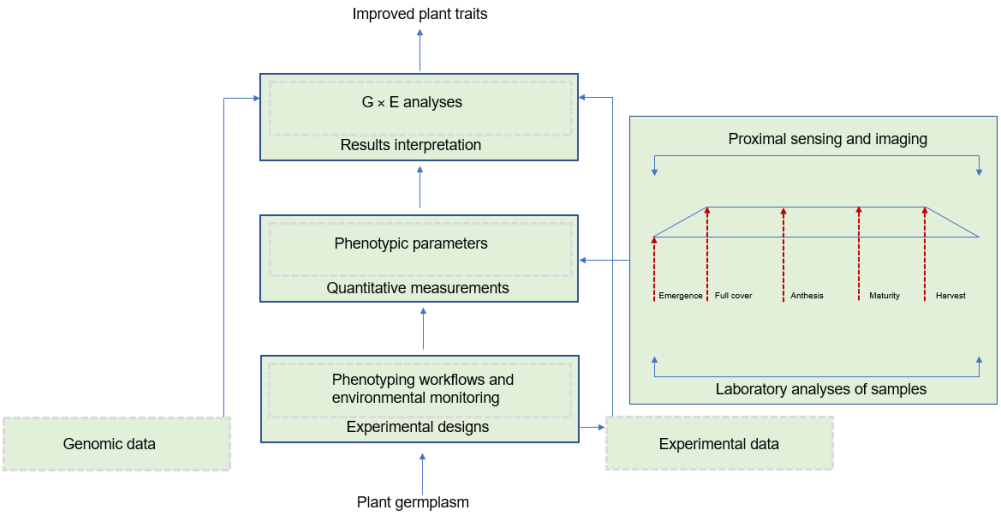

Figure 2.1. A scheme for plant phenotyping. Adapted from Li et al., 2014.

2.1.1 Proximal and remote sensing in plant phenotyping

Plant phenotyping increasingly employs PRS techniques because of their advantages in multi-dimensional phenotypic data acquisition, processing and analysis (Qiu et al., 2018; Machwitz et al., 2021; Tao et al., 2022). These techniques are used for characterising and monitoring crop or vegetation reflectance properties at reasonable temporal and spatial resolutions. PS is the employment of sensors close to plants to acquire spectral information. Remote sensing (RS) on the other hand is the acquisition of spectral information of plants without contact (Cavender-Bares et al., 2020; Tao et al., 2022). RS has been widely used in geoscience and engineering and may be applied to plant phenotyping and PA (Sishodia et al., 2020; Araus et al., 2022; Ahmed et al., 2023).

In the context of this PhD thesis, PS is the acquisition of spectral information using optical handheld devices or spectrometers contacting a leaf or in close range (non-contact) at a canopy scale. For example, the Soil Plant Analysis Development (SPAD) and PolyPen RP410 used in this work are typical types of contact spectrometers that generate spectral data at the leaf level. The Tec5 spectroradiometer on the other hand collects spectral data in close range at the canopy level. RS is the assessment of spectral information at a distance from the plant using a UAV (i.e., drone). Both PS and RS techniques are integrated into plant phenotyping for efficient data collection and monitoring of crop physiological status. For instance, the nutritional status of many crops has been assessed using PRS (e.g., Gabriel et al., 2017; Gordillo-Salinas et al., 2021; Zheng et al., 2022). However, little is known about quinoa and cowpea. The next section reviews the status of PRS for nutritional status assessment in the studied crops including quinoa, cowpea, and wheat.

2.1.2 Current state-of-the-art proximal and remote sensing techniques for nutritional status assessment in crops: special focus on quinoa, cowpea and wheat

This section of the literature review focuses on the current state-of-the-art PRS techniques employing handheld optical sensors and UAV drone imagery for nutritional status (N and P) monitoring in wheat, quinoa and cowpea. Farmers and agricultural producers are interested in systematically monitoring and assessing the nutritional status of crops at crucial times throughout the growing stages to supply adequate amounts of fertilisers (i.e., N and P fertilisers) for optimal crop growth, health monitoring and

performance prediction. Thus, a well-known strategy for achieving a high yield with minimal negative environmental impact is to match nutrient supply with crop nutritional needs (Feng et al., 2016). On a field scale, destructive sampling and laboratory chemical analysis are traditional methods of crop nutritional status evaluation that are accurate yet time and labour-intensive and expensive for rapid and precise nutritional status assessment (Yang et al., 2020; de Castro et al., 2021). Therefore, quick and non-destructive assessments of crop nutritional status at wide spatial and temporal scales are essential.

In recent years, PRS has played an important role in offering a quick, non-destructive and accurate assessment of crop nutritional status which is crucial for optimised fertiliser application and precision crop management decisions (Maes and Steppe, 2019; Sishodia et al., 2020). Its ability to measure the biophysical parameters of crops and detect spatiotemporal variability using appropriate platforms and techniques makes it one of the most promising approaches to assessing crop nutritional status (Fiorentini et al., 2021). Based on spectral data gathered by PRS, SRIs have been proposed as proxy techniques for evaluating the biophysical characteristics of vegetation at leaf and canopy scales (Skendžić et al., 2023).

In wheat, extensive studies have been conducted on nutritional status employing various combinations of PRS techniques (e.g., Aracena Santos et al., 2021; Fiorentini et al., 2021; Song et al., 2022; Zheng et al., 2022). Among the most recent approaches, UAVs or drones equipped with multispectral sensors have demonstrated efficiency in tracking and monitoring the nutritional status of wheat crops under field conditions (Walsh et al., 2018; Gordillo-Salinas et al., 2021; Nduku et al., 2023). Their usefulness relies on the capability to fly at low altitudes delivering imagery with high spatial resolution, ease of operation and the opportunity to mount various sensors to capture spectral data at different regions of the electromagnetic spectrum including the visible, near-infrared (NIR) and thermal (del Cerro et al., 2021). This enables high spatial-temporal resolution of crop monitoring during the production season. In addition, they are rapid, non-destructive and correlate closely with key physiological and agronomical crop characteristics (Lu et al., 2019). For instance, Walsh et al. (2018), evaluated the performance of SRIs derived from UAV images for quantification of plant N

concentration of spring wheat. The results indicated that red-edge and green-based SRIs including Red Edge Normalised Difference Vegetation Index ($NDVI_{rededge}$), Red Edge Simple Ratio ($SR_{rededge}$), Red Edge Chlorophyll Index ($CI_{rededge}$) and Green Chlorophyll Index (CI_{green}) showed higher correlation with plant N concentration compared to the red-based SRIs at the Feekes 5 growth stage. The strong correlations between SRIs obtained from UAV and plant N concentrations suggest the significance of the derived SRIs for early in-season N status detection in spring wheat. In another study, Fiorentini et al. (2021) demonstrated the utility of the NIR band-based vegetation indices such as Normalised Difference Vegetation Index (NDVI) and Normalised Difference Red Edge (NDRE) in detecting durum wheat N status (R^2=0.70 on average) under Mediterranean conditions.

A few studies have been focusing on determining the appropriate PRS tools for P status in wheat (Pimstein et al., 2011; Mahajan et al., 2014; Aracena Santos et al., 2021). For example, Mahajan et al. (2014) used leaf and canopy hyperspectral reflectance data coupled with linear correlation analysis to identify responsive wavelengths sensitive to biomass-based P status in wheat. A new proposed P-sensitive SRI based on 1080 nm and 1460 nm wavelengths predicted P content with high and significant accuracy (correlation coefficient (r) 0.42 and root means square error (RMSE) 0.180 g m^{-2}) at the booting stage of the wheat crop. Recently, Aracena Santos et al. (2021) used a spectroradiometer to determine key wavelengths in the visible and NIR spectra (418, 563, 639, 756 and 1000 nm) associated with P limitations at tillering (GS25) and heading (GS55) growth stages in wheat.

Most studies employing PRS techniques on crop nutritional status assessment have focused largely on wheat with limited research on tropical and semi-arid crops such as quinoa and cowpea. For quinoa, Alvar-Beltrán et al. (2020) tested proximal optical sensing tools to monitor quinoa growth in the field under various N input conditions. The researchers demonstrated that SPAD-502 and GreenSeeker had good accuracy in predicting crop biomass at harvest (R^2=0.68 and 0.82, respectively). Similarly, Cudjoe et al. (2023b) investigated how PS parameters (SPAD chlorophyll meter values and NDVI) could be used as indicators for N status and how they can be linked to quinoa performance in terms of photosynthesis and yield. The results showed that both SPAD

and NDVI correlated strongly with the leaf N content at 60 DAS (R^2=0.76, R^2=0.82, p<0.001), net CO_2 assimilation rate (R^2=0.86, R^2=0.81, p<0.001) and grain yield (R^2=0.68, R^2=0.80, p<0.001) respectively.

In cowpea, Amaral et al. (2022) employed a spectroradiometer-based hyperspectral RS to quantify the levels of P in cowpea leaves at different phenological stages. The study used single band, band ratio and partial least squares regression (PLSR) models to estimate the P content. The model showing the best fit was used to predict the P content in the single-band (R^2=0.62; RMSE=0.54 and RPD=1.61), band ratio (R^2=0.66; RMSE =0.65 and RPD=1.52) and PLSR models, using data from each of the phenological stages (R^2=0.80; RMSE=0.47 and RPD=1.66). The spectroscopy-related PLSR demonstrated the significant potential for the development of nutritional prediction models in cowpea. The authors concluded that the bands in the visible and NIR regions appeared to hold promise for determining the amount of nutrients (P) contents in the leaves of cowpea. Given the limited application of PRS in quinoa and cowpea, more advances in research are needed on these crops using the emerging PRS tools to monitor the nutritional status and improve their fertilisation management. These advances will be beneficial to farmers and the environment.

2.1.3 Physiological limitations of quinoa, cowpea and wheat to yield: source and sink dynamics in relation to N, P and water stress

The yield potential of quinoa, cowpea and wheat can be influenced by their physiological limitations, particularly through source-sink dynamics during critical growth phases (Lesjak, 2014; Chang and Zhu, 2017). Sources are plant parts like leaves that produce and export nutrients, while sinks are parts like seeds that import and use these nutrients. The balance between source strength (photosynthesis) and sink capacity (seed development) is crucial for optimal yield (Fang et al., 2024). Critical growth phases such as anthesis and seed filling are key phases where source-sink balance impacts yield (Carrera et al., 2024). For instance, a high source-sink ratio can enhance seed size but may lead to disorders if unbalanced (Fang et al., 2024). Adequate N boosts source activity by enhancing photosynthesis, while P supports root development, crucial for nutrient uptake (Martínez-Peña et al., 2022). Water stress affects both source activity (i.e., photosynthesis) and sink development (seed filling), potentially reducing yield

(Fang et al., 2024). Understanding these interactions helps in managing nutrient and water stresses to optimise crop yields.

Source-sink interactions significantly impact the yield of quinoa, cowpea and wheat by influencing the balance between the production of photoassimilates (source) and their utilisation for grain development (sink). Quinoa yield is often limited by sink capacity, as quinoa's ability to fill seeds depends on the plant's capacity to mobilise and allocate resources efficiently (Lesjak, 2014). Source-sink dynamics in cowpea are crucial during pod filling (Smith et al., 2018). The balance affects seed size and number, with N availability playing a significant role in enhancing source strength. Wheat yields are generally sink-limited, meaning that the number and size of grains determine yield potential (Miralles and Slafer, 2007). Enhancing sink capacity through breeding can improve yield. Overall, understanding these interactions helps optimise breeding strategies for better yield outcomes.

2.2 Field phenotyping for African crops: overview and perspectives

(This part of the literature review is based on Cudjoe et al., 2023a published in Frontiers in Plant Science, 14, https://doi.org/10.3389/fpls.2023.1219673 with minor modifications to the text, figures, tables and reformatting of the sections in general to improve clarity).

Daniel K. Cudjoe[1,2], Nicolas Virlet[1], March Castle[1], Andrew B. Riche[1], Manal Mhada[3], Toby W. Waine[2*], Fady Mohareb[2*] and Malcolm J. Hawkesford[1*]

[1]Rothamsted Research, Sustainable Soils and Crops, Harpenden, AL5 2JQ, United Kingdom.
[2]School of Water, Energy and Environment, Cranfield University, Cranfield, Bedfordshire, MK43 0AL, United Kingdom.
[3]AgroBiosciences Department, Mohammed VI Polytechnic University (UM6P), Lot 660 Hay My Rachid, 43150, Benguérir, Morocco.

***Correspondence:**
Corresponding Author: Malcolm J. Hawkesford
Email: malcolm.hawkesford@rothamsted.ac.uk

Corresponding Author: Toby W. Waine
Email: t.w.waine@cranfield.ac.uk

Corresponding Author: Fady Mohareb
Email: f.mohareb@cranfield.ac.uk

Abstract

Improvements in crop productivity are required to meet the dietary demands of the rapidly increasing African population. The development of key staple crop cultivars that are high-yielding and resilient to biotic and abiotic stresses is essential. To contribute to this objective, high-throughput plant phenotyping approaches are important enablers for the African plant science community to measure complex quantitative phenotypes and to establish the genetic basis of agriculturally relevant traits. These advances will facilitate the screening of germplasm for optimum performance and adaptation to low-input agriculture and resource-constrained environments. Increasing the capacity to investigate plant function and structure through non-invasive technologies is an effective strategy to aid plant breeding and additionally may contribute to precision agriculture (PA). However, despite the significant global advances in basic knowledge and sensor technology for plant phenotyping, Africa still lags behind in the development and implementation of these systems due to several practical, financial, geographical and political barriers. Currently, field phenotyping is mostly carried out by manual methods that are prone to error, costly, labour-intensive and may come with adverse

economic implications. Therefore, improvements in advanced field phenotyping capabilities and appropriate implementation are key factors for success in modern breeding and agricultural monitoring. In this review, we provide an overview of the current state of field phenotyping and the challenges limiting its implementation in some African countries. We suggest that the lack of appropriate field phenotyping infrastructures is impeding the development of improved crop cultivars and will have a detrimental impact on the agricultural sector and food security. We highlight the prospects for integrating emerging and advanced low-cost phenotyping technologies into breeding protocols and characterising crop responses to environmental challenges in field experimentation. Finally, we explore strategies for overcoming the barriers and maximising the full potential of emerging field phenotyping technologies in African agriculture. This review paper will open new windows and provide new perspectives for breeders and the entire plant science community in Africa.

Keywords: African crops, phenotypes, field phenotyping, high-throughput phenotyping, phenotyping infrastructures, low-cost phenotyping, African agriculture, precision agriculture

2.2.1 Introduction

The global demand for food is projected to increase in the coming decades, driven by population growth, climate change, pandemics, shifts in food consumption and biofuel use (Tilman et al., 2011; Godfray and Robinson, 2015; van Dijk et al., 2021). Ensuring that crop production is sufficient to meet future goals is a challenge for plant and agricultural sciences.

In Africa, agricultural crops provide food and income for smallholder farmers and consumers. Despite the huge agricultural potential, agricultural productivity in African countries continues to remain the lowest in the world (Bjornlund et al., 2020). Many studies have indicated that yields of several important staple crops may be stagnating or even declining across the continent (Roudier et al., 2011; Knox et al., 2012; Ray et al., 2012; Parkes et al., 2018). This is the case for key staple crops such as maize, rice, wheat, millet, sorghum, cowpea, cassava and yam, which together account for a large portion of the population's diet. Therefore, food supply systems would be negatively affected if yield gains in these crops continue to slow due to environmental stresses and production constraints.

Addressing food security in Africa is a vast challenge that needs to be tackled in many complementary directions. Infrastructure development adapted to local needs, good farming practices, management and political will are some of the major axes of development for food security. Improving crop performance and tolerance/resistance to biotic and abiotic conditions is the challenge facing the scientific community and innovative methods are needed. Advanced field phenotyping, e.g., using digital approaches, has developed substantially over the past decade and provides means for real-time monitoring of response to environmental stresses and nutrition, and aids in unravelling the relationships between yield and complex genotypic traits. The identification of genotypes with superior traits of agricultural interest remains one of the major targets for the genetic improvement of crops (Varshney et al., 2021).

The genomes of many agricultural crops such as rice (Matsumoto et al., 2005), sorghum (Paterson et al., 2009), maize (Schnable et al., 2009), soybean (Schmutz et al., 2010) and recently wheat (Appels et al., 2018) have been sequenced. However, the advances made in genomic approaches such as maker-assisted selection and high-throughput sequencing (Crossa et al., 2017; Scheben et al., 2018) are yet to be complemented with accurate field phenotyping methods (Minervini et al., 2015). Most of the traits of agronomic relevance (e.g., yield) are complex and quantitative, requiring tools for their phenotypic assessment in the field (Reynolds et al., 2020). Furthermore, open field rather than controlled environment measurements are more likely to be useful in identifying genotypes that will perform better in farming practice, especially when large plots that mimic real farm conditions (i.e., environmental and management conditions) are employed (Rebetzke et al., 2014).

In addition, PA is becoming increasingly important in today's technologically advanced world (Langemeier and Boehlje, 2021; Gobezie and Biswas, 2023) and PA remains one of the cardinal principles of field phenotyping. The PA farming management concept relies on modern digital techniques to monitor and optimise agricultural production processes to improve crop performance (Hedley, 2015; Gokool et al., 2023). Despite PA's contributions to sustainable agriculture, its use in resource-constrained smallholder farming environments, particularly in Sub-Saharan Africa (SSA), has been very limited (Gobezie and Biswas, 2023). Recent developments in sensor technologies, machine vision and higher-resolution digital cameras, in tandem with advanced data

processing power and other portable tools have paved the way for high-throughput plant phenotyping in the field to benefit crop breeding programmes (Deery et al., 2014; Zhang et al., 2016; Araus et al., 2022; Ahmed et al., 2023). From the field phenotyping perspective, these emerging technologies are enabling automated intensive data collection and increasing the ability to investigate plant function and structure through non-invasive methods with high accuracy. Such field phenotyping methods will aid crop improvement efforts to meet the expected demand for food and agricultural products in the future.

The development and application of these high-throughput tools for field phenotyping are currently focused on the main staple crops grown in the most developed agricultural regions. Over the decades, breeders and agronomists in Africa have used traditional phenotyping based on manual methods either for selecting traits or for improving yields through changes in agronomic practices (Iizumi and Sakai, 2020). However, traditional phenotyping in breeding is time-consuming and laborious, and data collection is insufficient to fulfil the needs of plant breeders which impedes breeding progress. Therefore, further advances in phenotyping methods and appropriate implementation are required to increase the effectiveness of selection in breeding programmes, speed up genetic gains, reduce costs and enable monitoring of plant status more efficiently than is currently feasible. The sophistication and cost of current plant phenotyping equipment (Reynolds et al., 2019) have restricted them from being widely applied in the developing world, especially in Africa. Additionally, insufficient technical, operational and regulatory restrictions and conceptual capacity in the plant science community have further limited implementation. Therefore, it is timely to begin to apply these technologies more widely, both geographically and with respect to target crops in Africa. Affordable high-throughput phenotyping aims to achieve reasonably priced solutions for all the components comprising the phenotyping pipeline which will promote their adoption for the breeding of African crops (Whalen and Yuhas, 2019; Bongomin et al., 2022).

Few studies have covered the use of modern field phenotyping approaches employing RS in Africa (e.g., Mutanga et al., 2016; Chivasa et al., 2017; Buchaillot et al., 2019; Bongomin et al., 2022; Kassim et al., 2022). For instance, Bongomin et al. (2022)

recently reviewed the status of field phenotyping in Uganda with a focus on the application of drones and image analytics.

In this review, we provide a background on African agriculture and cover the concept of digital field phenotyping, focused on traits that may be measured by emerging technologies and which could be applicable to African crops. The current developments of field phenotyping in Africa, including initiatives, implementation challenges and prospects are comprehensively reviewed. We observed that the lack of suitable field phenotyping infrastructures and approaches using digital technologies is limiting the development of improved crop cultivars and will negatively affect the agricultural industry and food security in Africa. We emphasise the potential for incorporating cutting-edge and low-cost phenotyping tools (i.e., portable field sensors, UAVs) into breeding schemes and for identifying agricultural crop responses to environmental constraints through field experimentation. Finally, we consider policy directions for tackling the implementation challenges (i.e., practical, financial, geographical and political) of digital field phenotyping and realising the full potential of available field phenotyping resources (i.e., technologies, tools and know-how) appropriate for African crops.

2.2.2 African crops and the production challenges

African countries are important producers of major crops with diverse agro-climatic and ecological conditions and cultural diversity (Leakey et al., 2022). Sub-Saharan West Africa is composed of a wide variety of ecosystems and an equally high number of production systems (https://www.fao.org/3/AC349E/ ac349e04.htm). Generally, crop production is concentrated in areas with a favourable combination of agro-bioclimatic conditions. In the Sahelian zone, cereals such as millet and sorghum are the predominant crops with annual rainfall (200-600 mm), transitioning to maize, groundnuts and cowpeas farther south in the Sudanian savannah zone (the so-called “Middle Belt”). These food crops are among the top five harvested crops in the Sahelian countries–Burkina Faso, Senegal, Mauritania, Mali, Chad and Niger. According to FAOSTAT (2018a) data, maize is the major essential staple food in SSA, accounting for nearly 20% of total calorie intake. The same source indicates that in Sub-Saharan West Africa, millet and sorghum account for roughly 64% of total cereal production. Across the rainy forests of the Guinean zone (1200-2200 mm of rainfall per year), crops are

predominantly root and tuber crops such as cassava and yams which are mostly cultivated in Ghana, Nigeria, Côte d'Ivoire and Sierra Leone. Yam is the second most important crop in Africa in terms of production after cassava (FAOSTAT, 2018a). Rice, on the other hand, is one of the most widely harvested crops in this humid zone, ranking first in Guinea, Liberia and Sierra Leone in terms of area harvested (Soullier et al., 2020; Duvallet et al., 2021).

Crop production in West Africa is mostly rainfed and crop production is vulnerable to climate change, which manifests itself in unpredictably high temperatures and erratic rainfall patterns (Sultan and Gaetani, 2016; Affoh et al., 2022). The five principal crops in West Africa in terms of harvested area (in millions of hectares per year on average in the last decade) are cassava (81), maize (19), millet (10), sorghum (12) and yam (57) (FAOSTAT, 2022). Major cash crops are cocoa, coffee and cotton. Declining soil fertility and unpredictable climate change impacts (among other factors) have made it difficult to maintain the yields of these major crops (Shimeles et al., 2018). Over the last three decades, the agricultural sector in West Africa has been characterised by strong production growth in some major staple crops culminating in increased production volumes for both domestic and export markets (Blein et al., 2008; FAO, 2015). Similarly to West Africa, Central Africa's principal food crops include cassava, peanuts, sorghum, millet, maize, sesame and plantains. Additionally, major cash crops for export include cotton, coffee and tobacco (Ochieng et al., 2020).

In Northern Africa, particularly Morocco, crop production is regionally diverse owing to different climatic conditions, agro-ecological zones, land-crop tenure and farming systems (Ouraich and Tyner, 2018). This geographical diversity results in varied agriculture, with crops ranging from cereals and vegetables to fruits and nuts, grains, legumes, etc., that contribute significantly towards the country's agricultural sustainability and food security. Cereal production accounts for 65% of cultivable agricultural areas (Ouraich and Tyner, 2018). Most cereal production occurs under rainfed conditions. As a result, productivity performance is influenced by precipitation levels. For instance, 7.3 million tonnes of wheat were produced in 2018 making it the 20th largest producer in the world, and 2.8 million tonnes of barley is the 15th largest producer in the world (FAOSTAT, 2018b). However, drought is a persistent threat to

crop production, especially in the lowlands where cereals are grown are particularly at risk because of the wide variations in annual precipitation (Verner et al., 2018; Meliho et al., 2020). In recent years, quinoa has sparked particular attention in Morocco (Choukr-Allah et al., 2016; Hirich et al., 2021). It remains one of the most nutrient-dense crops and is recognised as a 'Super Food' due to its nutritional benefits. Thus, Morocco is one of the few North African countries capable of achieving self-sufficiency in food production (Saidi and Diouri, 2017).

Grains and cereals (e.g., maize, wheat, barley, oats and sorghum) are South Africa's most important crops occupying more than 60% of the acreage under cultivation (FAO, 2022). Together, these crops account for one of the largest agricultural industries contributing more than 30% to the total gross value of agricultural production (FAO, 2022). Maize, the country's most important crop and largest locally produced field crop is a dietary staple supplying most of the carbohydrate needs, a source of livestock feed and an export crop (Epule et al., 2022). The country has emerged as the largest maize producer and exporter in the Southern African Development Community (SADC) region and Africa as a whole (Fisher et al., 2015; FAO, 2022). According to the FAO, 2022, in 2021 South Africa produced 17 million metric tonnes of maize, making it the 9th largest producer in the world. Moreover, it produced 2.6 million metric tonnes of potato and 2.3 million metric tonnes of wheat. Largely, South Africa has a semi-arid climate characterised by summer and winter rainfall seasons. Unpredictable weather conditions due to climate change have a severe impact on maize and wheat production which accounts for more than 36% of the total value of field crops (Bradshaw et al., 2022).

Smallholder farmers dominate agriculture in East African countries, contributing up to 90% of total agricultural production (Salami et al., 2010; Livingston et al., 2011). A cereal□legume mixed cropping pattern is the dominant system that includes maize, millet, sorghum and wheat (Van Duivenbooden et al., 2000). Over 40% of the region is covered by the maize mixed cropping system, which is followed by the pastoral (14%), root crop (12%) and cereal-root crop mixed system (11%) (Adhikari et al., 2015). Teff is a significant crop in the Ethiopian highlands, while other significant crops in the area include cassava, bananas and rice. The mixed cropping system in East Africa is based

on millet in the drier regions and maize and cassava in the humid regions (Adhikari et al., 2015). The main cash crops in most of the East African countries in SSA are coffee, tea, cotton, tobacco and sugarcane. Rainfall variability negatively impacts crop production in East African countries (Palmer et al., 2023). Generally, the major challenges to crop production in Africa are unproductive soils, pests and diseases, drought and poor crop management (Tadele, 2017). The distribution of major crops in each sub-region except Northern Africa is summarised in Figure 2.2.

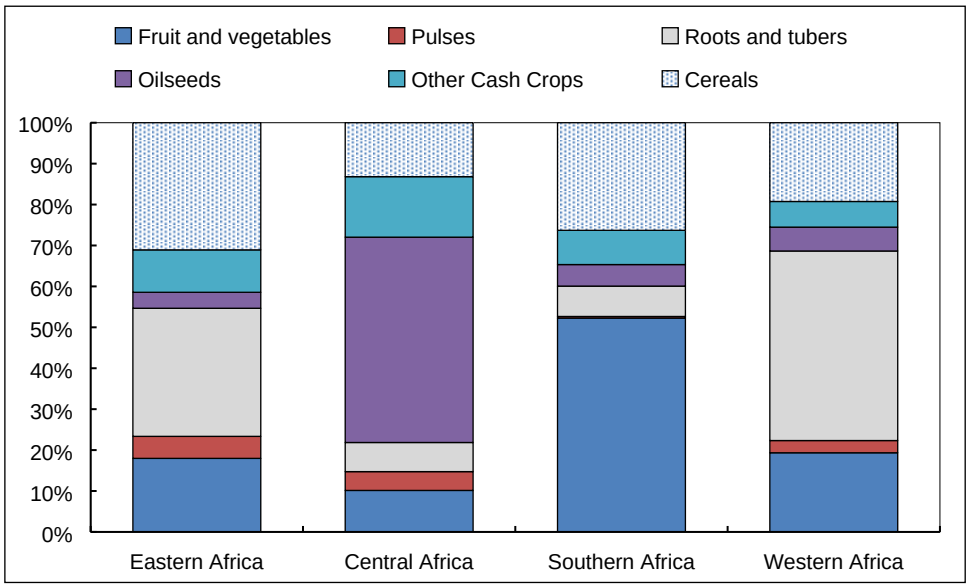

Figure 2.2. Major crop distribution in the Sub-Saharan African region based on average production values between 2011-13. Adapted from FAOSTAT. (2016). FAO, http://faostat3.fao.org/.

2.2.3 Digital and image-based field phenotyping

Experiments with repeated trials in diverse environments are often necessary to screen plants for desirable traits. This becomes problematic when there is the need to screen a large panel of genotypes for valuable traits (i.e., yield potential or abiotic and biotic stress tolerance) to assess genotype, environment and management (G×E×M) interactions (Araus and Cairns, 2014). Over the years, the measurement of individual plants in controlled conditions has dominated most of the phenotyping research. However, controlled environments often do not accurately mimic plant growth and development in field conditions (White et al., 2012). Field phenotyping is becoming more widely recognised as the approach that gives the most accurate representation of traits in real-world cropping systems (Tariq et al., 2020). Thus, field phenotyping is an

important component of crop improvement to assess how the genotype, the environment and their interaction (G×E) influence quantitative traits in a complex and dynamic manner (Fiorani and Schurr, 2013; Araus and Cairns, 2014; Neilson et al., 2015). Furthermore, field phenotyping is employed to discover novel traits, identify new germplasm carrying relevant but complex traits for breeding, and for testing proof of concept to validate traits (Watt et al., 2020). Traditionally, destructive sampling has been used to quantify certain observable plant traits, including laboratory analysis to characterise phenotypes based on their genetic and physiological functions. Digital phenotyping approaches seek to reduce this need (Tripodi et al., 2022; Virlet et al., 2022).

Different measurement approaches including novel technologies such as non-invasive imaging, robotics and sensor positioning systems have been incorporated in well-designed field phenotyping installations for high-throughput phenotyping (e.g., Araus and Cairns, 2014; Kirchgessner et al., 2017; Shakoor et al., 2017; Virlet et al., 2017; Pieruschka and Schurr, 2022). These significant strides in field phenotyping have fostered a major international collaborative effort directed toward data and protocol standardisation (Pieruschka and Schurr, 2019; Lorence and Jimenez, 2022). The appeal of these platforms is the increased throughput and objectivity in data collection compared to traditional field approaches. Non-invasive portable devices, ground-wheeled, motorised gantry scanalyzer systems, agricultural robots and aerial vehicles that deploy a wide range of cameras and sensors, together with high-performance computing are currently required to conduct field phenotyping in a timely and economical manner (Figure 2.3). Together, these platforms can phenotype plant characteristics throughout the season in field environments (White et al., 2012; Fritsche-Neto and Borém, 2015; Jimenez-Berni et al., 2018; Furbank et al., 2019; Li et al., 2021).

In recent years, manned and UAV-RS platforms have emerged as convenient high-throughput tools for field phenotyping (Pajares, 2015; Shi et al., 2016; Feng et al., 2021). These RS approaches, particularly UAVs enable quick and non-destructive high throughput phenotyping, with the benefit of adaptable and convenient operation (Yang et al., 2017a). These phenotyping platforms can combine multiple sensors such as digital cameras, infrared thermal imagers, light detection and ranging (LiDAR),

multispectral cameras and hyperspectral sensors for various assessments of morphological and physiological plant traits (Gonzalez-Dugo et al., 2015; Yang et al., 2017a; Camino et al., 2018; Roitsch et al., 2019).

Alternatively, field phenotyping can be accomplished on the ground utilising a fully automated fixed-site phenotyping platform (e.g., Kirchgessner et al., 2017; Virlet et al., 2017; Bai et al., 2019), hand-held sensors, portable spectroradiometers, hand-pushed carts or high-clearance tractors carrying multiple high-resolution sensors to measure phenotypic features non-destructively (Comar et al., 2012; Andrade-Sanchez et al., 2014; Crain et al., 2016). The use of rapid non-invasive portable devices that carry sensors for crop status monitoring has advanced field data collection due to their applicability and ease of operation (Parks et al., 2012; Yang et al., 2014; Condorelli et al., 2018). Recently, field phenotyping has become more flexible by integrating ground-based and aerial platforms (Potgieter et al., 2018; Furbank et al., 2019; Ninomiya, 2022). Table 2.1 summarises the diverse ground-based and aerial field phenotyping platforms, their applications, advantages and limitations.

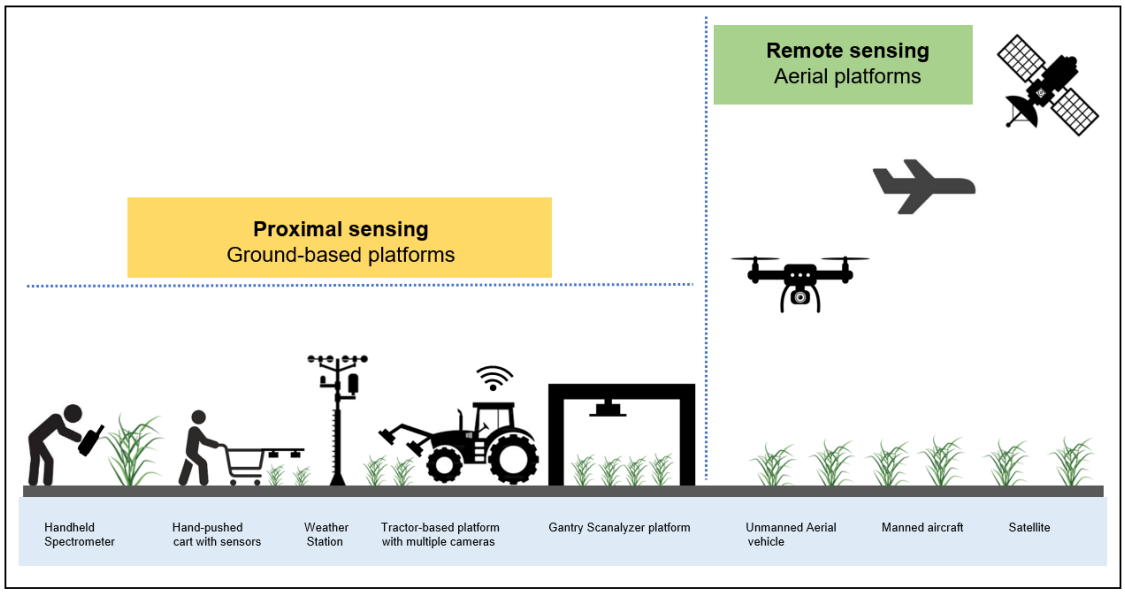

Figure 2.3. Overview of the most common field phenotyping systems and approaches at proximal and remote sensing (PRS) scales. The proximal sensing (PS) approach is based on ground-based platforms such as handheld spectrometers, hand-pushed carts equipped with sensors, tractor-based platforms fitted with multiple cameras and gantry scanalyzer systems that collect spectral information of crops in close range or contact. On the other hand, the remote sensing (RS) technique is based on aerial platforms including unmanned aerial vehicles (i.e., drones), manned aircraft and satellites that

acquire spectral imagery of crops without making physical contact but at a distance. Modified from (Pineda et al., 2021).

Table 2.1. Applications and limitations of field phenotyping platforms. Modified from Li et al., 2014 and Deery et al., 2014.

Phenotyping platform	Examples	Applications	Advantages	Limitations	References
Ground-based platforms					
Fixed-site systems	Field scanalyzers (i.e., Rothamsted field scanalyzer, Maricopa field scanalyzer)	Ground cover, canopy height, plant geometry, growth, growth stages, vegetation indices, chlorophyll fluorescence parameters	Unmanned continuous operation with good repeatability, deploy a wide range of sensors, fully automated. Not limited by soil conditions	Expensive, monitor a limited number of plots, limited by weather conditions	Virlet et al., 2017; Burnette et al., 2018
Permanent platforms based on a cable-suspended multi-sensor system	The ETH field phenotyping platform, the University of Nebraska phenotyping system	Monitor canopy cover, canopy height, and traits related to thermal and multi-spectral imaging with selected examples from winter wheat, maize, and soybean	Produce precise, high-resolution images, deploy a wide range of sensors, fully automated	Monitor a limited area of crop, difficult to move, expensive, and limited by weather conditions	Kirchgessner et al., 2017; Bai et al., 2019
Handheld sensors	Point spectroradiometers, thermal sensors, chlorophyll meters, imagers	Estimate chlorophyll fluorescence, canopy temperature, nitrogen status, leaf area, plant height, yield	Ground truth reference to validate aerial measurements (UAVs) and airplanes, low-cost and easy-to-use	Labour intensive and time-consuming, limited plot coverage, measurement bias	Yang et al., 2014; Andrianto et al., 2017; Garriga et al., 2017
In-field mobile platforms	Phenocart, proximal sensing cart, phenomobiles, manned buggies	Estimate biomass, leaf area index, counting plants, plant height, early vigour, and plant maturity	Manually operated, low-cost, easier to construct, multiple traits evaluations, deploy more sensors, flexibility with payload and view angle geometry; very adaptable	The motorised platforms are costly to construct and run, need technical expertise, hard to operate for large-scale experiments. Limited by weather and soil conditions	White and Conley, 2013; Andrade-Sanchez et al., 2014; Deery et al., 2014; Crain et al., 2016

Aerial platforms

Unmanned aerial vehicles (UAVs)	Broadly classified into Rotocopters, fixed wing systems, parachutes, and blimps	Traits such as canopy cover, canopy height, crop lodging, growth indices, and canopy temperature can be estimated from the imagery	Rotocopters (i.e., drones) can deploy a wide range of sensors, including thermal, multispectral, and hyperspectral cameras, high hovering capabilities, better flight time	Lower speeds for image stitching, lens distortion, and overlap of the acquired images can affect orthomosaic, battery use and flying time may be limited by the payload, and operability is limited in windy, wet, dull, variable light, or cold conditions	Sankaran et al., 2015; Zaman-Allah et al., 2015; Chawade et al., 2019; Holman, 2020
Satellite imaging	Digital Globe WorldView-2 satellite, WorldView-3 satellite, RADARSAT-2	In precision agriculture for germplasm evaluation, multi-location yield trials, field observation of crop biophysical parameters, weather predictions	Evaluation of moderate to large-sized trial, multi-location evaluation; provides automated coverage of isolated field trials across a larger geographical area	Affected by weather conditions, resolution, frequency of imaging, takes a long time from image acquisition to access, costly, higher frequency of satellite revisits, cloud cover can interfere with imaging	Tattaris et al., 2016; Yang et al., 2017b; Yang, 2018

2.2.4 Traits assessed by sensor platforms and their relevance for field phenotyping

For field phenotyping, traits that have been evaluated by sensors in the field have been reviewed recently by Watt et al. (2020) and include for example; (a) plant morphological development (i.e., including seed establishment and growth of the crop, the timing and dynamics of flower and fruit development); (b) functional traits that are related to the photosynthetic capacity and carbon uptake during the phenological growth phase; (c) traits related to biotic and abiotic stress resistance/tolerance; (d) traits that determine crop water status (e.g., water uptake and transpiration and water-use efficiency) of plants; (e) yield-related traits and harvest quality of crops (i.e., biomass yield) and (f) the structural and functional root traits (i.e., root architecture). These traits have been previously classified into morphometric and physiological parameters (Qiu et al., 2018). Traits such as plant height, stem diameter, leaf area or leaf area index, leaf angle, stalk length and in-plant space are morphometric parameters. Physiological parameters include traits such as photosynthetic rate, chlorophyll content, water stress, leaf water content, biomass and salt resistance, which together can impact plant growth. It should be emphasised that different phenotypic traits have specific time frames within the phenological cycle of the plant when they are relevant for the breeder and farmer. Currently, the most researched crops in field phenotyping are economic crops, such as wheat, maize, barley, sorghum, tomato, bean and grape because they have significant economic value for agricultural development. A challenge is to extend phenotyping into the vast range of African crops, some of which may be of only local importance.

Field phenotyping makes use of a variety of sensors due to the large number of phenotypic traits that must be measured. Several conventional and novel sensors such as digital cameras, range cameras, depth cameras, spectral sensors, lidar or laser sensors, thermal sensors, fluorescence sensors, multispectral cameras, hyperspectral cameras and others are employed and integrated for plant trait measurement in field phenotyping (Qiu et al., 2018; Roitsch et al., 2019; Xie and Yang, 2020). Since plants develop rapidly during their early growth stages, frequent measurements during their establishment are a prerequisite for the quantitative selection of vigour phenotypes. Drones fitted with conventional red-green-blue (RGB) cameras, in combination with advanced image processing pipelines, can automatically detect crop stands (single plants) and determine seed emergence, germination rates and timing under extreme

climatic events in the field (Liu et al., 2017). Most plants display strong morphological changes during their phenological development, which is greatly influenced by the availability of resources and changes in abiotic and biotic factors. Therefore, the development of robust, automated and precise methods to measure morphological plant traits in field conditions is still required (Gibbs et al., 2017).

The leaf is one of the important components of a plant. It plays a major role in plant growth given that its growing status influences the efficiency of the direct solar energy utilisation by plants. Hence, it is a significant parameter in plant phenotyping. Measurements of morphometric parameters of the leaf and other canopy features (i.e., leaf area, stem height, number of tillers and inflorescence architecture) have been evaluated using non-destructive multi-sensor approaches (Busemeyer et al., 2013; Fiorani and Schurr, 2013; Rahaman et al., 2015). However, the most frequently used geometric measure of plant canopy is the green leaf area index (GLAI), which relates the one-sided green leaf area per unit projected ground area (Chen and Black, 1992). For instance, UAV multispectral imagery has been used to characterise GLAI dynamics of a large maize panel under contrasted environmental conditions and thus holds great potential for yield predictions in breeding programmes (Blancon et al., 2019). LAI can also be evaluated, indicating plant coverage from spectral images (Dammer et al., 2016; Schirrmann et al., 2016).

Plant canopy architecture and other morphological traits of plant organs have been measured concurrently with 3D PS techniques. A body of recent reviews has compared the performances of the most common 3D sensors for high-throughput plant phenotyping (Li et al., 2014; Qiu et al., 2019). The 3D acquisition devices and approaches commonly used are LiDAR time-of-flight cameras, mono, multi-view stereo vision and structure-from-motion (SfM). The LiDAR sensors can scan and extract morphological traits of plant organs from 3D point clouds. For example, LiDAR was used to estimate plant height, ground cover and above-ground biomass in wheat (Jimenez-Berni et al., 2018). However, LiDAR sensors are expensive (Li et al., 2014), take significant time and there is a need to increase scanning time to increase the spatial resolution. Deploying a UAV-based system may reduce this challenge. Plant height is a key indicator of canopy structure, yield, carbohydrate storage capacity and lodging

occurrence (Holman et al., 2016; Hassan et al., 2019). Additionally, it has significant applications in predicting biomass, identifying plant cultivars, plant stress and phenological stages (Aasen et al., 2015). The traditional method of measuring height using a metre rule is labour-intensive, cumbersome and low throughput. In recent years, the development of drones and imaging sensors that capture high-resolution images has enabled high-throughput plant height estimation. For instance, Holman et al. (2016) estimated wheat height using UAV-based RGB images and terrestrial LiDAR.

Chlorophyll is a vital plant trait because it is strongly related to crop physiological status and may be indicative of photosynthetic rate, crop stress, nutrition status, yield and plant productivity (Peng et al., 2011; Maimaitijiang et al., 2017). The most popular tools for evaluating vegetation health using visible and NIR light are spectral sensors. Chlorophyll meters such as the SPAD-502 are frequently used instruments to measure the relative chlorophyll content. Handheld chlorophyll meters and fluorescence meters have been used to assess plant N status, photosynthesis, yield and its components in crops (Yang et al., 2014; Andrianto et al., 2017; Fernández-Calleja et al., 2020). Additionally, chlorophyll can be measured using NDVI sensors and portable spectrometers in the field (Bai et al., 2016).

Crop N content can serve as a proxy for soil fertiliser availability, assisting farmers in precision N application to the soil. UAV-based hyperspectral imaging and ground-level optical sensors (SPAD-502, Duplex and Multiplex) have been employed to estimate N fertilisation status in maize (Quemada et al., 2014). In another study, Zaman-Allah et al. (2015) used a UAV equipped with a multispectral sensor (Green, Red and NIR) to assess low N stress tolerance in corn. Additionally, vegetation indices (VIs) derived from spectral reflectance data captured by sensor devices such as the CropScan multispectral radiometer (Zhu et al., 2008), handheld spectroradiometers, the FieldSpec (Fitzgerald et al., 2006; Tilling et al., 2007; Feng et al., 2008) and Tec5 spectroradiometer (Erdle et al., 2013) can accurately measure N status in wheat and rice.

The above-ground biomass reflects light use efficiency and growth and is vital for carbon (C) stock accumulation and monitoring (Swinfield et al., 2019). Brocks and Bareth (2018) estimated the biomass in barley using RGB images collected by UAV.

Thermal NIR sensors are mostly used to detect crop water stress since they can provide temperature information for the crop (Park et al., 2017; Poblete et al., 2018; Bian et al., 2019). Thermal NIR sensors enable the estimation of canopy temperature which is a reflection of plant transpiration and plant water status. Kumar et al. (2020) used a proximal phenotyping cart (Phenocart) mounted with low-cost consumer-grade digital cameras to characterise wheat germplasm for drought tolerance under field conditions. Plant yield has been considered an important agronomic trait for field phenotyping. Bascon et al. (2022) estimated rice yield using multispectral images.

Additionally, roots play a crucial role in the uptake of N and P, essential nutrients for plant growth. They facilitate the absorption of these nutrients from the soil, which are vital for photosynthesis, energy transfer and overall plant health. Efficient root systems can enhance nutrient uptake efficiency, contributing to better growth and yield.
RS and root phenotyping with thermal imaging can help detect plant stresses by measuring leaf and canopy temperatures, which can indirectly reflect root activity (Li et al., 2014; Pineda et al., 2021). Thermal imaging capture emitted radiation, providing temperature readings that can indicate water stress and nutrient uptake efficiency (Smigaj et al., 2024; Wen et al., 2023). By combining thermal imaging with other spectral data, researchers can phenotype crops under various stress conditions (Sharma et al., 2023). Thermal imaging can be used in controlled environments to monitor early stress symptoms, aiding in the selection of genotypes with improved nutrient uptake capabilities (Sharma et al., 2023; Pineda et al., 2021). Overall, RS with thermal imaging offers a non-invasive method to study root phenotypes by analysing plant stress responses related to nutrient uptake.

The features of the sensors (e.g., spectral resolution, spatial resolution, specificity and cost) should be considered according to the specific applications, phenotyping needs and context. In the African context, low-cost sensors and analysis pipelines that are not complex would benefit a broader user base for plant phenotypic trait assessments. The most successful trait assessment approach incorporates in time (throughout the crop cycle) and space (at the canopy level) the performance of the crop with respect to capturing resources (e.g., radiation, water and nutrients) and the efficiency of resource utilisation (Araus et al., 2008). The aforementioned traits are discussed here with

specific examples of sensors and automated measurement approaches used for their evaluation in the field (see Table 2.2). The advantages and limitations of each type of sensor are indicated.

Table 2.2. Emerging high-throughput phenotyping techniques and integrated sensor platforms applicable for plant trait assessment for field phenotyping. Modified from Zhao et al., 2019.

Sensor	**Examples**	**Crop species**	**Trait/phenotypic parameter**	**Applications**	**Advantages**	**Limitation**	**References**
Hyperspectral sensor	VNIR, SWIR	Rice, Wheat	N status, NUE, water content, yield estimation, canopy components	Evaluate spectral properties, explore hyperspectral bands, estimate indices for fertiliser accumulated in plant organs, early detection of plant stress	Accurate estimation of N content and other biochemical or physiological status	Update model for new crop species, image processing is challenging, sensors are costly, large data size	Seiffert et al., 2010; Deery et al., 2014; Sadeghi-Tehran et al., 2021; Wang et al., 2021
Thermal sensor	Thermal infrared sensor, near-infrared camera, FLIR sensor	Wheat	Canopy temperature, drought tolerance, water use efficiency, root traits	Monitor crop temperature for abiotic stresses e.g., drought tolerance	Low-cost, precise and reliable in repeated experiments	Environmental factors have an impact on performance, very small temperature variations are undetectable, and cameras with higher resolution are heavier	Costa et al., 2013; Deery et al., 2019; Sagan et al., 2019 ; Pineda et al., 2021
Visible light sensor	RGB sensor, visible light camera	Rice	Shoot growth, phenology, greenness, plant vigour, leaf area	Visible phenotype parameters, classification of crop organs, greenness, growth and health, time series of vegetation indices	Affordable sensors are available	Visual spectral bands and properties are limited, Changes in illumination conditions cause image blur and noise errors	Kipp et al., 2014; Guo et al., 2015
3D sensor	LIDAR (Light Detection and Ranging) sensor, 3D laser scanner	Maize, Wheat	Plant height, canopy cover, above-ground biomass, crop architecture	Extract morphological traits of plants organs from 3D point clouds; measuring crop height and volume	3D plant information can be quickly captured through close-range observation	LIDAR can be sensitive to small variations in path length, field applications can be challenging	Müller-Linow et al., 2015; Guo et al., 2018; Jimenez-Berni et al., 2018; Qiu et al., 2019
Fluorescence sensor	Fluorescence camera, LIFT fluorometer	Wheat	Photosynthetic capacity, chlorophyll content, quantum yield	Measure photosynthesis, chlorophyll, water stress	Automatic and rapid measurement of photosynthetic parameters	Limited for UAV imagery, can be affected by background noise, difficult to use in the field	Chaerle and Van Der Straeten, 2000; Zendonadi dos Santos et al., 2021

Multispectral sensor	Sorghum, Maize	Disease resistance, nutrient use efficiency, N content, biomass, grain yield	Multiple plant responses to nutrient deficiency, water stress, diseases, etc.,	High-resolution, fast	Sensors can be expensive, limited to a few spectral bands	Zaman-Allah et al., 2015; Zhao et al., 2021
Spectrometer	Maize	Water content, seed composition, yield	Leaf and canopy growth, disease evaluation, leaf area, chlorophyll content, canopy temperature, and crop responses	Handy and easy to use, inexpensive	The quality of the data may be affected by soil background, spectral mixing could occur, and sensor calibration required	Cozzolino, 2014; Andrianto et al., 2017; Chivasa et al., 2020; Cavaco et al., 2022

2.2.5 Overview of the status of field phenotyping in Africa

Despite the recent advances in high-throughput field phenotyping based on the non-destructive analysis of plant traits, Africa has yet to consolidate the gains of these cutting-edge technologies for research into agricultural productivity. In terms of the deployment of high-end field phenotyping tools and approaches, Africa cannot keep pace with many regions, even in the era of artificial intelligence (AI), 'internet-of-things' (IoT) and technological advancements, although more affordable and lean phenotyping systems are now becoming available. Community-wide surveys and exchanges conducted by the International Plant Phenotyping Network (IPPN) and European Infrastructure for Multi-Scale Plant Phenomics and Simulation (EMPHASIS) within the growing phenotyping community in recent years have identified focus areas to assess the status of global plant phenotyping and crucial bottlenecks in the emerging field.

The major bottlenecks for developing field phenotyping in Africa were non-invasive phenotyping approaches, data management and cost among others (IPPN, 2016; Rosenqvist et al., 2019). This survey further reveals that in terms of using high-intensity field approaches (e.g., automation, robotics, image analysis and data storage management) for field phenotyping, Africa ranks lowest around the world. A recent survey conducted in the framework of the IPPN and EMPHASIS projects in 2020 (IPPN, 2020) which was reported by Yang et al. (2020) and Fahrner et al. (2021), indicated that Africa is still behind in the implementation of high-throughput field phenotyping. This highlights the need for a broader deployment of high-throughput field phenotyping techniques, which are essential enablers or resources for agricultural sciences and breeding to address upcoming crop production challenges.

The IPPN over the years has been promoting the idea of strengthening modern plant phenotyping in African countries by giving travel grants to Africa and inviting students and researchers for International Plant Phenotyping symposia and internships. However, only a few institutional members are identified for collaboration in the region. In recent times, there has been some high-throughput field phenotyping research and initiatives in African countries such as South Africa, Ghana, Senegal, Morocco, Nigeria, Ethiopia,

Kenya, Egypt and Zimbabwe which is encouraging for the emerging field and will be highlighted in this review (see section 2.2.5.2 and Table 2.3).

Like in many developing countries, field phenotyping in African countries is mostly based on conventional and traditional methodologies that rely heavily on manually recorded measurements of phenotypic data or visual assessment of plant parameters. It entails manually inspecting crops and measuring several crop characteristics that affect yield traits, including plant height, number of tillers, leaf colour, leaf shape, LAI, chlorophyll content, growth stages, above-ground biomass and stress tolerance (Gedil and Menkir, 2019; Bongomin et al., 2022; Badu-Apraku et al., 2023). In practice, in traditional field phenotyping, breeders or research evaluators inspect the trial fields and rate the plots according to how they feel, taste, smell and appear (Kim, 2020). Such phenotyping methods have several disadvantages such as being low-throughput, time-consuming, laborious, expensive and error-prone (Chapu et al., 2022; Xiao et al., 2022). Although these methods have been beneficial in developing new crop cultivars and improved yields, more effective phenotyping methods must be used to increase the accuracy of data collection.

In parallel, field phenotyping is undertaken to evaluate the agronomic performance of crops in breeding programmes, germplasm collections and in biotechnology programmes to deliver improved cultivars that can cope with environmental stresses (e.g., Asare-Bediako et al., 2019; Gedil and Menkir, 2019; Rezende et al., 2020; Kavhiza et al., 2022). These phenotyping research targets are focused on key crops for food security but are predominantly low-throughput phenotyping based on field trials. In SSA, breeding programmes championed by the Alliance for a Green Revolution in Africa (AGRA) have been dedicated to priority crops such as rice, maize, cassava, yam, beans, cowpea and vegetables under various regional breeding networks for improved varieties and seed systems (FAO, 2011; AGRA, 2019).

Previous studies have used a variety of calibration data, including ground-based survey methods and crop model simulations, to predict yield in smallholder systems (Burke and Lobell, 2017; Ogutu et al., 2018). However, there has been emerging evidence in SSA suggesting inaccurate farmer-reported crop production estimates in smallholder production systems (World Bank, 2010; Gourlay et al., 2017; Abay et al., 2019; Wahab,

2020). These anomalies in crop yield estimation at smallholder, country and regional levels can cause price fluctuations (i.e., inflation), wrong national policy decisions and food insecurity among others. High-throughput and/or digital phenotyping might offer a better estimation of regional and national crop production. Recent advances in sensor technology and the availability of free high-resolution (spatial and temporal) multispectral satellite images have also presented an opportunity to predict the yield of maize (Chivasa et al., 2017) and detect leaf spot diseases in groundnut (Sie et al., 2022), adaptation responses to early drought stress in sorghum (Gano et al., 2021) as well as mapping spatial distribution on a near real-time basis for a region, which hitherto was not feasible.

2.2.5.1 Field phenotyping initiatives and programmes in Africa

Despite the low implementation of high-throughput field phenotyping in Africa, there are some efforts by research organisations to adopt the technology in some countries. Prominent among these initiatives is a global network for precision field-based wheat phenotyping (https://globalrust.org/content/global-network-precision-field-based-wheat-phenotyping). Based on a global network of wheat partners, field phenotyping platforms are being developed with the support of the Consultative Group on International Agricultural Research (CGIAR) research programme on wheat and co-investing national agricultural research centres around the world, including some African countries such as Kenya, Ghana, Nigeria, Ethiopia and Morocco.

The main goal of this network is to generate high-quality phenotypic data to assist plant breeders in developing disease and drought-resistant and high-yielding wheat varieties with a broad genetic base and maximising the potential of new genotyping technologies. Additional but vital goals are to share knowledge and germplasm to accelerate new germplasm development and dissemination as well as develop capacities of breeders and plant scientists in precision field phenotyping. Some examples of these field phenotyping interventions being implemented include the development and application of precise phenotyping approaches, standardised protocols and novel tools for heat stress assessment in Sudan, *Septoria tritici* blotch in durum wheat in Tunisia (Ben M'Barek et al., 2022), *Septoria tritici* blotch in durum wheat and wheat rusts in Ethiopia (Kidane et al., 2017; https://globalrust.org/content/sources-resistance-septoria-tritici-

blotch-identified-ethiopian-durum-wheat), heat and drought tolerance in spring wheat in Morocco, yield potential in Egypt and Zimbabwe and drought and yield potential in Kenya (https://globalrust.org/content/global-network-precision-field-based-wheat-phenotyping). Additionally, low-cost high-throughput phenotyping tools for field selection for disease, drought and crop variety performance are currently being developed. These tools will be used in breeding programmes in Senegal, Ghana and Uganda and will serve as "centres of excellence for peanut breeding" in West and Eastern Africa (https://ftfpeanutlab.caes.uga.edu/Research/variety-development/high-throughput-phenotyping-in-senegal–ghana-and-uganda.html).

In West Africa, the field phenotyping network, since its inception in 2016 in the sub-region, has implemented high-throughput UAV (drone-based) phenotyping methodologies which are functional for sorghum, cowpea, peanut and pearl millet (Gano et al., 2021; Audebert et al., 2022). The network is advancing breeding activities through 'fine phenotyping', varietal evaluations in diverse environments to identify hot spots for specific stresses, including farmers' fields to test promising breeding lines in participating countries such as Senegal, Ghana, Mali and Burkina Faso.

The establishment of the network has facilitated infrastructure development, equipment acquisition and data management paired with long-term training of dedicated students, technicians and breeders capable of doing both breeding and carrying out high-throughput phenotyping measurements. In the sub-region, three sites have been chosen as prospective hubs for high-throughput phenotyping. Each hub including Bambey (ISRA research station, Senegal), Sotouba (IER research station, Bamako, Mali) and Farako-ba (INERA research Station, Bobo Dioulasso, Burkina Faso) exemplifies the diversity of soil and climate conditions in the region. According to Audebert et al. (2022), the network setup in Senegal is the most advanced while Mali and Burkina Faso lag behind mainly due to limited phenotyping equipment and funding challenges.

Similarly, the Regional Study Centre for the Improvement of Drought Adaptation (CERAAS) in complementing the field phenotyping initiatives of the West African field phenotyping network, has developed robust UAV imagery-based data collection and spatial modelling methodologies to accurately measure key traits of cereal crops to

advance plant breeding programmes. UAVs equipped with a multispectral imaging system coupled with a fully automated image processing pipeline can indirectly measure agronomic and phenological characteristics of cereal crops in agricultural field trials (Mbaye et al., 2022). Moreover, to advance the promotion and advancement of PA in Africa, the African Association for Precision Agriculture (AAPA), an initiative of the African Plant Nutrition Institute (APNI) is spearheading this goal (https://paafrica.org/AAPA). Since its establishment in 2020, the AAPA has worked in partnership with academia, research institutions, agri-food industry, financial institutions and public and private sector organisations to develop and scale up PA strategies and innovations through sustainable integration into African agriculture to address food security (i.e., reduce yield gaps) climate change and land degradation challenges.

2.2.5.2 Field phenotyping research in African countries

2.2.5.2.1 The case in Ghana

Digitalisation of agriculture is a new trend facilitated by digital platforms aimed at transforming small-scale agriculture by providing agricultural services to smallholder farmers in Ghana (Atanga, 2020; Abdulai et al., 2023). These digital platforms include simple devices such as mobile phones or radios to more sophisticated devices (e.g., field sensors, GIS, drones, field sensors, machinery sensors and diagnostics precision systems).

In Ghana, some of the notable digital platforms transforming the small-scale farming sector include the TROTRO Tractor Limited (an agritech company) that combines mechanisation with IoT and technology to make agricultural machinery (i.e., tractors and combined harvesters) available, accessible and affordable to farmers thereby enhancing their efficiency and productivity (https://www.trotrotractor.com). The use of RS as a decision support system (DSS) tool to optimise irrigation and farm management towards increasing yields has also been demonstrated (Kpienbaareh et al., 2019). These innovations primarily address the numerous issues smallholders and rural farmers confront in the present food systems, such as climate change, low access to inputs and restricted access to information (Degila et al., 2023).

As in many African countries breeding and field phenotyping is mostly based on conventional manual methods. However, to evaluate crop performance and improve breeding competitiveness, modern technologies using high-throughput techniques are being implemented but at a slow pace (e.g., Hall et al., 2018; Kassim et al., 2022; Sie et al., 2022). For instance, the responses of two populations of groundnut genotypes with various maturities to early and late leaf spot diseases were assessed under field conditions using UAV imagery (Kassim et al., 2022). In another breeding programme, smartphone-based RGB images detected leaf spot resistance and predicted yield in groundnuts (Sie et al., 2022). In a resource-constrained economy, Ghana is faced with numerous challenges such as lack of research funding, phenotyping infrastructures and technical personnel among others that can advance rapid characterisation of agriculturally relevant traits (e.g., growth, yield and stress resistance). Increasing its phenotyping capabilities will require a concerted effort from all stakeholders across the crop production value chain.

2.2.5.2.2 The case in Senegal

Senegal is making strides in PA by employing digital tools to address crop production challenges (https://www.apni.net/wp-content/uploads/2020/02/WAFPA-Tine.pdf). Even though advancement in modern breeding and field phenotyping methodologies has been slower and predominantly based on conventional methods (e.g., Dingkuhn et al., 2015), the use of drones for agricultural monitoring (i.e., stress detection, disease surveillance and crop performance) aided by high-throughput phenotyping has been exploited thanks to initiatives by the CERAAS and West African field phenotyping network. For instance, UAV multi-spectral imaging has been employed for the estimation of shoot biomass, LAI and plant height of West African sorghum varieties under severe drought conditions (Gano et al., 2021). The drone-based field phenotyping approach developed could help identify essential traits and cultivars for drought tolerance in sorghum breeding. The main challenges confronting crop field phenotyping in Senegal are a lack of equipment, technical personnel and funding (Audebert et al., 2022). However, Senegal being a hub for field phenotyping in West Africa, has the potential to increase its field phenotyping capabilities in the future.

2.2.5.2.3 The case in Nigeria

According to a recent review by Izuogu et al. (2023), the digitalisation of agriculture in Nigeria has reduced middlemen's participation in agriculture, offered small-holder farmers opportunities to improve their productivity and markets and strengthened the connections between extension and research facilities. The authors demonstrated that for effective digitalisation of agriculture, training was required in the areas of skills development, use of demand-driven digital services, digital privacy and security issues. The challenges of digitalisation of agriculture identified were lack of technical expertise, inadequate infrastructure and high purchase and maintenance costs. The use of RS techniques for precision crop production and monitoring has been implemented but to a lesser extent. Ifeanyieze et al. (2014) have previously reviewed the RS techniques needed for the smooth implementation of precision crop management by farmers as a climate change adaptation strategy in Nigeria. Few research groups have utilised RS for field phenotyping. For instance, Ejikeme et al. (2017) used a satellite-based crop prediction model to estimate crop statistics of major crops including rice, cassava, yam and maize.

Recently, the Institute of Tropical Agriculture (IITA) through its collaborative soybean breeding programmes has implemented machine learning (ML) models and multispectral high-resolution UAV imagery to aid rapid high-throughput phenotypic workflow for soybean yield estimation (Alabi et al., 2022). Other breeding programmes used manual field evaluation coupled with digital imaging analysis for phenotyping tomato breeding population (Daniel et al., 2016). The use of a handheld optical NDVI sensor for the evaluation of shoot biomass in field-grown staking yam has been implemented (Iseki and Matsumoto, 2019). Altogether, Nigeria has great potential for improving its field phenotyping capabilities.

2.2.5.2.4 The case in Morocco

Morocco is among the few African countries well-positioned for widespread agricultural digitalisation for PA and field phenotyping to increase crop production and cope with adverse environmental conditions such as drought. Jabir and Falih (2020) recently reviewed the state of digital agriculture in Morocco and highlighted the opportunities and challenges that need to be addressed. The design and implementation

of a wireless sensor network (WSN) and decision support tools (i.e., drones) for monitoring the agricultural environment have been demonstrated (Jabir and Falih, 2020). Nevertheless, challenges such as sensor deployment and inadequate software analytics still exist (Kobo et al., 2017). Morocco is home to the International Centre for Agricultural Research in the Dry Areas (ICARDA's) phenotyping facilities (ICARDA phenotyping platforms in Morocco), including a precision phenotyping platform at Sidi el Aidi (Settat) (Figure 2.4) and a phenomobile system (PhenoBuggy) situated at the main research station in Marchouch (Rabat) designed for drought and heat stress tolerance studies (https://www.cgiar.org/news-events/news/icardas-phenotyping-facilities-a-game-changing-solution-for-abiotic-stress-tolerance-in-crops/). The PhenoMA is another high-throughput phenotyping platform currently installed in Benguerir (Quahir et al., 2022). Field phenotyping using various RS techniques has been deployed for drought monitoring (Bijaber et al., 2018; Bouras et al., 2020; Laachrate et al., 2020), and grain yield prediction (Belmahi et al., 2023).

Figure 2.4. The ICARDA's precision field phenotyping platforms installed at Sidi el Aidi (Settat) in Morocco. Images are in courtesy of Andrea Visioni of ICARDA-Morocco.

2.2.5.2.5 The case in Egypt

Digital agriculture appears promising in addressing the major challenges facing the agri-food sector in Egypt and across the Middle East and North Africa (MENA) countries (Bahn et al., 2021). Available evidence indicates that the adoption of digital and PA technologies is still in its infancy and is typically driven by high-value agricultural production (Elsafty and Atallah, 2022; Sayed et al., 2023). However, Egypt has made

strides in the utilisation of modern technologies for agricultural crop management employing big data in tandem with cloud support systems, IoT, UAVs, satellite imagery, AI, ML and RS (Shokr, 2020; Abdelnabby and Khalil, 2023; Sayed et al., 2023). Typical high-throughput field phenotyping methodologies have been implemented in various crops for quantifying wheat characteristics in the Nile Delta (Elmetwalli et al., 2022) and estimating the growth performance and yield of soybean exposed to different drip irrigation regimes under arid conditions (Elmetwalli et al., 2020). Additionally, RS techniques based on thermal imaging and passive reflectance have been used to estimate the crop water status and grain yield in wheat (El-Shirbeny et al., 2014; Elsayed et al., 2017).

2.2.5.2.6 The case in South Africa

The agricultural sector in South Africa has been developing and moving towards becoming a knowledge-intensive enterprise due to new innovations and technologies incorporated in the digital economy (Baumüller and Kah, 2019; Born et al., 2021; Smidt and Jokonya, 2022). Due to this transformation, conventional production methods have gradually been replaced with more advanced, efficient and innovative systems (e.g., RS) for crop breeding and phenotyping (Mutanga et al., 2016).

Field phenotyping using modern high-throughput infrastructures and PA techniques is better developed in South Africa compared to other countries on the continent (Nyaga et al., 2021; Mukhawana et al., 2023). Some research groups are making efforts to champion field phenotyping and PA through workshops and implementation of UAV and RS applications and other approaches for agricultural monitoring (stress detection, nutrient and irrigation management) (https://www.fabinet.up.ac.za/index.php/research-groups/remote-sensing). For example, the Forestry and Agricultural Biotechnology Institute (FABI) and the Agricultural Research Council (ARC) (https://www.arc.agric.za/Pages/Home.aspx) are committed to building phenotyping infrastructures and disseminating emerging technologies for agricultural development.

Various RS applications have been employed targeted at different scales of crop monitoring (e.g., crop water use efficiency) in PA (e.g., Munghemezulu et al., 2023; Wellington, 2023). For instance, foliar temperature and stomatal conductance have been

used as indicators of water stress in maize based on optical and thermal imagery acquired using a UAV platform (Brewer et al., 2022a). The utility of multispectral UAV imagery as a proxy for predicting the chlorophyll content of maize at various growth stages in smallholder farming systems has been reported (Brewer et al., 2022b). The physiological processes of the maize canopy are intimately tied to and influenced by LAI, which is closely related to its productivity (Peng et al., 2021). Another study has focused on estimating the LAI of maize in smallholder farms across the growing season using UAV-derived multi-spectral data (Buthelezi et al., 2023). Maize is a major crop in South Africa, therefore, significant research on the crop using high-throughput techniques will aid in developing improved cultivars for farmers. South Africa has a great potential for becoming the field phenotyping hub of Africa due to the massive investment in modern technologies.

2.2.5.2.7 The case in Zimbabwe

In Zimbabwe, the implementation of digitalised agriculture is low and tilted toward commercial farmers rather than smallholder community farmers (Parwada and Marufu, 2023). Specifically, highly literate and resource-rich farming communities tend to use digitalised agriculture more frequently than farmers with fewer resources. At the communal level, farmers use mobile phones to obtain farming information relating to crop management, climate and weather information (Musungwini, 2018; Zimbabwe Centre for High-Performance Computing, 2021). The application of modern digital agriculture tools and infrastructure (i.e., sensors, robotics, AI, UAVs and other advanced machinery) is common in a few well-resourced commercial farms notably, those managed by large multinational companies (Shonhe and Scoones, 2022). Parwada and Marufu (2023) recently reviewed the challenges and opportunities for digitalisation of the Zimbabwean agriculture.

Key challenges such as lack of high-throughput infrastructures, digital illiteracy and strict regulations for drone deployment among others have been highlighted for limiting digital agriculture applications. However, according to the authors, Zimbabwe has the potential to improve its digital agriculture for crop management, yield prediction, disease detection, climate forecasting and soil management through PA. In recent years, few high-throughput phenotyping has been implemented in Zimbabwe using RGB

picture vegetation indexes (Kefauver et al., 2015), and multi-spectral imaging for field phenotyping of maize (Zaman-Allah et al., 2015). Other studies include RS methodologies for crop monitoring under conservation agriculture (Gracia-Romero et al., 2018; Gracia-Romero et al., 2020), affordable UAV-based RGB phenotyping techniques for evaluating maize performance under low N conditions (Buchaillot et al., 2019), and accelerating crop improvement in response to changing climate conditions employing UAV-based multispectral phenotyping for disease resistance in maize (Chivasa et al., 2020). Zimbabwe is among the few African countries capable of advancing its field phenotyping capabilities in the future.

2.2.5.2.8 The case in Kenya

Although there are several technologies currently available to Kenya's agricultural sector, they have not yet become widely used (Osiemo et al., 2021). Large-scale adoption of digital solutions is hampered by a lack of digital literacy and infrastructure. Only a few research groups are skilled in using and maintaining back-end service operations like data management, blockchain, ML, IoT, GIS and drones (Osiemo et al., 2021). However, the application of GIS and RS techniques have been used to map frost hotspots for mitigating agricultural losses (Kotikot and Onywere, 2015), climate-smart crop management (Manzi and Gweyi-Onyango, 2021) and assessment of yield variations and its determinants in smallholder systems (Burke and Lobell, 2017). Similarly, high-throughput phenotyping platforms based on multi-spectral imaging and RGB VIs have been implemented for field phenotyping of maize (Kefauver et al., 2015; Zaman-Allah et al., 2015). Kenya has the potential to expand its phenotyping capacities through low-cost PA and breeding.

2.2.5.2.9 The case in Ethiopia

Digital agricultural innovations in PA have the potential to increase productivity while minimising harmful environmental impacts along the value chains of agriculture and the food systems in Ethiopia (Alemaw and Agegnehu, 2019; Tamene and Ashenafi, 2022). In recent years, there have been some improvements in digital infrastructure in Ethiopia (Abdulai, 2022). However, the majority of Ethiopia’s smallholder farmers have limited access to digital farming technologies (Tamene and Ashenafi, 2022). According to Tamene and Ashenafi (2022), several challenges such as inadequate technological

capacity, limited funding to develop and disseminate digital tools and lack of data-sharing channels hampers the development of digital agriculture in Ethiopia. These barriers restrict the deployment of modern technologies for crop breeding and field phenotyping. Field phenotyping has relied largely on conventional methods as in the studies of eco-geographic adaptation and phenotypic diversity of Ethiopian teff across its cultivation range (Woldeyohannes et al., 2020) and genetic diversity in Ethiopian durum wheat (Mengistu et al., 2018). Field phenotyping using high-throughput techniques has been introduced in recent times. RS and GIS based methods have been used as crop yield predictors in wheat and maize (Beyene et al., 2022; Debalke and Abebe, 2022) as well as physical land suitability analysis for major cereal crops (Debesa et al., 2020). In essence, Ethiopia has the potential to accelerate its phenotyping capabilities. Table 2.3 summarises some key field phenotyping activities that exist in the African countries discussed in this review.

Table 2.3. Summary of some major characteristics of field phenotyping activities implemented in some African countries.

Region	Country	Area of high-throughput field phenotyping research	Prospects	Reference/weblink
West Africa	Ghana	Exploration of digital agriculture, deployment of low-cost sensors and technologies for breeding, exploration of RS for PA, GIS	Digital agriculture, low-cost PA and breeding, use of high-throughput tools	Hall et al., 2018; Kpienbaareh et al., 2019; Kassim et al., 2022; Sie et al., 2022; https://ftfpeanutlab.caes.uga.edu/Research/variety-development/high-throughput-phenotyping-in-senegal--ghana-and-uganda.html
	Senegal	Exploration of digital agriculture, exploration of UAV imagery, multi-spectral imaging, GIS	Development of high-throughput approaches, digital agriculture, low-cost precision breeding	Dingkuhn et al., 2015; Gano et al., 2021; https://www.devdiscourse.com/article/other/523595-senegals-embrace-of-the-digital-revolution-in-agriculture-marks-the-way-forward-for-africa
	Nigeria	Use of field mobile agricultural robots, digital imaging, RS, ML, GIS, site-specific analytics, drone imagery	Development of high-throughput approaches, digital agriculture, low-cost precision breeding, deployment of digital technologies and innovations	Ifeanyieze et al., 2014; Daniel et al., 2016; Ejikeme et al., 2017; Iseki and Matsumoto, 2019; Alabi et al., 2022; Izuogu et al., 2023; https://nitda.gov.ng/wp-content/uploads/2020/11/Digital-Agriculture-Strategy-NDAS-In-Review_Clean.pdf
North Africa	Morocco	High-throughput phenotyping, precision field-based phenotyping platform for drought/heat tolerance, development of quinoa phenotyping methodologies, expanding the precision and prediction value of phenotyping/genotypic data for new germplasm emerging from the wheat, adding an HTPP system for wheat abiotic stresses	Expanding phenotyping capabilities, low-cost precision breeding, deployment of digital technologies and innovations, expansion in RS capabilities	Bijaber et al., 2018; Danzi et al., 2019; Bouras et al., 2020; Laachrate et al., 2020; Jabir and Falih, 2020; Quahir et al., 2022; https://www.fao.org/in-action/plant-breeding/nuestrosasociados/africa/morocco/es/; https://www.icarda.org/research/projects/precision-field-based-phenotyping-platform-droughtheat-tolerance-morocco-pwpp
	Egypt	High-throughput precision phenotyping for improvement of drought and salt tolerance in wheat genotypes, implementation of digital technology (mobile applications) for field phenotyping, AI-enabled system to enhance agriculture process, satellite imagery for crop monitoring	Expanding phenotyping capacities, low-cost PA and breeding	El-Shirbeny et al., 2014; Elsayed et al., 2017; Shokr, 2020; Bahn et al., 2021; Elmetwalli et al., 2022; Elsafty et al., 2022; Abdelnabby and Khalil, 2023; Mahdy and Ahmad, 2023; Sayed et al., 2023; https://globalrust.org/geographic/egypt; https://www.fao.org/e-agriculture/news/egypt-turns-fao-digital-transformation-agriculture; https://dailynewsegypt.com/2021/12/07/government-launches-ai-enabled-system-to-enhance-agriculture-process/

Southern Africa	South Africa	Deployment of field scanalyzer (FieldScan) for spectral crop measurement, RS for PA	Expanding phenotyping capacities, low-cost PA and breeding, advancing RS capabilities	Mutanga et al., 2016; Brewer et al., 2022a; Buthelezi et al., 2023
	Zimbabwe	UAV-based high-throughput phenotyping, multispectral RS in maize varietal response to maize streak virus (MSV) disease, high-throughput phenotyping of maize performance under phosphorus fertilization, RS methodologies for crop monitoring under conservation agriculture	Expanding phenotyping capacities, low-cost PA and breeding	Kefauver et al., 2015; Zaman-Allah et al., 2015; Gracia-Romero et al., 2018, Musungwini, 2018; Buchaillot et al., 2019; Chivasa et al., 2020; Gracia-Romero et al., 2020; Shonhe and Scoones, 2022; Parwada et al., 2023;
East Africa	Kenya	Satellite-based assessment of maize yield variations in smallholder farms, GIS and RS capabilities	Expanding phenotyping capacities, low-cost PA and breeding	Kefauver et al., 2015; Kotikot and Onywere, 2015; Zaman-Allah et al., 2015; Burke and Lobell, 2017; Manzi and Gweyi-Onyango, 2021
	Ethiopia	GIS for PA, imaging technologies for crop trait analysis	Expanding phenotyping capacities, low-cost PA and breeding	Alemaw and Agegnehu, 2019; Bontpart et al., 2020; Debesa et al., 2020; Beyene et al., 2022; Debalke and Abebe, 2022

2.2.5.3 Current developing field phenotyping platforms in Africa

UAVs have been selected as the technical solution that is most suited for deployment across sites and trials throughout the several initiatives that made it possible for the West African field phenotyping network to get started (Audebert et al., 2022). For instance, in Senegal, the UAV platform comprises a FeHexaCopterV2 HexaCopter UAV system (Flying Eye Ltd., Sophia Antipolis, France) fitted with three cameras mounted on a two-axis gimbal pointing vertically downward. The camera consists of an RGB ILCE-6000 digital camera (Sony Corporation, New York, NY, USA), AIRPHEN multispectral camera (Hiphen, Avignon, France), and NIR thermographic camera Tau 2 (FLIR system, Oregon, USA) that collects spectral imagery of crops such as sorghum, pearl millet and peanut and cowpea (Gano et al., 2021; Diop et al., 2021).

The ARC of South Africa has installed a Phenospex planteye multispectral 3D laser scanner (the first of its kind in Africa) in the field (https://phenospex.com/products/plant-phenotyping/fieldscan-high-throughput-field-phenotyping/fieldscan-3d-spectral-plant-measurements-in-the-field-south-africa/). This state-of-the-art facility is fully automated, carrying a high-resolution sensor that combines the strength of 3D vision with the power of multispectral imaging. It captures plant data non-destructively and delivers precise and accurate plant parameters in real time. Plant phenotypic features such as digital biomass, plant height, 3D leaf area, projected leaf area, LAI, leaf inclination, etc., can be measured. The spectral information allows for the quantification of plant health, disease, senescence, N-content, chlorophyll levels, etc. Therefore, this phenotyping facility could assist in the characterisation and development of varieties with improved biotic and abiotic stress resistance for key crops such as grapefruit, sunflower, green maize and other cereals in Southern Africa.

Recently, a unique close-to-field high-throughput plant phenotyping platform “PhenoMA’’ has been installed in Benguerir, in the arid region of Morocco by the UM6P. PhenoMA consists of a 1440 fully automated lysimetric mini-plot system that can track the dynamics of water use and simulate drought scenarios. A critical component is a fully autonomous phenotyping robot (Hiphen PhenoMobile) that enables plant measurements at the canopy scale, using a range of sensors including

RGB, multispectral, IR and LiDAR cameras to monitor canopy development (Quahir et al., 2022).

Overall, due to the rich agricultural biodiversity of Africa, phenotyping in Africa has great potential to contribute to the development of improved crop varieties and enhanced food security. The utilisation of high-throughput tools can boost the elucidation of new agriculturally proven traits and catalogue these phenotypes in their natural environment.

2.2.5.4 Challenges limiting the application of high-throughput field phenotyping in Africa and the way forward

The application of emerging field phenotyping technologies has the potential to accelerate plant breeding efforts and crop production in Africa. On the other hand, most of these approaches reviewed here are at best relatively new or unknown to some of the plant science community in Africa. Field phenotyping is a critical component of crop improvement but remains a major bottleneck in African agriculture, as is the case globally. Some of the key challenges limiting the application of high-throughput field phenotyping in Africa are highlighted below.

2.2.5.4.1 Lack of appropriate high-throughput field phenotyping approaches

Phenotypic analysis has become a major limiting factor in genetic and physiological analyses in plant sciences as well as in plant breeding in Africa. The inadequate phenotyping infrastructures and software analytical tools that can be used by agricultural practitioners to make sense of simple to complicated phenotypic datasets have contributed to the low implementation of high-throughput phenotyping. The operational complexity of supporting both data acquisition and analysis has limited the use of these platforms for research activities worldwide (Chapman et al., 2014), including developing continents like Africa. To this end, training in image analytics, software and computer vision to provide a new generation of skilled personnel must be implemented by African governments, universities and the private sector. Phenotyping advancement is critical for current breeding progress for crop improvement in Africa. While the development of efficient high-throughput field phenotyping remains a challenge for future breeding progress, the growing interest in low-cost solutions for RS

approaches, machine vision, as well as data management, may facilitate technological adoption.

2.2.5.4.2 Cost of phenotyping infrastructures and maintenance

As a developing continent comprising highly indebted poor countries (HIPC) (Henri, 2019) and faced with multi-faceted economic hardships, the major limitation to the adoption and implementation of high-tech field phenotyping in Africa is the perceived high entry costs associated with the longer-term footprint of prototypical platforms (Reynolds et al., 2019). In several African countries, especially those discussed in this review, basic phenotyping tools and infrastructure even for the simplest field measurements and experimentation are scarce.

This prevents many research organisations in Africa such as IITA, International Centre for Tropical Agriculture (CIAT) and Africa Rice, from implementing demand-driven approaches due to a lack of investment budget or avoiding the significant follow-up costs on maintenance of large phenotyping infrastructures. For instance, the use of ground vehicles, aerial vehicles and gantries may require huge investment costs (Pauli et al., 2016; Vergara-Díaz et al., 2016).

Therefore, the requirements for such specialised equipment may be a bottleneck for widespread use in breeding programmes in poor countries. To alleviate this challenge, low-cost concepts and methods of HTPPs (e.g., sensors and platforms) that rely on easy-to-use technology must be disseminated in Africa by identifying demands and relevance, and adopting the required approach given the current financial constraints. For instance, conventional digital cameras (i.e., digital photography) could provide a more convenient method since they are more affordable, portable and easy to use (Casadesús et al., 2014).

2.2.5.4.3 Limited investment and funding

Limited investments in science, technology and innovation (STI) on the part of African governments, research institutions (e.g., academia) and the private sector have partly contributed to the poor implementation of high-throughput field phenotyping. The budgetary allocations dedicated to research, development and innovation are small. For example, in Ghana, a minimum of 1% of gross domestic product (GDP) is applied towards research and development (https://mesti.gov.gh/government-increase-research-

funding/). Similarly, in Morocco, the percentage of GDP to research as of 2010 was 0.63% (Hamidi and Benabdeljalil, 2013). This research funding gap is pervasive across the African continent.

Whereas research institutions and universities in developed economies, such as Europe (https://eppn2020.plant-phenotyping.eu/EPPN2020_installations#/), Australia, North America and Asia, have in recent years invested heavily in large-scale research infrastructure for automated and high-throughput field phenotyping, the same cannot be said for Africa. These large investments for plant phenotyping include funding, research hours and high-throughput installations (Costa et al., 2019; Rosenqvist et al., 2019; https://eppn2020.plant-phenotyping.eu/).

Furthermore, crops grown in Africa are frequently too local to attract international research funding for field phenotyping. Only a few essential African crop commodities, such as cassava and sweet potatoes are funded solely by extrabudgetary sources. Most of the main staple crops are exclusively funded for phenotyping exploitation outside of Africa. In addition to the above considerations, African governments and the Science Granting Councils Initiative (SGCI) in SSA countries mandated to support the Science Granting Councils (SGCs), must dedicate enough funding for low-cost plant phenotyping research infrastructure in the sub-region in the short to medium term. This could be achieved by developing financing mechanisms and collaborating with private sector partners. Donor support to Africa for agriculture and food security research should also consider projects in modern plant phenotyping and digital agriculture.

2.2.5.4.4 Lack of skilled technical personnel

A serious deficit of skilled technical personnel in the plant sciences and phenotyping ecosystem is evident in African countries. The building up of such competencies and the development of human resource capacity is necessary to operate simple-to-sophisticated equipment to accelerate breeding efforts through high-throughput phenotyping techniques. Another major barrier is the loss of talented and skilled personnel who were trained in developed nations and have contributed to the brain drain due to inadequate job prospects in Africa. Mostly, funds to pay salaries and absorb project operating costs are either limited or insufficient, resulting in a reduction of skilled personnel. Furthermore, due to the inadequacies in research and infrastructure in

many African nations, training acquired overseas is sometimes unsuited to local demands. To address this constraint, digital agricultural competencies and sensor technologies should be integrated into undergraduate and postgraduate learning curricula to allow students to specialise in digital agriculture through their projects. This will create a plethora of career opportunities for competent skilled personnel who can adapt to the emerging technologies for field phenotyping.

2.2.5.4.5 Regulations controlling emerging technologies

Emerging technologies such as UAVs offer the advantages of being flexible, real-time and non-destructive for agricultural phenotyping, but they must adhere to strict operational standards to ensure their safe use. Strict airspace regulations in many jurisdictions around the world and particularly in African countries due to the impact of political instability and military governments on UAV deployment may prohibit their use or make them unfeasible in practice (Gago et al., 2015; Yang et al., 2017a; Ayamga et al., 2021). For instance, authorisation from regulatory authorities, such as the Air Force, civil aviation and police, are required to undertake UAV flight campaigns, which mostly take time to be approved causing issues in time-critical data collection applications. According to Ayamga et al. (2021), in Africa, countries with regulations include Ghana, South Africa, Zimbabwe, Nigeria, Cameroon, Benin, Gabon, Senegal, Botswana, Namibia, Malawi, Tanzania, Zambia, Madagascar, Rwanda and Kenya. However, the lack of proper regulation and enforcement continues to limit the widespread adoption of drones. Unfortunately, these regulations combine to mean that most high-throughput techniques can only be implemented by multinational research institutions, even in those organisations, deployment of systems is limited to a few high-priority projects. The commitment of African governments and relevant stakeholders is crucial in the implementation and enforcement of regulations. The widespread deployment of drones stands to benefit farmers hence concerted effort needs to be made to sustain its adoption by promoting public digital literacy on the technology, skill development for potential users and farmers on drone operation and developing the necessary policy framework with regulatory agencies to increase the safety and acceptability of using agricultural drones in Africa.

2.2.5.4.6 Weakness of phenotyping linkages

At the regional and continental levels, networking is a powerful tool for increasing scientific collaboration and fostering information sharing. There seems to be weak collaborations between the African plant science community and international phenotyping partners which hampers technological transfer and adoption. As high-throughput field phenotyping initiatives have started in Africa, there is a need to strengthen national and institutional efforts within the continent for the development and application of accurate and high-throughput field phenotyping capabilities. The West Africa field phenotyping network should be strengthened and better resourced to carry out their mandate. Similar initiatives such as the EMPHASIS (https://emphasis.plant-phenotyping.eu) should be experimented to provide a more practical use of the available phenotyping data and infrastructure. The IPPN should spread its operations to Africa to develop programmes and establish synergies geared towards face-lifting plant phenotyping projects in the continent. Again, African governments and their partners should invest in building a centre of excellence or shared facilities for African plant scientists. Finally, a more urgent challenge is, however, that the international phenotyping community needs to bridge the gap between advanced economies and developing regions of the world such as Africa to benefit from the huge research efforts made internationally.

2.2.6 Concluding remarks and future perspectives

This review provides an overview of high-throughput field phenotyping and its implications for African crops. It highlights the prospects of emerging high-throughput phenotyping techniques and integrated sensor platforms for plant trait assessment for field phenotyping that could apply to African crops. High-throughput field phenotyping has superior advantages that facilitate quick, non-destructive and high-throughput detection, thus overcoming the shortcomings of conventional approaches. The readiness and the potential adoption of high-throughput field phenotyping for practical implementation in Africa are of paramount interest and should be demonstrated.

Field phenotyping solutions of immediate to long-term feasibility for African crops will likely rely on a combination of available techniques or prototypes of low-cost sensors and imaging approaches to study crop performance. Manual methods dominate the field

phenotyping ecosystem with only a few countries beginning to explore high-throughput techniques through digital and PA. Notably, high-throughput phenotyping cannot yet completely replace manual measurements but should be promoted. The implementation of high-throughput phenotyping in general, and low-cost methods for field evaluation is still fraught with challenges in Africa. Challenges identified by this present review include the high upfront cost of the prototypical platforms, huge funding gap, lack of conceptual and technical capacity, lack of technology transfer infrastructure and methodological approaches, lack of phenotyping network on the continent and the needed legislation in some cases, amongst others.

Lack of financial resources, a problem pervasive in African countries needs to be tackled holistically. Public-private partnerships could support resolving these financial and investment challenges to foster political will. Although in some countries, this public-private drive is already being implemented through close collaboration between universities and agricultural research organisations, these efforts need to be stepped up. In parallel, African governments should dedicate enough funding, incentives and tools to breeders to advance research and innovations regarding high-end plant breeding. We suggest that donor support to Africa for agriculture and food security research should also consider projects in modern plant phenotyping to cope with current and projected climate change.

This will open the possibility of investing more in current sensor and imaging technologies for field data collection and the use of cost-effective phenotyping technologies that are already available to increase the throughput, quantity and quality of phenotypic data. The wide range of applications for these phenotyping technologies makes them good candidates and feasible choices for adoption in Africa which hitherto were prohibitive in terms of cost and deployment. The advantages of improved sensor-platform integration have facilitated the development of complete phenotyping systems that can gather, integrate and store data for many subsystems concurrently in a structured, efficient and cost-effective way. Such platforms have been widely adopted by research groups in developed countries and are gradually adopted by plant breeders in Africa as the technology develops and the benefits are proven.

In addition to the adoption of high-throughput field phenotyping approaches in African countries, PA will also greatly benefit and revitalise the establishment of closer interaction between breeders and farmers to develop protocols mutually for the optimal use of improved crop varieties. The tools and knowledge exchange are expected to spur a second green revolution to meet the agricultural challenges to feed the ever-increasing African population. In terms of advancing field crop phenotyping in Africa for agricultural crop sustainability, we propose that breeding priority should be given to the most important staple crops such as maize, wheat, yam, cassava, cowpea, sorghum, etc. These crops form the backbone for food security and hence their improvement is crucial in the wake of prevailing climate change and production constraints. We suggest that each country selects traits that are of high demand and relevance by farmers and consumers when designing breeding strategies. In parallel, high-throughput phenotyping should be incorporated into national agricultural research policies and prioritise the practical implementation of field phenotyping. By and large, these could be achieved when governmental and private sector participation, as well as financial support is readily available.

To overcome the challenges with the deployment of phenotyping tools and the integration of software to deliver accurate data acquisition, processing, analysis and management, a multidisciplinary team of expert-level skills and competencies may be required. This will necessitate deliberate training and capacity improvement of African plant scientists and students in software engineering and computer science domains, including AI, demanding true interdisciplinary partnerships to provide meaningful results and inform decision making, while addressing the issue of training cost and related risks. In this instance, we recommend technological adoption rather than complete technological development considering the financial constraints and the low-level expertise in software and equipment development. However, as the plant phenotyping industry develops the development of new technologies from scratch may be feasible in Africa.

Furthermore, we propose encouraging collaborations between the African plant science community with their international counterparts to foster collaborative research, effective technological transfer and adoption. This review recommends close collaboration with the IPPN and similar phenotyping networks to benefit from the

unprecedented investments made in field phenotyping infrastructures globally. Consequently, crop scientists may leverage ground-breaking advancements in high-throughput field data collection, image analysis and data management. Efforts should be made to foster synergies among different African countries by establishing transnational interdisciplinary networks that incorporate expertise in all aspects of plant breeding.

To address the limited investments in STI, a commitment to expanded and long-term funding of agricultural research and development is essential. At the policy and operational levels, barriers must be overcome to allow the smooth establishment of public-private partnerships for transformational change in research and demand-driven technologies for breeders and farmers. There is renewed interest both from private and public institutions in developed countries to support African agriculture. Hence, African agricultural institutions need to develop strategies and synergies that include building partnerships that must be implemented to tackle the challenges, especially in the face of climate change and food insecurity.

The widespread adoption of high-throughput field phenotyping techniques in African countries could only be made possible in plant breeding programmes if it can be proven as something worthwhile in terms of genetic gains attained with resources invested. Hence, costs must be reasoned in relation to the precision, repeatability, heritability, cost per unit plot or trait, prevailing climatic and economic condition, etc., required in a particular phenotyping activity. Given what has been said, to ensure that such implementation of field phenotyping can be translated into yield gains, low-cost phenotyping tools must be adopted. On this basis, affordable, easy-to-handle, reliable tools and phenotyping infrastructures for small to large-scale field phenotyping may become a strategic choice and pave the way for practical implementation. Such technologies applicable to phenotyping methodologies should be available soon due to the high demands and efforts by the phenotyping community in Africa.

References

Aasen, H., Burkart, A., Bolten, A., and Bareth, G. (2015). Generating 3D hyperspectral information with lightweight UAV snapshot cameras for vegetation monitoring: From camera calibration to quality assurance. *ISPRS Journal of Photogrammetry and Remote Sensing*, 108, 245-259.

Abay, K. A., Abate, G. T., Barrett, C. B., and Bernard, T. (2019). Correlated non-classical measurement errors, 'Second best' policy inference, and the inverse size-productivity relationship in agriculture. *Journal of Development Economics*, 139, 171-184. https://doi.org/10.1016/j.jdeveco.2019.03.008

Abdelnabby, M and Khalil, T. (2023). Assessing precision agriculture applicability in agriculture sector in Egypt. Fayoum *Journal of Agricultural Research* and *Development*, 37 (1), 54-62. https://doi.org/10.21608/fjard.2023.281055

Abdulai, A. R. (2022). Toward digitalisation futures in smallholder farming systems in Sub-Sahara Africa: A social practice proposal. *Frontiers in Sustainable Food Systems*, 6. https://doi.org/10.3389/fsufs.2022.866331

Abdulai, A. R., Kc, K. B., and Fraser, E. (2023). What factors influence the likelihood of rural farmer participation in digital agricultural services? experience from smallholder digitalisation in Northern Ghana. *Outlook on Agriculture*, 52 (1), 57-66. https://doi.org/10.1177/00307270221144641

Adhikari, U., Nejadhashemi, A. P., and Woznicki, S. A. (2015). Climate change and Eastern Africa: a review of impact on major crops. *Food and Energy Security*, 4 (2), 110-132. https://doi.org/10.1002/fes3.61

Affoh, R., Zheng, H., Dangui, K., and Dissani, B. M. (2022). The impact of climate variability and change on food security in sub-saharan Africa: Perspective from panel data analysis. *Sustainability*, 14 (2), 759.

AGRA. (2019). *A handbook of plant breeding: Case studies from Africa 2019*. Available at:https://agra.org/wp-content/uploads/2022/09/Handbook-of-Plant-Breeding-Case-Studies-from-Africa-2019.pdf (Accessed July 15, 2023)

Ahmed, H. G. M. D., Zeng, Y., Fiaz, S., and Rashid, A. R. (2023). "Applications of high-throughput phenotypic phenomics," *in Sustainable agriculture in the era of the OMICs revolution*. Eds. C. S. Prakash, S. Fiaz, M. A. Nadeem, F. S. Baloch and A. Qayyum (Cham: Springer). https://doi.org/10.1007/978-3-031-15568-06

Alabi, T. R., Abebe, A. T., Chigeza, G., and Fowobaje, K. R. (2022). Estimation of soybean grain yield from multispectral high-resolution UAV data with machine learning models in West Africa. *Remote Sensing Applications: Society and Environment*, 27, 100782. https://doi.org/10.1016/j.rsase.2022.100782

Alemaw, G and Agegnehu, G. (2019). Precision agriculture and the need to introduce in Ethiopia. *Ethiopian Journal of Agricultural Sciences*, 29 (3), 139-158.

Alvar-Beltrán, J., Fabbri, C., Verdi, L., Truschi, S., Dalla Marta, A., and Orlandini, S. (2020). Testing proximal optical sensors on quinoa growth and development. *Remote Sensing*, 12 (12),1958. https://doi.org/10.3390/rs12121958.

Amaral, J. B. C., Lopes, F. B., Magalhães, A. C. M. D., Kujawa, S., Taniguchi, C. A. K., Teixeira, A. D. S., and Niedbała, G. (2022). Quantifying nutrient content in the leaves of cowpea using remote sensing. *Applied Sciences*, 12 (1), 458. https://doi.org/10.3390/app12010458

Andrade-Sanchez, P., Gore, M. A., Heun, J. T., Thorp, K. R., Carmo-Silva, A. E., French, A. N., et al. (2014). Development and evaluation of a field-based high-throughput phenotyping platform. *Functional Plant Biology*, 41 (1), 68-79. https://doi.org/10.1071/FP13126

Andrianto, H., Suhardi, S., and Faizal, A. (2017). "Measurement of chlorophyll content to determine nutrition deficiency in plants: A systematic literature review," in *2017 International Conference on Information Technology Systems and Innovation, ICITSI 2017 - Proceedings*, 2018-January. (Piscataway, New Jersey, United States: Institute of Electrical and Electronics Engineers (IEEE)), pp. 392-397. https://doi.org/10.1109/ICITSI.2017.8267976

Appels, R., Eversole, K., Feuillet, C., Keller, B., Rogers, J., Stein, N., et al. (2018). Shifting the limits in wheat research and breeding using a fully annotated reference genome. *Science*, 361 (6403). https://doi.org/10.1126/science.aar7191

Aracena Santos, P., Hakki, E. E., Gezgin, S., Topal, A., and Dedeoglu, M. (2021). Determination of phosphorus status in bread wheat leaves by visible and near-infrared spectral discriminant analysis. *Journal of Applied Remote Sensing*, 15 (1), 014503-014503. https://doi.org/10.1117/1.JRS.15.014503

Araus, J. L and Cairns, J. E. (2014). Field high-throughput phenotyping: The new crop breeding frontier. *Trends in Plant Science*, 19 (1), 52-61. https://doi.org/10.1016/j.tplants.2013.09.008

Araus, J. L., Kefauver, S. C., Vergara-Dıaz, O., Gracia-Romero, A., Rezzouk, F. Z., Segarra, J., et al. (2022). Crop phenotyping in a context of global change: What to measure and how to do it. *Journal of Integrative Plant Biology*, 64 (2), 592-618. https://doi.org/10.1111/jipb.13191

Araus, J. L., Slafer, G. A., Royo, C., and Serret, M. D. (2008). Breeding for yield potential and stress adaptation in cereals. *Critical Reviews in Plant Science*, 27 (6), 377-412. https://doi.org/10.1080/07352680802467736

Asare-Bediako, E., Taah, K. J., van der Puije, G., Amenorpe, G., Appiah-Kubi, A., and Akuamoa-Boateng, S. (2019). Evaluation of maize (*Zea mays* L.) genotypes for high grain yield and resistance to maize streak virus infections under diverse agro-ecological zones. *Research Journal of Plant Pathology*, 2 (2), 11. https://doi.org/10.36648/plantpathology.2.2.11

Atanga, S. N. (2020). Digitalisation of agriculture: how digital technology is transforming small-scale farming in Ghana. *Agrarian, Food and*

Environmental Studies (AFES). A research paper submitted to Erasmus University in partial fulfilment of the requirements for the degree of Master of Arts in Development Studies at the International Institute of Social Studies.

Audebert, A., Luquet, D., Vadez, V., Fonceka, D., and Kane, N. A. (2022). *Toward a regional field phenotyping network in West Africa*. Available at: https://agritrop.cirad.fr/604058/2/ID604058.pdf.

Ayamga, M., Tekinerdogan, B., and Kassahun, A. (2021). Exploring the challenges posed by regulations for the use of drones in agriculture in the African context. *Land*, 10 (2), 164. https://doi.org/10.3390/land10020164

Badu-Apraku, B., Fakorede, M. A., Nelimor, C., Osuman, A. S., Bonkoungou, T. O., Muhyideen, O., et al. (2023). Recent advances in breeding maize for drought, heat and combined heat and drought stress tolerance in sub-saharan Africa. *CABI Reviews*, Volume 2023. https://doi.org/10.1079/cabireviews.2023.0011

Bahn, R. A., Yehya, A. A. K., and Zurayk, R. (2021). Digitalisation for sustainable agri-food systems: Potential, status, and risks for the MENA Region. *Sustainability*, 13, 3223. https://doi.org/10.3390/su13063223

Bai, G., Ge, Y., Hussain, W., Baenziger, P. S., and Graef, G. (2016). A multi-sensor system for high throughput field phenotyping in soybean and wheat breeding. *Computers and Electronics in Agriculture*, 128, 181-192.

Bai, G., Ge, Y., Scoby, D., Leavitt, B., Stoerger, V., Kirchgessner, N., et al. (2019). NU-Spidercam: a large-scale, cable-driven, integrated sensing and robotic system for advanced phenotyping, remote sensing, and agronomic research. *Computers and Electronics in Agriculture*, 160, 71-81.

Bascon, M. V., Nakata, T., Shibata, S., Takata, I., Kobayashi, N., Kato, Y., et al. (2022). Estimating yield-related traits using UAV-derived multispectral images to improve rice grain yield prediction. *Agriculture, (Switzerland)* 12 (8), 1141. https://doi.org/10.3390/agriculture12081141

Baumüller, H and Kah, M. M. (2019). Going digital: Harnessing the power of emerging technologies for the transformation of Southern African agriculture. *Transforming Agriculture in Southern Africa: Constraints, Technologies, Policies and Policies and Processes* (Routledge: Taylor and Francis Inc., Milton Park, Abingdon in the United Kingdom), 179-187.

Belmahi, M., Hanchane, M., Krakauer, N. Y., Kessabi, R., Bouayad, H., Mahjoub, A., et al. (2023). Analysis of relationship between grain yield and NDVI from MODIS in the Fez-Meknes region, Morocco. *Remote Sensing*, 15 (11), 2707. https://doi.org/10.3390/rs15112707

Ben M'Barek, S., Laribi, M., Kouki, H., Castillo, D., Araar, C., Nefzaoui, M., et al. (2022). Phenotyping Mediterranean durum wheat landraces for resistance to *Zymoseptoria tritici* in Tunisia. *Genes*, 13 (2), 355. https://doi.org/10.3390/genes13020355

Beyene, A. N., Zeng, H., Wu, B., Zhu, L., Gebremicael, T. G., Zhang, M., et al. (2022). Coupling remote sensing and crop growth model to estimate national wheat yield in Ethiopia. *Big Earth Data*, 6 (1), 18-35.

Bian, J., Zhang, Z., Chen, J., Chen, H., Cui, C., Li, X., et al. (2019). Simplified evaluation of cotton water stress using high resolution unmanned aerial vehicle thermal imagery. *Remote Sensing*, 11 (3), 267.

Bijaber, N., El Hadani, D., Saidi, M., Svoboda, M. D., Wardlow, B. D., Hain, C. R., et al. (2018). Developing a remotely sensed drought monitoring indicator for Morocco. *Geosciences (Switzerland)*, 8 (2), 55.

Bjornlund, V., Bjornlund, H., and Van Rooyen, A. F. (2020). Why agricultural production in sub-Saharan Africa remains low compared to the rest of the world–a historical perspective. *International Journal of Water Resources Development*, 36 (sup1), S20–S53, 1-34.

Blancon, J., Dutartre, D., Tixier, M. H., Weiss, M., Comar, A., Praud, S., et al. (2019). A high-throughput model-assisted method for phenotyping maize green leaf area index dynamics using unmanned aerial vehicle imagery. *Frontiers in Plant Science*, 10. https://doi.org/10.3389/ fpls.2019.00685

Blein, R., Soule, B. G., Dupaigre, B. F., and Yerima, B. (2008). "Agricultural potential of west Africa," in *Economic community of West African States (ECOWAS)* (Foundation pour l'agriculture et la ruralité dans le monde (FARM), 118.

Bongomin, O., Lamo, J., Guina, J., Okello, C., Ocen, G., Obura, M., et al. (2022). *Applications of Drones and Image Analytics in Field Phenotyping: A Potential Breakthrough in Uganda's Agricultural Research*. *SSRN Electronic Journal*. Available at SSRN 4158755. https://dx.doi.org/10.2139/ssrn.4158755.

Bontpart, T., Concha, C., Giuffrida, M. V., Robertson, I., Admkie, K., Degefu, T., et al. (2020). Affordable and robust phenotyping framework to analyse root system architecture of soil□grown plants. *Plant Journal*, 103 (6), 2330-2343. https://doi.org/10.1111/tpj.14877

Born, L., Chirinda, N., Mabaya, E., Afun-Ogidan, O., Girvetz, E. H., Jarvis, A., et al. (2021). *Digital agriculture profile: South Africa* (FAO). Available at: http://www.fao.org/3/cb2506en/CB2506EN.pdf (Accessed August 4, 2023).

Bouras, E. H., Jarlan, L., Er-Raki, S., Albergel, C., Richard, B., Balaghi, R., et al. (2020). Linkages between rainfed cereal production and agricultural drought through remote sensing indices and a land data assimilation system: A case study in Morocco. *Remote Sensing*, 12 (24), 4018. https://doi.org/10.3390/rs12244018

Bradshaw, C. D., Pope, E., Kay, G., Davie, J. C., Cottrell, A., Bacon, J., et al. (2022). Unprecedented climate extremes in South Africa and implications for maize production. *Environmental Research Letters*, 17 (8), 084028. https://doi.org/10.1088/1748-9326/ac816d

Brewer, K., Clulow, A., Sibanda, M., Gokool, S., Naiken, V., and Mabhaudhi, T. (2022b). Predicting the chlorophyll content of maize over phenotyping as a

proxy for crop health in smallholder farming systems. *Remote Sensing*, 14 (3), 518. https://doi.org/10.3390/rs14030518

Brewer, K., Clulow, A., Sibanda, M., Gokool, S., Odindi, J., Mutanga, O., et al. (2022a). Estimation of maize foliar temperature and stomatal conductance as indicators of water stress based on optical and thermal imagery acquired using an unmanned aerial vehicle (UAV) platform. *Drones*, 6 (7), 169.

Brocks, S and Bareth, G. (2018). Estimating barley biomass with crop surface models from oblique RGB imagery. *Remote Sensing*, 10 (2), 268. https://doi.org/10.3390/rs10020268

Buchaillot, M. L., Gracia-Romero, A., Vergara-Diaz, O., Zaman-Allah, M. A., Tarekegne, A., Cairns, J. E., et al. (2019). Evaluating maize genotype performance under low nitrogen conditions using RGB UAV phenotyping techniques. *Sensors (Switzerland)*, 19 (8), 1815.

Burke, M and Lobell, D. B. (2017). Satellite-based assessment of yield variation and its determinants in smallholder African systems. Proceedings of the National Academy of Sciences. United States of America, 114 (9), 2189-2194. https://doi.org/10.1073/pnas.1616919114

Burnette, M., Kooper, R., Maloney, J. D., Rohde, G. S., Terstriep, J. A., Willis, C., et al. (2018). TERRA-REF data processing infrastructure. In *Proceedings of the Practice and Experience on Advanced Research Computing*, pp. 1-7. https://doi.org/10.1145/3219104.3219152

Busemeyer, L., Mentrup, D., Möller, K., Wunder, E., Alheit, K., Hahn, V., et al. (2013). Breedvision–A multi-sensor platform for non-destructive field-based phenotyping in plant breeding. *Sensors (Switzerland)*, 13 (3), 2830-2847. https://doi.org/10.3390/s130302830

Buthelezi, S., Mutanga, O., Sibanda, M., Odindi, J., Clulow, A. D., Chimonyo, V. G., et al. (2023). Assessing the prospects of remote sensing maize leaf area index using UAV-derived multi-spectral data in smallholder farms across the growing season. *Remote Sensing*, 15 (6), 1597. https://doi.org/10.3390/rs15061597

Camino, C., González-Dugo, V., Hernández, P., Sillero, J. C., and Zarco-Tejada, P. J. (2018). Improved nitrogen retrievals with airborne-derived fluorescence and plant traits quantified from VNIR-SWIR hyperspectral imagery in the context of precision agriculture. *International Journal of Applied Earth Observation and Geoinformation*, 70, 105-117. https://doi.org/10.1016/j.jag.2018.04.013

Casadesús, J and Villegas, D. (2014). Conventional digital cameras as a tool for assessing leaf area index and biomass for cereal breeding. *Journal of Integrative Plant Biology*, 56 (1), 7-14. https://doi.org/10.1111/jipb.12117

Cavaco, A. M., Utkin, A. B., da Silva, J. M., and Guerra, R. (2022). Making sense of light: The use of optical spectroscopy techniques in plant sciences and agriculture. *Applied Science (Switzerland)*, 12 (3), 997.

Cavender-Bares, J., Gamon, J. A., and Townsend, P. A., (2020). Remote Sensing of Plant Biodiversity. p. 581. *Springer Nature*. https://doi.org/10.1007/978-3-030-33157-3.

Carrera, C. S., Savin, R., and Slafer, G. A. (2024). Critical period for yield determination across grain crops. *Trends in Plant Science*, 29 (3), 329-342.

Chaerle, L and Van Der Straeten, D. (2000). Imaging techniques and the early detection of plant stress. *Trends in Plant Science*, 5 (11), 495-501. https://doi.org/10.1016/S1360-1385(00)01781-7

Chang, T. G and Zhu, X. G. (2017). Source–sink interaction: a century old concept under the light of modern molecular systems biology. *Journal of Experimental Botany*, 68 (16), 4417-4431.

Chapman, S. C., Merz, T., Chan, A., Jackway, P., Hrabar, S., Dreccer, M. F., et al. (2014). Pheno-copter: A low-altitude, autonomous remote-sensing robotic helicopter for high-throughput field-based phenotyping. *Agronomy*, 4 (2), 279-301. https://doi.org/10.3390/agronomy4020279

Chapu, I., Okello, D. K., Okello, R. C. O., Odong, T. L., Sarkar, S., and Balota, M. (2022). Exploration of alternative approaches to phenotyping of late leaf spot and groundnut rosette virus disease for groundnut breeding. *Frontiers in Plant Science*, 13. https://doi.org/10.3389/fpls.2022.912332

Chawade, A., Van Ham, J., Blomquist, H., Bagge, O., Alexandersson, E., and Ortiz, R. (2019). High-throughput field-phenotyping tools for plant breeding and precision agriculture. *Agronomy*, 9 (5), 258.

Chen, J. M and Black, T. A. (1992). Defining leaf area index for non-flat leaves. *Plant, Cell and Environment*, 15 (4), 421-429. https://doi.org/10.1111/j.1365-3040.1992.tb00992.x

Chivasa, W., Mutanga, O., and Biradar, C. (2017). Application of remote sensing in estimating maize grain yield in heterogeneous African agricultural landscapes: A review. *International Journal of Remote Sensing*, 38 (23), 6816-6845. https://doi.org/10.1080/01431161.2017.1365390

Chivasa, W., Mutanga, O., and Biradar, C. (2020). UAV-based multispectral phenotyping for disease resistance to accelerate crop improvement under changing climate conditions. *Remote Sensing*, 12 (15), 2445. https://doi.org/10.3390/RS12152445

Choukr-Allah, R., Rao, N. K., Hirich, A., Shahid, M., Alshankiti, A., Toderich, K., et al. (2016). Quinoa for marginal environments: toward future food and nutritional security in MENA and Central Asia regions. *Frontiers in Plant Science*, 7. https://doi.org/10.3389/fpls.2016.00346

Comar, A., Burger, P., De Solan, B., Baret, F., Daumard, F., and Hanocq, J. F. (2012). A semi-automatic system for high throughput phenotyping wheat cultivars in-field conditions: Description and first results. *Functional Plant Biology*, 39 (11), 914-924. https://doi.org/10.1071/FP12065

Condorelli, G. E., Maccaferri, M., Newcomb, M., Andrade-Sanchez, P., White, J. W., French, A. N., et al. (2018). Corrigendum: Comparative aerial and ground based high throughput phenotyping for the genetic dissection of NDVI as a proxy for drought adaptive traits in durum wheat. *Frontiers in Plant Science*, 9. https://doi.org/10.3389/fpls.2018.01885

Costa, J. M., Grant, O. M., and Chaves, M. M. (2013). Thermography to explore plant-environment interactions. *Journal of Experimental Botany*, 64 (13), 564-584. https://doi.org/10.1093/jxb/ert029

Costa, J. M., Marques da Silva, J., Pinheiro, C., Barón, M., Mylona, P., Centritto, M., et al. (2019). Opportunities and limitations of crop phenotyping in Southern European Countries. *Frontiers in Plant Science*, 10.

Cozzolino, D. (2014). Use of infrared spectroscopy for in-field measurement and phenotyping of plant properties: Instrumentation, data analysis, and examples. *Applied Spectroscopy Review*, 49 (7), 564-584.

Crain, J. L., Wei, Y., Barker, J., Thompson, S. M., Alderman, P. D., Reynolds, M., et al. (2016). Development and deployment of a portable field phenotyping platform. *Crop Science*, 56 (3), 965-975. https://doi.org/10.2135/cropsci2015.05.0290

Crossa, J., Pérez-Rodríguez, P., Cuevas, J., Montesinos-López, O., Jarquín, D., de los Campos, G., et al. (2017). Genomic selection in plant breeding: Methods, models, and perspectives. *Trends in Plant Science*, 22 (11), 961-975. https://doi.org/10.1016/j.tplants.2017.08.011

Cudjoe, D. K., Okyere, F. G., Virlet, N., Castle, M., Buchner, P., Parmar, S., Sadeghi-Tehran, P., Riche, A., Sohail, Q., Mhada, M., Ghanem, M., Waine, T. W., Mohareb, F., and Hawkesford, M. J. (2023b). Using proximal sensing parameters linked to the photosynthetic capacity to assess the nutritional status and yield potential in quinoa. *Acta Horticulturae*, 1360, 373-379 https://doi.org/10.17660/ActaHortic.2023.1360.45

Dammer, K. H., Dworak, V., and Selbeck, J. (2016). On-the-go phenotyping in field potatoes using camera vision. *Potato Research*, 59 (2), 113-127. https://doi.org/10.1007/s11540-016-9315-y

Daniel, I. O., Atinsola, K. O., Ajala, M. O., and Popoola, A. R. (2016). Phenotyping a tomato breeding population by manual field evaluation and digital imaging analysis. *International Journal of Plant Breeding and Genetics*, 11 (1), 19-24. https://doi.org/10.3923/ijpbg.2017.19.24

Danzi, D., Briglia, N., Petrozza, A., Summerer, S., Povero, G., Stivaletta, A., et al. (2019). Can high throughput phenotyping help food security in the Mediterranean area? *Frontiers in Plant Science*, 10.

de Castro, A. I., Shi, Y., Maja, J. M., and Peña, J. M. (2021). UAVs for vegetation monitoring: Overview and recent scientific contributions. *Remote Sensing*, 13 (11), 2139. https://doi.org/10.3390/rs13112139

Debalke, D. B and Abebe, J. T. (2022). Maize yield forecast using GIS and remote sensing in Kaffa Zone, South-West Ethiopia. *Environmental Systems Research*, 11 (1), 1. https://doi.org/10.1186/s40068-022-00249-5

Debesa, G., Gebre, S. L., Melese, A., Regassa, A., and Teka, S. (2020). GIS and remote sensing-based physical land suitability analysis for major cereal crops in Dabo Hana District, South-West Ethiopia. *Cogent Food and Agriculture*, 6 (1), 1780100. https://doi.org/10.1080/23311932.2020.1780100

Deery, D. M., Rebetzke, G. J., Jimenez-Berni, J. A., Bovill, W. D., James, R. A., Condon, A. G., et al. (2019). Evaluation of the phenotypic repeatability of canopy temperature in wheat using continuous-terrestrial and airborne measurements. *Frontiers in Plant Science*, 10.

Deery, D., Jimenez-Berni, J., Jones, H., Sirault, X., and Furbank, R. (2014). Proximal remote sensing buggies and potential applications for field-based phenotyping. *Agronomy*, 4 (3), 875. https://doi.org/10.3390/agronomy4030349

Degila, J., Sodedji, F. A. K., Avakoudjo, H. G. G., Tahi, S. P. G., Houetohossou, S. C. A., Honfoga, A. C., et al. (2023). Digital agriculture policies and strategies for innovations in the agri-food systems–cases of five West African Countries. *Sustainability*, 15 (12), 9192. https://doi.org/10.3390/su15129192

del Cerro, J., Cruz Ulloa, C., Barrientos, A., and de León Rivas, J. (2021). Unmanned Aerial Vehicles in Agriculture: A Survey. *Agronomy*, 11 (2), 203. https://doi.org/10.3390/agronomy11020203

Dhondt, S., Wuyts, N., and Inzé, D. (2013). Cell to whole-plant phenotyping: the best is yet to come. *Trends in Plant Science*, 18 (8), 428-439.

Dingkuhn, M., Sow, A., Manneh, B., Radanielina, T., Raboin, L. M., Dusserre, J., et al. (2015). Field phenomics for response of a rice diversity panel to ten environments in Senegal and Madagascar. 1. Plant phenological traits. *Field Crops Research*, 183, 342-355. https://doi.org/10.1016/j.fcr.2015.07.027

Duvallet, M., Dumas, P., Makowski, D., Boé, J., del Villar, P. M., and Ben-Ari, T. (2021). Rice yield stability compared to major food crops in West Africa. *Environmental Research Letters*, 16 (12), 124005. https://doi.org/10.1088/1748-9326/ac343a

Ejikeme, J. O., Ojiako, J. C., Onwuzuligbo, C. U., and Ezeh, F. C. (2017). Enhancing food security in Anambra state, Nigeria using remote sensing data. *Environmental Reviews*, 6 (1), 27-44.

Elmetwalli, A. H., El-Hendawy, S., Al-Suhaibani, N., Alotaibi, M., Tahir, M. U., Mubushar, M., et al. (2020). Potential of hyperspectral and thermal proximal sensing for estimating growth performance and yield of soybean exposed to different drip irrigation regimes under arid conditions. *Sensors*, 20 (22), 6569. https://doi.org/10.3390/s20226569

Elmetwalli, A. H., Mazrou, Y. S. A., Tyler, A. N., Hunter, P. D., Elsherbiny, O., Yaseen, Z. M., et al. (2022). Assessing the efficiency of remote sensing and

machine learning algorithms to quantify wheat characteristics in the Nile delta region of Egypt. *Agriculture*, 12 (3), 332.

Elsafty, A and Atallah, A. (2022). Factors influencing precision agriculture tools or technologies adoption in Egypt. *Business Management Studies*, 8 (2). https://doi.org/10.11114/bms.v8i2.5598

Elsayed, S., Elhoweity, M., Ibrahim, H. H., Dewir, Y. H., Migdadi, H. M., and Schmidhalter, U. (2017). Thermal imaging and passive reflectance sensing to estimate the water status and grain yield of wheat under different irrigation regimes. *Agricultural Water Management*, 189, 98-110. https://doi.org/10.1016/j.agwat.2017.05.001

El-Shirbeny, M. A., Ali, A., and Saleh, N. H. (2014). Crop water requirements in Egypt using remote sensing techniques. *Journal of Agricultural Chemistry and Environment*, 3 (2), 57-65. https://doi.org/10.4236/jacen.2014.32B010

Epule, T. E., Chehbouni, A., and Dhiba, D. (2022). Recent patterns in maize yield and harvest area across Africa. *Agronomy*, 12 (2), 374.

Erdle, K., Mistele, B., and Schmidhalter, U. (2013). Spectral assessments of phenotypic differences in spike development during grain filling affected by varying N supply in wheat. *Journal of Plant Nutrition and Soil Science*, 176, 952-963. https://doi.org/10.1002/jpln.201300247

Fahrner, S., Janni, M., Pieruschka, R., Vincenz-Donnelly, L., and von Gillhaussen, P. (2021). *Global plant phenotyping survey 2020/21* (Zenodo). https://doi.org/10.5281/zenodo.4723409

Fang, L., Struik, P. C., Girousse, C., Yin, X., and Martre, P. (2024). Source–sink relationships during grain filling in wheat in response to various temperature, water deficit, and nitrogen deficit regimes. *Journal of Experimental Botany*, erae310.

FAO. (2011). Evolving a plant breeding and seed system in sub-Saharan Africa in an era of donor dependence. *A report for the Global Partnership Initiative for Plant Breeding Capacity Building (GIPB) of the Food and Agricultural Organisation*. FAO plant production and protection paper 210, pp. 21-30. Available at: https://www.fao.org/3/at535e/at535e.pdfb.

FAO. (2015). FAOSTAT. *Food and Agricultural Organisation of the United Nations*. Available at: http://www.fao.org/faostat/en/#data/.

FAO. (2022). FAOSTAT. *Database of the Food and Agriculture Organisation United Nations*. Available at: www.fao.org/faostat/en/.

FAOSTAT. (2016). FAOSTAT statistical database. *Food and Agriculture Organisation of the United Nations, Rome, Italy*. Accessed on August 12, 2023.

FAOSTAT. (2018a). *Database of the Food and Agriculture Organisation United Nations*. Available at: www.fao.org/faostat/en/.

FAOSTAT. (2018b). *Morocco production in 2018*. Available at: https://www.fao.org/faostat/en/#data/QCL.

FAOSTAT. (2022). *Database of the Food and Agriculture Organisation of the United Nations, Rome, Italy*. Available at: https://www.fao.org/faostat/en/. Accessed on August 12, 2023.

Feng, L., Chen, S., Zhang, C., Zhang, Y., and He, Y. (2021). A comprehensive review on recent applications of unmanned aerial vehicle remote sensing with various sensors for high-throughput plant phenotyping. *Computers and Electronics in Agriculture*, 182, https://doi.org/106033. 10.1016/j.compag.2021.106033

Feng, W., Yao, X., Zhu, Y., Tian, Y. C., and Cao, W. X. (2008). Monitoring leaf nitrogen status with hyperspectral reflectance in wheat. *European Journal of Agronomy*, 28 (3), 394-404. https://doi.org/10.1016/j.eja.2007.11.005

Feng, W., Zhang, H. Y., Zhang, Y. S., Qi, S. L., Heng, Y. R., Guo, B. B., and Guo, T. C. (2016). Remote detection of canopy leaf nitrogen concentration in winter wheat by using water resistance vegetation indices from in-situ hyperspectral data. *Field Crops Research*, 198, 238-246.

Fernández-Calleja, M., Monteagudo, A., Casas, A. M., Boutin, C., Pin, P. A., Morales, F., et al. (2020). Rapid on-site phenotyping via field fluorimeter detects differences in photosynthetic performance in a hybrid–parent barley germplasm set. *Sensors (Switzerland)*, 20 (5), 1486. https://doi.org/10.3390/s20051486

Fiorani, F and Schurr, U. (2013). Future scenarios for plant phenotyping. *Annual Review of Plant Biology*, 64, 267-291. https://doi.org/10.1146/annurev-arplant-050312-120137

Fiorentini, M., Zenobi, S., and Orsini, R. (2021). Remote and proximal sensing applications for durum wheat nutritional status detection in Mediterranean area. *Agriculture*, 11 (1), 39. https://doi.org/10.3390/agriculture11010039

Fisher, M., Abate, T., Lunduka, R. W., Asnake, W., Alemayehu, Y., and Madulu, R. B. (2015). Drought tolerant maize for farmer adaptation to drought in sub-Saharan Africa: Determinants of adoption in eastern and southern Africa. *Climatic Change*, 133, 283-299. https://doi.org/10.1007/s10584-015-1459-2

Fitzgerald, G. J., Rodriguez, D., Christensen, L. K., Belford, R., Sadras, V. O., and Clarke, T. R. (2006). Spectral and thermal sensing for nitrogen and water status in rainfed and irrigated wheat environments. *Precision Agriculture*, 7 (4), 233-248. https://doi.org/10.1007/s11119-006-9011-z

Fritsche-Neto, R and Borém, A. (2015). Phenomics: How next-generation phenotyping is revolutionizing plant breeding. In *Phenomics: How Next-Generation Phenotyping is Revolutionizing Plant Breeding*. (Switzerland: Springer International Publishing). https://doi.org/10.1007/978-3-319-13677-6

Furbank, R. T., Jimenez-Berni, J. A., George-Jaeggli, B., Potgieter, A. B., and Deery, D. M. (2019). Field crop phenomics: enabling breeding for radiation use

efficiency and biomass in cereal crops. *New Phytologist*, 223 (4), 1714-1727. https://doi.org/10.1111/nph.15817

Gago, J., Douthe, C., Coopman, R. E., Gallego, P. P., Ribas-Carbo, M., Flexas, J., et al. (2015). UAVs challenge to assess water stress for sustainable agriculture. *Agricultural Water Management*, 153, 9-19.

Gano, B., Dembele, J. S. B., Ndour, A., Luquet, D., Beurier, G., Diouf, D., et al. (2021). Adaptation responses to early drought stress of West Africa sorghum varieties. *Agronomy*, 11 (5), 850. https://doi.org/10.3390/agronomy11050850

Garriga, M., Romero-Bravo, S., Estrada, F., Escobar, A., Matus, I. A., del Pozo, A., et al. (2017). Assessing wheat traits by spectral reflectance: Do we really need to focus on predicted trait-values or directly identify the elite genotypes group? *Frontiers in Plant Science*, 8. https://doi.org/10.3389/fpls.2017.00280

Gedil, M and Menkir, A. (2019). An integrated molecular and conventional breeding scheme for enhancing genetic gain in maize in Africa. *Frontiers in Plant Science*, 10. https://doi.org/10.3389/fpls.2019.01430

Gibbs, J. A., Pound, M., French, A. P., Wells, D. M., Murchie, E., and Pridmore, T. (2017). Approaches to three-dimensional reconstruction of plant shoot topology and geometry. *Functional Plant Biology*, 44 (1), 62-75.

Gobezie, T. B and Biswas, A. (2023). The need for streamlining precision agriculture data in Africa. *Precision Agriculture*, 24 (1), 375-383.

Godfray, H. C. J and Robinson, S. (2015). Contrasting approaches to projecting long-run global food security. *Oxford Reviews on Economic Policy*, 31 (1), 26-44. https://doi.org/10.1093/oxrep/grv006

Gokool, S., Mahomed, M., Kunz, R., Clulow, A., Sibanda, M., Naiken, V., et al. (2023). Crop monitoring in smallholder farms using unmanned aerial vehicles to facilitate precision agriculture practices: a scoping review and bibliometric analysis. *Sustainability*, 15 (4), 3557. https://doi.org/10.3390/su15043557

Gonzalez-Dugo, V., Hernandez, P., Solis, I., and Zarco-Tejada, P. J. (2015). Using high-resolution hyperspectral and thermal airborne imagery to assess physiological condition in the context of wheat phenotyping. *Remote Sensing*, 7 (10), 13586-13605. https://doi.org/10.3390/rs71013586

Gordillo-Salinas, V. M., Flores-Magdaleno, H., Ortiz-Solorio, C. A., and Arteaga-Ramírez, R. (2021). Evaluation of nitrogen status in a wheat crop using unmanned aerial vehicle images. *Chilean Journal of Agricultural Research*, 81 (3), 408-419. https://doi.org/10.4067/S0718-58392021000300408

Gourlay, S., Kilic, T., and Lobell, D. (2017). Could the debate be over? Errors in farmer-reported production and their implications for the inverse scale-productivity relationship in Uganda. *Technical Report, Policy Research Working Paper No. 8192*. (Washington, D C: World Bank). https://doi.org/10.1596/1813-9450-8192

Gracia-Romero, A., Kefauver, S. C., Vergara-Díaz, O., Hamadziripi, E., Zaman-Allah, M. A., Thierfelder, C., et al. (2020). Leaf versus whole-canopy remote sensing methodologies for crop monitoring under conservation agriculture: a case of study with maize in Zimbabwe. *Scientific Reports*, 10 (1), 16008. https://doi.org/10.1038/s41598-020-73110-3

Gracia-Romero, A., Vergara-Díaz, O., Thierfelder, C., Cairns, J. E., Kefauver, S. C., and Araus, J. L. (2018). Phenotyping conservation agriculture management effects on ground and aerial remote sensing assessments of maize hybrids performance in Zimbabwe. *Remote Sensing*, 10 (2), 349. https://doi.org/10.3390/rs10020349

Großkinsky, D. K., Svensgaard, J., Christensen, S., and Roitsch, T. (2015). Plant phenomics and the need for physiological phenotyping across scales to narrow the genotype-to-phenotype knowledge gap. *Journal of Experimental Botany*, 66, 5429-5440. https://doi.org/10.1093/jxb/erv345

Guo, Q., Wu, F., Pang, S., Zhao, X., Chen, L., Liu, J., et al. (2018). Crop 3D–a LiDAR based platform for 3D high-throughput crop phenotyping. *Science China Life Sciences*, 61 (3), 328-339. https://doi.org/10.1007/s11427-017-9056-0

Guo, W., Fukatsu, T., and Ninomiya, S. (2015). Automated characterisation of flowering dynamics in rice using field-acquired time-series RGB images. *Plant Methods*, 11 (1), 1-15. https://doi.org/10.1186/s13007-015-0047-9

Hall, O., Dahlin, S., Marstorp, H., Archila Bustos, M. F., Öborn, I., and Jirström, M. (2018). Classification of maize in complex smallholder farming systems using UAV imagery. *Drones*, 2 (3), 22. https://doi.org/10.3390/drones2030022

Hamidi, S and Benabdeljalil, N. (2013). National innovation systems: The Moroccan case. *Procedia-Social and Behavioural Sciences*, 75, 119-128.

Hassan, M. A., Yang, M., Fu, L., Rasheed, A., Zheng, B., Xia, X., et al. (2019). Accuracy assessment of plant height using an unmanned aerial vehicle for quantitative genomic analysis in bread wheat. *Plant Methods*, 15 (1), 1-12. https://doi.org/10.1186/s13007-019-0419-7

Hedley, C. (2015). The role of precision agriculture for improved nutrient management on farms. *Journal of the Science of Food and Agriculture*, 95 (1), 12-19. https://doi.org/10.1002/jsfa.6734

Henri, A. O. (2019). Heavily indebted poor countries initiative (HIPC), debt relief, economic stability and economic growth in Africa. *Economic Change Restructuring*, 52, 89-121. https://doi.org/10.1007/s10644-017-9218-1

Hickey, L. T., Hafeez, A. N., Robinson, H., Jackson, S. A., Leal-Bertioli, S. C., Tester, M., and Wulff, B. B. (2019). Breeding crops to feed 10 billion. *Nature Biotechnology*, 37 (7), 744-754. https://doi.org/10.1038/s41587-019-0152-9

Hirich, A., Rafik, S., Rahmani, M., Fetouab, A., Azaykou, F., Filali, K., et al. (2021). Development of quinoa value chain to improve food and nutritional security in

rural communities in Rehamna, Morocco: lessons learned and perspectives. *Plants*, 10 (2), 301. https://doi.org/10.3390/plants10020301

Holman, F. (2020). *Development and evaluation of unmanned aerial vehicles for high throughput phenotyping of field-based wheat trials*. (Doctoral dissertation, King's College London).

Holman, F. H., Riche, A. B., Michalski, A., Castle, M., Wooster, M. J., and Hawkesford, M. J. (2016). High throughput field phenotyping of wheat plant height and growth rate in field plot trials using UAV based remote sensing. *Remote Sensing*, 8 (12), 1031. https://doi.org/10.3390/rs8121031

ICARDA phenotyping platforms in Morocco. Available at: https://www.cgiar.org/news-events/news/icardas-phenotyping-facilities-a-game-changing-solution-for-abiotic-stress-tolerance-in-crops/.

Ifeanyieze, F. O., Ikehi, M. E., and Isiwu, E. (2014). Techniques in utilising remote sensor technology for precision crop production by farmers as climate change adaptation strategy in Nigeria. *Agricultural Sciences*, 5 (14), 1476.

Iizumi, T and Sakai, T. (2020). The global dataset of historical yields for major crops 1981–2016. *Scientific Data*, 7 (1), 97. https://doi.org/10.1038/s41597-020-0433-7

IPPN. (2016). The international plant phenotyping network. In: Survey 2016. Available at:http://www.plant-phenotyping.org/lw_resource/datapool/systemfiles/elements/files/ba090795-026e-11e7-8c78-dead53a91d31/live/document/Survey_2016_final_2.pdf (Accessed June 20, 2023).

IPPN. (2020). Survey. Available at: https://globalplantcouncil.org/global-plant-phenotyping-survey-2020-21/.

Iseki, K and Matsumoto, R. (2019). Non-destructive shoot biomass evaluation using a handheld NDVI sensor for field-grown staking Yam (*Dioscorea rotundata* Poir.). *Plant Production Science*, 22 (2), 301-310.

Izuogu, C. U., Njoku, L. C., Olaolu, M. O., Kadurumba, P. C., Azuamairo, G. C., and Agou, G. D. (2023). A review of the digitalisation of agriculture in Nigeria. *Journal of Agricultural Extension*, 27 (2), 47-64.

Jabir, B and Falih, N. (2020). Digital agriculture in Morocco, opportunities and challenges. In *Proceedings of the 2020 6th International Conference on Optimisation and Applications* (ICOA), Beni Mellal, Morocco. (Piscataway, New Jersey, United States: Institute of Electrical and Electronics Engineers (IEEE), 1-5, IEEE. https://doi.org/10.1109/ICOA49421.2020.9094450

Jimenez-Berni, J. A., Deery, D. M., Rozas-Larraondo, P., Condon, A. T. G., Rebetzke, G. J., James, R. A., et al. (2018). High throughput determination of plant height, ground cover, and above-ground biomass in wheat with LiDAR. *Frontiers in Plant Science*, 9. https://doi.org/10.3389/fpls.2018.00237

Johannsen, W. (1911). The genotype conception of heredity. *The American Naturalist*, 45 (531), 129-159.

Kassim, Y. B., Oteng-Frimpong, R., Puozaa, D. K., Sie, E. K., Abdul Rasheed, M., Abdul Rashid, I., et al. (2022). High-throughput plant phenotyping (HTPP) in resource-constrained research programmes: A working example in Ghana. *Agronomy*, 2 (11), 2733. https://doi.org/10.3390/agronomy12112733

Kavhiza, N. J., Zargar, M., Prikhodko, S. I., Pakina, E. N., Murtazova, K. M. S., and Nakhaev, M. R. (2022). Improving crop productivity and ensuring food security through the adoption of genetically modified crops in sub-saharan Africa. *Agronomy*, 12 (2), 439. https://doi.org/10.3390/agronomy12020439

Kefauver, S. C., El-Haddad, G., Vergara-Diaz, O., and Araus, J. L. (2015). RGB picture vegetation indexes for high-throughput phenotyping platforms (HTPPs). *Remote Sensing for Agriculture, Ecosystems and Hydrology, XVII 9637*, 82-90. SPIE. https://doi.org/10.1117/12.2195235

Kidane, Y. G., Hailemariam, B. N., Mengistu, D. K., Fadda, C., Pè, M. E., and Dell'Acqua, M. (2017). Genome-wide association study of Septoria tritici blotch resistance in Ethiopian durum Wheat Landraces. *Frontiers in Plant Science*, 8. https://doi.org/10.3389/fpls.2017.01586

Kim, J. Y. (2020). Roadmap to high throughput phenotyping for plant breeding. *Journal of Biosystems Engineering*, 45, 43-55. https://doi.org/10.1007/s42853-020-00043-0

Kipp, S., Mistele, B., and Schmidhalter, U. (2014). Identification of stay-green and early senescence phenotypes in high-yielding winter wheat, and their relationship to grain yield and grain protein concentration using high-throughput phenotyping techniques. *Functional Plant Biology*, 41 (3), 227-235.

Kirchgessner, N., Liebisch, F., Yu, K., Pfeifer, J., Friedli, M., Hund, A., et al. (2017). The ETH field phenotyping platform FIP: A cable-suspended multi-sensor system. *Functional Plant Biology*, 44 (1), 154-168. https://doi.org/10.1071/FP16165

Knox, J., Hess, T., Daccache, A., and Wheeler, T. (2012). Climate change impacts on crop productivity in Africa and South Asia. *Environmental Research Letters*, 7 (3), 034032. https://doi.org/10.1088/1748-9326/7/3/034032

Kobo, H. I., Abu-Mahfouz, A. M., and Hancke, G. P. (2017). A survey on software-defined wireless sensor networks: Challenges and design requirements. *IEEE Access* 5, 1872-1899. https://doi.org/10.1109/ACCESS.2017.2666200

Kotikot, S. M and Onywere, S. M. (2015). Application of GIS and remote sensing techniques in frost risk mapping for mitigating agricultural losses in the Aberdare ecosystem, Kenya. *Geocarto International*, 30 (1), 104-121.

Kpienbaareh, D., Kansanga, M., and Luginaah, I. (2019). Examining the potential of open-source remote sensing for building effective decision support systems for

precision agriculture in resource-poor settings. *GeoJournal*, 84 (6), 1481-1497. https://doi.org/10.1007/s10708-018-9932-x

Kumar, D., Kushwaha, S., Delvento, C., Liatukas, Ž., Vivekanand, V., Svensson, J. T., et al. (2020). Affordable phenotyping of winter wheat under field and controlled conditions for drought tolerance. *Agronomy*, 10 (6), 882.

Laachrate, H., Fadil, A., and Ghafiri, A. (2020). Drought monitoring of some Moroccan agricultural areas: Settat and Meknes using remote sensing techniques and a soil moisture-based drought index. In *Proceedings-2020 IEEE International Conference of Moroccan Geomatics*, Morgeo 2020.

Langemeier, M and Boehlje, M. (2021). What will be the capabilities and skills needed to manage the farm of the future? *Farmdoc Daily*, 11, 1-4. Department of Agricultural and Consumer Economics, University of Illinois at Urbana-Champaign.

Leakey, R. R., Tientcheu Avana, M. L., Awazi, N. P., Assogbadjo, A. E., Mabhaudhi, T., Hendre, P. S., et al. (2022). The future of food: Domestication and commercialization of indigenous food crops in Africa over the third decade, (2012-2021). *Sustainability*, 14 (4), 2355. https://doi.org/10.3390/su14042355

Lesjak, J. (2014). Effect of increased temperature and reduced source-sink ratio on grain yield of quinoa (*Chenopodium quinoa* Willd.). Thesis submitted to the Faculty of Agricultural Sciences of the Universidad Austral de Chilein partial fulfillment of the requirements for the degree of Master in Plant Sciences

Li, D., Quan, C., Song, Z., Li, X., Yu, G., Li, C., and Muhammad, A. (2021). High-throughput plant phenotyping platform (HT3P) as a novel tool for estimating agronomic traits from the lab to the field. *Frontiers in Bioengineering and Biotechnology*, 8, 623705. https://doi.org/10.3389/fbioe.2020.623705

Li, D., Quan, C., Song, Z., Li, X., Yu, G., Li, C., et al. (2021). High-throughput plant phenotyping platform (HT3P) as a novel tool for estimating agronomic traits from the lab to the field. *Frontiers in Bioengineering and Biotechnology*, 8. https://doi.org/10.3389/fbioe.2020.623705

Li, L., Zhang, Q., and Huang, D. (2014). A review of imaging techniques for plant phenotyping. *Sensors (Switzerland)*, 14 (11), 20078-20111. https://doi.org/10.3390/s141120078

Liu, T., Li, R., Jin, X., Ding, J., Zhu, X., Sun, C., et al. (2017). Evaluation of seed emergence uniformity of mechanically sown wheat with UAV RGB imagery. *Remote Sensing*, 9 (12), 1241. https://doi.org/10.3390/rs9121241

Livingston, G., Schonberger, S., and Delaney, S. (2011). Sub-Saharan Africa: The state of smallholders in agriculture. *Paper presented at the Conference on New Directions for Smallholder Agriculture*. (Rome: International Fund for Agricultural Development (IFAD) 24, 25.

Lorence, A and Jimenez, K. M. (Eds.) (2022). *High-throughput plant phenotyping: Methods and Protocols*, volume 2539 (New York, USA: Springer Nature). Available at: https://doi.org/10.1007/978-1-0716-2537-8

Lu, N., Zhou, J., Han, Z., Li, D., Cao, Q., Yao, X., and Cheng, T. (2019). Improved estimation of aboveground biomass in wheat from RGB imagery and point cloud data acquired with a low-cost unmanned aerial vehicle system. *Plant Methods*, 15 (1), 1-16. https://doi.org/10.1186/s13007-019-0402-3

Machwitz, M., Pieruschka, R., Berger, K., Schlerf, M., Aasen, H., Fahrner, S., and Rascher, U. (2021). Bridging the gap between remote sensing and plant phenotyping–Challenges and opportunities for the next generation of sustainable agriculture. *Frontiers in Plant Science*, 12, 749374.

Maes, W. H and Steppe, K. (2019). Perspectives for remote sensing with unmanned aerial vehicles in precision agriculture. *Trends in Plant Science*, 24 (2), 152-164. https://doi.org/10.1016/j.tplants.2018.11.007

Mahajan, G. R., Sahoo, R. N., Pandey, R. N., Gupta, V. K., and Kumar, D. (2014). Using hyperspectral remote sensing techniques to monitor nitrogen, phosphorus, sulphur and potassium in wheat (*Triticum aestivum* L.). *Precision Agriculture*, 15, 499- 522. https://doi.org/10.1007/s11119-014-9348-7

Mahdy, E. M. B and Ahmad, H. (2023). A study of Corchorus L. diversity in Egypt using high-throughput phenotyping platform (HTPP): an Egyptian gene bank example. *Genetic Resources and Crop Evolution*, 70, 1-11.

Maimaitijiang, M., Ghulam, A., Sidike, P., Hartling, S., Maimaitiyiming, M., Peterson, K., et al. (2017). Unmanned Aerial System (UAS)-based phenotyping of soybean using multi-sensor data fusion and extreme learning machine. *ISPRS Journal of Photogrammetry and Remote Sensing*, 134, 43-58.

Manzi, H and Gweyi-Onyango, J. P. (2021). "Agro-ecological lower midland zones IV and V in Kenya using GIS and remote sensing for climate-smart crop management," in *African handbook of climate change adaptation*. Eds. N. Oguge, D. Ayal, L. Adeleke and I. da Silva (Cham: Springer).

Martínez-Peña, R., Schlereth, A., Höhne, M., Encke, B., Morcuende, R., Nieto-Taladriz, M. T., and Vicente, R. (2022). Source-sink dynamics in field-grown durum wheat under contrasting nitrogen supplies: key role of non-foliar organs during grain filling. *Frontiers in Plant Science*, 13, 869680.

Matsumoto, T., Wu, J., Kanamori, H., Katayose, Y., Fujisawa, M., Namiki, N., et al. (2005). The map-based sequence of the rice genome. *Nature*, 436 (7052), 793-800. https://doi.org/10.1038/nature03895

Mbaye, M., Ndour, A., Gano, B., Dembele, J. S. B., Luquet, D., Beurier, G., et al. (2022). "UAV method based on multispectral imaging for field phenotyping," in *Crop adaptation and improvement for drought-prone environments*. Eds. Kane, N. A. Daniel, K and Dalton, T. J (Manhattan: New Prairie Press), 173-187, ISBN.

Meliho, M., Khattabi, A., Jobbins, G., and Sghir, F. (2020). Impact of meteorological drought on agriculture in the Tensift watershed of Morocco. *Journal of Water and Climate Change*, 11 (4), 1323-1338. https://doi.org/10.2166/wcc.2019.279

Mengistu, D. K., Kidane, Y. G., Fadda, C., and Pè, M. E. (2018). Genetic diversity in Ethiopian durum wheat (*Triticum turgidum* var durum) inferred from phenotypic variations. *Plant Genetic Resources*, 16 (1), 39-49.

Minervini, M., Scharr, H., and Tsaftaris, S. A. (2015). Image analysis: The new bottleneck in plant phenotyping (applications corner). *IEEE Signal Process*. *Magazine*, 32 (4), 126–131. https://doi.org/10.1109/MSP.2015.2405111

Miralles, D. J and Slafer, G. A. (2007). Sink limitations to yield in wheat: how could it be reduced? *The Journal of Agricultural Science* 145, 139–150.

Mukhawana, M. B., Kanyerere, T., and Kahler, D. (2023). Review of in-Situ and remote sensing-based indices and their Applicability for integrated drought monitoring in South Africa. *Water*, 15 (2), 240. https://doi.org/10.3390/w15020240

Müller-Linow, M., Pinto-Espinosa, F., Scharr, H., and Rascher, U. (2015). The leaf angle distribution of natural plant populations: Assessing the canopy with a novel software tool. *Plant Methods*, 11 (1), 1-16.

Munghemezulu, C., Mashaba-Munghemezulu, Z., Ratshiedana, P. E., Economon, E., Chirima, G., and Sibanda, S. (2023). Unmanned aerial vehicle (UAV) and spectral datasets in South Africa for precision agriculture. *Data*, 8 (6), 98. https://doi.org/10.3390/data8060098

Musungwini, S. (2018). Mobile phone use by Zimbabwean smallholder farmers: A baseline study. *African Journal of Information and Communication*, 22, 29-52. https://doi.org/10.23962/10539/26171

Mutanga, O., Dube, T., and Ahmed, F. (2016). Progress in remote sensing: vegetation monitoring in South Africa. *South African Geographical Journal*, 98 (3), 461-471. https://doi.org/10.1080/03736245.2016.1208586

Nduku, L., Munghemezulu, C., Mashaba-Munghemezulu, Z., Kalumba, A. M., Chirima, G. J., Masiza, W., and De Villiers, C. (2023). Global research trends for unmanned aerial vehicle remote sensing application in wheat crop monitoring. *Geomatics*, 3 (1), 115-136. https://doi.org/10.3390/geomatics3010006

Neilson, E. H., Edwards, A. M., Blomstedt, C. K., Berger, B., Møller, B. L., and Gleadow, R. M. (2015). Utilisation of a high-throughput shoot imaging system to examine the dynamic phenotypic responses of a C4 cereal crop plant to nitrogen and water deficiency over time. *Journal of Experimental Botany*, 66 (7), 1817-1832. https://doi.org/10.1093/jxb/eru526

Ninomiya, S. (2022). High-throughput field crop phenotyping: current status and challenges. *Breeding Science*, 72 (1), 3-18. https://doi.org/10.1270/jsbbs.21069

Nyaga, J. M., Onyango, C. M., Wetterlind, J., and Söderström, M. (2021). Precision agriculture research in sub-Saharan Africa countries: A systematic map.

Precision Agriculture, 22, 1217-1236. https://doi.org/10.1007/s11119-020-09780-w

Ochieng, J., Knerr, B., Owuor, G., and Ouma, E. (2020). Food crops commercialisation and household livelihoods: Evidence from rural regions in Central Africa. *Agribusiness*, 36 (2), 318-338. https://doi.org/10.1002/agr.21619

Ogutu, G. E. O., Franssen, W. H. P., Supit, I., Omondi, P., and Hutjes, R. W. A. (2018). Probabilistic maize yield prediction over East Africa using dynamic ensemble seasonal climate forecasts. *Agriculture and Forest Meteorology*, 250-251, 243-261. https://doi.org/10.1016/j.agrformet.2017.12.256

Osiemo, J., Girvetz, E. H., Hasiner, E., Schroeder, K., Treguer, D., Juergenliemk, A., et al. (2021). *Digital agriculture profile: Kenya* (Rome: FAO). Available at: https://www.fao.org/3/cb3958en/cb3958en.pdf (Accessed August 8, 2023).

Ouraich, I and Tyner, W. E. (2018). Moroccan agriculture, climate change, and the Moroccan Green Plan: A CGE analysis. *African Journal of Agricultural and Resource Economics*, 13 (311-2019-681), 307-330.

Pajares, G. (2015). Overview and current status of remote sensing applications based on unmanned aerial vehicles (UAVs). *Photogrammetric Engineering and Remote Sensing*, 81 (4), 281-330. https://doi.org/10.14358/PERS.81.4.281

Palmer, P. I., Wainwright, C. M., Dong, B., Maidment, R. I., Wheeler, K. G., Gedney, N., et al. (2023). Drivers and impacts of Eastern African rainfall variability. *Nature Reviews Earth and Environment*, 4 (4), 254-270.

Park, S., Ryu, D., Fuentes, S., Chung, H., Hernández-Montes, E., and O'Connell, M. (2017). Adaptive estimation of crop water stress in nectarine and peach orchards using high-resolution imagery from an unmanned aerial vehicle (UAV). *Remote Sensing*, 9 (8), 828. https://doi.org/10.3390/rs9080828

Parkes, B., DeFrance, D., Sultan, B., Ciais, P., and Wang, X. (2018). Projected changes in crop yield mean and variability over West Africa in a world 1.5K warmer than the pre-industrial era. *Earth System Dynamics*, 9 (1), 119-134.

Parks, S. E., Irving, D. E., and Milham, P. J. (2012). A critical evaluation of on-farm rapid tests for measuring nitrate in leafy vegetables. *Scientia Horticulturae*, 134, 1-6. https://doi.org/10.1016/j.scienta.2011.10.015

Parwada, C and Marufu, H. (2023). Digitalisation of agriculture in Zimbabwe: Challenges and opportunities. *International Journal of Sustainable Agricultural Research*, 10 (1), 32-41. https://doi.org/10.18488/ijsar.v10i1.3280

Paterson, A. H., Bowers, J. E., Bruggmann, R., Dubchak, I., Grimwood, J., Gundlach, H., et al. (2009). The Sorghum bicolour genome and the diversification of grasses. *Nature*, 457 (7229), 551-556. https://doi.org/10.1038/nature07723

Pauli, D., Andrade-Sanchez, P., Carmo-Silva, A. E., Gazave, E., French, A. N., Heun, J., et al. (2016). Field-based high-throughput plant phenotyping reveals the

temporal patterns of quantitative trait loci associated with stress-responsive traits in cotton. *G3: Genes Genomes, Genetics*, 6 (4), 865-879.

Peng, X., Han, W., Ao, J., and Wang, Y. (2021). Assimilation of LAI derived from UAV multispectral data into the SAFY model to estimate maize yield. *Remote Sensing*, 13 (6), 1094. https://doi.org/10.3390/rs13061094

Peng, Y., Gitelson, A. A., Keydan, G., Rundquist, D. C., and Moses, W. (2011). Remote estimation of gross primary production in maize and support for a new paradigm based on total crop chlorophyll content. *Remote Sensing of Environment*, 115 (4), 978–989. https://doi.org/10.1016/j.rse.2010.12.001

Pieruschka, R and Lawson, T. (2015). Phenotyping in Plants. Preface. *Journal of Experimental Botany*, 66 (18), 5385-5387. https://doi.org/10.1093/jxb/erv395

Pieruschka, R and Schurr, U. (2019). Plant phenotyping: Past, present, and future. *Plant Phenomics* 2019. https://doi.org/10.34133/2019/7507131

Pieruschka, R and Schurr, U. (2022). "Origins and drivers of crop phenotyping," in *Advances in plant phenotyping for more sustainable crop production*. Ed. A. Walter (Cambridge, UK: Burleigh Dodds Science Publishing Limited), 1-25

Pimstein, A., Karnieli, A., Bansal, S. K., and Bonfil, D. J. (2011). Exploring remotely sensed technologies for monitoring wheat potassium and phosphorus using field spectroscopy. *Field Crops Research*, 121 (1), 125-135.

Pineda, M., Barón, M., and Pérez-Bueno, M. L. (2021). Thermal imaging for plant stress detection and phenotyping. *Remote Sensing*, 13 (1), 68.

Poblete, T., Ortega-Farías, S., and Ryu, D. (2018). Automatic co-registration algorithm to remove canopy shaded pixels in UAV-borne thermal images to improve the estimation of crop water stress index of a drip-irrigated cabernet sauvignon vineyard. *Sensors (Switzerland)*, 18 (2), 397. https://doi.org/10.3390/s18020397

Potgieter, A. B., Watson, J., Eldridge, M., Laws, K., George-Jaeggli, B., Hunt, C., et al. (2018). Determining crop growth dynamics in sorghum breeding trials through remote and proximal sensing technologies. *International Geoscience and Remote Sensing Symposium* (IGARSS), Valencia, Spain. (Piscataway, New Jersey, United States: The Institute of Electrical and Electronics Engineers (IEEE)). https://doi.org/10.1109/IGARSS.2018.8519296

Qiu, Q., Sun, N., Bai, H., Wang, N., Fan, Z., Wang, Y., et al. (2019). Field-based high-throughput phenotyping for maize plant using 3D LIDAR point cloud generated with a "phenomobile". *Frontiers in Plant Science*, 10.

Qiu, R., Wei, S., Zhang, M., Li, H., Sun, H., Liu, G., et al. (2018). Sensors for measuring plant phenotyping: A review. *International Journal of Agricultural Biotechnology and Engineering*, 11 (2), 1-17.

Quahir, S., et al. (2022). Drought research in the dry areas of Africa: the case of PhenoMA the high throughput phenotyping Platform in Morocco. Available at: https://www.plantphenotyping.org/lw_resource/datapool/systemfiles/elements/fi

les/0dec546e-673e-11ed-9086-dead53a91d31/current/document/abstract_Book_IPPS_2022.pdf.

Quemada, M., Gabriel, J. L., and Zarco-Tejada, P. (2014). Airborne hyperspectral images and ground-level optical sensors as assessment tools for maize nitrogen fertilisation. *Remote Sensing*, 6 (4), 2940-2962.

Rahaman, M. M., Chen, D., Gillani, Z., Klukas, C., and Chen, M. (2015). Advanced phenotyping and phenotype data analysis for the study of plant growth and development. *Frontiers in Plant Science*, 6.

Ray, D. K., Ramankutty, N., Mueller, N. D., West, P. C., and Foley, J. A. (2012). Recent patterns of crop yield growth and stagnation. *Nature Communications*, 3, 1293. https://doi.org/10.1038/ncomms2296

Rebetzke, G. J., Fischer, R. A., Van Herwaarden, A. F., Bonnett, D. G., Chenu, K., Rattey, A. R., et al. (2014). Plot size matters: Interference from intergenotypic competition in plant phenotyping studies. *Functional Plant Biology*, 41 (2), 107-118. https://doi.org/10.1071/FP13177

Reynolds, D., Baret, F., Welcker, C., Bostrom, A., Ball, J., Cellini, F., et al. (2019). What is cost-efficient phenotyping? Optimising costs for different scenarios. *Plant Science*, 282, 14-22. https://doi.org/10.1016/j.plantsci.2018.06.015

Reynolds, M., Chapman, S., Crespo-Herrera, L., Molero, G., Mondal, S., Pequeno, D. N. L., et al. (2020). Breeder friendly phenotyping. *Plant Science*, 295, 110396. https://doi.org/10.1016/j.plantsci.2019.110396

Rezende, W. S., Beyene, Y., Mugo, S., Ndou, E., Gowda, M., Sserumaga, J. P., et al. (2020). Performance and yield stability of maize hybrids in stress-prone environments in Eastern Africa. *Crop Journal*, 8 (1), 107-118. https://doi.org/10.1016/j.cj.2019.08.001

Roitsch, T., Cabrera-Bosquet, L., Fournier, A., Ghamkhar, K., Jiménez-Berni, J., Pinto, F., et al. (2019). Review: New sensors and data-driven approaches–A path to next generation phenomics. *Plant Science*, 282, 2-10.

Rosenqvist, E., Großkinsky, D. K., Ottosen, C. O., and van de Zedde, R. (2019). The phenotyping dilemma–the challenges of a diversified phenotyping community. *Frontiers in Plant Science*, 10. https://doi.org/10.3389/fpls.2019.00163

Roudier, P., Sultan, B., Quirion, P., and Berg, A. (2011). The impact of future climate change on West African crop yields: What does the recent literature say*? Global Environmental Change*, 21 (3), 1073-1083.

Sadeghi-Tehran, P., Virlet, N., and Hawkesford, M. J. (2021). A neural network method for classification of sunlit and shaded components of wheat canopies in the field using high-resolution hyperspectral imagery. *Remote Sensing*, 13 (5), 898. https://doi.org/10.3390/rs13050898

Sagan, V., Maimaitijiang, M., Sidike, P., Eblimit, K., Peterson, K. T., Hartling, S., et al. (2019). UAV-based high resolution thermal imaging for vegetation monitoring,

and plant phenotyping using ICI 8640 P, FLIR Vue Pro R 640, and thermomap cameras. *Remote Sensing*, 11 (3), 330. https://doi.org/10.3390/rs11030330

Saidi, A. S and Diouri, M. (2017). Food self-sufficiency under the Green-Morocco Plan. *Journal of Experimental Biology and Agricultural Sciences*, 5 (Spl-1-SAFSAW), 33-40. https://doi.org/10.18006/2017.5(Spl-1-SAFSAW).S33.S40

Salami, A., Kamara, A. B., and Schwidrowski, Z. B. (2010). *Smallholder agriculture in East Africa: Trends, constraints and opportunities* (Tunis, Tunisia: African Development Bank).

Sankaran, S., Khot, L. R., Espinoza, C. Z., Jarolmasjed, S., Sathuvalli, V. R., Vandemark, G. J., et al. (2015). Low-altitude, high-resolution aerial imaging systems for row and field crop phenotyping: A review. *European Journal of Agronomy*, 70, 112-123. https://doi.org/10.1016/j.eja.2015.07.004

Sayed, S. A., Mahmoud, A. S., Farg, E., Mohamed, A. M., Saleh, A. M., AbdelRahman, M. A., et al. (2023). A comparative study of big data use in Egyptian agriculture. *Journal of Electrical Systems and Information Technology*, 10 (1), 21. https://doi.org/10.1186/s43067-023-00090-5

Scheben, A., Batley, J., and Edwards, D. (2018). Revolution in genotyping platforms for crop improvement. *Advances in Biochemical Engineering/Biotechnology*, 164, 37-52. https://doi.org/10.1007/10_2017_47

Schirrmann, M., Hamdorf, A., Garz, A., Ustyuzhanin, A., and Dammer, K. H. (2016). Estimating wheat biomass by combining image clustering with crop height. *Computers and Electronics in Agriculture*, 121, 374-384.

Schmutz, J., Cannon, S. B., Schlueter, J., Ma, J., Mitros, T., Nelson, W., et al. (2010). Genome sequence of the palaeopolyploid soybean. *Nature*, 463 (7278), 178-183. https://doi.org/10.1038/nature08670

Schnable, P. S., Ware, D., Fulton, R. S., Stein, J. C., Wei, F., Pasternak, S., et al. (2009). The B73 maize genome: Complexity, diversity, and dynamics. *Science*, 326 (5956), 1112-1115. https://doi.org/10.1126/science.1178534

Seiffert, U., Bollenbeck, F., Mock, H. P., and Matros, A. (2010). Clustering of crop phenotypes by means of hyperspectral signatures using artificial neural networks. *2nd Workshop on Hyperspectral Image and Signal Processing: Evolution in Remote Sensing, WHISPERS 2010–Workshop Programme*, Reykjavik, Iceland. (Piscataway, New Jersey, United States: The Institute of Electrical and Electronics Engineers (IEEE)), 1-4.

Shakoor, N., Lee, S., and Mockler, T. C. (2017). High throughput phenotyping to accelerate crop breeding and monitoring of diseases in the field. *Current Opinion in Plant Biology*, 38, 184-192. https://doi.org/10.1016/j.pbi.2017.05.006

Sharma, N., Banerjee, B. P., Hayden, M., and Kant, S. (2023). An Open-Source Package for Thermal and Multispectral Image Analysis for Plants in Glasshouse. *Plants*, 12 (2), 317. https://doi.org/10.3390/plants12020317

Shi, Y., Alex Thomasson, J., Murray, S. C., Ace Pugh, N., Rooney, W. L., Shafian, S., et al. (2016). Unmanned aerial vehicles for high-throughput phenotyping and agronomic research. *PLoS One*, 11 (7), e0159781. https://doi.org/10.1371/journal.pone.0159781

Shimeles, A., Verdier-Chouchane, A., and Boly, A. (2018). Introduction: Understanding the Challenges of the Agricultural Sector in Sub-Saharan Africa. In: A. Shimeles, A. Verdier-Chouchane and A. Boly (eds) *Building a Resilient and Sustainable Agriculture in Sub-Saharan Africa*. (Cham., Switzerland: Palgrave Macmillan), 1-12. https://doi.org/10.1007/978-3-319-76222-7_1

Shokr, M. E. (2020). Environmental Applications of Remote Sensing in Egypt: A Review and an Outlook. In: S. Elbeih, A. Negm and A. Kostianoy (eds) *Environmental Remote Sensing in Egypt*. (Cham, Switzerland: Springer Geophysics. Springer), 95–126. https://doi.org/10.1007/978-3-030-39593-3_4

Shonhe, T and Scoones, I. (2022). Private and state-led contract farming in Zimbabwe: Accumulation, social differentiation and rural politics. *Journal of Agrarian Change*, 22 (1), 118-138. https://doi.org/10.1111/joac.12473

Sie, E. K., Oteng-Frimpong, R., Kassim, Y. B., Puozaa, D. K., Adjebeng-Danquah, J., Masawudu, A. R., et al. (2022). RGB-image method enables indirect selection for leaf spot resistance and yield estimation in a groundnut breeding programme in Western Africa. *Frontiers in Plant Science*, 13.

Sishodia, R. P., Ray, R. L., and Singh, S. K. (2020). Applications of Remote Sensing in Precision Agriculture: A Review. *Remote Sensing*, 12 (19), 3136. http://dx.doi.org/10.3390/rs12193136

Skendžić, S., Zovko, M., Lešić, V., Pajač Živković, I., and Lemić, D. (2023). Detection and evaluation of environmental stress in winter wheat using remote and proximal sensing methods and vegetation indices–A review. *Diversity*, 15 (4), 481. https://doi.org/10.3390/ d15040481

Smidt, H. J and Jokonya, O. (2022). Factors affecting digital technology adoption by small-scale farmers in agriculture value chains (AVCs) in South Africa. *Information Technology for Development*, 28 (3), 558-584. https://doi.org/10.1080/02681102.2021.1975256

Smigaj, M., Agarwal, A., Bartholomeus, H., Decuyper, M., Elsherif, A., de Jonge, A., and Kooistra, L. (2024). Thermal infrared remote sensing of stress responses in forest environments: a review of developments, Challenges, and Opportunities. *Current Forestry Reports*, 10 (1), 56-76.

Smith, M. R., Rao, I. M., and Merchant, A. (2018). Source-sink relationships in crop plants and their influence on yield development and nutritional quality. *Frontiers in Plant Science*, *9*, 1889.

Song, X., Yang, G., Xu, X., Zhang, D., Yang, C., and Feng, H. (2022). Winter Wheat Nitrogen Estimation Based on Ground-Level and UAV-Mounted Sensors. *Sensors*, 22 (2), 549. http://dx.doi.org/10.3390/s22020549

Soullier, G., Demont, M., Arouna, A., Lançon, F., and Del Villar, P. M. (2020). The state of rice value chain upgrading in West Africa. *Global Food Security*, 25, 100365. https://doi.org/10.1016/j.gfs.2020.100365

Sultan, B and Gaetani, M. (2016). Agriculture in West Africa in the twenty-first century: climate change and impacts scenarios, and potential for adaptation. *Frontiers in Plant Science*, 7. https://doi.org/10.3389/fpls.2016.01262

Swinfield, T., Lindsell, J. A., Williams, J. V., Harrison, R. D., Agustiono, Habibi, et al. (2019). Accurate measurement of tropical forest canopy heights and aboveground carbon using structure from motion. *Remote Sensing*, 11 (8), 928. https://doi.org/10.3390/rs11080955

Tadele, Z. (2017). Raising crop productivity in Africa through intensification. *Agronomy*, 7 (1), 22. https://doi.org/10.3390/agronomy7010022

Tamene, L. D and Ashenafi, A. (2022). Digital agriculture profile: Ethiopia. *Addis Ababa (Ethiopia): Alliance of Biodiversity International and International Centre for Tropical Agriculture (CIAT)*. CIAT publication. p. 20. Available at: https://hdl.handle.net/10568/119309

Tao, H., Xu, S., Tian, Y., Li, Z., Ge, Y., Zhang, J., Wang, Y., Zhou, G., Deng, X., Zhang, Z., Ding, Y., Jiang, D., Guo, Q., and Jin, S. (2022). Proximal and remote sensing in plant phenomics: 20 years of progress, challenges, and perspectives. *Plant Communications*, 3 (6), 100344.

Tariq, M., Ahmed, M., Iqbal, P., Fatima, Z., and Ahmad, S. (2020). Crop phenotyping. In: M. Ahmed (eds) *Systems modelling* (Singapore: Springer), 45-60. https://doi.org/10.1007/978-981-15-4728-7_2

Tattaris, M., Reynolds, M. P., and Chapman, S. C. (2016). A direct comparison of remote sensing approaches for high-throughput phenotyping in plant breeding. *Frontiers in Plant Science*, 7. https://doi.org/10.3389/fpls.2016.01131

Thakur, S., Sharma, S., Barela, A., and Nagre, S. P. (2023). Plant phenomics through proximal remote sensing: A review for improved crop yield. *The Pharma Innovation Journal*, 12 (3), 2432-2442.

Tilling, A. K., O'Leary, G. J., Ferwerda, J. G., Jones, S. D., Fitzgerald, G. J., Rodriguez, D., et al. (2007). Remote sensing of nitrogen and water stress in wheat. *Field Crops Research*, 104 (1-3), 77-85. https://doi.org/10.1016/j.fcr.2007.03.023

Tilman, D., Balzer, C., Hill, J., and Befort, B. L. (2011). Global food demand and the sustainable intensification of agriculture. *Proceedings of the National Academy of Sciences of the United States of America*. 108 (50), 20260-20264. https://doi.org/10.1073/pnas.1116437108

Tripodi, P., Nicastro, N., Pane, C., and Cammarano, D. (2022). Digital applications and artificial intelligence in agriculture toward next-generation plant phenotyping. *Crop and Pasture Science*, 18. https://doi.org/10.1071/CP21387

Van Dijk, M., Morley, T., Rau, M. L., and Saghai, Y. (2021). A meta-analysis of projected global food demand and population at risk of hunger for the period 2010–2050. *Nature Food*, 2 (7), 494-501. https://doi.org/10.1038/s43016-021-00322-9

Van Duivenbooden, N., Pala, M., Studer, C., Bielders, C. L., and Beukes, D. J. (2000). Cropping systems and crop complementarity in dryland agriculture to increase soil water use efficiency: a review. *NJAS: Wageningen Journal of Life Sciences*, 48 (3), 213-236. https://doi.org/10.1016/S1573-5214(00)80015-9

Varshney, R. K., Bohra, A., Yu, J., Graner, A., Zhang, Q., and Sorrells, M. E. (2021). Designing future crops: Genomics-assisted breeding comes of age. *Trends in Plant Science*, 26 (6), 631-649. https://doi.org/10.1016/j.tplants.2021.03.010

Vergara-Díaz, O., Zaman-Allah, M. A., Masuka, B., Hornero, A., Zarco-Tejada, P., Prasanna, B. M., et al. (2016). A novel remote sensing approach for prediction of maize yield under different conditions of nitrogen fertilization. *Frontiers in Plant Science*, 7. https://doi.org/10.3389/fpls.2016.00666

Verner, D., Treguer, D., Redwood, J., Christensen, J., McDonnell, R., Elbert, C., et al. (2018). *Climate variability, drought, and drought management in Morocco's agricultural sector* (Washington, D. C., USA: World Bank). Available at: https://openknowledge.worldbank.org/handle/10986/30603.

Virlet, N., Lyra, D. H., and Hawkesford, M. J. (2022). Digital phenotyping and genotype-to-phenotype (G2P) models to predict complex traits in cereal crops. in: A Walter (ed.) *Advances in Plant Phenotyping for More Sustainable Crop Production*. (Cambridge: Burleigh Dodds Science Publishing), p. 40.

Virlet, N., Sabermanesh, K., Sadeghi-Tehran, P., and Hawkesford, M. J. (2017). Field Scanalyzer: An automated robotic field phenotyping platform for detailed crop monitoring. *Functional Plant Biology*, 44 (1), 143-153.

Wahab, I. (2020). In-season plot area loss and implications for yield estimation in smallholder rainfed farming systems at the village level in Sub-Saharan Africa. *GeoJournal*, 85 (6), 1553-1572. https://doi.org/10.1007/s10708-019-10039-9

Walsh, O. S., Shafian, S., Marshall, J. M., Jackson, C., McClintick-Chess, J. R., Blanscet, S. M., and Walsh, W. L. (2018). Assessment of UAV-based vegetation indices for nitrogen concentration estimation in spring wheat. *Advances in Remote Sensing*, 7 (2), 71-90. https://doi.org/10.4236/ars.2018.72006

Wang, J., Wu, B., Kohnen, M. V., Lin, D., Yang, C., Wang, X., et al. (2021). Classification of rice yield using UAV-based hyperspectral imagery and lodging feature. *Plant Phenomics* 2021, 9765952.

Watt, M., Fiorani, F., Usadel, B., Rascher, U., Muller, O., and Schurr, U. (2020). Phenotyping: New windows into the plant for breeders. *Annual Review of Plant Biology*, 71, 689-712. https://doi.org/10.1146/annurev-arplant-042916-041124

Wen, T., Li, J. H., Wang, Q., Gao, Y. Y., Hao, G. F., and Song, B. A. (2023). Thermal imaging: The digital eye facilitates high-throughput phenotyping traits of plant growth and stress responses. *Science of The Total Environment*, 165626.

Wellington, M. (2023). *Remote Sensing of Croplands, Crop Productivity, and Water use Efficiency with a Focus on Smallholder Systems in Southern Africa (Doctoral dissertation* (Australia: The Australian National University).

Whalen, K and Yuhas, C. (2019). *Low-cost drone and sensor for agricultural applications on small farms in Tanzania*. Available at: https://globalwater.osu.edu/files/Drone-Final-Design-Report-1.pdf (Accessed 4 January 2023).

White, J. W and Conley, M. M. (2013). A flexible, low-cost cart for proximal sensing. *Crop Science*, 53 (4), 1646-1649. https://doi.org/10.2135/cropsci2013.01.0054

White, J. W., Andrade-Sanchez, P., Gore, M. A., Bronson, K. F., Coffelt, T. A., Conley, M. M., et al. (2012). Field-based phenomics for plant genetics research. *Field Crops Research*, 133, 101-112. https://doi.org/10.1016/j.fcr.2012.04.003

Woldeyohannes, A. B., Accotto, C., Desta, E. A., Kidane, Y. G., Fadda, C., Pè, M. E., et al. (2020). Current and projected eco-geographic adaptation and phenotypic diversity of Ethiopian teff (*Eragrostis teff*) across its cultivation range. *Agriculture, Ecosystems and Environment*, 300, 107020. https://doi.org/10.1016/j.agee.2020.107020

World Bank (2010). "Global strategy to improve agricultural and rural statistics," in *Economic sector work no. 56719-GLB* (Washington DC: The International Bank for Reconstruction and Development / The World Bank).

Xiao, Q., Bai, X., Zhang, C., and He, Y. (2022). Advanced high-throughput plant phenotyping techniques for genome-wide association studies: A review. *Journal of Advanced Research*, 35, 215-230. https://doi.org/10.1016/j.jare.2021.05.002

Xie, C and Yang, C. (2020). A review on plant high-throughput phenotyping traits using UAV-based sensors. *Computers and Electronics in Agriculture*, 178, 105731. https://doi.org/10.1016/j.compag.2020.105731

Yang, G., Liu, J., Zhao, C., Li, Z., Huang, Y., Yu, H., et al. (2017a). Unmanned aerial vehicle remote sensing for field-based crop phenotyping: Current status and perspectives. *Frontiers in Plant Science*, 8.

Yang, H., Yang, J., Lv, Y., and He, J. (2014). SPAD values and nitrogen nutrition index for the evaluation of rice nitrogen status. *Plant Production Science*, 17 (1), 81-92. https://doi.org/10.1626/pps.17.81

Yang, M., Hassan, M. A., Xu, K., Zheng, C., Rasheed, A., Zhang, Y., and He, Z. (2020). Assessment of water and nitrogen use efficiencies through UAV-based

multispectral phenotyping in winter wheat. *Frontiers in Plant Science*, 11, 927. https://doi.org/10.3389/fpls.2020.00927

Yang, W., Feng, H., Zhang, X., Zhang, J., Doonan, J. H., Batchelor, W. D., et al. (2020). Crop phenomics and high-throughput phenotyping: past decades, current challenges, and future perspectives. *Molecular Plant*, 13 (2), 187-214. https://doi.org/10.1016/j.molp.2020.01.008

Yang, Z., Shao, Y., Li, K., Liu, Q., Liu, L., and Brisco, B. (2017b). An improved scheme for rice phenology estimation based on time-series multispectral HJ-1A/B and polarimetric RADARSAT-2 data. *Remote Sensing of Environment*, 195. https://doi.org/10.1016/j.rse.2017.04.016

Zaman-Allah, M., Vergara, O., Araus, J. L., Tarekegne, A., Magorokosho, C., Zarco-Tejada, P. J., et al. (2015). Unmanned aerial platform-based multi-spectral imaging for field phenotyping of maize. *Plant Methods*, 11 (1), 1–10. https://doi.org/10.1186/s13007-015-0078-2

Zendonadi dos Santos, N., Piepho, H. P., Condorelli, G. E., Licieri Groli, E., Newcomb, M., Ward, R., et al. (2021). High-throughput field phenotyping reveals genetic variation in photosynthetic traits in durum wheat under drought. *Plant, Cell and Environment*, 44 (9), 2858–2878. https://doi.org/10.1111/pce.14136

Zhang, J., Yang, C., Song, H., Hoffmann, W. C., Zhang, D., and Zhang, G. (2016). Evaluation of an airborne remote sensing platform consisting of two consumer-grade cameras for crop identification. *Remote Sensing*, 8 (3), 257. https://doi.org/10.3390/rs8030257

Zhao, C., Zhang, Y., Du, J., Guo, X., Wen, W., Gu, S., et al. (2019). Crop phenomics: Current status and perspectives. *Frontiers in Plant Science*, 10. https://doi.org/10.3389/fpls.2019.00714

Zhao, Y., Zheng, B., Chapman, S. C., Laws, K., George-Jaeggli, B., Hammer, G. L., et al. (2021). Detecting sorghum plant and head features from multispectral UAV imagery. *Plant Phenomics* 2021. https://doi.org/10.34133/2021/9874650

Zhu, Y., Yao, X., Tian, Y. C., Liu, X. J., and Cao, W. X. (2008). Analysis of common canopy vegetation indices for indicating leaf nitrogen accumulations in wheat and rice. *International Journal of Applied Earth Observation and Geoinformation*, 10 (1), 1–10. https://doi.org/10.1016/j.jag.2007.02.006

Zimbabwe Centre for High Performance Computing. (2021). Zimbabwe centre for high performance computing. Available at: https://zchpc.ac.zw/history

CHAPTER 3

Determination of optimal spectral reflectance indices for monitoring the nutritional status and agro-morpho-physiological responses in quinoa and cowpea under varying nitrogen and phosphorus availability using proximal sensing

(This chapter is based on Cudjoe et al., 2023b: Acta Horticulturae, https://doi.org/10.17660/ActaHortic.2023.1360.45, Appendix B-1 and with the addition of cowpea data included and analysed to satisfy this chapter's objectives. Accordingly, minor modifications of the text and data analysis were necessary compared with the published article and manuscript under review).

Daniel K. Cudjoe[1,2], Frank G. Okyere[1,2], Suzanne J. Clark[3], Nicolas Virlet[1], March Castle[1], Andrew B. Riche[1], Toby W. Waine[2], Fady Mohareb[2*] and Malcolm J. Hawkesford[1*]

[1]Rothamsted Research, Sustainable Soils and Crops, Harpenden, Hertfordshire, AL5 2JQ, United Kingdom.
[2]School of Water, Energy and Environment, Cranfield University, Cranfield, Bedfordshire, MK43 0AL, United Kingdom.
[3]Rothamsted Research, Intelligent Data Ecosystems, Harpenden, Hertfordshire, AL5 2JQ, United Kingdom.

***Correspondence**
Malcolm J. Hawkesford
Email: malcolm.hawkesford@rothamsted.ac.uk

Fady Mohareb
Email: f.mohareb@cranfield.ac.uk

Abstract

Nitrogen (N) and phosphorus (P) are the two most crucial mineral nutrients used by plants for optimum growth and crop yield improvement in agricultural production. However, the use of spectral reflectance indices (SRIs) at the leaf level using proximal sensing (PS) to assess effects of N and P stress separately and in combination on the nutritional status, morphology, physiology and agronomy of quinoa (*Chenopodium quinoa* Willd.) and cowpea (*Vigna unguiculata* L. Walp) has not been extensively studied. In the present study, the potential of SRIs to track the nutritional status and crop performance of quinoa and cowpea grown under glasshouse conditions with varying combinations of N and P availability were assessed. Using a handheld proximal sensor, SRIs computed from multiple wavelengths were measured along with agro-morpho-

physiological parameters indicative of N and P stress. Repeated measures ANOVA (RMA) was used to select optimal SRIs specific to N and P stress, both separately and in combination. RMA was also used to assess the effects of N and P treatments (and their interaction) on the agro-morpho-physiological parameters and SRIs. The relationship between optimal SRIs and the agro-morpho-physiological status of quinoa and cowpea was evaluated using correlation analysis. The results showed that SRIs including NDVI, OSAVI, G, MCARI, TCARI, ZMI, SPRI, NPQI, NPCI, Ctr2, Lic1, SIPI, CRI1, CRI2, RDVI, GNDVI_780 and SRa_790 demonstrated specificity for N stress detection in quinoa. On the other hand, SRIs that indicated specificity for N stress detection in cowpea included G and rDVI_790. For P status, the two SRIs that demonstrated specificity for detection in quinoa were mNDblue_730 and PRI_550. However, no SRI was identified to be specific for P status in cowpea. This study demonstrated the potential of using SRIs to identify early nutritional variations in quinoa and cowpea. Furthermore, our findings showed that the concurrent application of different N and P availabilities resulted in an overall positive response, as evidenced by the increases in agro-morpho-physiological parameters. The SRIs specific for assessing the N and P status also showed strong significant relationships with the agro-morpho-physiological parameters assessed in both crops. Altogether, our study demonstrated the utility of SRIs from the low-cost proximal sensor for discriminating N and P status and assessing the crop performance in quinoa and cowpea. Future work into this study will concentrate on applying these findings to field phenotyping in Africa, which may be essential for precision agriculture (PA) and aid in the advancement of portable sensor technology.

Keywords: Proximal sensing, nutritional status, quinoa, cowpea, spectral reflectance indices, agro-morpho-physiological responses

3.1 Introduction

Quinoa (*Chenopodium quinoa* Willd.) is a unique annual pseudocereal grain crop originating from the Andean region of South America (Adolf et al., 2013). The Lake Titicaca region of Bolivia and Peru is where quinoa was domesticated, and these countries are still the leading producers and exporters of quinoa. Quinoa has attracted global attention as an important food crop because of its versatility as having

exceptional nutritional qualities, health benefits and resilience to various abiotic stresses (Bazile et al., 2016; Hinojosa et al., 2018; Dakhili et al., 2019; Noratto et al., 2019). Quinoa is highly adaptable to climate change scenarios and has a high economic value, making it a potential novel crop in other parts of the world (Bazile et al., 2016; Hinojosa et al., 2019; Ain et al., 2023; Taaime et al., 2023). The introduction of high-yielding quinoa into the cropping system and diet has the potential to improve food and nutritional security in developing countries, especially in Africa (Maliro and Guwela, 2015; Maliro and Njala, 2019; Fathi and Kardoni, 2020). Quinoa was first introduced to Africa in the late 1990s (Oyoo et al., 2010; Maliro and Guwela, 2015). However, more research is required to better understand its production techniques and how it responds to various environmental conditions for farming in the semi-arid region. Quinoa is well adapted to marginal soil conditions (Choukr-Allah et al., 2016). However, crop productivity is limited by nutrient deficiency (Jacobsen et al., 2016; Wang et al., 2020).

On the other hand, cowpea (*Vigna unguiculata* L. Walp) is one of the most economically important indigenous African leguminous crops grown in the tropical and subtropical regions of the world for vegetables, grains and fodder (Singh et al., 2003; Fang et al., 2007; Abebe et al., 2022). It is a major cash crop and provides livelihoods to millions of people specifically smallholder farmers in many African countries (Kebede and Bekeko, 2020). In SSA, most of the cowpea cultivation occurs in West Africa, contributing to about 60% of global production (Kamara et al., 2018; Nwagboso et al., 2024). It is a source of nutritious grain and provides relatively cheap and high-quality protein for both rural and urban poor consumers (Kamara et al., 2018; Horn et al., 2022). In addition, cowpea serves as a protective cover crop and enhances soil fertility through the process of atmospheric N fixation. Thus, cowpea is a vital multipurpose crop crucial for food security in Africa.

Improved agronomic techniques and the breeding of more nutrient-efficient crops are required by farmers and breeders to meet the growing demand for crops such as quinoa and cowpea particularly in low-productivity areas (Keneni and Imtiaz, 2010; Choukr-Allah et al., 2016). Therefore, adjusting crop macronutrient needs based on the prediction of potential yield is a crucial component of PA for making in-season

management decisions, sustaining the crop metabolism for optimal growth and development and increasing profitability.

Plant growth is frequently limited by N and P (Elser et al., 2007; Agren et al., 2012; Dong et al., 2023). Therefore, understanding crop responses to the availability of these nutrients, their coordinated acquisition and biological interactions are vital for achieving nutritional balance and optimal growth under fluctuating nutritional conditions while reducing/optimising fertiliser use in agriculture (Luo et al., 2016; Medici et al., 2019; Alvar-Beltrán et al., 2021). To date, the effects of N and P fertilisation on crops, particularly quinoa and cowpea, have been largely studied separately or in isolation, but recent findings suggest interactions between the macronutrients at several levels of integration (Agren et al., 2012; Grohskopf et al., 2019; Krouk and Kiba, 2020; Alvar-Beltrán et al., 2021; Xia et al., 2023).

The amount of N and P in the soil changes through time, which can create interactions between the nutrients and result in synergistic or antagonistic combinations (Rietra et al., 2017; Grohskopf et al., 2019). This might directly or indirectly affect crop responses to the co-fertilisation of N and P (Groot et al., 2003; Duncan et al., 2018b). For instance, P deficiency in the soil could limit the plant response to N fertilisation (Setiyono et al., 2010) and negatively affect N uptake and assimilation (Gniazdowska and Rychter, 2000; Gan et al., 2016). Hence, the concomitant supply of these nutrients in the soil could lead to changes in chemical, physical and biological features that can alter the dynamics of N and P elements and ultimately crop response (Chen et al., 2017).

Unfortunately, the traditional methods of monitoring these essential nutrients and their complex interactions in plants require time-consuming, labour-intensive sampling and costly laboratory chemical analyses, all of which are not environmentally acceptable or economically viable on a large scale. The costs and destructive nature of these measurements limit determination of the spatial variability of soil and crop parameters. Therefore, to improve current farming practices and optimise input supply, especially in developing nations where conventional agricultural systems are challenged with the demands of a rapidly expanding population, farmers need innovative, accurate and efficient methods for detecting nutrient stresses in crops.

PS through plant phenotyping and phenomics technologies offers fast, timely, non-destructive and accurate assessments of crop nutritional status, which is crucially important for optimised fertiliser application and precision crop management (Chawade et al., 2019; Alvar-Beltrán et al., 2020; Huang et al., 2020; Stanschewski et al., 2021). SRIs computed from multiple wavelengths are among the many metrics provided by spectroscopy technologies (single point or image-based) and have been employed to assess the nutritional status of crops, detect nutrient deficiency, monitor growth and predict crop yields (Padilla et al., 2018; Darra et al., 2021; Rehman et al., 2022).

Numerous studies have proposed SRIs, the majority of which are based on spectral wavelengths, to non-destructively estimate the N status of plants and provide a measure of the stress caused by N deficiency (Li et al., 2008; Eitel et al., 2008; Wei et al., 2012; Lunagaria et al., 2015; Li et al., 2021). For instance, Wei et al. (2012) demonstrated the satisfactory performance of SRIs in estimating leaf N accumulation (LNA) in rice and wheat. The authors reported that the optimum SRI for estimating LNA during the early mid-season from jointing to booting was the Soil Adjusted Vegetation Index (SAVI) and Ratio Vegetation Index (RVI) for the mid-late season from heading to grain filling. Li et al. (2008) also showed the utility of Simple Ratio Vegetation Indices (SRVIs) including the Red Vegetation Index (ReVI) and Green Vegetation Index (GVI) as well as Normalised Difference Vegetation Indices (NDVI and GNDVI) among others for estimating the N uptake of winter wheat varieties at different growth stages. The authors concluded that using RVI showed the highest prediction (R^2=0.60) for N uptake across different years, varieties and growth stages.

In quinoa, Alvar-Beltrán et al. (2020) tested proximal optical sensors and derived NDVI to assess the N status. The GreenSeeker-derived NDVI was effective at making in-season predictions of crop biomass at harvest. Additionally, only a few studies have concentrated on selecting optimal wavelengths and SRIs for estimating crop P status using PS (e.g., Osborne et al., 2002; Alharbi, 2018; Pinit et al., 2022). For example, Alharbi (2018) demonstrated the effectiveness of NDVI for determining P deficiency in winter wheat due to a strong correlation with yield under low P conditions. However, no SRI has been found for determining quinoa P status yet. Therefore, to improve quinoa

productivity and nutrient use efficiency, more research is required to develop PS for P and to understand the specificity of estimating quinoa P status using spectroscopy.

Recently, Cudjoe et al. (2023b) assessed the combined impact of N and P stress on quinoa employing PS. However, there is no extensive research on the application of SRIs at the leaf level using PS to evaluate N and P stress separately and in combination on the morphology, physiology and agronomy of quinoa. This knowledge gap could compromise fertilisation management by resulting in incorrect diagnosis when monitoring the effects of N and P stress in quinoa. Therefore, it is essential to evaluate SRIs for more accurate and timely detection and phenotyping of the nutritional status to support PA and increase quinoa and cowpea productivity, as most farmers deal with both N and P nutrient stress management. The use of handheld sensors for field phenotyping and stress responses in crops in developing nations has garnered more attention recently due to the affordability, ease of use and potential lack of significant pre-processing of spectral data (Cudjoe et al., 2023a).

In the present study, quinoa and cowpea grown in different combinations of N and P availabilities under glasshouse conditions were evaluated to assess SRIs capable of monitoring their nutritional status and crop performance. The overall aim was to identify SRIs from a handheld proximal sensor capable of distinguishing between N and P stress in these crops and relating the spectral responses to the nutritional status, morpho-physiology and how they reflect crop performance. The specific objectives were (i) to identify optimal SRIs indicative of N and P status separately or the combined effect and their interactions, (ii) to assess the time-course response of optimal SRIs to identify early nutritional variations, (iii) to assess the agro-morpho-physiological responses under the different N and P availabilities and (iv) to examine the relationships between optimal SRIs and agro-morpho-physiological parameters.

3.2 Materials and methods

3.2.1 Plant materials and growth conditions

Seeds of quinoa (*Chenopodium quinoa* Willd.) and cowpea (*Vigna unguiculata* L. Walp) were obtained from Magic Garden Seeds GmbH (Regensburg, Germany) and were used for this study based on their significance to African agriculture but as these are understudied. A pot experiment was installed in the glasshouse at the Plant Growth

Facility at Cranfield University, United Kingdom (52° 4' 28.61" N, 0° 37' 41.819" W) from September 2020 to January 2021. The glasshouse conditions were set as follows: relative humidity (RH) of 50-65%; day/night temperature 24/21±2 °C; photoperiod of 14 h and natural light intensity of 400 µmol m^{-2} s^{-1} with supplemental light of 460 µmol m^{-2} s^{-1}. Before sowing, quinoa and cowpea seeds were stratified at 4 °C for three days.

After stratification, cowpea seeds were sown directly into pots while quinoa seeds were pre-germinated by sowing in wet vermiculite compost on a mini pot tray and incubated in the dark. After 3 days, germinated quinoa seeds were illuminated to prevent etiolation. Seedlings of similar size (5 cm) were transplanted into pots (21×19 cm). At the two-leaf stage, the seedlings were thinned to one plant per pot. Quinoa and cowpea were intercropped (Figure 3.1) and grown to physiological maturity on a reconstituted Levington F1, low-nutrient compost (ICL, Everris, Ipswich, Suffolk, England, United Kingdom).

Figure 3.1. Crop establishment and experimental setup of quinoa intercropped with cowpea in the glasshouse at the Plant Growth Facility at Cranfield University. The photograph was taken 44 days after sowing (DAS).

3.2.2 Preparation of compost and application of nutrient treatments

The Levington F1 low-nutrient compost, supplied by ICL, Everris, Ipswich, United Kingdom, was used in the experiment. The compost was first washed to remove soluble nutrients, by flooding one part of the compost with five-part deionised water, mixing,

breaking up aggregates and draining the mixture through a double 0.8 mm sieve (adapted from Masters-Clark et al., 2020; Cudjoe et al., 2023b) (Appendix B, Figure B-1). After five rounds of repeated washing, the washed compost was oven-dried at 105 °C for 48 h until no further water loss occurred. Dried samples of the washed compost were assessed by elemental analysis to determine that the washed compost had no or little nutrients remaining (Appendix B, Figure B-1).

A modified Letcombe nutrient solution was used to reconstitute nutrients in the washed compost, along with the supply of macro and micronutrients (Masters-Clark et al., 2020). Four nutritional treatments based on all combinations of two levels of N (high N; low N) and two levels of P (high P; low P) were tested. The combined treatment factors were designated as HNHP, HNLP, LNHP and LNLP with H and L for high and low levels, respectively. The N and P levels were varied to create a range in the N-P status and test the effectiveness of spectral reflectance measurement to detect these differences (Ansari et al., 2016; Skendžić et al., 2023). The macro-nutritional composition for each treatment is summarised in Table 3.1. The concentrations for HN and LN were 42.6 mM and 13.0 mM, respectively, and HP and LP were 13.4 mM and 3.3 mM, respectively. Each pot (of size 21×19 cm) was filled with 1500 g of washed compost mixed with 242 g of silver sand and 790 ml of nutrient solution. Based on the assigned treatments, pots were replenished with 790 ml of nutrient solution at 23, 44, 65 and 79 DAS. Equal amounts of deionised water were used to irrigate the plants at regular intervals.

Table 3.1. The composition of the modified Letcombe nutrient solution based on HNHP, HNLP, LNHP and LNLP input conditions. The concentrations of the treatment conditions are indicated. Nutrient solutions were prepared at p^H=6.

	Final concentration (mM)			
Macronutrient Stock Solution	**HNHP**	**HNLP**	**LNHP**	**LNLP**
1 M $Ca(NO_3)_2$ x $4H_2O$	6.4	6.4	1.6	1.6
1 M KNO_3	26.3	26.3	6.6	6.6
1 M CH_4N_2O	9.9	9.9	2.5	2.5
1 M $MgSO_4$	6.6	6.6	6.6	6.6
1 M KH_2PO_4 1 M K_2HPO_4	13.4	3.3	13.4	3.3
1 M KCl	0.0	10.0	19.7	29.7
1 M $CaCl_2$	0.0	0.0	4.8	4.8
50 mM FeEDTA	0.3	0.3	0.3	0.3

3.2.3 Statistical design

Quinoa and cowpea plants were arranged on a 550×180 cm bench and were spaced 50 cm apart within each row (Figure 3.2). The basic design comprised a 2×2 factorial set of N and P treatments which were allocated to pots according to a five-block randomised complete block design (RCBD). Hence, each of the four nutritional treatments was replicated five times. Each pot was sampled for spectral reflectance and morpho-physiological parameters on up to 13 successive occasions (DAS) hence, the maximal design structure comprised a 2×2×13 factorial, with a nested blocking structure, expressed as block/pot/sample, i.e., samples nested within pots nested within blocks. Shading effects during later growth stage of the crops in the glasshouse were managed by adjusting spacing between plants in a way that allowed for optimal light distribution. This included rotating pots or altering the positioning of plants to ensure all receive adequate light. Additionally, experimental errors such as shading and random effects were also considered during data analysis.

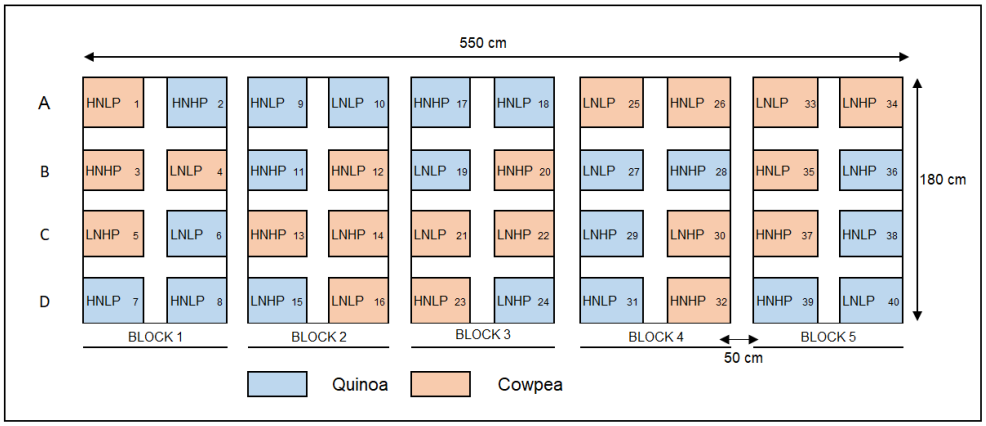

Figure 3.2. The statistical design employed for the experiment showing the allocation of the 2×2 factorial set of N and P treatments according to a 5-block randomised complete block design. Quinoa was intercropped with cowpea. The experimental area measured 550×180 cm with pots spaced 50 cm apart in each row (A-D). The rectangles are individual pots (plants) that have varying amounts of N and P supplied. The N and P treatments were randomly applied within each block. Pots are numbered from 1 to 40.

3.2.4 Data collection

3.2.4.1 Measurement of spectral reflectance

Leaf spectral reflectance data were collected using the PolyPen RP410/UVIS handheld contact spectroradiometer (Photon Systems Instruments, Drasov, Czech Republic), which can measure the wavelength range of 320-790 nm of the electromagnetic spectrum at intervals of 1.9 nm. Spectral reflectance was obtained from the uppermost fully expanded leaf of quinoa whereas in cowpea, the fully expanded trifoliate leaf from the top was used between 11:00 and 16:00 GMT repeatedly at 23, 30, 37, 44, 51, 58, 65, 72, 79, 86, 93, 100, 107 and 114 DAS. Three readings were made on each leaf and then averaged. A diffuse white reference standard (Spectralon®, Labsphere, Inc., North Sutton, USA) was used to calibrate the spectrometer sensor before and periodically during measurements. A xenon incandescent light source, emitting radiation in the range of 380–1050 nm is integrated into the PolyPen RP410 device. Along with manually computed SRIs from multiple wavelengths, the PolyPen RP410 incorporates predefined formulae for calculating frequently used SRIs. Initially, the spectra from each treatment were averaged, and the overall mean spectrum was analysed to look for variations in the spectral signature obtained from the different nutrient treatment combinations (Figures 3.3 and 3.4). Table 3.2 shows the SRIs that were computed from narrow-bands wavelengths for this study.

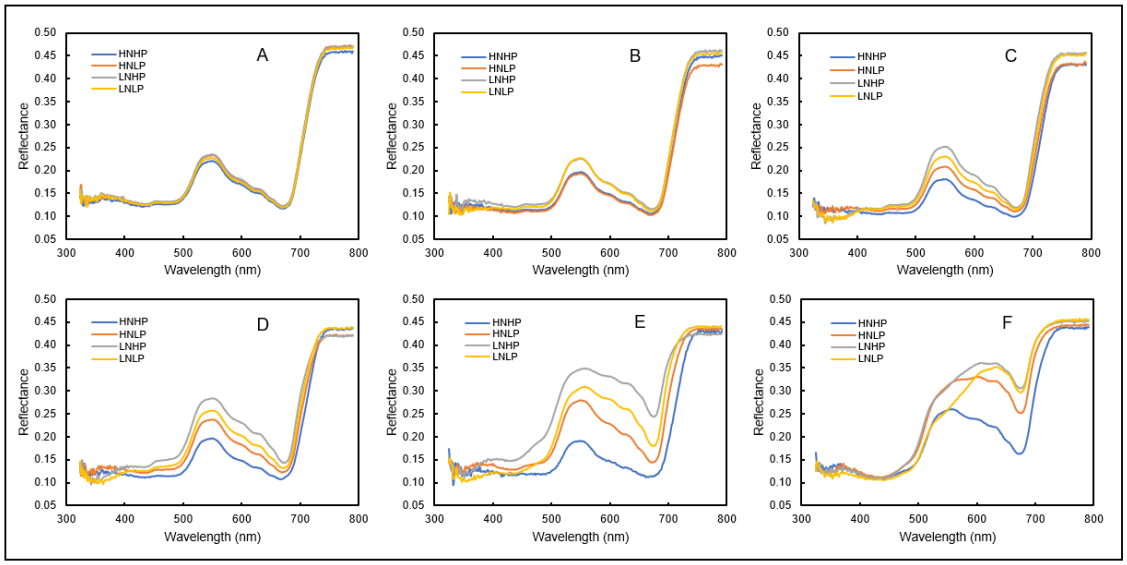

Figure 3.3. Reflectance spectra of quinoa leaves exposed to varying combinations of nitrogen (N) and phosphorus (P) treatments at different days after sowing (DAS) (A, 23 DAS), (B, 37 DAS), (C, 65 DAS), (D, 86 DAS), (E, 93 DAS) and (F, 107 DAS).

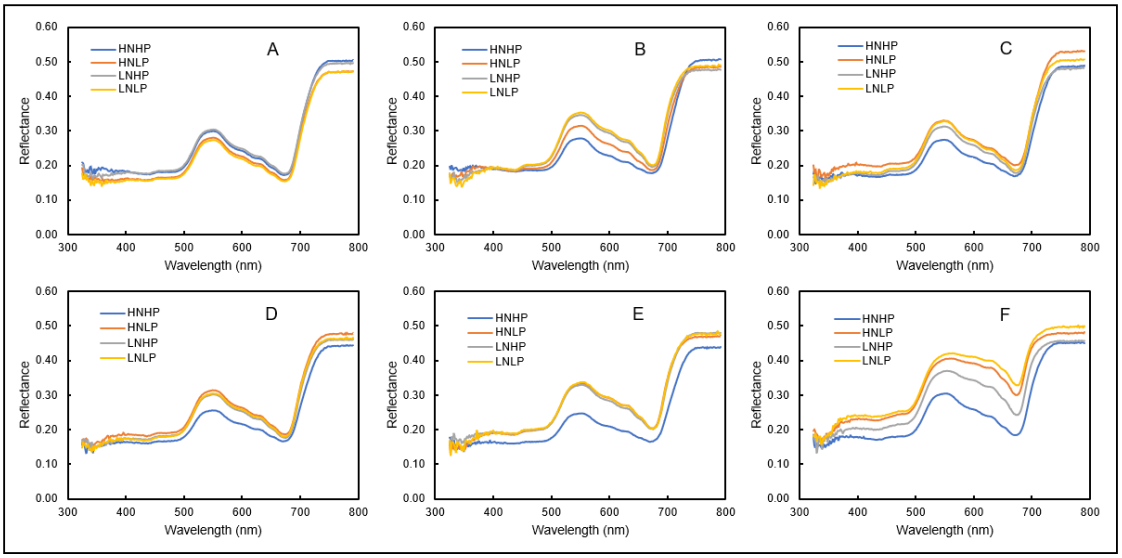

Figure 3.4. Reflectance spectra of cowpea leaves exposed to varying combinations of nitrogen (N) and phosphorus (P) treatments at different days after sowing (DAS) (A, 30 DAS), (B, 65 DAS), (C, 72 DAS), (D, 100 DAS), (E, 107 DAS) and (F, 114 DAS).

Table 3.2. Summary of the SRIs used in this study.

Spectral Reflectance Index	Acronym	Formulation/wavebands	Traits	References
Automatic computed indices from the PolyPen RP410				
Normalised Difference Vegetation Index	NDVI	$(R_{780} - R_{680})/(R_{780} + R_{680})$	Leaf greenness, canopy cover, stress levels, LAI, biomass, photosynthetic activity, vigor, plant health, N status	Rouse et al., 1974
Simple Ratio	SR	(R_{780}/R_{680})	Leaf greenness, vegetation cover, chlorophyll content, vigor, plant health	Chen, 1996
Modified Chlorophyll Absorption in Reflectance Index	MCARI1	$1.2 * [2.5 * (R_{790} - R_{670}) - 1.3 * (R_{790} - R_{550})]$	Chlorophyll concentration, vigor, LAI, stress levels	Haboudane et al., 2004
Optimised Soil-Adjusted Vegetation Index	OSAVI	$(1 + 0.16) * (R_{790} - R_{670}) / (R_{790} - R_{670} + 0.16)$	Greenness, canopy cover, vigor, biomass	Rondeaux et al., 1996
Greenness Index	G	(R_{554}/R_{677})	Chlorophyll content, biomass, photosynthetic activity, vigor, LAI, plant health	Roujean and Breon, 1995
Modified Chlorophyll Absorption in Reflectance Index	MCARI	$[(R_{700} - R_{670}) - 0.2 * (R_{700} - R_{550})] * (R_{700}/ R_{670})$	Chlorophyll concentration, vigor, LAI, stress levels	Daughtry et al., 2000
Transformed Chlorophyll Absorption in Reflectance Index	TCARI	$3 \times [(R700 - R670) - 0.2 * (R700 - R550) * (R700/R670)]$	Chlorophyll concentration, vigor, LAI, stress levels	Haboudane et al., 2002
Triangular Vegetation Index	TVI	$0.5 * [120 * (R_{750} - R_{550}) - 200 * (R_{670} - R_{550})]$	Chlorophyll content, greenness, stress levels, nutrient status, photosynthetic activity	Zarco-Tejada et al., 2005
Zarco-Tejada and Miller Index	ZMI	(R_{750} / R_{710})	Chlorophyll concentration, LAI, stress levels, photosynthetic activity	Zarco-Tejada et al., 2001
Simple Ratio Pigment Index	SRPI	(R_{430} / R_{680})	Chlorophyll concentration, photosynthetic activity, LAI, vegetation cover, green biomass	Peñuelas et al., 1995
Normalised Phaeophytinisation Index	NPQI	$(R_{415} - R_{435}) / (R_{415} + R_{435})$	Leaf senescence, drought, nutrient stress, plant health, vigor, crop maturity	Barnes et al., 1992

Photochemical Reflectance Index	PRI	$(R_{531}- R_{570}) / (R_{531}+ R_{570})$	Photosynthetic stress, water stress, light use efficiency, leaf pigment composition	Gamon et al., 1992
Normalised Pigment Chlorophyll Index	NPCI	$(R_{680}- R_{430}) / (R_{680}+ R_{430})$	Chlorophyll content, photosynthetic activity, stress levels, N status	Peñuelas et al., 1994
Carter Indices	Ctr1 and Ctr2	$Ctr1 = (R_{695} / R_{420})$; $Ctr2 = (R_{695} / R_{760})$	Chlorophyll concentration, vigor, LAI, stress levels	Carter and Miller, 1994
Lichtenthaler Indices	Lic1 and Lic2	$Lic1 = (R_{790} - R_{680}) / (R_{790} + R_{680})$; $Lic2 = (R_{440} / R_{690})$	Chlorophyll content, carotenoid content, greenness, photosynthetic activity, stress levels	Lichtenthaler et al., 1996
Structure Intensive Pigment Index	SIPI	$(R_{790}- R_{450}) / (R_{790}+ R_{650})$	Pigment concentration, leaf angle, canopy density, canopy structure, chlorophyll content, photosynthetic activity	Peñuelas et al., 1995
Gitelson and Merzlyak Indices	GM1 and GM2	$GM1 = (R_{750}/ R_{550})$; $GM2 = (R_{750}/ R_{700})$	Chlorophyll concentration, greenness, plant health status, vegetation biomass	Gitelson and Merzlyak, 1997
Anthocyanin Reflectance Indices	ARI1 and ARI2	$ARI1 = (1/R_{550}-1/R_{700})$; $ARI2 = R_{790}*(1/R_{550}-1/R_{700})$	Stress levels, phenological stage, anthocyanin concentration, leaf coloration, fruit maturity	Gitelson et al., 2009
Carotenoid Reflectance Indices	CRI1 and CRI2	$CRI1 = (1/R_{510}-1/R_{550})$; $CRI2 = (1/R_{510}-1/R_{700})$	Carotenoid to chlorophyll ratio, photosynthetic efficiency, leaf senescence, environmental stress response	Gitelson et al., 2002
Renormalised Difference Vegetation Index	RDVI	$(R_{780}-R_{670})/((R_{780}+R_{670}) \wedge 0.5)$	Leaf greenness, canopy cover, stress levels, LAI, biomass, photosynthetic activity, vigor, plant health	Roujean and Breon, 1995
Manually computed indices derived from the PolyPen RP410				
Photochemical Reflectance Index	PRI_{550} and PRI_{norm}	$PRI_{550} = (R_{549.1}- R_{530.6}) / (R_{549.1}+ R_{530.6})$; $PRI_{norm} = PRI_{550}/(RDVI*(R_{699.9} / R_{669.4}))$	Photosynthetic stress, water stress, light use efficiency, leaf pigment composition	Gamon et al., 1992
Green Normalised Difference Vegetation Index	$GNDVI_{780}$	$(R_{780.7} - R_{549.1})/(R_{780.7} + R_{549.1})$	Chlorophyll content, biomass, photosynthetic activity, vigor, LAI, plant health	Goodwin et al., 2018

Modified Red Edge Simple Ratio	MRESR	$(R_{749.3} - R_{444.7})/(R_{705.2} - R_{444.7})$	Chlorophyll content, LAI, stress levels, biomass, canopy density, early signs of senescence	Sims and Gamon, 2002
Red Edge Normalised Difference Vegetation Index	RENDVI	$(R_{749.3} - R_{705.2})/(R_{749.3} + R_{705.2})$	Chlorophyll concentration, stress levels, LAI, vigor, plant health, early growth stage monitoring	Sims and Gamon, 2002
Normalised Difference Red Edge	NDRE	$(R_{789.4} - R_{719.4})/(R_{789.4} + R_{719.4})$	Chlorophyll concentration, stress levels, LAI, vigor, plant health, early growth stage monitoring	Sharifi and Felegari, 2023
Chlorophyll Index Green	CIgreen	$(R_{791.1}/R_{549.1}) - 1$	Chlorophyll concentration, stress levels, senescence, N status, yield, growth	Muramatsu, 2019
Chlorophyll Index Red Edge	CIrededge	$(R_{791.1}/R_{719.4}) - 1$	Chlorophyll concentration, vigor, LAI, stress levels, N status	Gitelson et al., 2005
Chlorophyll Index	$mNDblue_{530}$ and $mNDblue_{730}$	$mNDblue_{530} = (R_{530.6} - R_{450.4})/(R_{791.1} + R_{450.4})$; $mNDblue_{730} = (R_{730} - R_{450.4})/(R_{791.1} + R_{450.4})$	Chlorophyll concentration, plant stress, N status, growth stage, potential yield	Shrestha et al., 2012
Red Difference Vegetation Index	$rDVI_{790}$	$(R_{789.4} - R_{680.2})$	Chlorophyll content, LAI, stress levels, biomass, vegetation density, vigor, plant health	Roujean and Breon, 1995
Green Simple Ratio	$gSRa_{790}$	$(R_{789.4}/R_{549.1})$	Leaf greenness, vegetation cover, chlorophyll content, vigor, plant health	Rouse et al., 1974
Red Simple Ratio	SRa_{790}	$(R_{789.4}/R_{680.2})$	Chlorophyll content, vegetation cover, plant stress, vigor, biomass, LAI	Rouse et al., 1974

3.2.4.2 Measurement of morpho-physiological parameters

3.2.4.2.1 Leaf-level photosynthesis measurement

The portable photosynthesis system LI-6400XT (LI-COR Biosciences Inc., Lincoln, NE, USA), equipped with the 6400-40 LCF chamber was used to measure the net CO_2 assimilation rate (A_n, µmol CO_2 m^{-2} s^{-1}) (Appendix B, Figure B-2). The uppermost fully expanded leaves of quinoa and the expanded trifoliate leaf of cowpea were used. Five plants per treatment were used for the photosynthesis measurement, which took place between 11:00 and 16:00 GMT at 44, 72 and 107 DAS. To account for any potential effects of the time of day on the measurements, the randomisation order of the experiment was followed. The flow rate was set at 200 µmol s^{-1}, leaf chamber CO_2 concentration was set to 400 µmol mol^{-1}, leaf temperature was maintained at 20 °C, relative humidity (RH) was adjusted between 60–65% and photosynthetically active radiation (PAR) was controlled to 1800 µmol m^{-2} s^{-1} to attain maximum photosynthetic capacity. Measurements were taken once gas exchange rates had stabilised within five minutes after the reading began.

3.2.4.2.2 SPAD measurement

The chlorophyll content was measured from the same leaves as above using a SPAD-502 chlorophyll meter (Soil Plant Analysis Development, Minolta Camera Co., Ltd., Japan). Three readings were made on each leaf and then averaged. SPAD measurements were done synchronously with the PolyPen RP410.

3.2.4.2.3 Plant height

The plant height (PH) was measured at indicative growth stages at 44, 72 and 107 DAS using a metre ruler placed at the soil level in the pot to the tip of the fully expanded leaf.

3.2.4.2.4 Leaf nitrogen content

Harvested leaf samples were taken at indicative stages of development (44, 72 and 107 DAS) for their nutrient status estimation. Fresh leaf samples were oven-dried at 80 °C for 24 h until no further water loss occurred and weighed to determine the dry weight (DW) expressed as gram per pot (g pot^{-1}). The dried samples were then milled to a fine powder at a speed of 17500 rpm using the Genogrinder (SPEX SamplePrep®, 2010, USA) for subsequent elemental analysis by the Analytical Chemistry Unit at Rothamsted Research. The leaf N content (LNC) (%) was determined by employing the

LECO combustion method (LECO CN628 Analyzer, LECO Corporation, St Joseph, Michigan, USA) as employed in earlier studies (Freidenreich et al., 2019).

3.2.4.2.5 Leaf phosphorus concentration

The same milled samples used for LNC were prepared for leaf P concentration (LPC). For the analysis of LPC, a total of 100 mg of sample was digested in acid for 24 h at 90 °C within Teflon vessels, using 2 ml of nitric acid (HNO_3) and 0.5 ml perchloric acid ($HClO_4$) with samples subsequently re-suspended in 25 ml of deionised water. Analyses were performed by the Inductively Coupled Plasma Optical Emission Spectroscopy (ICP-OES) using a Perkin-Elmer Optima 3200RL Spectrometer (Perkin-Elmer, Massachusetts, EEUU). LPC was expressed in ppm of dry matter (DM).

3.2.4.3 Measurement of agronomic parameters

Agronomic parameters including vegetative biomass (VB), total plant biomass (TPB), thousand-grain weight (TGW) and grain yield (GY) were determined at the final harvest. Manual destructive harvest of quinoa plants was done to separate seed heads from the vegetative parts (i.e., panicles, stems). The fresh vegetative parts were weighed using the Sartorius weighing balance (Sartorius Lab Instruments GmbH and Co.KG, Goettingen, Germany) and dried at 80 °C in a forced-air oven for 48 h. The dry vegetative biomass (VB) per plant (g $plant^{-1}$) was determined. The TPB was determined by weighing both dried seed heads and VB together and expressed as (g $plant^{-1}$). Additionally, TGW was determined by counting 1000 grains of quinoa using the Elmor seed counter (Elmor AG, SA, Ltd, Switzerland). The GY (g pot^{-1}) was also determined. For cowpea, agronomic parameters including fresh weight (FW), dry weight (DW), number of pods, number of seeds, hundred seed weight (HSW) and seed yield (SY) were determined.

3.2.5 Statistical analysis

Agronomic responses were analysed using analysis of variance (ANOVA) incorporating the 2×2 factorial treatment structure and RCBD blocking structure. F-statistics were employed to test all fixed terms (i.e., main effects and interaction), with all tests conducted at the 5% significance level. Spectral responses and agro-morpho-physiological variables measured on successive occasions were analysed using repeated

measures ANOVA (RMA) that incorporates an adjustment for the presence of autocorrelation between sample occasions (Greenhouse and Geisser, 1959; Girden, 1992; Keselman et al., 2000). These analyses incorporated the 3-way factorial treatment structure and the nested split-plot blocking structure. The RMA estimates a parameter (epsilon) that reflects the level of autocorrelation in the data (Greenhouse and Geisser, 1959) which is then used to adjust (reduce) the degrees of freedom (df) in the block.pot.sample stratum (i.e., the lowest stratum). F-statistics were then assessed on these reduced df, effectively meaning that the F-tests are more conservative the more evidence there is for autocorrelation (i.e., as epsilon gets smaller).

A $\log_{10}$ transformation was implemented to satisfy assumptions and achieve homogeneity of the residuals of some of the agronomic parameters where necessary. The residuals were examined to verify variance homogeneity (through fitted values plots) and normality assumptions (using histograms and Q-Q plots). Means plots were produced and differences between fitted means for the N and P treatment combinations on each sampling occasion were assessed against the approximate least significant difference (LSD) at a 5% level of significance. The relationship between responsive SRIs and agro-morpho-physiological traits was examined using the Pearson correlation coefficient (r). GenStat 22nd edition (VSN International Ltd., Hemel Hempstead, United Kingdom) was used for all analysis and visualisations.

3.3 Results

3.3.1 Quinoa

3.3.1.1 Identification of optimal spectral reflectance indices for N and P status in quinoa

RMA was employed to identify SRIs sensitive to N and P stresses both individually and in combination using the PolyPen RP410 spectrometer (Appendix B, Figure B-3). A wide range of SRIs, including NDVI, SR, OSAVI, G, MCARI, TCARI, ZMI, SPRI, NPQI, PRI, NPCI, Ctr1, Ctr2, Lic1, Lic2, SIPI, GM1, GM2, CRI1, CRI2, RDVI, GNDVI_780, MRESR, RENDVI, NDRE, CIgreen, CIrededge, mNDblue_530, gSRa_790 and SRa_790 were responsive to N stress (Table 3.3). SRIs that were responsive to P included SR, PRI, Ctr1, Lic2, GM1, GM2, PRI_550, MRESR, RENDVI, NDRE, CIgreen, CIrededge, mNDblue_530, mNDblue_730 and gSRa_790

(Table 3.3). Additionally, SRIs including SR, PRI, Ctr1, Lic2, GM1, GM2, MRESR, RENDVI, NDRE, CIgreen, CIrededge, mNDblue_530 and gSRa_790 showed high response to the combined N and P stress. Based on the results presented in Table 3.3, SRIs that were responsive to only N stress were NDVI, OSAVI, G, MCARI, TCARI, ZMI, SPRI, NPQI, NPCI, Ctr2, Lic1, SIPI, CRI1, CRI2, RDVI, GNDVI_780 and SRa_790 which indicates specificity for their detection (Table 3.3; Figure 3.5). The raw data distribution and residual plots for some of the N stress-specific SRIs are shown in Appendix B, Figure B-4. For P stress, the only SRIs that were responsive and indicated specificity for their detection were mNDblue_730 and PRI_550 (Table 3.3; Figure 3.6). Appendix B, Figure B-5 shows the raw data distribution and residual plots for the P stress-specific SRIs. The SRIs that showed no response to either N or P and their combined effect included MCARI1, TVI, ARI1, ARI2, PRI_norm, PRI/NDVI and rDVI_790 (Table 3.3). Additionally, a wide range of SRIs including NDVI, SR, OSAVI, ZMI, RENDVI, NDRE etc., were effective in detecting N×P interaction.

Table 3.3. F-tests from repeated measures ANOVA (RMA) for main effects of N and P on spectral reflectance indices (SRIs) in quinoa. The RMA analysis was done considering all treatment combinations and time points (DAS). The Statistically significant results (p<0.05) indicating differences between means for levels of N or P are shown in bold. Full results are given in Appendix B, Table B-1.

Index	N	P	N×P
NDVI	$F_{1,12}$=93.618, p<**0.001**	$F_{1,12}$=3.895, p=0.072	$F_{1,12}$=30.052, p<**0.001**
SR	$F_{1,12}$=144.270, p<**0.001**	$F_{1,12}$=9.031, p<**0.05**	$F_{1,12}$=44.955, p<**0.001**
MCARI1	$F_{1,12}$=0.159, p=0.697	$F_{1,12}$=0.028, p=0.870	$F_{1,12}$=1.977, p=0.185
OSAVI	$F_{1,12}$=31.695, p<**0.001**	$F_{1,12}$=0.932, p=0.353	$F_{1,12}$=16.811, p<**0.01**
G	$F_{1,12}$=14.128, p<**0.01**	$F_{1,12}$=0.984, p=0.341	$F_{1,12}$=4.861, p<**0.05**
MCARI	$F_{1,12}$=41.319, p<**0.001**	$F_{1,12}$=3.400, p=0.090	$F_{1,12}$=2.552, p=0.136
TCARI	$F_{1,12}$=51.418, p<**0.001**	$F_{1,12}$=0.794, p=0.391	$F_{1,12}$=11.627, p<**0.01**
TVI	$F_{1,12}$=0.112, p=0.744	$F_{1,12}$=0.065, p=0.803	$F_{1,12}$=4.311, p=0.060
ZMI	$F_{1,12}$=87.508, p<**0.001**	$F_{1,12}$=3.566, p=0.083	$F_{1,12}$=18.871, p<**0.001**
SPRI	$F_{1,12}$=43.292, p<**0.001**	$F_{1,12}$=4.581, p=0.054	$F_{1,12}$=1.056, p=0.324
NPQI	$F_{1,12}$=7.493, p<**0.05**	$F_{1,12}$=1.323, p=0.272	$F_{1,12}$=2.879, p=0.116
PRI	$F_{1,12}$=71.065, p<**0.001**	$F_{1,12}$=10.129, p<**0.01**	$F_{1,12}$=1.537, p=0.239
NPCI	$F_{1,12}$=32.916, p<**0.001**	$F_{1,12}$=3.642, p=0.081	$F_{1,12}$=0.783, p=0.394
Ctr1	$F_{1,12}$=78.080, p<**0.001**	$F_{1,12}$=9.731, p<**0.01**	$F_{1,12}$=2.110, p=0.172
Ctr2	$F_{1,12}$=81.244, p<**0.001**	$F_{1,12}$=3.237, p=0.097	$F_{1,12}$=23.513, p<**0.001**
Lic1	$F_{1,12}$=33.269, p<**0.001**	$F_{1,12}$=0.960, p=0.346	$F_{1,12}$=13.029, p<**0.01**
Lic2	$F_{1,12}$=98.123, p<**0.001**	$F_{1,12}$=10.519, p<**0.01**	$F_{1,12}$=6.008, p<**0.05**
SIPI	$F_{1,12}$=65.267, p<**0.001**	$F_{1,12}$=0.510, p=0.489	$F_{1,12}$=47.186, p<**0.001**
GM1	$F_{1,12}$=118.366, p<**0.001**	$F_{1,12}$=6.127, p<**0.05**	$F_{1,12}$=51.745, p<**0.001**

GM2	$F_{1,12}$=129.417, p<**0.001**	$F_{1,12}$=8.692, p<**0.05**	$F_{1,12}$=34.177, p<**0.001**
ARI1	$F_{1,12}$=2.492, p=0.140	$F_{1,12}$=1.162, p=0.302	$F_{1,12}$=6.302, p<**0.05**
ARI2	$F_{1,12}$=2.305, p=0.155	$F_{1,12}$=1.187, p=0.297	$F_{1,12}$=8.190, p<**0.05**
CRI1	$F_{1,12}$=81.086, p<**0.001**	$F_{1,12}$=0.263, p=0.617	$F_{1,12}$=25.724, p<**0.001**
CRI2	$F_{1,12}$=27.284, p<**0.001**	$F_{1,12}$=0.924, p=0.355	$F_{1,12}$=23.756, p<**0.001**
RDVI	$F_{1,12}$=21.289, p<**0.001**	$F_{1,12}$=0.803, p=0.388	$F_{1,12}$=18.592, p<**0.01**
PRI_550	$F_{1,12}$=2.916, p=0.113	$F_{1,12}$=7.991, p<**0.05**	$F_{1,12}$=2.279, p=0.157
PRI_norm	$F_{1,12}$=0.297, p=0.596	$F_{1,12}$=0.013, p=0.910	$F_{1,12}$=1.650, p=0.223
PRI/NDVI	$F_{1,12}$=2.850, p=0.117	$F_{1,12}$=0.013, p=0.910	$F_{1,12}$=1.315, p=0.274
GNDVI_780	$F_{1,12}$=61.883, p<**0.001**	$F_{1,12}$=3.118, p=0.103	$F_{1,12}$=55.354, p<**0.001**
MRESR	$F_{1,12}$=128.244, p<**0.001**	$F_{1,12}$=16.706, p<**0.01**	$F_{1,12}$=46.811, p<**0.001**
RENDVI	$F_{1,12}$=129.217, p<**0.001**	$F_{1,12}$=12.446, p<**0.01**	$F_{1,12}$=55.461, p<**0.001**
NDRE	$F_{1,12}$=133.386, p<**0.001**	$F_{1,12}$=18.080, p<**0.01**	$F_{1,12}$=57.081, p<**0.001**
CIgreen	$F_{1,12}$=76.664, p<**0.001**	$F_{1,12}$=6.938, p<**0.05**	$F_{1,12}$=63.164, p<**0.001**
CIrededge	$F_{1,12}$=132.412, p<**0.001**	$F_{1,12}$=19.031, p<**0.001**	$F_{1,12}$=57.428, p<**0.001**
mNDblue_530	$F_{1,12}$=79.911, p<**0.001**	$F_{1,12}$=5.736, p<**0.05**	$F_{1,12}$=37.803, p<**0.001**
mNDblue_730	$F_{1,12}$=1.993, p=0.183	$F_{1,12}$=8.454, p<**0.05**	$F_{1,12}$=20.623, p<**0.001**
rDVI_790	$F_{1,12}$=4.316, p=0.060	$F_{1,12}$=0.432, p=0.523	$F_{1,12}$=10.946, p<**0.05**
gSRa_790	$F_{1,12}$=76.664, p<**0.001**	$F_{1,12}$=6.938, p<**0.05**	$F_{1,12}$=63.164, p<**0.001**
SRa_790	$F_{1,12}$=45.166, p<**0.001**	$F_{1,12}$=3.663, p=0.080	$F_{1,12}$=30.725, p<**0.001**

3.3.1.2 Time course response of spectral reflectance indices to N and P variations

Figures 3.5 and 3.6 show the time course responses of the SRIs that indicated specificity for N and P stress in Table 3.3. The results as presented in Figures 3.5 and 3.6 revealed the earliest response of SRIs comprising GNDVI_780 and SRa_790 to detecting N and P nutritional variations first at 37 DAS (vegetative stage) and consistently from the mid-growth stage (anthesis) at 58 to 107 DAS (physiological maturity) stage of quinoa (Figure 3.5). These SRIs also displayed better separation of nutritional treatments particularly at the mid-growth and physiological maturity stages (Figure 3.5). Higher values were generally obtained for the HNHP treatment for GNDVI_780 and SRa_790.

Close to a week after 37 DAS, NDVI, MCARI, G, TCARI, Ctr2 and ZMI showed similar patterns in detecting N and P nutritional variations first at 44 DAS and consistently from 58 to 107 DAS with good separation between treatment conditions (Figure 3.5). Except for G, MCARI and Ctr2, high mean values were obtained under HNHP treatment by NDVI, TCARI and ZMI (Figure 3.5). For mNDblue_730, N and P nutritional variation during anthesis was first detected at 51 DAS and at later stages at 86, 93 and 100 DAS with corresponding separation between treatments (Figure 3.6A). NPQI showed the detection of N and P variations at late anthesis (65 DAS) and grain

development (79 and 86 DAS) with good separation between treatments (Figure 3.5H). Additionally, SIPI observed the detection of N and P variations at late anthesis (65 DAS) and later stages at 79, 86, 93, 100 and 107 DAS with good separation between treatments. Higher values were recorded for the HNHP treatment over time (Figure 3.5L).

SRIs such as OSAVI and Lic1 detected N and P nutritional variations at later growth stages at 79, 86, 93 and 100 DAS coupled with good separation between treatments (Figure 3.5). Higher values were obtained for the HNHP treatment for OSAVI and Lic1. At 86, 93, 100 and 107 DAS, RDVI detected changes in N and P nutrition with good separation between treatments (Figure 3.5N). A similar trend of N and P nutritional variation detection was observed for SPRI, NPCI and PRI_550 at physiological maturity at 93, 100 and 107 DAS with good separation between treatments (Figure 3.5). Generally, SRIs that were optimal for N stress such as SRa_790, GNDVI_780, NDVI, G, MCARI, CRI1, TCARI and ZMI showed early detection of variations in N and P nutrition compared to P-specific indices (mNDblue_730 and PRI_550) (Figure 3.5 and 3.6).

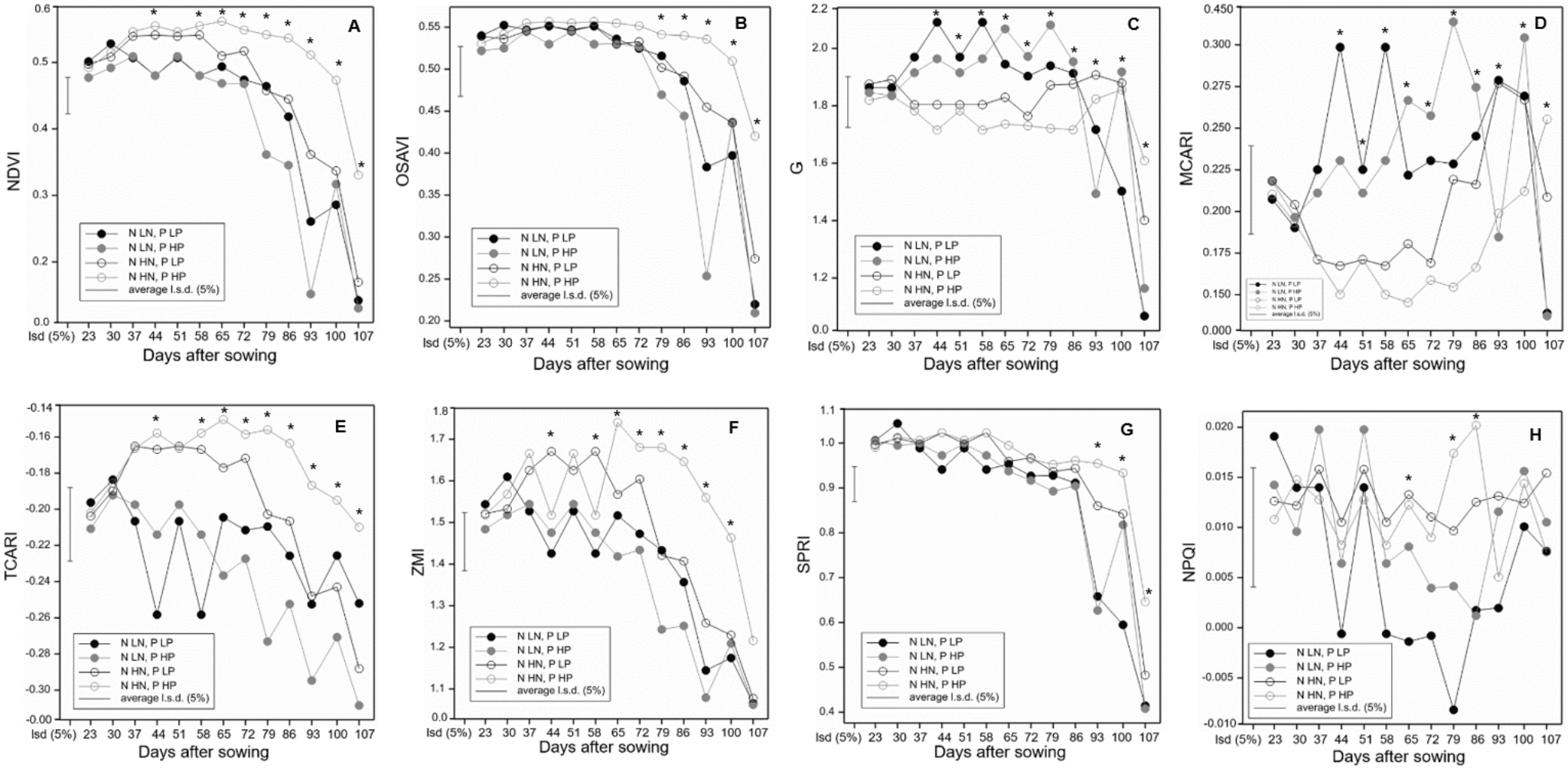
A
NDVI
B
OSAVI
C
G
D
MCARI
E
TCARI
F
ZMI
G
SPRI
H
NPQI
N LN, P LP
N LN, P HP
N HN, P LP
N HN, P HP
average l.s.d. (5%)
lsd (5%) 23 30 37 44 51 58 65 72 79 86 93 100 107
Days after sowing

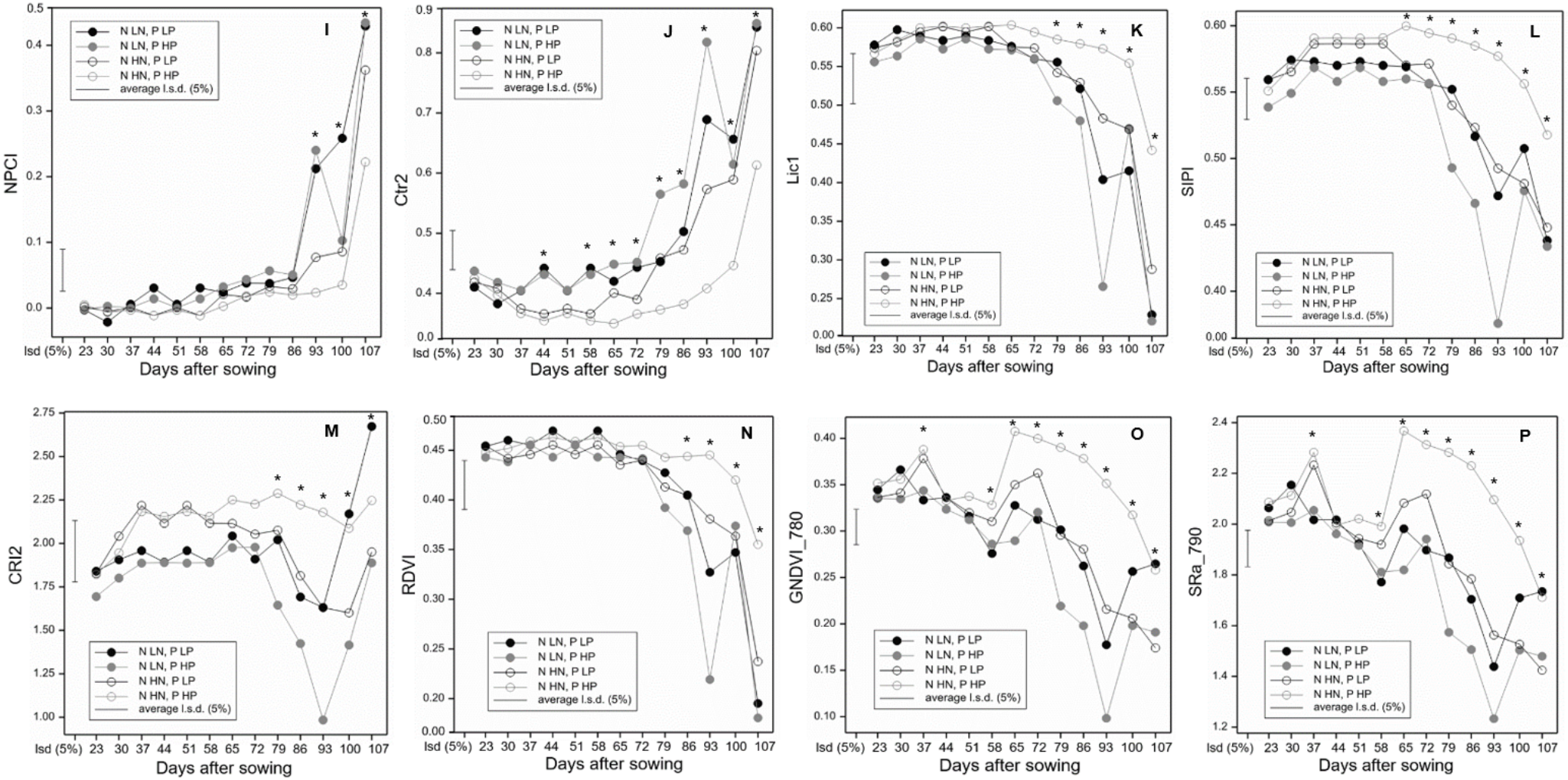

Figure 3.5. Time course of N stress responsive SRIs including (A) NDVI, (B) OSAVI, (C) G, (D) MCARI, (E) TCARI, (F) ZMI, (G) SPRI, (H) NPQI, (I) NPCI, (J) Ctr2, (K) Lic1, (L) SIPI, (M) CRI2, (N) RDVI, (O) GNDVI_780 and (P) SRa_790 showing their responses to N and P nutritional variations at specific days after sowing (DAS) during quinoa crop cycle from 23 to 107 DAS. Mean values represent five replicates per treatment condition. Bars indicate the average least significant difference (LSD) at the 5% significance level. Asterisks (*) indicate significant difference between treatments at 5% significance level at different DAS.

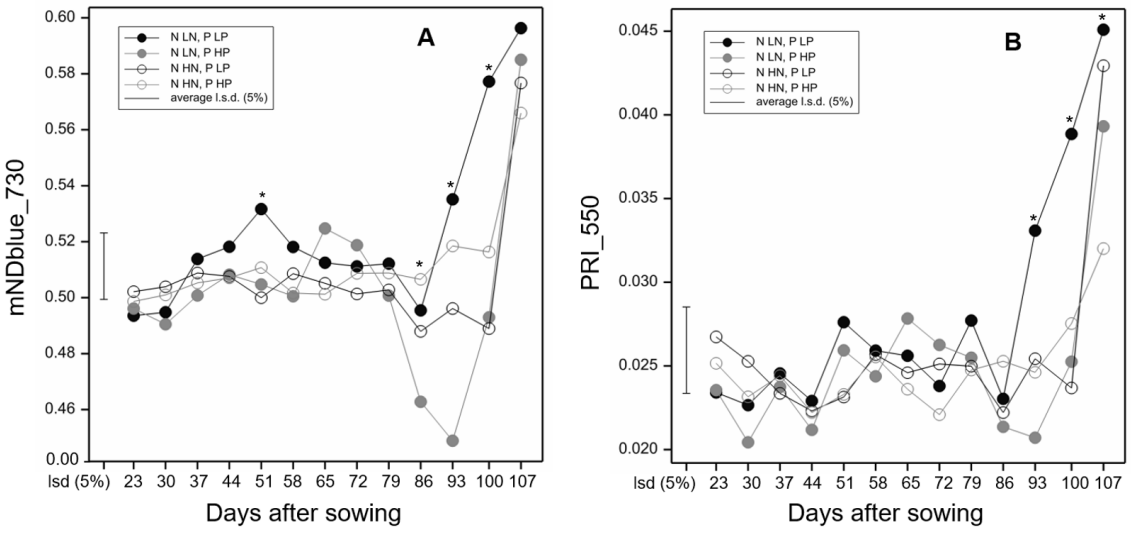

Figure 3.6. Time course of P stress specific SRIs including (A) mNDblue_730 and (B) PRI_550, showing their responses to N and P nutritional variations at specific days after sowing (DAS) during quinoa crop cycle from 23 to 107 DAS. Mean values represent five replicates per treatment condition. Bars indicate the average least significant difference (LSD) at the 5% significance level. Asterisks (*) indicate significant difference between treatments at 5% significance level at different DAS.

3.3.1.3 Assessment of quinoa agro-morpho-physiological responses under varying N and P availabilities

3.3.1.3.1 Morpho-physiological responses

Figure 3.7 shows a pictorial morpho-physiological response of quinoa assessed under different N and P availabilities. The mean values of LNC and LPC increased with increasing N and P supply over time with statistically significant differences between treatments observed at 44, 72 and 107 DAS (Figure 3.8). The raw data distribution of the different N and P treatments and their residual plots with fitted values for LNC and LPC are shown in Appendix B, Figure B-6. The HNHP treatment achieved high mean values in both variables (Figure 3.8). LNC responded significantly to N stress (p<0.001) and P stress (p<0.001) with a significant interaction (p<0.001) between the two stress factors (Table 3.4). A significant N×P×DAS interaction was observed (p<0.001) indicating the influence of all factors on LNC (Table 3.4). Similarly, LPC responded significantly to N stress (p<0.001) and P stress (p<0.001) but only the effect of P changed over time (P×DAS, p<0.001).

SPAD values increased with increasing N and P availability with significant differences between treatments observed over time except at 23 and 30 DAS (Figure 3.8C). High

SPAD values were recorded for the HNHP treatment (Figure 3.8C). SPAD values responded significantly to N stress ($p<0.001$) and P stress ($p<0.01$) with a significant N×P interaction ($p<0.001$) (Table 3.4). SPAD values indicated N×P×DAS interaction ($p<0.001$).

Additionally, A_n increased with a corresponding increase in N and P supply with significant differences between treatments observed at 44, 72 and 107 DAS (Figure 3.8D). The A_n values obtained for the HNHP treatment were high compared to the other treatments. A_n responded significantly to N stress ($p<0.001$) and P stress ($p<0.001$) and these effects changed over time (DAS, $p<0.001$) (Table 3.4).

PH increased with increasing N and P supply with a significant difference between treatments indicated at 72 and 107 DAS (Figure 3.8E). Except for 44 DAS, the HNHP treatment led to high mean values. PH responded significantly to N stress ($p<0.001$) and P stress ($p<0.05$) and the effects of both factors changed over time (N×DAS, $p<0.001$, and P×DAS, $p<0.05$) (Table 3.4).

Figure 3.7. Morpho-physiological responses of quinoa assessed under different N and P availabilities. A, B, C and D indicate quinoa plants grown under HNHP, HNLP, LNHP and LNLP nutrient conditions respectively. The photograph was taken 74 days after sowing (DAS).

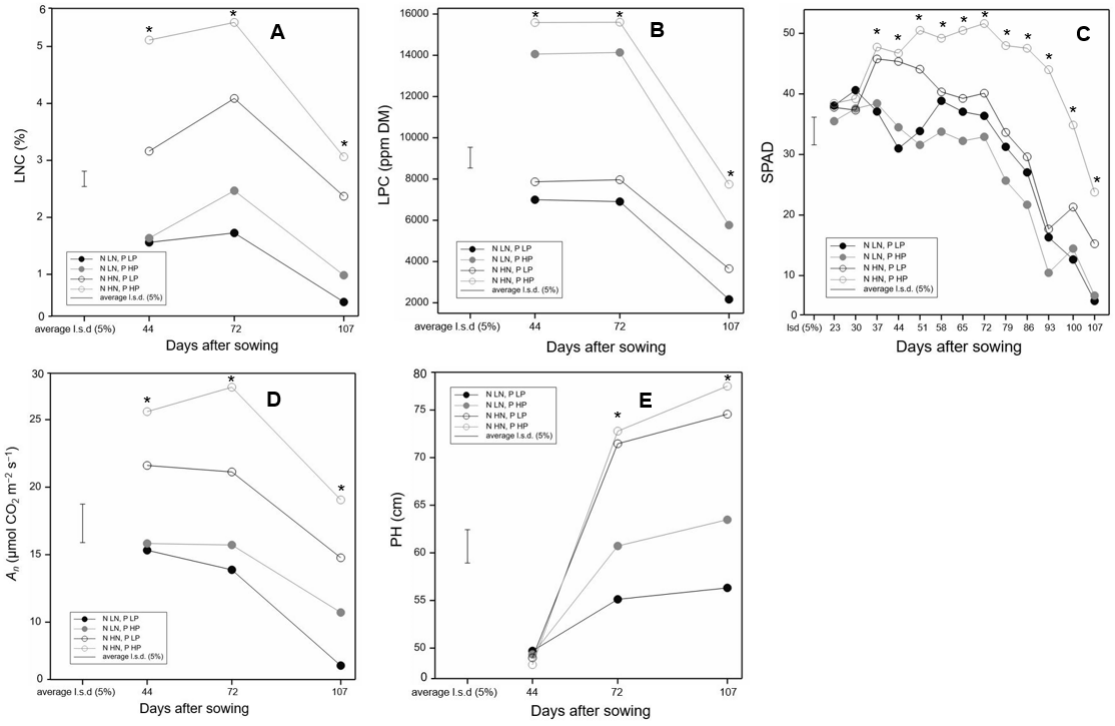

Figure 3.8. Mean values and time course of morpho-physiological parameters measured in response to different levels of N and P availability and assessed by repeated measures ANOVA. (A) LNC, (B) LPC, (C) SPAD, (D) A_n and (E) PH. Mean values represent five replicates per treatment. Bars indicate the average least significant difference (LSD) at the 5% significance level. Significant differences between treatments at 5% significance level at different days after sowing (DAS) are indicated with asterisks (*).

Table 3.4. F-tests from repeated measures ANOVA to assess the main effects of (and interactions between) N, P and days after sowing (DAS) on quinoa morpho-physiological parameters: leaf nitrogen content (LNC), leaf phosphorus concentration (LPC), SPAD, photosynthetic net CO_2 assimilation (A_n) and plant height (PH). Statistically significant results (p<0.05) are shown in bold.

Parameter	**N**	**P**	**N×P**	**DAS**	**N×DAS**	**P×DAS**	**N×P×DAS**
LNC (%)	$F_{1,12}$=2784.511, p<**0.001**	$F_{1,12}$=375.809, p<**0.001**	$F_{1,12}$=98.300, p<**0.001**	$F_{1.5,24.5}$=315.179, p<**0.001**	$F_{1.5,24.5}$=14.404, p<**0.001**	$F_{1.5,24.5}$=6.960, p=**0.007**	$F_{1.5,24.5}$=19.920, p<**0.001**
LPC (ppm DM)	$F_{1,12}$=28.573, p<**0.001**	$F_{1,12}$=566.097, p<**0.001**	$F_{1,12}$=0.979, p=0.342	$F_{1,17}$=673.838, p<**0.001**	$F_{1,17}$=1.073, p=0.319	$F_{1,17}$=53.861, p<**0.001**	$F_{1,17}$=0.053, p=0.833
SPAD	$F_{1,12}$=233.951, p<**0.001**	$F_{1,12}$=26.702, p<**0.001**	$F_{1,12}$=72.752, p<**0.001**	$F_{5.4,85.8}$=144.743, p<**0.001**	$F_{5.4,85.8}$=11.487, p<**0.001**	$F_{5.4,85.8}$=4.092, p<**0.05**	$F_{5.4,85.8}$=9.580, p<**0.001**
A_n (μmol CO_2 m^{-2} s^{-1})	$F_{1,12}$=122.208, p<**0.001**	$F_{1,12}$=20.124, p<**0.001**	$F_{1,12}$=3.177, p=0.100	$F_{1.4,22.6}$=94.404, p<**0.001**	$F_{1.4,22.6}$=0.991, p=0.360	$F_{1.4,22.6}$=1.767, p=0.198	$F_{1.4,22.6}$=1.782, p=0.196
PH (cm)	$F_{1,12}$=91.591, p<**0.001**	$F_{1,12}$=6.717, p<**0.05**	$F_{1,12}$=2.075, p=0.175	$F_{1.2,19.5}$=528.766, p<**0.001**	$F_{1.2,19.5}$=111.227, p<**0.001**	$F_{1.2,19.5}$=10.611, p<**0.05**	$F_{1.2,19.5}$=1.613, p=0.223

3.3.1.3.2 Assessment of agronomic responses

Table 3.5 and Figure 3.9 show the responses of agronomic variables under different N and P availabilities. All agronomic variables were responsive to N and P stress except for TGW (Table 3.5). Mean values of VB, TPB and GY increased with increased N and P supply, and statistically significant differences between treatments were observed (Table 3.5). Mean values of all agronomic variables obtained under HNHP treatment were high except for TGW (Table 3.5). No N×P interaction was observed for any of these agronomic variables (Table 3.5).

Table 3.5. Mean values of quinoa agronomic variables: vegetative biomass (VB), total plant biomass (TPB), thousand-grain weight (TGW) and grain yield (GY) in response to different N and P supplies. Values of VB, TPB and GY were log_{10}-transformed to achieve homogeneity of the residuals. Statistically significant results (p<0.05) are shown in bold.

Parameter	**log_{10}VB (g plant^{-1})**	**log_{10} TPB (g plant^{-1})**	**TGW (g plant^{-1})**	**log_{10} GY (g pot^{-1})**
Treatment	**Means**	**Means**	**Means**	**Means**
HNHP	1.88	2.17	2.73	1.87
HNLP	1.78	2.04	2.97	1.70
LNHP	1.59	1.80	3.05	1.36
LNLP	1.48	1.66	2.93	1.18
N	p<**0.001**	p<**0.001**	p=0.259	p<**0.001**
P	p<**0.001**	p<**0.001**	p=0.636	p<**0.001**
N×P	p=0.655	p=0.865	p=0.162	p=0.861

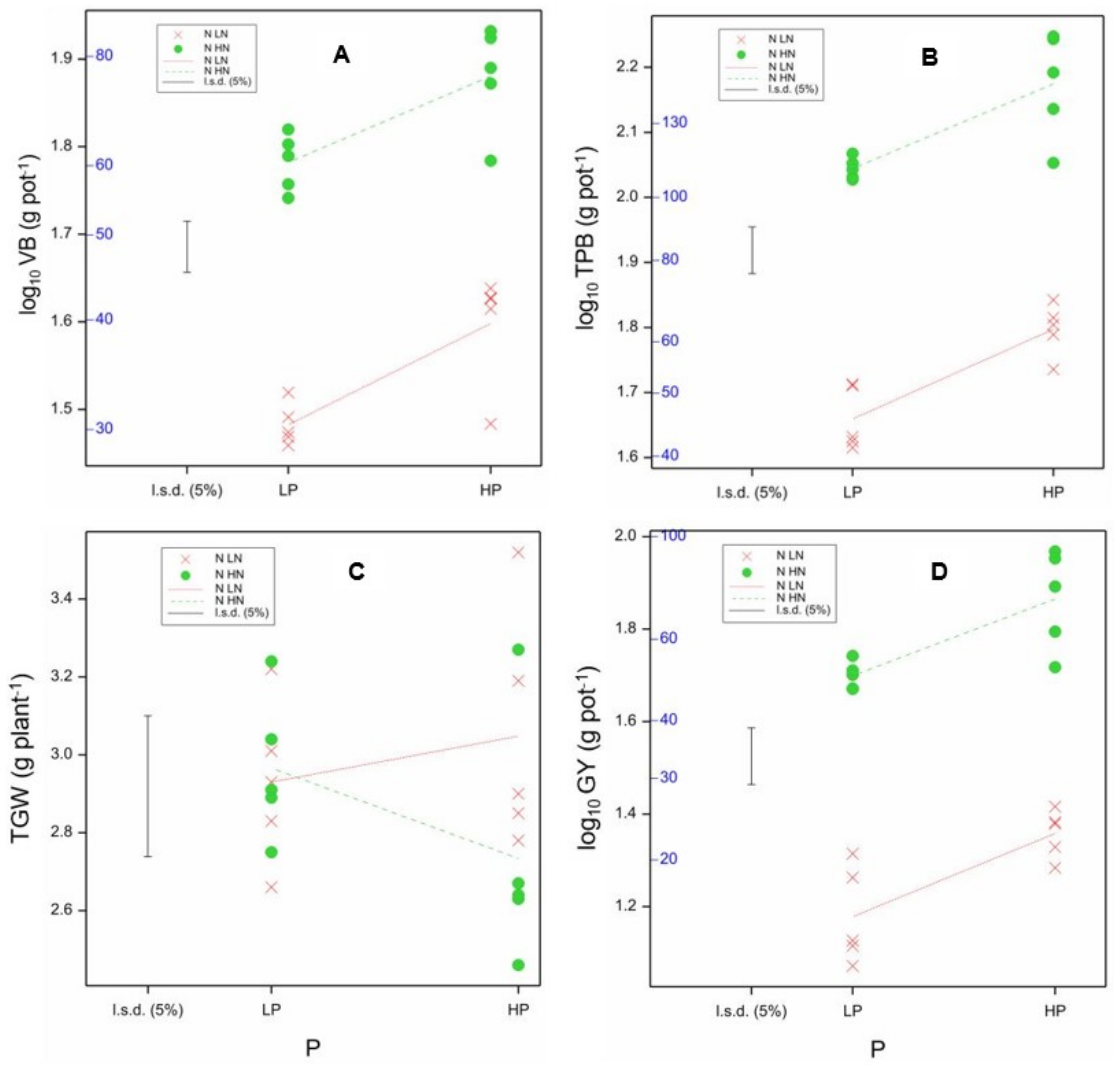

Figure 3.9. Responses of quinoa agronomic variables to different N and P supplies: (A) vegetative biomass (VB), (B) total plant biomass (TPB), (C) thousand-grain weight (TGW) and (D) grain yield (GY). Variables VB, TPB and GY were log_{10}-transformed to achieve homogeneity of the residuals. Mean values represent five replicates per treatment. Bars indicate the least significant difference (LSD) at the 5% significance level.

3.3.1.4 Assessing the relationship between spectral response and agro-morpho-physiological status

To evaluate the relationships between SRIs and quinoa agro-morpho-physiological parameters, correlation coefficients (r) were calculated for the SRIs that were specific to N and P stress (p<0.05) (Table 3.3). Results from the correlation analysis (Table 3.6) showed several of the SRIs significantly correlated with LNC except for G, MCARI, NPQI and CRI2. The highest correlation coefficients with LNC were obtained by NDVI, SIPI, CRI1, Ctr2 and ZMI (Table 3.6). A similar pattern of correlation was achieved for LPC where NDVI, Ctr2, SIPI, SPRI and SRa_790 showed the highest correlations, whereas MCARI, NPQI and CRI2 were non-significantly correlated (Table 3.6).

Almost all the SRIs significantly correlated with SPAD except for NPQI. The highest correlation coefficient with SPAD was recorded by NDVI, Ctr2, ZMI, SIPI and SRa_790 (Table 3.6). For A_n, a wide range of the SRIs significantly correlated with the photosynthetic parameter except for MCARI, NPCI and CRI2 (Table 3.6). The highest correlation with A_n was achieved by NDVI, Ctr2, SIPI, ZMI and CRI1. Several of the SRIs significantly correlated with PH, with SPRI, NPCI, PRI_550, Ctr2 and NDVI having the highest correlations with the plant growth indicator (Table 3.6). The only SRIs that were poorly correlated with PH included MCARI, TCARI, ZMI and CRI2.

Additionally, most of the SRIs significantly correlated with VB except for MCARI, TCARI, NPQI, CRI1, CRI2, GNDVI_780, SRa_790, mNDblue_730 and PRI_550. SRIs that achieved the highest correlation coefficient with VB included ZMI, NDVI, Ctr2, G and SIPI. A similar trend of correlation was observed for TPB. For TGW, none of the SRIs correlated with the agronomic parameter. However, most of the SRIs significantly correlated with GY except for TCARI, NPCI, CRI1, CRI2, GNDVI_780 and PRI_550 (Table 3.6). The highest correlation coefficient with GY was obtained by ZMI, NDVI, SPRI, SIPI and G.

Altogether, it is observed that the N-specific SRIs such as NDVI, ZMI, Ctr2, SIPI, SPRI, G, etc., achieved the highest correlation with several of the agro-morpho-physiological parameters. Contrarily, the two P-specific SRIs (mNDblue_730 and PRI_550) showed a non-significant correlation with all agronomic parameters (VB, TPB, TGW and GY) except mNDblue_730 which correlated significantly with GY (Table 3.6).

Table 3.6. Correlation analysis between optimal SRIs and quinoa agro-morpho-physiological parameters assessed by Pearson correlation. The data from spectral reflectance measurements and agro-morpho-physiological parameters measured at the same time were used. For LNC, LPC, A_n and PH, correlations with SRIs were implemented at 44, 72 and 107 DAS. SPAD and SRIs were correlated using data from 23 to 107 DAS. Agronomic parameters such as VB, TPB, TGW and GY were correlated with SRIs at 107 DAS at final harvest. Values are Pearson correlation coefficient (r) between SRIs and morpho-physiological parameters. Significant r values (p<0.05) are indicated in bold.

	Agro-morpho-physiological parameters								
Nutrient specific indices	**LNC (%)**	**LPC (ppm DM)**	**SPAD**	**A_n (µmol CO_2 m^{-2} s^{-1})**	**PH (cm)**	**VB (g $plant^{-1}$)**	**TPB (g $plant^{-1}$)**	**TGW (g $plant^{-1}$)**	**GY (g pot^{-1})**
NDVI	**0.61**	**0.68**	**0.88**	**0.66**	**-0.32**	**0.52**	**0.58**	-0.12	**0.62**
OSAVI	**0.52**	**0.62**	**0.77**	**0.56**	**-0.30**	**0.45**	**0.51**	-0.03	**0.54**
G	0.26	**0.48**	**0.33**	**0.31**	**-0.29**	**0.50**	**0.54**	-0.15	**0.56**
MCARI	-0.13	0.04	**-0.36**	-0.12	-0.06	0.37	0.42	0.06	**0.45**
TCARI	**0.57**	**0.43**	**0.71**	**0.55**	-0.13	0.12	0.17	0.25	0.20
ZMI	**0.58**	**0.57**	**0.83**	**0.62**	-0.25	**0.56**	**0.62**	-0.26	**0.65**
SPRI	**0.54**	**0.66**	**0.78**	**0.60**	**-0.39**	**0.47**	**0.53**	-0.12	**0.57**
NPQI	0.14	-0.09	0.09	**0.13**	**0.29**	0.11	0.10	-0.20	**0.09**
NPCI	**-0.53**	**-0.64**	**-0.74**	-0.58	**0.35**	**-0.46**	**-0.52**	0.08	-0.55
Ctr2	**-0.61**	**-0.68**	**-0.87**	**-0.65**	**0.32**	**-0.52**	**-0.58**	0.14	**-0.62**
Lic1	**0.53**	**0.62**	**0.78**	**0.57**	**-0.31**	**0.45**	**0.50**	-0.03	**0.54**
SIPI	**0.61**	**0.67**	**0.83**	**0.64**	**-0.30**	**0.48**	**0.54**	-0.04	**0.57**
CRI1	**0.59**	**0.62**	**0.79**	**0.62**	**-0.30**	0.31	0.34	-0.05	0.36
CRI2	0.02	-0.10	**0.33**	-0.01	0.02	-0.26	-0.25	0.30	-0.23
RDVI	**0.50**	**0.60**	**0.74**	**0.54**	**-0.31**	**0.44**	**0.50**	-0.02	**0.53**
GNDVI_780	**0.51**	**0.59**	**0.80**	**0.52**	**-0.27**	-0.15	-0.11	0.28	-0.07
SRa_790	**0.52**	**0.65**	**0.82**	**0.55**	**-0.33**	0.42	**0.48**	-0.08	**0.52**
mNDblue_730	**-0.50**	**-0.61**	**-0.32**	**-0.57**	**0.31**	-0.40	-0.44	0.22	**-0.46**
PRI_550	**-0.45**	**-0.61**	**-0.50**	**-0.53**	**0.34**	-0.32	-0.37	-0.01	-0.40

3.3.2 Cowpea

3.3.2.1 Identification of optimal spectral reflectance indices for N and P status in cowpea

To select the optimal SRIs sensitive to N and P stress separately and their combined effect in cowpea, RMA reflecting a degree of autocorrelation was used as employed in quinoa. Many different SRIs were responsive to N stress, including NDVI, SR, OSAVI, G, MCARI, TCARI, ZMI, SPRI, PRI, NPCI, Ctr1, Ctr2, Lic1, Lic2, GM1, GM2, RDVI, PRI_550, PRI_norm, PRI/NDVI, GNDVI_780, MRESR, RENDVI, NDRE, CIgreen, CIrededge, mNDblue_530, rDVI_790, gSRa_790 and SRa_790 according to the F-statistics and F-Test probabilities at the $p<0.05$ significance level (Table 3.7).

The NDVI, SR, OSAVI, MCARI, TCARI, ZMI, SPRI, PRI, NPCI, Ctr1, Ctr2, Lic1, Lic2, GM1, GM2, RDVI, PRI_550, PRI_norm, PRI/NDVI, GNDVI_780, MRESR, RENDVI, NDRE, CIgreen, CIrededge, mNDblue_530, gSRa_790 and SRa_790 were among the SRIs that responded to P stress (Table 3.7). Additionally, SRIs that were responsive to the combined N and P stress effect were NDVI, SR, OSAVI, MCARI, TCARI, ZMI, SPRI, PRI, NPCI, Ctr1, Ctr2, Lic1, Lic2, GM1, GM2, RDVI, PRI_550, PRI_norm, PRI/NDVI, GNDVI_780, MRESR, RENDVI, NDRE, CIgreen, CIrededge, mNDblue_530, gSRa_790 and SRa_790 (Table 3.7; Figure 3.11). Generally, the response of SRIs for N was greater compared to P (Table 3.7).

Based on the results presented in Table 3.7, SRIs that were responsive to only N stress were G and rDVI_790 which suggests they may be best suited for N-detection. The raw data distribution of the different treatments and residual plots of the N-specific SRIs for cowpea are shown in Appendix B, Figure B-7. However, no SRI was identified to be useful for P stress in cowpea (Table 3.7). The SRIs that showed no response to either N or P and their combined effect included MCARI1, TVI, NPQI, SIPI, ARI1, ARI2, CRI1, CRI2 and mNDblue_730 (Table 3.7). The NDVI, SR, MCARI, TCARI, ZMI, MRESR, CIrededge were among SRIs that were responsive in detecting N×P interaction in cowpea.

Table 3.7. Test for main effects of SRIs in response to N and P stress separately and their combined effects in cowpea. The responses of the spectral indices to N and P stresses and their interactions were tested using the F-statistics and F-Test probability via repeated measures ANOVA (RMA). The RMA analysis was done considering all treatment combinations and time points (DAS). The statistically significant results (p<0.05) indicating differences between means for levels of N or P are shown in bold. Full results are presented in Appendix B, Table B-2.

Index	N	P	N×P
NDVI	$F_{1,12}$=25.143, p<**0.01**	$F_{1,12}$=13.557, p<**0.05**	$F_{1,12}$=8.511, p<**0.05**
SR	$F_{1,12}$=24.744, p<**0.01**	$F_{1,12}$=10.751, p<**0.05**	$F_{1,12}$=7.666, p<**0.05**
MCARI1	$F_{1,12}$=0.003, p=0.955	$F_{1,12}$=0.004, p=0.953	$F_{1,12}$=1.308, p=0.275
OSAVI	$F_{1,12}$=9.122, p<**0.05**	$F_{1,12}$=7.659, p<**0.05**	$F_{1,12}$=3.820, p=0.074
G	$F_{1,12}$=23.461, p<**0.01**	$F_{1,12}$=2.429, p=0.145	$F_{1,12}$=4.343, p=0.059
MCARI	$F_{1,12}$=36.796, p<**0.001**	$F_{1,12}$=11.570, p<**0.05**	$F_{1,12}$=7.256, p<**0.05**
TCARI	$F_{1,12}$=16.668, p<**0.05**	$F_{1,12}$=15.365, p<**0.05**	$F_{1,12}$=6.580, p<**0.05**
TVI	$F_{1,12}$=0.729, p=0.410	$F_{1,12}$=0.178, p=0.681	$F_{1,12}$=0.392, p=0.543
ZMI	$F_{1,12}$=46.102, p<**0.001**	$F_{1,12}$=19.752, p<**0.01**	$F_{1,12}$=13.619, p<**0.05**
SPRI	$F_{1,12}$=31.313, p<**0.01**	$F_{1,12}$=22.642, p<**0.01**	$F_{1,12}$=1.322, p=0.273
NPQI	$F_{1,12}$=1.835, p=0.201	$F_{1,12}$=0.276, p=0.609	$F_{1,12}$=0.039, p=0.847
PRI	$F_{1,12}$=39.830, p<**0.001**	$F_{1,12}$=21.786, p<**0.01**	$F_{1,12}$=2.553, p=0.136
NPCI	$F_{1,12}$=24.277, p<**0.01**	$F_{1,12}$=19.903, p<**0.01**	$F_{1,12}$=0.750, p=0.404
Ctr1	$F_{1,12}$=41.462, p<**0.001**	$F_{1,12}$=15.159, p<**0.05**	$F_{1,12}$=2.678, p=0.128
Ctr2	$F_{1,12}$=30.144, p<**0.01**	$F_{1,12}$=19.676, p<**0.01**	$F_{1,12}$=9.259, p<**0.05**
Lic1	$F_{1,12}$=5.004, p<**0.05**	$F_{1,12}$=6.333, p<**0.05**	$F_{1,12}$=3.270, p=0.096
Lic2	$F_{1,12}$=40.725, p<**0.001**	$F_{1,12}$=18.699, p<**0.01**	$F_{1,12}$=3.512, p=0.085
SIPI	$F_{1,12}$=4.182, p=0.063	$F_{1,12}$=2.743, p=0.124	$F_{1,12}$=3.779, p=0.076
GM1	$F_{1,12}$=39.312, p<**0.001**	$F_{1,12}$=13.747, p<**0.05**	$F_{1,12}$=14.016, p<**0.05**
GM2	$F_{1,12}$=38.419, p<**0.001**	$F_{1,12}$=15.816, p<**0.05**	$F_{1,12}$=10.764, p<**0.05**
ARI1	$F_{1,12}$=0.045, p=0.835	$F_{1,12}$=0.606, p=0.451	$F_{1,12}$=3.191, p=0.099
ARI2	$F_{1,12}$=0.060, p=0.811	$F_{1,12}$=1.509, p=0.243	$F_{1,12}$=8.808, p<**0.05**
CRI1	$F_{1,12}$=0.296, p=0.596	$F_{1,12}$=0.078, p=0.784	$F_{1,12}$=0.344, p=0.568
CRI2	$F_{1,12}$=0.415, p=0.710	$F_{1,12}$=0.001, p=0.973	$F_{1,12}$=0.629, p=0.443
RDVI	$F_{1,12}$=12.260, p<**0.05**	$F_{1,12}$=6.450, p<**0.05**	$F_{1,12}$=2.721, p=0.125
PRI_550	$F_{1,12}$=22.013, p<**0.01**	$F_{1,12}$=12.702, p<**0.05**	$F_{1,12}$=0.000, p=0.979
PRI_norm	$F_{1,12}$=22.013, p<**0.01**	$F_{1,12}$=12.702, p<**0.05**	$F_{1,12}$=0.001, p=0.979
PRI/NDVI	$F_{1,12}$=4.962, p<**0.05**	$F_{1,12}$=11.827, p<**0.05**	$F_{1,12}$=0.015, p=0.905
GNDVI_780	$F_{1,12}$=45.426, p<**0.001**	$F_{1,12}$=14.389, p<**0.05**	$F_{1,12}$=5.474, p<**0.05**
MRESR	$F_{1,12}$=167.352, p<**0.001**	$F_{1,12}$=52.680, p<**0.001**	$F_{1,12}$=11.288, p<**0.05**
RENDVI	$F_{1,12}$=55.619, p<**0.001**	$F_{1,12}$=20.721, p<**0.01**	$F_{1,12}$=4.695, p=0.051
NDRE	$F_{1,12}$=57.549, p<**0.001**	$F_{1,12}$=18.749, p<**0.01**	$F_{1,12}$=6.782, p<**0.05**
CIgreen	$F_{1,12}$=54.387, p<**0.001**	$F_{1,12}$=15.770, p<**0.05**	$F_{1,12}$=5.392, p<**0.05**
CIrededge	$F_{1,12}$=65.525, p<**0.001**	$F_{1,12}$=20.862, p<**0.01**	$F_{1,12}$=7.150, p<**0.05**
mNDblue_530	$F_{1,12}$=134.749, p<**0.001**	$F_{1,12}$=37.657, p<**0.001**	$F_{1,12}$=8.687, p<**0.05**
mNDblue_730	$F_{1,12}$=0.002, p=0.967	$F_{1,12}$=0.036, p=0.852	$F_{1,12}$=0.924, p=0.355
rDVI_790	$F_{1,12}$=21.864, p<**0.01**	$F_{1,12}$=2.757, p=0.123	$F_{1,12}$=2.757, p=0.123
gSRa_790	$F_{1,12}$=54.387, p<**0.001**	$F_{1,12}$=15.770, p<**0.05**	$F_{1,12}$=5.392, p<**0.05**
SRa_790	$F_{1,12}$=14.442, p<**0.05**	$F_{1,12}$=6.607, p<**0.05**	$F_{1,12}$=0.469, p=0.506

3.3.2.2 Time course response of spectral reflectance indices to N and P variations in cowpea

Figures 3.10 and 3.11 show the time course response of the SRIs that were indicative of the combined N and P stress and optimal for N stress detection respectively. The results showed that SRIs including MCARI, Ctr1 (Figure 3.10) and G (Figure 3.11A) demonstrated the earliest detection of N and P nutritional variations with the first response at 23 DAS (early vegetative stage) and at different time points during the growing season. These SRIs also showed good separation between nutritional treatments. Lower values were obtained for the HNHP treatment in MCARI, Ctr1 and G. SRIs such as GNDVI_780, MRESR, RENDVI, NDRE, CIrededge, Lic2 and gSRa_790 displayed similar patterns for detecting N and P variations with first response at 44 DAS (reproductive stage) and various time points such as 51, 58, 65, 72, 79, 86, 93, 100, 107 and 114 DAS (Figure 3.10). A good separation between treatments was achieved by these SRIs with high values obtained for the HNHP treatment for GNDVI_780, MRESR, RENDVI, NDRE, CIrededge, Lic2 and gSRa_790 (Figure 3.10).

Additionally, rDVI_790 was responsive to detecting N and P variations first at 51 DAS (reproductive stage), 58 and 114 DAS but with poor separation between treatments (Figure 3.11B). SRIs including NDVI, SR, NPCI, PRI, SPRI, Ctr2 and GM2 were responsive to N and P variations first at 65 DAS (anthesis) and at multiple time points such as 72, 79, 93, 100, 107 and 114 DAS with good separation between treatments (Figure 3.10). Except for Ctr2, high values were generally obtained for HNHP treatment in NDVI, SR, PRI, SPRI and GM2.

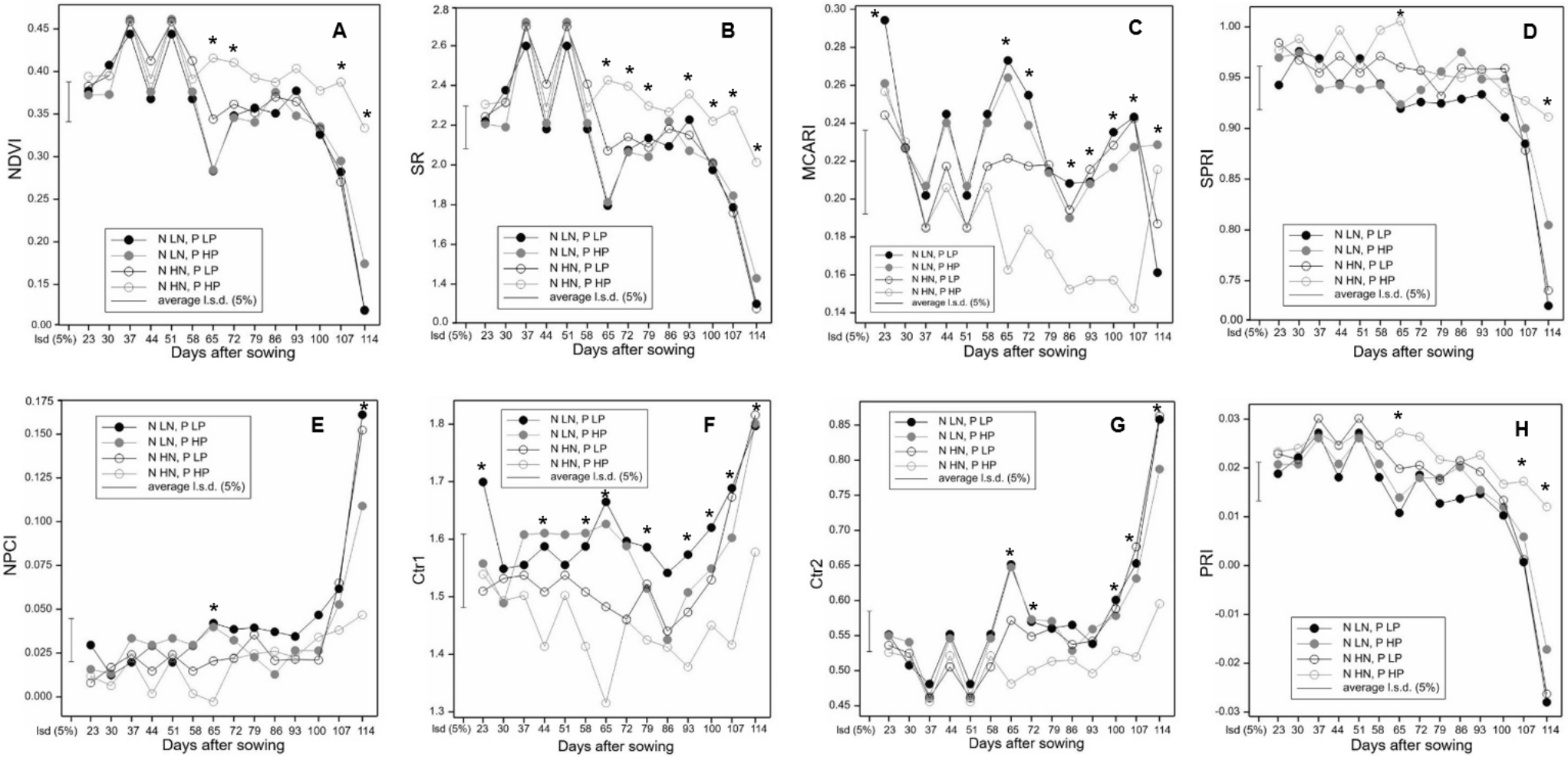
A
NDVI
B
SR
C
MCARI
D
SPRI
E
NPCI
F
Ctr1
G
Ctr2
H
PRI
N LN, P LP
N LN, P HP
N HN, P LP
N HN, P HP
average l.s.d. (5%)
lsd (5%) 23 30 37 44 51 58 65 72 79 86 93 100 107 114
Days after sowing

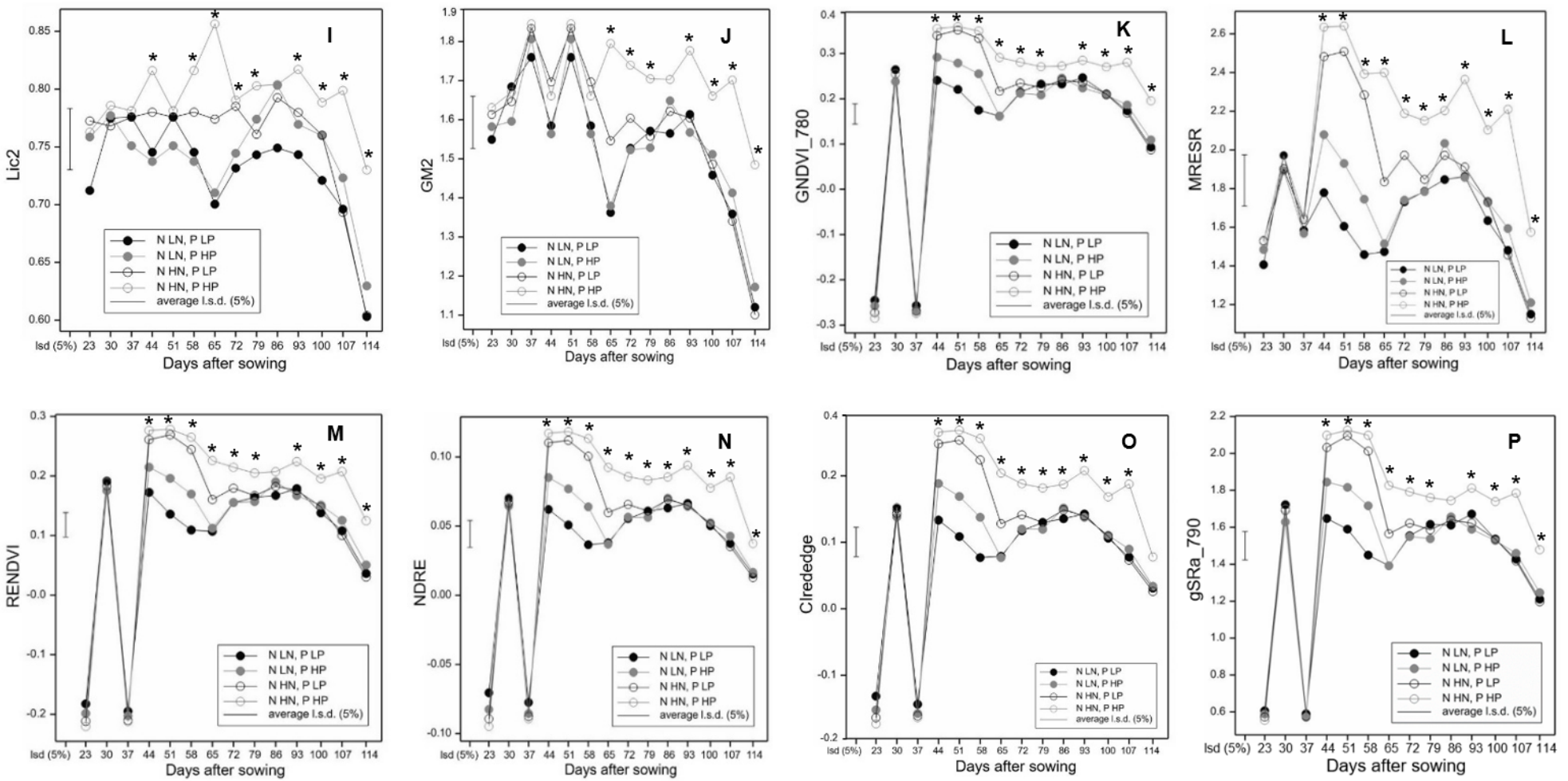

Figure 3.10. Time course of SRIs that were indicative of the combined N and P stress effect in cowpea including (A) NDVI, (B) SR, (C) MCARI, (D) SPRI, (E) NPCI, (F) Ctr1 (G) Ctr2 (H) PRI, (I) Lic2, (J) GM2, (K) GNDVI_780, (L) MRESR, (M) RENDVI, (N) NDRE, (O) CIrededge and (P) gSRa_790 showing their responses to N and P nutritional variations at several days after sowing (DAS) during the crop cycle from 23 to 114 DAS. Mean values represent five replicates per treatment condition. Bars indicate the average least significant difference (LSDs) at a 5% significance level. Asterisks (*) indicate significant difference between treatments at 5% significance level at different DAS.

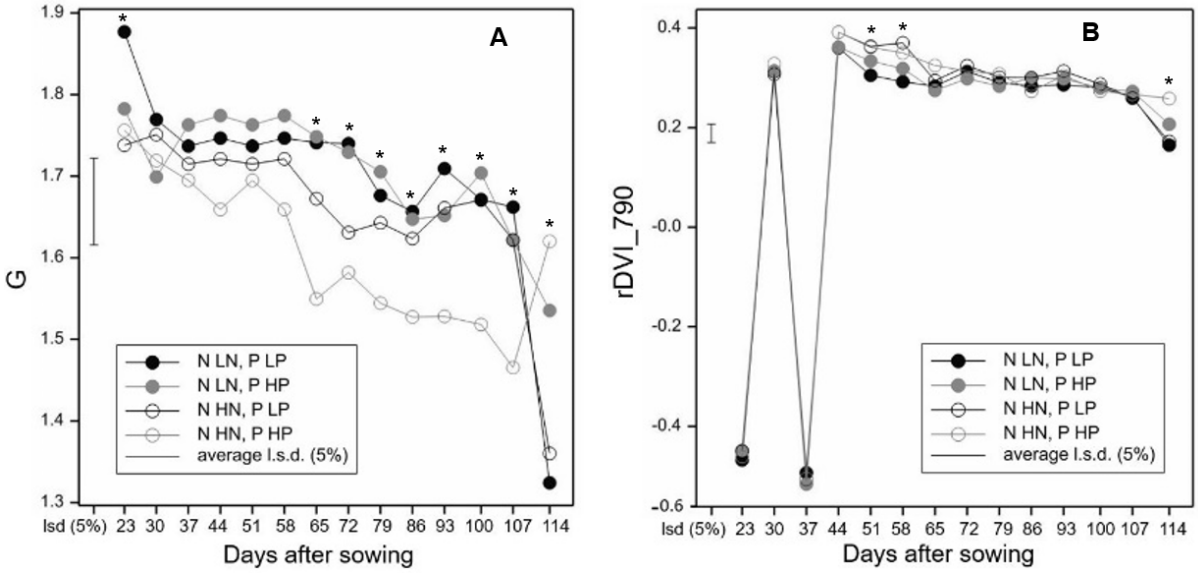

Figure 3.11. Time course of optimal N stress SRIs including (A) G and (B) rDVI_790 showing their responses to N and P nutritional variations at different days after sowing (DAS) during cowpea crop cycle from 23 to 114 DAS. Mean values represent five replicates per treatment condition. Bars indicate the average least significant difference (LSDs) at a 5% significant level. Asterisks (*) indicate significant difference between treatments at 5% significance level at different DAS.

3.3.2.3 Evaluating the agro-morpho-physiological responses under different N and P availabilities in cowpea

3.3.2.3.1 Morpho-physiological responses

The morpho-physiological responses of cowpea under varying N and P availabilities are displayed in Figure 3.12. The results showed that the mean values of LNC and LPC increased with increasing N and P supply over time with statistically significant differences between treatments observed at 44, 72 and 107 DAS (Figure 3.13A-B). High mean values were obtained for both variables in the HNHP treatment. The results as shown in Table 3.8 indicated that LNC responded significantly to N stress (p<0.001) and P stress (p<0.001) with significant (p<0.05) N×P interaction. The application of N had a significant (p<0.05) interactive effect with DAS on LNC (Table 3.8). Likewise, LPC responded significantly to both N (p<0.001) and P stress (p<0.001) but with non-significant N×P interaction (Table 3.8). Both N and P fertilisation interacted significantly (p<0.001) and (p<0.001) with DAS respectively.

SPAD values increased with increasing N and P fertilisation with significant differences between treatments observed over time except 30 and 37 DAS (Figure 3.13C). High SPAD values were obtained for HNHP treatment (Figure 3.13C). SPAD values responded

significantly to N stress (p<0.001) and P stress (p<0.001) with significant N×P interactions (p<0.01) (Table 3.8). SPAD values were significantly impacted by N×P×DAS interactions (p<0.05).

Furthermore, A_n increased along with an increase in N and P fertilisation with significant differences between treatments observed at 44, 72 and 107 DAS (Figure 3.13D). A_n values recorded for HNHP were high compared to the other treatments. The results indicate that A_n responded significantly to only N stress (p<0.001) but not P stress and was impacted significantly by DAS (p<0.001) (Table 3.8). The PH increased with increasing N and P supply with a significant difference between treatments observed at 37 and 51 DAS (Figure 3.13E). High values of PH were recorded in HNHP compared to the other treatments. The PH responded significantly to only N stress (p<0.001) and was affected significantly by DAS (p<0.001) (Table 3.8).

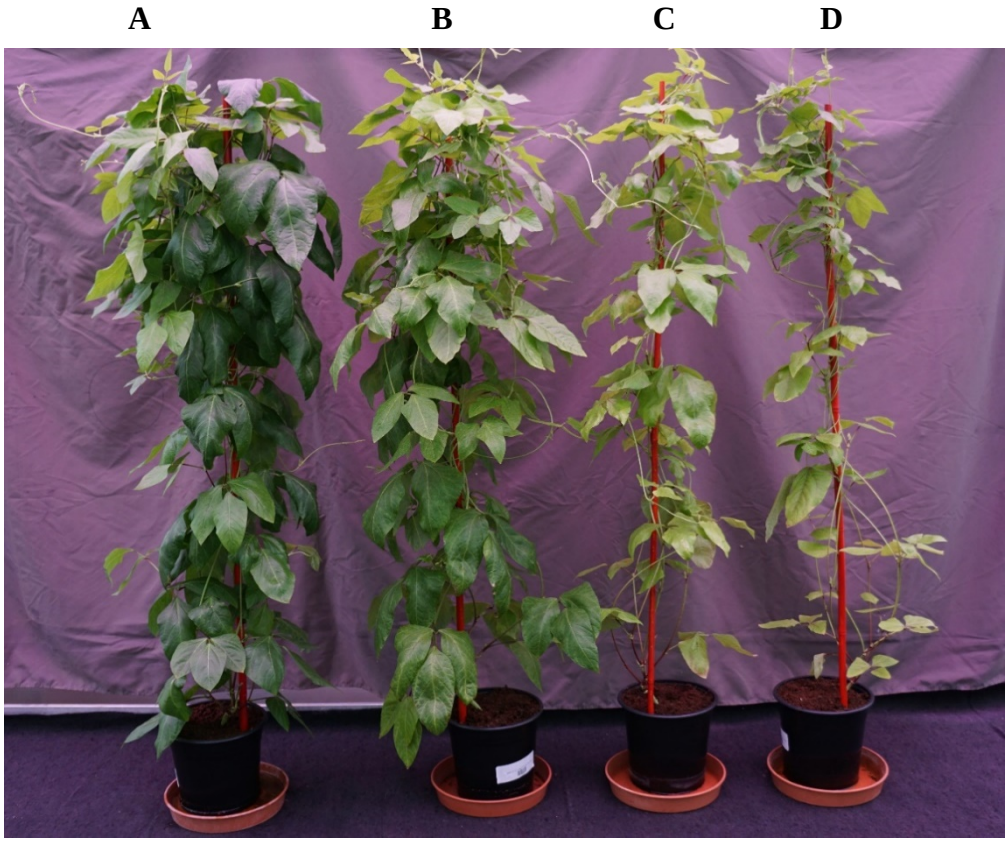

Figure 3.12. Morpho-physiological responses of cowpea assessed under different N and P availabilities. A, B, C and D indicate cowpea plants grown under HNHP, HNLP, LNHP and LNLP nutrient conditions respectively. The photograph was taken 74 days after sowing (DAS).

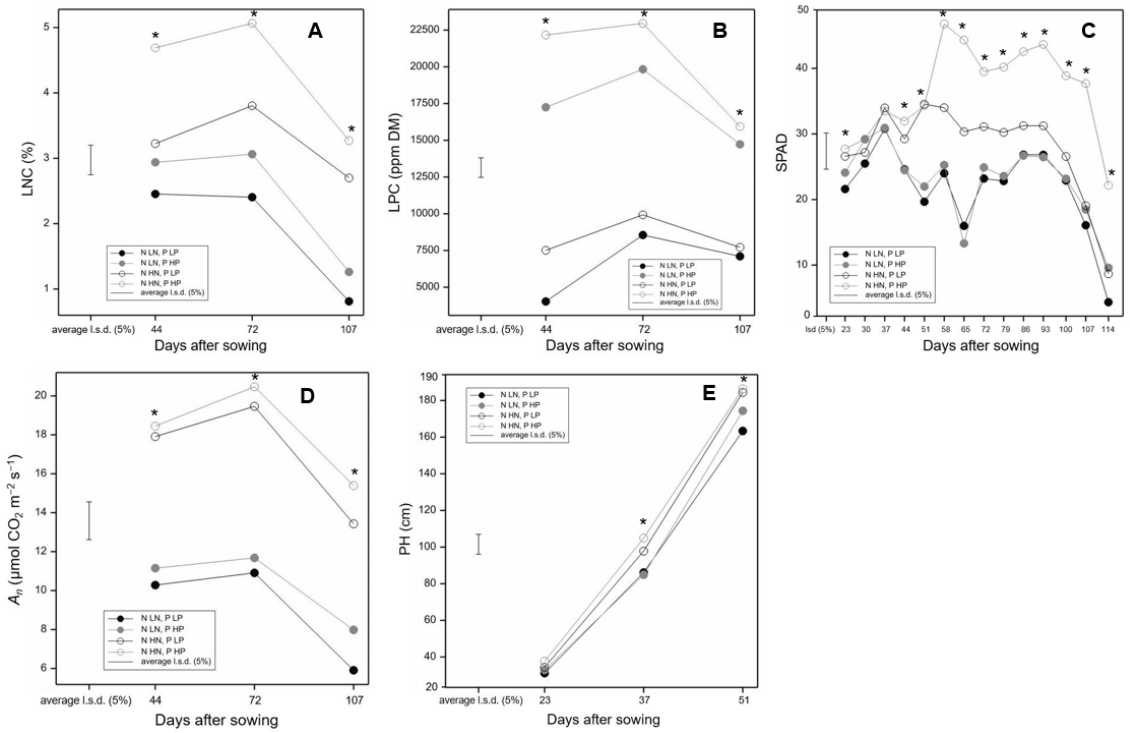

Figure 3.13. Morpho-physiological parameters including (A) LNC, (B) LPC, (C) SPAD, (D) A_n and (E) PH to different N and P availability assessed by repeated measures ANOVA (RMA). Mean values are untransformed and represent five replicates per treatment condition. Bars indicate the average least significant difference (LSD) at a 5% significance level. Asterisks (*) indicate significant difference between treatments at 5% significance level at different DAS.

Table 3.8. Test for fixed and main effects of cowpea morpho-physiological parameters including leaf nitrogen content (LNC), leaf phosphorus concentration (LPC), SPAD, photosynthetic net CO_2 assimilation (A_n) and plant height (PH) in response to the combined N and P stress assessed by repeated measures ANOVA. The F-statistics and F-Test probabilities were used to test the effects/responses of the morpho-physiological parameters to the combined nutrient stress factors as well as their interactions. Significant results are set at $p<0.05$ and are shown in bold.

Index	**N**	**P**	**N×P**	**DAS**	**N×DAS**	**P×DAS**	**N×P×DAS**
LNC (%)	$F_{1,12}$=264.951, $p<$**0.001**	$F_{1,12}$=65.707, $p<$**0.001**	$F_{1,12}$=7.995, $p<$**0.05**	$F_{2,31.6}$=125.447, $p<$**0.001**	$F_{2,31.6}$=5.339, $p<$**0.05**	$F_{2,31.6}$=3.049, p=0.062	$F_{2,31.6}$=2.042, p=0.147
LPC (ppm DM)	$F_{1,12}$=39.591, $p<$**0.001**	$F_{1,12}$=845.892, $p<$**0.001**	$F_{1,12}$=2.617, p=0.132	$F_{1.9,31}$=127.236, $p<$**0.001**	$F_{1.9,31}$=21.684, $p<$**0.001**	$F_{1.9,31}$=75.563, $p<$**0.001**	$F_{1.9,31}$=0.706, p=0.497
SPAD	$F_{1,12}$=194.851, $p<$**0.001**	$F_{1,12}$=45.860, $p<$**0.001**	$F_{1,12}$=25.748, $p<$**0.01**	$F_{5.5,88}$=32.917, $p<$**0.001**	$F_{5.5,88}$=8.391, $p<$**0.001**	$F_{5.5,88}$=2.683, $p<$**0.05**	$F_{5.5,88}$=3.120, $p<$**0.05**
A_n (µmol CO_2 m^{-2} s^{-1})	$F_{1,12}$=928.544, $p<$**0.001**	$F_{1,12}$=21.710, p=0.089	$F_{1,12}$=0.018, p=0.959	$F_{1.4,22.4}$=133.862, $p<$**0.001**	$F_{1.4,22.4}$=2.428, p=0.073	$F_{1.4,22.4}$=2.534, p=0.067	$F_{1.4,22.4}$=0.101, p=0.799
PH (cm)	$F_{1.5,24}$=35.601, $p<$**0.001**	$F_{1.5,24}$=3.826, p=0.074	$F_{1.5,24}$=0.005, p=0.946	$F_{1.5,24}$=1446.302, $p<$**0.001**	$F_{1.5,24}$=3.484, p=0.059	$F_{1.5,24}$=0.330, p=0.660	$F_{1.5,24}$=1.338, p=0.274

3.3.2.3.2 Assessment of agronomic parameters

Table 3.9 and Figure 3.14 show the responses of agronomic parameters assessed in cowpea under different N and P availabilities. All agronomic variables were responsive to N and P stress except for HSW and SY which responded only to N (Table 3.9). Mean values of the number of pods, number of seeds, HSW and SY increased with increased N and P supply except for FW and DW which had the LNLP treatment slightly higher than LNHP (Table 3.9 and Figure 3.14). The mean values of all agronomic variables obtained under the HNHP treatment were high compared to the other treatments (Table 3.9). Statistically significant differences between treatments were observed. N×P interaction was observed only for FW and DW agronomic variables (Table 3.9).

Table 3.9. Mean values and responses of cowpea agronomic parameters including fresh weight (FW), dry weight (DW), number of pods, number of seeds, hundred seed weight (HSW) and seed yield (SY) to different N and P supply. The mean values of the number of pods and number of seeds were transformed based on the $\log_{10}$ scale to achieve homogeneity of the residuals. Significant levels of agronomic responses to N, P and their interactions are set at $p<0.05$ and are shown in bold.

Parameter	**FW (g plant^{-1})**	**DW (g plant^{-1})**	**Number of pods**	**Number of seeds**	**HSW (g plant^{-1})**	**SY (g pot^{-1})**
Treatment	**Means**	**Means**	**Means**	**Means**	**Means**	**Means**
HNHP	251.90	59.55	1.70	2.65	9.01	40.60
HNLP	186.10	47.91	1.57	2.54	8.67	30.40
LNHP	76.30	29.51	1.30	2.30	7.44	14.50
LNLP	76.40	28.44	1.19	2.27	7.68	14.20
N	*p*<**0.001**	*p*<**0.001**	*p*<**0.001**	*p*<**0.001**	*p*<**0.001**	*p*<**0.001**
P	*p*<**0.05**	*p*<**0.05**	*p*<**0.001**	*p*<**0.05**	*p*=0.820	*p*=0.032
N×P	*p*<**0.05**	*p*<**0.05**	*p*=0.513	*p*=0.113	*p*=0.196	*p*=0.042

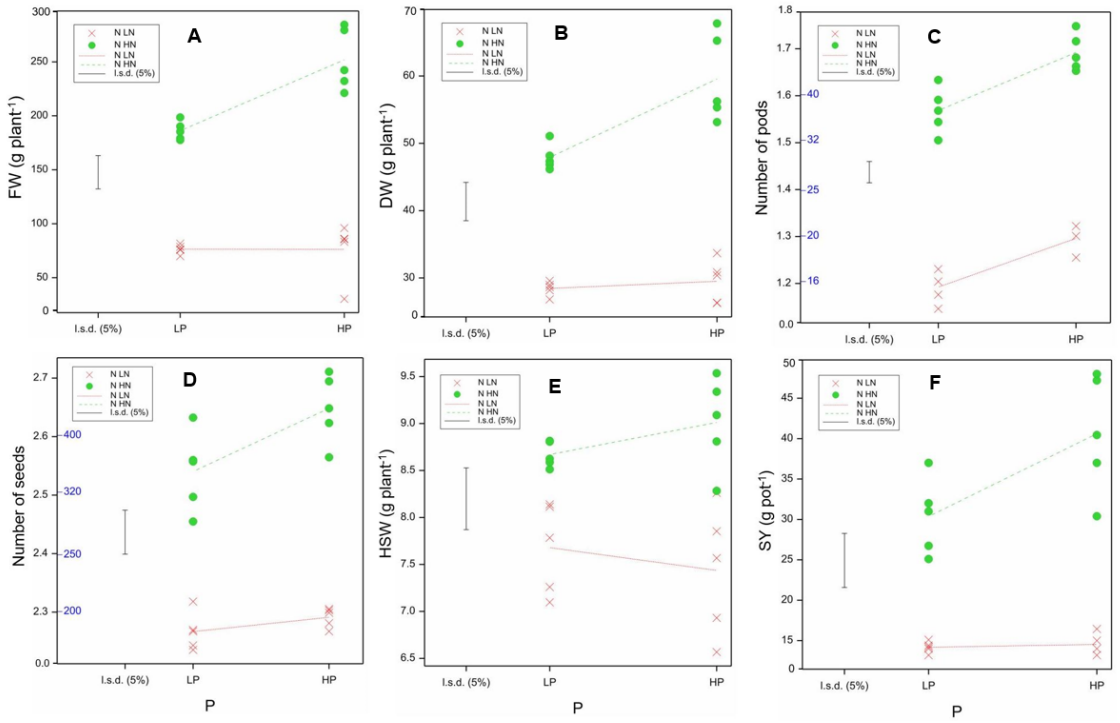

Figure 3.14. Responses of cowpea agronomic parameters including (A) FW, (B) DW, (C) number of pods, (D) number of seeds, (E) HSW and (F) SY. The mean and plotted values of the number of pods and number of seeds were transformed based on the $\log_{10}$ scale to achieve homogeneity of the residuals. Mean values represent five replicates per treatment condition. Bars indicate the average least significant difference (LSD) at a 5% significance level.

3.3.2.4 Assessing the relationship between spectral response and agro-morpho-physiological status in cowpea

To evaluate the relationships between the spectral response and cowpea agro-morpho-physiological parameters, correlation coefficients were calculated for the SRIs that were specific to N and P stress (p<0.05) (Table 3.10). Except for G, several of the SRIs significantly correlated with LNC according to the correlation analysis results (Table 3.10). The highest correlation coefficients with LNC were found among the red-edge group indices (i.e., MRESR, RENDVI, CIrededge, CIgreen, NDRE) and PRI (Table 3.10). A wide range of SRIs significantly correlated with LPC with mNDblue_530, PRI, Lic2, PRI/NDVI, GNDVI and including the red-edge group indices (i.e., MRESR, RENDVI, CIrededge, CIgreen, NDRE) obtaining the highest correlation coefficients. SRIs such as OSAVI, G, Lic1, RDVI, rDVI_790 and SRa_790 non-significantly correlated with LPC.

Almost all the SRIs significantly correlated with SPAD except for G and rDVI_790. The highest correlation coefficient with SPAD was achieved by ZMI, MRESR, Lic2, GM1, GM2, Ctr1 and Ctr2. For A_n, almost all the SRIs significantly correlated with the photosynthetic parameter except for G (Table 3.10). The highest correlation with A_n was recorded by the red-edge group indices (i.e., MRESR, RENDVI, CIrededge, NDRE) including PRI and mNDblue_530. Several of the SRIs significantly correlated with PH, with mNDblue_530, PRI_550, PRI_norm, GNDVI_780 and RENDVI obtaining the highest correlations with the plant growth parameter (Table 3.10). The SRIs that non-significantly correlated with PH included SPRI, NPCI, Ctr1, Lic2, RDVI and PRI/NDVI.

Additionally, most of the SRIs significantly correlated with FW except for G, MCARI, PRI_550, PRI_norm, PRI/NDVI and rDVI_790 (Table 3.10). A similar pattern of correlation was observed for DW, number of pods, number of seeds and SY with a wide range of SRIs significantly correlating with the agronomic variables. The highest correlation coefficients were recorded across the agronomic variables by SRIs including the red-edge group indices (i.e., MRESR, RENDVI, CIrededge, NDRE, CIgreen), GM1, GM2 and ZMI. However, SRIs such as G, MCARI, PRI_550, PRI_norm, PRI/NDVI and rDVI_790 non-significantly correlated with the agronomic variables (Table 3.10). All SRIs except for mNDblue_530 showed no significant correlation with HSW (Table 3.10).

Table 3.10. Correlation analysis between nutrient stress (N and P) responsive spectral indices and agro-morpho-physiological parameters assessed in cowpea. The data from spectral reflectance measurements and sampling points of agro-morpho-physiological parameters measured at the same time were used. For LNC, LPC and A_n, correlations with SRIs were implemented at 44, 72 and 107 DAS. PH and SRIs were correlated using data at 23, 37 and 51 DAS. Correlation between SPAD and SRIs were correlated using data from 23 to 114 DAS. Additionally, correlation between agronomic parameters including FW, DW, number of pods, number of seeds, HSW and SY and SRIs were achieved at 114 DAS at final harvest. Values are Pearson correlation coefficient (r) between spectral reflectance indices and agro-morpho-physiological stress parameters. Significant r values at $p<0.05$ are indicated in bold.

Index	LNC (%)	LPC (ppm DM)	SPAD	A_n (µmol CO_2 m^{-2} s^{-1})	PH (cm)	FW (g $plant^{-1}$)	DW (g $plant^{-1}$)	Number of Pods	Number of Seeds	HSW (g $plant^{-1}$)	SY (g pot^{-1})
NDVI	**0.59**	**0.33**	**0.64**	**0.57**	**0.68**	**0.56**	**0.55**	**0.58**	**0.55**	0.35	**0.54**
SR	**0.59**	**0.32**	**0.61**	**0.58**	**0.68**	**0.59**	**0.57**	**0.59**	**0.57**	0.39	**0.56**
OSAVI	**0.52**	0.23	**0.55**	**0.48**	**0.44**	**0.47**	**0.47**	**0.52**	**0.48**	0.26	**0.47**
G	-0.13	-0.21	-0.08	-0.23	**-0.35**	0.28	0.28	0.37	0.32	0.07	0.30
MCARI	**-0.36**	**-0.34**	**-0.42**	**-0.41**	**-0.65**	0.07	0.08	0.18	0.15	-0.13	0.13
TCARI	**0.40**	**0.31**	**0.58**	**0.38**	**0.69**	**0.49**	**0.49**	**0.52**	**0.45**	0.34	**0.45**
ZMI	**0.57**	**0.34**	**0.74**	**0.58**	**0.64**	**0.60**	**0.58**	**0.61**	**0.58**	0.43	**0.58**
SPRI	**0.54**	**0.34**	**0.58**	**0.52**	-0.14	**0.48**	**0.49**	**0.52**	**0.45**	0.23	0.43
PRI	**0.65**	**0.39**	**0.65**	**0.60**	**0.40**	**0.54**	**0.54**	**0.56**	**0.51**	0.29	**0.50**
NPCI	**-0.54**	**-0.34**	**-0.57**	**-0.52**	0.22	**-0.45**	**-0.46**	**-0.49**	-0.42	-0.21	-0.40
Ctr1	**-0.50**	**-0.36**	**-0.68**	**-0.54**	-0.16	**-0.52**	**-0.53**	**-0.50**	-0.44	-0.34	-0.43
Ctr2	**-0.57**	**-0.34**	**-0.68**	**-0.55**	**-0.68**	**-0.55**	**-0.54**	**-0.57**	**-0.54**	-0.34	**-0.53**
Lic1	**0.49**	0.22	**0.52**	**0.44**	**0.55**	**0.47**	**0.46**	**0.51**	**0.47**	0.26	**0.46**
Lic2	**0.52**	**0.37**	**0.70**	**0.54**	0.24	**0.58**	**0.59**	**0.58**	**0.51**	0.37	**0.50**
GM1	**0.57**	**0.32**	**0.68**	**0.59**	**0.71**	**0.61**	**0.60**	**0.60**	**0.58**	0.43	**0.57**
GM2	**0.58**	**0.33**	**0.70**	**0.59**	**0.67**	**0.60**	**0.59**	**0.61**	**0.58**	0.42	**0.58**
RDVI	**0.51**	0.20	**0.55**	**0.49**	-0.16	**0.46**	**0.45**	**0.51**	**0.47**	0.23	**0.46**
PRI_550	**-0.55**	**-0.35**	**-0.17**	**-0.59**	**0.90**	-0.36	-0.39	-0.39	-0.30	-0.10	-0.28
PRI_norm	**-0.55**	**-0.35**	**-0.17**	**-0.59**	**0.90**	-0.36	-0.39	-0.39	-0.30	-0.10	-0.28
PRI/NDVI	**0.58**	**0.37**	**0.45**	**0.52**	0.18	0.35	0.36	0.42	0.34	0.14	0.33
GNDVI_780	**0.62**	**0.37**	**0.18**	**0.57**	**0.89**	**0.58**	**0.57**	**0.57**	**0.54**	0.37	**0.53**
MRESR	**0.66**	**0.42**	**0.70**	**0.64**	**0.72**	**0.62**	**0.63**	**0.62**	**0.59**	0.40	**0.58**

RENDVI	**0.64**	**0.39**	**0.23**	**0.60**	**0.88**	**0.60**	**0.60**	**0.60**	**0.57**	0.38	**0.56**
NDRE	**0.63**	**0.39**	**0.26**	**0.59**	**0.87**	**0.58**	**0.57**	**0.60**	**0.57**	0.38	**0.56**
CIgreen	**0.61**	**0.36**	**0.30**	**0.56**	**0.88**	**0.60**	**0.59**	**0.58**	**0.55**	0.39	**0.54**
CIrededge	**0.63**	**0.39**	**0.30**	**0.59**	**0.87**	**0.59**	**0.58**	**0.60**	**0.57**	0.38	**0.56**
mNDblue_530	**-0.59**	**-0.43**	**-0.20**	**-0.62**	**0.92**	**-0.54**	**-0.54**	-0.44	-0.41	**-0.48**	-0.41
rDVI_790	**0.44**	0.09	0.02	**0.35**	**0.87**	0.38	0.38	0.44	0.40	0.12	0.38
gSRa_790	**0.61**	**0.36**	**0.30**	**0.56**	**0.88**	**0.60**	**0.59**	**0.58**	**0.55**	0.39	**0.54**
SRa_790	**0.48**	0.23	**0.21**	**0.39**	**0.88**	**0.48**	**0.48**	**0.51**	**0.48**	0.26	**0.46**

3.4 Discussion

3.4.1 Identification of optimal spectral reflectance indices for N and P status in quinoa and cowpea

One of the key objectives of this study was to identify optimal SRIs capable of distinguishing between individual and combined N and P stresses in quinoa and cowpea. The results revealed a wide range of SRIs including NDVI, SR, OSAVI, G, MCARI, TCARI, ZMI, SPRI, PRI, NPCI, Ctr1, Ctr2, Lic1, Lic2, GM1, GM2, GNDVI_780, MRESR, RENDVI, NDRE, CIgreen, CIrededge, mNDblue_530, gSRa_790 and SRa_790 that were responsive to N stress in both crops (Table 3.3 and Table 3.7). The high response of these SRIs to N stress could be explained by their sensitivity to the leaf chlorophyll content and the LNC, which is directly related to the N status (Prey and Schmidhalter, 2019). As there is less chlorophyll in the leaves when there is N deficiency, the spectral reflectance of the leaves is generally higher in the green and red edge regions (Tian et al., 2014; Zhao et al., 2018). Most of these SRIs are responsive to N stress in several crops (Kanke et al., 2011; Ranjan et al., 2012; Li et al., 2014; Lu et al., 2023).

SRIs comprising SR, PRI, Ctr1, Lic2, GM1, GM2, PRI_550, MRESR, RENDVI, NDRE, CIgreen, CIrededge, mNDblue_530 and gSRa_790 were responsive to P stress in both crops (Table 3.3 and Table 3.7). Leaf spectral reflectance in the visible range (350-750 nm) may increase when there is a P deficiency (Zhang et al., 2023). One of the distinctive responses of plants to P deficiency is the apparent accumulation of anthocyanin which enhances the red coloration of the leaf and further alters the spectral reflectance characteristics of leaves (Wang et al., 2020; El-Mejjaouy et al., 2023; Siedliska et al., 2023). In a study, Kawamura et al. (2011), demonstrated many of the SRIs identified in this study to be responsive to P stress in a legume-based pasture. According to the authors, the PRI showed the highest coefficient of determination for most of the P status variables.

In this study, the combined N and P stress was detected in both crops by similar SRIs such as SR, PRI, Ctr1, Lic2, GM1, GM2, MRESR, RENDVI, NDRE, CIgreen, CIrededge, mNDblue_530 and gSRa_790 (Table 3.3 and Table 3.7), suggesting that these indices could be indicative of both stresses but may not be specific for their

detection. Therefore, based on the present results, SRIs that indicate specificity and are optimal for N stress detection in quinoa are NDVI, OSAVI, G, MCARI, TCARI, ZMI, SPRI, NPQI, NPCI, Ctr2, Lic1, SIPI, CRI1, CRI2, RDVI, GNDVI_780 and SRa_790 (Table 3.3; Figure 3.5). On the other hand, SRIs that indicated specificity and were optimal for N stress detection in cowpea included G and rDVI_790 (Table 3.7; Figure 3.11). The SRIs including RVI, RDVI and OSAVI were used to determine optimal wavebands to discriminate N status in wheat (Lunagaria et al., 2015). The authors revealed that the red edge inflection point (REIP) at 733–736 nm was found to be the most responsive to N status among all SRIs. Furthermore, the results presented here show that the two SRIs that indicated specificity for P stress detection in quinoa included mNDblue_730 and PRI_550 (Table 3.3; Figure 3.6). However, no SRI was identified to be optimal for P stress detection in cowpea (Table 3.7), necessitating further studies.

In this study, SRIs such as MCARI1, TVI, ARI1 and ARI2 showed no response to N and P stresses in both crops (Table 3.3 and Table 3.7) and could be due to the saturation of these indices which resulted in insensitivity to both stress factors (Mutanga et al., 2023). Generally, SRIs may not respond to N and P stress because the changes in crop growth, reduced canopy cover, chlorophyll content and biomass production caused by nutrient deficiency do not significantly affect the spectral reflectance (Peng et al., 2020). However, it is important to note that the effectiveness of responsive SRIs can vary depending on factors such as crop type, growth stage and environmental conditions.

3.4.2 Detection of nutritional variations by spectral reflectance indices

The application of spectral reflectance technologies for early detection of crop nutritional status is vital for precision fertilisation management and ensuring sustainable and efficient agricultural practices (Huang et al., 2020; Lu et al., 2023). With the use of spectral sensors, this method measures crop reflectance at different wavelengths, which can be indicative of specific nutrient deficiency at a particular crop growth stage (Siedliska et al., 2021). However, there is limited research on the use of this technology for monitoring the complex nutritional status of quinoa and cowpea. This present study sought to bridge this gap by monitoring both N and P status in these crops during the entire growth period using SRIs derived from a contact proximal sensor. The results showed the early detection of N and P nutritional variations coupled with better

separation between the treatment conditions at the early growth stage in quinoa by SRIs including MCARI, GNDVI_780, SRa_790, NDVI, G, TCARI and ZMI from 37-44 DAS (Figure 3.5). For cowpea, SRIs such as MCARI, Ctr1 and G demonstrated early detection of N and P nutritional variations at 23 DAS (Figure 3.10). This result suggests that these SRIs could be effective for monitoring the complex nutritional status of these crops throughout the growing season and most importantly, at the early growth stages. Real-time and early detection of nutritional variations enables growers to fine-tune their fertilisation regime, minimise stress conditions, maintain optimal plant growth, reduce significant yield losses, and ultimately maximise crop productivity (Huang et al., 2020; Lu et al., 2023). Additionally, early detection of nutritional variations is important for ensuring efficient use of resources and reducing environmental pollution. In this study, detection of N and P nutritional variations by SRIs was faster in cowpea compared to quinoa. The ability of leguminous crops to fix atmospheric N could alter spectral reflectance to nutrient variations.

The use of spectral reflectance to detect N and P variations in various crops has been reported (Osborne, 1999; Patil et al., 2007; Özyiğit et al., 2013; Cudjoe et al., 2023b). For instance, NDVI was effective in detecting early N and P variations in quinoa and at various time points during the crop cycle (Cudjoe et al., 2023b).

This study also revealed the effectiveness of SRIs comprising OSAVI, SPRI, NPCI and PRI_550 that detected N and P nutritional variations only at later growth stages, especially for quinoa (Figure 3.5). The late detection of crop nutritional stress may limit the timely implementation of corrective fertilisation measures, leading to potential yield losses and reduced plant health. Therefore, it is crucial to employ effective monitoring and detection techniques (i.e., optimal SRIs) to identify and address crop nutritional stress promptly to mitigate its implications on crop yield and plant health. The impact of late detection of crop nutritional stress can vary depending on the specific nutrient deficiency and the stage of plant growth. While SRIs can respond to N and P stress, the response is complex and can be influenced by various factors, including the specific plant species, growth stage, the nutrients involved and the environmental conditions (Peng et al., 2020). Therefore, it is crucial to consider these factors when interpreting spectral reflectance data in the context of complex nutrient stress. Further work is required to validate the findings beyond the glasshouse settings for wider applicability.

3.4.3 Morpho-physiological responses under varying N and P availabilities

These findings showed an overall positive response to the simultaneous application of the different levels of N and P treatments, which was mainly reflected in the significant increases in morpho-physiological metrics measured in both crops (Figure 3.8; Figure 3.13). This result can be explained by the fact that there was an increase in N uptake and LNA when P levels in the plant were adequate or high while increasing the N supply increased the P uptake and concentration (Agren et al., 2012; Duncan et al., 2018a). This N-P nutritional interaction influenced the SPAD chlorophyll content and C assimilation for photosynthesis. The N:P ratio in plant tissues, particularly leaves, is a widely used indicator to predict N or P limitation to plant productivity (Cleveland et al., 2011; Jiang et al., 2019). A large body of research has proven synergetic plant growth responses and N and P uptake on a global scale (Schleuss et al., 2020; Wang et al., 2022; Xia et al., 2023). The mechanisms that cause synergistic responses of plant growth to multiple nutrient addition have been shown that plants and microbes adapt mechanisms of nutrient uptake or change allocation patterns, in the way that they trade one nutrient they have in excess into the acquisition of a limiting nutrient until their growth is co-limited by both nutrients (Jiang et al., 2019; Xia et al., 2023).

Recently, Hu and Chu (2020) assessed the growth performance and N/P utilisation of plants under different N–P conditions. The authors demonstrated that due to imbalanced N–P nutrition, a high P supply cannot stimulate plant growth under low N conditions. However, plant growth can be effectively stimulated by a high P supply in high N availability when they receive an optimally balanced N–P nutrition and this reflects the results in this present study (Figure 3.8; Figure 3.13). The findings reported in this thesis contradict Taaime et al. (2023) where high N and P fertilisation did not result in a concomitant increase in chlorophyll content and PH in quinoa grown under semi-arid conditions.

3.4.4 Agronomic responses under varying N and P availabilities

A positive effect of the combined application of N and P was observed on agronomic metrics: VB, TPB and GY but not TGW in quinoa (Table 3.5 and Figure 3.9). However, no interactive effect of N and P was observed in all these variables probably due to the enhanced N limitation. For cowpea, the average values for agronomic metrics such as

the number of pods, number of seeds, HSW and SY demonstrated an upward trend with higher N and P supply. However, in the case of FW and DW, the treatment with LNLP showed marginally higher values compared to the treatment with LNHP with N×P interaction (Table 3.9; Figure 3.14). The individual and combined application of N and P significantly increased the aboveground biomass with uniformly synergistic interaction (Jiang et al., 2019). Likewise, a synergistic interaction of N and P co-fertilisation on yield in many crops including wheat, millet, rice, sorghum, corn, etc., has been reported (Aulakh and Aulakh, 2005; Rietra et al., 2017; Schlegel and Bond, 2017; Grohskopf et al., 2019). The present results disagree with Taaime et al. (2023) who reported a high biomass and GY in quinoa with low N and high P fertilisation in the dry areas of Morocco. This highlights the need to maintain an optimally balanced nutrient for plant growth, biomass accumulation, tissue nutrient concentrations and crop productivity.

3.4.5 Assessing how well the spectral response reflected the morpho-physiology and crop performance

In the present study, SRIs that were optimal for assessing the N and P status separately in quinoa and cowpea were evaluated for their relationship with the morpho-physiological and agronomic parameters through correlation analysis (Table 3.6 and Table 3.10). Remarkably, the present findings showed a wide range of significant correlations between the SRIs (e.g., NDVI, SR, MCARI, OSAVI, Ctr2, Lic1, Lic2, GM1, GM2, PRI_norm RDVI, GNDVI_780, MRESR, RENDVI, NDRE, CIrededge, SRa_790, SIPI, SPRI, mNDblue_730 and PRI_550) with LNC, LPC, SPAD, A_n and PH in quinoa and cowpea (Table 3.6 and Table 3.10).

The sensitivity of these SRIs to the physiological changes in different leaf pigment pools (i.e., chlorophyll and anthocyanin) may be the cause of the significant correlations between the indices and the morpho-physiological parameters (Sims and Gamon, 2002; Hallik et al., 2017). Several of these SRIs have been reported to correlate significantly with crop morpho-physiological parameters under different stress conditions (Patil et al., 2007; Rodriguez et al., 2006). For instance, NDVI showed a significant relationship with morpho-physiological parameters (i.e., chlorophyll content and PH) under multiple stress conditions that resulted in the discrimination of stressed and unstressed soybean crops (Patil et al., 2007). The present results suggest that many of these SRIs could be

used for non-destructive monitoring of quinoa and cowpea morpho-physiological status under complex nutrient deficit conditions.

Furthermore, SRIs comprising NDVI, OSAVI, G, ZMI, Ctr2, Lic1, RDVI, SIPI and SPRI correlated significantly with agronomic parameters (VB, TPB and GY) except for TGW in quinoa. In cowpea, SRIs such as NDVI, SR, OSAVI, TCARI, ZMI, SPRI, PRI, Lic1, Lic2, GM1, GM2, GNDVI_780, MRESR, RENDVI, NDRE, CIrededge and gSRa_790 correlated strongly with agronomic parameters: FW, DW, number of pods, number of seeds and SY except for HSW. A study on maize varieties with different N efficiencies found that N fertilisation significantly increased SRIs such as NDVI and GOSAVI, and these indices were highly correlated with yield, dry matter and LNC at different grain filling stages (Zhao et al., 2023). The present results suggest that these SRIs could be used as predictors to assess the crop performance of quinoa but not for TGW and HSW in cowpea. A study on wheat grain development suggested that the regulation of carbohydrate levels during development is highly sophisticated and may impact grain weight (Whan et al., 2014). Therefore, the relationship between spectral indices and TGW and HSW is complex and may be influenced by multiple factors that can vary depending on the specific stress conditions and crop types.

3.5 Conclusions

The potential of SRIs for distinguishing between the N and P nutritional status in quinoa and cowpea at the leaf scale using contact PS is demonstrated in this study. The results revealed a wide range of SRIs including NDVI, SR, OSAVI, G, MCARI, TCARI, ZMI, SPRI, PRI, NPCI, Ctr1, Ctr2, Lic1, Lic2, GM1, GM2, GNDVI_780, MRESR, RENDVI, NDRE, CIgreen, CIrededge, mNDblue_530, gSRa_790 and SRa_790 that were responsive to N stress in both crops. However, SRIs that indicated specificity and optimal for N stress detection in quinoa were NDVI, OSAVI, G, MCARI, TCARI, ZMI, SPRI, NPQI, NPCI, Ctr2, Lic1, SIPI, CRI1, CRI2, RDVI, GNDVI_780 and SRa_790. On the other hand, SRIs that indicated specificity and were optimal for N stress detection in cowpea included G and rDVI_790. For P status, the two SRIs that were optimal and showed specificity for their detection in quinoa were mNDblue_730 and PRI_550. Contrarily, no SRI was identified to be specific for P status in cowpea requiring further research.

In this study, the feasibility of applying spectral reflectance data to detect early nutritional variations during the crop cycle of quinoa and cowpea was evaluated. The results indicated that it was possible to detect early N and P nutritional variations in tandem with better separation between the treatment conditions at the early critical growth stages by SRIs including GNDVI_780, SRa_790, MCARI, NDVI, G, TCARI, Ctr2 and ZMI in quinoa from 37-44 DAS. For cowpea, SRIs such as MCARI, Ctr1 and G demonstrated early detection of N and P nutritional variations at 23 DAS. The implications for this result are that growers of these crops can adjust their fertilisation schedule, reduce stress conditions, maintain optimal plant growth, minimise significant yield losses and increase their crop productivity when nutritional variations are detected in real-time and at an early stage.

Additionally, the present findings showed that the concurrent application of the various levels of N and P nutrients produced an overall positive response. This was primarily reflected by the notable increases in morpho-physiological parameters including LNC, LPC, SPAD, A_n and PH in both crops. Again, applying N and P together had a beneficial impact on agronomic parameters such as VB, TPB and GY but not for TGW in quinoa. For cowpea, the average values for agronomic metrics such as FW, DW, number of pods, number of seeds and SY demonstrated an upward trend with higher N and P supply. This highlights the need to maintain optimally balanced nutrients for tissue nutrient concentrations, chlorophyll content, photosynthetic capacity, plant growth, biomass accumulation and crop productivity.

In the present study, several SRIs that were optimal for assessing the N and P status in both crops also showed strong significant relationships with the agro-morpho-physiological parameters investigated. The strong significant relationships suggest that these SRIs hold the potential to accurately estimate different agro-morpho-physiological traits in a rapid, low-cost and non-destructive manner under controlled conditions. Validation using a spectroradiometer with a wider wavelength range or a RS tool over various plant species exposed to varying levels of N and P supplies is necessary to ensure the applicability of these findings as a guide for monitoring the nutritional status and agro-morpho-physiological crop performance in these crops. Future work on this study will focus on scaling up these findings for field phenotyping in Africa, which

could be crucial for PA and provide support for the development of portable sensors for field phenotyping.

References

Abebe, B. K and Alemayehu, M. T. (2022). A review of the nutritional use of cowpea (*Vigna unguiculata* L. Walp) for human and animal diets. *Journal of Agriculture and Food Research*, 10, 100383. https://doi.org/10.1016/j.jafr.2022.100383

Adolf, V. I., Jacobsen, S.-E., and Shabala, S. (2013). Salt tolerance mechanisms in quinoa (*Chenopodium quinoa* Willd.). *Environmental and Experimental Botany*, 92:43-54. https://doi.org/10.1016/j.envexpbot.2012.07.004

Agren, G. I., Wetterstedt, J. A., and Billberger, M. F. (2012). Nutrient limitation on terrestrial plant growth–modelling the interaction between nitrogen and phosphorus. *New Phytologist*, 194, 953-960. https://doi.org/10.1111/j.1469-8137.2012.04116.x

Ahamed, N. T., Singhal, R. S., Kulkarni, P. R., and Pal, M. (1998). A lesser-known grain, Chenopodium quinoa: Review of the chemical composition of its edible parts. *Food and Nutrition Bulletin*, 19 (1), 61-70.

Ain, Q. T., Siddique, K., Bawazeer, S., Ali, I., Mazhar, M., Rasool, R., and Jafar, T. H. (2023). Adaptive mechanisms in quinoa for coping in stressful environments: an update. *PeerJ*, 11, e14832. https://doi.org/10.7717/peerj.14832

Alharbi, S. F. (2018). Evaluation of Phosphorus Use Efficiency in Winter Wheat Varieties and Using Optical Sensors to Predict the Maize Population (*Zea mays* L.) (Doctoral dissertation, Oklahoma State University).

Aluwi, N., Murphy, K. M., and Ganjyal, G. M. (2017). Physicochemical characterisation of different varieties of quinoa. *Cereal Chemistry*, 94, 847-856.

Alvar-Beltrán, J., Fabbri, C., Verdi, L., Truschi, S., Dalla Marta, A., and Orlandini, S. (2020). Testing proximal optical sensors on quinoa growth and development. *Remote Sensing*, 12 (12), 1958. https://doi.org/10.3390/rs12121958.

Alvar-Beltrán, J., Napoli, M., Dao, A., Ouattara, A., Verdi, L., Orlandini, S., and Dalla Marta, A. (2021). Nitrogen, phosphorus and potassium mass balances in an irrigated quinoa field. *Italian Journal of Agronomy*, 16 (3).

Aulakh, M. S and Aulakh, N. S. (2005). Interactions of nitrogen with other nutrients and water: effect on crop yield and quality, nutrient use efficiency, carbon sequestration and environmental pollution. *Advances in Agronomy*, 86:341-409. https://doi.org/10.1016/S0065-2113(05)86007-9

Barnes, J. D., Balaguer, L., Manrique, E., Elvira, S., and Davison, A. W. (1992). A reappraisal of the use of DMSO for the extraction and determination of chlorophylls a and b in lichens and higher plants. *Environmental and Experimental Botany*, 32 (2), 85-100.

Bazile, D., Jacobsen, S.-E., and Verniau, A. (2016). The global expansion of quinoa: Trends and limits. *Frontiers in Plant Science*, 7, 622.

Carter, G. A and Miller, R. L. (1994). Early detection of plant stress by digital imaging within narrow stress-sensitive wavebands. *Remote Sensing of Environment*, 50 (3), 295-302. https://doi.org/10.1016/0034-4257(94)90079-5

Chawade, A., van Ham, J., Blomquist, H., Bagge, O., Alexandersson, E., and Ortiz, R. (2019). High-throughput field phenotyping tools for plant breeding and precision agriculture. *Agronomy*, 9, 258.

Chen, H., Zhang, W., Gurmesa, G. A., Zhu, X., Li, D., and Mo, J. (2017). Phosphorus addition affects soil nitrogen dynamics in a nitrogen□saturated and two nitrogen□ limited forests. *European Journal of Soil Science*, 68 (4), 472-79. https://doi.org/10.1111/ejss.12428

Chen, J. M. (1996). Evaluation of vegetation indices and a modified simple ratio for boreal applications. *Canadian Journal of Remote Sensing*, 22 (3), 229-242. https://doi.org/10.1080/07038992.1996.10855178

Chlingaryan, A., Sukkarieh, S., and Whelan, B. (2018). Machine learning approaches for crop yield prediction and nitrogen status estimation in precision agriculture: A review. *Computers and Electronics in Agriculture*, 151, 61-69.

Choukr-Allah, R., Rao, N. K., Hirich, A., Shahid, M., Alshankiti, A., Toderich, K., and Butt, K. U. R. (2016). Quinoa for marginal environments: toward future food and nutritional security in MENA and Central Asia regions. *Frontiers in Plant Science*, 7, 346. https://doi.org/10.3389/fpls.2016.00346

Cleveland, C. C., Townsend, A. R., Taylor, P., Alvarez□Clare, S., Bustamante, M. M., Chuyong, G., and Wieder, W. R. (2011). Relationships among net primary productivity, nutrients and climate in tropical rain forest: a pan□tropical analysis. *Ecology letters*, 14 (9), 939-947.

Cudjoe, D. K., Virlet, N., Castle, M., Riche, A. B., Mhada, M., Waine, T. W., Mohareb, F., and Hawkesford, M. J. (2023a). Field phenotyping for African crops: overview and perspectives. *Frontiers in Plant Science*, 14. https://doi.org/10.3389/fpls.2023.1219673

Cudjoe, D. K., Okyere, F. G., Virlet, N., Castle, M., Buchner, P., Parmar, S., Sadeghi-Tehran, P., Riche, A., Sohail, Q., Mhada, M., Ghanem, M., Waine, T. W., Mohareb, F., and Hawkesford, M. J. (2023b). Using proximal sensing parameters linked to the photosynthetic capacity to assess the nutritional status and yield potential in quinoa. *Acta Horticulturae*, 1360, 373-379. https://doi.org/10.17660/ActaHortic.2023.1360.45

Dakhili, S., Abdolalizadeh, L., Hosseini, S. M., Shojaee-Aliabadi, S., and Mirmoghtadaie, L. (2019). Quinoa protein: Composition, structure and functional properties. *Food Chemistry*, 299, 125161.

Darra, N., Psomiadis, E., Kasimati, A., Anastasiou, A., Anastasiou, E., and Fountas, S. (2021). Remote and proximal sensing-derived spectral indices and biophysical

variables for spatial variation determination in vineyards. *Agronomy*, 11 (4), 741. https://doi.org/10.3390/agronomy11040741

Daughtry, C. S., Walthall, C. L., Kim, M. S., De Colstoun, E. B., and McMurtrey Iii, J. E. (2000). Estimating corn leaf chlorophyll concentration from leaf and canopy reflectance. *Remote Sensing of Environment*, 74 (2), 229-239. https://doi.org/10.1016/S0034-4257(00)00113-9

Dong, K., Li, W., Tang, Y., Ma, S., and Jiang, M. (2023). Co-limitation of N and P is more prevalent in the Qinghai-Tibetan Plateau grasslands. *Frontiers in Plant Science*, 14, 1140462. https://doi.org/10.3389/fpls.2023.1140462

Duncan, E. G., O'Sullivan, C. A., Roper, M. M., Palta, J., Whisson, K., and Peoples, M. B. (2018a). Yield and nitrogen use efficiency of wheat increased with root length and biomass due to nitrogen, phosphorus, and potassium interactions. *Journal of Plant Nutrition and Soil Science*, 181 (3), 364-373. https://doi.org/10.1002/jpln.201700376.

Duncan, E. G., O'Sullivan, C. A., Roper, M. M., Biggs, J. S., and Peoples, M. B. (2018b). Influence of co-application of nitrogen with phosphorus, potassium and sulphur on the apparent efficiency of nitrogen fertiliser use, grain yield and protein content of wheat. *Field Crops Research*, 226, 56-65.

Eitel, J. U. H., Long, D. S., Gessler, P. E., and Hunt, E. R. (2008). Combined spectral index to improve ground□based estimates of nitrogen status in dryland wheat. *Agronomy Journal*, 100 (6), 1694-1702.

El-Mejjaouy, Y., Belmrhar, L., Zeroual, Y., Dumont, B., Mercatoris, B., and Oukarroum, A. (2023). PCA-based detection of phosphorous deficiency in wheat plants using prompt fluorescence and 820 nm modulated reflection signals. *Plos One*, 18 (5), e0286046.

Elser, J. J., Bracken, M. E., Cleland, E. E., Gruner, D. S., Harpole, W. S., Hillebrand, H., and Smith, J. E. (2007). Global analysis of nitrogen and phosphorus limitation of primary producers in freshwater, marine and terrestrial ecosystems. *Ecology Letters*, 10 (12), 1135-1142. https://doi.org/10.1111/j.1461-0248.2007.01113.x

Fang, J., Chao, C. C., Roberts, P., and Ehlers, J. (2007) Genetic Diversity of Cowpea (*Vigna unguiculata* (L.) Walp.) in Four West African and USA Breeding Programmes as Determined by AFLP Analysis. *Genetic Resources and Crop Evolution*, 54, 1197-1209. https://doi.org/10.1007/s10722-006-9101-9

Fathi, A and Kardoni, F. (2020). The importance of Quinoa (Quinoa Chenopodium Willd.) cultivation in developing countries: a review. *Cercetari Agronomice in Moldova*, 53 (3), 337-356.

Freidenreich, A., Barraza, G., Jayachandran, K., and Khoddamzadeh, A. A. (2019). Precision agriculture application for sustainable nitrogen management of

Justicia brandegeana using optical sensor technology. *Agriculture*, 9 (5), 98. https://doi.org/10.3390/agriculture9050098

Galieni, A., D'Ascenzo, N., Stagnari, F., Pagnani, G., Xie, Q., and Pisante, M. (2021). Past and future of plant stress detection: an overview from remote sensing to positron emission tomography. *Frontiers in Plant Science*, 11, 609155. https://doi.org/10.3389/fpls.2020.609155

Gamon, J. A., Penuelas, J., and Field, C. B. (1992). A narrow-waveband spectral index that tracks diurnal changes in photosynthetic efficiency. *Remote Sensing of Environment*, 41 (1), 35-44. https://doi.org/10.1016/0034-4257(92)90059-S

Gan, H., Jiao, Y., Jia, J., Wang, X., Li, H., Shi, W., Peng, C., Polle, A., and Luo, Z. B. (2016). Phosphorus and nitrogen physiology of two contrasting poplar genotypes when exposed to phosphorus and/or nitrogen starvation. *Tree Physiology*, 36 (1), 22-38. https://doi.org/10.1093/treephys/tpv093

Girden, E. R. (1992). *ANOVA: Repeated measures*. Newbury Park, CA: Sage. (No. 84).

Gitelson, A and Merzlyak, M. N. (1997). Remote estimation of chlorophyll content in higher plant leaves. *International Journal of Remote Sensing*, 18 (12), 2691-2697. https://doi.org/10.1080/014311697217558

Gitelson, A. A., Chivkunova, O. B., and Merzlyak, M. N. (2009). Non-destructive estimation of anthocyanins and chlorophylls in anthocyanic leaves. *American Journal of Botany*, 96 (10), 1861-1868. https://doi.org/10.3732/ajb.0800395

Gitelson, A. A., Kaufman, Y. J., Stark, R., and Rundquist, D. (2002). Novel algorithms for remote estimation of vegetation fraction. *Remote sensing of Environment*, 80 (1), 76-87. https://doi.org/10.1016/S0034-4257(01)00289-9

Gitelson, A. A., Viña, A., Ciganda, V., Rundquist, D. C., and Arkebauer, T. J. (2005). Remote estimation of canopy chlorophyll content in crops. *Geophysical Research Letters*, 32 (8). https://doi.org/10.1029/2005GL022688

Gniazdowska, A and Rychter, A. M. (2000). Nitrate uptake by bean (*Phaseolus vulgaris* L.) roots under phosphate deficiency. *Plant and Soil*, 226, 79-85. https://doi.org/10.1023/A:102646330

Goodwin, A. W., Lindsey, L. E., Harrison, S. K., and Paul, P. A. (2018). Estimating wheat yield with Normalised difference vegetation index and fractional green canopy cover. *Crop, Forage and Turfgrass Management*, 4 (1), 1-6. https://doi.org/10.2134/cftm2018.04.0026

Greenhouse, S. W and Geisser, S. (1959). On methods in the analysis of profile data. *Psychometrika*, 24 (2), 95-112. https://doi.org/10.1007/BF02289823

Grohskopf, M. A., Corrêa, J. C., Fernandes, D. M., Teixeira, P. C., Cruz, C. V., and Mota, S. C. A. (2019). Interaction between phosphorus and nitrogen in

organomineral fertiliser. *Communications in Soil Science and Plant Analysis*, 50 (21), 2742-2755. https://doi.org/10.1080/00103624.2019.1678632

Groot, C. C., Marcelis, L. F. M., van Den Boogard, R., Kaiser, W. N., and Lambers, H. (2003). Interaction of nitrogen and phosphorus nutrition in determining growth. *Plant and Soil*, 248, 257-68. https://doi.org/10.1023/A:1022323215010

Haboudane, D., Miller, J. R., Pattey, E., Zarco-Tejada, P. J., and Strachan, I. B. (2004). Hyperspectral vegetation indices and novel algorithms for predicting green LAI of crop canopies: Modelling and validation in the context of precision agriculture. *Remote Sensing of Environment*, 90 (3), 337-352.

Haboudane, D., Miller, J. R., Tremblay, N., Zarco-Tejada, P. J., and Dextraze, L. (2002). Integrated narrow-band vegetation indices for prediction of crop chlorophyll content for application to precision agriculture. *Remote Sensing of Environment*, 81 (2-3), 416-426. https://doi.org/10.1016/S0034-4257(02)00018-4

Hallik, L., Kazantsev, T., Kuusk, A., Galmés, J., Tomás, M., and Niinemets, Ü. (2017). Generality of relationships between leaf pigment contents and spectral vegetation indices in Mallorca (Spain). *Regional Environmental Change*, 17, 2097-2109. https://doi.org/10.1007/s10113-017-1202-9

Hank, T. B., Berger, K., Bach, H., Clevers, J. G., Gitelson, A., Zarco-Tejada, P., and Mauser, W. (2019). Spaceborne imaging spectroscopy for sustainable agriculture: Contributions and challenges. *Surveys in Geophysics*, 40, 515-551. https://doi.org/10.1007/s10712-018-9492-0

Hinojosa, L., González, J. A., Barrios-Masias, F. H., Fuentes, F., and Murphy, K. M. (2018). Quinoa abiotic stress responses: A review. *Plants*, 7 (4), 106. https://doi.org/10.3390/plants7040106

Hinojosa, L., Kumar, N., Gill, K. S., and Murphy, K. M. (2019). Spectral reflectance indices and physiological parameters in quinoa under contrasting irrigation regimes. *Crop Science*, 59 (5), 1927-1944.

Horn, L., Nghituwamata, S. N., and Ueitele, I. (2022). Cowpea production challenges and contribution to livelihood in Sub-Sahara region. *Agricultural Sciences*, 13, 25-32. https://doi.org/10.4236/as.2022.131003

Hu, B and Chu, C. (2020). Nitrogen-phosphorus interplay: old story with molecular tale. *The New Phytologist*, 225 (4), 1455-1460. https://doi.org/10.1111/nph.16102

Huang, C. H., Singh, G. P., Park, S. H., Chua, N. H., Ram, R. J., and Park, B. S. (2020). Early diagnosis and management of nitrogen deficiency in plants utilising Raman spectroscopy. *Frontiers in Plant Science*, 11, 663. https://doi.org/10.3389/fpls.2020.00663

Huete, A. R. (1988). A soil-adjusted vegetation index (SAVI). *Remote Sensing of Environment*, 25 (3), 295-309. https://doi.org/10.1016/0034-4257(88)90106-X

Jacobsen, S. E and Christiansen, J. L. (2016). Some agronomic strategies for organic quinoa (*Chenopodium quinoa* Willd.). *Journal of Agronomy and Crop Science*, 202 (6), 454-463. https://doi.org/10.1111/jac.12174

Jay, S., Maupas, F., Bendoula, R., and Gorretta, N. (2017). Retrieving LAI, chlorophyll and nitrogen contents in sugar beet crops from multi-angular optical remote sensing: Comparison of vegetation indices and PROSAIL inversion for field phenotyping. *Field Crops Research*, 210, 33-46.

Jiang, J., Wang, Y. P., Yang, Y., Yu, M., Wang, C., and Yan, J. (2019). Interactive effects of nitrogen and phosphorus additions on plant growth vary with ecosystem type. *Plant and Soil*, 440, 523-537. https://doi.org/10.1007/s11104-019-04119-5

Kamara, A. Y., Omoigui, L. O., Kamai, N., Ewansiha, S. U., and Ajeigbe, H. A. (2018). Improving cultivation of cowpea in West Africa. In: Achieving sustainable cultivation of grain legumes Volume 2: Improving cultivation of particular grain legumes. Burleigh Dodds Series in Agricultural Science. Burleigh Dodds Science Publishing, pp. 1-18. ISBN 978-1786761408

Kanke, Y., Raun, W., Solie, J., Stone, M., and Taylor, R. (2012). Red edge as a potential index for detecting differences in plant nitrogen status in winter wheat. *Journal of Plant Nutrition*, 35 (10), 1526-1541.

Kawamura, K., Mackay, A. D., Tuohy, M. P., Betteridge, K., Sanches, I. D., and Inoue, Y. (2011). Potential for spectral indices to remotely sense phosphorus and potassium content of legume-based pasture as a means of assessing soil phosphorus and potassium fertility status. *International Journal of Remote Sensing*, 32 (1), 103-124. https://doi.org/10.1080/01431160903439908

Kebede, E and Bekeko, Z. (2020). Expounding the production and importance of cowpea (*Vigna unguiculata* (L.) Walp.) in Ethiopia. *Cogent Food and Agriculture*, 6 (1), 1769805. https://doi.org/10.1080/23311932.2020.1769805

Keselman, H. J., Algina, J., and Kowalchuk, R. K. (2001). The analysis of repeated measures designs: a review. *British Journal of Mathematical and Statistical Psychology*, 54 (1), 1-20. https://doi.org/10.1348/000711001159357

Kowalski, R. J., Medina-Meza, I. G., Thapa, B. B., Murphy, K. M., and Ganjyal, G. M. (2016). Extrusion processing characteristics of quinoa (*Chenopodium quinoa* Willd.) var. Cherry Vanilla. *Journal of Cereal Science*, 70, 91-98. https://doi.org/10.1016/j.jcs.2016.05.024

Krouk, G and Kiba, T. (2020). Nitrogen and Phosphorus interactions in plants: from agronomic to physiological and molecular insights. *Current Opinion in Plant Biology*, 57, 104-109. https://doi.org/10.1016/j.pbi.2020.07.002

Lemaire, G., Jeuffroy, M. H., and Gastal, F. (2008). Diagnosis tool for plant and crop N status in vegetative stage: Theory and practices for crop N

management. *European Journal of Agronomy*, 28 (4), 614-624. https://doi.org/10.1016/j.eja.2008.01.005

Li, F., Gnyp, M. L., Jia, L., Miao, Y., Yu, Z., Koppe, W., and Zhang, F. (2008). Estimating N status of winter wheat using a handheld spectrometer in the North China Plain. *Field Crops Research*, 106 (1), 77-85.

Li, F., Li, D., Elsayed, S., Hu, Y., and Schmidhalter, U. (2021). Using optimised three-band spectral indices to assess canopy N uptake in corn and wheat. *European Journal of Agronomy*, 127, 126286. https://doi.org/10.1016/j.eja.2021.126286

Li, F., Miao, Y., Feng, G., Yuan, F., Yue, S., Gao, X., and Chen, X. (2014). Improving estimation of summer maize nitrogen status with red edge-based spectral vegetation indices. *Field Crops Research*, 157, 111-123.

Lichtenthaler, H. K. (1996). Vegetation stress: an introduction to the stress concept in plants. *Journal of Plant Physiology*, 148 (1-2), 4-14. https://doi.org/10.1016/S0176-1617(96)80287-2

Lu, Y., Zhang, X., Cui, Y., Chao, Y., Song, G., Nie, C., and Wang, L. (2023). Response of different varieties of maize to nitrogen stress and diagnosis of leaf nitrogen using hyperspectral data. *Scientific Reports*, 13 (1), 5890. https://doi.org/10.1038/s41598-023-31887-z

Lunagaria, M. M., Karande, B. I., Patel, K. I., and Pandey, V. (2015). Determination of optimal narrow bands for vegetation indices to discriminate nitrogen status in wheat crop. *Journal of Agrometeorology*, 17 (1), 23-29.

Luo, X., Mazer, S. J., Guo, H., Zhang, N., Weiner, J., and Hu, S. (2016). Nitrogen: phosphorous supply ratio and allometry in five alpine plant species. *Ecology and Evolution*, 6 (24), 8881-8892. https://doi.org/10.1002/ece3.2587

Maliro, M. F. A., Guwela, V. F., Nyaika, J., and Murphy, K. M. (2017) Preliminary Studies of the Performance of Quinoa (*Chenopodium quinoa* Willd.) Genotypes under Irrigated and Rainfed Conditions of Central Malawi. *Frontiers in Plant Science*, 8, 227. https://doi.org/10.3389/fpls.2017.00227

Maliro, M. F and Guwela, V. (2015). Quinoa breeding in Africa: history, goals, and progress. *Quinoa: Improvement and Sustainable Production*, 161-172. https://doi.org/10.1002/9781118628041.ch9

Maliro, M and Njala, A. L. (2019). Agronomic performance and strategies of promoting Quinoa (*Chenopodium quinoa* Willd) in Malawi. *Ciencia e investigación agraria: revista latinoamericana de ciencias de la agricultura*, 46 (2), 82-99.

Medici, A., Szponarski, W., Dangeville, P., Safi, A., Dissanayake, I. M., Saenchai, C., et al. (2019). Identification of molecular integrators shows that nitrogen actively controls the phosphate starvation response in plants. *Plant Cell*, 31, 1171-1184. https://doi.org/10.1105/tpc.18.00656

Muramatsu, K. (2019). Use of chlorophyll index-green and the red-edge chlorophyll index to derive an algorithm for estimating gross primary production capacity. In *Remote Sensing for Agriculture, Ecosystems, and Hydrology XXI* (Vol. 11149, pp. 54-61). SPIE. https://doi.org/10.1117/12.2532468

Murphy, K. M., Bazile, D., Kellogg, J., and Rahmanian, M. (2016). Development of a worldwide consortium on evolutionary participatory breeding in quinoa. *Frontiers in Plant Science*, 7, 184074.

Mutanga, O., Masenyama, A., and Sibanda, M. (2023). Spectral saturation in the remote sensing of high-density vegetation traits: A systematic review of progress, challenges, and prospects. *ISPRS Journal of Photogrammetry and Remote Sensing*, 198, 297-309. https://doi.org/10.1016/j.isprsjprs.2023.03.010

Noratto, G. D., Murphy, K., and Chew, B. P. (2019). Quinoa intake reduces plasma and liver cholesterol, lessens obesity-associated inflammation, and helps to prevent hepatic steatosis in obese db/db mouse. *Food Chemistry*, 287, 107-114. https://doi.org/10.1016/j.food-chem.2019.02.061

Nwagboso, C., Andam, K. S., Amare, M., Bamiwuye, T., and Fasoranti, A. (2024). The economic importance of cowpea in Nigeria trends and Implications for achieving agri-food system transformation. IFPRI Discussion Paper 2241. Washington, DC: International Food Policy Research Institute.

Okyere, F. G., Cudjoe, D., Sadeghi-Tehran, P., Virlet, N., Riche, A. B., Castle, M., Greche, L., Simms, D., Mhada, M., Mohareb, F., and Hawkesford, M. J. (2023). Modeling the spatial-spectral characteristics of plants for nutrient status identification using hyperspectral data and deep learning methods. *Frontiers in Plant Science*, 14, 1209500. https://doi.org/10.3389/fpls.2023.1209500

Osborne, S. L. (1999). Separating spectral signatures for detecting nitrogen, phosphorus and water stress in corn. Doctor of Philosophy thesis. The University of Nebraska-Lincoln.

Osborne, S. L., Schepers, J. S., Francis, D. D., and Schlemmer, M. R. (2002). Detection of phosphorus and nitrogen deficiencies in corn using spectral radiance measurements. *Agronomy Journal*, 94 (6), 1215-1221.

Oyoo, M. E., Githiri, S. M., and Ayiecho, P. O. (2010). Performance of some quinoa (*Chenopodium quinoa* Willd.) genotypes in Kenya. *South African Journal of Plant and Soil*, 27 (2), 187-190. https://hdl.handle.net/10520/EJC87969

Özyiğit, Y. A. Ş. A. R and Bilgen, M. E. H. M. E. T. (2013). Use of spectral reflectance values for determining nitrogen, phosphorus, and potassium contents of rangeland plants. *Journal of Agricultural Science and Technology*, 15 (7), 1537-1545. http://dorl.net/dor/20.1001.1.16807073.2013.15.7.8.7

Padilla, F. M., Gallardo, M., Peña-Fleitas, M. T., de Souza, R., and Thompson, R. B. (2018). Proximal optical sensors for nitrogen management of vegetable crops: A review. *Sensors*, 18, 2083. https://doi.org/10.3390/s18072083.

Pathan, S, Ndunguru, G, Clark, K., and Ayele, A. G. (2023) Yield and nutritional responses of quinoa (*Chenopodium quinoa* Willd.) genotypes to irrigated, rainfed, and drought stress environments. *Frontiers in Sustainable Food Systems*, 7, 1242187. https://doi.org/10.3389/fsufs.2023.1242187

Patil, V. D., Adsul, P. B., and Deshmukh, L. S. (2007). Studies on spectral reflectance under normal and nitrogen, phosphorus and pest and disease stress condition in soybean (*Glycine max* L.). *Journal of Indian Society of Remote Sensing*, 35, 351-359. https://doi.org/10.1007/BF02990790

Peng, Y., Zhang, M., Xu, Z., Yang, T., Su, Y., Zhou, T., Wang, H., Wang, Y., and Lin, Y. (2020). Estimation of leaf nutrition status in degraded vegetation based on field survey and hyperspectral data. *Scientific Reports*, 10 (1), 4361. https://doi.org/10.1038/s41598-020-61294-7

Peñuelas, J., Baret, F., and Filella, I. (1995). Semi-empirical indices to assess carotenoids/chlorophyll a ratio from leaf spectral reflectance. *Photosynthetica*, 31 (2), 221-230.

Peñuelas, J., Gamon, J. A., Fredeen, A. L., Merino, J., and Field, C. B. (1994). Reflectance indices associated with physiological changes in nitrogen-and water-limited sunflower leaves. *Remote Sensing of Environment*, 48 (2), 135-146. https://doi.org/10.1016/0034-4257(94)90136-8

Pinit, S., Ruengchaijatuporn, N., Sriswasdi, S., Buaboocha, T., Chadchawan, S., and Chaiwanon, J. (2022). Hyperspectral and genome-wide association analyses of leaf phosphorus status in local Thai indica rice. *Plos One*, 17 (4), e0267304. https://doi.org/10.1371/journal.pone.0267304

Prey, L and Schmidhalter, U. (2019). Sensitivity of Vegetation Indices for Estimating Vegetative N Status in Winter Wheat. *Sensors (Basel, Switzerland)*, 19 (17), 3712. https://doi.org/10.3390/s19173712

Ranjan, R., Chopra, U. K., Sahoo, R. N., Singh, A. K., and Pradhan, S. (2012). Assessment of plant nitrogen stress in wheat (*Triticum aestivum* L.) through hyperspectral indices. *International Journal of Remote Sensing*, 33(20), 6342-6360. https://doi.org/10.1080/01431161.2012.687473

Rehman, T. H., Lundy, M. E., and Linquist, B. A. (2022). Comparative sensitivity of vegetation indices measured via proximal and aerial sensors for assessing n status and predicting grain yield in rice cropping systems. *Remote Sensing*, 14 (12), 2770. https://doi.org/10.3390/rs14122770

Rietra, R. P., Heinen, M., Dimkpa, C. O., and Bindraban, P. S. (2017). Effects of nutrient antagonism and synergism on yield and fertiliser use

efficiency. *Communications in Soil Science and Plant Analysis*, 48 (16), 1895-1920. https://doi.org/10.1080/00103624.2017.1407429

Rodriguez, D., Fitzgerald, G. J., Belford, R., and Christensen, L. K. (2006). Detection of nitrogen deficiency in wheat from spectral reflectance indices and basic crop eco-physiological concepts. *Australian Journal of Agricultural Research*, 57 (7), 781-789. https://doi.org/10.1071/AR05361

Rondeaux, G., Steven, M., and Baret, F. (1996). Optimisation of soil-adjusted vegetation indices. *Remote Sensing of Environment*, 55 (2), 95-107.

Roujean, J. L and Breon, F. M. (1995). Estimating PAR absorbed by vegetation from bidirectional reflectance measurements. *Remote Sensing of Environment*, 51 (3), 375-384. https://doi.org/10.1016/0034-4257(94)00114-3

Rouse, J. W., Haas, R. H., Schell, J. A., and Deering, D. W. (1974). Monitoring vegetation systems in the Great Plains with ERTS. *NASA Special Publication*, 351 (1), 309.

Sadeghi-Tehran, P., Virlet, N., and Hawkesford, M. J. (2021). A neural network method for classification of sunlit and shaded components of wheat canopies in the field using high-resolution hyperspectral imagery. *Remote Sensing*, 13 (5). https://doi.org/10.3390/rs13050898

Sankaran, S., Espinoza, C. Z., Hinojosa, L., Ma, X., and Murphy, K. (2019). High□Throughput Field Phenotyping to Assess Irrigation Treatment Effects in Quinoa. *Agrosystems, Geosciences and Environment*, 2 (1), 1-7.

Schlegel, A. J and Bond, H. D. (2019). Long-Term Nitrogen, Phosphorus, and Potassium Fertilisation of Irrigated Grain Sorghum. *Kansas Agricultural Experiment Station Research Reports*, 5 (4), 1. https://doi.org/10.4148/2378-5977.7753

Schleuss, P. M., Widdig, M., Heintz□Buschart, A., Kirkman, K., and Spohn, M. (2020). Interactions of nitrogen and phosphorus cycling promote P acquisition and explain synergistic plant□growth responses. *Ecology*, 101 (5), e03003. https://doi.org/10.1002/ecy.3003

Setiyono, T. D., Walters, D. T., Cassman, K. G., Witt, C., and Dobermann, A. (2010). Estimating maize nutrient uptake requirements. *Field Crops Research*, 118, 158-68. https://doi.org/10.1016/j.fcr.2010.05.006.

Sharifi, A and Felegari, S. (2023). Remotely sensed Normalised difference red-edge index for rangeland biomass estimation. *Aircraft Engineering and Aerospace Technology*, 95 (7), 1128-1136. https://doi.org/10.1108/AEAT-07-2022-0199

Shrestha, S., Brueck, H., and Asch, F. (2012). Chlorophyll index, photochemical reflectance index and chlorophyll fluorescence measurements of rice leaves supplied with different N levels. *Journal of Photochemistry and Photobiology B: Biology*, 113, 7-13. https://doi.org/10.1016/j.jphotobiol.2012.04.008

Siedliska, A., Baranowski, P., Pastuszka-Woźniak, J., Zubik, M., and Krzyszczak, J. (2021). Identification of plant leaf phosphorus content at different growth stages based on hyperspectral reflectance. *BMC Plant Biology*, 21, 1-17.

Sims, D. A and Gamon, J. A. (2002). Relationships between leaf pigment content and spectral reflectance across a wide range of species, leaf structures and developmental stages. *Remote Sensing of Environment*, 81 (2-3), 337-354. https://doi.org/10.1016/S0034-4257(02)00010-X

Singh, B. B., Ajeigbe, H. A., Tarawali, S. A., Fernandez-Rivera, S., and Abubakar, M. (2003). Improving the production and utilisation of cowpea as food and fodder. *Field Crops Research*, 84 (1-2), 169-177. https://doi.org/10.1016/S0378-4290(03)00148-5

Skendžić, S., Zovko, M., Lešić, V., Pajač Živković, I., and Lemić, D. (2023). Detection and evaluation of environmental stress in winter wheat using remote and proximal sensing methods and vegetation indices–A review. *Diversity*, 15 (4), 481. https://doi.org/10.3390/ d15040481

Stanschewski, C. S., Rey, E., Fiene, G., Craine, E. B., Wellman, G., and Melino, V. J. (2021). Quinoa phenotyping methodologies: An international consensus. Quinoa Phenotyping Consortium, *Plants*, 10 (9), 1759.

Taaime, N., El Mejahed, K., Choukr-Allah, R., Bouabid, R., Oukarroum, A., and El Gharous, M. (2023) Optimisation of macronutrients for improved grain yield of quinoa (*Chenopodium quinoa* Wild.) crop under semi-arid conditions of Morocco. *Frontiers in Plant Science*, 14, 1146658.

Tian, Y.-C., Gu, K.-J., Chu, X., Yao, X., Cao, W.-X., and Zhu, Y. (2014). Comparison of different hyperspectral vegetation indices for canopy leaf nitrogen concentration estimation in rice. *Plant Soil*, 376 (1), 193-209. https://doi.org/10.1007/s11104-013-1937-0

Vilcacundo, R and Hernández-Ledesma, B. (2017). Nutritional and biological value of quinoa (*Chenopodium quinoa* Willd.). *Current Opinion in Food Science*, 14, 1-6. https://doi.org/10.1016/j.cofs.2016.11.007

Wang, J., Wu, B., Kohnen, M. V., Lin, D., Yang, C., Wang, X., Qiang, A., Liu, W., Kang, J., Li, H., Shen, J., Yao, T., Su, J., Li, B., and Gu, L. (2021). Classification of rice yield using UAV-based hyperspectral imagery and lodging feature. *Plant Phenomics*, *2021*. https://doi.org/10.34133/2021/9765952

Wang, N., Wang, F., Shock, C. C., Meng, C., and Qiao, L. (2020). Effects of management practices on quinoa growth, seed yield, and quality. *Agronomy*, 10 (3), 445. https://doi.org/10.3390/agronomy10030445

Wang, R., Bicharanloo, B., Hou, E., Jiang, Y., and Dijkstra, F. A. (2022). Phosphorus supply increases nitrogen transformation rates and retention in soil: A global meta-analysis. *Earth's Future*, 10, e2021EF002479.

Wang, W. D., Chang, Q. R., and Wang, Y. N. (2020). Hyperspectral monitoring of anthocyanins relative content in winter wheat leaves. *Journal of Triticeae Crops*, 40 (6), 754-761. https://doi.org/10.7606/j.issn.1009-1041.2020.06.14

Wei, W., Xia, Y., TIAN, Y. C., LIU, X. J., Jun, N. I., CAO, W. X., and Yan, Z. H. U. (2012). Common spectral bands and optimum vegetation indices for monitoring leaf nitrogen accumulation in rice and wheat. *Journal of Integrative Agriculture*, 11 (12), 2001-2012. https://doi.org/10.1016/S2095-3119(12)60457-2

Whan, A., Dielen, A. S., Mieog, J., Bowerman, A. F., Robinson, H. M., Byrne, K., and Ral, J. P. (2014). Engineering α-amylase levels in wheat grain suggests a highly sophisticated level of carbohydrate regulation during development. *Journal of Experimental Botany*, 65 (18), 5443-5457. https://doi.org/10.1093/jxb/eru299

Wu, G. (2015). Nutritional properties of quinoa. In: K. Murphy and J. Matanguihan, editors, Quinoa: Improvement and sustainable production. John Wiley and Sons, Hoboken, NJ. pp. 193–210. https://doi.org/10.1002/9781118628041.ch11

Wu, G., Morris, C. F., and Murphy, K. M. (2017). Quinoa starch characteristics and their correlations with the texture profile analysis (TPA) of cooked quinoa. *Journal of Food Science*, 82, 2387-2395. https://doi.org/10.1111/1750-3841.13848

Xia, S., Jiang, J., Liu, F., Chang, Z., Yu, M., Liu, C., and Yan, J. (2023). Phosphorus addition promotes plant nitrogen uptake mainly via enhancing microbial activities: A global meta-analysis. *Applied Soil Ecology*, 188, 104927. https://doi.org/10.1016/j.apsoil.2023.104927

Zarco-Tejada, P. J., Miller, J. R., Noland, T. L., Mohammed, G. H., and Sampson, P. H. (2001). Scaling-up and model inversion methods with narrowband optical indices for chlorophyll content estimation in closed forest canopies with hyperspectral data. *IEEE Transactions on Geoscience and Remote Sensing*, 39 (7), 1491-1507. https://doi.org/10.1109/36.934080

Zarco□Tejada, P. J., Ustin, S. L., and Whiting, M. L. (2005). Temporal and spatial relationships between within□field yield variability in cotton and high□spatial hyperspectral remote sensing imagery. *Agronomy Journal*, 97 (3), 641-653. https://doi.org/10.2134/agronj2003.0257

Zhang, Y., Wang, T., Li, Z., Wang, T., and Cao, N. (2023). Based on machine learning algorithms for estimating leaf phosphorus concentration of rice using optimised spectral indices and continuous wavelet transform. *Frontiers in Plant Science*, 14, 1185915. https://doi.org/10.3389/fpls.2023.1185915

Zhao, B., Duan, A., Ata-Ul-Karim, S. T., Liu, Z., Chen, Z., Gong, Z., et al. (2018). Exploring new spectral bands and vegetation indices for estimating nitrogen nutrition index of summer maize. *European Journal of Agronomy*, 93, 113-125. https://doi.org/10.1016/j.eja.2017.12.006

Zhao, X., Wang, S., Wen, T., Xu, J., Huang, B., Yan, S., Gao, G., Zhao, Y., Li, H., Qiao, J., Yang, J., Wu, L., Wang, H., Liu, T., and Mu, X. (2023). On correlation between canopy vegetation and growth indexes of maize varieties with different nitrogen efficiencies. *Open Life Sciences*, 18 (1), 20220566. https://doi.org/10.1515/biol-2022-0566

CHAPTER 4

Interaction of water and nitrogen stress in wheat and the potential for independent detection using a handheld proximal sensor

(This chapter is based on a manuscript under review at the Plant Phenomics Journal with manuscript number: PlantPhenomics-D-24-00072. Accordingly, minor modifications of the text were necessary compared with the submitted manuscript under review).

Daniel K. Cudjoe[1,2], Frank G. Okyere[1,2], Suzanne J. Clark[3], Nicolas Virlet[1], Parul Sehrawat[1], March Castle[1], Andrew B. Riche[1], Toby W. Waine[2], Fady Mohareb[2*] and Malcolm J. Hawkesford[1*]

[1]Rothamsted Research, Sustainable Soils and Crops, Harpenden, Hertfordshire, AL5 2JQ, United Kingdom.
[2]School of Water, Energy and Environment, Cranfield University, Cranfield, Bedfordshire, MK43 0AL, United Kingdom.
[3]Rothamsted Research, Intelligent Data Ecosystems, Harpenden, Hertfordshire, AL5 2JQ, United Kingdom.

***Correspondence**
Malcolm J. Hawkesford
Email: malcolm.hawkesford@rothamsted.ac.uk

Fady Mohareb
Email: f.mohareb@cranfield.ac.uk

Abstract

Water and nitrogen (N) limitation and their interactions continue to be the key limiting factors for the agronomic production of wheat (*Triticum aestivum* L.). In this study, the morpho-physiological responses to drought at high and low Nitrogen (N) conditions and the potential of spectral reflectance indices (SRIs) to discriminate drought and N stresses at the leaf scale, in spring wheat grown under controlled glasshouse conditions, were assessed. Morpho-physiological parameters indicative of water and N stress were measured in tandem with SRIs computed from multiple wavelengths using a handheld proximal sensor. These responses were analysed using linear mixed models (LMMs) fitted using residual maximum likelihood (REML) and with an autocorrelation (AR1) model to assess the effects of N and water stress and their interactions. Correlation analysis was employed to assess the relationship between effective SRIs and wheat morpho-physiological status. The results demonstrated a greater amplitude of drought response under HN compared to LN with interactive effects except for leaf N content (LNC). In an ensemble of 39 SRIs, only the Renormalised Difference Vegetation Index

(RDVI) and Red Difference Vegetation Index (rDVI_790) indicated higher specificity for drought stress detection. The results showed that the chlorophyll-sensitive indices including the chlorophyll Index (mNDblue_730), Greenness Index (G), Lichtenthaler Index (Lic2) and the red-edge indices: Modified Red-Edge Simple Ratio (MRESR), chlorophyll Index Red-Edge (CIrededge) and Normalised Difference Red-Edge (NDRE) showed higher specificity for N-stress detection. Correlation analysis revealed that the morpho-physiological status under water deficit and N availability is best estimated using several of the SRIs. The results indicated the feasibility of using a low-cost handheld proximal sensor for monitoring the morpho-physiological status in a rapid and non-destructive manner and discriminating drought and N stresses in spring wheat.

Keywords: Wheat, water and N interaction, proximal sensor, spectral reflectance indices, morpho-physiological status, drought response, N status

4.1 Introduction

Agriculture is currently facing unprecedented challenges due to the increasing human population, depleting natural resources and climate change scenarios (FAO, 2023). Wheat (*Triticum aestivum* L.), the third-most important crop after rice and maize and is cultivated widely throughout the world to meet global food needs (Ray et al., 2013). The improvement of both yields and resource use efficiency (water and nutrient use efficiency) presents major challenges. Therefore, the development and adoption of innovative technology and optimal management practices, especially for water and N input, which are key limiting factors of crop production, are crucial for increasing global future food supply and ecological sustainability (Erenstein et al., 2022).

Water stress (drought) occurs when the plant water requirement cannot be fully met through precipitation or irrigation, affecting the normal functioning of the plant (e.g., growth and development, photosynthetic rate and stomatal conductance) (Camaille et al., 2021). Several knowledge gaps such as understanding the competitive dynamics under water stress and elucidating the mechanisms underlying stress tolerance and recovery in crops can be identified despite the recent advances in understanding plant responses to water stress (dos Santos et al., 2022). Many of these gaps are linked to unidentified interactions between various environmental factors. The existence of an initial or prior stress that modifies a plant's typical response to a subsequent stress

because of an acclimation response is referred to as an ‘interaction’ between the stress factors (Atkinson et al., 2012). However, from a pragmatic perspective, research must address intricate interactions among complex environmental factors.

From the perspective of agricultural practice, the most crucial interaction with water stress is N availability. N is the main macronutrient for plant growth and function and is the principal regulator of many physiological, morphological and biochemical processes (Mu and Chen, 2021). Furthermore, spatial variation in the soil and temporal changes in meteorological conditions cause spatiotemporal variability in water and N availability. Therefore, matching water supply to N availability is critical to ensure optimal crop performance, providing opportunities for PA. A robust method that can detect small changes in crop growth and physiology in response to water and N availability is needed to rapidly monitor heterogeneity, optimise input supply and prevent detrimental effects on crop productivity and the environment.

Recent advancements in spectroscopic techniques for plant phenotyping and phenomics offer opportunities to measure spectral reflectance at the leaf scale in response to the physiological and biophysical status of crops (Skendžić et al., 2023). This technique provides a promising tool to rapidly and non-destructively phenotype plant leaf traits (Kothari and Schweiger, 2022). Numerous studies have linked spectral reflectance, transmittance or absorption responses in leaves and plant canopies to physiological status and plant adaptation to the environment (Kothari and Schweiger, 2022). These optical spectra rely on the amount of leaf pigment present at different absorption wavelengths and corresponding leaf spectral signatures. Due to the correlation between leaf spectral reflectance and leaf chlorophyll concentration, several studies (eg., Katsoulas et al., 2016) have linked reflectance in the green and red bands with water and nutrient stress.

Many SRIs have been proposed to remotely estimate the water content of plant tissues to offer a measure of the water deficit stress (Zhang and Zhou, 2019; Skendžić et al., 2023). For example, Zhang and Zhou, 2019 demonstrated the utility of the Green Chlorophyll Index (CIgreen), Red-Edge Normalised Ratio (NRrededge) and Red-Edge Chlorophyll Index (CIrededge) as the most sensitive SRIs responsive to water variations and being optimal for predicting canopy water status in maize.

Additionally, several studies have focused on determining the appropriate SRIs for the estimation of N status in crops (Prey and Schmidhalter, 2019). Among the several SRIs investigated, the red-edge region and indices have been proposed as most suitable for estimating chlorophyll content and for detecting the N status in crops as they were found to be superior to classical NIR/red indices such as the NDVI. For instance, the red-edge group indices such as the REIP, CIrededge and CIgreen (Klem et al., 2014; Prey and Schmidhalter, 2019) have been proposed as predictors of N status. It has been demonstrated that the red-edge region reduces the rapid saturation effects of spectral indices based on reflectance in the blue and red bands (Zhang et al., 2022), hence their high response to the chlorophyll content and N status. Additionally, the shortwave infrared (SWIR) spectral region (around 1000-2500 nm) is strongly correlated with leaf N content because the vibrational modes of N-containing organic compounds produce distinct absorption features in this spectral region, enabling direct quantification of plant N status (Herrmann et al., 2010).

Most of the studies employing SRIs concentrated on identifying water or N stress separately. The combined effect of water and N stress on spectral reflectance in crops has only been investigated in a few studies using RS (Klem et al., 2018; Sellami et al., 2022). For instance, Klem et al. (2018) evaluated the interactive effects of water deficit and N nutrition in winter wheat under rainout shelter field experiments using remote sensing data. The authors demonstrated that stomatal response to water deficit was best estimated using the Normalized Pigment Chlorophyll Index (NPCI) and Crop Water Stress Index (CWSI). While none of the indices accurately detected N content in plants, the total N uptake in wheat grain was reliably estimated using the Transformed Chlorophyll Absorption Reflectance Index/Optimized Soil-Adjusted Vegetation Index (TCARI/OSAVI).

However, the use of SRIs at the leaf level using PS to simultaneously assess the combined impacts of water and N stress and their interactions on morpho-physiological responses in wheat has not been widely investigated. Optimising the availability of both water and N for wheat cultivation can be extremely challenging due to the interactions and confounding factors (Li et al., 2020). This knowledge gap may lead to wrong diagnosis in monitoring the impact of water stress and compromise fertilisation

management on N nutrition. Since most farmers are confronted with both water and nutrient stress management, it is crucial to assess novel and existing SRIs for more precise identification and phenotyping of crop status to support PA and improve wheat productivity.

Recently, increased attention has been devoted to the use of handheld PS for field phenotyping and stress responses in crops in developing countries because of their ease of operation, non-destructive nature, low cost and because they may not require substantial pre-processing of spectral data such as soil, geometric and atmospheric corrections (Cudjoe et al., 2023a). However, little is known about the potential of using this technique in discriminating water and N stresses at the leaf scale.

Therefore, the overall aim of this study was to assess the morpho-physiological drought responses at high and low N conditions and examine the potential of a wide range of SRIs measured at the leaf scale to discriminate individual and combined drought and N stress effects in spring wheat. The specific objectives were to (1) assess the morpho-physiological drought responses at high and low N conditions, (2) assess the time-course response of SRIs to identify early drought responses under high and low N conditions, (3) identify effective SRIs specific for discriminating between drought and N stress and (4) to examine the relationships between spectral response and morpho-physiological status.

4.2 Materials and methods

4.2.1 Plant materials and growth conditions

A spring wheat (Cadenza cv.) was selected for this study based on its genetic background, breeding history and agronomical significance (Fernández-Gómez et al., 2020). A pot experiment was conducted in the glasshouse at the Plant Growth Facility at Cranfield University, United Kingdom; 52° 4' 28.61" N 0° 37' 41.819" W, from October 2022 to December 2022. The glasshouse conditions were set as: day/night temperature 24/21±2 °C, RH 50-60 %, and a photoperiod of 14 h with a supplemental light intensity of 20 klx (equivalent to 460 µmol m^{-2} s^{-1}). Before sowing, wheat seeds were soaked in tap water and stratified at 4 °C for 3 days. After stratification, four seeds were sowed into each pot (13.7×13.3×11 cm). At the growth stage GS13-15 (based on the Zadoks scale), (Zadoks et al., 1974) the seedlings were thinned to one plant per pot. Wheat

plants were grown on equal volumes of Levington Advance Seed and Modular F1 low nutrient compost (ICL, Everris, Ipswich, Suffolk, England, United Kingdom) containing 96 N, 49 P and 159 K mg/L. All plants were irrigated manually with deionised water under well-watered (WW) before the imposition of water stress (WS). Pests and diseases (aphids and powdery mildew) were controlled chemically by spraying with Talius® fungicide (1.66 ml/L) and following standard greenhouse procedures. The experiment was structured in a 3-way (2×2×6) factorial split-plot randomised complete block design (RCBD) with twelve (12) replications per treatment. Plants were arranged in a 4 by 12 array on a bench with dimensions: 550 cm length and 180 cm width (Figure 4.1). The intra-row distance between plants was 50 cm. The microclimate data in the glasshouse are reported in Figure 4.2.

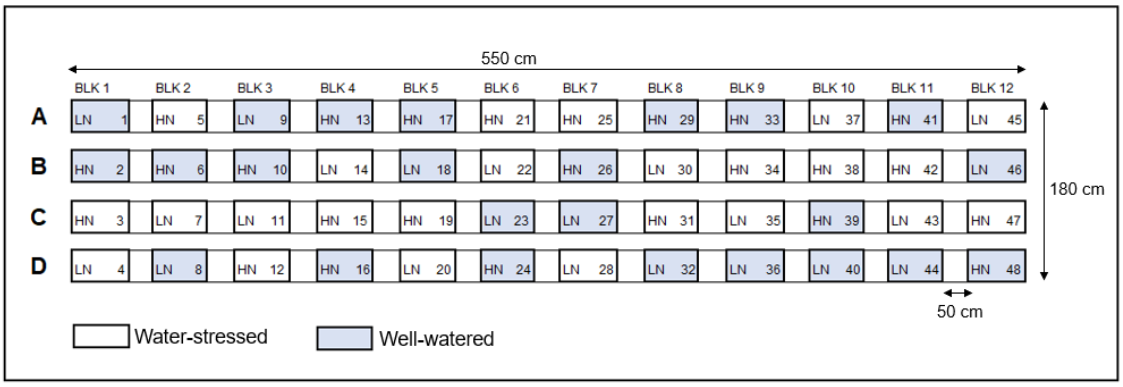

Figure 4.1. The statistical design used for the trial showing the allocation of the 2×2 (i.e., N×irrigation) factorial set of treatments according to a randomised complete block (BLK) design. The experimental area had dimensions of 550×180 cm with 50 cm inter- and intra-row distance between pots. The rectangles are individual pots and those coloured in light blue were kept under well-watered (WW) conditions while non-coloured pots were water-stressed (WS). Pots are numbered from 1 to 48. LN = low N, HN = high N. A-D are individual rows.

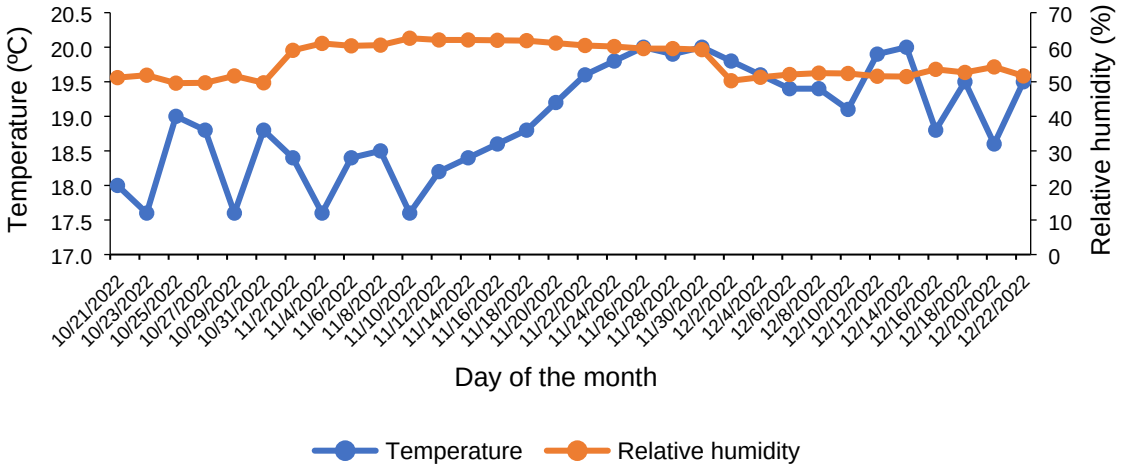

Figure 4.2. The microclimate data showing mean temperature and relative humidity every other day in the glasshouse during the experiment.

4.2.2 Application of nutrient and drought treatments and statistical design

Four treatments based on combinations of two levels of N (high N (HN) and low N (LN) and two levels of irrigation; well-watered (WW) and water-stressed (WS) were tested. The combined treatments were designated as HN-WW, HN-WS, LN-WW and LN-WS. The water and N levels were chosen to create a range in the N-water status and test the utility of spectral reflectance sensing to detect these differences. Before the imposition of WS, plants were supplied with modified Letcombe nutrient solution in accordance with their respective treatments as adopted recently by Cudjoe et al. (2023b). A total volume of 900 mL of the nutrient solution was applied to each pot with saucers containing 615 g compost in staggered applications. The N concentrations for HN and LN were 58.7 mM and 5.8 mM, respectively. Plants grown under HN received 769.9 mg N per pot while LN plants were supplied with 76.99 mg N per pot. A week after the last N application at 50 DAS, WS was imposed during stem elongation (GS33) by withholding water for two weeks (14 days). Before the imposition of WS, 91 g of plastic poly pellets (Hugge Design Ltd., UK) were added to each pot to cover the soil surface to reduce excessive evaporative loss from the soil. WW conditions were maintained at 80% field/pot capacity of the soil. To keep the soil moisture constant, pots were manually weighed and the weight of the pots was recorded every other day using an analytical balance. In parallel, soil moisture content (SMC) was monitored with the aid of a two-pin SM150T soil moisture sensor (Delta-T Devices Ltd., Cambridge, England, UK).

4.2.3 Data collection

4.2.3.1 Spectral reflectance measurements

The PolyPen RP410/UVIS handheld contact spectroradiometer (Photon Systems Instruments, Drasov, Czech Republic), capable of measuring the wavelength range of 320-790 nm of the electromagnetic spectrum at intervals of 1.9 nm, was used to collect leaf spectral reflectance data. Spectral reflectance data was collected from the uppermost fully expanded leaf of the plants from 11:00 to 16:00 h GMT. Spectral data were measured using the same fully expanded leaf of the main stem at GS33 to GS39 during the 14-d drought period on days 0, 3, 6, 9, 12 and 14. Measurements were acquired from five plants for each treatment selected at random from the trial. Three readings were made on a single leaf per plant and then averaged. The spectrometer sensor was calibrated before measurement and periodically with a diffuse white reference standard (Spectralon®, Labsphere, Inc., North Sutton, USA). The PolyPen RP410 device integrates a xenon incandescent lamp as an internal light source, with radiation emitted between 380-1050 nm. The PolyPen RP410 incorporates pre-defined formulae for calculating commonly used SRIs in addition to indices that were manually computed. Initially, to detect differences in the spectral signature acquired from the various treatment combinations, the spectra from each treatment were averaged and the total mean spectrum was examined (Figure 4.3). The SRIs used in this study were computed from narrow-band wavelengths and are reported in Table 4.1.

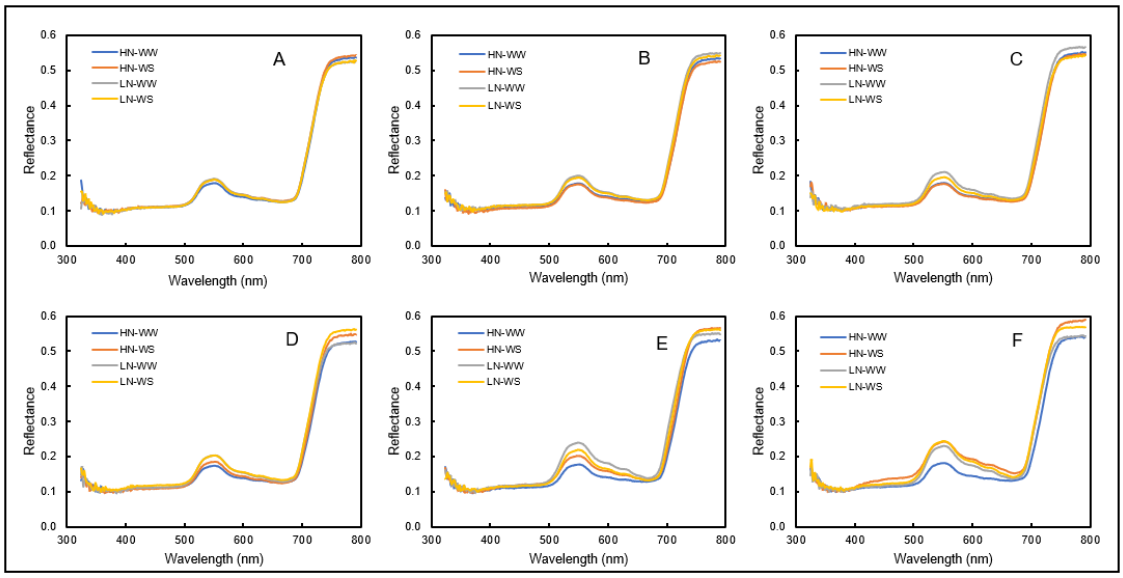

Figure 4.3. Reflectance spectra of wheat leaves exposed to irrigation and N treatments at different numbers of days after water stress (DAWS). It can be observed from the reflectance spectra that treatments were resolved at (C) 6 DAWS around 500-600 nm in the green region and 700-790 nm in the near-infrared region. By (E) 12 DAWS, a clear separation of the treatment spectra was indicated with spectral reflectance peaking at 550 nm and 790 nm as stressed treatments reflected more pigments (i.e., chlorophyll) to obtain high reflectance values except for LN-WW. Resolution of the treatment spectra was observed at (F) 14 DAWS with stressed treatments (HN-WS and LN-WS) achieving higher reflectance values compared to unstressed treatments (HN-WW and LN-WW). A-F = 0, 3, 6, 9, 12, and 14 DAWS, respectively. HN = high N, LN = low N, WW = well-watered, WS = water stressed.

Table 4.1. List of SRIs computed from narrow-bands and used in this study.

Spectral Reflectance Index	Acronym	Formulation/wavebands	Traits	References
Automatic computed indices from the PolyPen RP410				
Normalised Difference Vegetation Index	NDVI	$(R_{780} - R_{680})/(R_{780} + R_{680})$	Leaf greenness, canopy cover, stress levels, LAI, biomass, photosynthetic activity, vigor, plant health, N status	Rouse et al., 1974
Simple Ratio	SR	(R_{780}/R_{680})	Leaf greenness, vegetation cover, chlorophyll content, vigor, plant health	Chen, 1996
Modified Chlorophyll Absorption in Reflectance Index	MCARI1	$1.2 * [2.5 * (R_{790} - R_{670}) - 1.3 * (R_{790} - R_{550})]$	Chlorophyll concentration, vigor, LAI, stress levels	Daughtry et al., 2000)
Optimised Soil-Adjusted Vegetation Index	OSAVI	$(1 + 0.16) * (R_{790} - R_{670}) / (R_{790} - R_{670} + 0.16)$	Greenness, canopy cover, vigor, biomass	Huete, 1988
Greenness Index	G	(R_{554}/R_{677})	Chlorophyll content, biomass, photosynthetic activity, vigor, LAI, plant health	Daughtry et al., 2000
Modified Chlorophyll Absorption in Reflectance Index	MCARI	$[(R_{700} - R_{670}) - 0.2 * (R_{700} - R_{550})] * (R_{700}/ R_{670})$	Chlorophyll concentration, vigor, LAI, stress levels	Daughtry et al., 2000
Transformed Chlorophyll Absorption in Reflectance Index	TCARI	$3 \times [(R700 - R670) - 0.2 * (R700-R550) * (R700/R670)]$	Chlorophyll concentration, vigor, LAI, stress levels	Daughtry et al., 2000
Triangular Vegetation Index	TVI	$0.5 * [120 * (R_{750} - R_{550}) - 200 * (R_{670} - R_{550})]$	Chlorophyll content, greenness, stress levels, nutrient status, photosynthetic activity	Zarco-Tejada et al., 2005
Zarco-Tejada and Miller Index	ZMI	(R_{750} / R_{710})	Chlorophyll concentration, LAI, stress levels, photosynthetic activity	Zarco-Tejada et al., 2001
Simple Ratio Pigment Index	SRPI	(R_{430} / R_{680})	Chlorophyll concentration, photosynthetic activity, LAI, vegetation cover, green biomass	Chen, 1996
Normalised Phaeophytinisation Index	NPQI	$(R_{415} - R_{435}) / (R_{415} + R_{435})$	Leaf senescence, drought, nutrient stress, plant health, vigor, crop maturity	Barnes et al., 1992

Photochemical Reflectance Index	PRI	$(R_{531}- R_{570}) / (R_{531}+ R_{570})$	Photosynthetic stress, water stress, light use efficiency, leaf pigment composition	Shrestha et al., 2012
Normalised Pigment Chlorophyll Index	NPCI	$(R_{680}- R_{430}) / (R_{680}+ R_{430})$	Chlorophyll content, photosynthetic activity, stress levels, N status	Daughtry et al., 2000
Carter Indices	Ctr1 and Ctr2	Ctr1 = (R_{695} / R_{420}); Ctr2 = (R_{695} / R_{760})	Chlorophyll concentration, vigor, LAI, stress levels	Carter and Miller, 1994
Lichtenthaler Indices	Lic1 and Lic2	Lic1 = $(R_{790} - R_{680}) / (R_{790} + R_{680})$; Lic2 = (R_{440} / R_{690})	Chlorophyll content, carotenoid content, greenness, photosynthetic activity, stress levels	Lichtenthaler et al., 1996
Structure Intensive Pigment Index	SIPI	$(R_{790}- R_{450}) / (R_{790}+ R_{650})$	Pigment concentration, leaf angle, canopy density, canopy structure, chlorophyll content, photosynthetic activity	Peñuelas et al., 1995
Gitelson and Merzlyak Indices	GM1 and GM2	GM1 = (R_{750}/ R_{550}); GM2 = (R_{750}/ R_{700})	Chlorophyll concentration, greenness, plant health status, vegetation biomass	Gitelson and Merzlyak, 1997
Anthocyanin Reflectance Indices	ARI1 and ARI2	ARI1 = $(1/R_{550}-1/R_{700})$; ARI2 = $R_{790}*(1/R_{550}-1/R_{700})$	Stress levels, phenological stage, anthocyanin concentration, leaf coloration, fruit maturity	Gitelson et al., 2009
Carotenoid Reflectance Indices	CRI1 and CRI2	CRI1 = $(1/R_{510}-1/R_{550})$; CRI2 = $(1/R_{510}-1/R_{700})$	Carotenoid to chlorophyll ratio, photosynthetic efficiency, leaf senescence, environmental stress response	Gitelson et al., 2002
Renormalised Difference Vegetation Index	RDVI	$(R_{780}-R_{670})/((R_{780}+R_{670}) \wedge 0.5)$	Leaf greenness, canopy cover, stress levels, LAI, biomass, photosynthetic activity, vigor, plant health	Daughtry et al., 2000
Manually computed indices derived from the PolyPen RP410				
Photochemical Reflectance Index	PRI_{550} and PRI_{norm}	$PRI_{550} = (R_{549.1}- R_{530.6}) / (R_{549.1}+ R_{530.6})$; $PRI_{norm} = PRI_{550}/(RDVI*(R_{699.9} / R_{669.4}))$	Photosynthetic stress, water stress, light use efficiency, leaf pigment composition	Shrestha et al., 2012; Sukhova et al., 2022
Green Normalised Difference Vegetation Index	$GNDVI_{780}$	$(R_{780.7} - R_{549.1})/(R_{780.7} + R_{549.1})$	Chlorophyll content, biomass, photosynthetic activity, vigor, LAI, plant health	Rouse et al., 1974

Modified Red Edge Simple Ratio	MRESR	$(R_{749.3} - R_{444.7})/(R_{705.2} - R_{444.7})$	Chlorophyll content, LAI, stress levels, biomass, canopy density, early signs of senescence	Chen, 1996
Red Edge Normalised Difference Vegetation Index	RENDVI	$(R_{749.3} - R_{705.2})/(R_{749.3} + R_{705.2})$	Chlorophyll concentration, stress levels, LAI, vigor, plant health, early growth stage monitoring	Rouse et al., 1974
Normalised Difference Red Edge	NDRE	$(R_{789.4} - R_{719.4})/(R_{789.4} + R_{719.4})$	Chlorophyll concentration, stress levels, LAI, vigor, plant health, early growth stage monitoring	Rouse et al., 1974
Chlorophyll Index Green	CIgreen	$(R_{791.1}/R_{549.1}) - 1$	Chlorophyll concentration, stress levels, senescence, N status, yield, growth	Daughtry et al., 2000
Chlorophyll Index Red Edge	CIrededge	$(R_{791.1}/R_{719.4}) - 1$	Chlorophyll concentration, vigor, LAI, stress levels, N status	Daughtry et al., 2000
Chlorophyll Index	$mNDblue_{530}$ and $mNDblue_{730}$	$mNDblue_{530} = (R_{530.6} - R_{450.4})/(R_{791.1} + R_{450.4})$; $mNDblue_{730} = (R_{730} - R_{450.4})/(R_{791.1} + R_{450.4})$	Chlorophyll concentration, plant stress, N status, growth stage, potential yield	Daughtry et al., 2000
Red Difference Vegetation Index	$rDVI_{790}$	$(R_{789.4} - R_{680.2})$	Chlorophyll content, LAI, stress levels, biomass, vegetation density, vigor, plant health	Rouse et al., 1974
Green Simple Ratio	$gSRa_{790}$	$(R_{789.4}/R_{549.1})$	Leaf greenness, vegetation cover, chlorophyll content, vigor, plant health	Chen, 1996
Red Simple Ratio	SRa_{790}	$(R_{789.4}/R_{680.2})$	Chlorophyll content, vegetation cover, plant stress, vigor, biomass, LAI	Chen, 1996

4.2.3.2 Measurement of morpho-physiological indicators

4.2.3.2.1 Leaf-level gas exchange measurement

Gas exchange parameters including A_n (µmol CO_2 m^{-2} s^{-1}), stomatal conductance (G_s, mmol H_2O m^{-2} s^{-1}), transpiration rate (E, mol H_2O m^{-2} s^{-1}) and intrinsic water use efficiency (WUE_i = A_n/G_s, µmol CO_2 mmol H_2O) were measured with a portable photosynthesis system LI-6400XT (LI-COR Biosciences Inc., Lincoln, NE, USA), equipped with the 6400-40 LCF chamber. Gas exchange measurements were conducted from 11:00 to 16:00 h GMT using the uppermost fully expanded leaves of the main stem from five plants in each treatment at stem elongation (GS33–GS39) during the drought phase at 0, 3, 6, 9, 12 and 14 DAWS. The randomisation order of the experimental layout was followed to account for the possible effects of the time of day on the measurements. The flow rate was set at 200 µmol s^{-1}, leaf chamber CO_2 concentration was set to 400 µmol mol^{-1}, leaf temperature was maintained at 20 °C, RH was adjusted between 60–65% and PAR was controlled to 1800 µmol m^{-2} s^{-1} to attain maximum photosynthetic capacity. Measurements were taken once gas exchange rates had stabilised within five minutes after the reading began. When the leaf was smaller than the cuvette, the area of the leaf was adjusted during data processing.

4.2.3.2.2 SPAD chlorophyll measurement

Chlorophyll content was measured using a SPAD-502 chlorophyll meter (Soil Plant Analysis Development, Minolta Camera Co., Ltd., Japan). Three readings were made on each leaf and then averaged. SPAD measurements were done synchronously with PolyPen RP410 and gas exchange.

4.2.3.2.3 Leaf area

Three wheat plants from each treatment were destructively harvested at 0, 9 and 14 DAWS for leaf area (LA) measurement. LA was measured with the Area Measurement System, WinDIAS 3 Image Analysis System (Delta-T Devices Ltd., Burwell, Cambridge, England). The video camera shutter speed was set to 10 ms at a resolution of 1280×1024. The WinDIAS 3 was calibrated first with a ruler and then a standard of a known area. The conveyer and ‘Long Leaf Mode’ were then enabled. Individual unfolded leaves were fed carefully through the conveyer one at a time to measure the accumulated area (in cm^2).

4.2.3.2.4 Relative water content

Relative water content (RWC) was measured in fully expanded leaves of the main stem of five plants per treatment at 9 and 14 DAWS. The fully expanded leaves were detached, and the FW was recorded using an analytical balance, Mettler PM 4600 Delta Range® (Mettler Instrument Ltd., Switzerland). The leaf samples were packed in a sealed plastic bag and maintained in a cooler at 5 °C until they reached the laboratory. The samples were immersed in a Duran bottle filled with 1000 mL of deionised water for 72 h at room temperature to regain turgidity. The samples were removed from the Duran bottle, and excess water was blotted with a paper towel and then weighed to determine the turgid weight (TW). Finally, leaf samples were oven-dried at 70 °C for 48 h until constant DW was achieved. RWC was estimated as follows:

$$RWC\ (\%) = (FW\text{-}DW)/(TW\text{-}DW) * 100 \qquad (4.1)$$

4.2.3.2.5 Shoot fresh weight

For shoot fresh weight (SFW), five wheat plants from each treatment were destructively harvested at 0, 9 and 14 DAWS and the FW (g pot^{-1}) was determined by weighing on an analytical balance, Mettler PM 4600 Delta Range® (Mettler Instrument Ltd., Switzerland).

4.2.3.2.6 Leaf nitrogen content

The leaf samples used for SFW were then oven-dried and milled at a speed of 17500 rpm using the Genogrinder (SPEX SamplePrep®, 2010, USA). The leaf N content (LNC) (%) was estimated for each treatment by laboratory chemical analysis employing the LECO combustion method (LECO CN628 Analyzer, LECO Corporation, St Joseph, Michigan, USA).

4.2.4 Statistical analysis

Spectral and morpho-physiological response variables measured on six successive occasions, i.e., at increasing numbers of days after water stress (DAWS), were analysed using linear mixed models (LMMs) fitted using residual (or restricted) maximum likelihood (REML) (Payne et al., 2011; Bolker, 2015). The repeated measurements over time were considered as split-plot measurements within pots of the basic design resulting in a 3-stratum nested blocking structure (block/pot/occasion). The fixed model

represented the resulting 3-way (2×2×6) factorial treatment structure (D×N×DAWS), with drought (D) and N treatments applied to pots (within blocks) and the DAWS effects (and interactions) tested within pots. F-statistics were used to test all fixed terms (i.e., main effects and interactions), with all tests done at the 5% significance level. Due to the non-orthogonality of the sampling protocol, the pot-level fixed model terms (i.e., D and N) were fitted in their two possible orders to check for consistency between orders of adding these terms into the models. Order of fitting generally had no marked effect on the results and so the 'D then N' order was adopted for presenting results.

The basic random model represented the blocking structure of the overall design and the split-plot nature of the repeated measurements within pots (i.e., block/pot/occasion, sample occasions nested within pots and pots nested within blocks). A pragmatic approach was taken to ignore the fact that the last two time points were only two days apart rather than three; hence, the time points were assumed to be equally spaced. The standard split-plot model was compared to an autocorrelation model with an AR1 covariance structure for the block.pot.occasion term and the need for this extra complexity was assessed via the change in deviance. The extra term was generally found to improve the model and hence the autocorrelation model was adopted as the final model from which to present all results. For all the analyses, variance components (VCs) were constrained to be positive to avoid computational issues. Residuals were inspected to check the assumptions of normality (via histograms and Q-Q plots) and variance homogeneity (via fitted values plots).

Means plots were produced and differences between fitted means for the WS and WW treatments at each level of N on each sampling occasion were assessed against the approximate least significant difference (LSD) at a 5% level of significance. Any of these 12 pairwise differences that exceeded the LSD were considered statistically significant. The Pearson correlation coefficient (r) was used to relate responsive SRIs with morpho-physiological/soil indicators. All analyses and graphics were done using GenStat 22nd edition (VSN International Ltd., Hemel Hempstead, United Kingdom).

4.3 Results

4.3.1 Morpho-physiological drought responses under HN and LN conditions

Under HN, the photosynthetic variables; A_n, G_s, E and WUEi showed a different baseline with higher values for WW plants at 0 DAWS before the irrigation was stopped on WS plants (Table 4.2; Figure 4.4A-D). From the 6th DAWS onwards, A_n and E showed lower significant values for the WS plants. G_s showed a statistically significant difference between WW and WS plants from 0 DAWS onwards (Table 4.2). However, this could not be attributed to the effect of drought as the irrigation was stopped on WS plants just after the measurement on day 0. This was due to the difference in baseline and the same could be said for the 3rd DAWS as the difference was in the same order as 0 DAWS. Apart from this, A_n, G_s and E showed a similar pattern over the 14 days of the drought, displaying a sharp decrease in the values for the WS plants from 6 DAWS (Table 4.2). Under LN, a similar pattern is observed for WS plants, with a sharp decrease observed later than HN plants from 12 DAWS for A_n and E, and from 9 DAWS for G_s (Table 4.2). Drought had significant interactive effects on A_n at 6, 9, 12 and 14 DAWS (D×DAWS), whereas N showed significant effects earlier at 0, 3, 6, 9 and 14 DAWS (N×DAWS) (Appendix C, Table C-1). Drought had a statistically significant effect on G_s at 3, 6, 9, 12 and 14 DAWS with an interactive effect (D×DAWS), while N had a significant effect earlier at time 0 and later at 14 DAWS, with an interactive effect (N×DAWS) (Appendix C, Table C-1). Similarly to G_s, drought had a statistically significant effect on E at 6, 9, 12 and 14 DAWS with an interactive effect (D×DAWS) (Appendix C, Table C-1), while N supply was significant at only 6 DAWS, indicating a lesser impact but with an interactive effect (N×DAWS) (Appendix C, Table C-1).

WUEi showed a different pattern to the three previous gas exchange variables (Table 4.2; Figure 4.4D). A sharp increase in WUEi was observed for WS plants from 6 DAWS for HN plants and from 9 DAWS for LN plants before dropping at 14 DAWS (Table 4.2; Figure 4.4D). Statistically significant differences were observed on the 6th, 9th and 12th DAWS for HN plants while it was only significant at the 12th DAWS for the LN plants (Table 4.2). Drought had significant interactions at 6, 9 and 12 DAWS, whereas N had a significant interactive effect at 6 and 9 DAWS (Appendix C, Table C-1).

The N status indicators: LNC and SPAD showed different drought response patterns (Table 4.2). The raw data distribution of the different treatments and residual plots for LNC and SPAD are provided in Appendix C, Figure C-1. For LNC, mean values of WS plants were slightly higher compared to WW plants except at 14 DAWS, with no significant difference observed under HN (Table 4.2; Figure 4.4F). A similar trend was observed under LN (Table 4.2). Consequently, drought and N supply did not have any significant effect or interaction on LNC (Appendix C, Table C-1). The WW plants recorded high mean SPAD values compared to WS plants, except for 0 DAWS under HN (Table 4.2; Figure 4.4E). A statistically significant difference between WW and WS plants was observed consistently at 3, 6, 9, 12 and 14 DAWS under HN (Table 4.2; Figure 4.4E). A similar trend was seen under LN as WW plants recorded high SPAD values compared to WS plants except for 0 and 3 DAWS (Table 4.2; Figure 4.4E). A significant difference between WW and WS plants was observed at 6, 9 and 14 DAWS (Table 4.2). Both drought and N stress had significant interactive effects on SPAD values at 6, 9, 12 and 14 DAWS (Appendix C, Table C-1).

Mean values of SFW recorded in WW plants were high compared to WS plants except at 0 DAWS under HN, with significant differences between treatment means indicated at 0, 9 and 14 DAWS (Table 4.2; Figure 4.4H). A similar observation was recorded under LN conditions with significant differences between treatments observed at 9 and 14 DAWS (Table 4.2). Both drought and N supply had significant interactions at 9 and 14 DAWS (Appendix C, Table C-1). Additionally, mean values of LA recorded in WW plants were high compared to WS plants except for 0 DAWS under HN, with a significant difference between treatments indicated at 14 DAWS (Table 4.2; Figure 4.4I). A similar trend was observed under LN but with a significant difference between treatment means observed at 9 and 14 DAWS (Table 4.2). Both drought and N had significant interactive effects on LA at 9 and 14 DAWS (Appendix C, Table C-1).

Drought stress indicators: RWC and SMC showed similar response trends (Table 4.2). Appendix C, Figure C-2 shows the data distribution of the different treatments and residual plots of RWC and SMC. Under both HN and LN conditions, mean values of RWC in WW plants were high compared to WS plants with a significant difference between treatments indicated at 9 and 14 DAWS (Table 4.2; Figure 4.4G). Interestingly, WS plants under LN recorded high RWC compared to WS plants under HN at 9 and 14

DAWS (Table 4.2). Only drought had significant interactive effects at 9 and 14 DAWS (D×DAWS) (Appendix C, Table C-1). The amplitude of drought responses was greater under HN compared to LN.

For SMC, under both HN and LN conditions, mean values of WW plants were high compared to WS plants except 0 DAWS with significant differences between treatments observed consistently at 3, 6, 9, 12 and 14 DAWS (Table 4.2; Figure 4.4J). Similarly to RWC, drought had a significant interactive effect on SMC at 9, 12 and 14 DAWS (Appendix C, Table C-1). Generally, the significant difference between treatment means observed in the variables discussed under both HN and LN at specific DAWS suggests a 3-way interactive effect (D×N×DAWS) (Table 4.2). In parallel, the amplitude of drought responses under HN was faster and greater compared to LN conditions in all variables except LNC (Table 4.2).

Table 4.2. Descriptive statistics (predicted means from LMMs and absolute differences between drought (D) and well-watered (WW) means with approximate LSD) for morpho-physiological parameters including net CO_2 assimilation rate (A_n), stomatal conductance (G_s), transpiration rate (E), intrinsic water use efficiency (WUEi), SPAD, leaf nitrogen content (LNC), relative water content (RWC), shoot fresh weight (SFW), leaf area (LA) and soil moisture content (SMC) in response to high nitrogen (HN) and low nitrogen (LN) conditions on six occasions after water stress was applied (DAWS). Absolute difference (Absolute Diff.) values greater than the approximate (Approx.) least significant differences (LSDs) are considered statistically significant at the 5% level and shown in bold. The full results are shown in Appendix C, Table C-1.

Model term		**D×N×DAWS**							
Treatment		**HN**				**LN**			
		Drought	**Well-watered**	**Absolute Diff.**	**Approx. LSD**	**Drought**	**Well-watered**	**Absolute Diff.**	**Approx. LSD**
Parameter	**DAWS**								
A_n **(µmol CO_2 m^{-2} s^{-1})**	0	23.49	27.59	4.10	4.33	20.75	20.99	0.24	4.33
	3	23.49	27.71	4.22	4.33	19.12	20.59	1.46	4.33
	6	16.91	28.25	**11.34**	4.33	19.49	19.29	0.20	4.33
	9	14.02	27.04	**13.02**	4.33	16.29	16.82	0.53	4.33
	12	3.24	23.55	**20.31**	4.33	7.82	13.82	**6.00**	4.33
	14	0.16	22.32	**22.16**	4.47	1.18	10.92	**9.74**	4.33
	Mean	13.55	26.08	**12.52**	4.35	14.11	17.07	3.03	4.33
G_s **(mmol H_2O m^{-2} s^{-1})**	0	0.27	0.35	**0.09**	0.06	0.25	0.25	0.01	0.06
	3	0.25	0.33	**0.08**	0.06	0.23	0.27	0.04	0.06
	6	0.13	0.36	**0.23**	0.06	0.25	0.26	0.01	0.06
	9	0.11	0.36	**0.25**	0.06	0.19	0.26	**0.07**	0.06
	12	0.02	0.31	**0.29**	0.06	0.07	0.21	**0.14**	0.06
	14	0.01	0.29	**0.28**	0.06	0.01	0.20	**0.18**	0.06
	Mean	0.13	0.33	**0.20**	0.06	0.17	0.24	**0.07**	0.06
E **(mol H_2O m^{-2} s^{-1})**	0	0.0034	0.0039	0.0005	0.0006	0.0034	0.0032	0.0001	0.0006
	3	0.0032	0.0037	0.0005	0.0006	0.0031	0.0034	0.0003	0.0006
	6	0.0020	0.0041	**0.0021**	0.0006	0.0039	0.0038	0.0001	0.0006
	9	0.0012	0.0028	**0.0016**	0.0006	0.0021	0.0024	0.0004	0.0006
	12	0.0003	0.0028	**0.0025**	0.0006	0.0011	0.0023	**0.0013**	0.0006
	14	0.0002	0.0032	**0.0031**	0.0006	0.0002	0.0023	**0.0021**	0.0006
	Mean	0.0017	0.0034	**0.0017**	0.0006	0.0023	0.0029	**0.0007**	0.0006

Table 4.2 continued

WUEi (µmol CO_2 mmol H_2O)	0	88.39	79.21	9.18	23.86	83.45	87.26	3.80	23.86
	3	95.14	84.43	10.71	23.86	83.72	76.72	7.01	23.86
	6	134.68	80.34	**54.35**	23.86	78.62	74.02	4.61	23.86
	9	140.10	76.56	**63.54**	23.86	84.87	63.37	21.50	23.86
	12	138.22	76.18	**62.04**	23.86	115.94	66.04	**49.90**	23.86
	14	73.81	77.12	3.30	25.82	75.49	52.43	23.06	23.86
	Mean	111.72	78.97	**33.85**	24.19	87.01	69.97	17.04	23.86
SPAD	0	44.72	44.04	0.68	4.42	43.0	40.2	2.79	4.42
	3	41.25	46.66	**5.41**	4.42	41.9	41.1	0.82	4.42
	6	40.10	50.34	**10.24**	4.42	36.8	42.0	**5.22**	4.42
	9	36.22	51.28	**15.06**	4.42	35.5	41.7	**6.21**	4.42
	12	34.45	48.48	**14.03**	4.42	32.0	35.6	3.60	4.42
	14	31.00	49.04	**18.04**	4.42	31.1	37.6	**6.50**	4.42
	Mean	37.96	48.31	**10.58**	4.42	36.7	39.7	4.19	4.42
LNC (%)	0	5.04	4.96	0.09	0.49	3.46	3.42	0.04	0.49
	3	-	-	-	-	-	-	-	-
	6	-	-	-	-	-	-	-	-
	9	5.15	5.11	0.04	0.55	2.56	2.62	0.06	0.49
	12	-	-	-	-	-	-	-	-
	14	4.70	4.90	0.20	0.38	2.36	2.29	0.07	0.38
	Mean	4.96	4.99	0.11	0.48	2.79	2.78	0.06	0.46
RWC (%)	0	-	-	-	-	-	-	-	-
	3	-	-	-	-	-	-	-	-
	6	-	-	-	-	-	-	-	-
	9	47.86	84.48	**36.62**	14.00	53.81	74.43	**20.62**	12.52
	12	-	-	-	-	-	-	-	-
	14	40.77	87.24	**46.47**	10.29	47.31	73.87	**26.56**	10.29
	Mean	44.32	85.86	**41.55**	12.15	50.56	74.15	**23.59**	11.41

Table 4.2 continued

SFW (g pot^{-1})	0	6.06	5.62	**0.44**	0.42	5.42	5.43	0.00	0.42
	3	-	-	-	-	-	-	-	-
	6	-	-	-	-	-	-	-	-
	9	5.39	6.70	**1.30**	0.47	5.32	5.87	**0.54**	0.42
	12	-	-	-	-	-	-	-	-
	14	4.38	8.12	**3.74**	0.33	4.57	5.87	**1.30**	0.35
	Mean	5.28	6.81	**1.83**	0.41	5.11	5.72	**0.61**	0.40
LA (cm^2)	0	32.36	31.01	1.35	2.57	26.58	26.27	0.31	2.76
	3	-	-	-	-	-	-	-	-
	6	-	-	-	-	-	-	-	-
	9	32.36	33.66	1.30	2.83	25.45	28.31	**2.86**	2.79
	12	-	-	-	-	-	-	-	-
	14	22.14	42.19	**20.05**	2.01	21.21	28.29	**7.08**	2.20
	Mean	28.95	35.62	**7.57**	2.47	24.41	27.62	**3.42**	2.58
SMC (%)	0	41.75	41.43	0.32	7.93	51.48	47.92	3.56	8.32
	3	29.0	48.3	**19.32**	7.93	44.2	61.4	**17.15**	8.32
	6	17.2	29.4	**12.20**	7.93	23.0	51.7	**28.78**	8.32
	9	10.09	40.47	**30.38**	7.93	13.22	66.12	**52.90**	8.32
	12	8.9	48.0	**39.14**	7.93	9.7	74.0	**64.29**	8.32
	14	6.63	53.07	**46.44**	7.93	7.04	66.57	**59.53**	8.32
	Mean	18.92	43.45	**24.63**	7.93	24.77	61.29	**37.70**	8.32

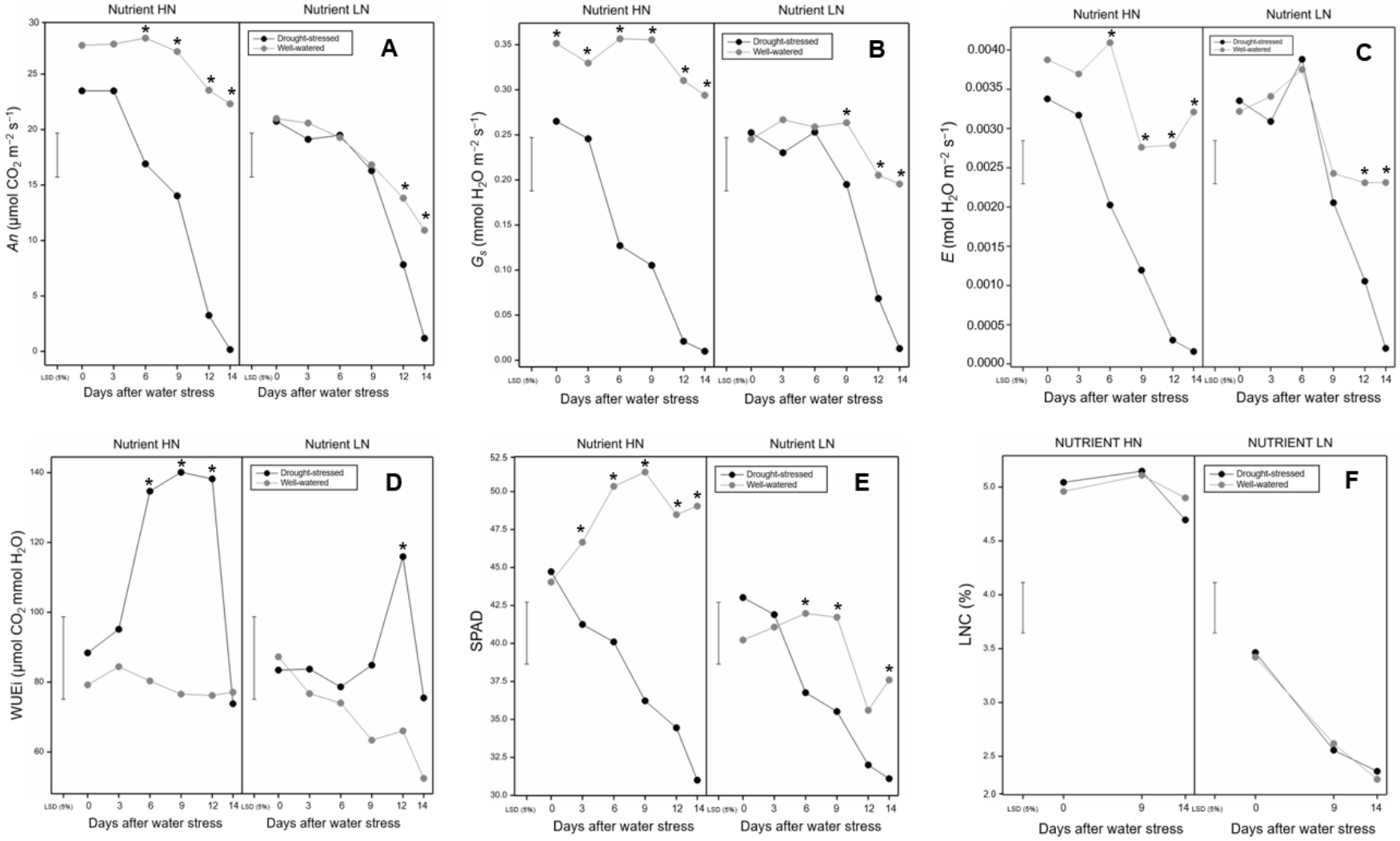
Nutrient HN
Nutrient LN
Drought-stressed
Well-watered
A
B
C
D
E
F
An (µmol CO2 m−2 s−1)
Gs (mmol H2O m−2 s−1)
E (mol H2O m−2 s−1)
WUEi (µmol CO2 mmol H2O)
SPAD
LNC (%)
LSD (5%)
Days after water stress

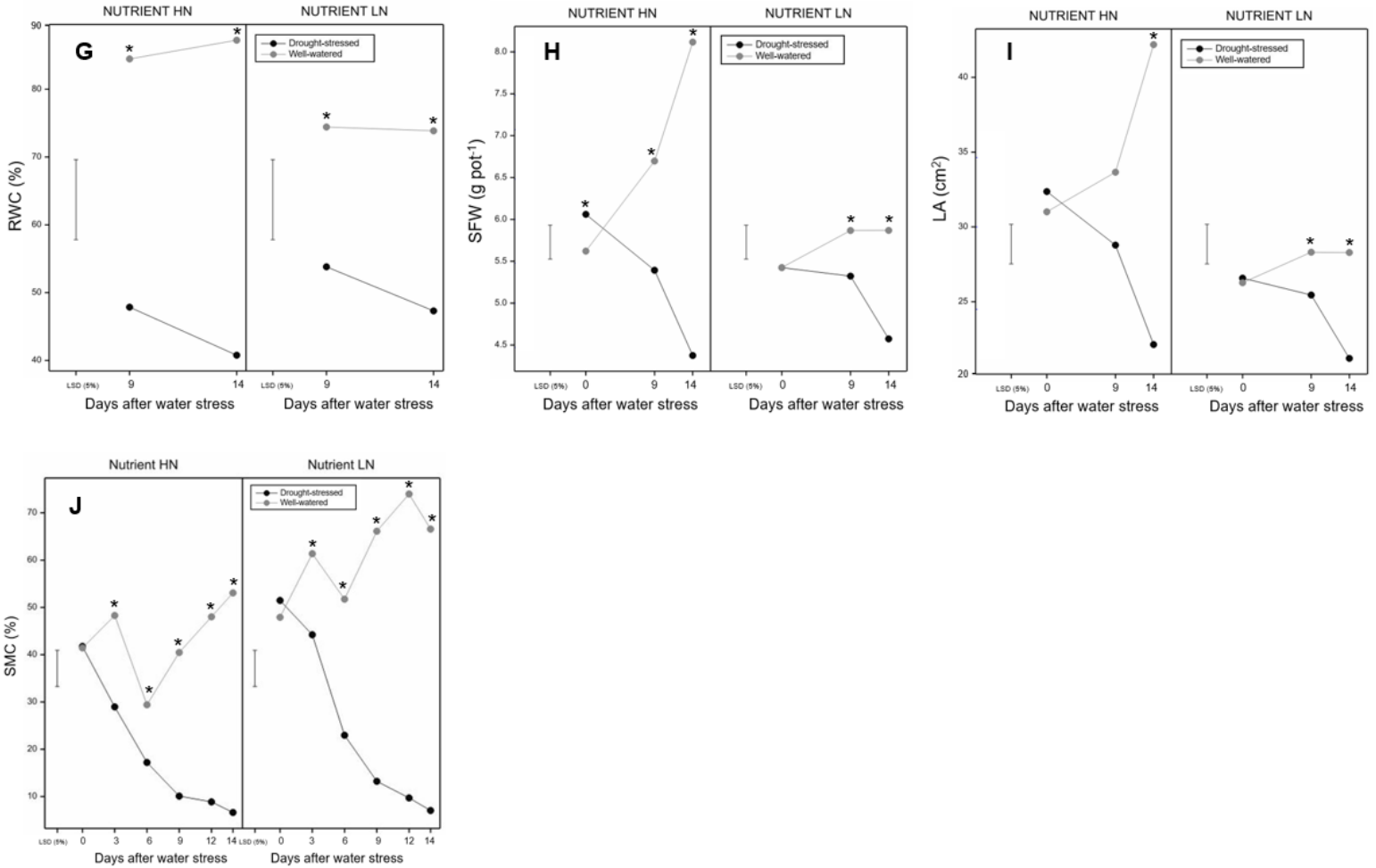

Figure 4.4. Time courses of spring wheat morpho-physiological responses under HN and LN nutrient, and drought-stressed and well-watered conditions: (A) A_n, (B) G_s, (C) E, (D) WUEi, (E) SPAD, (F) LNC, (G) RWC, (H) SFW, (I) LA and (J) SMC. Plotted means are predictions from linear mixed models (LMMs). Bars represent average approximate LSDs at the 5% significance level. Asterisks (*) indicate significant difference between drought-stressed and well-watered treatments under different N availabilities at 5% significance level.

4.3.2 Does drought response measured by spectral reflectance affected by the nitrogen input?

Similarly to the morpho-physiological measurements, the estimated means values from the 3-way component (D×N×DAWS) (Table 4.3) and 2-way component (D×DAWS) and (N×DAWS) (Appendix C, Table C-2) of the REML model were evaluated to look at the drought responses of the SRIs under HN and LN. Among all the SRIs, TVI, RDVI and rDVI_790 showed the earliest response to drought with a significant difference between WW and WS plants observed from 9 DAWS under HN (Table 4.3). MCARI1, ARI1, ARI2 and CRI2 showed significant differences from 12 DAWS while all other SRIs (e.g., NDVI, SR, G, ZMI, TCARI, PRI, Ctr1, SIPI, NPQI, GM1, GM2, CRI1, PRI/NDVI, GNDVI_780, MRESR, RENDVI, NDRE, CIgreen, CIrededge and gSRa_790) displayed either a significant difference between WW and WS plants at 14 DAWS or were not showing any significance difference (OSAVI, SPRI, NPCI, Ctr2, PRI_550, PRI_norm and mNDblue_730) (Table 4.3).

Under LN, the earliest response to drought with a significant difference between WW and WS plants was observed by NPQI at 3 DAWS (Table 4.3). TVI showed a significant difference between WW and WS from 6 DAWS. Only rDVI_790 showed a statistically significant difference between WW and WS plants from 9 DAWS (Table 4.3). SRIs including ARI1, Lic1, Lic2 and SRa_790 showed a statistically significant difference between treatments from 12 DAWS. ARI2 showed a significant difference between WW and WS first at 14 DAWS while all the other SRIs did not show any significant differences between WW and WS treatments (Table 4.3).

Generally, the significant difference between WW and WS treatments observed by SRIs under either HN, LN or both at specific DAWS indicates a 3-way interactive effect (D×N×DAWS) (Table 4.3). The earliest (D×DAWS) interaction was observed from 9 DAWS by MCARI1, TVI, RDVI and rDVI_790 (Appendix C, Table C-2). SRIs including OSAVI, NPCI, ARI1 and ARI2 showed (D×DAWS) interaction from 12 DAWS. SR, G, PRI, GMI, CRI1, CRI2, PRI/NDVI, GNDVI_780, CIgreen and gSRa_790 showed (D×DAWS) interaction at 14 DAWS (Appendix C, Table C-2).

The earliest (N×DAWS) interaction was observed from the onset of WS at 0 DAWS by GNDVI_780 since N fertilisation was initiated several weeks before the imposition of

WS (Appendix C, Table C-2). SRIs that showed (N×DAWS) interaction from 3 DAWS include MCARI1, G, TVI, NPCI, GM1, ARI1, ARI2, MRESR, CIgreen and gSRa_790 (Appendix C, Table C-2). From 6 DAWS, ZMI, Ctr1, Lic2, GM2, PRI_550, NDRE, CIrededge, mNDblue_530 and mNDblue_730 showed (N×DAWS) interaction (Appendix C, Table C-2). Additionally, TCARI, Ctr2, CRI1 and RENDVI showed (N×DAWS) interaction from 12 DAWS while only CRI2 showed (N×DAWS) interaction from 14 DAWS (Appendix C, Table C-2). SRIs that showed both (D×DAWS) and (N×DAWS) interactions were MCARI1, TVI, ARI1, ARI2, NPCI, GM1, CRI2, GNDVI_780 and gSRa_790 (Appendix C, Table C-2).

Table 4.3. Descriptive statistics (predicted means from LMMs and absolute differences between drought (WS) and well-watered (WW) means with approximate LSD) for spectral reflectance indices in response to high nitrogen (HN) and low nitrogen (LN) conditions on six occasions after water stress was applied (DAWS). Absolute difference (Absolute Diff.) values greater than the approximate (Approx.) least significant differences (LSDs) are considered statistically significant at the 5% level and shown in bold. The full results are shown in Appendix C, Table C-2.

Model term		D×N×DAWS							
Treatment		HN				LN			
		Drought	Well-watered	Absolute Diff.	Approx. LSD	Drought	Well-watered	Absolute Diff.	Approx. LSD
Index	DAWS								
NDVI	0	0.60	0.60	0.01	0.04	0.60	0.59	0.01	0.04
	3	0.60	0.60	0.00	0.04	0.59	0.59	0.00	0.04
	6	0.61	0.60	0.00	0.04	0.59	0.58	0.01	0.04
	9	0.60	0.60	0.00	0.04	0.59	0.57	0.01	0.04
	12	0.59	0.59	0.01	0.04	0.58	0.54	0.03	0.04
	14	0.54	0.60	**0.06**	0.04	0.55	0.55	0.00	0.04
	Mean	0.59	0.60	0.01	0.04	0.58	0.57	0.01	0.04
SR	0	3.95	4.03	0.08	0.39	3.96	3.88	0.08	0.39
	3	3.98	4.00	0.02	0.39	3.85	3.87	0.02	0.39
	6	4.07	4.02	0.05	0.39	3.87	3.80	0.07	0.39
	9	4.02	4.00	0.01	0.39	3.86	3.70	0.16	0.39
	12	3.83	3.93	0.09	0.39	3.74	3.46	0.28	0.39
	14	3.36	3.97	**0.61**	0.39	3.50	3.47	0.04	0.39
	Mean	3.87	3.99	0.15	0.39	3.80	3.70	0.11	0.39
MCARI1	0	0.70	0.67	0.03	0.05	0.68	0.68	0.00	0.05
	3	0.66	0.66	0.00	0.05	0.69	0.71	0.02	0.05
	6	0.68	0.68	0.00	0.05	0.69	0.74	0.05	0.05
	9	0.70	0.65	0.05	0.05	0.72	0.68	0.04	0.05
	12	0.73	0.65	**0.08**	0.05	0.75	0.75	0.00	0.05
	14	0.77	0.67	**0.10**	0.05	0.78	0.73	0.05	0.05
	Mean	0.71	0.66	0.04	0.05	0.72	0.72	0.03	0.05
OSAVI	0	0.58	0.58	0.00	0.02	0.58	0.57	0.00	0.02
	3	0.57	0.57	0.00	0.02	0.57	0.58	0.01	0.02
	6	0.58	0.58	0.00	0.02	0.57	0.58	0.00	0.02
	9	0.58	0.57	0.01	0.02	0.58	0.56	0.01	0.02
	12	0.58	0.57	0.01	0.02	0.58	0.56	0.02	0.02
	14	0.56	0.57	0.01	0.02	0.57	0.56	0.01	0.02
	Mean	0.58	0.57	0.01	0.02	0.60	0.60	0.00	0.02
G	0	1.45	1.39	0.05	0.13	1.49	1.49	0.00	0.13
	3	1.38	1.38	0.00	0.13	1.46	1.49	0.03	0.13
	6	1.37	1.36	0.01	0.13	1.47	1.52	0.05	0.13
	9	1.44	1.34	0.09	0.13	1.48	1.55	0.07	0.13
	12	1.47	1.35	0.12	0.13	1.62	1.65	0.03	0.13
	14	1.55	1.35	**0.20**	0.13	1.65	1.64	0.01	0.13
	Mean	1.44	1.36	0.08	0.13	1.53	1.56	0.03	0.13
MCARI	0	0.12	0.10	0.02	0.06	0.12	0.12	0.00	0.06
	3	0.10	0.09	0.01	0.06	0.12	0.13	0.01	0.06
	6	0.09	0.09	0.00	0.06	0.12	0.14	0.02	0.06
	9	0.11	0.09	0.02	0.06	0.13	0.15	0.02	0.06
	12	0.12	0.09	0.03	0.06	0.17	0.22	0.05	0.06
	14	0.15	0.09	0.06	0.06	0.20	0.20	0.00	0.06
	Mean	0.11	0.09	0.02	0.06	0.14	0.16	0.02	0.06
TCARI	0	-0.15	-0.14	0.01	0.04	-0.15	-0.15	0.00	0.04
	3	-0.14	-0.14	0.00	0.04	-0.15	-0.16	0.00	0.04
	6	-0.14	-0.14	0.00	0.04	-0.15	-0.17	0.01	0.04
	9	-0.15	-0.14	0.01	0.04	-0.16	-0.16	0.00	0.04
	12	-0.16	-0.14	0.02	0.04	-0.18	-0.21	0.03	0.04
	14	-0.19	-0.14	**0.05**	0.04	-0.20	-0.19	0.01	0.04
	Mean	-0.16	-0.14	0.02	0.04	-0.17	-0.17	0.01	0.04

Table 4.3 continued

TVI	0	27.04	25.85	1.19	1.61	25.85	26.00	0.15	1.61
	3	25.42	25.47	0.04	1.61	26.49	27.20	0.71	1.61
	6	26.10	26.16	0.06	1.61	26.50	28.16	**1.66**	1.61
	9	26.70	25.02	**1.68**	1.61	27.64	26.11	1.53	1.61
	12	27.74	25.13	**2.61**	1.61	28.65	28.33	0.32	1.61
	14	28.98	25.78	**3.20**	1.61	29.44	27.65	**1.79**	1.61
	Mean	27.00	25.57	1.46	1.61	27.43	27.24	1.03	1.61
ZMI	0	1.86	1.82	0.04	1.61	1.83	1.82	0.02	1.61
	3	1.94	1.83	0.11	1.61	1.84	1.83	0.02	1.61
	6	1.99	1.79	0.21	1.61	1.84	1.79	0.06	1.61
	9	1.93	1.73	0.20	1.61	1.83	1.73	0.10	1.61
	12	1.93	1.63	0.29	1.61	1.77	1.63	0.14	1.61
	14	1.76	1.63	0.13	1.61	1.70	1.63	0.07	1.61
	Mean	1.90	1.74	0.17	1.61	1.80	1.74	0.07	1.61
SPRI	0	0.84	0.85	0.01	0.03	0.85	0.84	0.00	0.03
	3	0.86	0.85	0.01	0.03	0.86	0.86	0.00	0.03
	6	0.86	0.86	0.00	0.03	0.84	0.86	0.01	0.03
	9	0.83	0.84	0.01	0.03	0.84	0.83	0.01	0.03
	12	0.84	0.84	0.00	0.03	0.83	0.81	0.02	0.03
	14	0.83	0.83	0.00	0.03	0.81	0.81	0.00	0.03
	Mean	0.84	0.84	0.00	0.03	0.84	0.84	0.01	0.03
NPQI	0	-0.006	-0.005	0.001	0.014	-0.002	-0.003	0.000	0.014
	3	-0.003	-0.017	0.014	0.014	0.001	-0.017	**0.018**	0.014
	6	-0.011	-0.004	0.007	0.014	-0.008	-0.006	0.001	0.014
	9	0.000	-0.005	0.005	0.014	-0.008	0.004	0.012	0.014
	12	-0.014	-0.007	0.007	0.014	-0.008	0.000	0.008	0.014
	14	-0.024	-0.009	**0.015**	0.014	-0.009	-0.005	0.004	0.014
	Mean	-0.010	-0.008	0.008	0.014	-0.006	-0.005	0.007	0.014
PRI	0	0.033	0.032	0.000	0.006	0.032	0.032	0.000	0.006
	3	0.028	0.031	0.003	0.006	0.031	0.031	0.000	0.006
	6	0.030	0.029	0.001	0.006	0.030	0.031	0.001	0.006
	9	0.028	0.028	0.000	0.006	0.029	0.030	0.001	0.006
	12	0.025	0.027	0.002	0.006	0.029	0.029	0.000	0.006
	14	0.017	0.030	**0.013**	0.006	0.027	0.026	0.001	0.006
	Mean	0.027	0.030	0.003	0.006	0.029	0.030	0.001	0.006
NPCI	0	0.086	0.081	0.005	0.016	0.084	0.085	0.001	0.016
	3	0.078	0.083	0.005	0.016	0.075	0.078	0.003	0.016
	6	0.075	0.074	0.001	0.016	0.084	0.077	0.008	0.016
	9	0.095	0.088	0.007	0.016	0.085	0.090	0.005	0.016
	12	0.089	0.087	0.002	0.016	0.092	0.103	0.011	0.016
	14	0.095	0.093	0.002	0.016	0.108	0.108	0.000	0.016
	Mean	0.086	0.084	0.004	0.016	0.088	0.090	0.005	0.016
Ctr1	0	1.54	1.49	0.05	0.15	1.52	1.54	0.02	0.15
	3	1.48	1.46	0.02	0.15	1.51	1.55	0.04	0.15
	6	1.42	1.43	0.01	0.15	1.54	1.57	0.03	0.15
	9	1.54	1.45	0.09	0.15	1.51	1.63	0.12	0.15
	12	1.56	1.44	0.11	0.15	1.63	1.79	0.15	0.15
	14	1.63	1.47	**0.16**	0.15	1.78	1.76	0.02	0.15
	Mean	1.53	1.46	0.07	0.15	1.58	1.64	0.06	0.15
Ctr2	0	0.31	0.31	0.01	0.05	0.32	0.32	0.00	0.05
	3	0.31	0.30	0.01	0.05	0.32	0.32	0.00	0.05
	6	0.30	0.30	0.00	0.05	0.32	0.33	0.01	0.05
	9	0.31	0.30	0.00	0.05	0.32	0.34	0.02	0.05
	12	0.32	0.31	0.01	0.05	0.33	0.38	0.05	0.05
	14	0.36	0.31	0.05	0.05	0.37	0.37	0.00	0.05
	Mean	0.32	0.30	0.01	0.05	0.33	0.35	0.01	0.05
Lic1	0	0.609	0.610	0.001	0.023	0.611	0.607	0.004	0.023
	3	0.606	0.608	0.002	0.023	0.601	0.606	0.004	0.023
	6	0.612	0.608	0.004	0.023	0.604	0.604	0.000	0.023
	9	0.613	0.603	0.010	0.023	0.602	0.594	0.008	0.023
	12	0.606	0.599	0.007	0.023	0.609	0.583	**0.026**	0.023
	14	0.578	0.602	0.023	0.023	0.586	0.584	0.002	0.023
	Mean	0.604	0.605	0.008	0.023	0.602	0.596	0.007	0.023

Table 4.3 continued

Lic2	0	0.768	0.789	0.021	0.042	0.769	0.763	0.006	0.042
	3	0.785	0.791	0.006	0.042	0.779	0.775	0.003	0.042
	6	0.802	0.793	0.009	0.042	0.764	0.764	0.000	0.042
	9	0.754	0.787	0.034	0.042	0.766	0.736	0.030	0.042
	12	0.755	0.773	0.018	0.042	0.736	0.688	**0.048**	0.042
	14	0.740	0.772	0.032	0.042	0.680	0.691	0.012	0.042
	Mean	0.767	0.784	0.020	0.042	0.749	0.746	0.017	0.042
SIPI	0	0.64	0.64	0.00	0.02	0.64	0.64	0.00	0.02
	3	0.64	0.64	0.00	0.02	0.63	0.63	0.01	0.02
	6	0.64	0.64	0.01	0.02	0.63	0.63	0.00	0.02
	9	0.64	0.64	0.01	0.02	0.63	0.63	0.00	0.02
	12	0.63	0.63	0.00	0.02	0.64	0.62	0.02	0.02
	14	0.60	0.64	**0.04**	0.02	0.62	0.62	0.00	0.02
	Mean	0.63	0.64	0.01	0.02	0.63	0.63	0.01	0.02
GM1	0	2.79	2.91	0.11	0.29	2.73	2.71	0.02	0.29
	3	2.90	2.93	0.03	0.29	2.72	2.70	0.02	0.29
	6	2.98	2.96	0.02	0.29	2.72	2.63	0.09	0.29
	9	2.86	2.95	0.09	0.29	2.70	2.55	0.16	0.29
	12	2.73	2.91	0.17	0.29	2.54	2.36	0.18	0.29
	14	2.40	2.92	**0.52**	0.29	2.38	2.36	0.02	0.29
	Mean	2.78	2.93	0.16	0.29	2.63	2.55	0.08	0.29
GM2	0	2.59	2.70	0.11	0.27	2.55	2.52	0.02	0.27
	3	2.67	2.71	0.04	0.27	2.55	2.53	0.03	0.27
	6	2.77	2.74	0.03	0.27	2.54	2.46	0.08	0.27
	9	2.67	2.73	0.06	0.27	2.52	2.38	0.15	0.27
	12	2.63	2.69	0.06	0.27	2.43	2.21	0.23	0.27
	14	2.35	2.69	**0.34**	0.27	2.28	2.20	0.08	0.27
	Mean	2.61	2.71	0.11	0.27	2.48	2.38	0.10	0.27
ARI1	0	0.37	0.39	0.02	0.09	0.36	0.37	0.01	0.09
	3	0.45	0.43	0.02	0.09	0.32	0.34	0.02	0.09
	6	0.40	0.41	0.02	0.09	0.35	0.32	0.03	0.09
	9	0.36	0.45	0.09	0.09	0.33	0.34	0.01	0.09
	12	0.19	0.42	**0.23**	0.09	0.20	0.29	**0.10**	0.09
	14	0.09	0.44	**0.35**	0.09	0.18	0.31	**0.13**	0.09
	Mean	0.31	0.43	**0.12**	0.09	0.29	0.33	0.05	0.09
ARI2	0	0.21	0.21	0.00	0.05	0.19	0.19	0.00	0.05
	3	0.24	0.23	0.01	0.05	0.17	0.18	0.01	0.05
	6	0.22	0.23	0.01	0.05	0.19	0.18	0.01	0.05
	9	0.19	0.24	0.04	0.05	0.19	0.18	0.01	0.05
	12	0.11	0.22	**0.12**	0.05	0.11	0.16	0.05	0.05
	14	0.05	0.24	**0.19**	0.05	0.10	0.17	**0.07**	0.05
	Mean	0.17	0.23	**0.06**	0.05	0.16	0.18	0.02	0.05
CRI1	0	2.47	2.44	0.03	0.32	2.68	2.65	0.03	0.32
	3	2.42	2.35	0.07	0.32	2.45	2.51	0.05	0.32
	6	2.30	2.26	0.04	0.32	2.53	2.43	0.10	0.32
	9	2.49	2.35	0.14	0.32	2.43	2.69	0.26	0.32
	12	2.19	2.35	0.16	0.32	2.62	2.45	0.17	0.32
	14	1.96	2.32	**0.36**	0.32	2.36	2.55	0.18	0.32
	Mean	2.30	2.35	0.13	0.32	2.51	2.54	0.13	0.32
CRI2	0	2.84	2.83	0.01	0.36	3.03	3.00	0.03	0.36
	3	2.87	2.79	0.09	0.36	2.76	2.83	0.07	0.36
	6	2.69	2.67	0.02	0.36	2.87	2.74	0.13	0.36
	9	2.85	2.80	0.05	0.36	2.76	3.03	0.26	0.36
	12	2.38	2.77	**0.39**	0.36	2.81	2.73	0.08	0.36
	14	2.05	2.76	**0.71**	0.36	2.54	2.85	0.31	0.36
	Mean	2.61	2.77	0.21	0.36	2.80	2.86	0.15	0.36
RDVI	0	0.51	0.50	0.01	0.02	0.50	0.50	0.00	0.02
	3	0.50	0.50	0.00	0.02	0.50	0.51	0.01	0.02
	6	0.51	0.51	0.00	0.02	0.50	0.51	0.01	0.02
	9	0.51	0.47	**0.04**	0.02	0.51	0.48	**0.03**	0.02
	12	0.52	0.49	**0.03**	0.02	0.52	0.49	**0.03**	0.02
	14	0.50	0.50	0.00	0.02	0.51	0.49	0.02	0.02
	Mean	0.51	0.50	0.01	0.02	0.51	0.50	0.01	0.02

Table 4.3 continued

PRI_550	0	0.031	0.032	0.002	0.005	0.035	0.035	0.001	0.005
	3	0.033	0.031	0.002	0.005	0.032	0.035	0.003	0.005
	6	0.029	0.029	0.000	0.005	0.033	0.036	0.003	0.005
	9	0.032	0.031	0.001	0.005	0.034	0.037	0.002	0.005
	12	0.032	0.032	0.000	0.005	0.039	0.035	0.004	0.005
	14	0.034	0.029	0.005	0.005	0.035	0.038	0.003	0.005
	Mean	0.032	0.031	0.002	0.005	0.035	0.036	0.003	0.005
PRI_norm	0	0.038	0.042	0.004	0.006	0.043	0.044	0.001	0.006
	3	0.043	0.041	0.002	0.006	0.041	0.043	0.002	0.006
	6	0.038	0.039	0.001	0.006	0.041	0.043	0.001	0.006
	9	0.040	0.043	0.003	0.006	0.042	0.045	0.003	0.006
	12	0.040	0.044	0.004	0.006	0.044	0.040	0.004	0.006
	14	0.042	0.039	0.002	0.006	0.039	0.044	0.004	0.006
	Mean	0.040	0.041	0.003	0.006	0.042	0.043	0.003	0.006
PRI/NDVI	0	0.055	0.054	0.001	0.009	0.054	0.054	0.000	0.009
	3	0.047	0.052	0.005	0.009	0.052	0.053	0.001	0.009
	6	0.049	0.048	0.001	0.009	0.050	0.053	0.003	0.009
	9	0.047	0.047	0.000	0.009	0.049	0.052	0.003	0.009
	12	0.043	0.046	0.004	0.009	0.050	0.052	0.003	0.009
	14	0.030	0.049	**0.019**	0.009	0.047	0.047	0.001	0.009
	Mean	0.045	0.049	0.005	0.009	0.051	0.052	0.002	0.009
GNDVI_780	0	0.48	0.50	0.01	0.05	0.47	0.47	0.01	0.05
	3	0.50	0.50	0.00	0.05	0.47	0.46	0.00	0.05
	6	0.51	0.50	0.00	0.05	0.47	0.46	0.02	0.05
	9	0.49	0.50	0.01	0.05	0.47	0.44	0.03	0.05
	12	0.47	0.50	0.02	0.05	0.44	0.40	0.04	0.05
	14	0.42	0.50	**0.08**	0.05	0.41	0.41	0.00	0.05
	Mean	0.48	0.50	0.02	0.05	0.45	0.44	0.01	0.05
MRESR	0	3.11	3.35	0.23	0.43	3.05	3.01	0.04	0.43
	3	3.41	3.46	0.05	0.43	3.12	3.01	0.10	0.43
	6	3.59	3.56	0.03	0.43	3.06	2.89	0.17	0.43
	9	3.28	3.54	0.26	0.43	3.05	2.71	0.33	0.43
	12	3.31	3.43	0.12	0.43	2.81	2.47	0.34	0.43
	14	2.87	3.49	**0.62**	0.43	2.56	2.47	0.10	0.43
	Mean	3.26	3.47	0.22	0.43	2.94	2.76	0.18	0.43
RENDVI	0	0.36	0.38	0.02	0.05	0.36	0.36	0.00	0.05
	3	0.38	0.39	0.00	0.05	0.36	0.36	0.01	0.05
	6	0.40	0.39	0.00	0.05	0.36	0.34	0.01	0.05
	9	0.38	0.39	0.01	0.05	0.36	0.33	0.03	0.05
	12	0.38	0.38	0.01	0.05	0.34	0.29	0.05	0.05
	14	0.33	0.39	**0.06**	0.05	0.31	0.30	0.01	0.05
	Mean	0.37	0.39	0.02	0.05	0.35	0.33	0.02	0.05
NDRE	0	0.20	0.21	0.01	0.03	0.19	0.18	0.01	0.03
	3	0.21	0.21	0.00	0.03	0.19	0.18	0.01	0.03
	6	0.22	0.22	0.01	0.03	0.19	0.18	0.01	0.03
	9	0.21	0.22	0.01	0.03	0.19	0.17	0.02	0.03
	12	0.21	0.22	0.00	0.03	0.17	0.15	0.03	0.03
	14	0.18	0.21	**0.04**	0.03	0.16	0.14	0.01	0.03
	Mean	0.21	0.21	0.01	0.03	0.18	0.17	0.01	0.03
CIgreen	0	1.88	1.98	0.10	0.30	1.81	1.77	0.03	0.30
	3	1.97	2.01	0.04	0.30	1.80	1.76	0.04	0.30
	6	2.06	2.06	0.00	0.30	1.79	1.68	0.11	0.30
	9	1.94	2.03	0.09	0.30	1.76	1.59	0.18	0.30
	12	1.81	1.98	0.18	0.30	1.58	1.38	0.20	0.30
	14	1.47	2.01	**0.54**	0.30	1.40	1.39	0.01	0.30
	Mean	1.86	2.01	0.16	0.30	1.69	1.59	0.10	0.30
CIrededge	0	0.49	0.52	0.03	0.10	0.47	0.45	0.02	0.10
	3	0.54	0.54	0.01	0.10	0.48	0.46	0.02	0.10
	6	0.58	0.56	0.01	0.10	0.48	0.44	0.04	0.10
	9	0.53	0.56	0.03	0.10	0.47	0.40	0.07	0.10
	12	0.55	0.55	0.01	0.10	0.42	0.34	0.08	0.10
	14	0.44	0.56	**0.11**	0.10	0.37	0.34	0.03	0.10
	Mean	0.52	0.55	0.03	0.10	0.45	0.41	0.04	0.10

Table 4.3 continued

mNDblue_530	0	0.10	0.09	0.01	0.03	0.10	0.11	0.00	0.03
	3	0.09	0.09	0.00	0.03	0.10	0.11	0.01	0.03
	6	0.08	0.08	0.00	0.03	0.10	0.11	0.01	0.03
	9	0.10	0.08	0.01	0.03	0.10	0.12	0.02	0.03
	12	0.10	0.09	0.02	0.03	0.13	0.15	0.02	0.03
	14	0.12	0.09	**0.04**	0.03	0.15	0.14	0.01	0.03
	Mean	0.10	0.09	0.01	0.03	0.11	0.12	0.01	0.03
mNDblue_730	0	0.52	0.51	0.01	0.02	0.52	0.53	0.01	0.02
	3	0.50	0.50	0.00	0.02	0.51	0.52	0.01	0.02
	6	0.49	0.50	0.00	0.02	0.52	0.52	0.01	0.02
	9	0.51	0.49	0.02	0.02	0.52	0.54	0.02	0.02
	12	0.50	0.50	0.00	0.02	0.54	0.55	0.01	0.02
	14	0.50	0.50	0.00	0.02	0.55	0.55	0.00	0.02
	Mean	0.51	0.50	0.00	0.02	0.53	0.53	0.01	0.02
rDVI_790	0	0.419	0.407	0.013	0.018	0.400	0.396	0.004	0.018
	3	0.400	0.404	0.004	0.018	0.407	0.413	0.006	0.018
	6	0.414	0.414	0.000	0.018	0.407	0.425	0.018	0.018
	9	0.417	0.397	**0.019**	0.018	0.420	0.391	**0.029**	0.018
	12	0.428	0.395	**0.032**	0.018	0.426	0.406	**0.020**	0.018
	14	0.432	0.404	**0.028**	0.018	0.420	0.398	**0.021**	0.018
	Mean	0.418	0.404	0.016	0.018	0.413	0.405	0.016	0.018
gSRa_790	0	2.87	2.99	0.11	0.30	2.81	2.76	0.05	0.30
	3	2.98	3.01	0.04	0.30	2.79	2.75	0.04	0.30
	6	3.07	3.04	0.03	0.30	2.79	2.68	0.11	0.30
	9	2.95	3.04	0.09	0.30	2.76	2.60	0.16	0.30
	12	2.80	2.97	0.17	0.30	2.59	2.39	0.20	0.30
	14	2.46	2.99	**0.53**	0.30	2.40	2.39	0.02	0.30
	Mean	2.86	3.01	0.16	0.30	2.69	2.60	0.10	0.30
SRa_790	0	4.12	4.15	0.03	0.26	4.16	4.09	0.07	0.26
	3	4.08	4.11	0.03	0.26	4.03	4.08	0.05	0.26
	6	4.16	4.11	0.05	0.26	4.06	4.03	0.02	0.26
	9	4.19	4.05	0.14	0.26	4.01	3.95	0.07	0.26
	12	4.09	3.98	0.11	0.26	4.13	3.83	**0.31**	0.26
	14	3.76	4.00	0.24	0.26	3.87	3.80	0.07	0.26
	Mean	4.07	4.07	0.10	0.26	4.04	3.96	0.10	0.26

4.3.3 Evaluation of spectral reflectance indices for drought and nitrogen stress responses detected individually

All the SRIs assessed in this work (Table 4.1) were subjected to F-statistics and F-Test probabilities via the LMM/REML with an autocorrelation (ARI) model fitted in the D-N order of factors to show their responsiveness to drought (D) and N stress and the underlying interactions (Appendix C, Figure C-3). The results which are summarised in part in Table 4.4 and in greater detail in Appendix C, Table C-3 indicated that SRIs comprising RDVI, rDVI_790, MCARI1, TVI, ARI1 and ARI2 were responsive to drought (Table 4.4). The time course of the drought responsive SRIs under HN and LN nutrient conditions are shown in Figure 4.5A-F. Drought responses were generally significant first at 9 DAWS except TVI which was significant at 6 DAWS under LN (Figure 4.5A-F). Drought responses for ARI1 and ARI2 were significant from 12 DAWS. Additionally, MCARI1, TVI, ARI1 and ARI2 were also responsive to N stress and hence may not be specific to drought or N stress (Table 4.4). Therefore, RDVI and

rDVI_790 are the only SRIs that have a specificity to drought detection (Table 4.4; Figure 4.5 A-B). Appendix C, Figure C-4 shows the raw data distribution of the different treatment conditions for RDVI and rDVI_790. Additionally, the residual plots are shown in Appendix C, Figure C-6.

There was a wide range of SRIs including the pigment (i.e., chlorophyll) based and red-edge group indices such as G, PRI_550, mNDblue_730, Lic2, MRESR, CIrededge, Ctr1, NDRE, mNDblue_530, ZMI, MCARI, CIgreen, gSRa_790, GM1, GM2, RENDVI, CRI1, GNDVI_780 and Ctr2 that showed high responses to only N and may be specific for their detection based on F-statistics and F-test probabilities (p<0.05) as shown in Table 4.4. The time course of the most responsive N specific SRIs under HN and LN nutrient conditions are shown in Figure 4.6A-F. Drought responses for G, MRESR, Ctr1 and NDRE were significant at 14 DAWS while PRI_550 and mNDblue_730 showed no significant difference under HN and LN nutrient conditions (Figure 4.6A-F). The raw data distribution of the different treatment conditions of some N stress-specific SRIs are shown in Appendix C, Figure C-5. Additionally, the residual plots for these SRIs are shown in Figure C-7. SRIs that did not show any responses to either drought or N stress included NDVI, SR, OSAVI, TCARI, SPRI, NPQI, PRI, NPCI, Lic1, SIPI, CRI2, PRI_norm, PRI/NDVI and SRa_790 (Table 4.4). No significant D×N interaction was observed across all SRIs (Table 4.4).

Table 4.4. F-tests from repeated measures ANOVA (RMA) for the main effects of drought (D) and nitrogen (N) on SRIs. The RMA analysis was done considering all treatment combinations and days after water stress (DAWS). Statistically significant results (p<0.05) indicating differences between means for levels of D or N are shown in bold. Full results are given in Appendix C, Table C-3.

Index	D	N	D×N
NDVI	$F_{1,13.17}$=0.86, p=0.371	$F_{1,13.17}$ =1.79, p=0.203	$F_{1,13.2}$=1.72, p=0.213
SR	$F_{1,13.0}$=1.05, p=0.325	$F_{1,13.0}$=2.08, p=0.173	$F_{1,13.0}$=2.50, p=0.138
MCARI1	$F_{1,14.0}$=9.86, p<**0.05**	$F_{1,14.0}$=10.58, p<**0.05**	$F_{1,14.0}$=4.42, p=0.054
OSAVI	$F_{1,13.8}$=1.29, p=0.276	$F_{1,13.8}$=0.40, p=0.538	$F_{1,13.8}$=0.36, p=0.559
G	$F_{1,15.7}$=3.67, p=0.074	$F_{1,15.7}$=18.69, p<**0.001**	$F_{1,15.7}$=3.13, p=0.096
MCARI	$F_{1,14.4}$=1.22, p=0.287	$F_{1,14.4}$=9.66, p<**0.05**	$F_{1,14.4}$=1.72, p=0.210
TCARI	$F_{1,16.6}$=1.91, p=0.185	$F_{1,16.6}$=4.23, p=0.056	$F_{1,16.6}$=1.77, p=0.201
TVI	$F_{1,14.0}$=10.72, p<**0.05**	$F_{1,14.0}$=11.09, p<**0.05**	$F_{1,14.0}$= 4.39, p=0.055
ZMI	$F_{1,11.8}$=0.93, p=0.353	$F_{1,11.8}$=10.93, p<**0.05**	$F_{1,11.8}$=3.13, p=0.103
SPRI	$F_{1,23.7}$=0.03, p=0.856	$F_{1,23.7}$=1.87, p=0.184	$F_{1, 23.7}$=0.47, p=0.500
NPQI	$F_{1,24.1}$=0.33, p=0.572	$F_{1,24.1}$= 2.91, p=0.101	$F_{1, 24.1}$=0.05, p=0.818

PRI	$F_{1,14.9}$ =1.85, p=0.194	$F_{1,14.9}$=1.09, p=0.313	$F_{1,14.9}$=2.06, p=0.172
NPCI	$F_{1,23.5}$=0.04, p=0.853	$F_{1,23.5}$=2.01, p=0.170	$F_{1,23.5}$=0.48, p=0.495
Ctr1	$F_{1,15.7}$=1.17, p=0.295	$F_{1,15.7}$=12.52, p<**0.05**	$F_{1,15.7}$=3.13, p=0.096
Ctr2	$F_{1,13.1}$=0.72, p=0.411	$F_{1,13.1}$=4.93, p<**0.05**	$F_{1,13.1}$=1.30, p=0.275
Lic1	$F_{1,13.9}$=0.02, p=0.878	$F_{1,13.9}$=1.02, p=0.330	$F_{1,13.9}$=0.79, p=0.388
Lic2	$F_{1,16.4}$=1.22, p=0.285	$F_{1,16.4}$=14.98, p<**0.05**	$F_{1,16.4}$=2.30, p=0.148
SIPI	$F_{1,13.8}$=0.34, p=0.567	$F_{1,13.8}$=0.41, p=0.534	$F_{1,13.8}$=1.02, p=0.330
GM1	$F_{1,12.0}$=3.00, p=0.109	$F_{1,12.0}$=8.66, p<**0.05**	$F_{1,12.0}$=3.79, p=0.075
GM2	$F_{1,11.4}$=1.23, p=0.291	$F_{1,11.4}$=8.54, p<**0.05**	$F_{1,11.4}$=3.08, p=0.106
ARI1	$F_{1,14.0}$=16.59, p<**0.05**	$F_{1,8.2}$=8.98, p<**0.05**	$F_{1,10.0}$=3.98, p=0.074
ARI2	$F_{1,13.8}$=15.16, p<**0.05**	$F_{1,8.7}$=8.90, p<**0.05**	$F_{1,10.6}$=3.71, p=0.081
CRI1	$F_{1,11.8}$=0.09, p=0.775	$F_{1,10.5}$=8.13, p<**0.05**	$F_{1,12.7}$=0.01, p=0.916
CRI2	$F_{1,12.4}$=1.38, p=0.262	$F_{1,10.3}$=2.77, p=0.126	$F_{1,12.4}$=0.31, p=0.590
RDVI	$F_{1,24.9}$=10.31, p<**0.05**	$F_{1,24.9}$=0.51, p=0.482	$F_{1,24.9}$=0.06, p=0.802
PRI_550	$F_{1,13.8}$=0.33, p=0.573	$F_{1,9.9}$=43.50, p<**0.001**	$F_{1,11.5}$=3.00, p=0.110
PRI_norm	$F_{1,13.8}$=0.99, p=0.338	$F_{1,10.7}$=2.31, p=0.157	$F_{1,12.2}$=0.00, p=0.969
PRI/NDVI	$F_{1,16.1}$=2.18, p=0.160	$F_{1,16.1}$=4.29, p=0.055	$F_{1,16.1}$=1.40, p=0.253
GNDVI_780	$F_{1,12.4}$=1.88, p=0.194	$F_{1,12.4}$=7.13, p<**0.05**	$F_{1,12.4}$=2.50, p=0.139
MRESR	$F_{1,12.2}$=2.05, p=0.178	$F_{1,12.2}$=18.10, p<**0.05**	$F_{1,12.2}$=4.15, p=0.064
RENDVI	$F_{1,11.7}$=0.97, p=0.345	$F_{1,11.7}$=8.06, p<**0.05**	$F_{1,11.7}$=2.26, p=0.159
NDRE	$F_{1,11.9}$=0.49, p=0.499	$F_{1,11.9}$=12.45, p<**0.05**	$F_{1,11.9}$=2.59, p=0.134
CIgreen	$F_{1,12.1}$=2.79, p=0.121	$F_{1,12.1}$=9.91, p<**0.05**	$F_{1,12.1}$=3.59, p=0.082
CIrededge	$F_{1,12.5}$=0.75, p=0.403	$F_{1,12.5}$=14.92, p<**0.05**	$F_{1,12.5}$=2.84, p=0.117
mNDblue_530	$F_{1,13.9}$=1.59, p=0.229	$F_{1,13.9}$=12.27, p<**0.05**	$F_{1,13.9}$=2.14, p=0.166
mNDblue_730	$F_{1,22.5}$=0.03, p=0.861	$F_{1,22.5}$=55.64, p<**0.001**	$F_{1,22.5}$=2.81, p=0.108
rDVI_790	$F_{1,16.4}$=18.86, p<**0.001**	$F_{1,29.9}$=0.45, p=0.507	$F_{1,28.6}$=1.60, p=0.216
gSRa_790	$F_{1,11.8}$=2.59, p=0.134	$F_{1,11.8}$=9.65, p<**0.05**	$F_{1,11.8}$=3.73, p=0.078
SRa_790	$F_{1,14.0}$=0.15, p=0.702	$F_{1,14.0}$=1.09, p=0.313	$F_{1,14.0}$=0.90, p=0.358

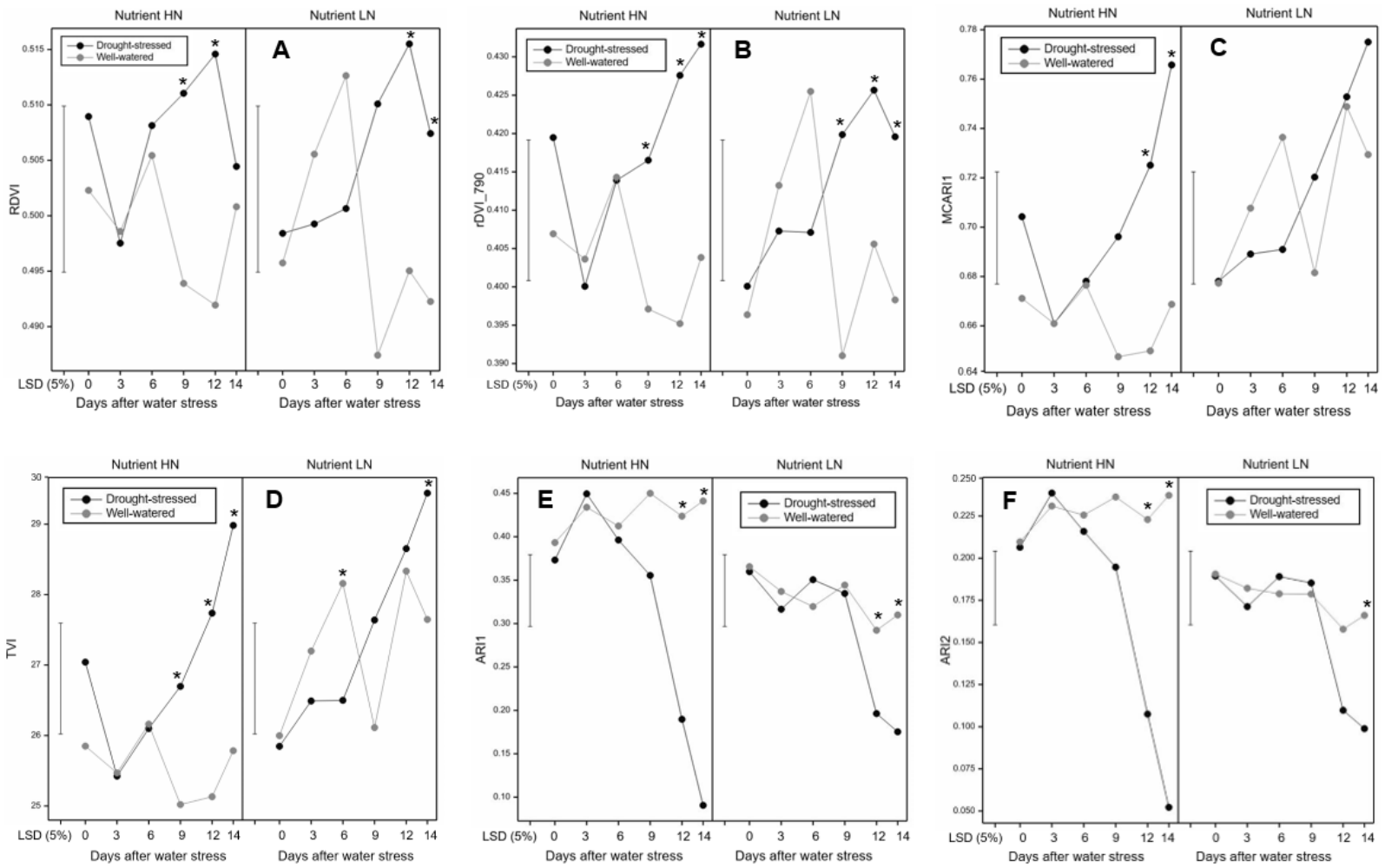

Figure 4.5. Time course of the drought-responsive SRIs comprising (A) RDVI, (B) rDVI_790, (C) MCARI1, (D) TVI, (E) ARI1 and (F) ARI2 under HN and LN nutrient conditions. Plotted means are estimations from the Autocorrelation (AR1) model. Bars represent average approximate LSDs significant at a 5% level of REML means in each treatment combination and days after water stress (DAWS). Asterisks (*) indicate significant difference between drought-stressed and well-watered treatments under different N availabilities at 5% significance level.

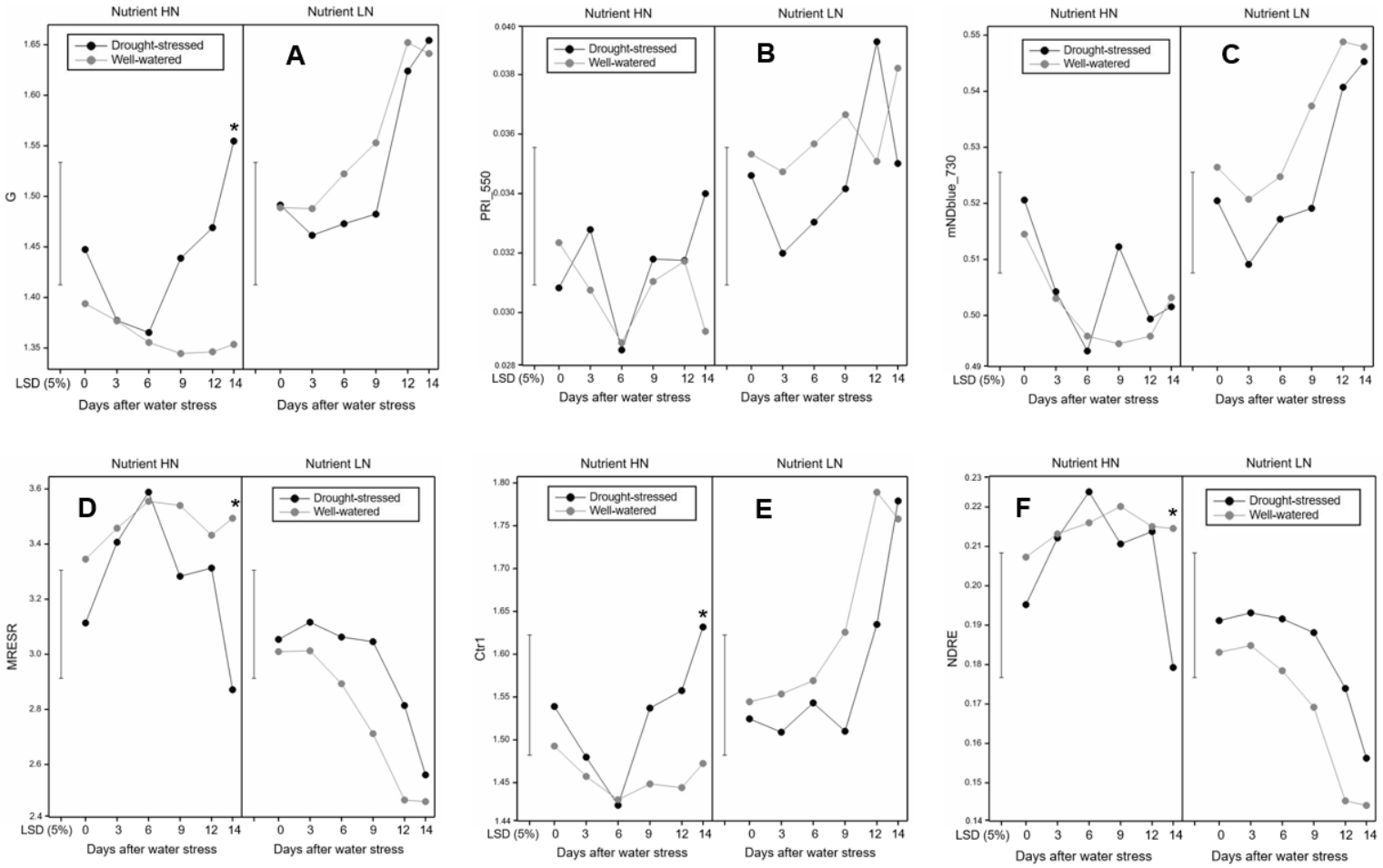

Figure 4.6. Time course of N responsive SRIs including (A) G, (B) PRI_550 (C) mNDblue_730, (D) MRESR, (E) Ctr1, (F) NDRE, and their drought responses under HN and LN nutrient conditions. Plotted means are estimations from the Autocorrelation (AR1) model. Bars represent average approximate LSDs with default significance set at a 5% level of REML means in each treatment combination and days after water stress (DAWS). Asterisks (*) indicate significant difference between drought-stressed and well-watered treatments under different N availabilities at 5% significance level.

4.3.4 Correlation between spectral reflectance indices and morpho-physiological status

The SRIs that were responsive to drought and N stress based on the F-statistics and F-test probabilities (p<0.05) (Table 4.4) were used for correlations with the morpho-physiological parameters indicative of water and N stress to assess their relationships (Table 4.5). The results of the correlation analysis showed that all SRIs significantly correlated with A_n and E regardless of water stress or N availability (Table 4.5). The SRIs with the highest values of correlation coefficient (r) with A_n and E were ARI1 and ARI2.

Almost all SRIs correlated significantly with SPAD values except for RDVI and CRI1 (Table 4.5). Except for RDVI, rDVI_790 and CRI1, all SRIs showed significant correlations with LNC (Table 4.5). The highest r with LNC was achieved by the chlorophyll and red-edge group indices, including mNDblue_730, G, MRESR, NDRE, CIrededge, CIgreen, RENDVI, etc., while RDVI and rDVI_790 recorded the lowest r (Table 4.5). For G_s, all SRIs showed significant correlations except for CRI1.

A similar pattern of correlation was observed for LA and SFW where most SRIs showed strong significant correlations with both parameters except for RDVI, rDVI_790 and CRI1 (Table 4.5). The only two SRIs that did not show a significant correlation with RWC were RDVI and mNDblue_730. Most of the SRIs significantly correlated with WUEi with GM2 recording the highest value of correlation coefficient (Table 4.5). However, only a few SRIs correlated significantly with SMC, particularly RDVI and rDVI_790 recording the highest value of correlation, while the chlorophyll and red-edge group SRIs showed poor and non-significant correlations with SMC (Table 4.5). Altogether, it is evident that the two morpho-physiological parameters that indicated drought and N stress based on their relationships with responsive SRIs are SMC and LNC respectively, and therefore are the potential indicators of water and N status in this study.

Table 4.5. Pearson correlation analysis between SRIs that were responsive to either drought, N stress or both and spring wheat morpho-physiological stress indicators. The data from spectral reflectance measurements and sampling points of morpho-physiological parameters measured at the same time were used. For A_n, G_s, E, WUE_i, SPAD and SMC, correlations with SRIs were done at 0, 3, 6, 9, 12 and 14 DAWS. Correlation between LNC, LA and SFW and SRIs were implemented using data at 0, 9 and 14 DAWS. Additionally, correlation between RWC and SRIs were achieved at 9 and 14 DAWS. Values are Pearson correlation coefficient (r) between SRIs and morpho-physiological stress parameters. Significant r values at $p<0.05$ are indicated in bold.

Responsive indices	**Morpho-physiological stress parameters**									
	***An* (µmol CO_2 m^{-2} s^{-1})**	***Gs* (mmol H_2O m^{-2} s^{-1})**	***E* (mol H_2O m^{-2} s^{-1})**	**WUEi (µmol CO_2 mmol H_2O)**	**SPAD**	**LNC (%)**	**RWC (%)**	**SFW (g pot^{-1})**	**LA (cm^2)**	**SMC (%)**
RDVI	**-0.20**	**-0.28**	**-0.21**	0.31	-0.16	-0.02	-0.13	-0.13	-0.10	**-0.39**
rDVI_790	**-0.39**	**-0.41**	**-0.36**	**0.12**	**-0.34**	-0.07	**-0.44**	-0.32	-0.28	**-0.45**
MCARI1	**-0.73**	**-0.64**	**-0.57**	-0.18	**-0.73**	**-0.43**	**-0.59**	**-0.51**	**-0.52**	**-0.26**
G	**-0.68**	**-0.55**	**-0.47**	**-0.25**	**-0.75**	**-0.59**	**-0.49**	**-0.54**	**-0.58**	-0.02
MCARI	**-0.60**	**-0.47**	**-0.42**	**-0.32**	**-0.67**	**-0.53**	**-0.40**	**-0.42**	**-0.46**	0.04
TVI	**-0.71**	**-0.62**	**-0.56**	-0.16	**-0.70**	**-0.42**	**-0.59**	**-0.50**	**-0.50**	**-0.28**
ZMI	**0.55**	**0.39**	**0.32**	**0.41**	**0.65**	**0.54**	**0.42**	**0.46**	**0.49**	-0.14
Ctr1	**-0.61**	**-0.49**	**-0.45**	**-0.29**	**-0.65**	**-0.51**	**-0.40**	**-0.42**	**-0.45**	0.04
Ctr2	**-0.57**	**-0.42**	**-0.40**	**-0.40**	**-0.62**	**-0.42**	**-0.37**	**-0.36**	**-0.39**	0.06
Lic2	**0.62**	**0.49**	**0.50**	**0.25**	**0.60**	**0.56**	**0.38**	**0.37**	**0.42**	-0.03
GM1	**0.68**	**0.52**	**0.47**	**0.38**	**0.72**	**0.51**	**0.51**	**0.50**	**0.53**	-0.01
GM2	**0.59**	**0.42**	**0.38**	**0.42**	**0.66**	**0.52**	**0.42**	**0.42**	**0.46**	-0.10
ARI1	**0.82**	**0.74**	**0.69**	0.09	**0.73**	**0.34**	**0.71**	**0.65**	**0.65**	**0.38**
ARI2	**0.82**	**0.74**	**0.69**	0.10	**0.73**	**0.33**	**0.70**	**0.66**	**0.65**	**0.36**
CRI1	**0.21**	0.17	**0.24**	0.18	0.11	-0.22	**0.29**	0.04	0.02	**0.28**
PRI_550	**-0.31**	**-0.25**	**-0.21**	-0.13	**-0.33**	**-0.54**	**-0.42**	**-0.46**	**-0.48**	0.10
GNDVI_780	**0.65**	**0.50**	**0.46**	**0.38**	**0.70**	**0.48**	**0.47**	**0.46**	**0.49**	-0.02
MRESR	**0.58**	**0.42**	**0.35**	**0.36**	**0.67**	**0.61**	**0.47**	**0.52**	**0.55**	-0.12
RENDVI	**0.56**	**0.40**	**0.35**	**0.40**	**0.64**	**0.51**	**0.40**	**0.43**	**0.46**	-0.12
NDRE	**0.52**	**0.37**	**0.30**	**0.41**	**0.63**	**0.55**	**0.38**	**0.42**	**0.45**	-0.16
CIgreen	**0.68**	**0.52**	**0.47**	**0.38**	**0.73**	**0.54**	**0.51**	**0.50**	**0.54**	-0.02
CIrededge	**0.53**	**0.38**	**0.31**	**0.39**	**0.64**	**0.58**	**0.41**	**0.47**	**0.50**	-0.15
mNDblue_530	**-0.64**	**-0.50**	**-0.46**	**-0.31**	**-0.69**	**-0.53**	**-0.42**	**-0.45**	**-0.48**	0.04

mNDblue_730	**-0.40**	**-0.29**	**-0.22**	-0.19	**-0.51**	**-0.65**	-0.23	**-0.37**	**-0.39**	**0.19**
gSRa_790	**0.68**	**0.52**	**0.47**	**0.39**	**0.72**	**0.52**	**0.50**	**0.49**	**0.52**	-0.02

4.4 Discussion

4.4.1 Morpho-physiological drought responses under HN and LN conditions

Plant physiological responses to either drought or N stress are well known, while their interactions remain less well understood. In this study, the morpho-physiological status of spring wheat was assessed to understand the complex drought responses under HN and LN nutrient conditions. Principal indicators of plant physiological status that were assessed were gas exchange parameters such as the A_n, G_s, E and WUEi (Table 4.2; Figure 4.4A-D). Drought effects on A_n under HN were coupled much earlier with greater amplitude of responses compared to LN (Table 4.2). The greater drought responses in A_n under HN compared to LN could be explained by the higher LNC attributable to N supply enhancing photosynthetic activity and leaf carboxylation efficiency (Ullah et al., 2019). These results are consistent with Shi et al. (2014) where the authors reported enhanced leaf photosynthesis under HN treatments compared to LN treatments during water deficit stress in wheat. It is also evident that the application of N had a rapid positive response on A_n at 0, 3, 6, 9 and 14 DAWS, while water stress (drought) was gradual at 6, 9, 12 and 14 DAWS (Appendix C, Table C-1). This may be explained by the fact that N treatments were applied several weeks before the imposition of water stress, even though N treatments were withheld a week before water stress. Moreover, the significant (D×N×DAWS) interaction observed suggests the positive impact of all the factors on A_n under the different N availabilities (Table 4.2).

The G_s measures the extent of stomatal opening and serves as an indicator of the water status of plants (Huang et al., 2021). The stomata impose a large limitation on the rate of CO_2 assimilation or water vapor exiting through the stomata and is more severe in stressed plants (Urban et al., 2017). In this present study, a very rapid response to drought was observed in G_s at 0, 3, 6, 9, 12 and 14 DAWS under HN, compared to LN which delayed until 9, 12 and 14 DAWS (Table 4.2; Figure 4.4B), suggesting that N availability influenced the rapidity of the response. Meanwhile, the significant difference observed on day 3 may be attributed to the WS. The G_s in wheat plants subjected to drought under HN was lower after 3 DAWS compared to droughted plants under LN (Table 4.2). These results are in line with the findings of Medici et al. (2007) who reported lower G_s in maize plants under drought and high N compared to plants under drought and low N in field conditions which indicated drought tolerance in maize.

This observation was reported by Li et al. (2020) for oats. The consistent effect of drought on G_s compared to N stress observed in this study indicates the greater impact of drought on wheat plants.

Transpiration is a physiological mechanism that allows plants to absorb water from the soil through the root and it is then evaporated at leaf level through the stomata and other plant surfaces (Yoo et al., 2009). The rate at which water moves through the plant due to transpiration plays a vital role in maintaining plant water balance, nutrient uptake, evaporative cooling under increasing air temperature, and maintaining optimal leaf temperature for photosynthesis (Houshmandfar et al., 2018). In this study, the consistent statistically significant difference observed between WW and WS plants in *E* under HN compared to LN suggests a greater amplitude of response in the former which may be influenced by a higher N supply (Table 4.2; Figure 4.4C). This observation conforms with those of Shi et al. (2014) who reported significantly higher transpiration under high water treatments compared to low water treatments, which further increased with increased N supply, especially in well-irrigated plants. Drought significantly reduced the *E* irrespective of N supply (Appendix C, Table C-1) suggesting that it was the most limiting factor. This observation is in support of Wang et al. (2016) and Akram et al. (2014) who both reported a noticeable decrease in *E* and G_s in wheat exposed to drought under different N levels. A significant interaction between drought, N stress and DAWS was found suggesting the influence of all factors on *E* in this study (Appendix C, Table C-1).

The observed significant difference between treatments on WUEi under HN compared to LN indicates a greater drought response which may be influenced by a higher N supply that impacted positively on Rubisco activity and stomatal regulation (Table 4.2; Figure 4.4D). In parallel, the increase in WUEi in response to drought was greater for HN plants than for LN. During drought stress, a sufficient supply of N can minimise the detrimental effects of the drought, maximise water use efficiency and speed up the recovery process (Gessler et al., 2017). These findings corroborate Shangguan et al. (2000) who reported a significantly higher WUEi in wheat plants under high N than in low N exposed to drought conditions. The authors discovered that depending on the availability of water, the effects of N nutrition on photosynthetic parameters differ. The

significant effect of both drought and N stress on WUEi indicates a synergistic effect with a significant water-by-N availability interaction.

This study noted high SPAD values in response to drought under HN compared to LN particularly at 6, 9 and 12 DAWS suggesting the influence of high N application that minimally raised the relative leaf chlorophyll content in HN plants (Table 4.2; Figure 4.4E). These results partly agree with Basal and Szabó (2020), who found that whereas drought significantly reduced SPAD values at the late reproductive stage, increasing N fertilisation rate was associated with increases in SPAD values in the early reproductive stage in soybean. The present findings indicate a greater amplitude of drought response in SPAD values under HN compared to LN (Table 4.2; Figure 4.4E). The significant effect of both drought and N stress indicates that SPAD values were sensitive to water deficit and N stress.

This study observed a non-significant drought response in LNC regardless of N availability and consequently, no significant drought and N effects and interactions (Table 4.2; Figure 4.4F). This observation suggests that the LNC was unaffected by both combined stress factors. According to the findings of Radin and Boyer (1982), the water relations of plants under drought stress are altered by N content and this could account for the results observed in this study. The RWC of leaves is a crucial marker of plant water status since it shows how well water is supplied to the leaf tissue while also reflecting the rate of transpiration (Lugojan and Ciulca, 2011). The greater drought response in RWC under HN compared to LN suggests the influence of high N supply. However, the overall effects of a high N supply on leaf RWC seem unclear Feng et al., 2009. Querejeta et al. (2022) reported that N supply can improve plant water relations and drought tolerance. Therefore, it is challenging to draw broad conclusions about how a high N supply affects leaf RWC without considering the specific context (i.e., plant species, N form and level and water availability). It is clear from the data presented in (Table 4.2; and Figure 4.4G) that only drought significantly affected the leaf RWC with no effect by N stress. A similar observation has been reported (Akram et al., 2014).

The SFW is considered a valuable measure of plant physiological status as it reflects light use efficiency and growth and is useful for C stock accumulation and assessment (Huang et al., 2022). The SFW in response to drought under HN was greater compared

to LN probably due to the influence of high N supply that increased the photosynthetic activities leading to more C stock accumulation in the leaf which could increase sensitivity to water stress (Huang et al., 2022). The interactive effect of drought and N stress indicates the co-limitation of both stress factors on SFW (Appendix C, Table C-1).

The LA growth determines the light interception capacity of a crop stand and is arguably the most frequently measured phenotypic feature of crop canopies in high-throughput phenotyping systems (Haghshenas and Emam, 2022). The observed greater drought response in LA under HN compared to LN (Table 4.2; Figure 4.4I) may be attributed to high N supply that influenced CO_2 assimilation resulting in LA expansion, increased crop photosynthesis and rate of water loss through transpiration (Lawson and Milliken, 2023). The data presented in (Appendix C, Table C-1) showed that both drought and N stress co-limited LA expansion. The interactive effect of co-occurring water and N stress on LA reduces LA development and can accelerate leaf senescence (Ghani et al., 2000).

The observed SMC in this study indicated that under HN, water was drawn faster than in LN to the root zone to facilitate photosynthesis and CO_2 assimilation for biomass production and LA expansion, resulting in higher water demand and thereby reducing the SMC significantly (Table 4.2; Figure 4.4J).

4.4.2 Spectral reflectance indices responses to drought under HN and LN conditions

There is limited information on how N availability affects spectral reflectance to drought stress. The SRIs response to drought under HN and LN differed among several indices (Table 4.3; Appendix C, Table C-2). Drought responses in SRIs were generally significant on the last day of water stress (14 DAWS) under HN compared to LN except for NPQI, Lic1, Lic2, and SRa_790. This finding indicates that the duration of water stress and N availability had a profound impact on plants responses to drought. Drought responses for SRIs such as MCARI1, G, TCARI, TVI, PRI, Ctr1, GM1, GM2, ARI1, ARI2, CRI1, CRI2, PRI/NDVI, GNDVI_780, MRESR, RENDVI, NDRE, CIgreen, CIrededge, mNDblue_530, rDVI_790 and gSRa_790 were significant with first response from either 9, 12 or 14 DAWS under HN compared to LN (Table 4.3). The

findings demonstrate that adding a high concentration of N before the onset of drought increased the sensitivity of wheat spectral reflectance of these SRIs to water stress. However, SRIs such as NPQI, TVI, RDVI, rDVI_790, Lic1, Lic2 and SRa_790 responded to water stress under LN supply with the earliest response from either 3, 9, 12 or 14 DAWS (Table 4.3). The findings also revealed no influence of N availability for some SRIs including OSAVI, MCARI, ZMI, SPRI, NPCI, Ctr2, RDVI, PRI_550, PRI_norm and mNDblue_730 on responses to water stress, suggesting that the stress effect was only dictated by water stress (Table 4.3). The findings also revealed some SRIs whose drought responses were not directly affected by either HN or LN and N×DAWS (e.g., SPRI and PRI_norm). However, SRIs such as OSAVI, MCARI, ZMI, NPCI, Ctr2, PRI_550 and mNDblue_730 were impacted by N×DAWS, yet drought responses were not influenced by HN or LN.

There was no significant D×N interaction observed by the SRIs (Table 4.4). The interaction between drought and N levels in wheat involves complex physiological and biochemical processes that may affect spectral reflectance of the crop. High N availability can enhance plant growth and increase water demand, potentially exacerbating water depletion under drought conditions. Conversely, low N levels may limit growth, reducing water use but also potentially decreasing drought resilience due to insufficient resources for stress response mechanisms (Wan et al., 2022). Drought stress reduces water availability, affecting nutrient uptake, including N which is crucial for protein synthesis and plant growth (Camaille et al., 2022). The interaction between drought and N levels influences wheat's ability to manage water efficiently and maintain productivity under adverse conditions (Sallam et al., 2019).

4.4.3 Assessment of spectral reflectance indices for discriminating between drought and nitrogen stress

SRIs were found to be useful tools for discriminating between drought and N stress in two recent studies (Rubo and Zinkernagel, 2021; Colovic et al., 2022). In the present study, the F-statistics and F-Test probabilities (p<0.05) were conducted to assess SRIs that were responsive for discriminating the combined drought and N stress during the stem elongation stage of spring wheat and further identify SRIs specific to these stress factors (Table 4.4; Appendix C, Table C-3). The present findings showed that RDVI, rDVI_790, MCARI1, TVI, ARI1 and ARI2 were responsive to drought (Table 4.4). The

results also showed that MCARI1, TVI, ARI1 and ARI2 were responsive to N stress and therefore they may be indicative of both stresses but may not be specific to none. On the other hand, RDVI and rDVI_790 were the only indices responsive to drought and therefore may show specificity for detection (Table 4.4; Figure 4.5A-B). Drought treatment impacted these drought-responsive indices with D×DAWS interaction (Appendix C, Table C-3).

The short wavelength range (320 to 790 nm) of the PolyPen RP410 spectroradiometer used for collecting spectral reflectance data in this study, limits its use for water stress detection. Therefore, a spectroradiometer with a wider wavelength range may be more appropriate. Generally, the spectral region from 800 to 2500 nm is more sensitive to plant water stress. This region encompasses the short-wave infrared (SWIR) range from 800 nm to 1600 nm (Kim et al., 2015) as well as wavelengths between 1300 and 2500 nm (Maimaitiyiming et al., 2017). Again, the shorter period of water stress might have affected spectral response to drought. Plants may employ photo-protection techniques in response to short-time water stress, such as reducing photosynthesis while increasing heat emission and chlorophyll fluorescence (Zhang and Zhou et al., 2019).

A wide range of SRIs including G, mNDblue_730, PRI_550, MRESR, Lic2, CIrededge, NDRE, RENDVI, CIgreen, GNDVI_780, mNDblue_530, gSRa_790, ZMI, Ctr1, GM1, GM2, Ctr2 and CRI1 showed high responses to only N stress and would be effective for N stress detection (Table 4.4; Figure 4.6). From the results presented in Table 4.4, the high response of these SRIs to N seems to be impacted heavily by HN supply coupled with N×DAWS interaction (Appendix C, Table C-3). The specific SRIs suitable to detect the combined drought and N stress in plants may vary depending on the plant species, the type and severity of stress conditions and the measurement technique used (Saud et al., 2017).

4.4.4 Linking the spectral reflectance responses to the morpho-physiological status

In the present study, the effectiveness of SRIs that were responsive for assessing the water and N status were evaluated for their relationship with the morpho-physiological indicators through correlation analysis (Table 4.5). The results of this study indicated a large range of significant correlations of the SRIs (e.g., ARI1, ARI2, GMI, GNDVI_780, CIgreen, MRESR, CIrededge, etc.) with gas exchange parameters such as

A_n, E, G_s and WUEi regardless of water stress or N availability and DAWS (Table 4.5). The strong relationship between SRIs and A_n observed could be explained by non-saturation of the indices especially their wavebands which made them more sensitive to changes in photosynthetic pigments (i.e., chlorophylls and carotenoids), plant tissues and absorption and scattering of light during photosynthesis, leading to corresponding changes in the spectral reflectance (Hejtmánek et al., 2022).

The significant correlation of the SRIs with E, G_s and WUEi could be accounted for by the sensitivity of the indices to variations of stomatal closure and water loss through transpiration (El-Hendawy et al., 2017; Ihuoma and Madramootoo, 2019a) which may be dictated by the photosynthetic efficiency, nutrient and water availability and plant water status. Several of these SRIs have been reported to correlate significantly with leaf gas exchange parameters in many studies (Sellami et al., 2022; Colovic et al., 2022; Hejtmánek et al., 2022). For instance, Colovic et al. (2022) demonstrated a significant correlation between the red-edge group indices (e.g., CIrededge and NDRE) with leaf gas exchange parameters which was influenced by responsiveness to the chlorophyll concentration. These results partly agree with Maimaitiyiming et al. (2017) who also reported a strong relationship between SRIs mostly from the red-edge region with G_s and A_n because of their sensitivity to subtle changes in chlorophyll. These findings suggest that most of the SRIs can be effective and non-destructive tools for evaluating plant leaf gas exchange parameters offering useful data for stress monitoring and plant growth.

A wide range of the SRIs correlated significantly with SPAD values which are proxies for relative chlorophyll content except for RDVI and CRI1 (Table 4.5). The highest correlation was achieved by chlorophyll indices (e.g., G, MCARI, CIgreen, GMI) and anthocyanin-based indices such as ARI1 and ARI2. The chlorophyll and anthocyanin-based indices correlated strongly with SPAD values under drought and N stress probably because they are all related to the leaf pigments (Sukhova et al., 2022). There have been strong relationships found between the SPAD index and leaf pigments (Hlavinka et al., 2013).

In the present study, almost all the SRIs significantly correlated with the LNC except for RDVI, rDVI_790 and CRI1 (Table 4.5). The highest correlation of the SRIs with

LNC was achieved by the chlorophyll-sensitive indices (e.g., mNDblue_730, G and Lic2) and the red-edge group indices (e.g., MRESR, CIrededge, NDRE, etc.,) (Table 4.5). These findings could be explained by the fact that the chlorophyll indices use wavelengths in the red-edge region due to their close relationship with chlorophyll content. The red edge is a spectral region between the visible red (e.g., 670 nm) and NIR (e.g., from 750 nm with the PolyPen RP410) wavelengths, and it is sensitive to changes in chlorophyll content, which is closely related to LNC (Kanke et al., 2012). As chlorophyll absorbs less in the red-edge region, the saturation effect is reduced using these wavelengths (Zhang et al., 2022).

The linkage between the red-edge region and plant N status explains why the red-edge indices correlated significantly with LNC (Kanke et al., 2012). The significance of employing red-edge indices to assess plant N deficiency and N requirement is highlighted by the great sensitivity to the leaf chlorophyll content. According to Sellami et al. (2022), the red-edge indices could separate different levels of water and N stress at the mid-season stage in maize. The authors observed a shift in the red-edge position (REP) which was attributed to variations in the width of the maximum chlorophyll absorption in the red spectral region due to reduced chlorophyll content and lower photosynthetic efficiency due to low N supply. Additionally, other studies reported the variations in REP (up to 10 nm) as the consequence of different factors, including plant disease (Gazala et al., 2013), nutrient deficit (Zhao et al., 2005) and water stress (Zhang and Zhou, 2019; Ballester et al., 2019).

Furthermore, Meer and De Jong (2006) have reported that the REP is affected by chlorophyll concentration, leaf mesophyll structure and LAI. The results in the present study are consistent with Colovic et al. (2022) who reported a higher sensitivity to N levels by the red-edge-based indices compared to the structural and water band indices in sweet maize. The significance of the chlorophyll and red-edge group indices which were identified by the F-statistics and F-Test probabilities is supported by this result and makes them optimal indices for N stress detection.

In this study, a wide range of SRIs (e.g., ARI1, ARI2, G, MRESR, CIgreen, MCARI1, GM1, gSRa_790, etc.,) showed a consistent trend of a strong relationship with the destructive morpho-physiological parameters (i.e., LA, SFW and RWC) (Table 4.5).

This result suggests that several SRIs examined in this study could be used to indirectly assess the growth and water status based on LA, SFW and RWC in a rapid, low-cost and non-destructive manner. However, for water status, they may not be specific in their assessment. The results also showed a few SRIs (e.g., RDVI, rDVI_790, ARI1, ARI2, MCARI1, TVI, CRI1 and mNDblue_730) that significantly correlated with SMC (Table 4.5). RDVI and rDVI_790 showed the strongest correlation with SMC but a very poor relationship with LNC (Table 4.5). It is evident that among all the morpho-physiological parameters assessed in this study, SMC and LNC clearly distinguish SRIs that indicate specificity for drought and N stress respectively. By this observation, RDVI and rDVI_790 are the only indices that indicate specificity for drought stress which confirms the earlier findings. Both RDVI $(R_{780}–R_{670})/((R_{780}+R_{670})^{1/2})$ and rDVI_790 $(R_{790}–R_{680})$ are narrow-band greenness SRIs that compare reflectance measurements from the reflectance peak in the NIR region to reflectance in the red region, including the red-edge where chlorophyll absorbs light energy for photosynthesis (Roujean and Breon, 1995). These combinations of reflectance measurements make them sensitive to the combined effects of chlorophyll content and canopy LA.

These findings are supported by Ihuoma and Madramootoo (2019a) who demonstrated the utility of RDVI and other SRIs for detecting water stress levels in greenhouse-based tomato plants where it showed a good correlation with SMC and other water stress indicators such as canopy temperature and RWC. In another study, RDVI was found to be one of the most useful SRIs for detecting water stress in bell pepper under greenhouse conditions (Ihuoma and Madramootoo, 2019b).

Rosa et al. (2023) explored many leaf-level spectroradiometer indices for their response to early drought stress in tomatoes. However, RDVI was not responsive to drought probably because their work was field-based which may have influenced spectral reflectance and the authors did not consider SMC as a water stress indicator. The present findings indicate that RDVI and rDVI_790 are the most sensitive indices for drought stress in spring wheat and may be specific for detection regardless of N stress using the low-cost handheld proximal sensor.

Collectively, the findings of this study suggest that the chlorophyll-sensitive and red-edge group SRIs including mNDblue_730, G, Lic2, MRESR, CIrededge, CIgreen and NDRE are the key mechanistic SRIs for N stress detection and may be related to autocorrelation because they capture spatial patterns in the leaf/vegetation that are often influenced by environmental factors like precipitation and nutrient availability which equally exhibit spatial autocorrelation. The RDVI and rDVI_790 are the key mechanistic SRIs for drought stress detection and may potentially relate to autocorrelation. The findings could inform better nutrient management strategies under drought conditions, leading to more resilient cropping systems. However, a validation in the field with a spectrometer of a wider wavelength range and crop varieties under multiple stress conditions may be required for generalisability of the findings.

To prioritise SRIs that best explain crop traits variations linked to the morpho-physiological status, further work should consider exploiting a more robust statistical analysis methods such as forward stepwise regression analysis. This method involves adding variables one at a time to a regression model based on their statistical significance in explaining the variation in crop traits (Saed-Moucheshi et al., 2013; Sardoei et al., 2023). This analysis method would help identify the most relevant SRIs by evaluating their contribution to the model incrementally (Naik et al., 2020; Wang et al., 2022). Additionally, Principal Component Analysis (PCA) reduces the dimensionality of spectral data by transforming it into a set of uncorrelated variables called principal components. These components capture the most variance in the data, allowing for the identification of key SRIs that could influence crop traits (Beattie and Esmonde-White, 2021). These methods would provide a robust framework for selecting and prioritising SRIs that are most informative for analysing crop traits variations under drought and N stress scenarios.

4.5 Conclusions

This study assessed the morpho-physiological drought responses at high and low N supplies and examined the feasibility of using SRIs at the leaf scale to discriminate the combined drought and N stress effects in spring wheat. A short period of water stress had a negative impact on the morpho-physiological parameters investigated and the

spectral reflectance of wheat plants. The results of this study demonstrated a faster response to drought for the HN plant compared to LN with a larger amplitude of response in morpho-physiological parameters including gas exchange parameters, SPAD values, RWC, SFW, LA and SMC with interactive effects except for LNC.

These findings imply that in water-limited scenarios, plants with an adequate or surplus of N may be more sensitive to drought stress; hence, N fertiliser management could be a key component in increasing water productivity during dry spells. The result of this study collectively indicates that N status is likely to have an impact on how spring wheat responds to water stress. It is suggested that SRIs can be used in wheat breeding programmes to quantify the morpho-physiological status quickly and non-destructively because of their close relationships.

This study demonstrated that the combined drought and N stress could be discriminated against using a low-cost handheld proximal sensor and identified key SRIs that were more responsive to drought and N stress. The narrow-band greenness SRIs which also use red-edge wavelengths (RDVI and rDVI_790) are the only indices that indicate higher specificity for drought stress detection. For N stress, the chlorophyll-sensitive indices (mNDblue_730, G and Lic2) and most importantly the red-edge group indices (e.g., MRESR, CIrededge and NDRE) showed higher specificity for their detection. Therefore, the application of SRIs in wheat during the stem elongation stage could improve PA by detecting stress patterns and helping growers make wise decisions, such as the optimisation of agricultural water use and crop fertilisation to reduce the negative effects of stress.

The applicability of these findings as a guide or methodology for monitoring the morpho-physiological status of crops in a rapid and non-destructive manner and discriminating the combined drought and N stress requires validation with a spectroradiometer of wider wavelength range, or RS tool over different plant species exposed to different levels of water stress and N availabilities. Scaling up these findings for field phenotyping in developing countries such as Africa is the future work of this research and may play a pivotal role in PA.

References

Akram, M., Iqbal, R. M., and Jamil, M. (2014). The response of wheat (*Triticum aestivum* L.) to integrating effects of drought stress and nitrogen management. *Bulgarian Journal of Agricultural Science*, 20 (2), 275-286.

Atkinson, N. J and Urwin, P. E. (2012). The interaction of plant biotic and abiotic stresses: from genes to the field. *Journal of Experimental Botany*, 63 (10), 3523-3543. https://doi.org/10.1093/jxb/ers100

Ballester, C., Brinkhoff, J., Quayle, W. C., and Hornbuckle, J. (2019). Monitoring the effects of water stress in cotton using the green-red vegetation index and red edge ratio. *Remote Sensing*, 11 (7), 873. https://doi.org/10.3390/rs11070873

Barnes, J. D., Balaguer, L., Manrique, E., Elvira, S., and Davison, A. W. (1992). A reappraisal of the use of DMSO for the extraction and determination of chlorophylls a and b in lichens and higher plants. *Environmental and Experimental Botany*, 32:85-100. https://doi.org/10.1016/0098-8472(92)90034-Y

Basal, O and Szabó, A. (2020). The combined effect of drought stress and nitrogen fertilisation on soybean. *Agronomy*, 10 (3), 384.

Bolker, B. M. (2015). Linear and generalized linear mixed models. Ecological statistics: contemporary theory and application, 309-333.

Camaille, M., Fabre, N., Clément, C., and Ait Barka, E. (2021). Advances in wheat physiology in response to drought and the role of plant growth promoting rhizobacteria to trigger drought tolerance. *Microorganisms*, 9 (4), 687. https://doi.org/10.3390/microorganisms9040687

Carter, G and Miller, R. L. (1994). Early detection of plant stress by digital imaging within narrow stress-sensitive wavebands. *Remote Sensing of Environment*, 50 (3), 295-302. https://doi.org/10.1016/0034-4257(94)90079-5

Chen, J. M. (1996). Evaluation of vegetation indices and a modified simple ratio for boreal applications. *Canadian Journal of Remote Sensing*, 22 (3), 229-242. https://doi.org/10.1080/07038992.1996.10855178

Colovic, M., Yu, K., Todorovic, M., Cantore, V., Hamze, M., Albrizio, R., and Stellacci, A. M. (2022). Hyperspectral Vegetation Indices to Assess Water and Nitrogen Status of Sweet Maize Crop. *Agronomy*, 12 (9), 2181. http://dx.doi.org/10.3390/agronomy12092181

Cudjoe, D. K., Virlet, N., Castle, M., Riche, A. B., Mhada, M., Waine, T. W., Mohareb, F., and Hawkesford, M. J. (2023a). Field phenotyping for African crops: overview and perspectives. *Frontiers in Plant Science*, 14. https://doi.org/10.3389/fpls.2023.1219673

Cudjoe, D. K., Okyere, F. G., Virlet, N., Castle, M., Buchner, P., Parmar, S., Sadeghi-Tehran, P., Riche, A., Sohail, Q., Mhada, M., Ghanem, M., Waine, T. W., Mohareb, F., and Hawkesford, M. J. (2023b). Using proximal sensing parameters linked to the photosynthetic capacity to assess the nutritional status and yield potential in quinoa. *Acta Horticulturae*, 1360, 373-379 https://doi.org/10.17660/ActaHortic.2023.1360.45

Beattie, J. R and Esmonde-White, F. W. (2021). Exploration of principal component analysis: deriving principal component analysis visually using spectra. *Applied Spectroscopy*, 75 (4), 361-375

Daughtry, C. S., Walthall, C. L., Kim, M. S., De Colstoun, E. B., and McMurtrey Iii, J. E. (2000). Estimating corn leaf chlorophyll concentration from leaf and canopy reflectance. *Remote Sensing of Environment*, 74 (2), 229-239. https://doi.org/10.1016/S0034-4257(00)00113-9

dos Santos, T. B., Ribas, A. F., de Souza, S. G. H., Budzinski, I. G. F., and Domingues, D. S. (2022). Physiological Responses to Drought, Salinity, and Heat Stress in Plants: A Review. *Stresses*, 2 (1), 113-135.

El-Hendawy, S., Hassan, W., Al-Suhaibani, N., and Schmidhalter, U. (2017). Spectral assessment of drought tolerance indices and grain yield in advanced spring wheat lines grown under full and limited water irrigation. *Agricultural Water Management*, 182, 1-12. https://doi.org/10.1016/j.agwat.2016.12.003

Erenstein, O., Jaleta, M., Mottaleb, K. A., Sonder, K., Donovan, J., and Braun, H. J. (2022). Global trends in wheat production, consumption and trade. In Wheat improvement: food security in a changing climate (pp. 47-66). Cham: Springer International Publishing. https://doi.org/10.1007/978-3-030-90673-3_4

FAO. (2020). Sustainable Food and Agriculture. Accessed on August 12, 2023. Available at: http://www.fao.org/sustainability/background/en/

Feng, L., Li, H., Jiao, J., Li, D., Zhou, L., Wan, J., and Li, Y. (2009). Reduction in SBPase activity by antisense RNA in transgenic rice plants: effect on photosynthesis, growth, and biomass allocation at different nitrogen levels. *Journal of Plant Biology*, 52, 382-394. https://doi.org/10.1007/s12374-009-9049-3

Fernández-Gómez, J., Talle, B., Tidy, A. C., and Wilson, Z. A. (2020). Accurate staging of reproduction development in Cadenza wheat by non-destructive spike analysis. *Journal of Experimental Botany*, 71 (12), 3475-3484. https://doi.org/10.1093/jxb/eraa156

Gazala, I. S., Sahoo, R. N., Pandey, R., Mandal, B., Gupta, V. K., Singh, R., and Sinha, P. (2013). Spectral reflectance pattern in soybean for assessing yellow mosaic disease. *Indian Journal of Virology*, 24, 242-249. https://doi.org/10.1007/s13337-013-0161-0

Gessler, A., Schaub, M., and McDowell, N. G. (2017). The role of nutrients in drought□ induced tree mortality and recovery. *New Phytologist*, 214 (2), 513-520. https://doi.org/10.1111/nph.14340

Ghani, A., Hussain, M., and Hassan, A. (2000). Interactive effect of nitrogen and water stress on leaf area of sunflower. *Pakistan Journal of Biological Sciences*, 3: 989-990.

Gitelson, A. A and Merzlyak, M. N. (1997). Remote estimation of chlorophyll content in higher plant leaves. *International Journal of Remote Sensing*, 18 (12), 2691-2697. https://doi.org/10.1080/014311697217558

Gitelson, A. A., Chivkunova, O. B., and Merzlyak, M. N. (2009). Nondestructive estimation of anthocyanins and chlorophylls in anthocyanic leaves. *American Journal of Botany*, 96 (10), 1861-1868. https://doi.org/10.3732/ajb.0800395

Gitelson, A. A., Kaufman, Y. J., Stark, R., and Rundquist, D. (2002). Novel algorithms for remote estimation of vegetation fraction. *Remote Sensing of Environment*, 80 (1), 76-87. https://doi.org/10.1016/S0034-4257(01)00289-9

Haghshenas, A and Emam, Y. (2022). Accelerating leaf area measurement using a volumetric approach. *Plant Methods*, 18 (1), 61. https://doi.org/10.1186/s13007-022-00896-w

Hejtmánek, J., Stejskal, J., Čepl, J., Lhotáková, Z., Korecký, J., Krejzková, A., Dvořák, J., and Gezan, S. A. (2022). Revealing the Complex Relationship Among Hyperspectral Reflectance, Photosynthetic Pigments, and Growth in Norway Spruce Ecotypes. *Frontiers in Plant Science*, 13, 721064. https://doi.org/10.3389/fpls.2022.721064

Herrmann, I., Karnieli, A., Bonfil, D. J., Cohen, Y., and Alchanatis, V. (2010). SWIR-based spectral indices for assessing nitrogen content in potato fields. *International Journal of Remote Sensing*, 31 (19), 5127-5143.

Hlavinka, J., Nauš, J., and Špundová, M. (2013). Anthocyanin contribution to chlorophyll meter readings and its correction. *Photosynthesis Research*, 118, 277-295. https://doi.org/10.1007/s11120-013-9934-y

Houshmandfar, A., Fitzgerald, G. J., O'Leary, G., Tausz□Posch, S., Fletcher, A., and Tausz, M. (2018). The relationship between transpiration and nutrient uptake in wheat changes under elevated atmospheric CO_2. *Physiologia Plantarum*, 163 (4), 516-529. https://doi.org/10.1111/ppl.12676

Huang, G., Yang, Y., Zhu, L., Peng, S., and Li, Y. (2021). Temperature responses of photosynthesis and stomatal conductance in rice and wheat plants. *Agricultural and Forest Meteorology*, 300, 108322.

Huang, W., Ratkowsky, D. A., Hui, C., Wang, P., Su, J., and Shi, P. (2019). Leaf fresh weight versus dry weight: which is better for describing the scaling relationship

between leaf biomass and leaf area for broad-leaved plants?. *Forests*, 10 (3), 256. https://doi.org/10.3390/f10030256

Huete A. R. (1988). A soil-adjusted vegetation index (SAVI). *Remote Sensing of Environment*, 25 (3), 295-309. https://doi.org/10.1016/0034-4257(88)90106-X

Ihuoma, S. O and Madramootoo, C. A. (2019a). Sensitivity of spectral vegetation indices for monitoring water stress in tomato plants. *Computers and Electronics in Agriculture*, 163, 104860. https://doi.org/10.1016/j.compag.2019.104860

Ihuoma, S. O and Madramootoo, C. A. (2019b). Crop reflectance indices for mapping water stress in greenhouse-grown bell pepper. *Agricultural Water Management*, 219, 49-58. https://doi.org/10.1016/j.agwat.2019.04.001

Kanke, Y., Raun, W., Solie, J., Stone, M., and Taylor, R. (2012). Red edge as a potential index for detecting differences in plant nitrogen status in winter wheat. *Journal of Plant Nutrition*, 35 (10), 1526-1541.

Katsoulas, N., Elvanidi, A., Ferentinos, K. P., Kacira, M., Bartzanas, T., and Kittas, C. (2016). Crop reflectance monitoring as a tool for water stress detection in greenhouses: A review. *Biosystems Engineering*, 151, 374-398. https://doi.org/10.1016/j.biosystemseng.2016.10.003

Kim, D. M., Zhang, H., Zhou, H., Du, T., Wu, Q., Mockler, T. C., and Berezin, M. Y. (2015). Highly sensitive image-derived indices of water-stressed plants using hyperspectral imaging in SWIR and histogram analysis. *Scientific Reports*, 5, 15919. https://doi.org/10.1038/srep15919

Klem, K., Rajsnerová, P., Novotná, K., Mìša, P., and Křen, J. (2014). Changes in vertical distribution of spectral reflectance within spring barley canopy as an indicator of nitrogen nutrition, canopy structure and yield parameters. *Agriculture*, 60 (2), 50-59. https://doi.org/10.2478/agri-2014-0006

Klem, K., Záhora, J., Zemek, F., Trunda, P., Tůma, I., Novotná, K., and Holub, P. (2018). Interactive effects of water deficit and nitrogen nutrition on winter wheat. Remote sensing methods for their detection. *Agricultural Water Management*, 210, 171-184. https://doi.org/10.1016/j.agwat.2018.08.004

Kothari, S and Schweiger, A. K. (2022). Plant spectra as integrative measures of plant phenotypes. *Journal of Ecology*, 110 (11), 2536-2554.

Lawson, T and Milliken, A. L. (2023). Photosynthesis–beyond the leaf. *New Phytologist*, 238 (1), 55-61. https://doi.org/10.1111/nph.18671

Li, L., Ma, H., Xing, J., Liu, F., and Wang, Y. (2020). Effects of water deficit and nitrogen application on leaf gas exchange, phytohormone signalling, biomass and water use efficiency of oat plants. *Journal of Plant Nutrition and Soil Science*, 183 (6), 695-704. https://doi.org/10.1002/jpln.202000183

Li, Z., Zhang, Q., Wei, W., Cui, S., Tang, W., and Li, Y. (2020). Determining effects of water and nitrogen inputs on wheat yield and water productivity and nitrogen use efficiency in China: A quantitative synthesis. *Agricultural Water Management*, 242, 106397. https://doi.org/10.1016/j.agwat.2020.106397

Lichtenthaler, H. K. (1996). Vegetation stress: an introduction to the stress concept in plants. *Journal of Plant Physiology*, 148 (1-2), 4-14.

Lugojan, C and Ciulca, S. (2011). Evaluation of relative water content in winter wheat. *Journal of Horticulture, Forestry and Biotechnology*, 15 (2), 173-177.

Maimaitiyiming, M., Ghulam, A., Bozzolo, A., Wilkins, J. L., and Kwasniewski, M. T. (2017). Early detection of plant physiological responses to different levels of water stress using reflectance spectroscopy. *Remote Sensing*, 9 (7), 745. https://doi.org/10.3390/rs9070745

Medici, L. O., Azevedo, R. A., Canellas, L. P., Machado, A. T., and Pimentel, C. (2007). Stomatal conductance of maize under water and nitrogen deficits. *Pesquisa Agropecuária Brasileira*, 42, 599-601. https://doi.org/10.1590/S0100-204X2007000400020

Meer, F. V. D and De Jong, S. M. (2006). Imaging spectrometry for agriculture applications. *Imaging spectrometry: Basic principal and prospective application*, eds. Clevers, J. G. P. W and Jongschaap, R. pp. 157-197. Dordrecht, the Netherlands: Springer

Mu, X and Chen, Y. (2021). The physiological response of photosynthesis to nitrogen deficiency. *Plant Physiology and Biochemistry*, 158, 76-82.

Naik, B. B., Naveen, H. R., Sreenivas, G., Choudary, K. K., Devkumar, D., and Adinarayana, J. (2020). Identification of water and nitrogen stress indicative spectral bands using hyperspectral remote sensing in maize during post-monsoon season. *Journal of the Indian Society of Remote Sensing*, 48, 1787-1795.

Payne, R., Welham, S., and Harding, S. (2011). A Guide to REML in GenStat. VSN International, Hemel Hempstead, United Kingdom.

Peñuelas, J., Baret, F., and Filella, I. (1995). Semi-empirical indices to assess carotenoids/chlorophyll a ratio from leaf spectral reflectance. *Photosynthetica*, 31 (2), 221-230.

Prey, L and Schmidhalter, U. (2019). Sensitivity of Vegetation Indices for Estimating Vegetative N Status in Winter Wheat. *Sensors*, 19 (17), 3712. https://doi.org/10.3390/s19173712

Querejeta, J. I., Prieto, I., Armas, C., Casanoves, F., Diémé, J. S., Diouf, M., and Rusch, G. M. (2022). Higher leaf nitrogen content is linked to tighter stomatal regulation of transpiration and more efficient water use across dryland trees. *New Phytologist*, 235 (4), 1351-1364.

Radin, J. W and Boyer, J. S. (1982). Control of leaf expansion by nitrogen nutrition in sunflower plants: role of hydraulic conductivity and turgor. *Plant Physiology*, 69 (4), 771-775. https://doi.org/10.1104/pp.69.4.771

Ray, D. K., Mueller, N. D., West, P. C., and Foley, J. A. (2013). Yield trends are insufficient to double global crop production by 2050. *Plos One*, 8 (6), e66428. https://doi.org/10.1371/journal.pone.0066428

Rosa, A. P., Barão, L., Chambel, L., Cruz, C., and Santana, M. M. (2023). Early identification of plant drought stress responses: changes in leaf reflectance and plant growth promoting rhizobacteria selection-the case study of tomato plants. *Agronomy*, 13 (1), 183. https://doi.org/10.3390/agronomy13010183

Roujean, J. L and Breon, F. M. (1995). Estimating PAR absorbed by vegetation from bidirectional reflectance measurements. *Remote Sensing of Environment*, 51 (3), 375-384. https://doi.org/10.1016/0034-4257(94)00114-3

Rouse, J. W., Haas, R. H., Schell, J. A., and Deering, D. W. (1974). Monitoring vegetation systems in the Great Plains with ERTS. *NASA Special Publications*, 351 (1), 309.

Rubo, S and Zinkernagel, J. (2022). Exploring hyperspectral reflectance indices for the estimation of water and nitrogen status of spinach. *Biosystems Engineering*, 214, 58-71. https://doi.org/10.1016/j.biosystemseng.2021.12.008

Sallam, A., Alqudah, A. M., Dawood, M. F., Baenziger, P. S., and Börner, A. (2019). Drought stress tolerance in wheat and barley: advances in physiology, breeding and genetics research. *International journal of molecular sciences*, 20 (13), 3137.

Saed-Moucheshi, A., Fasihfar, E., Hasheminasab, H., Rahmani, A., and Ahmadi, A. (2013). A review on applied multivariate statistical techniques in agriculture and plant science. *International Journal of Agronomy and Plant Production*, 4 (1):127-141, 2013.

Sardoei, A. S., Sharifani, M., Sarmast, M. K., and Ghasemnejhad, M. (2023). Stepwise regression analysis of citrus genotype under cold stress. *Gene, Cell and Tissue*, 10 (2).

Saud, S., Fahad, S., Yajun, C., Ihsan, M. Z., Hammad, H. M., Nasim, W., Amanullah, Arif, M., and Alharby, H. (2017). Effects of Nitrogen Supply on Water Stress and Recovery Mechanisms in Kentucky Bluegrass Plants. *Frontiers in Plant Science*, 8, 983. https://doi.org/10.3389/fpls.2017.00983

Sellami, M. H. Albrizio, R., Čolović, M., Hamze, M., Cantore, V., Todorovic, M., Piscitelli, L., and Stellacci, A. M. (2022). Selection of Hyperspectral Vegetation Indices for Monitoring Yield and Physiological Response in Sweet Maize under Different Water and Nitrogen Availability. *Agronomy*, 12, 489. https://doi.org/10.3390/agronomy12020489

Shangguan, Z. P., Shao, M. A., and Dyckmans, J. (2000). Nitrogen nutrition and water stress effects on leaf photosynthetic gas exchange and water use efficiency in winter wheat. *Environmental and Experimental Botany*, 44 (2), 141-149. https://doi.org/10.1016/S0098-8472(00)00064-2

Shi, J., Yasuor, H., Yermiyahu, U., Zuo, Q., and Ben-Gal, A. (2014). Dynamic responses of wheat to drought and nitrogen stresses during re-watering cycles. *Agricultural Water Management*, 146, 163-172.

Shrestha, S., Brueck, H., and Asch, F. (2012). Chlorophyll index, photochemical reflectance index and chlorophyll fluorescence measurements of rice leaves supplied with different N levels. *Journal of Photochemistry and Photobiology B: Biology*, 113, 7-13. https://doi.org/10.1016/j.jphotobiol.2012.04.008

Skendžić, S., Zovko, M., Lešić, V., Pajač Živković, I., and Lemić, D. (2023). Detection and Evaluation of Environmental Stress in Winter Wheat Using Remote and Proximal Sensing Methods and Vegetation Indices–A Review. *Diversity*, 15, 481. https://doi.org/10.3390/ d15040481

Sukhova, E., Yudina, L., Kior, A., Kior, D., Popova, A., Zolin, Y., Gromova, E., and Sukhov, V. (2022). Modified Photochemical Reflectance Indices as New Tool for Revealing Influence of Drought and Heat on Pea and Wheat Plants. *Plants*, 11 (10), 1308. https://doi.org/10.3390/plants11101308

Ullah, H., Santiago-Arenas, R., Ferdous, Z., Attia, A., and Datta, A. (2019). Improving water use efficiency, nitrogen use efficiency, and radiation use efficiency in field crops under drought stress: A review. *Advances in Agronomy*, 156, 109-157. https://doi.org/10.1016/bs.agron.2019.02.002

Urban, J., Ingwers, M., McGuire, M. A., and Teskey, R. O. (2017). Stomatal conductance increases with rising temperature. *Plant Signaling and Behavior*, 12 (8), e1356534. https://doi.org/10.1080/15592324.2017.1356534

Wan, C., Dang, P., Gao, L., Wang, J., Tao, J., Qin, X., and Gao, J. (2022). How does the environment affect wheat yield and protein content response to drought? A meta-analysis. *Frontiers in Plant Science*, 13, 896985.

Wang, J., Zhang, X., Han, Z., Feng, H., Wang, Y., Kang, J., and Ma, G. (2022). Analysis of physiological indicators associated with drought tolerance in wheat under drought and re-watering conditions. *Antioxidants*, 11 (11), 2266.

Wang, X., Wang, L., and Shangguan, Z. (2016). Leaf Gas Exchange and Fluorescence of Two Winter Wheat Varieties in Response to Drought Stress and Nitrogen Supply. *Plos One*, 11 (11), e0165733.

Yoo, C. Y., Pence, H. E., Hasegawa, P. M., and Mickelbart, M. V. (2009). Regulation of transpiration to improve crop water use. *Critical Reviews in Plant Science*, 28 (6), 410-431. https://doi.org/10.1080/07352680903173175

Zadoks, J. C., Chang, T. T., and Konzak, C. F. (1974). A decimal code for the growth stages of cereals. *Weed Research*, 14 (6), 415-421. https://doi.org/10.1111/j.1365-3180.1974.tb01084.x

Zarco-Tejada, P. J., Miller, J. R., Noland, T. L., Mohammed, G. H., and Sampson, P. H. (2001). Scaling-up and model inversion methods with narrowband optical indices for chlorophyll content estimation in closed forest canopies with hyperspectral data. *IEEE Transactions on Geoscience and Remote Sensing*, 39 (7), 1491-1507.

Zarco□Tejada, P. J., Ustin, S. L., and Whiting, M. L. (2005). Temporal and spatial relationships between within□field yield variability in cotton and high□spatial hyperspectral remote sensing imagery. *Agronomy Journal*, 97 (3), 641-653. https://doi.org/10.2134/agronj2003.0257

Zhang, F and Zhou, G. (2019). Estimation of vegetation water content using hyperspectral vegetation indices: A comparison of crop water indicators in response to water stress treatments for summer maize. *BMC Ecology*, 19, 1-12. https://doi.org/10.1186/s12898-019-0233-0

Zhang, H., Li, J., Liu, Q., Lin, S., Huete, A., Liu, L., and Yu, W. (2022). A novel red□edge spectral index for retrieving the leaf chlorophyll content. *Methods in Ecology and Evolution*, 13 (12), 2771-2787.

Zhao, D., Reddy, K. R., Kakani, V. G., and Reddy, V. R. (2005). Nitrogen deficiency effects on plant growth, leaf photosynthesis, and hyperspectral reflectance properties of sorghum. *European Journal of Agronomy*, 22 (4), 391-403. https://doi.org/10.1016/j.eja.2004.06.005

Zhao, D., Reddy, K. R., Kakani, V. G., and Reddy, V. R. (2005). Nitrogen deficiency effects on plant growth, leaf photosynthesis, and hyperspectral reflectance properties of sorghum. *European Journal of Agronomy*, 22 (4), 391-403. https://qadoi.org/10.1016/j.eja.2004.06.0aqq

CHAPTER 5

Multiscale assessment of aerial drone imagery and ground-based proximal sensors for assessing the nitrogen status and agronomic performance in winter wheat

Daniel K. Cudjoe[1,2], Frank G. Okyere[1,2], Suzanne J. Clark[3], Nicolas Virlet[1], March Castle[1], Andrew B. Riche[1], Toby W. Waine[2], Fady Mohareb[2*] and Malcolm J. Hawkesford[1*]

[1]Rothamsted Research, Sustainable Soils and Crops, Harpenden, Hertfordshire, AL5 2JQ, United Kingdom.
[2]School of Water, Energy and Environment, Cranfield University, Cranfield, Bedfordshire, MK43 0AL, United Kingdom.
[3]Rothamsted Research, Intelligent Data Ecosystems, Harpenden, Hertfordshire, AL5 2JQ, United Kingdom.

***Correspondence**
Malcolm J. Hawkesford; Email: malcolm.hawkesford@rothamsted.ac.uk
Fady Mohareb; Email: f.mohareb@cranfield.ac.uk

Abstract

In contemporary agricultural research, the integration of cutting-edge technologies has become imperative for precise and efficient crop management. The present study focused on multiscale assessment, employing a comprehensive approach that compares aerial drone imagery and ground-based proximal sensors. The primary objective of this study was to evaluate the nitrogen (N) status and agronomic performance in winter wheat through the quantitative comparison of aerially sensed Normalised Difference Vegetation Index (NDVI) and a ground-based proximally sensed NDVI derived at both canopy and leaf scales. This study used data collected from the Wheat Genetic Improvement Network (WGIN) diversity field trial at Rothamsted Research during the 2020/2021 growing season. N fertiliser treatments were applied as ammonium nitrate (NH_4NO_3) at 3 N levels –100, 200 and 350 kg N ha^{-1} applied as 50:50 (N1), 50:100:50 (N2) and 50:250:50 (N3) splits respectively. The trial was structured in 3-fold replication in a split-plot randomised design. Aerially sensed NDVI was acquired using an RGB/NIR adapted camera fitted to a drone whereas the canopy and leaf scales NDVI were measured using a handheld TEC5 spectrometer and handheld contact spectrometer (PolyPen RP410) respectively. Crop parameters indicative of N status including the leaf N content (LNC) and SPAD chlorophyll were measured. Additionally, agronomic parameters such as leaf area index (LAI), number of tillers, straw yield and grain yield

(GY) were determined. F-tests from repeated measures ANOVA (RMA) were used to assess the sensitivity of the sensors to N treatments. Linear Pearson correlation analysis was employed to assess the relationships between sensors (NDVI) to the N status and agronomic parameters. The findings showed that NDVI (PolyPen) was more sensitive than NDVI (Drone) and NDVI (TEC5) to the N status and for evaluating the agronomic performance of wheat. The results indicated that NDVI (PolyPen) demonstrated the earliest detection of nutritional N variations compared to NDVI (Drone) and NDVI (TEC5). At the early to mid-season stage (anthesis), the NDVI (PolyPen) is a good leaf-level indicator for wheat LNC and SPAD chlorophyll content estimation. However, at the late wheat growth stage, NDVI (Drone) was more sensitive to the LNC and SPAD chlorophyll content. The NDVI (Drone), NDVI (PolyPen) and NDVI (TEC5) were strongly correlated to each other validating their alternative use and effectiveness for N status monitoring in winter wheat during the growing season. This study demonstrated that the LAI, number of tillers and straw yield of winter wheat could be effectively assessed non-destructively at mid-season with NDVI (Drone) and NDVI (PolyPen) but more limited with NDVI (TEC5). However, all derived NDVIs irrespective of their proximity showed promise as effective predictors of GY early in the season. The results presented in this study will be useful for understanding and integrating NDVI data across various spatial scales. Overall, the findings of this study may form the basis for developing a decision support tool for farmers, leading to better N management and improved N use efficiency.

Keywords: Aerial drone imagery, remote sensing, proximal sensors, N status, winter wheat

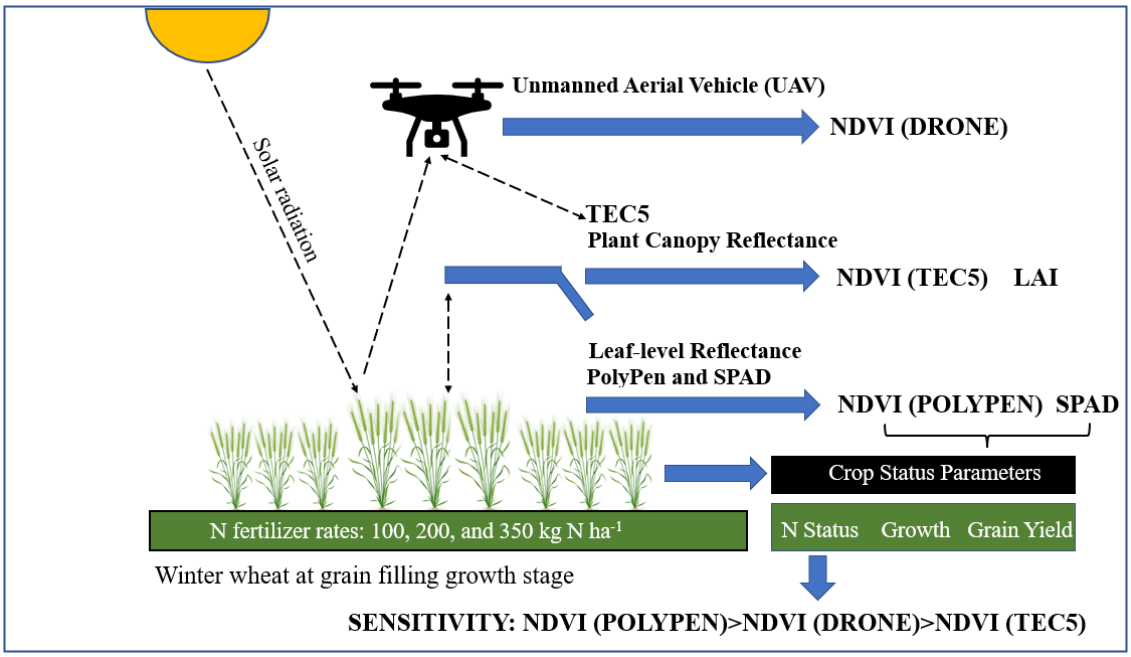

Figure 5.1. Graphical abstract.

5.1 Introduction

Winter wheat (*Triticum aestivum* L.), a major staple food crop, is vital to global food security and sustainable agriculture. N plays a crucial role in determining wheat growth, development and a sufficient supply is fundamental to maximising grain yield and quality (She et al., 2023; Wang et al., 2023). However, optimising N management to achieve high crop yield and high N use efficiency (NUE) is a major challenge in the production of winter wheat. Additionally, excessive N fertiliser application in wheat and other crops has been linked to lower yields, reduced farm economic benefits and detrimental effects on the environment (Li et al., 2018; Shakoor et al., 2018; Wu and Ge, 2019; Hou et al., 2023). Therefore, matching N fertiliser supply to crop needs is essential to ensure optimal crop performance and safeguard the environment.

In agricultural practice, farmers or practitioners frequently estimate the crop N status employing traditional methods that involve destructive sampling and plant tissue chemical analysis or leaf colour charts (Witt et al., 2005). However, despite these manual methods often producing accurate results, they are laborious and time-consuming. Additionally, laboratory results are often delayed which hampers decision making. Moreover, given the extreme spatial and temporal variability of the crop N status within and between fields, these manual methods are not appropriate for

evaluating the crop N status at large scales (Fu et al., 2020). A detailed assessment of the crop N status across time and space using PRS techniques has become the frontier of plant phenotyping and PA (Sishodia et al., 2020; Gordillo-Salinas et al., 2021; Ruan et al., 2023).

PRS are valuable techniques for informing sustainable agronomic management as they allow for quick and accurate assessment of the status of developing crops non-destructively in a dynamic way (Hatfield et al., 2008; Mezera et al., 2021; Yoosefzadeh-Najafabadi et al., 2023). The basis of agricultural PRS is the gathering of crop leaf or canopy reflectance spectra at specific electromagnetic spectrum wavelengths, which typically correspond to areas of the leaf/canopy that strongly absorb or reflect incoming radiation (Xue et al., 2017). A popular technique for interpreting leaf/canopy reflectance data is to use the wavelengths to develop SRIs, which is a mathematical combination of wavelengths associated with specific biophysical characteristics of the plant (Zou and Mõttus, 2017). The NDVI is one of the SRIs that has been widely explored for assessing the biophysical status of developing crops to quantify various agronomic parameters, e.g., nutrient status, LA, crop canopy cover, biomass, crop type and yield (Viña et al., 2011; Tenreiro et al., 2021; Farias et al., 2023). It is calculated using the ratio of red and NIR wavelengths from proximally or remotely sensed data, providing an index/indication of crop vegetation health, vigour, photosynthetic activity or greenness (Huang et al., 2021).

Notably, the NDVI is a commonly used SRI for assessing the N status of crops (Rehman et al., 2019). Based on the physiological intercorrelation between N and chlorophylls, the spectral reflectance of crop leaves or canopies can be used to determine the N status. In wheat, NDVI has been used for assessing the N status, helping to optimise N application, improve nutrient uptake and predict yield (Mitra et al., 2023). The use of NDVI sensors for N management in wheat has been associated with improved economic NUE, particularly with lower rates of N application, indicating the potential for significant N savings (Mitra et al. 2023). Additionally, the NDVI can be used to improve NUE by estimating in-season crop needs and addressing nutrient management through variable-rate applications (Ali et al., 2022; Miller et al., 2023). Therefore, by estimating the early to mid-season N requirement, the NDVI could act as a framework for rational N management in cereals. Despite its limitations in dealing

with soil background, atmospheric and saturation effects, NDVI is still the most adopted SRI due to its simplicity of use and interpretation (Huang et al., 2021). Thus, correlates with the status of a broad array of vegetation properties, making it easier to classify and quantify vegetation. Again, it is readily available from most satellite and other RS platforms which is valuable in commercial agriculture and precision farming (Scheftic et al., 2014).

NDVI data can be collected using a variety of platforms, including proximal handheld sensors and aerial sensors mounted on aircraft, satellites or UAVs (Toth and Jóźków, 2016; Rehman et al., 2022). The use of proximal sensors, particularly those that make use of an active light source, has been the main focus of agricultural RS research over the past 20 years (Saberioon et al., 2014). NDVI values obtained from PS tools have been used to track the crop N status throughout the wheat growing season and predicted yield, aiding in finding the balance between crop N requirements and fertiliser application (Aranguren et al., 2020).

Moreover, a growing number of studies are using low-altitude UAV-based platforms due to the recent development of low-cost and small aerial sensors that are simple to mount to a UAV (e.g., drone) (Colomina and Molina, 2014; Sørensen et al., 2017; Lu et al., 2019; Fu et al., 2020; Liu et al., 2022). Among studies that solely used aerial sensors to evaluate N status, Dunn et al. (2016) reported strong correlations between NDVI and NDRE and N uptake in rice. The authors found that NDVI saturated more than NDRE.

In recent times, numerous studies have embarked on a novel exploration within the realm of PA, focusing on the comparative analysis of aerially sensed and proximally sensed SRI measurements to assess the N status of crops. For instance, Rehman et al. (2023) compared the sensitivity of proximally sensed NDVI and aerially sensed NDRE to crop N status and predicted GY in rice. The authors reported that despite the differences between the sensors used for measurement, both the proximally and aerially measured SRIs can be used to assess the in-season crop N status and predict the GY response to top-dress N with similar precision. When proximal NDVI and aerial NDRE were measured in maize, Sumner et al. (2021) discovered that they were both more responsive to variations in N fertiliser rate than aerial NDVI.

Furthermore, Rehman et al. (2022) quantitatively compared the sensitivity of aerially sensed NDVI and NDRE and proximally sensed NDVI for assessing total N uptake at panicle initiation and predicting GY in a rice cropping system. The authors concluded that both proximally sensed NDVI and aerially sensed NDRE produced measurements sensitive enough to inform N fertiliser management in this system, whereas aerially sensed NDVI was more limited.

Although numerous studies have demonstrated the ability of NDVI and other SRIs (e.g., NDRE) to assess crop N status and predict yields using either a proximal sensor, aerial sensor or both, few studies have directly compared NDVI measured from proximal and aerial sensors side-by-side at different scales. Among the few studies that have, Zheng et al. (2018) reported that NDVI measured with a proximal sensor correlated more strongly with rice N concentration than aerial NDVI. In another study, Ryu et al. (2020) evaluated the performance of garlic and onion using data from a leaf spectrometer, field spectrometers, ground-installed spectral reflectance sensors, a multispectral camera onboard a UAV and Sentinel-2 satellites. The authors reported that the ground-based NDVI data can be used to validate UAV-derived NDVI data without further processing and UAV-derived NDVI data can be used to validate Sentinel-2 NDVI data after upscaling to the Sentinel-2 pixel size. While Duan et al. (2017) reported that aerial NDVI measurements were limited to a narrower range than proximal NDVI, Duan et al. (2017) and Hassan et al. (2018) both found that proximal and aerial NDVI measurements were well-correlated to each other across a wide range of growth stages in wheat.

Given the backdrop of increasing demands for precision in agricultural management, the present study is positioned at the intersection of technological advancement and agronomic necessity. The primary objective is to quantitatively compare the sensitivity and effectiveness of NDVI derived from two distinct scales: aerial imagery and ground-based proximal sensors. This comparison is aimed at assessing their respective capabilities in evaluating the N status and overall agronomic performance of winter wheat, a staple crop with significant global importance.

The rationale for this research stems from the recognition that while both aerial and proximal sensing technologies have individually shown promise in PA, there is a

paucity of studies that systematically compare their performance, especially in the context of NDVI for winter wheat cultivation. Aerial imagery, facilitated by UAVs, offers broad-scale observations, whereas proximal sensors provide high-resolution data at a closer range, potentially capturing more detailed information about the crop canopy and leaf characteristics (Ryu et al., 2020; Alexopoulos et al., 2023).

This study seeks to bridge this gap by employing a multiscale approach to sensor data analysis, hypothesising that integrating insights from both aerial RS and PS modalities could lead to a more accurate, comprehensive understanding of winter wheat N status and agronomic performance. Such an integrated approach could not only enhance the precision of N management strategies but also contribute to the broader goals of sustainable agriculture by optimising resource use and minimising environmental footprint.

5.2 Materials and methods

5.2.1 Plant material and field site

A winter wheat cultivar (*Triticum aestivum* L. cv. KWS Zyatt) was chosen from an existing long-term diversity field trial (Figure 5.2; Appendix D, Figure D-1), Wheat Genetic Improvement Network (WGIN, funded by Defra grant CH0109) at West Barnfield, Rothamsted Experimental Farm, Harpenden, UK (51°48'34.56"N, 0°21'22.68"W). The soil is a well-drained, silty clay loam surface (25% clay) overlying clay with flints (50% clay) at a depth of several metres. According to the UK Soil Classification, the soil at Rothamsted is designated as "Batcombe Series", "Aquic Paleudalf," in the USDA system and "Chromic Luvisol" in the FAO system (Avery and Catt, 1995). Poulton et al. (2003) have provided a thorough description of the experimental site.

The WGIN diversity field trial constitutes a wide range of wheat germplasm which are tested under multiple levels of N inputs (https://www.rothamsted.ac.uk/projects/wheat-genetic-improvement-network). The choice for selecting cv. KWS Zyatt for this study was due to its breeding history, response to N fertilisation, nutritional and bakery quality as well as its agronomical significance. This study used data collected over the WGIN diversity field trial during the 2020/2021 growing season on cv. KWS Zyatt sown on 28th September 2020 and harvested in August 2021.

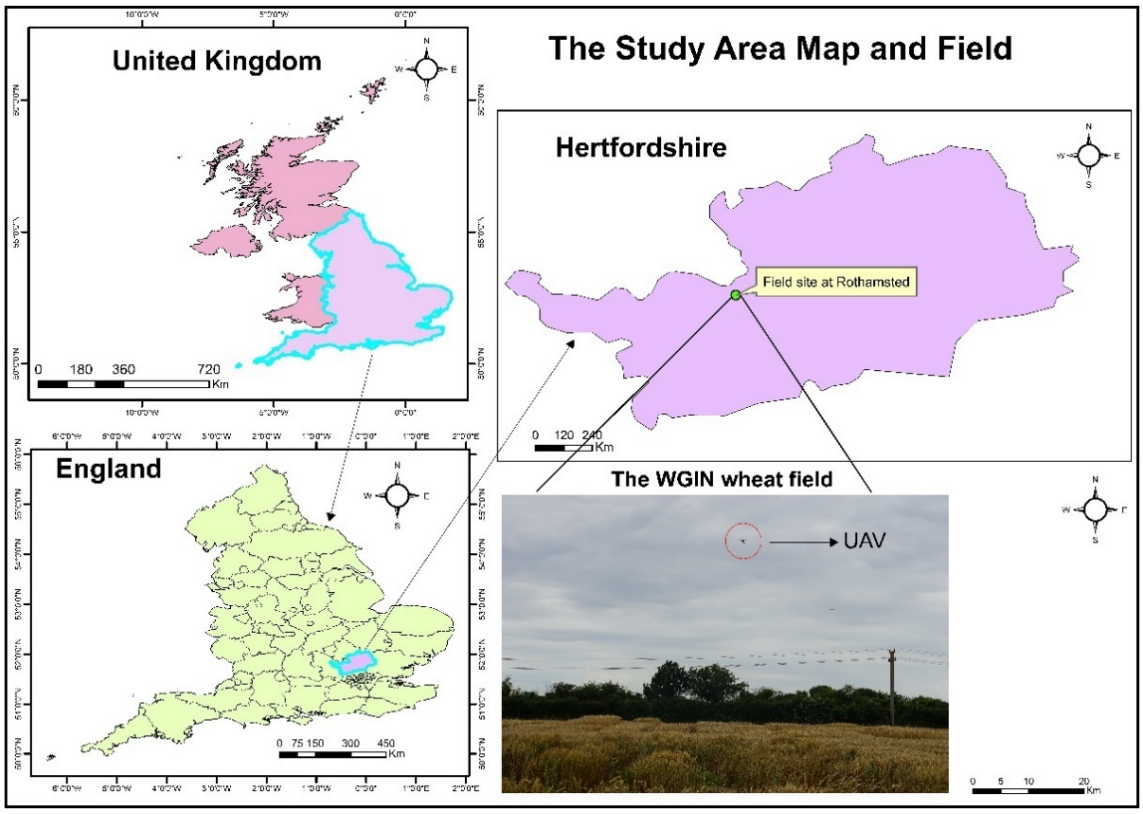

Figure 5.2. WGIN diversity field trial. The photograph was taken at post-anthesis. QGIS software version 3.0.0-Girona was used to prepare maps. Coordinates are displayed in the WGS 1984 Coordinate System.

5.2.2 Agro-climatic conditions of the growing season

Daily measures of meteorological data were collected by the Rothamsted Research weather station and made available by the electronic Rothamsted Archive (Perryman et al., 2018). From this, daily rainfall (mm), daily sunshine (hrs) and average minimum and maximum daily temperatures (°C) were extracted throughout the growing season and used to assess and understand variability in environmental conditions between seasons. At Rothamsted, annual rainfall is typically 700 mm, which is dispersed throughout the year. Rainfall in October 2020 was the highest (200 mm) throughout the experiment (Figure 5.3). The lowest was recorded in April 2021. Sunshine hours in April and July 2021 were extremely high in the UK (Figure 5.3). The highest maximum temperature was 29.4 °C and was recorded in July 2021 whereas the lowest minimum temperature was -4.9 °C recorded in February 2021 (Figure 5.4).

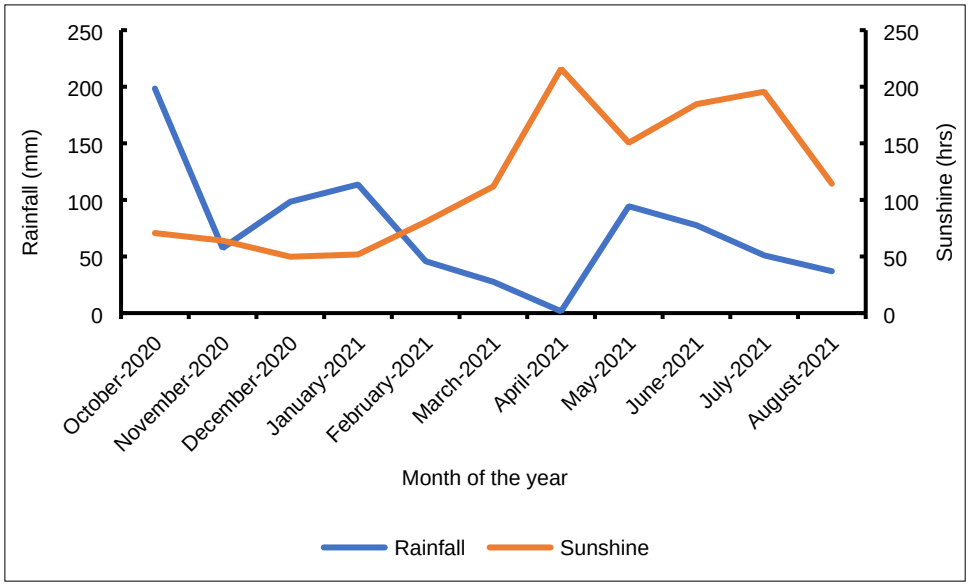

Figure 5.3. Cumulative monthly rainfall and sunshine hours between October 2020 and August 2021 during the experimental period.

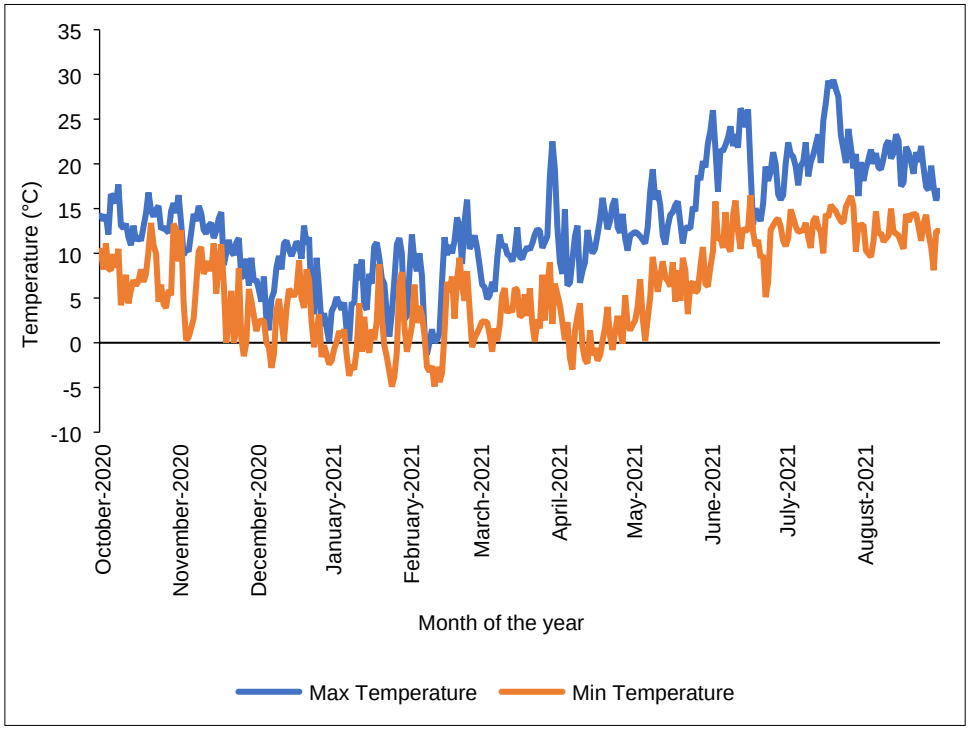

Figure 5.4. Daily minimum (min) and maximum (max) temperatures were recorded between October 2020 and August 2021 during the experimental period.

5.2.3 Experimental treatments, field design and farm practice

N treatments were applied as ammonium nitrate (NH_4NO_3) at 3 N levels-100, 200 and 350 kg N ha^{-1} applied in 50:50 (N1), 50:100:50 (N2) and 50:250:50 (N3) splits respectively (Table 5.1; Figure 5.5). The N levels were varied to create a range in the N nutritional status and test the suitability of sensors to detect these differences. The trial was structured in 3-fold replication in a split-plot randomised design. The plot dimensions were 9 m×1.8 m, at a planting density of ~350 plants m^{-2}. A 2.5 m×1.8 m sampling plot was used for destructive sampling. All plots were separated by 0.5 m uncropped buffer zones. There was an additional treatment of standard farm practice with the applications of pesticides (fungicides) to control disease and insect pest pressure.

Table 5.1. Details of the three (3) N fertiliser treatments applied as ammonium nitrate (NH_4NO_3) in splits to the field plots.

Nitrogen treatment level	Total Nitrogen Application (Kg N ha^{-1})	Application Dates	Amount of Nitrogen Applied (Kg N ha^{-1})
N1	100	25/02/2021	50
		19/04/2021	50
		25/05/2021	0
N2	200	25/02/2021	50
		19/04/2021	100
		25/05/2021	50
N3	350	25/02/2021	50
		19/04/2021	250
		25/05/2021	50

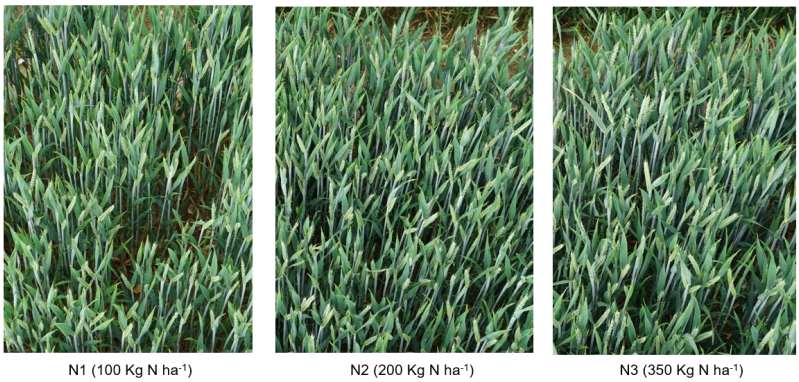

Figure 5.5. Digital images highlighting the impact of 100 kg N ha^{-1} (N1), 200 kg N ha^{-1} (N2) and 350 kg N ha^{-1} (N3) N fertiliser application on canopy development of winter wheat. Images were acquired 2 m above *Triticum aestivum* L. cv. KWS Zyatt canopies on 2nd June 2021.

5.2.4 Data collection

5.2.4.1 Acquisition of aerial drone imagery

In the 2021 season, 14 flight campaigns were conducted at the WGIN diversity field trial (by March Castle, Rothamsted Research) from 02 March 2021 to 27 July 2021 which commenced at stem elongation to physiological maturity. A DJI S900 UAV (Da-Jiang Innovations, Shengzhen, China) (Figure 5.6) equipped with a DJI flight controller was flown at 25 m altitude over the field site according to a pre-established flight plan. The flight plan was designed to guarantee that an 80% overlap between concurrent images was obtained. Two Sony RGB/NIR α5100 mirrorless adapted cameras (Tokyo, Japan) (Table 5.2) mounted on the UAV were used to capture RGB and NIR images as previously deployed by Holman et al. (2020). Both cameras have 20 mm F2.8 Sony prime lenses, and complementary metal-oxide semiconductor (CMOS) sensors with a resolution of 24.3 MP. The NIR-adapted camera had its internal blocking filter replaced with a long-range 830 nm wavelength filter to prevent capturing visible light and enable the acquisition of NIR waveband imagery (Berra et al., 2017; Holman et al., 2019). The RGB camera captures from around 400 to 800 nm and generates 3 bands (Red, Green and Blue) of the electromagnetic spectrum compared to the single band of the NIR-adapted camera.

The cameras were programmed to shutter priority to capture images at 1-sec intervals and in raw format, with the focus set to 25 m to correspond with the UAV flight height. Shutter speed was fixed at 1/1000 sec while ISO and aperture were left on automatic mode to reduce motion blur. The DJI S900 was flown at a speed of 4 m/s providing a total flight time of 12 minutes to cover the whole field. All UAV imagery over the field site was collected close to solar noon under clear sky conditions with image collection taken between 10:00 am to 1:30 pm.

The DJI S900 relies on Ground Control Points (GCPs) whose positions were measured and recorded with a Trimble Geo 7 DGPS (Trimble, Inc., Sunnyvale, CA, USA) for ortho-rectification. Twelve GCPs (100 cm^2) each made of concrete painted with circular patterns, mounted on 5 mm foamboard with a weatherproof lamination, which can be automatically detected by the software were used for georeferencing final RGB and NIR orthomosaics (Figure 5.7; Figure 5.8). The Tec5 HandySpec Field Spectrometer (Tec5,

Oberursel, Germany) equipped with a cosine-corrected downwelling optic was placed at a fixed point next to the field and programmed to measure at 1-second intervals to produce measurements of the total incoming solar irradiance to adjust for variation in ambient light during the flight. Spectral measurements were acquired at 10 nm spectral resolution within 360–1000 nm wavelength range.

Figure 5.6. The DJI S900 UAV (drone) with RGB/NIR adapted camera used for collecting aerial images.

Table 5.2. Sensitivities of Sony α5100 mirrorless adapted camera band. A double monochromator equipped with an integrating sphere was used to measure the sensitivities. Adapted from Holman et al., 2019.

Model	Channel	Number of Channels	Waveband Range (nm)
RGB camera	Red	3	580-660
	Green		420-610
	Blue		410-540
NIR camera	NIR (Blue channel)	1	800-900

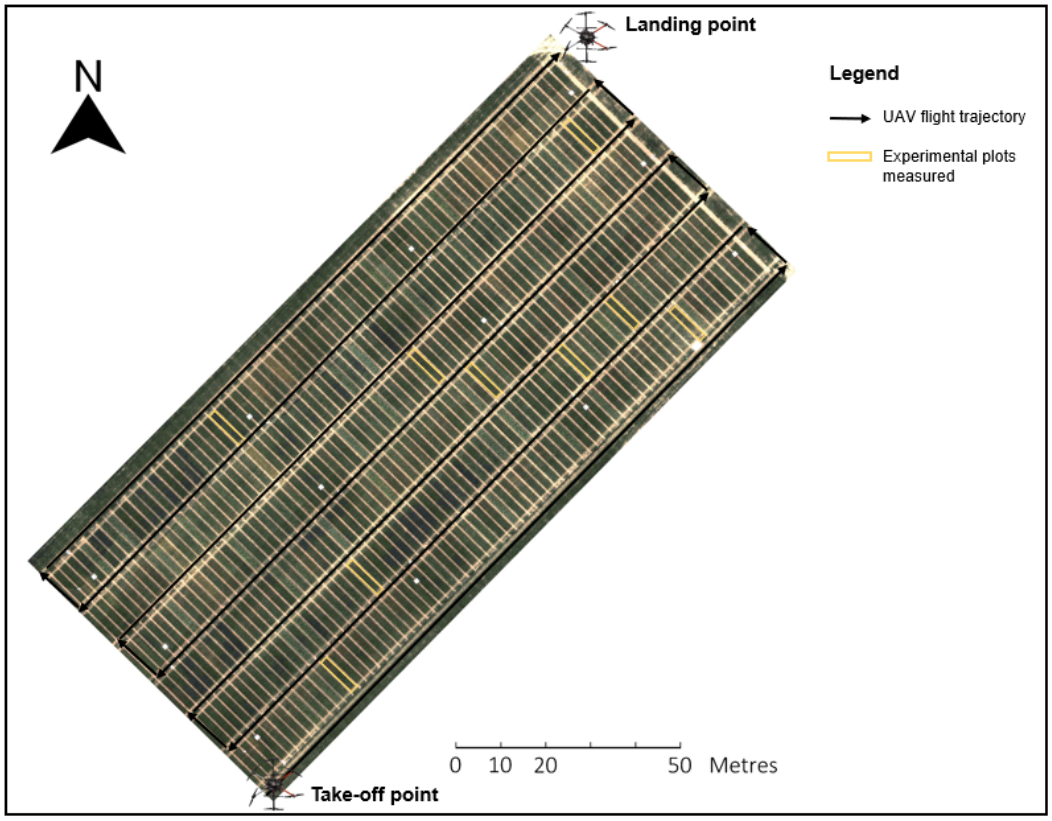

Figure 5.7. Orthomosaic of the experimental field, showing the location of Ground Control Points (GCPs) as white squares, measured plots marked in orange colour and the UAV flight trajectory used in black arrows. Coordinates are displayed in the WGS 1984 Coordinate System.

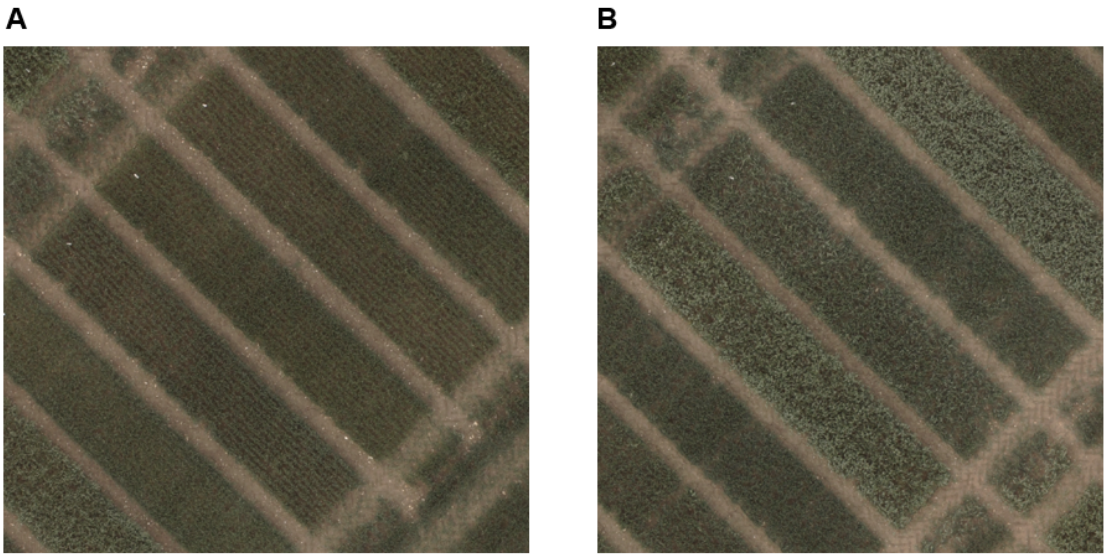

Figure 5.8. UAV imagery (orthomosaic) collected at a flying height of 25 m of (A) N1 (100 kg N ha^{-1}) fertiliser treatment plots compared to (B) N3 (350 kg N ha^{-1}) fertiliser treatment plots. Wheat cultivar Zyatt compared in both scenarios.

5.2.4.2 UAV image processing and data extraction

To process UAV images, both sets of images (RGB and NIR) were corrected using the ground-based Tec5 HandySpec Field spectrometer data (collected at the same time as the images were taken). The Tec5 HandySpec uses a downwelling optic with a cosine diffuser to compensate for variations in sun illumination between measurements (Holman et al., 2019). This is done using the 'Image Calibration' tool contained within the 'UAVImageConverter' software. The camera captures the data in 'RAW' format and outputs as 'TIF' format. This means that no compression algorithms are used and that all image data is preserved. The images (either RGB or NIR) were aligned using the Agisoft Metashape Professional version 2.0.0 (Agisoft LLC, St. Petersburg, Russia).

The global positioning system (GPS) data captured with the Trimble Geo7 DGPS logger (Trimble, Inc., Sunnyvale, CA, USA) was manually assigned to the GCPs shown within image data (http://www.agisoft.com/downloads/user-manuals/). This will 'orthorectify' to give scale and location information to the orthomosaic with precision or georeferenced (Ruiz et al., 2013). A dense point cloud is generated from SfM at high quality and using mild depth filtering to prevent removing points representing plant canopies to produce a georeferenced orthomosaic (image orthomosaic) and digital elevation model (DEM) in the case of height data.

The data extraction tool from the 'UAVImageConverter' software was used to extract the data from each plot. This data extraction step requires, a bare soil DEM (height data from the first flight of the season showing bare soil or newly established canopy), RGB and NIR orthomosaics, a DEM generated from data captured at the same time as the RGB/NIR image data. Furthermore, 'shapefiles'–which in this case are several 'polygons' that define the identity, size and location of each plot from the trial from which the image data was collected (Sangjan et al., 2022) are constructed using the ArcMap version 10.4 (ESRI®, Germany) and QGIS software version 3.0.0-Girona (http://qgis.org). Once processing is complete the 'UAVImageConverter' software generates an Excel file with Red, Green, Blue and NIR channel mean values, as well as NDVI and height data for each plot as outputs of the RGB/NIR orthomosaics as described in Table 5.3. Orthomosaics were generated at a ground sampling distance (GSD) of approximately 1 cm/pixel. Image processing and regression analysis were performed using the statistical software R version 3.5.1 (R Core Team, 2018). The

parameter settings used for the UAV imagery and Agisoft Metashape software are summarised in Table 5.4. The workflow used for processing the UAV images is also summarised in Figure 5.9.

NDVI (Drone) orthomosaics were generated using Equation 5.1.

$$\text{NDVI (Drone)} = R_{NIR} - R_R / R_{NIR} + R_R \quad (5.1)$$

Where R_R is the measured reflectance in the red waveband and R_{NIR} is the measured reflectance in the NIR waveband. The wavebands for the NIR and R were 780 nm and 680 nm respectively.

Table 5.3. Definitions of parameters derived from orthomosaics of the UAV imagery.

Model	Description
NDVI	NDVI calculated from the red and NIR reflectance imagery wavebands
NIR	NIR extracted from the near-infrared reflectance spectrum with values > 0
R	R channel (colour space) by pixels classified as the red spectrum of the vegetation with values > 0
G	G channel (colour space) by pixels classified as green spectrum of the vegetation with values > 0
B	B channel (colour space) by pixels classified as the blue spectrum of the vegetation with values > 0

Table 5.4. Parameters of the UAV flights, camera settings and Agisoft Metashape processing parameters.

Process	Parameter	Setting
UAV flight	Altitude (m)	25 m
	Overlaps (front and side)	80% overlaps
	Speed	4 m/s
	Flight time	12 min
	Number of GCPs	12
	Size of GCPs	100 cm^2
	Coordinate system	WGS 1984 Coordinate System
Cameras (Sony RGB/NIR)	Accuracy	Highest
	Adapted camera model	Yes
	Resolution (both cameras)	24.3 MP
	Aperture (both cameras)	f/2.8
	ISO (both cameras)	100
	Shutter speed (Sony RGB)	1/3 s
	Shutter speed (Sony NIR)	8 s
	Light range (Sony RGB)	350-850 nm
	Light range (Sony NIR)	750-1150 nm
	Storage format	16 bits TIFF
Agisoft metashape processing	DEM parameters	Dense cloud
	DEM resolution (m)	0.02 m
	Dense point cloud	High disabled
	Alignment accuracy	Highest
	Mesh	High
	GSD (m)	0.01m/pixel
	Orthomosaic	Blending disabled

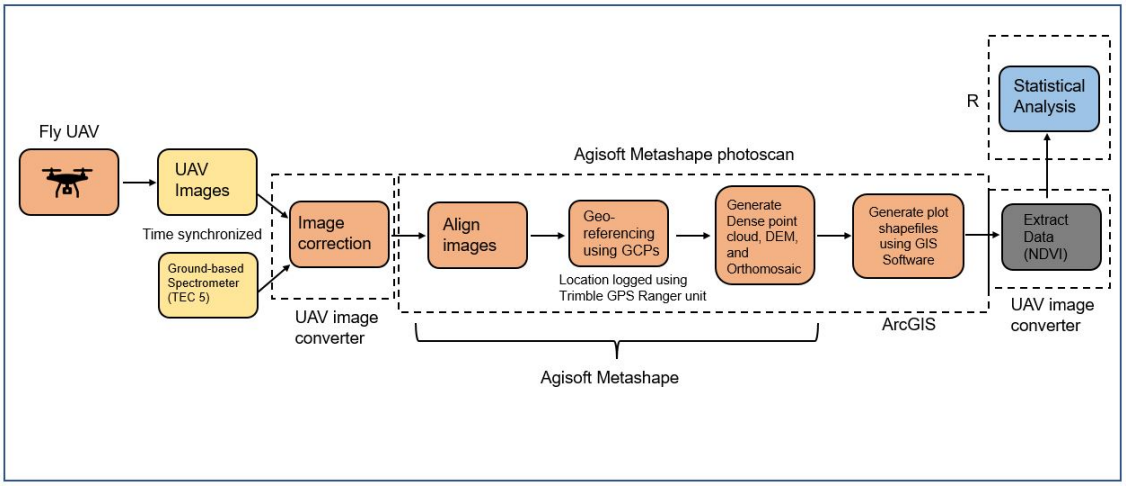

Figure 5.9. Workflow for processing the UAV imagery and extracting NDVI and NIR values for each plot. Adapted from Holman, 2020.

5.2.4.3 Ground-based proximal sensor measurements

5.2.4.3.1 Canopy scale NDVI measurement

For canopy reflectance measurements, a radiometrically calibrated portable Tec5 HandySpec Field Spectrometer (Oberursel, Germany) was used. It provides hyperspectral point measurements in the range of 360-1000 nm with a spectral resolution of 10 nm. To collect the spectrometer measurements, a single scan of each plot canopy was collected with the spectrometer optic held approximately 1 m above the plot (Holman et al., 2019). Each scan produced one spectral reflectance measure for the plot at 10 nm spectral resolution across the wavelength range 360–1000 nm. The canopy reflectance was measured weekly starting from stem elongation and continuing through to physiological maturity. NDVI (TEC5) was extracted from the same wavebands as in NDVI (Drone). The spectra from each treatment were first averaged and the total mean spectrum was examined to detect differences in the spectral signature acquired from the different N treatments (Figure 5.10).

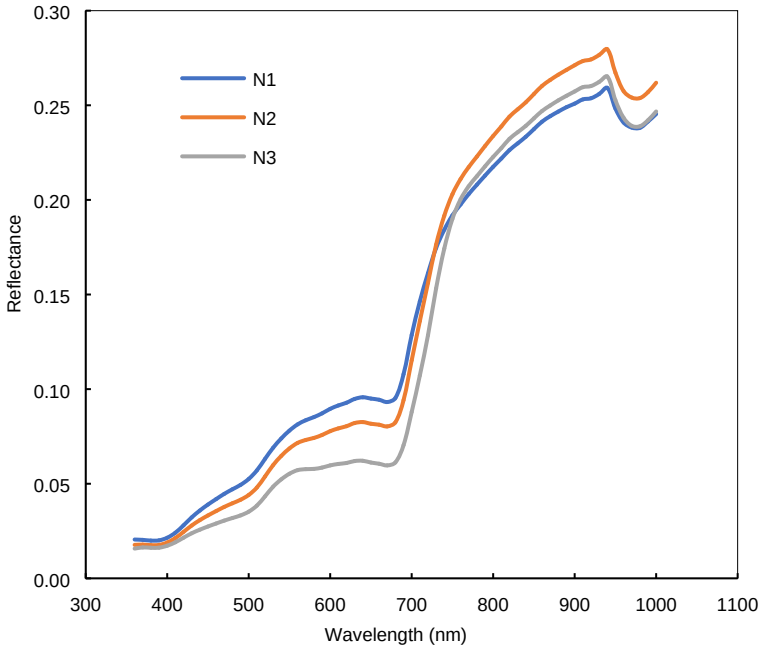

Figure 5.10. Reflectance spectra of winter wheat leaves exposed to different N levels and measured with the TEC5 spectrometer at anthesis. N1, N2 and N3 represent 100, 200 and 350 kg N ha^{-1} respectively.

5.2.4.3.2 Leaf level NDVI measurement

The PolyPen RP410/UVIS handheld contact spectroradiometer (Photon Systems Instruments, Drasov, Czech Republic), capable of measuring the wavelength range of 320-790 nm of the electromagnetic spectrum at intervals of 1.9 nm, was used to collect leaf spectral reflectance data as employed in Chapters 3 and 4. Spectral reflectance data was collected from the uppermost fully expanded leaf of the plants from 11:00 to 16:00 h GMT. Spectral data were measured weekly using the fully expanded leaf of the main stem from stem elongation to physiological maturity. Measurements were acquired from five plants for each treatment selected at random from the plot. Three readings were made on a single leaf per plant and then averaged. The spectrometer sensor was calibrated before measurement and periodically with a diffuse white reference standard (Spectralon®, Labsphere, Inc., North Sutton, USA). The PolyPen RP410 device integrates a xenon incandescent lamp as an internal light source, with radiation emitted between 380-1050 nm. The PolyPen RP410 incorporates pre-defined formulae for calculating commonly used SRIs. NDVI (PolyPen) was derived from similar wavelengths used for NDVI (Drone) and NDVI (TEC5) to set a baseline for all the derived NDVIs. To detect differences in the spectral signature acquired from the

different N treatments, the spectra from each treatment were first averaged and the total mean spectrum was examined as in NDVI (TEC5) (Figure 5.11).

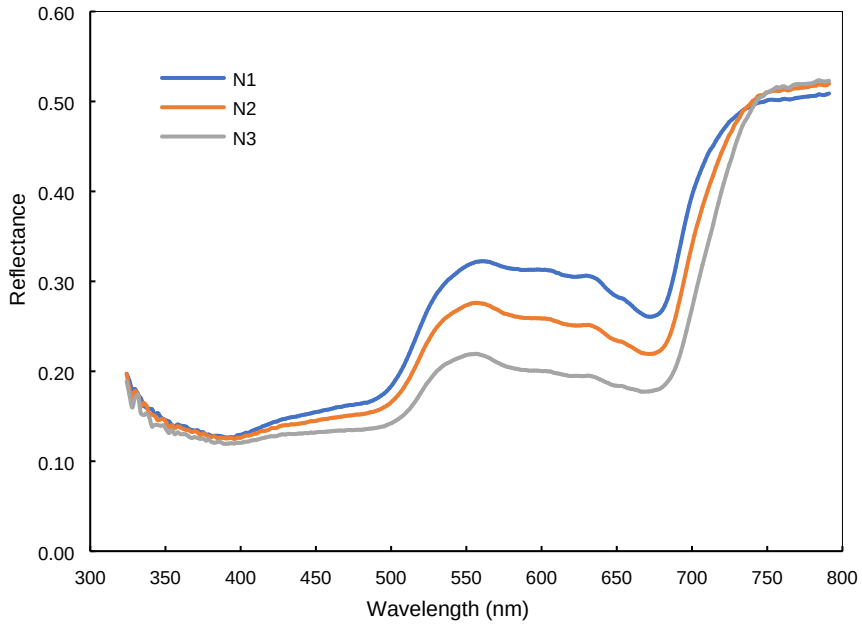

Figure 5.11. Reflectance spectra of winter wheat leaves exposed to different N levels and measured with the PolyPen RP410 spectrometer at anthesis. N1, N2 and N3 represent 100, 200 and 350 kg N ha^{-1} respectively.

5.2.4.4 Determination of N status

5.2.4.4.1 SPAD measurement

The SPAD-502 chlorophyll meter (Soil Plant Analysis Development, Minolta Camera Co., Ltd., Japan) was used to measure the relative leaf chlorophyll content. Five measurements were made on each plot with three readings taken from each leaf and then averaged. SPAD measurements were done synchronously with the PolyPen RP410.

5.2.4.4.2 Leaf nitrogen content

The fully expanded leaves of five wheat plants from each treatment plot were destructively harvested for the LNC. The leaf samples were then oven-dried and milled at a speed of 17500 rpm using the Genogrinder (SPEX SamplePrep®, 2010, USA). The LNC was determined for each treatment by laboratory chemical analysis employing the LECO combustion method (LECO CN628 Analyzer, LECO Corporation, St Joseph, Michigan, USA) at anthesis and post-anthesis growth stages.

5.2.4.5 Measurement of agronomic parameters

5.2.4.5.1 Leaf area index

The LAI-2200C Plant Canopy Analyzer (LI-COR, Biosciences, Lincoln, NE, USA) employs a non-destructive method and was used to measure the LAI. The LAI was measured at anthesis. Before LAI measurement, the LAI-2200C optical sensor (wand) was levelled and placed closely over the canopy with a 90° view restricting cap. One above-canopy reading followed by two below-canopy readings were taken at a short time interval under a uniform overcast (clear, blue sky) early in the morning. Measurements made above and below the canopy were used to calculate canopy light interception at five zenith angles, from which LAI was computed using a model of radiative transfer in vegetative canopies within a wavelength range (320-490 nm).

5.2.4.5.2 Number of tillers

The number of tillers was determined by counting the number of side shoots (tillers) formed around the main stem within an m^2 area of treatment plots. The counting was performed along the 1 m rule at 3 random locations within the plot and the average was recorded.

5.2.4.5.3 Straw and grain yield

Before harvest, preharvest sampling of 100 stems was collected at plot level and the harvested samples were threshed to separate the grains and straw. The FW of the straw was recorded and oven-dried for 48 h at 105 °C. The DW was determined and extrapolated to straw yield in tonnes per hectare (t ha^{-1}). At the final harvest, plots were harvested, and fresh grains were weighed using a Haldrup GMbH C-85 specialist plot combine harvester (Haldrup, Ilshofen, Germany). The GY (85% dry matter) in tonnes per hectare (t ha^{-1}) was also determined.

5.2.5 Statistical analysis

Spectral responses and variables measured on successive occasions were analysed using repeated measures ANOVA (RMA) that incorporates an adjustment for the presence of autocorrelation between sample occasions (Greenhouse and Geisser, 1959; Keselman et al., 2000). F-statistics were employed to test all fixed terms (i.e., main effects and interactions), with all tests conducted at the 5% significance level. Pearson's correlation coefficient was used to assess the linear relationships between pairs of variables. All

analyses and visualisations were conducted using GenStat 22nd edition (VSN International Ltd., Hemel Hempstead, United Kingdom).

5.3 Results

5.3.1 Detection of nutritional variations across sensors

Figure 5.12 demonstrates the time course response of NDVI derived from the drone imagery, PolyPen and TEC5 spectroradiometer to detect N nutritional variations from the stem elongation to the physiological maturity growth stages of winter wheat. The results showed the early response of NDVI (PolyPen) to detecting N nutritional variations first at 252 DAS (anthesis) and consistently from 266 to 301 DAS except for 273 DAS along with good separation between treatments (Figure 5.12B). Two weeks post-anthesis, NDVI (Drone) detected N nutritional variations at 266 DAS (14 DPA) and consistently to 301 DAS (Figure 5.12A). A good separation between treatments was observed at these time points by NDVI (Drone). Contrarily, NDVI (TEC5) only showed the detection of N nutritional variations at 294 DAS during physiological maturity (Figure 5.12C). Generally, higher NDVI values were obtained for the N3 treatment compared to N2 and N1 across the three sensors.

Additionally, the F-tests from RMA showed a higher sensitivity ($p<0.001$) of the NDVI (PolyPen) to N stress followed by NDVI (Drone) ($p<0.05$) with corresponding (N×DAS) interaction (Table 5.5). However, the NDVI (TEC5) did not show sensitivity to N stress and was only affected by DAS. Based on the results, the sensitivity of the three sensors to N treatment is ranked as NDVI (PolyPen) > NDVI (Drone) > NDVI (TEC5) (Table 5.5).

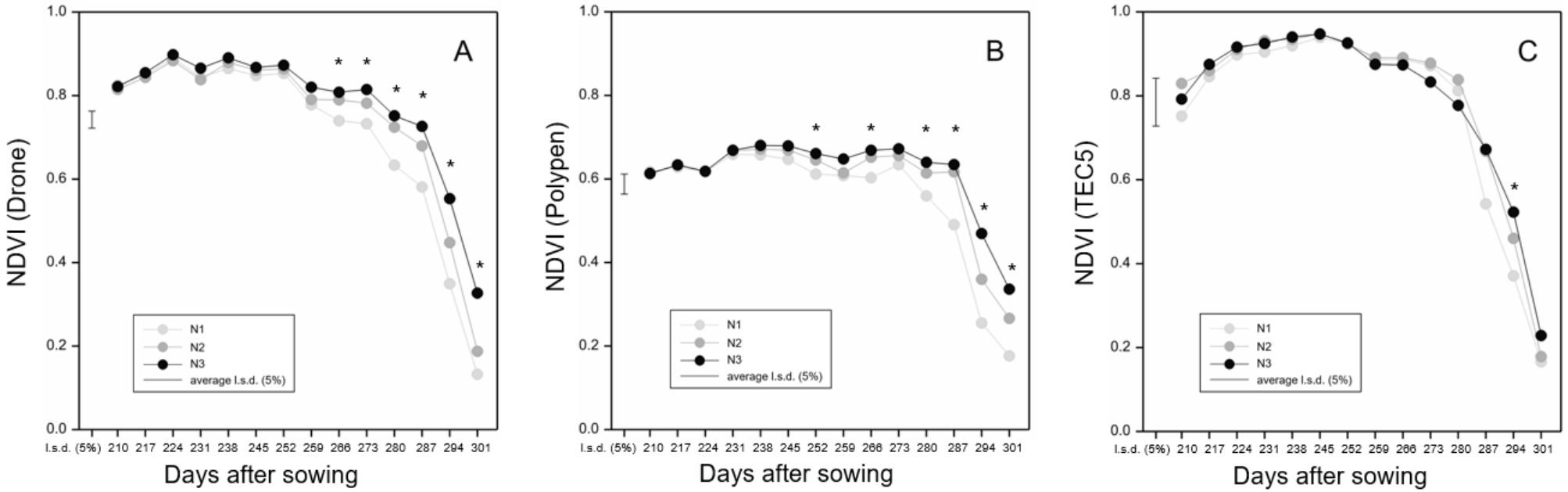

Figure 5.12. Time course responses of (A) NDVI (Drone), (B) NDVI (PolyPen) and (C) NDVI (TEC5) spectroradiometers to N nutritional variations at specific days after sowing (DAS) during the crop cycle from 210 to 301 DAS. Mean values represent three replicates per N treatment. Bars indicate the average least significant difference (LSD) at the 5% significance level. Asterisks (*) indicate significant difference between treatments at 5% significance level. N1, N2 and N3 represent 100, 200 and 350 kg N ha^{-1} respectively.

Table 5.5. F-tests from repeated measures ANOVA (RMA) to assess the sensitivity or main effects of (and interactions between) N and days after sowing (DAS) on NDVI derived from the drone imagery, PolyPen and TEC5 spectroradiometers. Statistically significant results (p<0.05) are shown in bold.

Parameter	N	DAS	N×DAS
NDVI (Drone)	$F_{2,4}$=22, p<**0.05**	$F_{2,13}$=680.3, p<**0.001**	$F_{2,26}$=8.5, p<**0.001**
NDVI (PolyPen)	$F_{2,4}$=464, p<**0.001**	$F_{2,13}$=167.8, p<**0.001**	$F_{2,26}$=4.5, p<**0.05**
NDVI (TEC5)	$F_{2,4}$=0.63, p=0.578	$F_{2,13}$=128.6, p<**0.001**	$F_{2,26}$=0.85, p=0.518

5.3.2 Correlation with N status indicators

5.3.2.1 Correlation with LNC

Figure 5.13 shows the linear relationship between LNC and the derived NDVI from the drone, PolyPen and TEC5 assessed by Pearson's correlation. The results showed a strong correlation (r=0.84) between LNC and NDVI (PolyPen) at 252 DAS (Figure 5.13A). A good correlation (r=0.59) was observed between LNC and NDVI (Drone) at the same time. However, the lowest correlation (r=-0.02) was observed between LNC and NDVI (TEC5) due to the high variability of the N2 and N3 treatments. Generally, higher data variation was seen for the lower values of LNC and NDVI across all sensors especially for N1 treatment, reflecting the observations on the linear relationship.

At 266 DAS, the linear relationship between LNC and NDVI (Drone) recorded the highest correlation (r=0.91) (Figure 5.13B). A good correlation (r=0.68) was observed between LNC and NDVI (PolyPen) and was driven by a high variability among N1 and N2 treatments during the same period. A negatively poor correlation (r=-0.17) was observed between LNC and NDVI (TEC5) probably due to the high variability among the N2 and N3 treatments.

Additionally, a strong correlation (r=0.85) was recorded between LNC and NDVI (Drone) at 273 DAS with variability shown among N1 and N2 treatments (Figure 5.13C). The linear relationship between LNC and NDVI (PolyPen) showed a good correlation (r=0.63) but with high variations among N1 and N2 treatments. A low linear relationship was observed between LNC and NDVI (TEC5) with a negatively poor correlation (r=-0.23) due to the high variability among treatments.

Similarly, at 280 DAS a strong correlation (r=0.85) was observed between LNC and NDVI (Drone) (Figure 5.13D). A good correlation (r=0.73) was observed between LNC and NDVI (PolyPen) with high variability among N1 and N2 treatments. A negatively poor correlation (r=-0.11) was observed between LNC and NDVI (TEC5) due to high variability among N2 and N3 treatments. Generally, higher data variation was seen for the lower values of LNC and NDVI across all sensors, reflecting the observations on the linear relationship.

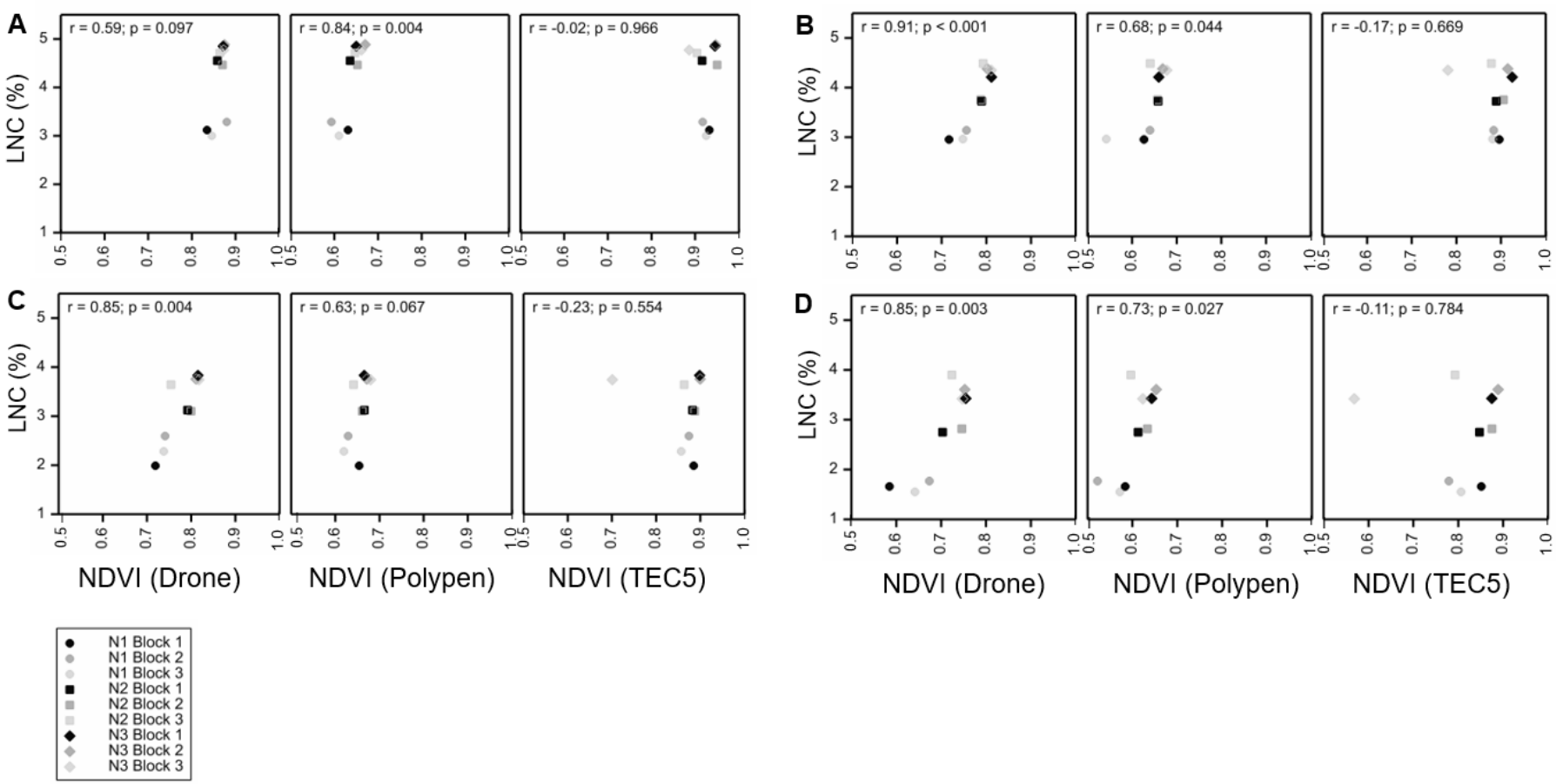

Figure 5.13. Linear association assessed by Pearson's correlation coefficient between NDVI derived from the drone imagery, PolyPen and TEC5 spectroradiometers and leaf nitrogen content (LNC) at (A) 252 DAS, (B) 266 DAS, (C) 273 DAS and (D) 280 DAS. Each N treatment represents three replicates from 3 blocks. N1, N2 and N3 represent 100, 200 and 350 kg N ha^{-1} respectively.

5.3.2.2 Correlation with SPAD

The linear relationship between SPAD and the derived NDVI from the drone imagery, PolyPen and TEC5, as determined by Pearson's correlation, are shown in Figure 5.14. The results showed a strong correlation (r=0.89) between SPAD and NDVI (PolyPen) at 231 DAS (Figure 5.14A). Concurrently, a good correlation (r=0.63) was found between SPAD and NDVI (TEC5). The high variability of the N2 and N3 treatments, however, resulted in the lowest correlation (r=0.07) between SPAD and NDVI (Drone).

A strong correlation (r=0.74) was observed at 238 DAS in the linear relationship between NDVI (PolyPen) and SPAD (Figure 5.14B). At the same time, a good correlation was observed between SPAD and NDVI (Drone) (r=0.38) and NDVI (TEC5) (r=0.51). A similar pattern of variability was more pronounced in N2 and N3 treatments across sensors at 238 DAS. At 266 DAS, the linear relationship between NDVI (Drone) and SPAD recorded the strongest correlation (r=0.95) (Figure 5.14C). The NDVI (PolyPen) and SPAD showed a good correlation (r=0.53) along with high variability in N1 treatments. A negatively poor correlation was observed between NDVI (TEC5) and SPAD with high variability among N treatments over the same time.

A similar trend of linear relationship was demonstrated at 273 DAS with a strong correlation (r=0.86) between NDVI (Drone) and SPAD with little variations among treatments (Figure 5.14D). A good correlation (r=0.69) was seen between NDVI (PolyPen) and SPAD with high variability especially among N1 treatments. At the same time, a negatively poor correlation (r=-0.17) was observed between NDVI (TEC5) and SPAD with high variability found among the N3 treatments.

Altogether, the NDVI (PolyPen) showed a stronger relationship with SPAD at the early growth stages (231 DAS and 238 DAS) (Figure 5.14A-B) while NDVI (Drone) demonstrated a stronger relationship with SPAD at the late growth stages (266 DAS and 273 DAS) (Figure 5.14C-D). Additionally, NDVI (TEC5) showed a good correlation with SPAD at the early growth stage (231 DAS and 238 DAS) (Figure 5.14A-B) but poorly at the later stage (266 DAS and 273 DAS) (Figure 5.14C-D). Higher data variation was seen for the lower values of NDVI and SPAD across all sensors especially for N1 treatment, reflecting the observations on the linear relationship (Figure 5.14).

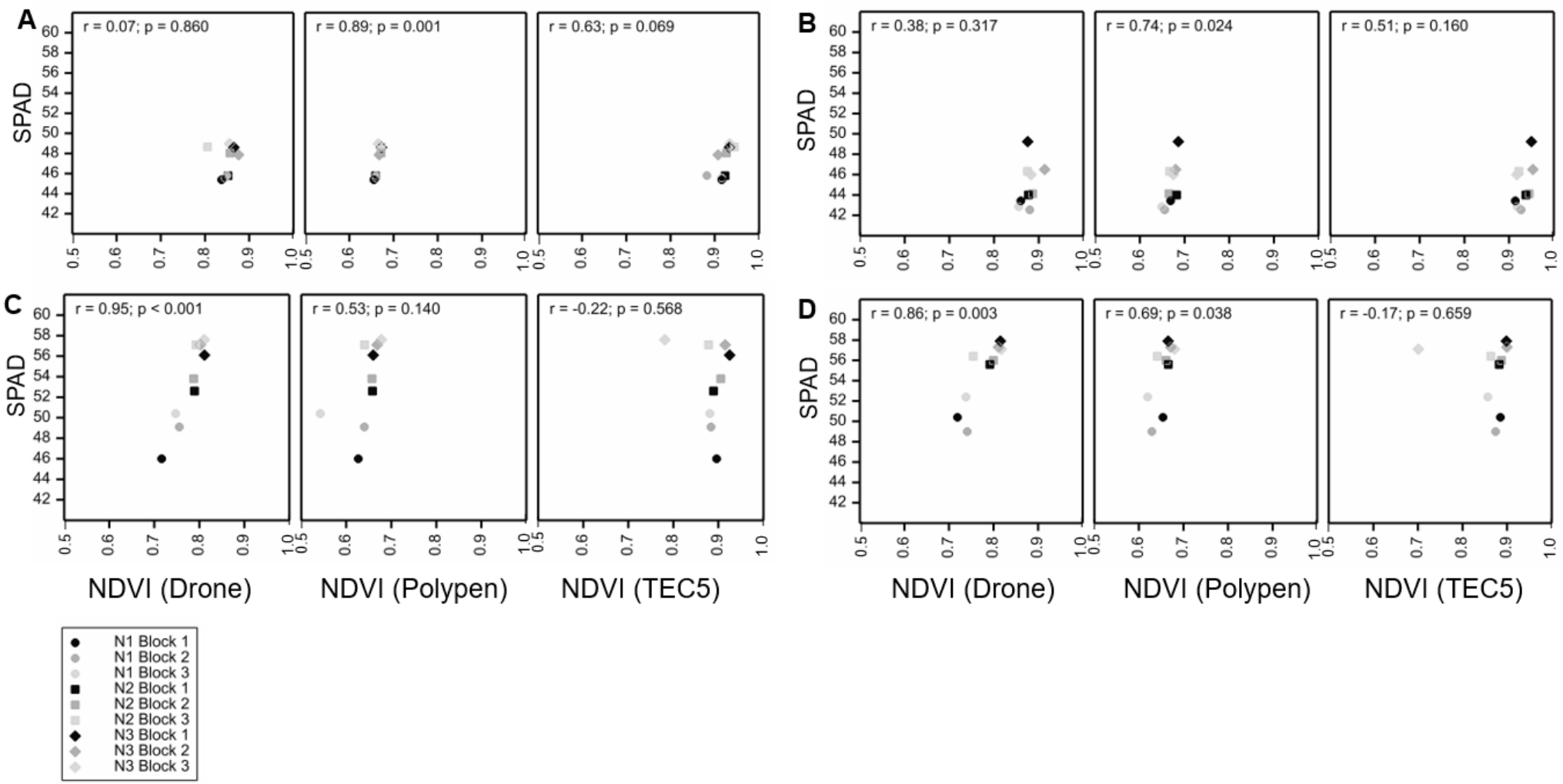

Figure 5.14. Linear association assessed by Pearson's correlation coefficient between NDVI derived from the drone imagery, PolyPen and TEC5 spectroradiometers and SPAD at (A) 231 DAS, (B) 238 DAS, (C) 266 DAS and (D) 273 DAS. Each N treatment represents three replicates from 3 blocks. N1, N2 and N3 represent 100, 200 and 350 kg N ha^{-1} respectively.

5.3.3 Assessment of relationships among sensors

To examine the relationships among aerial drone imagery and ground-based spectral reflectance (PolyPen and TEC5) spectroradiometers, correlation analysis was conducted with their derived NDVI values (Figure 5.15). Generally, strong correlations were recorded between the various derived NDVIs across sensors. The highest linear relationship was observed between NDVI (Drone) and NDVI (PolyPen) with a correlation coefficient (r=0.94) (Figure 5.15A). Similarly, a strong linear relationship (r=0.92) was observed between NDVI (Drone) and NDVI (TEC5) (Figure 5.15B). The linear relationship between NDVI (PolyPen) and NDVI (TEC5) also showed a strong correlation (r=0.89) (Figure 5.15C). Generally, a high variation is observed across N1, N2 and N3 treatments at lower NDVI values across sensors as data points are spread and hence confidence in the correlation is likely to be low. However, at higher NDVI values, tight clustering of data points drives a stronger confidence in the correlation reflecting in the r values. Additionally, the relative sensitivity of the sensors to N1, N2 and N3 may be proportional as each treatment seem to contribute equally to the variations in the data.

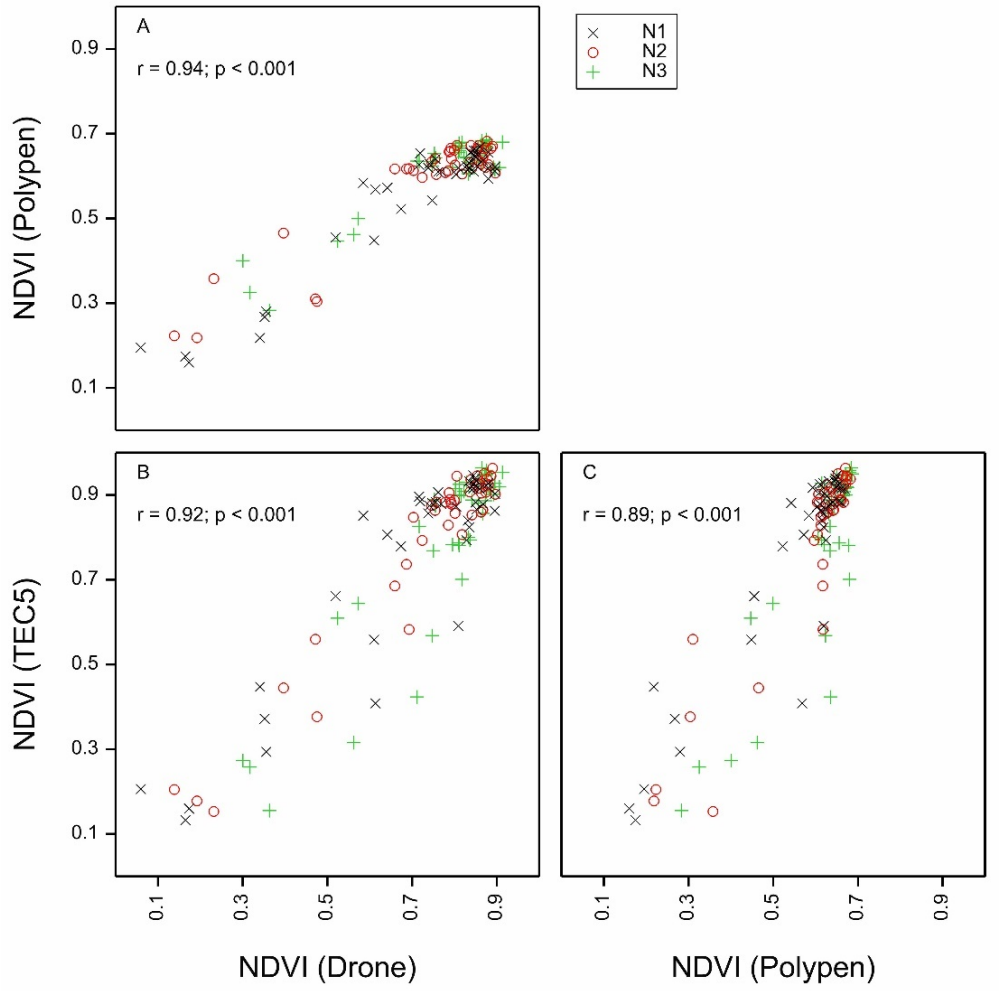

Figure 5.15. Linear relationships between (A) NDVI (Drone) and NDVI (PolyPen), (B) NDVI (Drone) and NDVI (TEC5) and (C) NDVI (PolyPen) and NDVI (TEC5) spectroradiometers assessed by Pearson's correlation. Spectral reflectance data from all time points were correlated. N1, N2 and N3 correspond to 100, 200 and 350 kg N ha^{-1} respectively.

5.3.4 Assessment of effectiveness of aerial drone imagery and proximal sensors in determining crop performance

Figure 5.16 shows the linear relationship between agronomic parameters and the derived NDVI values from the drone imagery, PolyPen and TEC5, as assessed by Pearson's correlation. The results showed a strong correlation (r=0.86) between NDVI (PolyPen) and LAI at 259 DAS (anthesis) with variability found among N2 and N3 treatments (Figure 5.16A). At the same time, a good correlation (r=0.65) was observed between NDVI (Drone) and LAI with high variability found among N1 and N2 treatments. A very low correlation (r=0.07) was found between NDVI (TEC5) and LAI with high variations observed among treatments, especially in N3. At the same time

(259 DAS), a strong correlation (r=0.82) was indicated between NDVI (PolyPen) and the number of tillers with N1 and N2 showing high variability (Figure 5.16B). An equally strong correlation (r=0.70) was observed between NDVI (Drone) and the number of tillers with high variability found among N1 and N2 treatments. However, a poor correlation (r=-0.11) was observed between NDVI (TEC5) and the number of tillers with widespread variations found among treatments.

Additionally, at final harvest, both NDVI (Drone) and NDVI (PolyPen) had similar correlations (r=0.46 and r=0.40) respectively with straw yield with widespread variations among N2 and N3 treatments (Figure 5.16C). NDVI (TEC5) correlated poorly (r=0.14) with straw yield and showed widespread nutritional variations among N2 and N3 treatments. For GY, NDVI (PolyPen) and NDVI (TEC5) showed a similarly strong correlation (r=0.85) with the agronomic parameter and showed a high variation in N2 and N3 treatments (Figure 5.16D). NDVI (Drone) also showed a good correlation (r=0.69) with GY but exhibited high variability among treatments, particularly in N2 and N3.

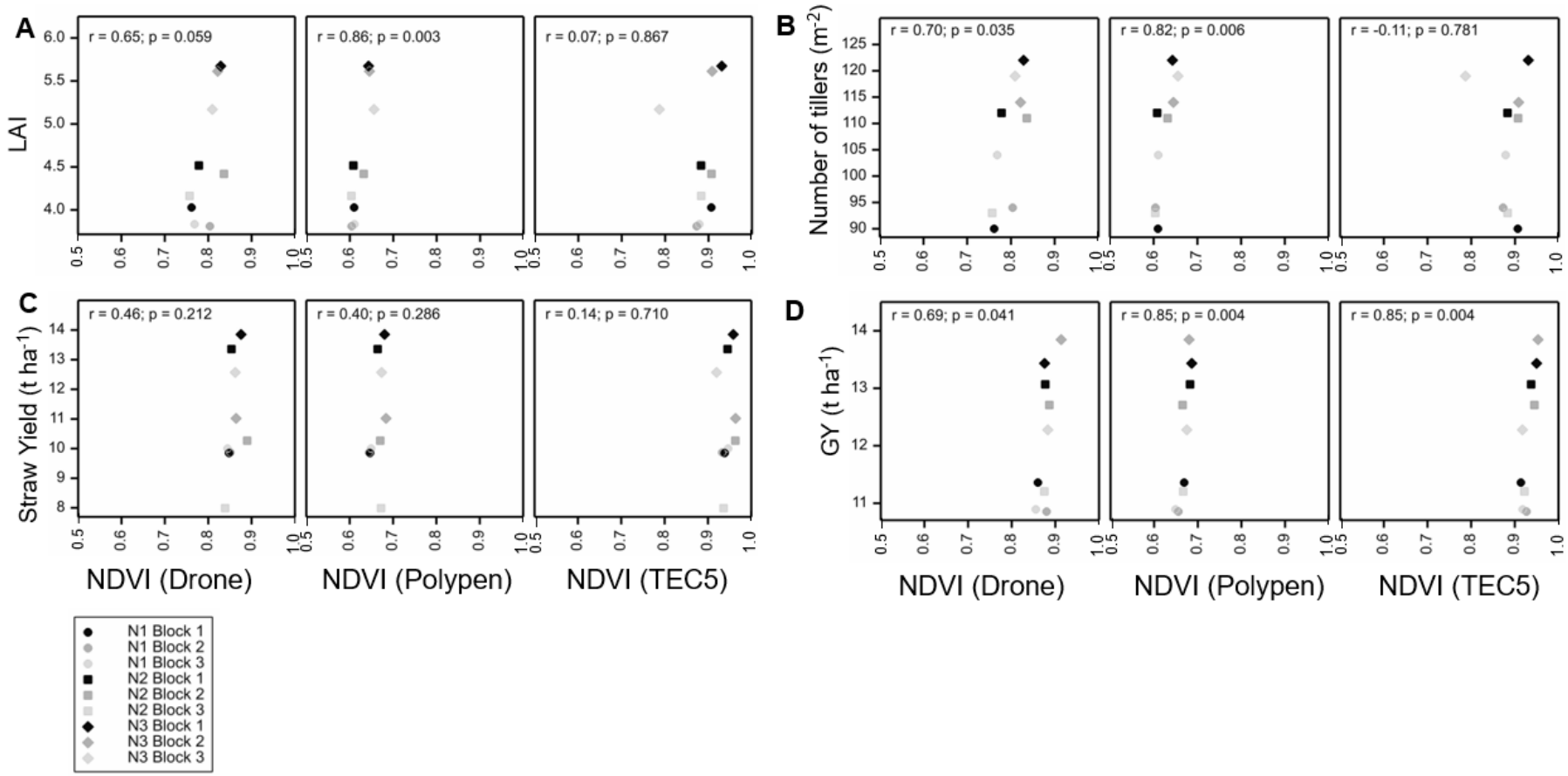

Figure 5.16. Linear association assessed by Pearson's correlation coefficient between NDVI values derived from the drone imagery, PolyPen and TEC5 spectroradiometers and (A) leaf area index (LAI) at 259 DAS during anthesis, (B) number of tillers at 259 DAS (anthesis), (C) NDVI (drone imagery, PolyPen and TEC5) at 245 DAS and straw yield at final harvest and (D) NDVI (drone imagery, PolyPen and TEC5) at 238 DAS and grain yield (GY) at harvest. Each N treatment represents three replicates from 3 blocks. N1, N2 and N3 represent 100, 200 and 350 kg N ha^{-1} respectively.

5.4 Discussion

5.4.1 Detection of nutritional variations and sensitivity of sensors to the N status

In this study, the response of NDVI derived from the PolyPen, TEC5 and drone imagery at the leaf, canopy and aerial scales respectively was assessed for their detection of nutritional N variations. The findings showed NDVI (PolyPen) showing the earliest detection of nutritional N variations first at 252 DAS (anthesis) compared to NDVI (Drone) and NDVI (TEC5) (Figure 5.12). The results are reflected in the higher sensitivity of NDVI (PolyPen) to nutritional N variations compared to NDVI (Drone) and NDVI (TEC5) (Table 5.5).

The NDVI is more sensitive to the N status at the leaf level compared to canopy and aerial scales due to the influence of factors such as LAI and the composition of the vegetation. Research suggests that NDVI is generally sensitive to LAI between 0 and 4.0 and becomes saturated as the LAI continues to increase (Quan et al., 2014). This means that at the canopy and aerial scales, where the LAI is higher, NDVI may become saturated and less sensitive to small changes in N status. As leaves are added to a canopy, there are changes in chlorophyll and structural complexities, leading to variations in red reflectance and NIR reflectance, which can affect the sensitivity of NDVI (Raper and Varco 2015; Sumner et al., 2021). A study on rice cropping systems found that proximal NDVI and aerial NDRE were more sensitive to changes in N compared to canopy-level measurements (Rehman et al., 2022) which aligns closely with the results found in this study.

Therefore, these factors contribute to the higher sensitivity of NDVI at the leaf level compared to canopy and aerial scales. The measurement of NDVI at the leaf level allows for a more direct and sensitive assessment of N status, as it is not affected by the saturation effect observed at higher LAI levels. Additionally, the use of SRIs at the leaf level, such as red edge indices, has been shown to differentiate N levels more effectively compared to canopy-level measurements (Prey and Schmidhalter, 2019). On the other hand, NDVI derived aerially, and at canopy level is affected by atmospheric conditions such as cloud cover, which can impact the reflectance of the wavelengths used in its calculation, leading to inaccurate values.

The NDVI measured at the leaf level directly captures the reflectance of leaves and is less affected by these factors, making it a more accurate measure of vegetation health and density at a local level (Perry and Davenport, 2007; Caruso et al., 2023). However, NDVI derived aerially using a drone is useful for large-scale monitoring of vegetation cover, such as changes in canopy cover, LAI and biomass, while NDVI measured at leaf level provides a more detailed and precise assessment of vegetation health at a smaller scale. This characteristic, along with the opportunity to quickly monitor large areas, enables fertilisation in accordance with crop spatial variability, enhancing farm-scale N fertilisation management. Therefore, the direct assessment of leaves using a handheld proximal sensor can provide a more sensitive indicator of early nutritional variations compared to the more general information obtained from the canopy and aerial level measurements.

5.4.2 Correlation with N status indicators

To assess the relationship between the different NDVIs with the N status, correlation analyses were done at critical stages of growth with the LNC and SPAD chlorophyll content which are reliable indicators of the N status (Figures 5.13 and 5.14). The high correlation between NDVI (PolyPen) measured at the leaf level and LNC, compared to NDVI (Drone) measured aerially and NDVI (TEC5) at the canopy scale during the early growth stage of winter wheat, can be attributed to the direct relationship between leaf-level physiological processes and NDVI. At the early growth stage, the NDVI measured at the leaf level is more closely linked to the LNC due to the active physiological processes in the leaves, which are directly related to N uptake and photosynthetic activity (Yang et al., 2017). This direct relationship diminishes as the plant matures and other factors start influencing NDVI measurements, such as canopy structure and density as discussed previously. Research studies on maize and winter wheat have shown that the correlation between spectral reflectance and LNC is significant at early growth stages, indicating the strong relationship between SRIs and leaf-level N content during this period (Jiang et al., 2020; Miller and Adkins, 2021; Zhao et al., 2023). Additionally, studies on maize and field pea have demonstrated the use of NDVI measures for estimating early season growth and biomass, further supporting the relevance of NDVI at the early growth stage of crops (Liebisch et al., 2015; Tefera et al., 2022). The findings of this study also showed a stronger correlation between NDVI

(Drone) and LNC at the later growth stages of winter wheat compared to NDVI (PolyPen) and NDVI (TEC5) (Figure 5.13B-D). This observation could be explained by the ability of aerial NDVI to capture the overall plant health and N status more effectively than NDVI measured at leaf and canopy levels. This is supported by research findings that showed significant correlations between NDVI measured from UAV and LNC during the late growth stages of wheat (Hassan et al., 2018; Miller and Adkins, 2021). Aerial NDVI provides a comprehensive view of the entire crop, integrating information from multiple plants, and can therefore better reflect the overall N status and health of the crop compared to measurements at the leaf and canopy levels (Hassan et al., 2018; Miller and Adkins, 2021).

The linear relationship between NDVI (Drone), NDVI (PolyPen) and NDVI (TEC5) with SPAD chlorophyll followed a similar pattern as observed with LNC (Figure 5.14). The high correlation between NDVI (PolyPen) with SPAD chlorophyll content, compared to NDVI (Drone) and NDVI (TEC5) during the early growth stage of winter wheat can be attributed to the direct relationship between leaf chlorophyll content and NDVI (Boiarskii and Hasegawa, 2019). At the early growth stage, the chlorophyll content in the leaves plays a crucial role in determining the future growth rate and final yield of wheat (Wang et al., 2022; Yin et al., 2023). This direct relationship between leaf chlorophyll content and NDVI makes the correlation higher when measured at the leaf level compared to the aerial scale and canopy levels. The relationship between NDVI and chlorophyll content has been widely studied and utilised for precision N management and yield prediction in various crops, including wheat (Kizilgeci et al., 2021). This correlation is significant for understanding the physiological status of the crop and can be leveraged for PA practices, such as targeted nutrient management and yield prediction. However, it is important to consider other factors that can influence NDVI measurements, such as soil background, crop structure, and sensor characteristics when interpreting the results (Kizilgeci et al., 2021). On the other hand, the high correlation between NDVI (Drone) and SPAD chlorophyll content at the late growth stage of wheat compared to NDVI (PolyPen) and NDVI (TEC5) can be attributed to the comprehensive assessment of the entire plot/field vegetation health and chlorophyll content provided by aerial NDVI measurements. This allows for a more holistic understanding of crop physiological status and consequently, N requirements. Aerial

NDVI measurements capture the overall plant health and can reflect variations in chlorophyll content across the entire plot or field, making them more indicative of the crop's N status compared to measurements at leaf and canopy levels, which may not capture the full variability across the field. The correlation between NDVI and SPAD chlorophyll content has been studied widely. For instance, a study on durum wheat cultivars under semi-arid conditions revealed that N fertilisation significantly influenced the SPAD and NDVI-attributed traits of durum wheat, highlighting the relationship between NDVI and chlorophyll content (Kizilgeci et al., 2021). Another study on winter wheat demonstrated a significant correlation between SPAD values and the chlorophyll content of wheat leaves, emphasising the relationship between these two parameters (Wang et al., 2022).

Additionally, a study on spring wheat based on multi-temporal UAV monitoring also focused on the estimation of relative chlorophyll content, further supporting the relationship between NDVI and chlorophyll content (Wu et al., 2023). Moreover, the correlation between stay-green (a trait related to chlorophyll content and plant health) and yield in spring wheat has been demonstrated in previous studies, further emphasising the importance of chlorophyll content to crop productivity (Lopes and Reynolds, 2012).

The findings of this study demonstrated a strong intercorrelation between NDVI (Drone), NDVI (PolyPen) and NDVI (TEC5) (Figure 5.15). The effectiveness of the proximally and remotely sensed NDVIs for monitoring N status in winter wheat during the growing season is validated by the strong intercorrelation that has been observed. The results demonstrate that NDVI (Drone), NDVI (PolyPen) and NDVI (TEC5) are comparable for accuracy in detecting differences in crop N status. However, as shown earlier, NDVI (PolyPen) can be useful to identify important N variations and can detect these variations at an early crop stage such as anthesis, when the N rate can still be adjusted by a further application of N fertiliser. Using NDVI (PolyPen) represents a low-cost approach for N fertilisation management compared to NDVI (Drone). This finding suggests that the NDVIs derived from the different sensors can be used alternatively for the assessment of crop N status, depending on the context where to use them (e.g., growth stage, crop type, cost, sensor, platform, weather, land size, etc.). Additionally, effective crop N status assessment across many sensors offers end-users a

distinct benefit by granting them the flexibility to select the sensor that best suits their needs.

5.4.3 Assessment of the relationship between NDVI and agronomic parameters

To assess how well the different NDVIs reflected crop performance, linear relationships were performed with agronomic parameters (Figure 5.16). The strong correlation between NDVI (PolyPen) with LAIccompared to NDVI (Drone) and NDVI (TEC5) can be attributed to the sensitivity of NDVI to the structural properties of the plant canopy, such as LAI, light interception and biomass as explained previously. This is also reflected in the correlation with the number of tillers. NDVI is useful for measuring these properties at the leaf level, as it reflects the amount of chlorophyll and the overall health of the vegetation. This sensitivity diminishes at the aerial and canopy levels due to saturation effects and interference from other factors such as soil and background reflectance. The spectral and spatial differences in the response to different measurement scales, as well as the limitations of NDVI, support the idea that NDVI measured at the leaf level is more closely related to LAI. Gracia-Romero et al. (2017) showed that NDVI measured at ground level with an active sensor correlates better with plant properties such as LAI and biomass compared to aerial or satellite-based measurements. It should be emphasised that although NDVI (PolyPen) correlates best with LAI and numbers of tillers in the present study compared to NDVI (Drone) and NDVI (TEC5), this may not be the case in other experiments with more genotypes and/or N treatments as NDVI (PolyPen) does not fully take account of canopy size/architecture effects.

For straw yield, both NDVI (Drone) and NDVI (PolyPen) showed similar correlations with the agronomic parameter (Figure 5.16C). This observation can be explained by the sensitivity of NDVI to various plant parameters such as LAI, green biomass and nutrient (particularly N) uptake. Research has shown that NDVI measured at the leaf level can efficiently predict crop yield and nutrient uptake, making it a valuable tool for PA (Aranguren et al., 2020). For example, a study on winter wheat demonstrated that NDVI sensor-based N management led to improved GY and nutrient use efficiency (Quebrajo et al., 2015). Additionally, the relationship between NDVI and GY, as well as straw yield, has been reported to be strong (Memon et al., 2019), further supporting

the use of NDVI for yield estimation. This sensitivity of NDVI to plant parameters at the leaf level makes it a more accurate indicator of crop health and productivity compared to NDVI measured at the canopy level (Walsh et al., 2020; Mitra et al., 2023).

The findings of this study demonstrated a strong correlation between NDVI (Drone), NDVI (PolyPen) and NDVI (TEC5) at the early growth stage (238 DAS) with GY at harvest (Figure 5.16D). Research has shown that NDVI at the leaf level and aerial scale during the early growth stage is strongly correlated with GY. For example, a study observed a strong correlation between NDVI and GY in the early season, indicating that an increase in NDVI during this period led to a significant increase in GY (Panek and Gozdowski, 2020). Similarly, other studies have reported a very strong correlation between NDVI and GY, with regression coefficients ranging from 0.77 to 0.89 (Belmahi et al., 2023). This sensitivity of NDVI at early growth stages to predict GY is further supported by research that evaluated the relationship between corn GY and early season NDVI, showing a strong correlation (Teal et al., 2006). Additionally, the NDVI at an early growth stage has been positively correlated with the final GY, indicating its utility for developing in-season yield predictions (Rehman et al., 2019). The sensitivity of NDVI at early growth stages to predict GY is further emphasised by a study that revealed a high correlation between NDVI and GY, indicating its potential for predicting GY in various crops (Walsh et al., 2020; Zhao et al., 2022). The present findings agree with Rehman et al. (2023) who reported that aerial and proximal sensor reflectance measurements showed comparable precision in forecasting the rice yield response to mid-season N applications. The findings of this study indicate that NDVI (Drone), NDVI (PolyPen) and NDVI (TEC5) could effectively be used as predictors of GY early in the season when N fertilisation could still be adjusted.

Overall, this study adopts a multiscale approach by combining aerial drone imagery with ground-based proximal sensors to evaluate N stress in winter wheat. This chapter focuses on the largest scale of analysis, linking leaf-level NDVI to canopy and aerial NDVI, which cover larger field areas. The use of drone technology enables more extensive and efficient field phenotyping, making it practical for large-scale agricultural applications. While leaf-level sensing offers detailed insights, this chapter demonstrates

that scaling up to drone imagery provides field-wide monitoring, making it a more viable option for larger operations.

5.5 Conclusions

A multiscale approach was used to assess the responses of NDVI derived from aerial drone imagery and ground-based proximal sensors at leaf and canopy scales in this study. Results indicated a stronger sensitivity of NDVI (PolyPen) to the N status and for assessing the agronomic performance of winter wheat compared to NDVI (Drone) and NDVI (TEC5). The findings showed NDVI (PolyPen) demonstrating the earliest detection of nutritional N variations compared to NDVI (Drone) and NDVI (TEC5). At the early to mid-season stage (anthesis), the NDVI (PolyPen) is a good leaf-level indicator for winter wheat LNC and SPAD chlorophyll content estimation. The results indicate that the measurement of NDVI at the leaf level allows for a more direct and sensitive assessment of winter wheat N status, as it is not affected by the saturation effect observed at higher LAI levels, atmospheric conditions and soil background. Therefore, the direct evaluation of leaves using a handheld proximal sensor can offer a low-cost and more sensitive indicator of early nutritional N variations in winter wheat.

The findings of this study also revealed that at the late winter wheat growth stage, NDVI (Drone) was more sensitive to the LNC and SPAD chlorophyll content as the plant canopy develops and matures. This suggests that drone-derived NDVI will be appropriate for large-scale monitoring of vegetation cover for N status estimation at the late wheat growth stage. The NDVI (Drone), NDVI (PolyPen) and NDVI (TEC5) were strongly correlated to each other validating their alternative use and effectiveness for N status monitoring in wheat during the growing season. The ability to assess crop status effectively across various sensors offers a unique benefit for end-users as it allows flexibility to choose the sensor most suitable for their needs, considering factors such as cost, expertise, weather, platform, crop type, growth stage, etc. The results further suggest that RS could be a helpful technique to extrapolate handheld measurements spatially throughout winter wheat growth and development, given the strong intercorrelations observed.

This study demonstrated that the LAI, number of tillers and straw yield of winter wheat could be effectively assessed mid-season with NDVI (Drone) and NDVI (PolyPen) but more limited with NDVI (TEC5). However, all derived NDVIs irrespective of their proximity to winter wheat plants showed promise as effective predictors of GY early in the season. Altogether, these results indicate that the ability of NDVI to inform crop management decisions depends on the measurement platform, sensor and time of measurement. Both NDVI (PolyPen) and NDVI (Drone) produced measurements sensitive enough to inform N fertiliser management, whereas NDVI (TEC5) was more limited. Future work into this study will explore different SRIs, platforms and sensors and, concentrate on applying these findings for field phenotyping in Africa.

References

Alexopoulos, A., Koutras, K., Ali, S. B., Puccio, S., Carella, A., Ottaviano, R., and Kalogeras, A. (2023). Complementary use of ground-based proximal sensing and airborne/spaceborne remote sensing techniques in precision agriculture: A systematic review. *Agronomy*, 13 (7), 1942.

Ali, A. M., Ibrahim, S. M., Salem, E. M., El-Sadek, A. N., and Salem, H. M. (2022). In-season estimation of wheat response to nitrogen using Normalised difference vegetation index. *International Journal of Plant Production*, 16 (4), 681-689. https://doi.org/10.1007/s42106-022-00207-2

Aranguren, M., Castellón, A., and Aizpurua, A. (2020). Wheat yield estimation with NDVI values using a proximal sensing tool. *Remote Sensing*, 12 (17), 2749. https://doi.org/10.3390/rs12172749

Avery, B. W and Catt, J. A. (1995). *The soil at Rothamsted*. Lawes Agricultural Trust.

Belmahi, M., Hanchane, M., Krakauer, N. Y., Kessabi, R., Bouayad, H., Mahjoub, A., and Zouhri, D. (2023). Analysis of Relationship between Grain Yield and NDVI from MODIS in the Fez-Meknes Region, Morocco. *Remote Sensing*, 15 (11), 2707. https://doi.org/10.3390/rs15112707

Benincasa, P., Antognelli, S., Brunetti, L., Fabbri, C. A., Natale, A., Sartoretti, V., and Vizzari, M. (2018). Reliability of NDVI derived by high resolution satellite and UAV compared to in-field methods for the evaluation of early crop N status and grain yield in wheat. *Experimental Agriculture*, 54 (4), 604-622. https://doi.org/10.1017/S0014479717000278

Berra, E. F., Gaulton, R., and Barr, S. (2017). Commercial off-the-shelf digital cameras on unmanned aerial vehicles for multitemporal monitoring of vegetation reflectance and NDVI. *IEEE Transactions on Geoscience and Remote Sensing*, 55 (9), 4878-4886. https://doi.org/10.1109/TGRS.2017.2655365

Boiarskii, B and Hasegawa, H. (2019). Comparison of NDVI and NDRE indices to detect differences in vegetation and chlorophyll content. *Journal of Mechanics of Continua and Mathematical Sciences*, 4, 20-29.

Caruso, G., Palai, G., Tozzini, L., D'Onofrio, C., and Gucci, R. (2023). The role of LAI and leaf chlorophyll on NDVI estimated by UAV in grapevine canopies. *Scientia Horticulturae*, 322, 112398.

Colomina, I and Molina, P. (2014). Unmanned aerial systems for photogrammetry and remote sensing: A review. *ISPRS Journal of Photogrammetry and Remote Sensing*, 92, 79-97. https://doi.org/10.1016/j.isprsjprs.2014.02.013

de la Iglesia Martinez, A and Labib, S. M. (2023). Demystifying Normalised difference vegetation index (NDVI) for greenness exposure assessments and policy interventions in urban greening. *Environmental Research*, 220, 115155. https://doi.org/10.1016/j.envres.2022.115155

Duan, T., Chapman, S. C., Guo, Y., and Zheng, B. (2017). Dynamic monitoring of NDVI in wheat agronomy and breeding trials using an unmanned aerial vehicle. *Field Crops Research*, 210, 71-80.

Dunn, B. W., Dunn, T. S., Hume, I., Orchard, B. A., Dehaan, R., and Robson, A. (2016). Remote Sensing PI Nitrogen Uptake in Rice. *IREC Newsletter*. 195, 48-50.

Farias, G. D., Bremm, C., Bredemeier, C., de Lima Menezes, J., Alves, L. A., Tiecher, T., and de Faccio Carvalho, P. C. (2023). Normalised Difference Vegetation Index (NDVI) for soybean biomass and nutrient uptake estimation in response to production systems and fertilisation strategies. *Frontiers in Sustainable Food Systems*, 6, 959681. https://doi.org/10.3389/fsufs.2022.959681

Fu, Y., Yang, G., Li, Z., Song, X., Li, Z., Xu, X., and Zhao, C. (2020). Winter wheat nitrogen status estimation using UAV-based RGB imagery and Gaussian processes regression. *Remote Sensing*, 12 (22), 3778.

Gordillo-Salinas, V. M., Flores-Magdaleno, H., Ortiz-Solorio, C. A., and Arteaga-Ramírez, R. (2021). Evaluation of nitrogen status in a wheat crop using unmanned aerial vehicle images. *Chilean Journal of Agricultural Research*, 81 (3), 408-419. http://dx.doi.org/10.4067/S0718-58392021000300408

Gracia-Romero, A., Kefauver, S. C., Vergara-Díaz, O., Hamadziripi, E., Zaman-Allah, M. A., Thierfelder, C., and Araus, J. L. (2020). Leaf versus whole-canopy remote sensing methodologies for crop monitoring under conservation agriculture: A case of study with maize in Zimbabwe. *Scientific Reports*, 10 (1), 16008. https://doi.org/10.1038/s41598-020-73110-3

Gracia-Romero, A., Kefauver, S. C., Vergara-Díaz, O., Zaman-Allah, M. A., Prasanna, B. M., Cairns, J. E., and Araus, J. L. (2017). Comparative performance of ground vs. aerially assessed RGB and multispectral indices for early-growth evaluation of maize performance under phosphorus fertilization. *Frontiers in Plant Science*, 8, 2004. https://doi.org/10.3389/fpls.2017.02004

Greenhouse, S. W and Geisser, S. (1959). On methods in the analysis of profile data. *Psychometrika*, 24 (2), 95-112. https://doi.org/10.1007/BF02289823

Hassan, M. A., Yang, M., Rasheed, A., Yang, G., Reynolds, M., Xia, X., and He, Z. (2019). A rapid monitoring of NDVI across the wheat growth cycle for grain yield prediction using a multi-spectral UAV platform. *Plant Science*, 282, 95-103. https://doi.org/10.1016/j.plantsci.2018.10.022

Hatfield, J. L., Gitelson, A. A., Schepers, J. S., and Walthall, C. L. (2008). Application of spectral remote sensing for agronomic decisions. *Agronomy Journal*, 100, S-117. https://doi.org/10.2134/agronj2006.0370c

Holman, F. (2020). Development and evaluation of unmanned aerial vehicles for high throughput phenotyping of field-based wheat trials. (Doctoral dissertation, King's College London).

Holman, F. H., Riche, A. B., Castle, M., Wooster, M. J., and Hawkesford, M. J. (2019). Radiometric calibration of 'commercial off the shelf' cameras for UAV-based high-resolution temporal crop phenotyping of reflectance and NDVI. *Remote Sensing*, 11 (14), 1657. https://doi.org/10.3390/rs11141657

Hou, S., Dang, H., Huang, T., Huang, Q., Li, C., Li, X., and Wang, Z. (2023). Targeting high nutrient efficiency to reduce fertiliser input in wheat production of China. *Field Crops Research*, 292, 108809.

Huang, S., Tang, L., Hupy, J. P., Wang, Y., and Shao, G. (2021). A commentary review on the use of Normalised difference vegetation index (NDVI) in the era of popular remote sensing. *Journal of Forestry Research*, 32 (1), 1-6.

Jiang, J., Zhang, Z., Cao, Q., Liang, Y., Krienke, B., Tian, Y., and Liu, X. (2020). Use of an active canopy sensor mounted on an unmanned aerial vehicle to monitor the growth and nitrogen status of winter wheat. *Remote Sensing*, 12 (22), 3684. https://doi.org/10.3390/rs12223684

Keselman, H. J., Algina, J., and Kowalchuk, R. K. (2001). The analysis of repeated measures designs: a review. *British Journal of Mathematical and Statistical Psychology*, 54 (1), 1-20. https://doi.org/10.1348/000711001159357

Kizilgeci, F., Yildirim, M., Islam, M. S., Ratnasekera, D., Iqbal, M. A., and Sabagh, A. E. (2021). Normalised difference vegetation index and chlorophyll content for precision nitrogen management in durum wheat cultivars under semi-arid conditions. *Sustainability*, 13 (7), 3725. https://doi.org/10.3390/su13073725

Li, W., Guo, S., Liu, H., Zhai, L., Wang, H., and Lei, Q. (2018). Comprehensive environmental impacts of fertiliser application vary among different crops: Implications for the adjustment of agricultural structure aimed to reduce fertiliser use. *Agricultural Water Management*, 210, 1-10.

Liebisch, F., Kirchgessner, N., Schneider, D., Walter, A., and Hund, A. (2015). Remote, aerial phenotyping of maize traits with a mobile multi-sensor approach. *Plant Methods*, 11 (1), 1-20. https://doi.org/10.1186/s13007-015-0048-8

Liu, J., Zhu, Y., Tao, X., Chen, X., and Li, X. (2022). Rapid prediction of winter wheat yield and nitrogen use efficiency using consumer-grade unmanned aerial vehicles multispectral imagery. *Frontiers in Plant Science*, 13, 1032170. https://doi.org/10.3389/fpls.2022.1032170

Lopes, M. S and Reynolds, M. P. (2012). Stay-green in spring wheat can be determined by spectral reflectance measurements (Normalised difference vegetation index) independently from phenology. *Journal of Experimental Botany*, 63 (10), 3789-3798. https://doi.org/10.1093/jxb/ers071

Lu, N., Wang, W., Zhang, Q., Li, D., Yao, X., Tian, Y., and Cheng, T. (2019). Estimation of nitrogen nutrition status in winter wheat from unmanned aerial vehicle based multi-angular multispectral imagery. *Frontiers in Plant Science*, 10, 1601. https://doi.org/10.3389/fpls.2019.01601

Maestrini, B and Basso, B. (2018). Predicting spatial patterns of within-field crop yield variability. *Field Crops Research*, 219, 106-112.

Memon, M. S., Jun, Z., Sun, C., Jiang, C., Xu, W., Hu, Q., and Ji, C. (2019). Assessment of wheat straw cover and yield performance in a rice-wheat cropping system by using Landsat satellite data. *Sustainability*, 11 (19), 5369. https://doi.org/10.3390/su11195369

Mezera, J., Lukas, V., Horniaček, I., Smutný, V., and Elbl, J. (2021). Comparison of Proximal and Remote Sensing for the Diagnosis of Crop Status in Site-Specific Crop Management. *Sensors*, 22 (1), 19. https://doi.org/10.3390/s22010019

Miller, J. O and Adkins, J. (2021). Monitoring winter wheat growth at different heights using aerial imagery. *Agronomy Journal*, 113 (2), 1586-1595. https://doi.org/10.1002/agj2.20539

Miller, J. O., Mondal, P., and Sarupria, M. (2023). Sensor-based measurements of NDVI in small grain and corn fields by tractor, drone, and satellite platforms. *Crop and Environment*. https://doi.org/10.1016/j.crope.2023.11.001

Mitra, B., Singha, P., Roy Chowdhury, A., Sinha, A. K., Skalicky, M., Brestic, M., and Hossain, A. (2023). Normalised difference vegetation index sensor-based nitrogen management in bread wheat (*Triticum aestivum* L.): Nutrient uptake, use efficiency, and partial nutrient balance. *Frontiers in Plant Science*, 14, 1153500. https://doi.org/10.3389/fpls.2023.1153500

Mulla, D. J. (2013). Twenty-five years of remote sensing in precision agriculture: Key advances and remaining knowledge gaps. *Biosystems Engineering*, 114 (4), 358-371. https://doi.org/10.1016/j.biosystemseng.2012.08.009

Panek, E and Gozdowski, D. (2020). Analysis of relationship between cereal yield and NDVI for selected regions of Central Europe based on MODIS satellite data. *Remote Sensing Applications: Society and Environment*, 17, 100286. https://doi.org/10.1016/j.rsase.2019.100286

Perry, E. M and Davenport, J. R. (2007). Spectral and spatial differences in response of vegetation indices to nitrogen treatments on apple. *Computers and Electronics in Agriculture*, 59 (1-2), 56-65. https://doi.org/10.1016/j.compag.2007.05.002

Perryman, S. A. M., Scott, T., and Hall, C. (2020). Annual mean air temperature at Rothamsted 1878-2019.

Poulton, P. R., Pye, E., Hargreaves, P. R., and Jenkinson, D. S. (2003). Accumulation of carbon and nitrogen by old arable land reverting to woodland. *Global Change Biology*, 9, 942-955. https://doi.org/10.1046/j.1365-2486.2003.00633.x.

Prey, L and Schmidhalter, U. (2019). Sensitivity of Vegetation Indices for Estimating Vegetative N Status in Winter Wheat. *Sensors*, 19 (17), 3712. https://doi.org/10.3390/s19173712

Quan, X., He, B., Wang, Y., Tang, Z., and Li, X. (2014). An extended Fourier approach to improve the retrieved leaf area index (LAI) in a time series from an alpine wetland. *Remote Sensing*, 6 (2), 1171-1190. https://doi.org/10.3390/rs6021171

Quebrajo, L., Pérez-Ruiz, M., Rodriguez-Lizana, A., and Agüera, J. (2015). An approach to precise nitrogen management using hand-held crop sensor measurements and winter wheat yield mapping in a Mediterranean environment. *Sensors*, 15 (3), 5504-5517. https://doi.org/10.3390/s150305504

Raper, T. B and Varco, J. J. (2015). Canopy-scale wavelength and vegetative index sensitivities to cotton growth parameters and nitrogen status. *Precision Agriculture*, 16, 62-76. https://doi.org/10.1007/s11119-014-9383-4

Rehman, T. H., Borja Reis, A. F., Akbar, N., and Linquist, B. A. (2019). Use of Normalised difference vegetation index to assess N status and predict grain yield in rice. *Agronomy Journal*, 111 (6), 2889-2898.

Rehman, T. H., Lundy, M. E., and Linquist, B. A. (2022). Comparative sensitivity of vegetation indices measured via proximal and aerial sensors for assessing N status and predicting grain yield in rice cropping systems. *Remote Sensing*, 14 (12), 2770. https://doi.org/10.3390/rs14122770

Ruan, G., Schmidhalter, U., Yuan, F., Cammarano, D., Liu, X., Tian, Y., and Cao, Q. (2023). Exploring the transferability of wheat nitrogen status estimation with multisource data and Evolutionary Algorithm-Deep Learning (EA-DL) framework. *European Journal of Agronomy*, 143, 126727.

Ruiz, J. J., Diaz-Mas, L., Perez, F., and Viguria, A. (2013). Evaluating the accuracy of DEM generation algorithms from UAV imagery. *International Archives of the Photogrammetry, Remote Sensing and Spatial Information Sciences* 40, 333–337.

Ryu, J. H., Na, S. I., and Cho, J. (2020). Inter-comparison of Normalised Difference Vegetation Index measured from different footprint sizes in cropland. *Remote Sensing*, 12 (18), 2980. https://doi.org/10.3390/rs12182980

Saberioon, M. M., Amin, M. S. M., Gholizadeh, A., and Ezri, M. H. (2014). A review of optical methods for assessing nitrogen contents during rice growth. *Applied Engineering in Agriculture*, 30 (4), 657-669.

Sangjan, W., McGee, R. J., and Sankaran, S. (2022). Optimisation of UAV-based imaging and image processing orthomosaic and point cloud approaches for estimating biomass in a forage crop. *Remote Sensing*, 14 (10), 2396. https://doi.org/10.3390/rs14102396

Scheftic, W., Zeng, X., Broxton, P., and Brunke, M. (2014). Intercomparison of seven NDVI products over the United States and Mexico. *Remote Sensing*, 6 (2), 1057-1084. https://doi.org/10.3390/rs6021057

Shakoor, A., Xu, Y., Wang, Q., Chen, N., He, F., Zuo, H., and Yang, S. (2018). Effects of fertiliser application schemes and soil environmental factors on nitrous oxide emission fluxes in a rice-wheat cropping system, East China. *PloS One*, 13 (8), e0202016. https://doi.org/10.1371/journal.pone.0202016

She, Y., Li, P., Qi, X., Rahman, S. U., and Guo, W. (2023). Effects of nitrogen application on winter wheat growth, water use, and yield under different shallow groundwater depths. *Frontiers in Plant Science*, 14, 1114611.

Sishodia, R. P., Ray, R. L., and Singh, S. K. (2020). Applications of remote sensing in precision agriculture: A review. *Remote Sensing*, 12 (19), 3136. https://doi.org/10.3390/rs12193136

Sørensen, L. Y., Jacobsen, L. T., and Hansen, J. P. (2017). Low Cost and Flexible UAV Deployment of Sensors. *Sensors*, 17 (1), 154. https://doi.org/10.3390/s17010154

Sumner, Z., Varco, J. J., Dhillon, J. S., Fox, A. A., Czarnecki, J., and Henry, W. B. (2021). Ground versus aerial canopy reflectance of corn: Red□edge and non□red edge vegetation indices. *Agronomy Journal*, 113 (3), 2782-2797.

Tan, C. W., Zhang, P. P., Zhou, X. X., Wang, Z. X., Xu, Z. Q., Mao, W., and Yun, F. (2020). Quantitative monitoring of leaf area index in wheat of different plant types by integrating NDVI and Beer-Lambert law. *Scientific Reports*, 10 (1), 929. https://doi.org/10.1038/s41598-020-57750-z

Teal, R. K., Tubana, B., Girma, K., Freeman, K. W., Arnall, D. B., Walsh, O., and Raun, W. R. (2006). In□season prediction of corn grain yield potential using Normalised Difference Vegetation Index. *Agronomy Journal*, 98 (6), 1488-1494. https://doi.org/10.2134/agronj2006.0103

Tefera, A. T., Banerjee, B. P., Pandey, B. R., James, L., Puri, R. R., Cooray, O., and Rosewarne, G. M. (2022). Estimating early season growth and biomass of field pea for selection of divergent ideotypes using proximal sensing. *Field Crops Research*, 277, 108407. https://doi.org/10.1016/j.fcr.2021.108407

Tenreiro, T. R., García-Vila, M., Gómez, J. A., Jiménez-Berni, J. A., and Fereres, E. (2021). Using NDVI for the assessment of canopy cover in agricultural crops within modelling research. *Computers and Electronics in Agriculture*, 182, 106038. https://doi.org/10.1016/j.compag.2021.106038

Toth, C and Jóźków, G. (2016). Remote sensing platforms and sensors: A survey. *ISPRS Journal of Photogrammetry and Remote Sensing*, 115, 22-36. https://doi.org/10.1016/j.isprsjprs.2015.10.004

Vergara-Díaz, O., Zaman-Allah, M. A., Masuka, B., Hornero, A., Zarco-Tejada, P., Prasanna, B. M., and Araus, J. L. (2016). A novel remote sensing approach for

prediction of maize yield under different conditions of nitrogen fertilisation. *Frontiers in Plant Science*, 7, 666.

Viña, A., Gitelson, A. A., Nguy-Robertson, A. L., and Peng, Y. (2011). Comparison of different vegetation indices for the remote assessment of green leaf area index of crops. *Remote Sensing of Environment*, 115 (12), 3468-3478.

Walsh, O. S., Torrion, J. A., Liang, X., Shafian, S., Yang, R., Belmont, K. M., and McClintick□Chess, J. R. (2020). Grain yield, quality, and spectral characteristics of wheat grown under varied nitrogen and irrigation. *Agrosystems, Geosciences and Environment*, 3 (1), e20104. https://doi.org/10.1002/agg2.20104

Wang, W., Cheng, Y., Ren, Y., Zhang, Z., and Geng, H. (2022). Prediction of Chlorophyll Content in Multi-Temporal Winter Wheat Based on Multispectral and Machine Learning. *Frontiers in Plant Science*, 13, 896408.

Wang, Y., Peng, Y., Lin, J., Wang, L., Jia, Z., and Zhang, R. (2023). Optimal nitrogen management to achieve high wheat grain yield, grain protein content, and water productivity: A meta-analysis. *Agricultural Water Management*, 290, 108587. https://doi.org/10.1016/j.agwat.2023.108587

Witt, C., Pasuquin, J. M. C. A., Mutters, R., and Buresh, R. J. (2005). New leaf colour chart for effective nitrogen management in rice. *Better Crops*, 89 (1), 36-39.

Wu, H and Ge, Y. (2019). Excessive application of fertiliser, agricultural non-point source pollution, and farmers' policy choice. *Sustainability*, 11 (4), 1165. https://doi.org/10.3390/su11041165

Wu, Q., Zhang, Y., Zhao, Z., Xie, M., and Hou, D. (2023). Estimation of Relative Chlorophyll Content in Spring Wheat Based on Multi-Temporal UAV Remote Sensing. *Agronomy*, 13 (1), 211. https://doi.org/10.3390/agronomy13010211

Xue, J and Su, B. (2017). Significant remote sensing vegetation indices: A review of developments and applications. *Journal of Sensors*, 1353691. https://doi.org/10.1155/2017/1353691

Yang, H., Yang, X., Heskel, M., Sun, S., and Tang, J. (2017). Seasonal variations of leaf and canopy properties tracked by ground-based NDVI imagery in a temperate forest. *Scientific Reports*, 7 (1), 1267.

Yin, Q., Zhang, Y., Li, W., Wang, J., Wang, W., Ahmad, I., and Huo, Z. (2023). Estimation of winter wheat SPAD values based on UAV multispectral remote sensing. *Remote Sensing*, 15 (14), 3595. https://doi.org/10.3390/rs15143595

Yoosefzadeh-Najafabadi, M., Singh, K. D., Pourreza, A., Sandhu, K. S., and Rajcan, I. (2023). Remote and proximal sensing: How far has it come to help plant breeders? *In Advances in Agronomy; Elsevier: Amsterdam, The Netherlands*. https://doi.org/10.1016/bs.agron.2023.05.004

Zhao, H., Pandey, B. R., Khansefid, M., Khahrood, H. V., Sudheesh, S., Joshi, S., and Rosewarne, G. M. (2022). Combining NDVI and bacterial blight score to predict grain yield in field pea. *Frontiers in Plant Science*, 13, 923381. https://doi.org/10.3389/fpls.2022.923381

Zhao, X., Wang, S., Wen, T., Xu, J., Huang, B., Yan, S., Gao, G., Zhao, Y., Li, H., Qiao, J., Yang, J., Wu, L., Wang, H., Liu, T., and Mu, X. (2023). On correlation between canopy vegetation and growth indexes of maize varieties with different nitrogen efficiencies. *Open Life Sciences*, 18 (1), 20220566.

Zheng, H., Cheng, T., Li, D., Yao, X., Tian, Y., Cao, W., and Zhu, Y. (2018). Combining unmanned aerial vehicle (UAV)-based multispectral imagery and ground-based hyperspectral data for plant nitrogen concentration estimation in rice. *Frontiers in Plant Science*, 9, 936. https://doi.org/10.3389/fpls.2018.00936

Zou, X and Mõttus, M. (2017). Sensitivity of common vegetation indices to the canopy structure of field crops. *Remote Sensing*, 9 (10), 994.

CHAPTER 6

6 GENERAL DISCUSSION, SUMMARY OF FINDINGS AND FUTURE OUTLOOK

6.1 Overview

This chapter provides an analytical synthesis of the thesis focused on the three research chapters (Chapters 3, 4 and 5) highlighting the general discussion, summary of key findings and scientific and practical applications of the findings. The chapter reviews how well the findings achieved the main research aims and objectives, makes recommendations for future research and gives concluding remarks for the PhD thesis. To achieve the set research objectives, a substantial amount of data was collected from different glasshouse and field experiments utilising quinoa, cowpea and wheat. New and untested experimental designs and phenotyping methodologies were employed in tandem with software tools for data processing and analysis. Collectively, this work produced findings that were not previously published in the scientific literature. The findings have implications for future research in PRS and plant physiology. Additionally, the findings hold the potential for the development of diagnostic tools to estimate the nutritional and water status of the studied crops.

6.2 General discussion

6.2.1 Nitrogen and phosphorus stress interactions in crops: focus on quinoa and cowpea

Crop growth and cultivation may be co-limited by N and P (Agren et al., 2012; Dong et al., 2023). Therefore, understanding how plants respond to nutrient availability, their synchronised uptake and biological interactions are crucial for attaining nutritional equilibrium and maximising growth amid varying nutrient fluctuations, thereby minimising or optimising fertiliser application in agriculture (Luo et al., 2016; Medici et al., 2019; Alvar-Beltrán et al., 2021).

So far, research has mostly examined the impact of N and P fertilisation on crops independently, but recent findings indicate that these macronutrients may interact with each other across various levels of integration (Agren et al., 2012; Grohskopf et al., 2019; Krouk and Kiba, 2020; Xia et al., 2023). Interactions between N and P are important for plant growth and ecosystem C sequestration (Wang et al., 2022). Plants

may use one element to acquire another (i.e., trading N for P and P for N) resulting from synergistic growth responses to NP addition (Schlegel and Bond, 2017). The mechanisms that cause synergistic responses of plant growth to multiple element addition have been shown that plants and microbes adapt mechanisms of element uptake or change allocation patterns, in the way that they trade one element they have in excess into the acquisition of a limiting element until their growth is equally limited by both elements (Davidson and Howarth, 2007; Schleuss et al., 2020; Wang et al., 2022; Xia et al., 2023).

There is an increase in N uptake and accumulation when P levels in the plant are adequate or high while increasing the N supply increases the P uptake (Agren et al., 2012; Duncan et al., 2018a). Therefore, there is a synergistic interaction between N and P. A synergistic interaction of N and P co-fertilisation on yield in many crops including wheat, millet, rice, sorghum, corn and cotton has been reported (Aulakh and Aulakh, 2005; Rietra et al., 2017; Schlegel and Bond, 2017; Grohskopf et al., 2019).

On the other hand, additive and antagonistic interactions can occur (Crain et al., 2008; Grohskopf et al., 2019; Jiang et al., 2019). For instance, P deficiency in the soil could limit the plant response to N fertilisation (Setiyono et al., 2010) and negatively affect N uptake and assimilation resulting in antagonistic interactions (Gniazdowska and Rychter, 2000; Gan et al., 2016). The main sources of N and P for plants are nitrate and phosphate, and they also function as signal molecules to initiate downstream N or P responses. In both Arabidopsis and rice, their respective signalling pathways have been well studied (Hu and Chu, 2020). Recently, Hu and Chu (2020) assessed the growth performance and N/P utilisation of plants under different N and P conditions (Figure 6.1).

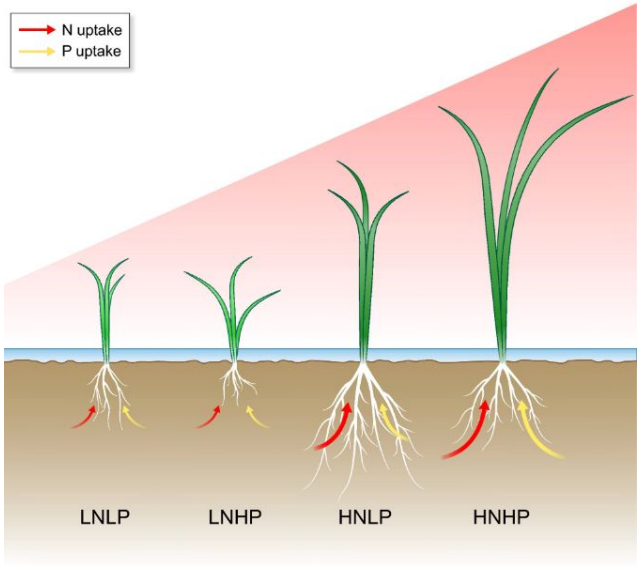

Figure 6.1. The growth performance and N/P uptake of plants under different N and P supplies. LN, low N; HN, high N; LP, low P; HP, high P. Source: Hu and Chu, 2020.

The interaction of N and P on the spectral reflectance of crops is a crucial aspect in determining the nutrient status and growth of plants non-destructively. Changes in N and P levels in plants can lead to variations in leaf pigments, affecting the spectral characteristics during plant growth (Okyere et al., 2023). In recent times, hyperspectral imaging systems have been utilised to collect spectral data at different growth stages of plants, enabling the identification of N and P status in cowpea, quinoa, grape leaves and tomato crops (Elvanidi et al., 2018; Siedliska et al., 2021; Peng et al., 2022; Okyere et al., 2023). However, these studies were limited in assessing the interaction of N and P on the spectral reflectance of these crops. Another key research gap is finding SRIs that can discriminate between N and P stress. This work has demonstrated the utility of SRIs to identify the N and P interactions (N×P) in quinoa and cowpea at leaf scale using a handheld proximal sensor (Chapter 3; Appendix B, Table B-1 and Table B-2). In quinoa, SRIs including NDVI, SR, OSAVI, G, TCARI, ZMI, Ctr2, Lic1, Lic2, SIPI, GM1, GM2, ARI1, ARI2, CRI1, CRI2, RDVI, GNDVI_780, MRESR, RENDVI, NDRE, CIgreen, CIrededge, mNDblue_530, mNDblue_730, rDVI_790, gSRa_790 and SRa_790 showed N×P interactions (Chapter 3; Appendices B, Table B-1). Also, morpho-physiological parameters; LNC and SPAD showed N×P interactions but no

interaction was observed for agronomic parameters (Chapter 3; Table 3.4 and Table 3.5).

For cowpea, SRIs including NDVI, SR, MCARI, TCARI, ZMI, Ctr2, GM1, GM2, ARI2, GNDVI_780, MRESR, NDRE, CIgreen, CIrededge, mNDblue_530 and gSRa_790 showed N×P interactions (Chapter 3; Appendix B, Table B-2). Similarly to quinoa, LNC and SPAD showed N×P interactions in cowpea (Chapter 3; Table 3.8). Further, the findings showed N×P interactions in FW and DW in cowpea (Chapter 3; Table 3.9).

This work therefore presents pertinent and valid research and provides a useful contribution to the body of work on N and P interactions. The findings suggest that these SRIs could non-destructively detect subtle changes in N and P variations due to their sensitivities to the leaf pigments which is essential for determining the nutrient status of these crops. Thus, the findings provide a physiological and agronomic basis for crop management, focusing on improving the nutrient status of quinoa and cowpea.

6.2.2 Delineating the complex drought and nitrogen stress responses and interactions in wheat using proximal sensing techniques

The interaction between drought and N availability in wheat evokes complex physiological and morphological responses and their combined impact can affect growth, development, yield and quality traits (Shi et al., 2014). The drought and N interaction can either mitigate or exacerbate the effects of each other on wheat. Drought stress reduces water availability, leading to physiological drought in plants, which affects various growth processes such as photosynthesis, stomatal conductance and nutrient uptake (Sallam et al., 2019; Ru et al., 2022; Ullah et al., 2022). N, being a vital nutrient for plant growth, influences the plant response to drought stress by affecting metabolic processes. Adequate N supply can mitigate the adverse effects of drought on wheat growth by maintaining cellular hydration, sustaining photosynthetic activity and promoting root growth to enhance water uptake (Abid et al., 2016; Ru et al., 2022; Biswas et al., 2023). However, a high N supply can increase the sensitivity of the plant to drought stress (Zhong et al., 2019).

Due to the complexity of drought and N interactions, PRS techniques are pivotal in understanding and managing the complex interactions between these two stress factors

in wheat. Several studies have shown the significance of PRS tools in assessing water and N status in wheat, aiding in reducing environmental impacts by detecting crop N levels and water status (Klem et al., 2018; Pancorbo et al., 2021).

In recent times, the selection of spectral bands and SRIs that are sensitive to the physiological and biochemical changes associated with drought and N stress in wheat has been investigated (Bandyopadhyay et al., 2014; Kusnierek and Korsaeth, 2015; Li et al., 2021). This selection has involved considering specific wavelengths known to be related to the chlorophyll content, leaf water status, N concentration, photosynthetic activity and other relevant parameters.

In the quest to look for new or existing SRIs to distinguish between drought and N stress and their interactions in wheat, this work attempted to identify novel wavelengths, but this goal did not look promising (Chapter 4). The shorter wavelength range of the PolyPen RP410 spectrometer used for measuring the spectral reflectance of the leaf limited its exploration for drought-sensitive wavelengths. Additionally, the statistical method used was not robust enough to identify effective wavelengths. Hence, 39 existing SRIs were explored for their response to the combined drought and N stress (Chapter 4; Table 4.1).

In Chapter 4; Table 4.3, it was demonstrated that the spectral reflectance of wheat at the leaf scale could be used to assess the interaction between drought (D) and N at different days after water stress (D×N×DAWS) using several SRIs. The findings showed that NPQI and TVI demonstrated the earliest (D×N×DAWS) interaction at 3 and 6 DAWS respectively, driven by LN (Chapter 4; Table 4.3). RDVI and rDVI_790 showed (D×N×DAWS) interaction at 9 DAWS and was driven by both HN and LN (Chapter 4; Table 4.3). At 12 DAWS, MCARI1, ARI1, ARI2 and CRI2 showed (D×N×DAWS) interaction mostly under HN. The majority of the SRIs including NDVI, SR, G, ZMI, TCARI, PRI, Ctr1, SIPI, GM1, GM2, CRI1, PRI/NDVI, GNDVI_780, MRESR, RENDVI, NDRE, CIgreen, CIrededge and gSRa_790 indicated (D×N×DAWS) interaction at 14 DAWS (Chapter 4; Table 4.3). In most cases, the (D×N×DAWS) interactions were driven by HN supply with a bigger amplitude of response compared to LN (Chapter 4; Table 4.3). The findings indicate that these SRIs could detect subtle changes in the water and N status due to their sensitivities to the chlorophyll content,

leaf water status and N concentration, providing valuable insights into plant stress responses (Muñoz-Huerta et al., 2013; Elsayed et al., 2021; El-Hendawy et al., 2022).

However, SRIs such as OSAVI, SPRI, NPCI, Ctr2, PRI_550, PRI_norm and mNDblue_730 did not show any (D×N×DAWS) interaction either under HN or LN. Additionally, the findings showed (D×N×DAWS) interaction in morpho-physiological parameters: A_n, G_s, E, WUEi, SPAD, RWC, SFW, LA, SMC except for LNC (Chapter 4; Table 4.2) reflecting their usefulness for assessing the physiological status of wheat and how they respond to stress conditions.

Collectively, this study is one of the few instances, if not the first in PS, where SRIs demonstrated utility in unravelling the complex drought and N interactions in spring wheat at the leaf scale. These advancements in PS techniques offer valuable insights into the responses of wheat crops to drought and N stress, enabling more informed agricultural practices for improved crop management.

6.2.3 Integrating aerial imagery (remote sensing) and proximal sensing for high-throughput phenotyping of the N status in winter wheat

The incorporation of cutting-edge technologies is essential to improving precision, accuracy, efficiency, throughput and productivity in modern agriculture (Shi et al., 2016). Among these technologies, aerial drone imagery and ground-based proximal sensors have emerged as powerful tools for monitoring crop health and nutrient status (Fiorentini et al., 2021; Mezera et al., 2022). Notably, a gap exists in the literature regarding integrating these two sensing methodologies, particularly in the context of assessing N status and agronomic performance in winter wheat using NDVI at different spatial scales. In Chapter 5 of this thesis, it is demonstrated that the N status and how it reflects the agronomic performance in winter wheat can be assessed through the quantitative multiscale comparison of aerially sensed NDVI and ground-based proximally sensed NDVI derived from both leaf and canopy scales. In sum, the findings showed that the NDVI (PolyPen) measured at leaf level was more sensitive to the N status and for assessing the agronomic performance of winter wheat compared to NDVI (Drone) and NDVI (TEC5) measured aerially and at canopy scale, respectively (Chapter 5; Figure 5.12; Table 5.5). Given the level of correlations observed in this study (Chapter 5; Figure 5.15), RS might be a useful tool to extrapolate handheld

measurements spatially throughout winter wheat growth and development. Moreover, there is compelling evidence of the utility of integrating PS and RS employing a multiscale approach to sensor data analysis to understand winter wheat N status and agronomic performance. This comprehensive approach has the potential to not just improve the accuracy of N management strategies but also advance the overarching goal of sustainable agriculture through efficient resource utilisation and reduced environmental impact.

6.3 Summary of findings and implications

This section assesses how successfully the research aims and objectives outlined in Chapter 1 of this thesis have been achieved based on the findings of the study. The overall aim of this thesis was to evaluate the feasibility of employing handheld proximal sensors and drone-based imagery to identify individual nutrient stresses and distinguish between combined nutrient stresses, as well as to examine how these stresses interact, in quinoa, cowpea and wheat. This evaluation aimed to determine their suitability for field phenotyping in Africa using quick and non-destructive phenotyping techniques. To address these research aims, a series of specific objectives were defined (Chapter 1, Section 1.2), and subsequently addressed and assessed (Chapters 3–5). In this section, an overview of the general findings and outcomes of each of these chapters is provided, relating the aims and relevant specific objectives outlined in this thesis. These findings embody new insights and knowledge that could impact not just techniques for PRS for stress detection in crops but also investigations into plant physiology, morphology and agronomy.

Chapter 3 aimed to select optimal SRIs that can effectively differentiate between N and P stress in quinoa and cowpea using a handheld proximal sensor (PolyPen RP410). This focussed on establishing the link between the spectral responses observed and the nutritional status, morpho-physiology and overall performance of the crops. This study has not been previously reported in the scientific literature, hence demonstrating its novelty in this thesis.

As outlined in Chapter 3; section 3.1, the specific objectives were (i) to identify optimal SRIs indicative of N and P status separately or the combined effect and their interactions, (ii) to assess the time course response of optimal SRIs to identify early

nutritional variations, (iii) to assess the agro-morpho-physiological responses under the different N and P availabilities and (iv) to examine the relationships between optimal SRIs and agro-morpho-physiological parameters.

The results showed that among the SRIs evaluated for quinoa, NDVI, OSAVI, G, MCARI, TCARI, ZMI, SPRI, NPQI, NPCI, Ctr2, Lic1, SIPI, CRI1, CRI2, RDVI, GNDVI_780 and SRa_790, were identified as indicators with specificity in detecting N stress (Chapter 3; Table 3.3; Figure 3.5). For P status, the two SRIs that were most effective and demonstrated specificity for their detection were mNDblue_730 and PRI_550 (Chapter 3; Table 3.3; Figure 3.6). Furthermore, SRIs including GNDVI_780, SRa_790, MCARI, NDVI, G, TCARI, Ctr2 and ZMI were effective in detecting early N and P nutritional variations from 37-44 DAS (vegetative stage) in quinoa (Chapter 3; Figure 3.5).

The results revealed that the simultaneous application of different levels of N and P nutrients elicited an overall positive response in quinoa (Chapter 3; Table 3.4; Figure 3.8) This was predominantly evidenced by significant increases in morpho-physiological indicators such as LNC, LPC, SPAD values, A_n and PH (Chapter 3; Figure 3.8). Once more, the simultaneous application of N and P exhibited a beneficial influence on agronomic parameters such as VB, TPB and GY but not for TGW in quinoa (Chapter 3; Table 3.5; Figure 3.9). In this study, most of the SRIs that were optimal for distinguishing the N and P status in quinoa also demonstrated robust and significant correlations with the agro-morpho-physiological parameters (Chapter 3; Table 3.6).

Moreover, the results indicated that for cowpea, SRIs including NDVI, SR, OSAVI, MCARI, TCARI, ZMI, SPRI, PRI, NPCI, Ctr1, Ctr2, Lic1, Lic2, GM1, GM2, RDVI, PRI_550, PRI_norm, PRI/NDVI, GNDVI_780, MRESR, RENDVI, NDRE, CIgreen, CIrededge, mNDblue_530, gSRa_790 and SRa_790 were responsive to the combined N and P stress (Chapter 3; Table 3.7). It is interesting to highlight that only G and rDVI_790 showed specificity for N stress detection in cowpea (Chapter 3; Table 3.7; Figure 3.11). However, no SRI was identified to be optimum for P stress in cowpea (Chapter 3; Table 3.7), requiring future research. The earliest detection of N and P nutritional variations in cowpea was demonstrated by SRIs such as MCARI, Ctr1 and G

(Chapter 3; Figures 3.10 and 3.11) at 23 DAS (early vegetative stage) compared to quinoa from 37-44 DAS.

The results showed that the measured morpho-physiological parameters for cowpea increased with increasing N and P availability (Chapter 3; Figure 3.13). The LNC, LPC and SPAD responded significantly to both N and P stress with N×P interactions observed for LNC and SPAD (Chapter 3; Table 3.8). However, A_n and PH responded to only N stress (Chapter 3; Table 3.8). Additionally, agronomic parameters such as FW, DW, number of pods and number of seeds responded significantly to N and P supply with N×P interactions observed for FW and DW (Chapter 3; Table 3.9). However, HSW and SY responded significantly only to P stress. Like quinoa, a wide range of SRIs also correlated significantly with agro-morpho-physiological parameters in cowpea (Chapter 3; Table 3.10). In the present study, a more effective and significant correlation is observed between several SRIs and agro-morpho-physiological metrics in quinoa and cowpea reflecting their usefulness in non-destructive assessment of the morpho-physiological status of these crops. A more effective correlation between SRIs and morpho-physiological parameters in quinoa and cowpea can be achieved by integrating knowledge of physiological mechanisms, environmental conditions, canopy structure and advanced analytical techniques. This holistic approach may enable better monitoring and management of these crops.

Due to the limitations of the PolyPen RP410 spectrometer in detecting P stress especially in cowpea, a spectrometer with a wider wavelength range could be more effective sensor for monitoring complex nutritional stresses. Hyperspectral sensors could be more effective than spectrometers with shorter wavelength ranges due to several factors. For instance, hyperspectral sensors capture a wide range of wavelengths, allowing for detailed analysis of subtle biochemical changes in plants, such as N content and chlorophyll levels, which are indicative of nutritional stress (Liu et al., 2020; Sanaeifar et al., 2023). This broad spectral coverage enables the detection of specific stress-related spectral signatures that might be missed by spectrometers with limited wavelength ranges. However, there should be a trade-off between cost and effectiveness when using a sensor.

The implications for these findings suggest that quinoa and cowpea growers can modify their N and P fertilisation schedules, alleviate nutrient stress conditions, sustain optimal plant growth, mitigate substantial yield losses and enhance overall crop productivity by promptly detecting and responding to nutritional fluctuations in real-time and at an early phase. This underscores the importance of maintaining a well-balanced nutrient regimen to ensure optimal tissue nutrient levels, chlorophyll content, photosynthetic efficiency, plant growth, biomass buildup and overall crop productivity. The robust and significant correlations indicate that these SRIs have the capacity to reliably estimate various agro-morpho-physiological characteristics swiftly, affordably and non-destructively in quinoa and cowpea grown under controlled environments. The demonstrated feasibility of using a handheld proximal sensor to distinguish between N and P can greatly aid in accurately estimating crop nutritional needs. By optimising fertiliser use and improving crop monitoring, this study supports PA, potentially leading to increased crop yields and sustainable farming practices. Additionally, the use of low-cost sensing technologies can make advanced crop phenotyping accessible to resource-limited settings, promoting PA in developing countries.

Chapter 4 of the thesis evaluated the morpho-physiological drought responses at HN and LN supplies and investigated the feasibility of using SRIs derived at the leaf scale using the handheld proximal sensor explored in Chapter 3, to distinguish between the combined effects of drought and N stress in spring wheat under glasshouse conditions. The findings of this research indicated that HN plants exhibited a swifter response to drought with a bigger amplitude of response in comparison to the LN plants as observed in morpho-physiological parameters including gas exchange parameters, SPAD values, RWC, SFW, LA and SMC with synergistic interactive effects except for LNC (Chapter 4; Table 4.2). These results suggest that in situations where water is scarce, plants possessing sufficient or excess N may experience heightened vulnerability to drought conditions. Consequently, managing N fertiliser could play a crucial role in enhancing water use efficiency during periods of drought.

So far, there is limited data on how N availability influences spectral reflectance in response to drought stress. This work has demonstrated the spectral response of several SRIs to drought under HN and LN conditions (Chapter 4; Table 4.3). Generally,

drought responses in SRIs were significant on the last day of water stress (14 DAWS) under HN compared to LN except for NPQI, Lic1, Lic2 and SRa_790 (Chapter 4; Table 4.3). Out of all the SRIs explored, NPQI and TVI exhibited the swiftest response to drought, with a noticeable significant difference between WW and WS plants becoming apparent from 3 and 6 DAWS under LN respectively (Chapter 4; Table 4.3). RDVI and rDVI_790 demonstrated significant difference between WW and WS plants starting from 9 DAWS and were driven by both HN and LN conditions (Chapter 4; Table 4.3). SRIs including MCARI1, ARI1, ARI2 and CRI2 showed significant difference between WW and WS treatments starting from 12 DAWS. Most of the SRIs (e.g., NDVI, SR, G, ZMI, TCARI, PRI, Ctr1, SIPI, GM1, GM2, CRI1, PRI/NDVI, GNDVI_780, MRESR, RENDVI, NDRE, CIgreen, CIrededge and gSRa_790) showed a significant difference between WS and WW plants at 14 DAWS (Chapter 4; Table 4.3).

It has been successfully demonstrated that drought and N stress could be distinguished in spring wheat at the leaf level using a low-cost handheld proximal sensor (PolyPen RP410), by identifying key SRIs that were more specific to drought and N stress (Chapter 4; Table 4.4). In an ensemble of 39 SRIs investigated, the narrow-band greenness SRIs (RDVI and rDVI_790) indicated higher specificity for drought stress detection (Chapter 4; Table 4.4; Figure 4.5A-B). On the other hand, the chlorophyll-sensitive indices (mNDblue_730, G and Lic2) and the red-edge group indices (MRESR, CIrededge and NDRE) exhibited greater specificity for detecting N stress (Chapter 4; Table 4.4; Figure 4.6). The findings also revealed strong correlations between a wide range of SRIs and morpho-physiological parameters suggesting their utility for non-destructive assessment of the morpho-physiological status in spring wheat (Chapter 4; Table 4.5). The ability to discriminate between drought and N stress using proximally sensed data has huge implications for detecting complex environmental stresses in a climate change scenario.

The findings provide new knowledge and a confirmation of established knowledge in understanding complex environmental stress which will be useful for advancing PA. The series of important ecophysiological thresholds and SRIs that are identified could be used by producers as references or guidelines for managing wheat production in the future. Most farmers are confronted with both nutrient and water stress management. Therefore, the use of spectral data from this work could enhance PA by identifying

stress patterns, and aid growers in making good decisions; for instance, optimisation of agricultural water use and N application to mitigate adverse stress effects. To this end, the findings of this work could be developed by agronomists to establish a fertiliser application and intervention protocol for farmers. The use of handheld proximal sensors represents a low-cost approach for non-destructive plant phenotyping of crop status. Low-cost handheld devices are well-suited for constantly tracking crop growth and will provide growers with timely information about crop performance.

Chapter 5 of this thesis focussed on assessing the N status and how it reflects agronomic performance in winter wheat through the quantitative multiscale comparison of aerially sensed NDVI and the ground-based proximally sensed NDVI derived from both leaf and canopy scales. In this study, NDVI has been compared side-by-side across three different spatial scales: aerial, canopy and leaf scales in winter wheat which represents a new approach. Existing work has either compared two spatial scales or different SRIs at the same time in other crops (eg., Rehman et al., 2019; 2022).

The findings showed that NDVI (PolyPen) was more sensitive than NDVI (Drone) imagery and NDVI (TEC5) to N status and for evaluating the agronomic performance of winter wheat (Chapter 5; Figure 5.12; Table 5.5). What is interesting is that while NDVI (PolyPen) shows stronger sensitivity to the N status at the early stage, NDVI (Drone) was sensitive at a later stage but was more limited with NDVI (TEC5) (Chapter 5; Figures 5.13 and 5.14). The direct evaluation of N status using a handheld proximal sensor NDVI (PolyPen) can offer a low-cost and more sensitive indicator of early nutritional N variations in winter wheat when N fertilisation can still be adjusted. On the other hand, NDVI (Drone) offers rapid and large-scale monitoring of vegetation cover for N status monitoring at the maturity stage. Additionally, NDVI (Drone), NDVI (PolyPen) and NDVI (TEC5) showed promise as accurate predictors of GY early in the season (Chapter 5; Figure 5.16D). These findings show that the time of measurement, measurement platform and sensor all affect how well the NDVI can guide crop management decisions.

The findings show that NDVI (Drone), NDVI (PolyPen) and NDVI (TEC5) could be used interchangeably because of their strong correlation to each other (Chapter 5; Figure 5.15). The results imply that RS could be a useful technique to extrapolate ground-based

handheld measurements spatially throughout winter wheat growth and development. Furthermore, it offers end-users the flexibility to choose the sensor and platform most suitable for their needs, considering factors such as cost, expertise, weather, geographical location, growth stage, etc., for practical agricultural applications, favoring ground-based methods for certain conditions. Collectively, the OCP and OCP Africa will aid in the dissemination of the findings or technologies of this PhD work down to potential end-users i.e., farmers. The summary of findings of key SRIs across the three research chapters and their implications for practice are shown in Table 6.1.

6.3.1 Impact of phenotyping scale

Chapters 3, 4 and 5 of the PhD thesis each assesses the impact of scale on SRIs for monitoring crop responses to different stresses, but with varying focus on crop types, stresses, and the scale of data collection. **Chapter 3** focuses on leaf-level proximal sensing for quinoa and cowpea, assessing their agro-morpho-physiological responses under different N and P stresses. This chapter determines optimal SRIs at a fine scale, aiming to detect early-stage nutrient stress, distinguish between stresses and understand how these stresses affect crop performance. The small-scale data collection (proximal sensors at leaf-level) is useful for highly controlled and specific identification of stress responses. However, this scale limits its broader applicability across larger fields.

Chapter 4 expands the scale slightly by exploring the interaction of drought and N stress in spring wheat, again using a proximal sensor at the leaf level. Here, the study not only measures the responses to combined stresses but also attempts to detect each stress independently. The leaf-level sensing still operates at a relatively small scale but introduces more complexity by evaluating how SRIs can distinguish between multiple, overlapping stressors. The effectiveness of detecting drought and N stresses independently shows that even at this level, scale limitations might hinder broader, field-scale applications.

Chapter 5 takes the analysis to a multiscale approach incorporating both aerial drone imagery and ground-based proximal sensors for assessing N stress in winter wheat. This chapter represents the largest scale of assessment, aiming to connect leaf-level NDVI to canopy and aerial imagery NDVI, which can capture larger field sections. The

integration of drone technology allows for broader, more efficient field phenotyping, suitable for practical agricultural applications at a commercial scale. This chapter shows that while leaf-level sensing provides detailed insight, scaling up to drone-based imagery allows for field-wide monitoring, making it a more feasible approach for larger operations.

The comparison across the chapters reveals that scale impacts both the precision of the data and the applicability of the findings. Leaf-level sensing in Chapters 3 and 4 is more precise but less scalable, while Chapter 5's multiscale approach sacrifices some detail for broader applicability across larger areas. Thus, integrating scales, as demonstrated in Chapter 5, offers a more comprehensive solution for agricultural phenotyping, addressing both precision and scalability. The findings suggest that smaller-scale sensing is critical for early detection and specific stress analysis, while larger-scale sensing enables more practical, large-field monitoring solutions, especially when dealing with complex environmental interactions. The scaling up from leaf-level to canopy and aerial imagery illustrates how spectral response accuracy and field-wide applicability can be balanced for optimal agricultural management.

Table 6.1. Summary of findings of key SRIs identified across the three research chapters and their implications for practice.

Chapter	**Specific objective**	**Key findings of effective SRIs**	**Implications for practice**
3	(1) To identify optimal SRIs indicative of N and P status separately or the combined effect and their interactions. (2) To assess the time course response of optimal SRIs to identify early nutritional variations. (3) To examine the relationships between optimal SRIs and agro-morpho-physiological parameters.	• NDVI, OSAVI, G, MCARI, TCARI, ZMI, SPRI, NPQI, NPCI, Ctr2, Lic1, SIPI, CRI1, CRI2, RDVI, GNDVI_780 and SRa_790 were specific for N stress detection in quinoa. • mNDblue_730 and PRI_550 were specific for detecting P stress in quinoa. • SRIs including GNDVI_780, SRa_790, MCARI, NDVI, G, TCARI, Ctr2 and ZMI were effective in detecting early N and P nutritional variations in quinoa. • G and rDVI_790 showed specificity for N stress detection in cowpea. MCARI, Ctr1 and G were effective for detecting early N and P nutritional variations in cowpea. • A wide range of SRIs correlated significantly with agro-morpho-physiological parameters in both crops.	When validated, these SRIs hold the potential for rapid and non-destructive assessment of complex nutritional stress and morpho-physiological status of the studied crops.
4	(1) Identify effective SRIs specific for discriminating between drought and N stress. (2) To examine the relationships between spectral response and morpho-physiological status.	• The chlorophyll-sensitive and red-edge group SRIs including mNDblue_730, G, Lic2, MRESR, CIrededge, CIgreen and NDRE are the key mechanistic SRIs for N stress detection in spring wheat. • The RDVI and rDVI_790 are the key mechanistic SRIs for drought stress detection and may potentially relate to autocorrelation because they capture spatial patterns in leaf/vegetation that correlate with environmental factors like water and nutrient availability which equally exhibit spatial autocorrelation. • These SRIs correlated significantly with the morpho-physiological metrics due to their sensitivity to subtle changes in pigments and leaf/canopy structure of wheat crop.	The SRIs hold the potential to differentiate between drought and N stress for strategic crop management. The use of handheld proximal sensors represents a low-cost approach for non-destructive plant phenotyping of crop status.

5	To assess the N status and how it reflects agronomic performance in winter wheat through the quantitative multiscale comparison of aerially sensed NDVI and the ground-based proximally sensed NDVI derived from both leaf and canopy scales.	• NDVI (PolyPen) was more sensitive to N status and for evaluating the agronomic performance of winter wheat compared to NDVI (Drone) imagery and NDVI (TEC5). • NDVI (PolyPen) demonstrated early detection of N nutritional variation and for estimating LNC and SPAD chlorophyll content at the early growth stage. • NDVI (Drone) was more sensitive at the late growth stage. • NDVI (Drone), NDVI (PolyPen) and NDVI (TEC5) were strongly correlated to each other, cross-validating their alternative use and effectiveness for N status monitoring.	Integrating proximal and remote sensing using NDVI at the leaf, canopy, and aerial scales for comprehensive crop N monitoring in winter wheat provides new insights that enhance the accuracy, efficiency, and reliability of N nutritional assessments.

6.4 Future research outlook

While the findings of this work are conclusive within the scope of the PhD thesis, they provide a foundation for further research in this area. Therefore, based on the findings and limitations of this thesis, the following future research directions are recommended.

1. In chapters 3 and 4, the purpose of the controlled/glasshouse experiments was not necessarily to build relationships that can be translated directly to the field and different geographical settings but to test when these proximal sensors could be used at different timings to monitor crop nutritional status. Control trials entail the precise control of environmental factors such as temperature, humidity, gas concentration, air volume, wind speed, light intensity, spectral range, photoperiod, nutrient content, irrigation, etc., which may differ from the changing field conditions. Again, pot size, soil volume and spacing could influence the morpho-physiological status of the crop (Poorter et al., 2012). Therefore, for the correlations established in controlled conditions to be applied in the field and different geographical settings, it will require building up specific field calibration/validation or new models that could mimic those field conditions and these are beyond the scope of the work. Overall, there is a lot of variation in how plants develop in pots, which can make it difficult to interpret and extrapolate to the field (Passioura 2006). Therefore, any activity undertaken in controlled, or glasshouse conditions must be properly validated with field measurements to be confident that the data are relevant and of value for field conditions (Rebetzke et al., 2013). The findings presented in this study represent an initial stage of research. The observed effects might not exist or could be more or less pronounced, in plants cultivated in natural field conditions. Further research is necessary to validate the findings beyond the controlled environment of the glasshouse settings. Additionally, extension of the SRIs to more genotypes and environments through validation studies should be considered.

2. In this work, the handheld proximal contact sensor (PolyPen RP410) demonstrated the capability to discriminate between the combined N and P in quinoa and cowpea (Chapter 3) as well as drought and N stress in spring wheat (Chapter 4). However, the PolyPen RP410 and the spectral analysis method

employed were limited in their response to detecting P and drought stress due to the shorter wavelength range (320–790 nm). Future research should consider the incorporation or deployment of a spectroradiometer of a wider wavelength range, or RS tool along with more robust and automated analysis methods such as ML and computer vision to increase detection power and phenotyping capabilities (Klem et al., 2018; Ahmad et al., 2021; Safdar et al., 2023). For instance, hyperspectral sensing and deep learning methods may be feasible choices for use (Osco et al., 2019; Okyere et al., 2023; Yu et al., 2023). Hyperspectral expands the number of wavebands accessible for phenotyping, thereby broadening the spectrum of measurable phenotypes (Kim et al., 2015; Corti et al., 2017; Brugger et al., 2019).

3. This thesis demonstrated the potential of using existing SRIs for discriminating N and P stress in quinoa and cowpea (Chapter 3) and drought and N in spring wheat (Chapter 4) at leaf scale. However, future research should consider examining the full spectrum and identify indicative or optimal wavelengths capable of distinguishing these stresses at leaf, canopy or aerial scales and build on that to develop novel SRIs for these crops. The reduction of the high dimensionality of the extracted spectral data could aid in the selection of optimal wavelengths. Elsewhere, Ansari et al. (2016) showed the utility of hyperspectral RS for determining a specific wavelength range for separating N and P stress in wheat.

4. P is an essential macronutrient crucial for the growth of plants and is among the least nutrients available in soil. P deficiency frequently serves as a significant limitation to plant growth on a global scale. Although P addition experiments have been carried out to study the long-term effects on yield, data on early P stress detection in spring wheat using PS at leaf and canopy scales are still scarce. This work intended to close this gap but did not materialise due to time constraints. Future work should consider this research direction.

5. This work demonstrated the integration of NDVI at leaf, canopy and aerial scales for assessing the N status in winter wheat. The integration of more SRIs at different spatial scales is highly recommended for further research.

6. Further work about genetic studies to identify molecular markers for key SRIs for application in plant breeding should be considered. For instance, Genome-Wide Association Studies (GWAS) can be used to associate specific genetic variants with SRIs that correlate with important crop traits. By analysing a large population, GWAS can identify loci linked to variations in spectral reflectance, providing potential markers for breeding and aiding in the development of crops with optimised traits for stress resistance and productivity.

6.5 Concluding remarks

This PhD work has developed and assessed PRS techniques for phenotyping the nutritional status of crops grown under glasshouse and field conditions using SRIs at different spatial scales. Conventional manual phenotyping has been a bottleneck to significant advances in assessing the nutritional status of crops required to meet the needs of a rapidly expanding global population. The phenotyping methods developed and assessed in this study represent a low-cost approach and offer superior temporal and spatial resolutions whilst achieving comparable accuracy for crop physiology, morphology, agronomy and spectral reflectance of crops. Field phenotyping methodologies for African crops with immediate to long-term feasibility are expected to depend on a blend of existing methods or emerging low-cost sensor prototypes and imaging techniques for evaluating the nutritional status and crop performance. This will aid the widespread adoption for practical implementation in Africa and may play a pivotal role in PA as demonstrated in Cudjoe et al. (2023a). The findings presented in this thesis indicate a direction for future research and have practical implications for field phenotyping in Africa.

References

Abid, M., Tian, Z., Ata-Ul-Karim, S. T., Cui, Y., Liu, Y., Zahoor, R., and Dai, T. (2016). Nitrogen nutrition improves the potential of wheat (*Triticum aestivum* L.) to alleviate the effects of drought stress during vegetative growth periods. *Frontiers in Plant Science*, 7, 981. https://doi.org/10.3389/fpls.2016.00981

Agren, G. I., Wetterstedt, J. A., and Billberger, M. F. (2012). Nutrient limitation on terrestrial plant growth–modeling the interaction between nitrogen and phosphorus. *New Phytologist*, 194, 953-960. https://doi.org/10.1111/j.1469-8137.2012.04116.x

Ahmad, U., Alvino, A., and Marino, S. (2021). A review of crop water stress assessment using remote sensing. *Remote Sensing*, 13 (20), 4155.

Alvar-Beltrán, J., Napoli, M., Dao, A., Ouattara, A., Verdi, L., Orlandini, S., and Dalla Marta, A. (2021). Nitrogen, phosphorus and potassium mass balances in an irrigated quinoa field. *Italian Journal of Agronomy*, 16 (3). https://doi.org/10.4081/ija.2021.1788

Ansari, M. S., Young, K. R., and Nicolas, M. E. (2016). Determining wavelength for nitrogen and phosphorus nutrients through hyperspectral remote sensing in wheat (*Triticum aestivum* L.) plant. *International Journal of Bio-resource and Stress Management*, 7, 653-662.

Aulakh, M. S and Aulakh, N. S. (2005). Interactions of nitrogen with other nutrients and water: effect on crop yield and quality, nutrient use efficiency, carbon sequestration and environmental pollution. *Advances in Agronomy*, 86:341-409. https://doi.org/10.1016/S0065-2113(05)86007-9

Bandyopadhyay, K. K., Pradhan, S., Sahoo, R. N., Singh, R., Gupta, V. K., Joshi, D. K., and Sutradhar, A. K. (2014). Characterisation of water stress and prediction of yield of wheat using spectral indices under varied water and nitrogen management practices. *Agricultural Water Management*, 146, 115-123. https://doi.org/10.1016/j.agwat.2014.07.017

Bashir, S., Anwar, S., Ahmad, B., Sarfraz, Q., Khatk, W., and Islam, M. (2015). Response of wheat crop to phosphorus levels and application methods. *Journal of Environment and Earth Science*, 5 (9), 151-5.

Biswas, D., Gjetvaj, B., St. Luce, M., Liu, K., and Asgedom, H. (2023). Effects of soil water and nitrogen on drought resilience, growth, yield, and grain quality of a spring wheat. *Canadian Journal of Plant Science*, 103 (4), 401-410. https://doi.org/10.1139/cjps-2022-0210

Brugger, A., Behmann, J., Paulus, S., Luigs, H. G., Kuska, M. T., Schramowski, P., and Mahlein, A. K. (2019). Extending hyperspectral imaging for plant phenotyping to the UV-range. *Remote Sensing*, 11 (12), 1401.

Corti, M., Gallina, P. M., Cavalli, D., and Cabassi, G. (2017). Hyperspectral imaging of spinach canopy under combined water and nitrogen stress to estimate biomass, water, and nitrogen content. *Biosystems Engineering*, 158, 38-50. https://doi.org/10.1016/j.biosystemseng.2017.03.006

Cudjoe, D. K., Virlet, N., Castle, M., Riche, A. B., Mhada, M., Waine, T. W., Mohareb, F., and Hawkesford, M. J. (2023a). Field phenotyping for African crops: overview and perspectives. *Frontiers in Plant Science*, 14. https://doi.org/10.3389/fpls.2023.1219673

Duncan, E. G., O'Sullivan, C. A., Roper, M. M., Palta, J., Whisson, K., and Peoples, M. B. (2018a). Yield and nitrogen use efficiency of wheat increased with root length and biomass due to nitrogen, phosphorus, and potassium interactions. *Journal of Plant Nutrition and Soil Science*, 181 (3), 364-373. https://doi.org/10.1002/jpln.201700376.

Dong, K., Li, W., Tang, Y., Ma, S., and Jiang, M. (2023). Co-limitation of N and P is more prevalent in the Qinghai-Tibetan Plateau grasslands. *Frontiers in Plant Science*, 14, 1140462. doi:10.3389/fpls.2023.1140462

El-Hendawy, S., Dewir, Y. H., Elsayed, S., Schmidhalter, U., Al-Gaadi, K., Tola, E., Refay, Y., Tahir, M. U., and Hassan, W. M. (2022). Combining Hyperspectral Reflectance Indices and Multivariate Analysis to Estimate Different Units of Chlorophyll Content of Spring Wheat under Salinity Conditions. *Plants*, 11 (3), 456. https://doi.org/10.3390/plants11030456

Elsayed, S., El-Hendawy, S., Dewir, Y. H., Schmidhalter, U., Ibrahim, H. H., Ibrahim, M. M., and Farouk, M. (2021). Estimating the leaf water status and grain yield of wheat under different irrigation regimes using optimised two-and three-band hyperspectral indices and multivariate regression models. *Water*, 13 (19), 2666. https://doi.org/10.3390/w13192666

Elvanidi, A., Katsoulas, N., Augoustaki, D., Loulou, I., and Kittas, C. (2018). Crop reflectance measurements for nitrogen deficiency detection in a soilless tomato crop. *Biosystems Engineering*, 176, 1-11.

Fiorentini, M., Zenobi, S., and Orsini, R. (2021). Remote and proximal sensing applications for durum wheat nutritional status detection in Mediterranean area. *Agriculture*, 11 (1), 39. https://doi.org/10.3390/agriculture11010039

Gan, H., Jiao, Y., Jia, J., Wang, X., Li, H., Shi, W., Peng, C., Polle, A., and Luo, Z. B. (2016). Phosphorus and nitrogen physiology of two contrasting poplar genotypes when exposed to phosphorus and/or nitrogen starvation. *Tree physiology*, 36 (1), 22–38. https://doi.org/10.1093/treephys/tpv093

Gniazdowska, A and Rychter, A. M. (2000). Nitrate uptake by bean (*Phaseolus vulgaris* L.) roots under phosphate deficiency. *Plant and Soil*, 226, 79-85. https://doi.org/10.1023/A:102646330

Grohskopf, M. A., Corrêa, J. C., Fernandes, D. M., Teixeira, P. C., Cruz, C. V., and Mota, S. C. A. (2019). Interaction between phosphorus and nitrogen in organomineral fertiliser. *Communications in Soil Science and Plant Analysis*, 50 (21), 2742-2755. https://doi.org/10.1080/00103624.2019.1678632

Hu, B and Chu, C. (2020). Nitrogen–phosphorus interplay: old story with molecular tale. *New Phytologist*, 225 (4), 1455-1460. https://doi.org/10.1111/nph.16102

Jiang, J., Wang, Y. P., Yang, Y., Yu, M., Wang, C., and Yan, J. (2019). Interactive effects of nitrogen and phosphorus additions on plant growth vary with ecosystem type. *Plant and Soil*, 440, 523-537. https://doi.org/10.1007/s11104-019-04119-5

Kim, D. M., Zhang, H., Zhou, H., Du, T., Wu, Q., Mockler, T. C., and Berezin, M. Y. (2015). Highly sensitive image-derived indices of water-stressed plants using hyperspectral imaging in SWIR and histogram analysis. *Scientific Reports*, 5 (1), 15919. https://doi.org/10.1038/srep15919

Klem, K., Záhora, J., Zemek, F., Trunda, P., Tůma, I., Novotná, K., and Holub, P. (2018). Interactive effects of water deficit and nitrogen nutrition on winter wheat. Remote sensing methods for their detection. *Agricultural Water Management*, 210, 171-184. https://doi.org/10.1016/j.agwat.2018.08.004

Krouk, G and Kiba, T. (2020). Nitrogen and Phosphorus interactions in plants: from agronomic to physiological and molecular insights. *Current Opinion in Plant Biology*, 57, 104-109. https://doi.org/10.1016/j.pbi.2020.07.002

Kusnierek, K and Korsaeth, A. (2015). Simultaneous identification of spring wheat nitrogen and water status using visible and near infrared spectra and Powered Partial Least Squares Regression. *Computers and Electronics in Agriculture*, 117, 200-213. https://doi.org/10.1016/j.compag.2015.08.001

Li, F., Li, D., Elsayed, S., Hu, Y., and Schmidhalter, U. (2021). Using optimised three-band spectral indices to assess canopy N uptake in corn and wheat. *European Journal of Agronomy*, 127, 126286. https://doi.org/10.1016/j.eja.2021.126286

Liu, H., Bruning, B., Garnett, T., and Berger, B. (2020). The Performances of Hyperspectral Sensors for Proximal Sensing of Nitrogen Levels in Wheat. *Sensors*, 20 (16), 4550. https://doi.org/10.3390/s20164550

Liu, J., Zhu, Y., Tao, X., Chen, X., and Li, X. (2022). Rapid prediction of winter wheat yield and nitrogen use efficiency using consumer-grade unmanned aerial vehicles multispectral imagery. *Frontiers in Plant Science*, 13, 1032170. https://doi.org/10.3389/fpls.2022.1032170

Luo, X., Mazer, S. J., Guo, H., Zhang, N., Weiner, J., and Hu, S. (2016). Nitrogen: phosphorous supply ratio and allometry in five alpine plant species. *Ecology and Evolution* 6: 8881-8892. https://doi.org/10.1002/ece3.2587

Medici, A., Szponarski, W., Dangeville, P., Safi, A., Dissanayake, I. M., Saenchai, C., et al. (2019). Identification of molecular integrators shows that nitrogen actively controls the phosphate starvation response in plants. *Plant Cell*, 31, 1171-1184. https://doi.org/10.1105/tpc.18.00656

Mezera, J., Lukas, V., Horniaček, I., Smutný, V., and Elbl, J. (2021). Comparison of proximal and remote sensing for the diagnosis of crop status in site-specific crop management. *Sensors*, 22 (1), 19. https://doi.org/10.3390/s22010019

Muñoz-Huerta, R. F., Guevara-Gonzalez, R. G., Contreras-Medina, L. M., Torres-Pacheco, I., Prado-Olivarez, J., and Ocampo-Velazquez, R. V. (2013). A review of methods for sensing the nitrogen status in plants: advantages, disadvantages, and recent advances. *Sensors*, 13 (8), 10823-10843.

Okyere, F. G., Cudjoe, D., Sadeghi-Tehran, P., Virlet, N., Riche, A. B., Castle, M., Greche, L., Simms, D., Mhada, M., Mohareb, F., and Hawkesford, M. J. (2023). Modeling the spatial-spectral characteristics of plants for nutrient status identification using hyperspectral data and deep learning methods. *Frontiers in Plant Science*, 14, 1209500. https://doi.org/10.3389/fpls.2023.1209500

Osco, L. P., Ramos, A. P. M., Moriya, É. A. S., Bavaresco, L. G., Lima, B. C. D., Estrabis, N., and Araújo, F. F. D. (2019). Modeling hyperspectral response of water-stress induced lettuce plants using artificial neural networks. *Remote Sensing*, 11 (23), 2797. https://doi.org/10.3390/rs11232797

Pancorbo, J. L., Camino, C., Alonso-Ayuso, M., Raya-Sereno, M. D., Gonzalez-Fernandez, I., Gabriel, J. L., and Quemada, M. (2021). Simultaneous assessment of nitrogen and water status in winter wheat using hyperspectral and thermal sensors. *European Journal of Agronomy*, 127, 126287.

Passioura J. B. (2006). The perils of pot experiments. *Functional Plant Biology*, 33, 1075-1079. https://doi.org/10.1071/FP06223

Peng, X., Chen, D., Zhou, Z., Zhang, Z., Xu, C., Zha, Q., and Hu, X. (2022). Prediction of the Nitrogen, Phosphorus and Potassium Contents in Grape Leaves at Different Growth Stages Based on UAV Multispectral Remote Sensing. *Remote Sensing*, 14 (11), 2659. https://doi.org/10.3390/rs14112659

Poorter, H., Bühler, J., van Dusschoten, D., Climent, J., and Postma, J. A. (2012). Pot size matters: a meta-analysis of the effects of rooting volume on plant growth. *Functional Plant Biology*, 39, 839-850. https://doi.org/10.1071/FP12049

Rebetzke, G. J., Fischer, R. T. A., Van Herwaarden, A. F., Bonnett, D. G., Chenu, K., Rattey, A. R., and Fettell, N. A. (2013). Plot size matters: interference from intergenotypic competition in plant phenotyping studies. *Functional Plant Biology*, 41 (2), 107-118. https://doi.org/10.1071/FP13177

Rehman, T. H., Borja Reis, A. F., Akbar, N., and Linquist, B. A. (2019). Use of Normalised difference vegetation index to assess N status and predict grain yield in rice. *Agronomy Journal*, 111 (6), 2889-2898.

Rehman, T. H., Lundy, M. E., and Linquist, B. A. (2022). Comparative sensitivity of vegetation indices measured via proximal and aerial sensors for assessing N status and predicting grain yield in rice cropping systems. *Remote Sensing*, 14 (12), 2770. https://doi.org/10.3390/rs14122770

Rietra, R. P., Heinen, M., Dimkpa, C. O., and Bindraban, P. S. (2017). Effects of nutrient antagonism and synergism on yield and fertiliser use efficiency. *Communications in Soil Science and Plant Analysis*, 48 (16), 1895-1920. https://doi.org/10.1080/00103624.2017.1407429

Ru, C., Hu, X., Chen, D., Song, T., Wang, W., Lv, M., and Hansen, N. C. (2022). Nitrogen modulates the effects of short-term heat, drought and combined stresses after anthesis on photosynthesis, nitrogen metabolism, yield, and water and nitrogen use efficiency of wheat. *Water*, 14 (9), 1407. https://doi.org/10.3390/w14091407

Safdar, M., Shahid, M. A., Sarwar, A., Rasul, F., Majeed, M. D., and Sabir, R. M. (2023). Crop Water Stress Detection Using Remote Sensing Techniques. *Environmental Sciences Proceedings*, 25 (1), 20. https://doi.org/10.3390/ECWS-7-14198

Sallam, A., Alqudah, A. M., Dawood, M. F. A., Baenziger, P. S., and Börner, A. (2019). Drought Stress Tolerance in Wheat and Barley: Advances in Physiology, Breeding and Genetics Research. *International Journal of Molecular Sciences*, 20 (13), 3137. https://doi.org/10.3390/ijms20133137

Sanaeifar, A., Yang, C., de la Guardia, M., Zhang, W., Li, X., and He, Y. (2023). Proximal hyperspectral sensing of abiotic stresses in plants. *Science of The Total Environment*, 861, 160652.

Schlegel, A. J and Bond, H. D. (2019). Long-Term Nitrogen, Phosphorus, and Potassium Fertilisation of Irrigated Grain Sorghum. *Kansas Agricultural Experiment Station Research Reports*, 5 (4), 1. https://doi.org/10.4148/2378-5977.7753

Sellami, M. H., Albrizio, R., Čolović, M., Hamze, M., Cantore, V., Todorovic, M., and Stellacci, A. M. (2022). Selection of hyperspectral vegetation indices for monitoring yield and physiological response in sweet maize under different water and nitrogen availability. *Agronomy*, 12 (2), 489. https://doi.org/10.3390/agronomy12020489

Setiyono, T. D., Walters, D. T., Cassman, K. G., Witt, C., and Dobermann, A. (2010). Estimating maize nutrient uptake requirements. *Field Crops Research*, 118, 158-68. https://doi.org/10.1016/j.fcr.2010.05.006.

Shi, J., Yasuor, H., Yermiyahu, U., Zuo, Q., and Ben-Gal, A. (2014). Dynamic responses of wheat to drought and nitrogen stresses during re-watering cycles. *Agricultural Water Management*, 146, 163-172. https://doi.org/10.1016/j.agwat.2014.08.006

Shi, Y., Thomasson, J. A., Murray, S. C., Pugh, N. A., Rooney, W. L., Shafian, S., and Yang, C. (2016). Unmanned aerial vehicles for high-throughput phenotyping and agronomic research. *PloS One*, 11 (7), e0159781.

Siedliska, A., Baranowski, P., Pastuszka-Woźniak, J., Zubik, M., and Krzyszczak, J. (2021). Identification of plant leaf phosphorus content at different growth stages based on hyperspectral reflectance. *BMC Plant Biology*, 21 (1), 28. https://doi.org/10.1186/s12870-020-02807-4

Statkevičiūtė, G., Liatukas, Ž., Cesevičienė, J., Jaškūnė, K., Armonienė, R., Kuktaite, R., and Brazauskas, G. (2022). Impact of combined drought and heat stress and nitrogen on winter wheat productivity and end-use quality. *Agronomy*, 12 (6), 1452. https://doi.org/10.3390/agronomy12061452

Ullah, A., Tian, Z., Xu, L., Abid, M., Lei, K., Khanzada, A., and Dai, T. (2022). Improving the effects of drought priming against post-anthesis drought stress in wheat (*Triticum aestivum* L.) using nitrogen. *Frontiers in Plant Science*, 13, 965996. https://doi.org/10.3389/fpls.2022.965996

Wang, R., Bicharanloo, B., Hou, E., Jiang, Y., and Dijkstra, F. A. (2022). Phosphorus supply increases nitrogen transformation rates and retention in soil: A global meta-analysis. *Earth's Future*, 10, e2021EF002479. https://doi.org/10.1029/2021EF002479

Xia, S., Jiang, J., Liu, F., Chang, Z., Yu, M., Liu, C., and Yan, J. (2023). Phosphorus addition promotes plant nitrogen uptake mainly via enhancing microbial activities: A global meta-analysis. *Applied Soil Ecology*, 188, 104927. https://doi.org/10.1016/j.apsoil.2023.104927

Yu, S., Fan, J., Lu, X., Wen, W., Shao, S., Liang, D., and Zhao, C. (2023). Deep learning models based on hyperspectral data and time-series phenotypes for predicting quality attributes in lettuces under water stress. *Computers and Electronics in Agriculture*, 211, 108034. https://doi.org/10.1016/j.compag.2023.108034

Zhong, S., Xu, Y., Meng, B., Loik, M. E., Ma, J. Y., and Sun, W. (2019). Nitrogen addition increases the sensitivity of photosynthesis to drought and re-watering differentially in C3 versus C4 grass species. *Frontiers in Plant Science*, 10, 815. https://doi.org/10.3389/fpls.2019.00815

APPENDICES

Appendix A Evidence of ethical approval letter for the PhD research project

24 March 2020

Dear Mr Cudjoe ,

Reference: CURES/9738/2020
Title: Phenotyping the nutritional status of crops using remote sensing technologies

Thank you for your application to the Cranfield University Research Ethics System (CURES).

We are pleased to inform you your CURES application, reference CURES/9738/2020 **has been reviewed. You may now proceed with the research activities you have sought approval for.**

If you have any queries, please contact CURES Support.

We wish you every success with your project.

Regards,

CURES Team

Appendix B Supplementary materials for Chapter 3

Appendix B-1. Using proximal sensing parameters linked to the photosynthetic capacity to assess the nutritional status and yield potential in quinoa (*Acta Horticulturae*, https://doi.org/10.17660/ActaHortic.2023.1360.45).

D.K. Cudjoe[1,2], F.G. Okyere[1,2], N. Virlet[1], M. Castle[1], P. Buchner[1], S. Parmar[1], P. Sadeghi-Tehran[1], A. Riche[1], Q. Sohail[3], M. Mhada[3], M. Ghanem[3], T.W. Waine[2], F. Mohareb[2] and M.J. Hawkesford[1]

[1]Rothamsted Research, Harpenden, Hertfordshire, AL5 2JQ, United Kingdom.
[2]School of Water, Energy and Environment, Cranfield University, Cranfield, Bedfordshire, MK43 0AL, United Kingdom.
[3]AgroBiosciences Department, Mohammed VI Polytechnic University (UM6P), Lot 660, Hay My Rachid, 43150, Benguérir, Morocco.

Correspondence: malcolm.hawkesford@rothamsted.ac.uk

Abstract

Proximal sensing has been used extensively for decades to assess crop nitrogen (N) status using either a handheld chlorophyll meter or vegetation indices such as the Normalized Difference Vegetation Index (NDVI) for various crops. However, little has been done on quinoa (*Chenopodium quinoa* Willd.). In this study, we investigated how the SPAD chlorophyll meter values and NDVI could be used as indicators for N status and how they can be linked to quinoa performance in terms of photosynthesis and yield. The objectives of this study were to: (1) evaluate SPAD values and NDVI as indicators of N status, (2) assess their relevance over the crop cycle, and (3) investigate their link to the performance in terms of net CO_2 assimilation and grain yield at harvest. A pot experiment based on varying nitrogen and phosphorus (P) input conditions was conducted in the glasshouse at Cranfield University, United Kingdom. The results showed that both SPAD and NDVI correlated similarly with the leaf N content (%) (R^2=0.76, R^2=0.82, p<0.001 respectively). High correlations between SPAD and NDVI were also observed at 58 DAS (R^2=0.67) and across the entire crop cycle (R^2=0.84), validating the utility of both parameters for N status monitoring. Furthermore, significant differences between treatments were observed at different growth stages when SPAD and NDVI were measured across the crop cycle. Strong significant correlations between SPAD and NDVI with the net CO_2 assimilation (A_{net}) (R^2=0.86, R^2=0.81, p<0.001 respectively) were recorded. SPAD values and NDVI significantly correlated with grain yield at harvest (R^2=0.68, R^2=0.80, p<0.001 respectively). While SPAD and NDVI are potentially useful tools to improve N fertilizer management and develop in-season yield predictions in quinoa at relatively low-cost, alternative non-saturating spectral indices need to be explored to improve accuracy.

Keywords: *Chenopodium quinoa*, SPAD, NDVI, N status, net CO_2 assimilation, photosynthesis

Introduction

Quinoa (*Chenopodium quinoa* Willd.) is a unique pseudocereal originating from the Andean region of South America. Quinoa has attracted global attention as an important food source having exceptional nutritional qualities, health benefits, and resilience to various abiotic stresses (Bazile et al., 2016; Hinojosa et al., 2018; Dakhili et al., 2019). To meet the ever-increasing demand for quinoa, farmers and breeders need improved agronomic practices combined with the breeding of more nutrient-efficient crops, especially in low-productivity regions. Therefore, adjusting N requirements based on the prediction of potential yield is a crucial part of precision agriculture for making in-season management decisions and increasing profitability.

Proximal sensing (PS) technologies offer quick, non-destructive, and accurate assessments of crop N status, which is crucial for optimised fertiliser application and precision crop management (Chawade et al., 2019; Alvar-Beltrán et al., 2020). Spectroscopy technologies (single point or imager) offer a wide range of metrics including computed spectral reflectance indices (SRIs) and have been used to assess the nutrient status of crops, diagnose nutrient deficiency, monitor growth, and predict crop yields (Padilla et al., 2018). Chlorophyll meters such as the SPAD-502 and SRIs such as NDVI (Normalised Difference Vegetation Index) are reliable indicators for assessing the N status of crop plants (Kizilgeci et al., 2019). The NDVI is a numerical indicator using a Normalised ratio of the difference between the near-infrared (NIR) and the red reflectance bands. For instance, Rehman et al. (2019) demonstrated the ability of NDVI to assess N status in rice and predict grain yield at harvest. The NDVI at panicle initiation was most closely related to crop N uptake and positively correlated (R^2=0.58) with grain yield at harvest. On the other hand, the SPAD-502 measures the relative leaf chlorophyll levels at light absorbances of 650 nm (red) and 940 nm NIR (Li et al., 2019). The SPAD has been successfully used as a selection criterion for nitrogen use efficiency and improved grain yield in durum wheat (Kizilgeci et al., 2019). In another study, Chetan and Potdar (2016) showed that yield potential in corn could be accurately predicted in-season with NDVI and SPAD. A strong correlation (r=0.98) was achieved between NDVI, SPAD, and grain yield at the tasselling stage.

Previously, most studies employing SRIs have focused largely on cereals. However, the use of PS parameters to assess the nutritional status and crop performance in quinoa has not been thoroughly studied. Recently, Alvar-Beltrán et al. (2020) tested proximal optical sensing tools to monitor quinoa growth in field conditions with various N inputs. The authors showed that SPAD-502 and GreenSeeker were effective at making in-season predictions of crop biomass at harvest (R^2=0.68 and 0.82, respectively).

As the amount of chlorophyll in the leaves provides valuable information on the physiological status and is directly linked to the photosynthetic capacity and therefore primary production (Li et al., 2019), we decided to focus the present study on these three components. The main objectives of this study were to: (1) evaluate the SPAD and leaf-level NDVI as indicators of N status in quinoa, (2) monitor N status across the season using SPAD and NDVI, and (3) assess how both reflect the crop performance in terms of net CO_2 assimilation and grain yield at harvest.

MATERIALS AND METHODS

Plant material, growth conditions, and crop establishment

A pot experiment with quinoa (*Chenopodium quinoa* Willd var. *temuco*) was conducted in the glasshouse at the Plant Growth Facility at Cranfield University, United Kingdom, from September 2020 to January 2021. The conditions were set as: day/night temperature 24/21±2 °C, relative humidity 60%, a photoperiod of 14 h with a light intensity of 400-500 µmol m^{-2} s^{-1}. Before sowing, quinoa seeds were stratified at 4°C for 3 days and sown in wet vermiculite compost on a mini pot tray and incubated in the dark. After 3 days, germinated seeds were illuminated to prevent etiolation. Seedlings of similar size (5 cm) were transplanted into pots. At the two-leaf stage, the seedlings were thinned to one plant per pot. Quinoa plants were grown to maturity on a reconstituted Levington F1, low-nutrient compost, as detailed in the following section.

Experimental design, compost preparation, and application of nutrient treatments

The experiment was structured in a randomized complete block design (RCBD) with five replications. The compost used was Levington F1, low-nutrient compost (ICL, Everris, United Kingdom). Compost was washed to remove soluble nutrients, by flooding one part of the compost with five-part deionised water, mixing, breaking up

aggregates, and draining through a double 0.8 mm sieve (adapted from Masters-Clark et al., 2020). The washing process was repeated five times and the washed compost was oven-dried at 80 °C. Nutrients were reconstituted in the washed compost with macro and micronutrients in a modified Letcombe nutrient solution (Masters-Clark et al., 2020). The N and P inputs were applied in four nutritional levels designated (HN-HP, HN-LP, LN-HP, and LN-LP, with H and L for high and low levels respectively). The concentrations for HN and LN were 49.12 mM and 14.59 mM and for HP and LP were, 13.38 mM and 3.33 mM respectively. Each pot (21 cm tall by 19 cm diameter) was filled with 360 g of washed compost and mixed with 58 g of silver sand and 790 ml of nutrient solution. Pots were replenished with 790 ml of nutrient solution at 23 DAS, 44 DAS, 65 DAS, and 79 DAS based on the designated treatments. Plants were irrigated with deionised water.

Measurement parameters

Weekly measurements

From 23 DAS, the chlorophyll index and spectral data were measured weekly using a SPAD-502 chlorophyll meter (Soil Plant Analysis Development, Minolta Camera Co., Ltd., Japan) and a PolyPen instrument (PolyPen, Photon Systems Instruments, Czech Republic). NDVI was extracted from the PolyPen data using the 780 nm and 630 nm wavelengths. At 58 DAS, NDVI was calculated by taking an average of the 51 and 65 DAS because the 58 DAS data was missing due to an instrument failure. Measurements were realized on fully expanded leaves at the top of the plants. Three readings were made and then averaged.

Gas-exchange measurement

The net CO_2 assimilation (A_{net}) was measured at 46 DAS in a fully expanded leaf from the top of each plant, employing a gas-exchange system (Li-6400XT, Li-COR Inc., Lincoln, NE, USA). The photosynthesis measurements were done between 10 AM and 2 PM. Additional SPAD data was collected on the same leaves.

Sampling for nitrogen content and yield determination

At 60 DAS, leaves were sampled for nitrogen content analysis. Total nitrogen (N) content (%) was determined by the LECO combustion method. At maturity, manual

harvesting was done to separate matured seed heads from the vegetative parts (i.e., panicles and stems). Harvested seed heads were dried at 40 °C for 48 h in a forced-air oven and threshed manually. Chaffs were removed to retain cleaned grains. The grain yield per pot (g pot^{-1}) was further determined based on 13% moisture content.

Statistical analysis

Data were analysed using linear regression to investigate the relationship between variables. Analysis of variance (ANOVA) using R software was employed to assess differences between treatments throughout the crop cycle. All results were evaluated at a 5% level of significance.

RESULTS

Evaluation of N status during the reproductive/inflorescence growth stage

Table 1 shows the summary statistics of leaf N content determined at 60 DAS, SPAD, and NDVI at 58 DAS for each treatment. An increase in the mean values for each variable was observed with the higher nutrient supply treatments, except for SPAD and NDVI for the LN-HP treatment, for which values were lower than the LN-LP. The linear regression of the leaf N content with SPAD and NDVI showed high correlations (R^2=0.76, R^2=0.82 respectively; Figure 1a, b). The relationship between the N predictors (SPAD and NDVI) was also high (R^2=0.67, Figure 1c).

Table 1. Descriptive statistics of leaf N content (%) at 60 DAS, and SPAD and NDVI at 58 DAS. Abbreviations used are minimum (Min); maximum (Max); standard deviation (SD); coefficient of variation (CV). Each treatment represents five replicates.

Parameter	Leaf N content (%)					SPAD					NDVI				
Treatment	Mean	Min	Max	SD	CV (%)	Mean	Min	Max	SD	CV (%)	Mean	Min	Max	SD	CV (%)
HN-HP	5.1	5.0	5.3	0.12	2.35	49.2	45.5	53.3	2.83	5.75	0.55	0.55	0.56	0.00	0.00
HN-LP	3.2	3.0	3.3	0.14	4.38	40.3	38.8	41.5	1.01	2.51	0.52	0.51	0.54	0.01	1.92
LN-HP	1.6	1.4	1.9	0.23	14.38	33.8	32.1	35.0	1.13	3.34	0.49	0.47	0.5	0.01	2.04
LN-LP	1.5	1.3	1.8	0.20	13.33	38.9	35.6	41.6	2.36	6.07	0.50	0.47	0.51	0.02	4.00

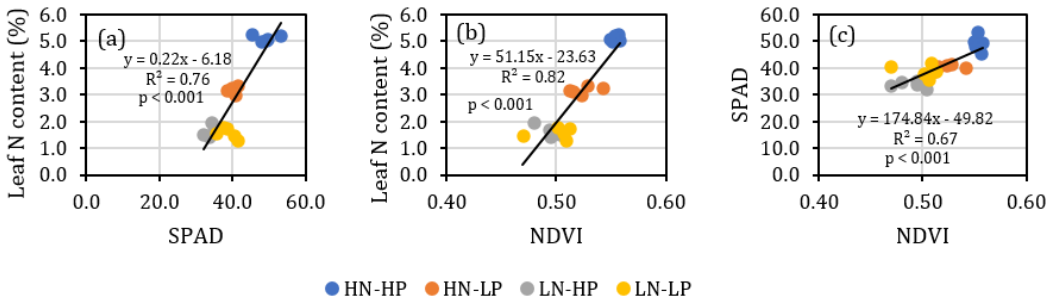

Figure 1. Linear regression between leaf N content at 60 DAS and SPAD (a), NDVI (b) at 58 DAS, and between NDVI and SPAD at 58 DAS (c). Each treatment represents five replicates. Significant level is ****p*<0.001.

Time course of proximal sensing parameters (SPAD and NDVI) and their relationship throughout the crop cycle

Figure 2 (a, b) displays the time course of SPAD and NDVI measured from 23 DAS to 93 DAS. A significant difference between treatments was observed from 37 DAS for SPAD (Figure 2a) and 30 DAS for NDVI. High statistical differences between treatments (p<0.001) were observed constantly from 37 DAS for SPAD and 44 DAS for NDVI. For both variables, higher values were obtained for the HN-HP treatment. The lowest SPAD values were observed for the LN-HP except at 44 DAS. Similarly, for NDVI, the lowest values were observed for the LN-HP treatment from 65 DAS. The relationship between SPAD and NDVI across the crop cycle is shown in Figure 2c. Non-linear regression was fitted to the data displaying a high R^2 (0.84). Higher data variation was seen for the lower values of SPAD and NDVI, reflecting the observations on the time course for the LN-LP and LN-HP treatments.

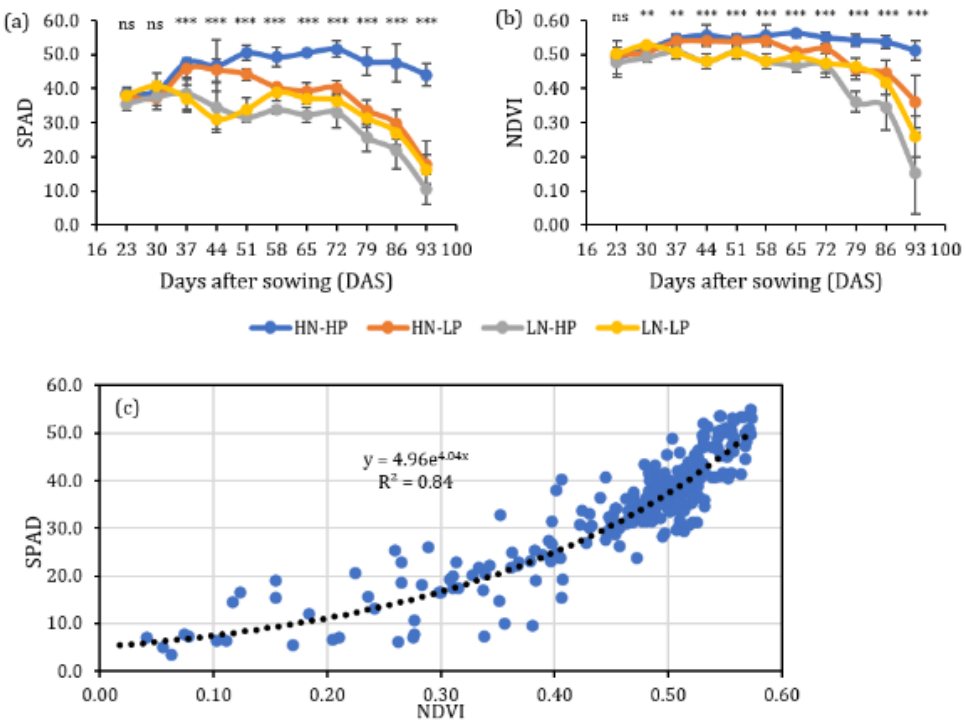

Figure 2. Time course of SPAD (a) and NDVI (b) from 23 to 93 DAS. Relationship between NDVI and SPAD over the same period (c). Error bars represent mean ± SD (n=5). Asterisks indicate significant difference between treatments (**p<0.01, ***p<0.001) using student's t-tests. Non-significant is denoted as ns (p>0.05).

Assessment of how well the proximal sensing parameters reflected crop performance

Table 2 highlights the summary statistics of the crop performance indicators under different nutritional treatments. An increase in the mean values for each variable was observed with the increase in nutrient supply. To assess how the N status predictors (SPAD and NDVI) reflected crop performance in terms of photosynthesis (net CO_2 assimilation) and grain yield at harvest, correlation analyses were performed (Figure 3). The results showed a strong significant correlation between A_{net} and leaf N content, SPAD, and NDVI (R^2=0.68, R^2=0.86, and R^2=0.81, respectively). In parallel, the N status predictors were significantly correlated with grain yield (R^2=0.86, R^2=0.68, R^2=0.80, respectively).

Table 2. Descriptive statistics of A_{net} measured at 46 DAS and grain yield at harvest. Abbreviations used are minimum (Min); maximum (Max); standard deviation (SD); coefficient of variation (CV). Each treatment represents five replicates, except HN-HP and HN-LP for A_{net} in which one of the replicates had wilted leaves and was removed.

Performance indicator	A_{net} (µmol m^2 s^{-1})					Grain yield (g pot^{-1})				
Treatment	Mean	Min	Max	SD	CV (%)	Mean	Min	Max	SD	CV (%)
HN-HP	25.10	20.01	28.03	3.60	14.34	75.0	52.2	92.8	17.5	23.33
HN-LP	21.37	17.04	23.19	2.91	13.61	50.1	46.8	55.2	3.47	6.93
LN-HP	15.83	11.91	17.84	2.50	15.79	22.9	19.2	26.1	2.68	11.70
LN-LP	15.32	11.95	18.97	3.11	20.30	15.4	11.8	20.6	3.82	24.81

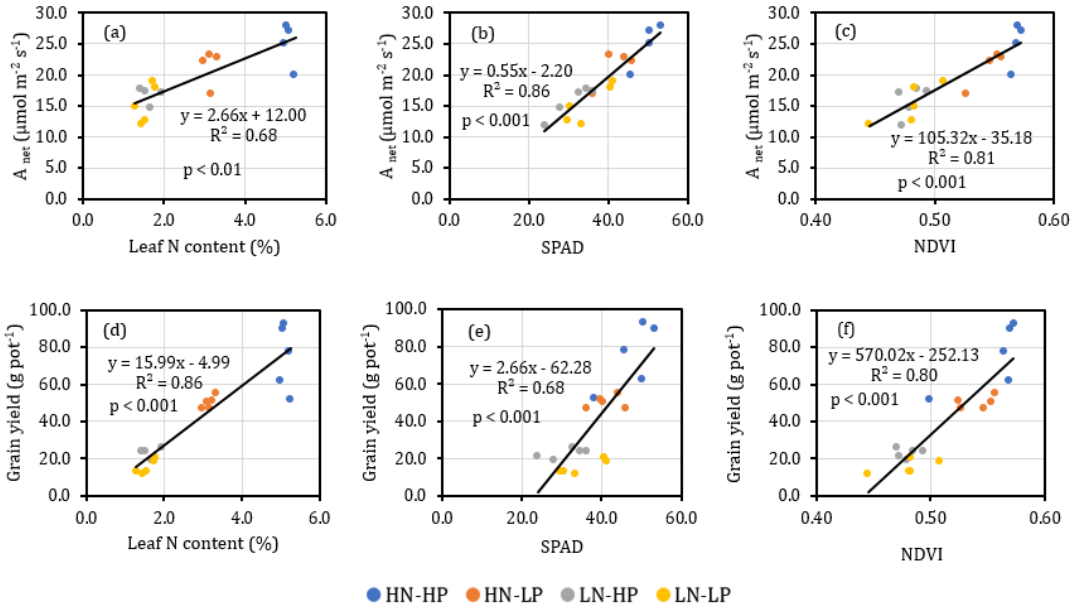

Figure 3. Correlations between leaf N content at 60 DAS and A_{net} at 46 DAS (a), SPAD at 46 DAS and A_{net} at 46 DAS (b), NDVI at 44 DAS and A_{net} at 46 DAS (c), leaf N content at 60 DAS and grain yield at harvest (d), SPAD at 46 DAS and grain yield at harvest (e), and NDVI at 44 DAS and grain yield at harvest (f). Each treatment represents five replicates, except HN-HP and HN-LP for A_{net} in which one of the replicates had wilted leaves and was removed. Significant levels are $^{**}p<0.01$, $^{***}p<0.001$. SPAD and NDVI values are dimensionless.

DISCUSSION

This study was conducted to evaluate the usefulness of proximal sensing and indices such as SPAD and NDVI measured at the leaf level, as indicators of N status and crop performance predictors in quinoa. As there is a strong relationship between chlorophyll content and the leaf N content, leaf chlorophyll content is considered a useful indicator

of the N status (Uddling et al., 2007). Here, both the SPAD and NDVI displayed similar efficiencies as indicators of N status, as they correlated strongly (R^2=0.76, R^2=0.82, respectively) with the leaf N content at 60 DAS (Figure 1a, b). As reported by Yang et al. (2010), the high correlation observed between NDVI and leaf N content at 60 DAS may be reasoned by the reflectivity of quinoa leaves as influenced by the amount of accumulated N, chlorophyll, and leaf area. The results are also consistent with Vian et al. (2018), where strong positive relationships were established between NDVI and leaf N content in wheat.

SPAD chlorophyll readings and NDVI have been established as reliable indicators to identify crop N status in many cereals (Kizilgeci et al., 2019; Rehman et al., 2019). However, as already mentioned, comparative research on their exploitation in quinoa remains scarce. Thus, the SPAD and leaf NDVI indices hold great potential to optimise N-use efficiency in quinoa. Furthermore, the strong relationship between SPAD and NDVI observed at 58 DAS during the inflorescence stage and throughout the crop cycle validates the suitability and precision of both parameters for rapid and non-destructive N status monitoring during the growing season (Figure 1c, 2c).

The time series of SPAD and NDVI showed strong significant differences between treatments at various growth stages of quinoa (Figure 2a, b). The results suggest that quinoa was very responsive to N fertilisation but also phosphorus fertilization. Generally, quinoa responds well to N applications due to enhanced photosynthetic capacity and production of photoassimilates (Murphy and Matanguihan 2015; Bascuñán-Godoy et al., 2018). This observation further demonstrates the utility of SPAD and NDVI in revealing nutritional variations during the growing season.

This study assessed how the N status predictors (SPAD and NDVI) reflected the crop performance in terms of photosynthesis and grain yield at harvest. It is well established that grain yield and net CO_2 assimilation are positively correlated to leaf or canopy N content, as both are responsive to an increase in nitrogen. Strong significant correlations were observed between A_{net} with leaf N content, SPAD, and NDVI in the present study (Figure 3). Our results indicate that SPAD and NDVI indices could reasonably and accurately assess the photosynthetic performance of quinoa when the proximal sensors are not saturated. Moreover, the linear regression with grain yield showed that grain yield is responding quite well to the increase in N and P fertilisation and that SPAD and

NDVI could reflect those changes. These findings demonstrate the utility of developing in-season yield predictors in quinoa based on proximal sensing.

CONCLUSIONS

This study demonstrated that SPAD and NDVI measured at the leaf level through proximal sensing are relevant as indicators of N status in quinoa. The strong relationship observed between SPAD and NDVI validates the effectiveness of both parameters for N status monitoring in quinoa during the growing season. Furthermore, the significant difference between treatments established at critical growth stages of the crop indicates the utility of both parameters in detecting nutritional variations during the growing season. Both SPAD and NDVI indices correlated strongly with net CO_2 assimilation and grain yield, indicating the utility for assessing the photosynthetic capacity and developing in-season yield predictions in quinoa. As SPAD and NDVI are potentially suitable proximal sensing parameters to improve N fertiliser management and develop in-season yield predictions in quinoa at a low cost. Alternative non-saturating spectral indices should be explored in quinoa to further improve accuracy.

ACKNOWLEDGEMENT

This research is funded by OCP S.A under the Mohammed VI Polytechnic University (UM6P), Rothamsted Research and Cranfield University programme. Rothamsted Research receives grant-aided support from the Biotechnology and Biological Sciences Research Council (BBSRC) through the Designing Future Wheat programme [BB/P016855/1].

References

Alvar-Beltrán, J., Fabbri, C., Verdi, L., Truschi, S., Dalla Marta, A., and Orlandini, S. (2020). Testing proximal optical sensors on quinoa growth and development. Remote Sensing. 12(12):1958. https://doi.org/10.3390/rs12121958.

Bascuñán-Godoy, L., Sanhueza, C., Hernández, C. E., Cifuentes, L., Pinto, K., Álvarez, R., et al. (2018). Nitrogen supply affects photosynthesis and photoprotective attributes during drought-induced senescence in quinoa. Front. Plant Sci., 9: 994. https://doi.org/10.3389/fpls.2018.00994.

Bazile, D., Jacobsen, S. E., and Verniau, A. (2016). The global expansion of quinoa: Trends and limits. Front. Plant Sci. 7, 622. https://doi.org/10.3389/fpls.2016.00622.

Chawade, A., van Ham, J., Blomquist, H., Bagge, O., Alexandersson, E., and Ortiz, R. (2019). High-throughput field phenotyping tools for plant breeding and precision agriculture. Agronomy, 9, 258. https://doi.org/10.3390/agronomy9050258.

Chetan, H. T., and Potdar, M. P. (2016). Yield prediction models in maize using SPAD and NDVI. Res. Environ. Life Sci. 9, 1002-1004.

Dakhili, S., Abdolalizadeh, L., Hosseini, S. M., Shojaee-Aliabadi, S., and Mirmoghtadaie, L. (2019). Quinoa protein: Composition, structure and functional properties [Review]. Food Chemistry, 299, 125161. https://doi.org/10.1016/j.foodchem.2019.125161.

Hinojosa, L., González, J., Barrios-Masias, F., Fuentes, F., and Murphy, K. (2018). Quinoa abiotic stress responses: a review. Plants 7(4), 106. https://doi.org/10.3390/plants7040106.

Kizilgeci, F., Akinci, C., and Yildirim, M. (2019). Improving grain yield, protein ratio and nitrogen use efficiency of durum wheat (Triticum durum Desf.) hybrids using SPAD meter as a selection criterion. Int. J. Agric. Environ. Food Sci., 3, 112-120. https://doi.org/10.31015/jaefs.2019.3.1.

Li, R., Chen, J., Qin, Y., and Fan, M. (2019). Possibility of using a SPAD chlorophyll meter to establish a Normalised threshold index of nitrogen status in different potato cultivars. Journal of Plant Nutrition, 42, 834-840. https://doi.org/10.1080/01904167.2019.1584215.

Masters-Clark, E., Shone, E., Paradelo, M., Hirsch, P. R., Clark, I. M., Otten, W., Brennan, F., and Mauchline, T. H. (2020). Development of a defined compost system for the study of plant-microbe interactions. Sci. Rep. 10, 7521. https://doi.org/10.1038/s41598-020-64249-0.

Murphy, K., and Matanguihan, J. (2015). Quinoa improvement and sustainable production. John Wiley and Sons, Hoboken, New Jersey, USA. https://doi.org/10.1002/9781118628041.

Padilla, F. M., Gallardo, M., Peña-Fleitas, M. T., de Souza, R., and Thompson, R. B. (2018). Proximal optical sensors for nitrogen management of vegetable crops: a review. Sensors 18, 2083. https://doi.org/10.3390/s18072083.

Rehman, T. H., Borja Reis, A. F., Akbar, N., and Linquist, B. A. (2019). Use of Normalised difference vegetation index to assess N status and predict grain yield in rice. Agron. J. 111:1-10. https://doi.org/10.2134/agronj2019.03.0217.

Uddling, J., Gelnag-Alfredsson, J., Piikki, K., and Pleijel, H. (2007). Evaluating the relationship between leaf chlorophyll concentration and SPAD-502 chlorophyll meter readings. Photosynth. Res. 91: 37-46. https://doi.org/10.1007/s11120-006-9077-5.

Vian, A. L., Bredemeier, C., Turra, M. A., Giordano, C. P. S., Fochesatto, E., Silva, J. A., and Drum, M. A. (2018). Nitrogen management in wheat based on the Normalised difference vegetation index (NDVI). Ciência Rural, 48. https://doi.org/10.1590/0103-8478cr20170743.

Yang, W., Nick, S., and Li, M. Z. (2010). Nitrogen content testing and diagnosing of cucumber leaves based on multispectral imagines. Guang, P., Xue, Y., Guang, P., Fen, X. 30(1):210-3. Chinese. PMID: 20302116. http://dx.doi.org/10.3964/j.issn.1000-0593(2010)01-0210-04.

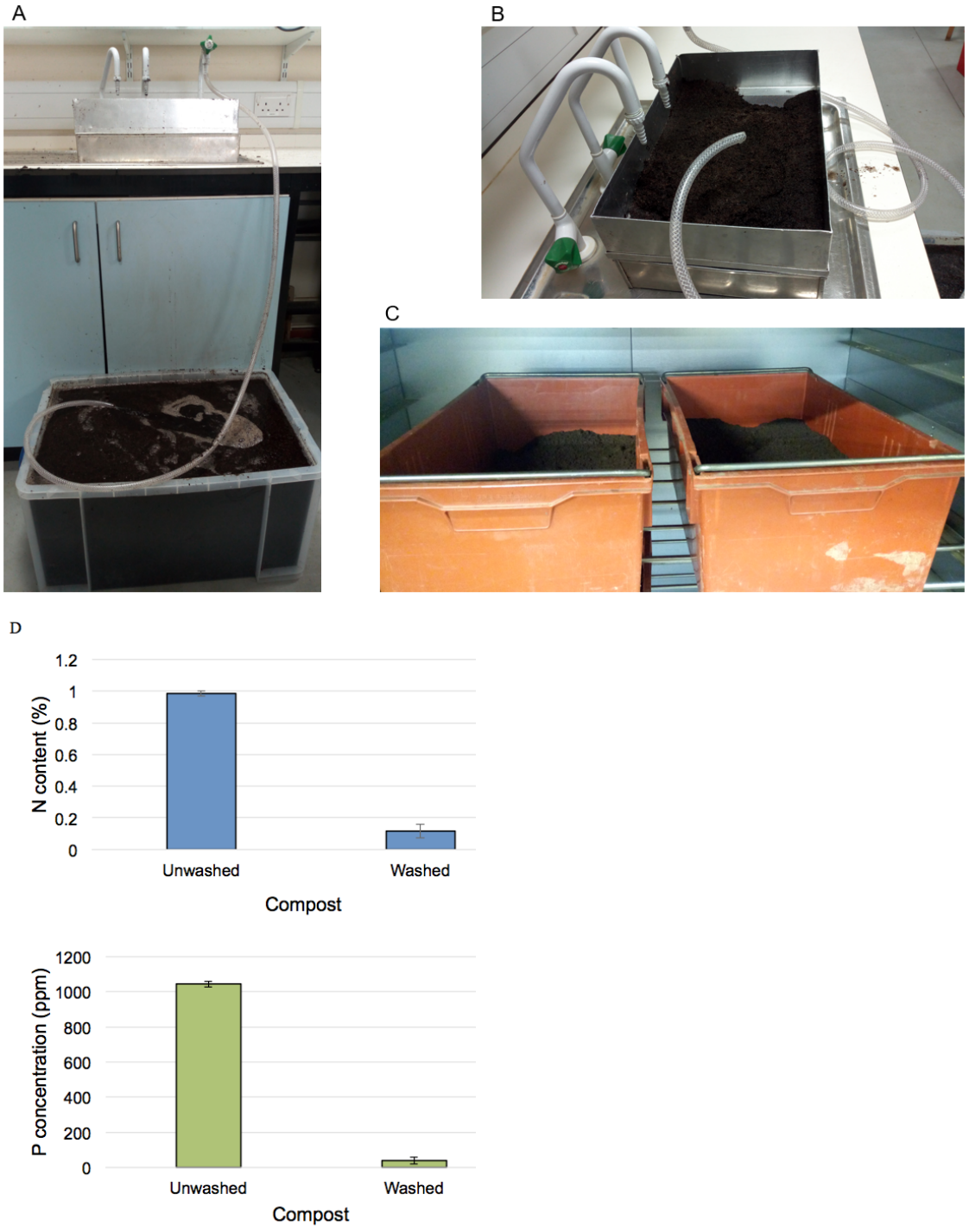

Figure B-1. The washing process of the compost is in three steps. These involve flooding one part of the compost with five-part deionised water, mixing, and breaking up aggregates (A), the compost mixture is then drained through a 0.8 mm double sieve (B) and after five repeated washings and draining, the washed compost is oven-dried at 105 °C for nutrient reconstitution (C) and N and P contents of the unwashed and washed compost (D).

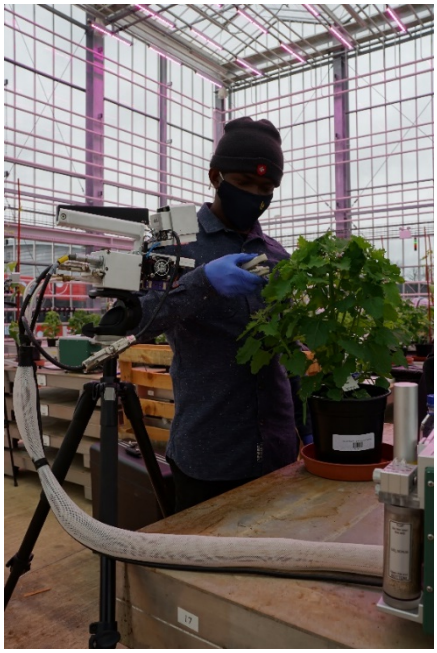

Figure B-2. The author taking gas exchange measurements for net CO_2 assimilation rate (A_n) using the portable photosynthetic system (Li-6400XT) along with SPAD measurement.

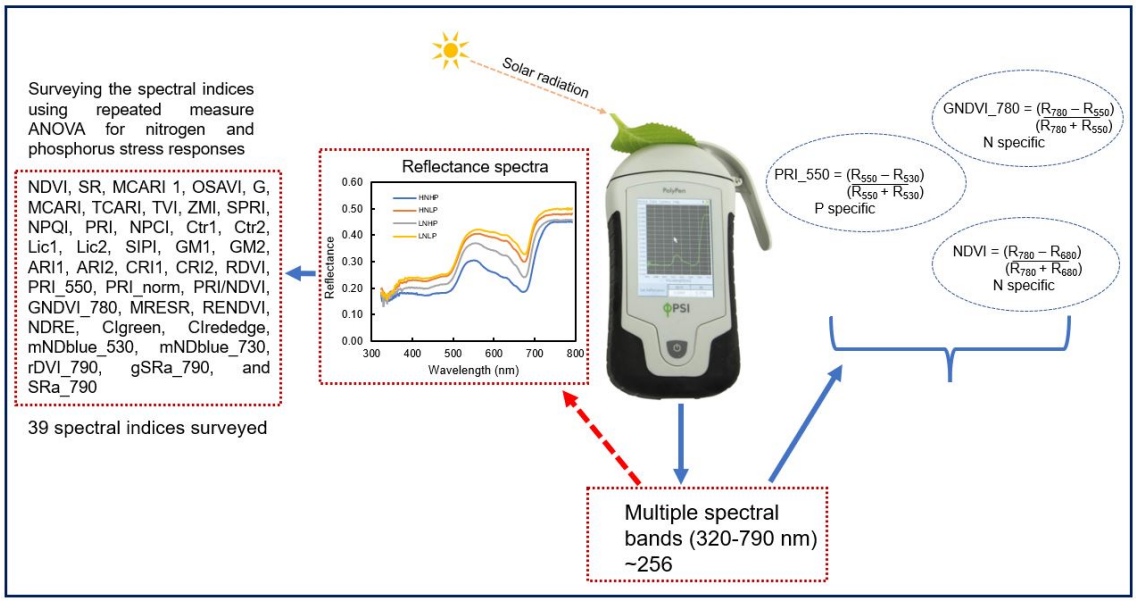

Figure B-3. Schematic measurement of spectral reflectance using the PolyPen RP410 spectrometer to identify responsive spectral reflectance indices (SRIs) by repeated measures ANOVA (RMA) for N and P status in quinoa. The same approach was used to identify SRIs specific for N and P status in cowpea.

Table B-1. Full results of the test for main effects of spectral reflectance indices (SRIs) in response to nitrogen (N) and phosphorus (P) stress separately and their combined effects in quinoa. The responses of the SRIs to N and P stresses and their interactions were tested using the F-statistics and F-Test probability via repeated measures ANOVA (RMA). The RMA analysis was done considering all treatment combinations and time points (DAS). The statistically significant results (p<0.05) indicating differences between means for levels of N or P and their interactions are shown in bold.

Index	N	P	N×P	DAS	N×DAS	P×DAS	N×P×DAS
NDVI	$F_{1,12}$=93.618, P<**0.001**	$F_{1,12}$=3.895, P=0.072	$F_{1,12}$=30.052, P<**0.001**	$F_{3,9,62}$=117.517, P<**0.001**	$F_{3,9,62}$=9.966, P<**0.001**	$F_{3,9,62}$=2.642, P<**0.05**	$F_{3,9,62}$=5.156, P<**0.01**
SR	$F_{1,12}$=144.270, P<**0.001**	$F_{1,12}$=9.031, P<**0.05**	$F_{1,12}$=44.955, P<**0.001**	$F_{4.7,74.6}$=136.037, P<**0.001**	$F_{4.7,74.6}$=9.278, P<**0.001**	$F_{4.7,74.6}$=3.089, P<**0.05**	$F_{4.7,74.6}$=5.982, P<**0.001**
MCARI1	$F_{1,12}$=0.159, P=0.697	$F_{1,12}$=0.028, P=0.870	$F_{1,12}$=1.977, P=0.185	$F_{1.4,22.4}$=24.506, P<**0.001**	$F_{1.4,22.4}$=6.942, P<**0.01**	$F_{1.4,22.4}$=1.231, P=0.297	$F_{1.4,22.4}$=1.184, P=0.308
OSAVI	$F_{1,12}$=31.695, P<**0.001**	$F_{1,12}$=0.932, P=0.353	$F_{1,12}$=16.811, P<**0.01**	$F_{2,31.6}$=59.964, P<**0.001**	$F_{2,31.6}$=7.312, P<**0.01**	$F_{2,31.6}$=1.728, P=0.194	$F_{2,31.6}$=2.391, P=0.108
G	$F_{1,12}$=14.128, P<**0.01**	$F_{1,12}$=0.984, P=0.341	$F_{1,12}$=4.861, P<**0.05**	$F_{2.2,36}$=26.081, P<**0.001**	$F_{2.2,36}$=11.636, P<**0.001**	$F_{2.2,36}$=2.507, P=0.090	$F_{2.2,36}$=1.902, P=0.160
MCARI	$F_{1,12}$=41.319, P<**0.001**	$F_{1,12}$=3.400, P=0.090	$F_{1,12}$=2.552, P=0.136	$F_{2.4,38}$=5.441, P<**0.01**	$F_{2.4,38}$=9.858, P<**0.001**	$F_{2.4,38}$=2.575, P=0.081	$F_{2.4,38}$=3.033, P=0.052
TCARI	$F_{1,12}$=51.418, P<**0.001**	$F_{1,12}$=0.794, P=0.391	$F_{1,12}$=11.627, P<**0.01**	$F_{1.8,28}$=14.000, P<**0.001**	$F_{1.8,28}$=3.209, P=0.062	$F_{1.8,28}$=0.683, P=0.495	$F_{1.8,28}$=4.622, P<**0.05**
TVI	$F_{1,12}$=0.112, P=0.744	$F_{1,12}$=0.065, P=0.803	$F_{1,12}$=4.311, P=0.060	$F_{1.5,23.8}$=28.176, P<**0.001**	$F_{1.5,23.8}$=6.916, P<**0.01**	$F_{1.5,23.8}$=1.231, P=0.299	$F_{1.5,23.8}$=1.303, P=0.282
ZMI	$F_{1,12}$=87.508, P<**0.001**	$F_{1,12}$=3.566, P=0.083	$F_{1,12}$=18.871, P<**0.001**	$F_{1.6,25}$=40.744, P<**0.001**	$F_{1.6,25}$=3.254, P=0.066	$F_{1.6,25}$=1.553, P=0.231	$F_{1.6,25}$=4.418, P<**0.05**
SPRI	$F_{1,12}$=43.292, P<**0.001**	$F_{1,12}$=4.581, P=0.054	$F_{1,12}$=1.056, P=0.324	$F_{2.7,43}$=123.454, P<**0.001**	$F_{2.7,43}$=9.661, P<**0.001**	$F_{2.7,43}$=3.175, P<**0.05**	$F_{2.7,43}$=1.973, P=0.138
NPQI	$F_{1,12}$=7.493, P<**0.05**	$F_{1,12}$=1.323, P=0.272	$F_{1,12}$=2.879, P=0.116	$F_{4.8,77}$=3.415, P<**0.01**	$F_{4.8,77}$=2.494, P<**0.05**	$F_{4.8,77}$=0.673, P=0.639	$F_{4.8,77}$=0.840, P=0.522
PRI	$F_{1,12}$=71.065, P<**0.001**	$F_{1,12}$=10.129, P<**0.01**	$F_{1,12}$=1.537, P=0.239	$F_{1.7,27.4}$=96.084, P<**0.001**	$F_{1.7,27.4}$=7.626, P<**0.01**	$F_{1.7,27.4}$=4.035, P<**0.05**	$F_{1.7,27.4}$=1.471, P=0.247
NPCI	$F_{1,12}$=32.916, P<**0.001**	$F_{1,12}$=3.642, P=0.081	$F_{1,12}$=0.783, P=0.394	$F_{1.9,30.8}$=89.249, P<**0.001**	$F_{1.9,30.8}$=7.572, P<**0.01**	$F_{1.9,30.8}$=2.281, P=0.121	$F_{1.9,30.8}$=1.735, P=0.194
Ctr1	$F_{1,12}$=78.080, P<**0.001**	$F_{1,12}$=9.731, P<**0.01**	$F_{1,12}$=2.110, P=0.172	$F_{1.7,27.5}$=93.230, P<**0.001**	$F_{1.7,27.5}$=6.008, P<**0.01**	$F_{1.7,27.5}$=2.227, P=0.133	$F_{1.7,27.5}$=1.584, P=0.224
Ctr2	$F_{1,12}$=81.244, P<**0.001**	$F_{1,12}$=3.237, P=0.097	$F_{1,12}$=23.513, P<**0.001**	$F_{3.5,56}$=112.713, P<**0.001**	$F_{3.5,56}$=9.600, P<**0.001**	$F_{3.5,56}$=2.505, P=0.060	$F_{3.5,56}$=4.643, P<**0.01**
Lic1	$F_{1,12}$=33.269, P<**0.001**	$F_{1,12}$=0.960, P=0.346	$F_{1,12}$=13.029, P<**0.01**	$F_{2,33}$=62.743, P<**0.001**	$F_{2,33}$=6.875, P<**0.01**	$F_{2,33}$=1.853, P=0.172	$F_{2,33}$=2.419, P=0.104
Lic2	$F_{1,12}$=98.123, P<**0.001**	$F_{1,12}$=10.519, P<**0.01**	$F_{1,12}$=6.008, P<**0.05**	$F_{3.3,53.4}$=162.341, P<**0.001**	$F_{3.3,53.4}$=10.183, P<**0.001**	$F_{3.3,53.4}$=3.988, P<**0.01**	$F_{3.3,53.4}$=2.216, P=0.091
SIPI	$F_{1,12}$=65.267, P<**0.001**	$F_{1,12}$=0.510, P=0.489	$F_{1,12}$=47.186, P<**0.001**	$F_{4.6,74.4}$=58.103, P<**0.001**	$F_{4.6,74.4}$=6.961, P<**0.001**	$F_{4.6,74.4}$=1.533, P=0.194	$F_{4.6,74.4}$=6.550, P<**0.001**
GM1	$F_{1,12}$=118.366, P<**0.001**	$F_{1,12}$=6.127, P<**0.05**	$F_{1,12}$=51.745, P<**0.001**	$F_{4,66.3}$=67.25, P<**0.001**	$F_{4,66.3}$=12.185, P<**0.001**	$F_{4,66.3}$=1.274, P=0.289	$F_{4,66.3}$=8.255, P<**0.001**
GM2	$F_{1,12}$=129.417, P<**0.001**	$F_{1,12}$=8.692, P<**0.05**	$F_{1,12}$=34.177, P<**0.001**	$F_{4.4,70.5}$=140.815, P<**0.001**	$F_{4.4,70.5}$=10.647, P<**0.001**	$F_{4.4,70.5}$=3.043, P<**0.05**	$F_{4.4,70.5}$=6.862, P<**0.001**
ARI1	$F_{1,12}$=2.492, P=0.140	$F_{1,12}$=1.162, P=0.302	$F_{1,12}$=6.302, P<**0.05**	$F_{1.6,25.5}$=35.815, P<**0.001**	$F_{1.6,25.5}$=4.375, P<**0.05**	$F_{1.6,25.5}$=1.985, P=0.165	$F_{1.6,25.5}$=1.548, P=0.232
ARI2	$F_{1,12}$=2.305, P=0.155	$F_{1,12}$=1.187, P=0.297	$F_{1,12}$=8.190, P<**0.05**	$F_{1.7,26.5}$=33.276, P<**0.001**	$F_{1.7,26.5}$=4.890, P<**0.05**	$F_{1.7,26.5}$=2.211, P=0.137	$F_{1.7,26.5}$=1.639, P=0.215
CRI1	$F_{1,12}$=81.086, P<**0.001**	$F_{1,12}$=0.263, P=0.617	$F_{1,12}$=25.724, P<**0.001**	$F_{4.8,77}$=38.096, P<**0.001**	$F_{4.8,77}$=4.845, P<**0.001**	$F_{4.8,77}$=1.113, P=0.360	$F_{4.8,77}$=4.459, P<**0.01**
CRI2	$F_{1,12}$=27.284, P<**0.001**	$F_{1,12}$=0.924, P=0.355	$F_{1,12}$=23.756, P<**0.001**	$F_{2.8,44}$=6.947, P<**0.001**	$F_{2.8,44}$=2.529, P=0.074	$F_{2.8,44}$=0.608, P=0.600	$F_{2.8,44}$=3.908, P<**0.05**
RDVI	$F_{1,12}$=21.289, P<**0.001**	$F_{1,12}$=0.803, P=0.388	$F_{1,12}$=18.592, P<**0.01**	$F_{1.9,30.5}$=55.647, P<**0.001**	$F_{1.9,30.5}$=7.373, P<**0.01**	$F_{1.9,30.5}$=1.486, P=0.242	$F_{1.9,30.5}$=2.275, P=0.122

PRI_550	$F_{1,12}$=2.916, *P*=0.113	$F_{1,12}$=7.991, *P*<**0.05**	$F_{1,12}$=2.279, *P*=0.157	$F_{2.4,38.6}$=26.449, *P*<**0.001**	$F_{2.4,38.6}$=2.443, *P*=0.091	$F_{2.4,38.6}$=2.651, *P*=0.074	$F_{2.4,38.6}$=3.328, *P*<**0.05**
PRI_norm	$F_{1,12}$=0.297, *P*=0.596	$F_{1,12}$=0.013, *P*=0.910	$F_{1,12}$=1.650, *P*=0.223	$F_{1,16}$=3.219, *P*=0.092	$F_{1,16}$=0.247, *P*=0.626	$F_{1,16}$=0.022, *P*=0.884	$F_{1,16}$=1.868, *P*=0.191
PRI/NDVI	$F_{1,12}$=2.850, *P*=0.117	$F_{1,12}$=0.013, *P*=0.910	$F_{1,12}$=1.315, *P*=0.274	$F_{1,16}$=9.658, *P*<**0.01**	$F_{1,16}$=1.804, *P*=0.198	$F_{1,16}$=0.031, *P*=0.866	$F_{1,16}$=1.741, *P*=0.206
GNDVI_780	$F_{1,12}$=61.883, *P*<**0.001**	$F_{1,12}$=3.118, *P*=0.103	$F_{1,12}$=55.354, *P*<**0.001**	$F_{4,65.6}$=61.495, *P*<**0.001**	$F_{4,65.6}$=12.543, *P*<**0.001**	$F_{4,65.6}$=0.784, *P*=0.543	$F_{4,65.6}$=9.305, *P*<**0.001**
MRESR	$F_{1,12}$=128.244, *P*<**0.001**	$F_{1,12}$=16.706, *P*<**0.01**	$F_{1,12}$=46.811, *P*<**0.001**	$F_{5.2,83.8}$=99.584, *P*<**0.001**	$F_{5.2,83.8}$=11.601, *P*<**0.001**	$F_{5.2,83.8}$=2.718, *P*<**0.05**	$F_{5.2,83.8}$=6.334, *P*<**0.001**
RENDVI	$F_{1,12}$=129.217, *P*<**0.001**	$F_{1,12}$=12.446, *P*<**0.01**	$F_{1,12}$=55.461, *P*<**0.001**	$F_{4.4,70}$=119.693, *P*<**0.001**	$F_{4.4,70}$=12.025, *P*<**0.001**	$F_{4.4,70}$=2.772, *P*<**0.05**	$F_{4.4,70}$=6.275, *P*<**0.001**
NDRE	$F_{1,12}$=133.386, *P*<**0.001**	$F_{1,12}$=18.080, *P*<**0.01**	$F_{1,12}$=57.081, *P*<**0.001**	$F_{5,80}$=108.917, *P*<**0.001**	$F_{5,80}$=10.836, *P*<**0.001**	$F_{5,80}$=2.872, *P*<**0.05**	$F_{5,80}$=7.181, *P*<**0.001**
CIgreen	$F_{1,12}$=76.664, *P*<**0.001**	$F_{1,12}$=6.938, *P*<**0.05**	$F_{1,12}$=63.164, *P*<**0.001**	$F_{4.8,76}$=61.198, *P*<**0.001**	$F_{4.8,76}$=12.624, *P*<**0.001**	$F_{4.8,76}$=1.529, *P=0.194*	$F_{4.8,76}$=8.514, *P*<**0.001**
CIrededge	$F_{1,12}$=132.412, *P*<**0.001**	$F_{1,12}$=19.031, *P*<**0.001**	$F_{1,12}$=57.428, *P*<**0.001**	$F_{5,81}$=103.713, *P*<**0.001**	$F_{5,81}$=10.827, *P*<**0.001**	$F_{5,81}$=2.936, *P*<**0.05**	$F_{5,81}$=7.264, *P*<**0.001**
mNDblue_530	$F_{1,12}$=79.911, *P*<**0.001**	$F_{1,12}$=5.736, *P*<**0.05**	$F_{1,12}$=37.803, *P*<**0.001**	$F_{4,66.6}$=71.269, *P*<**0.001**	$F_{4,66.6}$=10.473, *P*<**0.001**	$F_{4,66.6}$=1.313, *P*=0.273	$F_{4,66.6}$=6.702, *P*<**0.001**
mNDblue_730	$F_{1,12}$=1.993, *P*=0.183	$F_{1,12}$=8.454, *P*<**0.05**	$F_{1,12}$=20.623, *P*<**0.001**	$F_{4,63.5}$=29.281, *P*<**0.001**	$F_{4,63.5}$=2.990, *P*<**0.001**	$F_{4,63.5}$=1.844, *P*=0.132	$F_{4,63.5}$=6.237, *P*<**0.001**
rDVI_790	$F_{1,12}$=4.316, *P*=0.060	$F_{1,12}$=0.432, *P*=0.523	$F_{1,12}$=10.946, *P*<**0.05**	$F_{1.9,30.6}$=37.901, *P*<**0.001**	$F_{1.9,30.6}$=5.941, *P*<**0.05**	$F_{1.9,30.6}$=0.694, *P*=0.501	$F_{1.9,30.6}$=2.662, *P*=0.088
gSRa_790	$F_{1,12}$=76.664, *P*<**0.001**	$F_{1,12}$=6.938, *P*<**0.05**	$F_{1,12}$=63.164, *P*<**0.001**	$F_{4.8,76}$=61.198, *P*<**0.001**	$F_{4.8,76}$=12.625, *P*<**0.001**	$F_{4.8,76}$=1.529, *P*=0.194	$F_{4.8,76}$=8.514, *P*<**0.001**
SRa_790	$F_{1,12}$=45.166, *P*<**0.001**	$F_{1,12}$=3.663, *P*=0.080	$F_{1,12}$=30.725, *P*<**0.001**	$F_{3.5,56.6}$=92.727, *P*<**0.001**	$F_{3.5,56.6}$=8.763, *P*<**0.001**	$F_{3.5,56.6}$=2.488, *P*=0.060	$F_{3.5,56.6}$=2.614, *P*=0.051

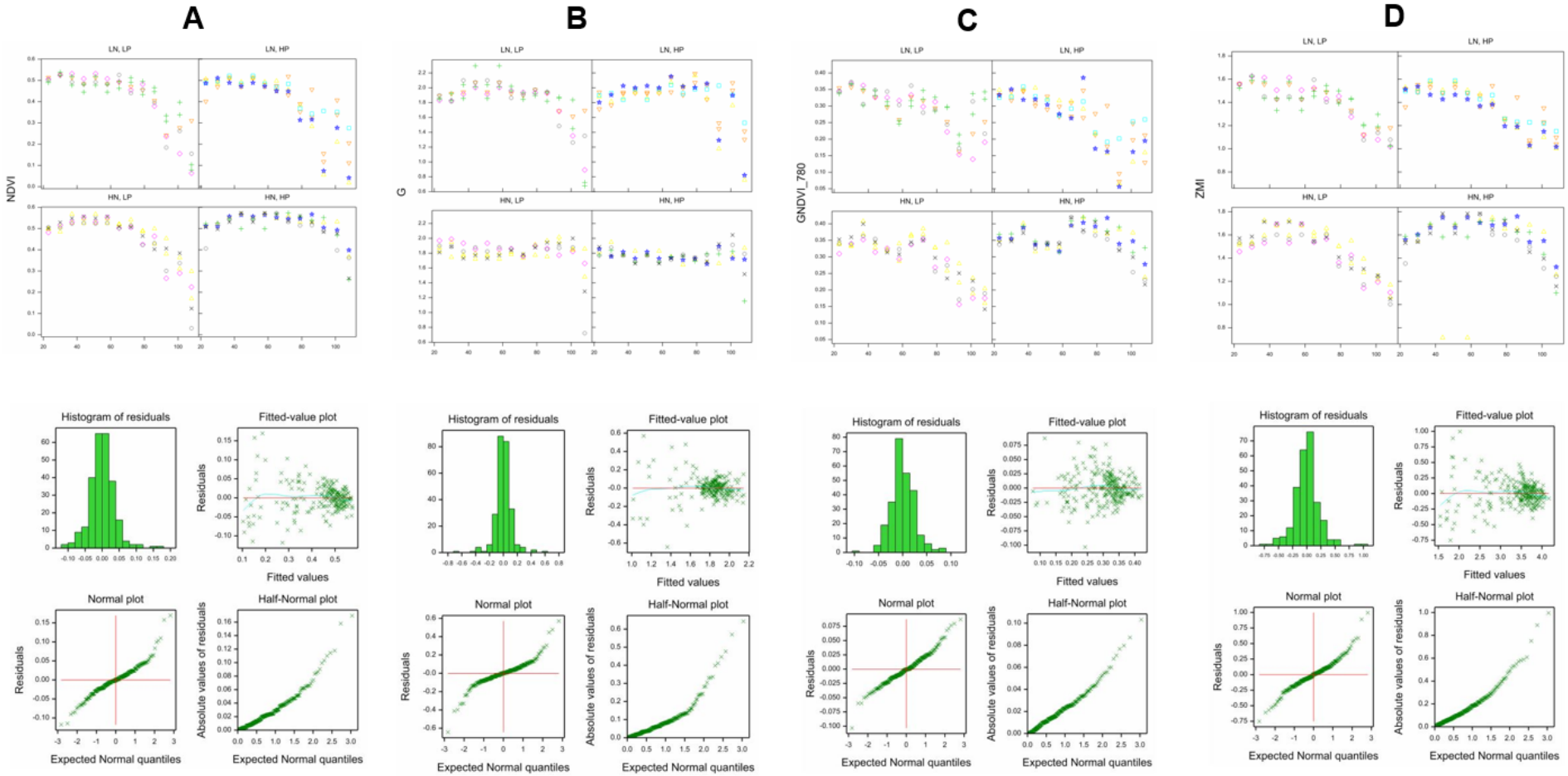

Figure B-4. Raw data distribution and residual plots of some N stress-specific SRIs for quinoa including (A) NDVI, (B) G, (C) GNDVI_780 and (D) ZMI. The residuals were examined to verify the assumptions of normality (using histograms) and homogeneity of variance (using plots of fitted values).

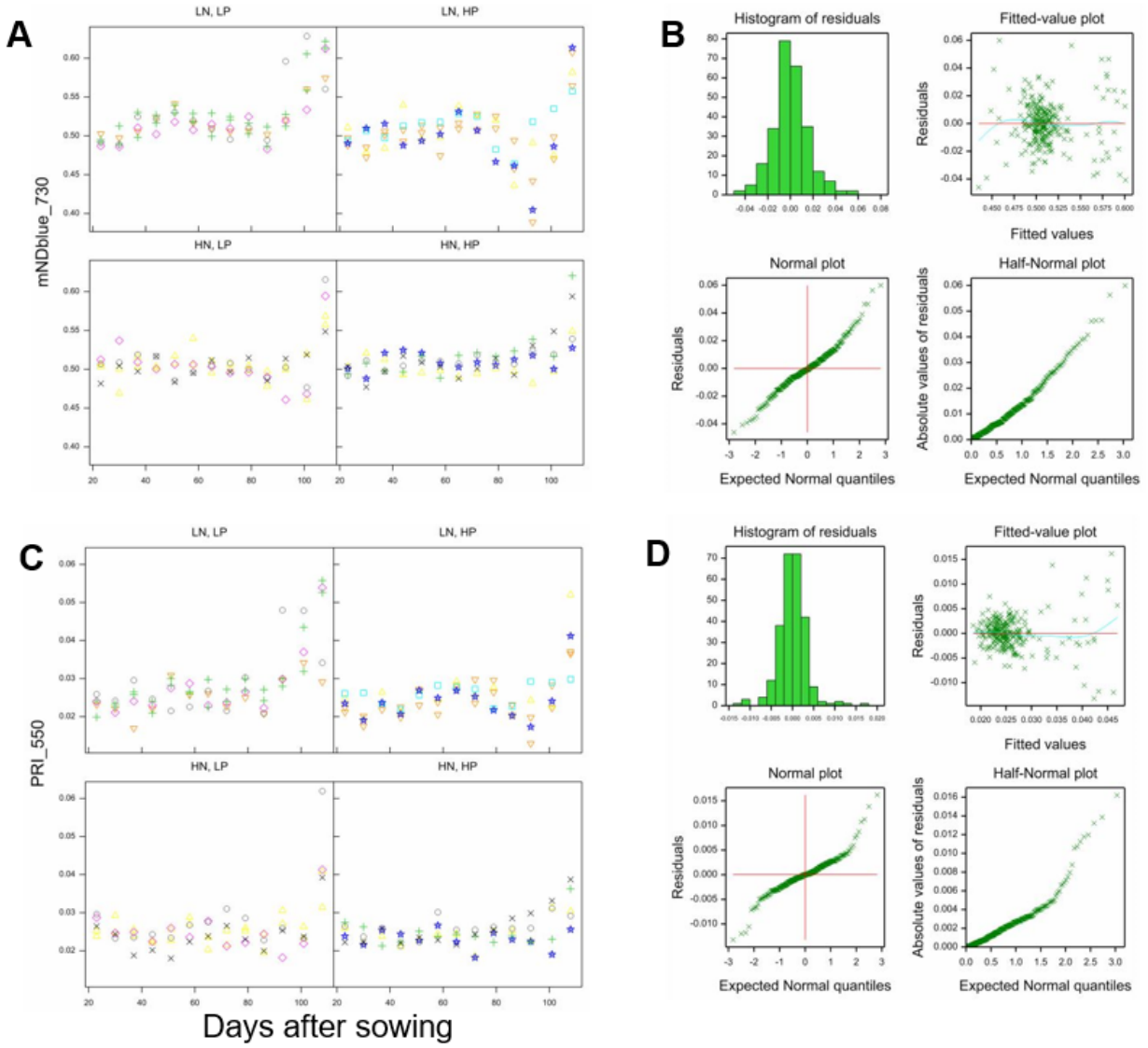

Figure B-5. Raw data distribution and residual plots of P stress-specific SRIs for quinoa. Raw data distribution for (A) mNDblue_780, residual plots for (B) mNDblue_780, raw data distribution for (C) PRI_550 and residual plots for (D) PRI_550. The residuals were examined to verify the assumptions of normality (using histogram plots) and homogeneity of variance (using plots of fitted values).

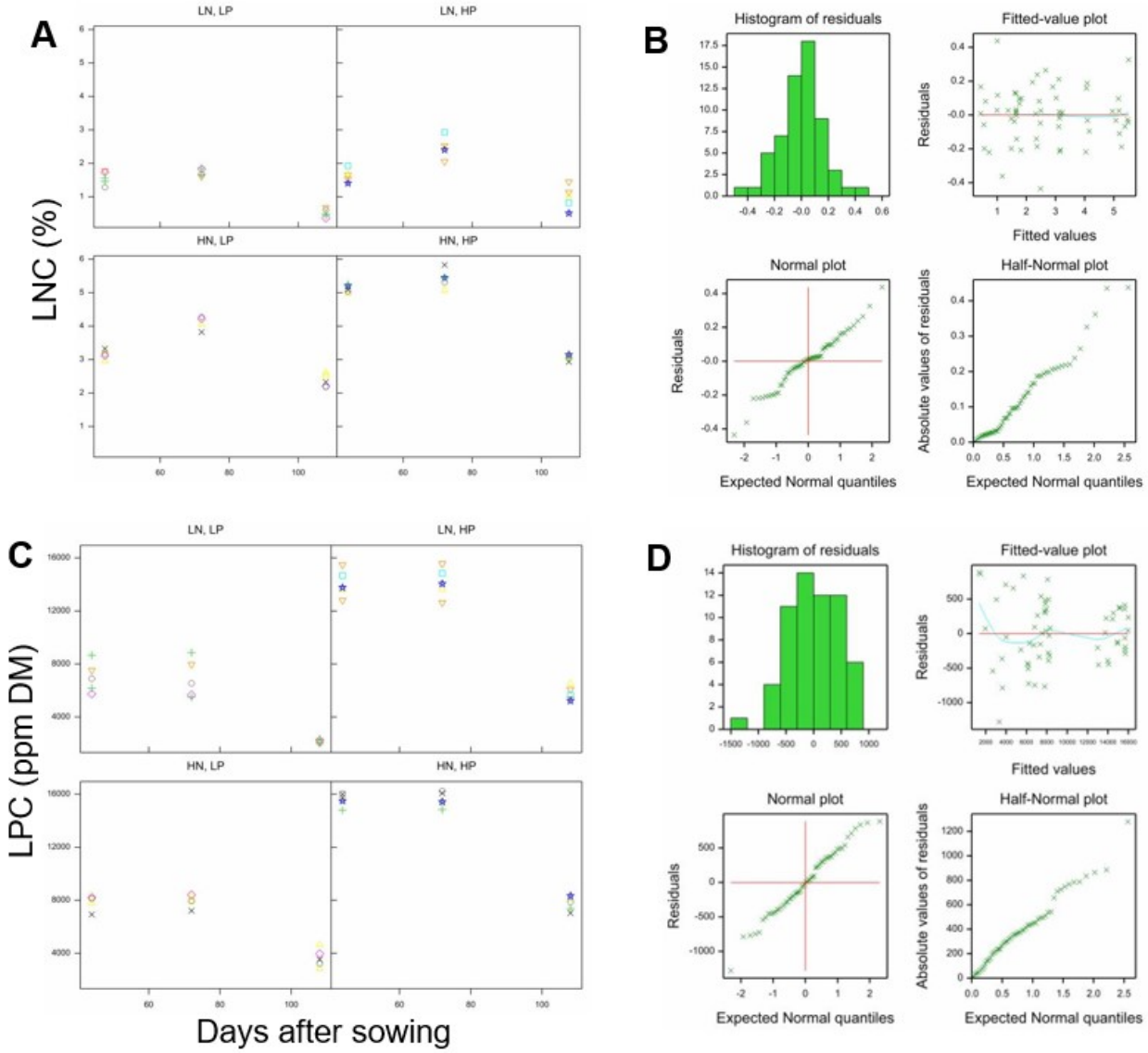

Figure B-6. Raw data distribution and residual plots of quinoa nutritional status parameters. Raw data distribution for (A) leaf nitrogen content (LNC), residual plots and fitted value plots for (B) LNC, raw data distribution for (C) leaf phosphorus concentration (LPC) and residual plots and fitted value plots for (D) LPC. Residuals were inspected to check the assumptions of normality (via histogram plots) and variance homogeneity (via fitted values plots).

Table B-2. Full results of the test for main effects of spectral reflectance indices (SRIs) in response to nitrogen (N) and phosphorus (P) stress separately and their combined effects in cowpea. The responses of the SRIs to N and P stresses and their interactions were tested using the F-statistics and F-Test probability via repeated measures ANOVA (RMA). The RMA analysis was done considering all treatment combinations and time points (DAS). The statistically significant results (p<0.05) indicating differences between means for levels of N or P and their interactions are shown in bold.

Index	**N**	**P**	**N×P**	**DAS**	**N×DAS**	**P×DAS**	**N×P×DAS**
NDVI	$F_{1,12}$=25.143, P<**0.01**	$F_{1,12}$=13.557, P<**0.05**	$F_{1,12}$=8.511, P<**0.05**	$F_{4.6,74}$=64.307, P<**0.001**	$F_{4.6,74}$=2.707, P<**0.05**	$F_{4.6,74}$=5.490, P<**0.01**	$F_{4.6,74}$=2.836, P<**0.05**
SR	$F_{1,12}$=24.744, P<**0.01**	$F_{1,12}$=10.751, P<**0.05**	$F_{1,12}$=7.666, P<**0.05**	$F_{6,95}$=61.718, P<**0.001**	$F_{6,95}$=2.279, P<**0.05**	$F_{6,95}$=3.441, P<**0.05**	$F_{6,95}$=2.670, P<**0.05**
MCARI1	$F_{1,12}$=0.003, P=0.955	$F_{1,12}$=0.004, P=0.953	$F_{1,12}$=1.308, P=0.275	$F_{4,60.6}$=22.638, P<**0.001**	$F_{4,60.6}$=0.944, P=0.441	$F_{4,60.6}$=3.878, P<**0.05**	$F_{4,60.6}$=1.142, P=0.344
OSAVI	$F_{1,12}$=9.122, P<**0.05**	$F_{1,12}$=7.659, P<**0.05**	$F_{1,12}$=3.820, P=0.074	$F_{2.7,43}$=60.677, P<**0.001**	$F_{2.7,43}$=2.098, P=0.120	$F_{2.7,43}$=7.520, P<**0.01**	$F_{2.7,43}$=1.623, P=0.201
G	$F_{1,12}$=23.461, P<**0.01**	$F_{1,12}$=2.429, P=0.145	$F_{1,12}$=4.343, P=0.059	$F_{5,80}$=19.883, P<**0.001**	$F_{5,80}$=1.899, P=0.104	$F_{5,80}$=4.800, P<**0.01**	$F_{5,80}$=1.188, P=0.322
MCARI	$F_{1,12}$=36.796, P<**0.001**	$F_{1,12}$=11.570, P<**0.05**	$F_{1,12}$=7.256, P<**0.05**	$F_{5.3,84}$=6.991, P<**0.001**	$F_{5.3,84}$=1.656, P=0.151	$F_{5.3,84}$=2.748, P<**0.05**	$F_{5.3,84}$=1.102, P=0.358
TCARI	$F_{1,12}$=16.668, P<**0.05**	$F_{1,12}$=15.365, P<**0.05**	$F_{1,12}$=6.580, P<**0.05**	$F_{4.3,68.3}$=23.753, P<**0.001**	$F_{4.3,68.3}$=1.868, P=0.122	$F_{4.3,68.3}$=4.161, P<**0.05**	$F_{4.3,68.3}$=1.751, P=0.145
TVI	$F_{1,12}$=0.729, P=0.410	$F_{1,12}$=0.178, P=0.681	$F_{1,12}$=0.392, P=0.543	$F_{3.7,60}$=25.607, P<**0.001**	$F_{3.7,60}$=1.014, P=0.404	$F_{3.7,60}$=4.029, P<**0.05**	$F_{3.7,60}$=1.086, P=0.370
ZMI	$F_{1,12}$=46.102, P<**0.001**	$F_{1,12}$=19.752, P<**0.01**	$F_{1,12}$=13.619, P<**0.05**	$F_{6,95}$=30.344, P<**0.001**	$F_{6,95}$=2.187, P=0.052	$F_{6,95}$=2.816, P<**0.05**	$F_{6,95}$=1.889, P=0.092
SPRI	$F_{1,12}$=31.313, P<**0.01**	$F_{1,12}$=22.642, P<**0.01**	$F_{1,12}$=1.322, P=0.273	$F_{4.2,66.8}$=35.836, P<**0.001**	$F_{4.2,66.8}$=1.896, P=0.119	$F_{4.2,66.8}$=4.690, P<**0.05**	$F_{4.2,66.8}$=1.956, P=0.109
NPQI	$F_{1,12}$=1.835, P=0.201	$F_{1,12}$=0.276, P=0.609	$F_{1,12}$=0.039, P=0.847	$F_{5.4,86.3}$=2.328, P<**0.05**	$F_{5.4,86.3}$=1.745, P=0.128	$F_{5.4,86.3}$=1.205, P=0.313	$F_{5.4,86.3}$=0.524, P=0.770
PRI	$F_{1,12}$=39.830, P<**0.001**	$F_{1,12}$=21.786, P<**0.01**	$F_{1,12}$=2.553, P=0.136	$F_{3.5,56}$=59.543, P<**0.001**	$F_{3.5,56}$=1.819, P=0.146	$F_{3.5,56}$=5.832, P<**0.01**	$F_{3.5,56}$=2.314, P=0.077
NPCI	$F_{1,12}$=24.277, P<**0.01**	$F_{1,12}$=19.903, P<**0.01**	$F_{1,12}$=0.750, P=0.404	$F_{3,49}$=36.979, P<**0.001**	$F_{3,49}$=1.725, P=0.173	$F_{3,49}$=5.667, P<**0.05**	$F_{3,49}$=1.739, P=0.170
Ctr1	$F_{1,12}$=41.462, P<**0.001**	$F_{1,12}$=15.159, P<**0.05**	$F_{1,12}$=2.678, P=0.128	$F_{6,94}$=9.332, P<**0.001**	$F_{6,94}$=1.544, P=0.174	$F_{6,94}$=1.270, P=0.279	$F_{6,94}$=1.444, P=0.207
Ctr2	$F_{1,12}$=30.144, P<**0.01**	$F_{1,12}$=19.676, P<**0.01**	$F_{1,12}$=9.259, P<**0.05**	$F_{4.7,75}$=56.460, P<**0.001**	$F_{4.7,75}$=2.628, P<**0.05**	$F_{4.7,75}$=5.639, P<**0.01**	$F_{4.7,75}$=2.582, P<**0.05**
Lic1	$F_{1,12}$=5.004, P<**0.05**	$F_{1,12}$=6.333, P<**0.05**	$F_{1,12}$=3.270, P=0.096	$F_{3,48}$=62.248, P<**0.001**	$F_{3,48}$=1.909, P=0.140	$F_{3,48}$=7.371, P<**0.01**	$F_{3,48}$=1.803, P=0.158
Lic2	$F_{1,12}$=40.725, P<**0.001**	$F_{1,12}$=18.699, P<**0.01**	$F_{1,12}$=3.512, P=0.085	$F_{5.8,93}$=14.832, P<**0.001**	$F_{5.8,93}$=2.012, P=0.074	$F_{5.8,93}$=1.816, P=0.107	$F_{5.8,93}$=1.398, P=0.225
SIPI	$F_{1,12}$=4.182, P=0.063	$F_{1,12}$=2.743, P=0.124	$F_{1,12}$=3.779, P=0.076	$F_{5,82.2}$=55.210, P<**0.001**	$F_{5,82.2}$=1.592, P=0.170	$F_{5,82.2}$=4.494, P<**0.05**	$F_{5,82.2}$=2.478, P<**0.05**
GM1	$F_{1,12}$=39.312, P<**0.001**	$F_{1,12}$=13.747, P<**0.05**	$F_{1,12}$=14.016, P<**0.05**	$F_{6,95}$=44.736, P<**0.001**	$F_{6,95}$=2.543, P<**0.05**	$F_{6,95}$=3.157, P<**0.05**	$F_{6,95}$=2.675, P<**0.05**
GM2	$F_{1,12}$=38.419, P<**0.001**	$F_{1,12}$=15.816, P<**0.05**	$F_{1,12}$=10.764, P<**0.05**	$F_{6,97}$=38.690, P<**0.001**	$F_{6,97}$=2.135, P=0.056	$F_{6,97}$=2.907, P<**0.05**	$F_{6,97}$=1.986, P=0.074
ARI1	$F_{1,12}$=0.045, P=0.835	$F_{1,12}$=0.606, P=0.451	$F_{1,12}$=3.191, P=0.099	$F_{4.8,76}$=20.859, P<**0.001**	$F_{4.8,76}$=0.795, P=0.551	$F_{4.8,76}$=0.775, P=0.565	$F_{4.8,76}$=2.711, P<**0.05**
ARI2	$F_{1,12}$=0.060, P=0.811	$F_{1,12}$=1.509, P=0.243	$F_{1,12}$=8.808, P<**0.05**	$F_{5.6,89.7}$=24.861, P<**0.001**	$F_{5.6,89.7}$=0.814, P=0.555	$F_{5.6,89.7}$=0.952, P=0.459	$F_{5.6,89.7}$=2.280, P<**0.05**
CRI1	$F_{1,12}$=0.296, P=0.596	$F_{1,12}$=0.078, P=0.784	$F_{1,12}$=0.344, P=0.568	$F_{4,65}$=36.406, P<**0.001**	$F_{4,65}$=0.809, P=0.525	$F_{4,65}$=2.067, P=0.094	$F_{4,65}$=1.360, P=0.257
CRI2	$F_{1,12}$=0.415, P=0.710	$F_{1,12}$=0.001, P=0.973	$F_{1,12}$=0.629, P=0.443	$F_{3.7,58}$=36.744, P<**0.001**	$F_{3.7,58}$=0.685, P=0.594	$F_{3.7,58}$=1.952, P=0.119	$F_{3.7,58}$=1.846, P=0.137
RDVI	$F_{1,12}$=12.260, P<**0.05**	$F_{1,12}$=6.450, P<**0.05**	$F_{1,12}$=2.721, P=0.125	$F_{2.8,45.3}$=50.550, P<**0.001**	$F_{2.8,45.3}$=1.841, P=0.156	$F_{2.8,45.3}$=6.374, P<0.05	$F_{2.8,45.3}$=1.339, P=*0.274*
PRI_550	$F_{1,12}$=22.013, P<**0.01**	$F_{1,12}$=12.702, P<**0.05**	$F_{1,12}$=0.000, P=0.979	$F_{5,80}$ =395.618, P<**0.001**	$F_{5,80}$ =1.640, P=0.159	$F_{5,80}$ =1.425, P=0.224	$F_{5,80}$ =1.062, P=0.388

PRI_norm	$F_{1,12}$=22.013, *P*<**0.01**	$F_{1,12}$=12.702, *P*<**0.05**	$F_{1,12}$=0.001, *P*=0.979	$F_{5,80}$=395.618, *P*<**0.001**	$F_{5,80}$=1.640, *P*=0.159	$F_{5,80}$=1.425, *P*=0.224	$F_{5,80}$=1.062, *P*=0.388
PRI/NDVI	$F_{1,12}$=4.962, *P*<**0.05**	$F_{1,12}$=11.827, *P*<**0.05**	$F_{1,12}$=0.015, *P*=0.905	$F_{1,16.7}$=20.330, *P*<**0.01**	$F_{1,16.7}$=1.400, *P*=0.255	$F_{1,16.7}$=7.536, *P*<**0.05**	$F_{1,16.7}$=0.059, *P*=0.822
GNDVI_780	$F_{1,12}$=45.426, *P*<**0.001**	$F_{1,12}$=14.389, *P*<**0.05**	$F_{1,12}$=5.474, *P*<**0.05**	$F_{3.7,60}$=614.263, *P*<**0.001**	$F_{3.7,60}$=8.426, *P*<**0.001**	$F_{3.7,60}$=2.602, *P*<**0.05**	$F_{3.7,60}$=3.040, *P*<**0.05**
MRESR	$F_{1,12}$=167.352, *P*<0**.001**	$F_{1,12}$=52.680, *P*<**0.001**	$F_{1,12}$=11.288, *P*<**0.05**	$F_{5,82}$=30.944, *P*<**0.001**	$F_{5,82}$=7.693, *P*<**0.001**	$F_{5,82}$=1.626, *P*=0.161	$F_{5,82}$=2.079, *P*=0.075
RENDVI	$F_{1,12}$=55.619, *P*<**0.001**	$F_{1,12}$=20.721, *P*<**0.01**	$F_{1,12}$=4.695, *P*=0.051	$F_{4.3,68.8}$=401.795, *P*<**0.001**	$F_{4.3,68.8}$=8.735, *P*<**0.001**	$F_{4.3,68.8}$=2.333, *P*=0.059	$F_{4.3,68.8}$=2.297, *P*=0.063
NDRE	$F_{1,12}$=57.549, *P*<**0.001**	$F_{1,12}$=18.749, *P*<**0.01**	$F_{1,12}$=6.782, *P*<**0.05**	$F_{5,80}$=289.325, *P*<**0.001**	$F_{5,80}$=9.651, *P*<**0.001**	$F_{5,80}$=2.085, *P*=0.076	$F_{5,80}$=2.119, *P*=0.072
CIgreen	$F_{1,12}$=54.387, *P*<**0.001**	$F_{1,12}$=15.770, *P*<**0.05**	$F_{1,12}$=5.392, *P*<**0.05**	$F_{3.7,59.3}$=260.367, *P*<**0.001**	$F_{3.7,59.3}$=8.905, *P*<**0.001**	$F_{3.7,59.3}$=2.020, *P*=0.108	$F_{3.7,59.3}$=2.916, *P*<**0.05**
CIrededge	$F_{1,12}$=65.525, *P*<**0.001**	$F_{1,12}$=20.862, *P*<**0.01**	$F_{1,12}$=7.150, *P*<**0.05**	$F_{4.8,77}$=229.619, *P*<**0.001**	$F_{4.8,77}$=9.816, *P*<**0.001**	$F_{4.8,77}$=1.938, *P*=0.100	$F_{4.8,77}$=2.152, *P*=0.070
mNDblue_530	$F_{1,12}$=134.749, *P*<**0.001**	$F_{1,12}$=37.657, *P*<**0.001**	$F_{1,12}$=8.687, *P*<**0.05**	$F_{5.3,84.7}$=993.998, *P*<**0.001**	$F_{5.3,84.7}$=8.906, *P*<**0.001**	$F_{5.3,84.7}$=1.567, *P*=0.175	$F_{5.3,84.7}$=2.437, *P*<**0.05**
mNDblue_730	$F_{1,12}$=0.002, *P*=0.967	$F_{1,12}$=0.036, *P*=0.852	$F_{1,12}$=0.924, *P*=0.355	$F_{4.3,69.5}$=2773.273, *P*<**0.001**	$F_{4.3,69.5}$=0.796, *P*=0.541	$F_{4.3,69.5}$=2.582, *P*<**0.05**	$F_{4.3,69.5}$=0.774, *P*=0.555
rDVI_790	$F_{1,12}$=21.864, *P*<**0.01**	$F_{1,12}$=2.757, *P*=0.123	$F_{1,12}$=2.757, *P*=0.123	$F_{4.6,73.8}$=1896.738, *P*<**0.001**	$F_{4.6,73.8}$=2.001, *P*=0.094	$F_{4.6,73.8}$=2.021, *P*=0.091	$F_{4.6,73.8}$=1.228, *P*=0.305
gSRa_790	$F_{1,12}$=54.387, *P*<**0.001**	$F_{1,12}$=15.770, *P*<**0.05**	$F_{1,12}$=5.392, *P*<**0.05**	$F_{3.7,59.3}$=260.367, *P*<**0.001**	$F_{3.7,59.3}$=8.905, *P*<**0.001**	$F_{3.7,59.3}$=2.020, *P*=0.108	$F_{3.7,59.3}$=2.916, *P*<**0.05**
SRa_790	$F_{1,12}$=14.442, *P*<**0.05**	$F_{1,12}$=6.607, *P*<**0.05**	$F_{1,12}$=0.469, *P*=0.506	$F_{3.6,57}$=269.367, *P*<**0.001**	$F_{3.6,57}$=4.831, *P*<**0.05**	$F_{3.6,57}$=2.533, *P*=0.057	$F_{3.6,57}$=1.773, *P*=0.154

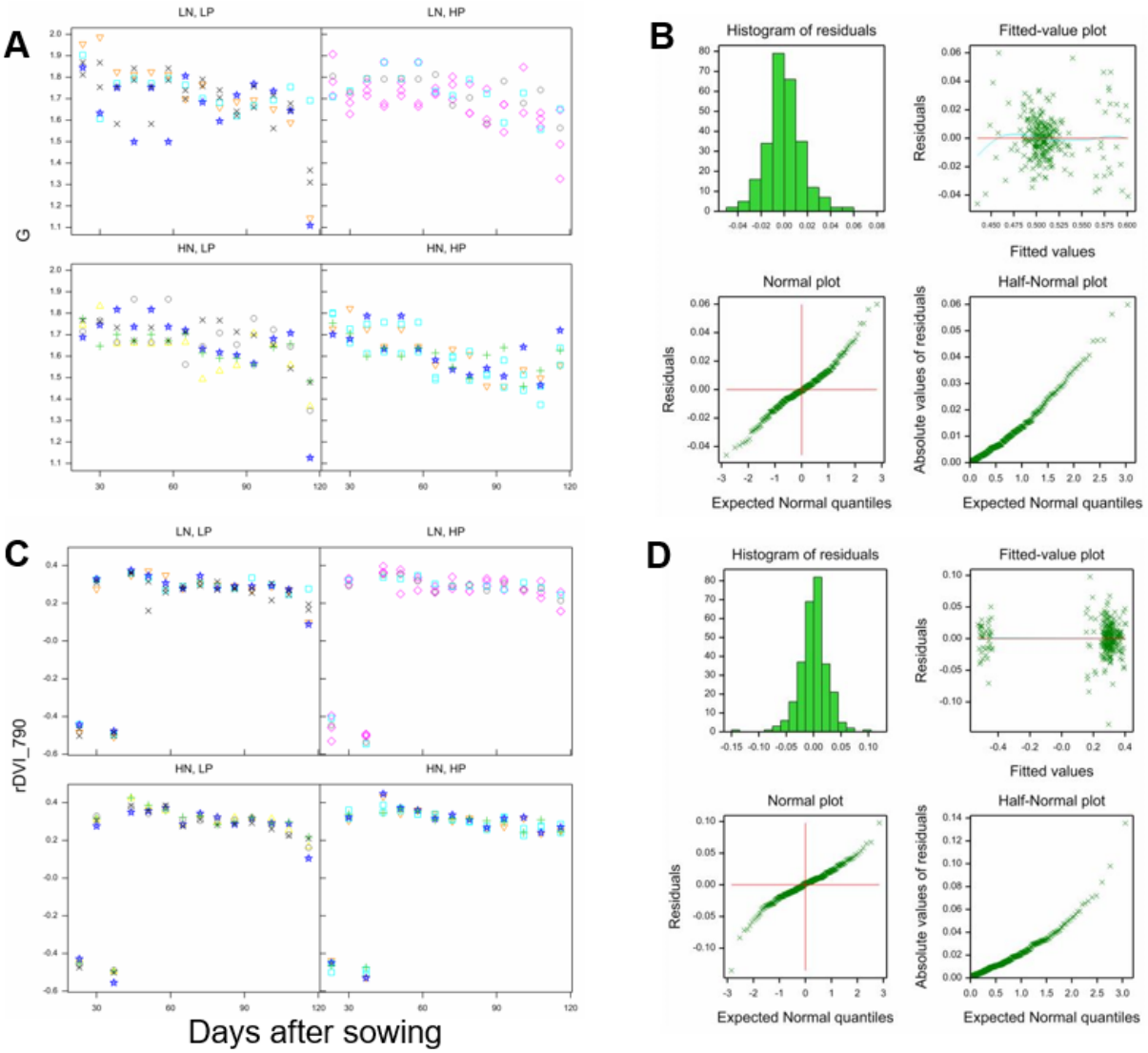

Figure B-7. Raw data distribution and residual plots of N stress-specific SRIs identified for cowpea. Raw data distribution for (A) G, residual plots for (B) G, raw data distribution for (C) rDVI_790 and residual plots for (D) rDVI_790. The residuals were inspected to verify the assumptions of normality (using histogram plots) and homogeneity of variance (using plots of fitted values).

Appendix C Supplementary materials for Chapter 4

Table C-1. Full results of descriptive statistics (Means, Absolute Diff., and Approx. LSD) of morpho-physiological parameters including net CO_2 assimilation rate (A_n), stomatal conductance (G_s), transpiration rate (E), intrinsic water use efficiency (WUEi), SPAD, leaf nitrogen content (LNC), relative water content (RWC), shoot fresh weight (SFW), leaf area (LA) and soil moisture content (SMC) in response to drought under high nitrogen (HN) and low nitrogen (LN) conditions and their interactions. Analysis was based on the LMM/REML Autocorrelation (AR1) model fitted in the D-N order of terms. The means are estimations from the Autocorrelation (AR1) model. Means of E, LA and SFW were squarely rooted to conform to the residuals of the analysis. Absolute difference (Absolute Diff) values or pairwise differences between treatment means and days after water stress (DAWS) greater than the approximate (Approx) least significant differences (LSDs) at a 5% level of REML means are considered statistically significant and bolded.

Model term		**D×N×DAWS**								**D×DAWS**				**N×DAWS**				**DAWS**
Treatment		**HN**				**LN**												
		Drought	**Well-watered**	**Absolute Diff.**	**Approx. LSD**	**Drought**	**Well-watered**	**Absolute Diff.**	**Approx. LSD**	**Drought**	**Well-watered**	**Absolute Diff.**	**Approx. LSD**	**HN**	**LN**	**Absolute Diff.**	**Approx. LSD**	**Mean**
Parameter	**DAWS**																	
***An* (µmol CO_2 m^{-2} s^{-1})**	0	23.49	27.59	4.10	4.33	20.75	20.99	0.24	4.33	22.12	24.29	2.17	3.06	25.54	20.87	**4.67**	3.06	23.21
	3	23.49	27.71	4.22	4.33	19.12	20.59	1.46	4.33	21.31	24.15	2.84	3.06	25.60	19.86	**5.75**	3.06	22.73
	6	16.91	28.25	**11.34**	4.33	19.49	19.29	0.20	4.33	18.20	23.77	**5.57**	3.06	22.58	19.39	**3.19**	3.06	20.99
	9	14.02	27.04	**13.02**	4.33	16.29	16.82	0.53	4.33	15.16	21.93	**6.77**	3.06	20.53	16.56	**3.97**	3.06	18.54
	12	3.24	23.55	**20.31**	4.33	7.82	13.82	**6.00**	4.33	5.53	18.68	**13.15**	3.06	13.40	10.82	2.58	3.06	12.11
	14	0.16	22.32	**22.16**	4.47	1.18	10.92	**9.74**	4.33	0.67	16.62	**15.95**	3.06	11.24	6.05	**5.19**	3.11	8.65
	Mean	13.55	26.08	**12.52**	4.35	14.11	17.07	3.03	4.33	13.83	21.57	**7.74**	3.06	19.82	15.59	**4.22**	3.07	17.70
***Gs* (mmol H_2O m^{-2} s^{-1})**	0	0.27	0.35	**0.09**	0.06	0.25	0.25	0.01	0.06	0.26	0.30	0.04	0.04	0.31	0.25	**0.06**	0.04	0.28
	3	0.25	0.33	**0.08**	0.06	0.23	0.27	0.04	0.06	0.24	0.30	**0.06**	0.04	0.29	0.25	0.04	0.04	0.27
	6	0.13	0.36	**0.23**	0.06	0.25	0.26	0.01	0.06	0.19	0.31	**0.12**	0.04	0.24	0.26	0.01	0.04	0.25
	9	0.11	0.36	**0.25**	0.06	0.19	0.26	**0.07**	0.06	0.15	0.31	**0.16**	0.04	0.23	0.23	0.00	0.04	0.23
	12	0.02	0.31	**0.29**	0.06	0.07	0.21	**0.14**	0.06	0.04	0.26	**0.21**	0.04	0.17	0.14	0.03	0.04	0.15
	14	0.01	0.29	**0.28**	0.06	0.01	0.20	**0.18**	0.06	0.01	0.24	**0.23**	0.04	0.15	0.10	**0.05**	0.04	0.13
	Mean	0.13	0.33	**0.20**	0.06	0.17	0.24	**0.07**	0.06	0.15	0.29	**0.14**	0.04	0.23	0.20	0.03	0.04	0.22
***E* (mol H_2O m^{-2} s^{-1})**	0	0.0034	0.0039	0.0005	0.0006	0.0034	0.0032	0.0001	0.0006	0.0034	0.0035	0.0002	0.0004	0.0036	0.0033	0.0003	0.0004	0.0035
	3	0.0032	0.0037	0.0005	0.0006	0.0031	0.0034	0.0003	0.0006	0.0031	0.0036	0.0004	0.0004	0.0034	0.0032	0.0002	0.0004	0.0033
	6	0.0020	0.0041	**0.0021**	0.0006	0.0039	0.0038	0.0001	0.0006	0.0030	0.0039	**0.0010**	0.0004	0.0031	0.0038	**0.0008**	0.0004	0.0034
	9	0.0012	0.0028	**0.0016**	0.0006	0.0021	0.0024	0.0004	0.0006	0.0016	0.0026	**0.0010**	0.0004	0.0020	0.0022	0.0003	0.0004	0.0021
	12	0.0003	0.0028	**0.0025**	0.0006	0.0011	0.0023	**0.0013**	0.0006	0.0007	0.0025	**0.0019**	0.0004	0.0015	0.0017	0.0001	0.0004	0.0016
	14	0.0002	0.0032	**0.0031**	0.0006	0.0002	0.0023	**0.0021**	0.0006	0.0002	0.0028	**0.0026**	0.0004	0.0017	0.0013	0.0004	0.0004	0.0015
	Mean	0.0017	0.0034	**0.0017**	0.0006	0.0023	0.0029	**0.0007**	0.0006	0.0020	0.0032	**0.0012**	0.0004	0.0026	0.0026	0.0004	0.0004	0.0026

Table C-1 continued

WUEi (µmol CO_2 mmol H_2O)	0	88.39	79.21	9.18	23.86	83.45	87.26	3.80	23.86	85.92	83.23	2.69	16.92	83.80	85.35	1.55	16.35	84.58
	3	95.14	84.43	10.71	23.86	83.72	76.72	7.01	23.86	89.43	80.57	8.86	16.92	89.79	80.22	9.57	16.35	85.00
	6	134.68	80.34	**54.35**	23.86	78.62	74.02	4.61	23.86	106.65	77.18	**29.48**	16.92	107.51	76.32	**31.19**	16.35	91.92
	9	140.10	76.56	**63.54**	23.86	84.87	63.37	21.50	23.86	112.48	69.97	**42.52**	16.92	108.33	74.12	**34.22**	16.35	91.23
	12	138.22	76.18	**62.04**	23.86	115.94	66.04	**49.90**	23.86	127.08	71.11	**55.97**	16.92	107.20	90.99	16.21	16.35	99.09
	14	73.81	77.12	3.30	25.82	75.49	52.43	23.06	23.86	74.65	64.77	9.88	16.92	75.46	63.96	11.50	17.03	69.71
	Mean	111.72	78.97	**33.85**	24.19	87.01	69.97	17.04	23.86	99.37	74.47	**24.90**	16.92	95.35	78.49	**17.37**	16.46	86.92
SPAD	0	44.72	44.04	0.68	4.42	43.0	40.2	2.79	4.42	43.87	42.13	1.74	3.13	44.38	41.62	2.76	3.13	43.00
	3	41.25	46.66	**5.41**	4.42	41.9	41.1	0.82	4.42	41.57	43.87	2.29	3.13	43.96	41.49	2.47	3.13	42.72
	6	40.10	50.34	**10.24**	4.42	36.8	42.0	**5.22**	4.42	38.43	46.16	**7.73**	3.13	45.22	39.37	**5.85**	3.13	42.29
	9	36.22	51.28	**15.06**	4.42	35.5	41.7	**6.21**	4.42	35.87	46.50	**10.63**	3.13	43.75	38.62	**5.13**	3.13	41.19
	12	34.45	48.48	**14.03**	4.42	32.0	35.6	3.60	4.42	33.22	42.04	**8.82**	3.13	41.47	33.80	**7.66**	3.13	37.63
	14	31.00	49.04	**18.04**	4.42	31.1	37.6	**6.50**	4.42	31.05	43.32	**12.27**	3.13	40.02	34.35	**5.67**	3.13	37.19
	Mean	37.96	48.31	**10.58**	4.42	36.7	39.7	4.19	4.42	37.34	44.00	**7.25**	3.13	43.13	38.21	**4.92**	3.13	40.67
LNC (%)	0	5.04	4.96	0.09	0.49	3.46	3.42	0.04	0.49	4.25	4.19	0.06	0.35	5.00	3.44	1.56	0.35	4.22
	3	-	-	-	-	-	-	-	-	-	-	-	-	-	-	-	-	-
	6	-	-	-	-	-	-	-	-	-	-	-	-	-	-	-	-	-
	9	5.15	5.11	0.04	0.55	2.56	2.62	0.06	0.49	3.85	3.86	0.01	0.37	5.13	2.59	2.54	0.37	3.86
	12	-	-	-	-	-	-	-	-	-	-	-	-	-	-	-	-	-
	14	4.70	4.90	0.20	0.38	2.36	2.29	0.07	0.38	3.53	3.59	0.06	0.27	4.80	2.32	2.47	0.27	3.56
	Mean	4.96	4.99	0.11	0.48	2.79	2.78	0.06	0.46	3.88	3.88	0.05	0.33	4.98	2.79	2.19	0.33	3.88
RWC (%)	0	-	-	-	-	-	-	-	-	-	-	-	-	-	-	-	-	-
	3	-	-	-	-	-	-	-	-	-	-	-	-	-	-	-	-	-
	6	-	-	-	-	-	-	-	-	-	-	-	-	-	-	-	-	-
	9	47.86	84.48	**36.62**	14.00	53.81	74.43	**20.62**	12.52	50.8	79.5	**28.6**	9.4	66.2	64.1	2.1	9.4	65.1
	12	-	-	-	-	-	-	-	-									
	14	40.77	87.24	**46.47**	10.29	47.31	73.87	**26.56**	10.29	44.0	80.6	**36.5**	7.3	64.0	60.6	3.4	7.3	62.3
	Mean	44.32	85.86	**41.55**	12.15	50.56	74.15	**23.59**	11.41	47.4	80.0	**32.6**	8.3	65.1	62.4	2.7	8.3	63.7

Table C-1 continued

SFW (g pot^{-1})	0	6.06	5.62	**0.44**	0.42	5.42	5.43	0.00	0.42	5.74	5.52	0.22	0.30	5.84	5.43	0.42	0.30	5.63
	3	-	-	-	-	-	-	-	-	-	-	-	-	-	-	-	-	-
	6	-	-	-	-	-	-	-	-	-	-	-	-	-	-	-	-	-
	9	5.39	6.70	**1.30**	0.47	5.32	5.87	**0.54**	0.42	5.36	6.28	**0.92**	0.32	6.05	5.60	**0.45**	0.32	5.82
	12	-	-	-	-	-	-	-	-	-	-	-	-	-	-	-	-	-
	14	4.38	8.12	**3.74**	0.33	4.57	5.87	**1.30**	0.35	4.47	6.99	**2.52**	0.23	6.25	5.22	**1.03**	0.24	5.73
	Mean	5.28	6.81	**1.83**	0.41	5.11	5.72	**0.61**	0.40	5.19	6.27	1.22	0.28	6.04	5.41	**0.63**	0.29	5.73
LA (cm^2)	0	32.36	31.01	1.35	2.57	26.58	26.27	0.31	2.76	29.47	28.64	0.83	1.94	31.69	26.42	**5.27**	1.96	29.05
	3	-	-	-	-	-	-	-	-	-	-	-	-	-	-	-	-	-
	6	-	-	-	-	-	-	-	-	-	-	-	-	-	-	-	-	
	9	32.36	33.66	1.30	2.83	25.45	28.31	**2.86**	2.79	27.12	30.98	**3.86**	2.06	31.22	26.88	**4.34**	2.03	29.05
	12	-	-	-	-	-	-	-	-	-	-	-	-	-	-	-	-	-
	14	22.14	42.19	**20.05**	2.01	21.21	28.29	**7.08**	2.20	21.67	35.24	**13.57**	1.72	32.16	24.75	**7.41**	1.54	28.46
	Mean	28.95	35.62	**7.57**	2.47	24.41	27.62	**3.42**	2.58	26.09	31.62	**6.09**	1.91	31.69	26.02	**5.67**	1.84	28.85
SMC (%)	0	41.75	41.43	0.32	7.93	51.48	47.92	3.56	8.32	46.61	44.68	1.93	20.63	41.59	49.70	8.11	20.63	45.64
	3	29.0	48.3	**19.32**	7.93	44.2	61.4	**17.15**	8.32	36.59	54.83	18.24	20.63	38.63	52.80	14.17	20.63	45.71
	6	17.2	29.4	**12.20**	7.93	23.0	51.7	**28.78**	8.32	20.08	40.58	20.50	20.63	23.31	37.35	14.04	20.63	30.33
	9	10.09	40.47	**30.38**	7.93	13.22	66.12	**52.90**	8.32	11.65	53.30	**41.65**	20.63	25.28	39.67	14.39	20.63	32.47
	12	8.9	48.0	**39.14**	7.93	9.7	74.0	**64.29**	8.32	9.28	61.00	**51.72**	20.63	28.44	41.85	13.41	20.63	35.14
	14	6.63	53.07	**46.44**	7.93	7.04	66.57	**59.53**	8.32	6.83	59.82	**52.99**	20.63	29.85	36.81	6.96	20.63	33.33
	Mean	18.92	43.45	**24.63**	7.93	24.77	61.29	**37.70**	8.32	21.84	52.37	**31.17**	20.63	31.18	43.03	11.85	20.63	37.10

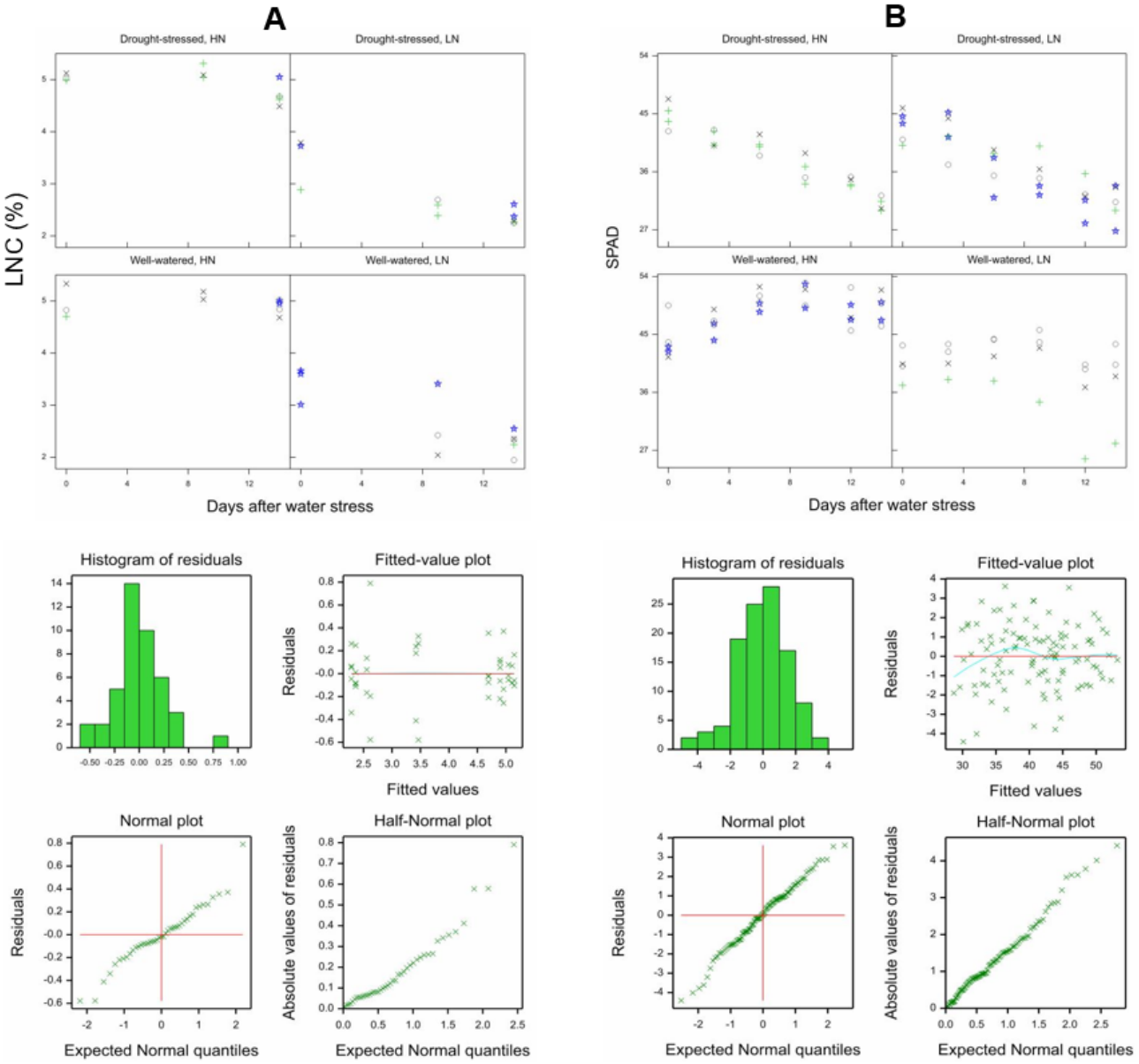

Figure C-1. Raw data distribution of the different treatments and residual plots of N stress morpho-physiological indicators in spring wheat. Raw data distribution and residual plots for (A) LNC and (B) SPAD. The residuals were inspected to verify the assumptions of normality (using histogram plots) and homogeneity of variance (using plots of fitted values).

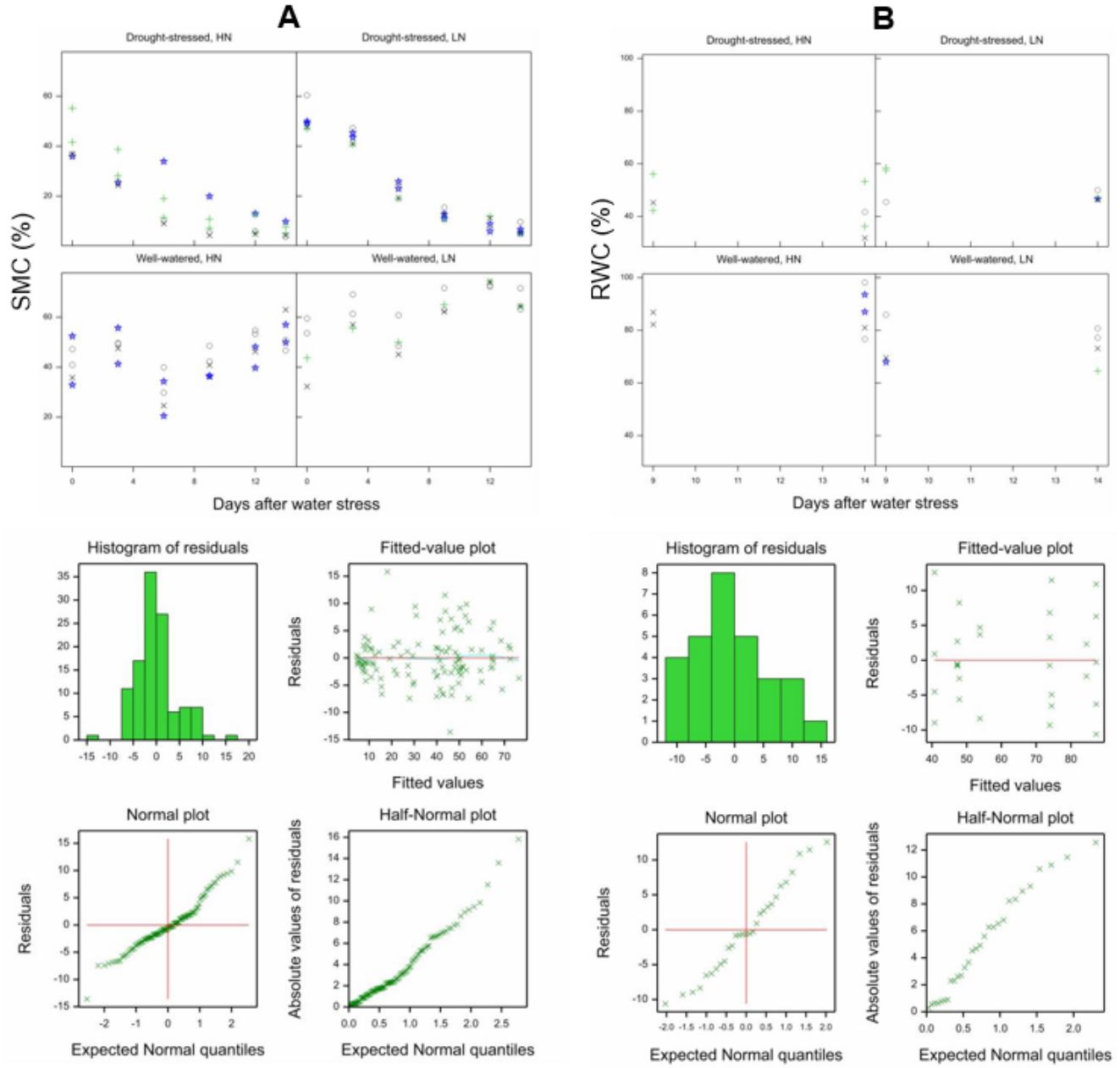

Figure C-2. Raw data distribution of the different treatments and residual plots of drought stress morpho-physiological indicators in spring wheat. Raw data distribution and residual plots for (A) SMC and (B) RWC. The residuals were inspected to verify the assumptions of normality (using histogram plots) and homogeneity of variance (using plots of fitted values).

Table C-2. Descriptive statistics (Means, Absolute difference and Approximate LSDs) of spectral reflectance indices (SRIs) in response to drought under high nitrogen (HN) and low nitrogen (LN) conditions and their interactions. Analysis was based on the REML Autocorrelation (AR1) model fitted in the D-N order of terms. Absolute difference (Absolute Diff) values or pairwise differences between treatment means and days after water stress (DAWS) greater than the approximate (Approx) least significant differences (LSDs) at a 5% level of REML means are considered statistically significant and bolded.

Model term		**D×N×DAWS**								**D×DAWS**				**N×DAWS**				**DAWS**
Treatment		**HN**				**LN**												
		Drought	**Well-watered**	**Absolute Diff.**	**Approx. LSD**	**Drought**	**Well-watered**	**Absolute Diff.**	**Approx. LSD**	**Drought**	**Well-watered**	**Absolute Diff.**	**Approx. LSD**	**HN**	**LN**	**Absolute Diff.**	**Approx. LSD**	**Mean**
Index	**DAWS**																	
NDVI	0	0.60	0.60	0.01	0.04	0.60	0.59	0.01	0.04	0.60	0.60	0.00	0.03	0.60	0.59	0.01	0.03	0.60
	3	0.60	0.60	0.00	0.04	0.59	0.59	0.00	0.04	0.59	0.59	0.00	0.03	0.60	0.59	0.01	0.03	0.59
	6	0.61	0.60	0.00	0.04	0.59	0.58	0.01	0.04	0.60	0.59	0.00	0.03	0.60	0.59	0.02	0.03	0.59
	9	0.60	0.60	0.00	0.04	0.59	0.57	0.01	0.04	0.59	0.59	0.01	0.03	0.60	0.58	0.02	0.03	0.59
	12	0.59	0.59	0.01	0.04	0.58	0.54	0.03	0.04	0.58	0.57	0.01	0.03	0.59	0.56	0.03	0.03	0.58
	14	0.54	0.60	**0.06**	0.04	0.55	0.55	0.00	0.04	0.54	0.57	0.03	0.03	0.57	0.55	0.02	0.03	0.56
	Mean	0.59	0.60	0.01	0.04	0.58	0.57	0.01	0.04	0.58	0.59	0.01	0.03	0.59	0.58	0.02	0.03	0.58
SR	0	3.95	4.03	0.08	0.39	3.96	3.88	0.08	0.39	3.95	3.96	0.00	0.28	3.99	3.92	0.07	0.28	3.95
	3	3.98	4.00	0.02	0.39	3.85	3.87	0.02	0.39	3.92	3.94	0.02	0.28	3.99	3.86	0.13	0.28	3.93
	6	4.07	4.02	0.05	0.39	3.87	3.80	0.07	0.39	3.97	3.91	0.06	0.28	4.04	3.83	0.21	0.28	3.94
	9	4.02	4.00	0.01	0.39	3.86	3.70	0.16	0.39	3.94	3.85	0.08	0.28	4.01	3.78	0.23	0.28	3.90
	12	3.83	3.93	0.09	0.39	3.74	3.46	0.28	0.39	3.79	3.69	0.10	0.28	3.88	3.60	0.28	0.28	3.74
	14	3.36	3.97	**0.61**	0.39	3.50	3.47	0.04	0.39	3.43	3.72	**0.29**	0.28	3.66	3.49	0.18	0.28	3.57
	Mean	3.87	3.99	0.15	0.39	3.80	3.70	0.11	0.39	3.83	3.84	0.09	0.28	3.93	3.75	0.18	0.28	3.84
MCARI1	0	0.70	0.67	0.03	0.05	0.68	0.68	0.00	0.05	0.69	0.67	0.02	0.03	0.69	0.68	0.01	0.03	0.68
	3	0.66	0.66	0.00	0.05	0.69	0.71	0.02	0.05	0.68	0.68	0.01	0.03	0.66	0.70	**0.04**	0.03	0.68
	6	0.68	0.68	0.00	0.05	0.69	0.74	0.05	0.05	0.68	0.71	0.02	0.03	0.68	0.71	**0.04**	0.03	0.70
	9	0.70	0.65	0.05	0.05	0.72	0.68	0.04	0.05	0.71	0.66	**0.04**	0.03	0.67	0.70	0.03	0.03	0.69
	12	0.73	0.65	**0.08**	0.05	0.75	0.75	0.00	0.05	0.74	0.70	**0.04**	0.03	0.69	0.75	**0.06**	0.03	0.72
	14	0.77	0.67	**0.10**	0.05	0.78	0.73	0.05	0.05	0.77	0.70	**0.07**	0.03	0.72	0.75	0.03	0.03	0.73
	Mean	0.71	0.66	0.04	0.05	0.72	0.72	0.03	0.05	0.71	0.69	0.03	0.03	0.68	0.72	**0.04**	0.03	0.70
OSAVI	0	0.58	0.58	0.00	0.02	0.58	0.57	0.00	0.02	0.58	0.57	0.00	0.01	0.58	0.57	0.00	0.01	0.58
	3	0.57	0.57	0.00	0.02	0.57	0.58	0.01	0.02	0.57	0.57	0.00	0.01	0.57	0.57	0.00	0.01	0.57
	6	0.58	0.58	0.00	0.02	0.57	0.58	0.00	0.02	0.58	0.58	0.00	0.01	0.58	0.58	0.00	0.01	0.58
	9	0.58	0.57	0.01	0.02	0.58	0.56	0.01	0.02	0.58	0.57	0.01	0.01	0.58	0.57	0.01	0.01	0.57
	12	0.58	0.57	0.01	0.02	0.58	0.56	0.02	0.02	0.58	0.56	**0.02**	0.01	0.57	0.57	0.00	0.01	0.57
	14	0.56	0.57	0.01	0.02	0.57	0.56	0.01	0.02	0.56	0.57	0.00	0.01	0.57	0.57	0.00	0.01	0.57
	Mean	0.58	0.57	0.01	0.02	0.58	0.57	0.01	0.02	0.58	0.57	0.01	0.01	0.57	0.57	0.00	0.01	0.57

Table C-2 continued

G	0	1.45	1.39	0.05	0.13	1.49	1.49	0.00	0.13	1.47	1.44	0.03	0.09	1.42	1.49	0.07	0.09	1.46
	3	1.38	1.38	0.00	0.13	1.46	1.49	0.03	0.13	1.42	1.43	0.01	0.09	1.38	1.47	**0.10**	0.09	1.43
	6	1.37	1.36	0.01	0.13	1.47	1.52	0.05	0.13	1.42	1.44	0.02	0.09	1.36	1.50	**0.14**	0.09	1.43
	9	1.44	1.34	0.09	0.13	1.48	1.55	0.07	0.13	1.46	1.45	0.01	0.09	1.39	1.52	**0.13**	0.09	1.45
	12	1.47	1.35	0.12	0.13	1.62	1.65	0.03	0.13	1.55	1.50	0.05	0.09	1.41	1.64	**0.23**	0.09	1.52
	14	1.55	1.35	**0.20**	0.13	1.65	1.64	0.01	0.13	1.60	1.50	**0.11**	0.09	1.45	1.65	**0.19**	0.09	1.55
	Mean	1.44	1.36	0.08	0.13	1.53	1.56	0.03	0.13	1.49	1.46	0.04	0.09	1.40	1.54	**0.14**	0.09	1.47
MCARI	0	0.12	0.10	0.02	0.06	0.12	0.12	0.00	0.06	0.12	0.11	0.01	0.04	0.11	0.12	0.01	0.04	0.12
	3	0.10	0.09	0.01	0.06	0.12	0.13	0.01	0.06	0.11	0.11	0.00	0.04	0.10	0.13	0.03	0.04	0.11
	6	0.09	0.09	0.00	0.06	0.12	0.14	0.02	0.06	0.11	0.12	0.01	0.04	0.09	0.13	0.04	0.04	0.11
	9	0.11	0.09	0.02	0.06	0.13	0.15	0.02	0.06	0.12	0.12	0.00	0.04	0.10	0.14	0.04	0.04	0.12
	12	0.12	0.09	0.03	0.06	0.17	0.22	0.05	0.06	0.14	0.15	0.01	0.04	0.10	0.19	**0.09**	0.04	0.15
	14	0.15	0.09	0.06	0.06	0.20	0.20	0.00	0.06	0.18	0.15	0.03	0.04	0.12	0.20	**0.08**	0.04	0.16
	Mean	0.11	0.09	0.02	0.06	0.14	0.16	0.02	0.06	0.13	0.13	0.01	0.04	0.10	0.15	**0.05**	0.04	0.13
TCARI	0	-0.15	-0.14	0.01	0.04	-0.15	-0.15	0.00	0.04	-0.15	-0.15	0.01	0.03	-0.15	-0.15	0.00	0.03	-0.15
	3	-0.14	-0.14	0.00	0.04	-0.15	-0.16	0.00	0.04	-0.15	-0.15	0.00	0.03	-0.14	-0.16	0.02	0.03	-0.15
	6	-0.14	-0.14	0.00	0.04	-0.15	-0.17	0.01	0.04	-0.15	-0.16	0.01	0.03	-0.14	-0.16	0.02	0.03	-0.15
	9	-0.15	-0.14	0.01	0.04	-0.16	-0.16	0.00	0.04	-0.15	-0.15	0.00	0.03	-0.14	-0.16	0.02	0.03	-0.15
	12	-0.16	-0.14	0.02	0.04	-0.18	-0.21	0.03	0.04	-0.17	-0.17	0.00	0.03	-0.15	-0.19	**0.04**	0.03	-0.17
	14	-0.19	-0.14	**0.05**	0.04	-0.20	-0.19	0.01	0.04	-0.20	-0.17	0.03	0.03	-0.17	-0.20	0.03	0.03	-0.18
	Mean	-0.16	-0.14	0.02	0.04	-0.17	-0.17	0.01	0.04	-0.16	-0.16	0.01	0.03	-0.15	-0.17	0.02	0.03	-0.16
TVI	0	27.04	25.85	1.19	1.61	25.85	26.00	0.15	1.61	26.44	25.92	0.52	1.14	26.45	25.92	0.52	1.14	26.18
	3	25.42	25.47	0.04	1.61	26.49	27.20	0.71	1.61	25.96	26.33	0.38	1.14	25.45	26.84	**1.40**	1.14	26.15
	6	26.10	26.16	0.06	1.61	26.50	28.16	**1.66**	1.61	26.30	27.16	0.86	1.14	26.13	27.33	**1.20**	1.14	26.73
	9	26.70	25.02	**1.68**	1.61	27.64	26.11	1.53	1.61	27.17	25.57	**1.60**	1.14	25.86	26.88	1.02	1.14	26.37
	12	27.74	25.13	**2.61**	1.61	28.65	28.33	0.32	1.61	28.19	26.73	**1.46**	1.14	26.43	28.49	**2.06**	1.14	27.46
	14	28.98	25.78	**3.20**	1.61	29.44	27.65	**1.79**	1.61	29.21	26.72	**2.50**	1.14	27.38	28.54	**1.16**	1.14	27.96
	Mean	27.00	25.57	1.46	1.61	27.43	27.24	1.03	1.61	27.21	26.41	**1.22**	1.14	26.28	27.33	**1.23**	1.14	26.81
ZMI	0	1.86	1.82	0.04	1.61	1.83	1.82	0.02	1.61	1.85	1.87	0.02	1.14	1.89	1.83	0.06	1.14	1.86
	3	1.94	1.83	0.11	1.61	1.84	1.83	0.02	1.61	1.89	1.89	0.00	1.14	1.94	1.84	0.11	1.14	1.89
	6	1.99	1.79	0.21	1.61	1.84	1.79	0.06	1.61	1.92	1.88	0.04	1.14	1.99	1.81	**0.17**	1.14	1.90
	9	1.93	1.73	0.20	1.61	1.83	1.73	0.10	1.61	1.88	1.85	0.03	1.14	1.96	1.78	**0.18**	1.14	1.87
	12	1.93	1.63	0.29	1.61	1.77	1.63	0.14	1.61	1.85	1.80	0.05	1.14	1.94	1.70	**0.24**	1.14	1.82
	14	1.76	1.63	0.13	1.61	1.70	1.63	0.07	1.61	1.73	1.80	0.07	1.14	1.86	1.66	**0.20**	1.14	1.76
	Mean	1.90	1.74	0.17	1.61	1.80	1.74	0.07	1.61	1.85	1.85	0.03	1.14	1.93	1.77	**0.16**	1.14	1.85

Table C-2 continued

SPRI	0	0.84	0.85	0.01	0.03	0.85	0.84	0.00	0.03	0.84	0.85	0.00	0.02	0.85	0.84	0.00	0.02	0.85
	3	0.86	0.85	0.01	0.03	0.86	0.86	0.00	0.03	0.86	0.85	0.01	0.02	0.85	0.86	0.01	0.02	0.85
	6	0.86	0.86	0.00	0.03	0.84	0.86	0.01	0.03	0.85	0.86	0.01	0.02	0.86	0.85	0.01	0.02	0.86
	9	0.83	0.84	0.01	0.03	0.84	0.83	0.01	0.03	0.84	0.84	0.00	0.02	0.83	0.84	0.01	0.02	0.84
	12	0.84	0.84	0.00	0.03	0.83	0.81	0.02	0.03	0.83	0.83	0.01	0.02	0.84	0.82	0.02	0.02	0.83
	14	0.83	0.83	0.00	0.03	0.81	0.81	0.00	0.03	0.82	0.82	0.00	0.02	0.83	0.81	0.02	0.02	0.82
	Mean	0.84	0.84	0.01	0.03	0.84	0.84	0.01	0.03	0.84	0.84	0.01	0.02	0.84	0.84	0.01	0.02	0.84
NPQI	0	-0.006	-0.005	0.001	0.014	-0.002	-0.003	0.000	0.014	-0.004	-0.004	0.001	0.010	-0.006	-0.003	0.003	0.010	0.00
	3	-0.003	-0.017	0.014	0.014	0.001	-0.017	**0.018**	0.014	-0.001	-0.017	0.016	0.010	-0.010	-0.008	0.002	0.010	-0.01
	6	-0.011	-0.004	0.007	0.014	-0.008	-0.006	0.001	0.014	-0.009	-0.005	0.004	0.010	-0.008	-0.007	0.001	0.010	-0.01
	9	0.000	-0.005	0.005	0.014	-0.008	0.004	0.012	0.014	-0.004	-0.001	-0.004	0.010	-0.003	-0.002	0.001	0.010	0.00
	12	-0.014	-0.007	0.007	0.014	-0.008	0.000	0.008	0.014	-0.011	-0.004	0.007	0.010	-0.011	-0.004	0.007	0.010	-0.01
	14	-0.024	-0.009	**0.015**	0.014	-0.009	-0.005	0.004	0.014	-0.016	-0.007	0.009	0.010	-0.016	-0.007	0.009	0.010	-0.01
	Mean	-0.010	-0.008	0.008	0.014	-0.006	-0.005	0.007	0.014	-0.008	-0.006	0.006	0.010	-0.009	-0.005	0.004	0.010	-0.01
PRI	0	0.033	0.032	0.000	0.006	0.032	0.032	0.000	0.006	0.033	0.032	0.000	0.004	0.033	0.032	0.001	0.004	0.03
	3	0.028	0.031	0.003	0.006	0.031	0.031	0.000	0.006	0.030	0.031	0.002	0.004	0.030	0.031	0.001	0.004	0.03
	6	0.030	0.029	0.001	0.006	0.030	0.031	0.001	0.006	0.030	0.030	0.000	0.004	0.029	0.030	0.001	0.004	0.03
	9	0.028	0.028	0.000	0.006	0.029	0.030	0.001	0.006	0.029	0.029	0.000	0.004	0.028	0.029	0.001	0.004	0.03
	12	0.025	0.027	0.002	0.006	0.029	0.029	0.000	0.006	0.027	0.028	0.001	0.004	0.026	0.029	0.002	0.004	0.03
	14	0.017	0.030	**0.013**	0.006	0.027	0.026	0.001	0.006	0.022	0.028	**0.006**	0.004	0.023	0.026	0.003	0.004	0.02
	Mean	0.027	0.030	0.003	0.006	0.029	0.030	0.001	0.006	0.028	0.030	0.002	0.004	0.028	0.030	0.002	0.004	0.03
NPCI	0	0.086	0.081	0.005	0.016	0.084	0.085	0.001	0.016	0.085	0.083	0.002	0.004	0.083	0.084	0.001	0.004	0.08
	3	0.078	0.083	0.005	0.016	0.075	0.078	0.003	0.016	0.077	0.080	0.004	0.004	0.081	0.076	**0.005**	0.004	0.08
	6	0.075	0.074	0.001	0.016	0.084	0.077	0.008	0.016	0.080	0.076	0.004	0.004	0.075	0.081	**0.006**	0.004	0.08
	9	0.095	0.088	0.007	0.016	0.085	0.090	0.005	0.016	0.090	0.089	0.001	0.004	0.091	0.088	0.004	0.004	0.09
	12	0.089	0.087	0.002	0.016	0.092	0.103	0.011	0.016	0.091	0.095	**0.005**	0.004	0.088	0.098	**0.009**	0.004	0.09
	14	0.095	0.093	0.002	0.016	0.108	0.108	0.000	0.016	0.101	0.100	0.001	0.004	0.094	0.108	**0.014**	0.004	0.10
	Mean	0.086	0.084	0.004	0.016	0.088	0.090	0.005	0.016	0.087	0.087	0.003	0.004	0.085	0.089	**0.006**	0.004	0.09
Ctr1	0	1.54	1.49	0.05	0.15	1.52	1.54	0.02	0.15	1.53	1.52	0.01	0.10	1.52	1.53	0.02	0.10	1.53
	3	1.48	1.46	0.02	0.15	1.51	1.55	0.04	0.15	1.49	1.51	0.01	0.10	1.47	1.53	0.06	0.10	1.50
	6	1.42	1.43	0.01	0.15	1.54	1.57	0.03	0.15	1.48	1.50	0.02	0.10	1.43	1.56	**0.13**	0.10	1.49
	9	1.54	1.45	0.09	0.15	1.51	1.63	0.12	0.15	1.52	1.54	0.01	0.10	1.49	1.57	0.08	0.10	1.53
	12	1.56	1.44	0.11	0.15	1.63	1.79	0.15	0.15	1.60	1.62	0.02	0.10	1.50	1.71	**0.21**	0.10	1.61
	14	1.63	1.47	**0.16**	0.15	1.78	1.76	0.02	0.15	1.71	1.62	0.09	0.10	1.55	1.77	**0.22**	0.10	1.66
	Mean	1.53	1.46	0.07	0.15	1.58	1.64	0.06	0.15	1.56	1.55	0.03	0.10	1.49	1.61	**0.12**	0.10	1.55

Table C-2 continued

Ctr2	0	0.31	0.31	0.01	0.05	0.32	0.32	0.00	0.05	0.32	0.31	0.00	0.03	0.31	0.32	0.01	0.03	0.31
	3	0.31	0.30	0.01	0.05	0.32	0.32	0.00	0.05	0.31	0.31	0.00	0.03	0.31	0.32	0.02	0.03	0.31
	6	0.30	0.30	0.00	0.05	0.32	0.33	0.01	0.05	0.31	0.31	0.00	0.03	0.30	0.33	0.03	0.03	0.31
	9	0.31	0.30	0.00	0.05	0.32	0.34	0.02	0.05	0.31	0.32	0.01	0.03	0.31	0.33	0.03	0.03	0.32
	12	0.32	0.31	0.01	0.05	0.33	0.38	0.05	0.05	0.33	0.35	0.02	0.03	0.31	0.36	**0.05**	0.03	0.34
	14	0.36	0.31	0.05	0.05	0.37	0.37	0.00	0.05	0.36	0.34	0.03	0.03	0.33	0.37	**0.04**	0.03	0.35
	Mean	0.32	0.30	0.01	0.05	0.33	0.35	0.01	0.05	0.32	0.32	0.01	0.03	0.31	0.34	0.03	0.03	0.32
Lic1	0	0.609	0.610	0.001	0.023	0.611	0.607	0.004	0.023	0.610	0.609	0.001	0.016	0.610	0.609	0.001	0.016	0.61
	3	0.606	0.608	0.002	0.023	0.601	0.606	0.004	0.023	0.604	0.607	0.003	0.016	0.607	0.603	0.004	0.016	0.61
	6	0.612	0.608	0.004	0.023	0.604	0.604	0.000	0.023	0.608	0.606	0.002	0.016	0.610	0.604	0.007	0.016	0.61
	9	0.613	0.603	0.010	0.023	0.602	0.594	0.008	0.023	0.607	0.599	0.009	0.016	0.608	0.598	0.011	0.016	0.60
	12	0.606	0.599	0.007	0.023	0.609	0.583	**0.026**	0.023	0.608	0.591	0.016	0.016	0.602	0.596	0.006	0.016	0.60
	14	0.578	0.602	0.023	0.023	0.586	0.584	0.002	0.023	0.582	0.593	0.010	0.016	0.590	0.585	0.005	0.016	0.59
	Mean	0.604	0.605	0.008	0.023	0.602	0.596	0.007	0.023	0.603	0.601	0.007	0.016	0.605	0.599	0.005	0.016	0.60
Lic2	0	0.768	0.789	0.021	0.042	0.769	0.763	0.006	0.042	0.768	0.776	0.007	0.030	0.778	0.766	0.012	0.030	0.77
	3	0.785	0.791	0.006	0.042	0.779	0.775	0.003	0.042	0.782	0.783	0.001	0.030	0.788	0.777	0.011	0.030	0.78
	6	0.802	0.793	0.009	0.042	0.764	0.764	0.000	0.042	0.783	0.778	0.004	0.030	0.797	0.764	**0.034**	0.030	0.78
	9	0.754	0.787	0.034	0.042	0.766	0.736	0.030	0.042	0.760	0.762	0.002	0.030	0.770	0.751	0.019	0.030	0.76
	12	0.755	0.773	0.018	0.042	0.736	0.688	**0.048**	0.042	0.745	0.730	0.015	0.030	0.764	0.712	**0.052**	0.030	0.74
	14	0.740	0.772	0.032	0.042	0.680	0.691	0.012	0.042	0.710	0.732	0.022	0.030	0.756	0.686	**0.070**	0.030	0.72
	Mean	0.767	0.784	0.020	0.042	0.749	0.746	0.017	0.042	0.758	0.760	0.009	0.030	0.776	0.743	**0.033**	0.030	0.76
SIPI	0	0.64	0.64	0.00	0.02	0.64	0.64	0.00	0.02	0.64	0.64	0.00	0.02	0.64	0.64	0.00	0.02	0.64
	3	0.64	0.64	0.00	0.02	0.63	0.63	0.01	0.02	0.63	0.64	0.00	0.02	0.64	0.63	0.01	0.02	0.63
	6	0.64	0.64	0.01	0.02	0.63	0.63	0.00	0.02	0.64	0.63	0.00	0.02	0.64	0.63	0.01	0.02	0.63
	9	0.64	0.64	0.01	0.02	0.63	0.63	0.00	0.02	0.64	0.63	0.01	0.02	0.64	0.63	0.01	0.02	0.64
	12	0.63	0.63	0.00	0.02	0.64	0.62	0.02	0.02	0.64	0.63	0.01	0.02	0.63	0.63	0.01	0.02	0.63
	14	0.60	0.64	**0.04**	0.02	0.62	0.62	0.00	0.02	0.61	0.63	0.02	0.02	0.62	0.62	0.00	0.02	0.62
	Mean	0.63	0.64	0.01	0.02	0.63	0.63	0.01	0.02	0.63	0.63	0.01	0.02	0.63	0.63	0.01	0.02	0.63
GM1	0	2.79	2.91	0.11	0.29	2.73	2.71	0.02	0.29	2.76	2.81	0.05	0.20	2.85	2.72	0.13	0.20	2.78
	3	2.90	2.93	0.03	0.29	2.72	2.70	0.02	0.29	2.81	2.81	0.01	0.20	2.91	2.71	**0.21**	0.20	2.81
	6	2.98	2.96	0.02	0.29	2.72	2.63	0.09	0.29	2.85	2.80	0.05	0.20	2.97	2.68	**0.29**	0.20	2.82
	9	2.86	2.95	0.09	0.29	2.70	2.55	0.16	0.29	2.78	2.75	0.03	0.20	2.91	2.63	**0.28**	0.20	2.77
	12	2.73	2.91	0.17	0.29	2.54	2.36	0.18	0.29	2.64	2.63	0.00	0.20	2.82	2.45	**0.37**	0.20	2.63
	14	2.40	2.92	**0.52**	0.29	2.38	2.36	0.02	0.29	2.39	2.64	**0.25**	0.20	2.66	2.37	**0.29**	0.20	2.52
	Mean	2.78	2.93	0.16	0.29	2.63	2.55	0.08	0.29	2.70	2.74	0.07	0.20	2.85	2.59	**0.26**	0.20	2.72

Table C-2 continued

GM2	0	2.59	2.70	0.11	0.27	2.55	2.52	0.02	0.27	2.57	2.61	0.05	0.19	2.65	2.54	0.11	0.19	2.59
	3	2.67	2.71	0.04	0.27	2.55	2.53	0.03	0.27	2.61	2.62	0.01	0.19	2.69	2.54	0.15	0.19	2.61
	6	2.77	2.74	0.03	0.27	2.54	2.46	0.08	0.27	2.65	2.60	0.05	0.19	2.76	2.50	**0.26**	0.19	2.63
	9	2.67	2.73	0.06	0.27	2.52	2.38	0.15	0.27	2.60	2.55	0.05	0.19	2.70	2.45	**0.25**	0.19	2.57
	12	2.63	2.69	0.06	0.27	2.43	2.21	0.23	0.27	2.53	2.45	0.08	0.19	2.66	2.32	**0.34**	0.19	2.49
	14	2.35	2.69	**0.34**	0.27	2.28	2.20	0.08	0.27	2.32	2.45	0.13	0.19	2.52	2.24	**0.28**	0.19	2.38
	Mean	2.61	2.71	0.11	0.27	2.48	2.38	0.10	0.27	2.55	2.55	0.06	0.19	2.66	2.43	**0.23**	0.19	2.55
ARI1	0	0.37	0.39	0.02	0.09	0.36	0.37	0.01	0.09	0.37	0.38	0.01	0.06	0.38	0.36	0.02	0.06	0.37
	3	0.45	0.43	0.02	0.09	0.32	0.34	0.02	0.09	0.38	0.39	0.00	0.06	0.44	0.33	**0.12**	0.06	0.38
	6	0.40	0.41	0.02	0.09	0.35	0.32	0.03	0.09	0.37	0.37	0.01	0.06	0.40	0.34	**0.07**	0.06	0.37
	9	0.36	0.45	0.09	0.09	0.33	0.34	0.01	0.09	0.35	0.40	0.05	0.06	0.40	0.34	0.06	0.06	0.37
	12	0.19	0.42	**0.23**	0.09	0.20	0.29	**0.10**	0.09	0.19	0.36	**0.17**	0.06	0.31	0.24	0.06	0.06	0.28
	14	0.09	0.44	**0.35**	0.09	0.18	0.31	**0.13**	0.09	0.13	0.38	**0.24**	0.06	0.27	0.24	0.02	0.06	0.25
	Mean	0.31	0.43	**0.12**	0.09	0.29	0.33	0.05	0.09	0.30	0.38	**0.08**	0.06	0.37	0.31	0.06	0.06	0.34
ARI2	0	0.21	0.21	0.00	0.05	0.19	0.19	0.00	0.05	0.20	0.20	0.00	0.03	0.21	0.19	0.02	0.03	0.20
	3	0.24	0.23	0.01	0.05	0.17	0.18	0.01	0.05	0.20	0.21	0.00	0.03	0.23	0.18	**0.06**	0.03	0.21
	6	0.22	0.23	0.01	0.05	0.19	0.18	0.01	0.05	0.20	0.20	0.00	0.03	0.22	0.18	**0.04**	0.03	0.20
	9	0.19	0.24	0.04	0.05	0.19	0.18	0.01	0.05	0.19	0.21	0.02	0.03	0.22	0.18	0.03	0.03	0.20
	12	0.11	0.22	**0.12**	0.05	0.11	0.16	0.05	0.05	0.11	0.19	**0.08**	0.03	0.17	0.13	0.03	0.03	0.15
	14	0.05	0.24	**0.19**	0.05	0.10	0.17	**0.07**	0.05	0.08	0.20	**0.13**	0.03	0.14	0.13	0.01	0.03	0.14
	Mean	0.17	0.23	**0.06**	0.05	0.16	0.18	0.02	0.05	0.16	0.20	**0.04**	0.03	0.20	0.17	0.03	0.03	0.18
CRI1	0	2.47	2.44	0.03	0.32	2.68	2.65	0.03	0.32	2.57	2.54	0.03	0.22	2.45	2.66	0.21	0.22	2.56
	3	2.42	2.35	0.07	0.32	2.45	2.51	0.05	0.32	2.44	2.43	0.01	0.22	2.39	2.48	0.09	0.22	2.43
	6	2.30	2.26	0.04	0.32	2.53	2.43	0.10	0.32	2.41	2.35	0.07	0.22	2.28	2.48	0.20	0.22	2.38
	9	2.49	2.35	0.14	0.32	2.43	2.69	0.26	0.32	2.46	2.52	0.06	0.22	2.42	2.56	0.14	0.22	2.49
	12	2.19	2.35	0.16	0.32	2.62	2.45	0.17	0.32	2.40	2.40	0.01	0.22	2.27	2.53	**0.26**	0.22	2.40
	14	1.96	2.32	**0.36**	0.32	2.36	2.55	0.18	0.32	2.16	2.43	**0.27**	0.22	2.14	2.46	**0.32**	0.22	2.30
	Mean	2.30	2.35	0.13	0.32	2.51	2.54	0.13	0.32	2.41	2.44	0.07	0.22	2.32	2.53	0.20	0.22	2.43
CRI2	0	2.84	2.83	0.01	0.36	3.03	3.00	0.03	0.36	2.94	2.92	0.02	0.25	2.84	3.02	0.18	0.25	2.93
	3	2.87	2.79	0.09	0.36	2.76	2.83	0.07	0.36	2.82	2.81	0.01	0.25	2.83	2.80	0.03	0.25	2.81
	6	2.69	2.67	0.02	0.36	2.87	2.74	0.13	0.36	2.78	2.71	0.08	0.25	2.68	2.81	0.12	0.25	2.75
	9	2.85	2.80	0.05	0.36	2.76	3.03	0.26	0.36	2.81	2.91	0.11	0.25	2.82	2.90	0.07	0.25	2.86
	12	2.38	2.77	**0.39**	0.36	2.81	2.73	0.08	0.36	2.59	2.75	0.16	0.25	2.58	2.77	0.19	0.25	2.67
	14	2.05	2.76	**0.71**	0.36	2.54	2.85	0.31	0.36	2.29	2.80	**0.51**	0.25	2.40	2.69	**0.29**	0.25	2.55
	Mean	2.61	2.77	0.21	0.36	2.80	2.86	0.15	0.36	2.71	2.82	0.15	0.25	2.69	2.83	0.15	0.25	2.76

Table C-2 continued

RDVI	0	0.51	0.50	0.01	0.02	0.50	0.50	0.00	0.02	0.50	0.50	0.00	0.01	0.51	0.50	0.01	0.01	0.50
	3	0.50	0.50	0.00	0.02	0.50	0.51	0.01	0.02	0.50	0.50	0.00	0.01	0.50	0.50	0.00	0.01	0.50
	6	0.51	0.51	0.00	0.02	0.50	0.51	0.01	0.02	0.50	0.51	0.00	0.01	0.51	0.51	0.00	0.01	0.51
	9	0.51	0.47	**0.04**	0.02	0.51	0.48	**0.03**	0.02	0.51	0.49	**0.02**	0.01	0.50	0.50	0.00	0.01	0.50
	12	0.52	0.49	**0.03**	0.02	0.52	0.49	**0.03**	0.02	0.52	0.49	**0.02**	0.01	0.50	0.51	0.00	0.01	0.50
	14	0.50	0.50	0.00	0.02	0.51	0.49	0.02	0.02	0.51	0.50	0.01	0.01	0.50	0.50	0.00	0.01	0.50
	Mean	0.51	0.50	0.01	0.02	0.51	0.50	0.01	0.02	0.51	0.50	0.01	0.01	0.50	0.50	0.00	0.01	0.50
PRI_550	0	0.031	0.032	0.002	0.005	0.035	0.035	0.001	0.005	0.033	0.034	0.001	0.003	0.032	0.035	0.003	0.003	0.03
	3	0.033	0.031	0.002	0.005	0.032	0.035	0.003	0.005	0.032	0.033	0.000	0.003	0.032	0.033	0.002	0.003	0.03
	6	0.029	0.029	0.000	0.005	0.033	0.036	0.003	0.005	0.031	0.032	0.001	0.003	0.029	0.034	**0.005**	0.003	0.03
	9	0.032	0.031	0.001	0.005	0.034	0.037	0.002	0.005	0.033	0.034	0.001	0.003	0.031	0.035	**0.004**	0.003	0.03
	12	0.032	0.032	0.000	0.005	0.039	0.035	0.004	0.005	0.035	0.033	0.002	0.003	0.032	0.037	**0.005**	0.003	0.03
	14	0.034	0.029	0.005	0.005	0.035	0.038	0.003	0.005	0.035	0.034	0.001	0.003	0.032	0.037	**0.005**	0.003	0.03
	Mean	0.032	0.031	0.002	0.005	0.035	0.036	0.003	0.005	0.033	0.033	0.001	0.003	0.031	0.035	**0.004**	0.003	0.03
PRI_norm	0	0.038	0.042	0.004	0.006	0.043	0.044	0.001	0.006	0.041	0.043	0.003	0.004	0.040	0.043	0.003	0.004	0.04
	3	0.043	0.041	0.002	0.006	0.041	0.043	0.002	0.006	0.042	0.042	0.000	0.004	0.042	0.042	0.001	0.004	0.04
	6	0.038	0.039	0.001	0.006	0.041	0.043	0.001	0.006	0.040	0.041	0.001	0.004	0.038	0.042	0.004	0.004	0.04
	9	0.040	0.043	0.003	0.006	0.042	0.045	0.003	0.006	0.041	0.044	0.003	0.004	0.041	0.043	0.002	0.004	0.04
	12	0.040	0.044	0.004	0.006	0.044	0.040	0.004	0.006	0.042	0.042	0.000	0.004	0.042	0.042	0.000	0.004	0.04
	14	0.042	0.039	0.002	0.006	0.039	0.044	0.004	0.006	0.040	0.041	0.001	0.004	0.041	0.041	0.001	0.004	0.04
	Mean	0.040	0.041	0.003	0.006	0.042	0.043	0.003	0.006	0.041	0.042	0.001	0.004	0.041	0.042	0.002	0.004	0.04
PRI/NDVI	0	0.055	0.054	0.001	0.009	0.054	0.054	0.000	0.009	0.055	0.054	0.001	0.007	0.055	0.054	0.001	0.007	0.05
	3	0.047	0.052	0.005	0.009	0.052	0.053	0.001	0.009	0.050	0.053	0.003	0.007	0.050	0.053	0.003	0.007	0.05
	6	0.049	0.048	0.001	0.009	0.050	0.053	0.003	0.009	0.050	0.051	0.001	0.007	0.048	0.052	0.003	0.007	0.05
	9	0.047	0.047	0.000	0.009	0.049	0.052	0.003	0.009	0.048	0.049	0.001	0.007	0.047	0.050	0.003	0.007	0.05
	12	0.043	0.046	0.004	0.009	0.050	0.052	0.003	0.009	0.046	0.049	0.003	0.007	0.044	0.051	0.007	0.007	0.05
	14	0.030	0.049	**0.019**	0.009	0.047	0.047	0.001	0.009	0.039	0.048	**0.009**	0.007	0.040	0.047	0.007	0.007	0.04
	Mean	0.045	0.049	0.005	0.009	0.051	0.052	0.002	0.009	0.048	0.051	0.003	0.007	0.047	0.051	0.004	0.007	0.05
GNDVI_780	0	0.48	0.50	0.01	0.05	0.47	0.47	0.01	0.05	0.48	0.48	0.00	0.01	0.49	0.47	**0.02**	0.01	0.48
	3	0.50	0.50	0.00	0.05	0.47	0.46	0.00	0.05	0.48	0.48	0.00	0.01	0.50	0.47	**0.03**	0.01	0.48
	6	0.51	0.50	0.00	0.05	0.47	0.46	0.02	0.05	0.49	0.48	0.01	0.01	0.51	0.46	**0.04**	0.01	0.49
	9	0.49	0.50	0.01	0.05	0.47	0.44	0.03	0.05	0.48	0.47	0.01	0.01	0.50	0.45	**0.04**	0.01	0.48
	12	0.47	0.50	0.02	0.05	0.44	0.40	0.04	0.05	0.46	0.45	0.01	0.01	0.49	0.42	**0.06**	0.01	0.45
	14	0.42	0.50	**0.08**	0.05	0.41	0.41	0.00	0.05	0.41	0.45	**0.04**	0.01	0.46	0.41	**0.05**	0.01	0.43
	Mean	0.48	0.50	0.02	0.05	0.45	0.44	0.01	0.05	0.47	0.47	0.01	0.01	0.49	0.45	**0.04**	0.01	0.47

Table C-2 continued

MRESR	0	3.11	3.35	0.23	0.43	3.05	3.01	0.04	0.43	3.08	3.18	0.09	0.30	3.23	3.03	0.20	0.30	3.13
	3	3.41	3.46	0.05	0.43	3.12	3.01	0.10	0.43	3.26	3.23	0.03	0.30	3.43	3.06	**0.37**	0.30	3.25
	6	3.59	3.56	0.03	0.43	3.06	2.89	0.17	0.43	3.33	3.22	0.10	0.30	3.57	2.98	**0.59**	0.30	3.27
	9	3.28	3.54	0.26	0.43	3.05	2.71	0.33	0.43	3.16	3.13	0.04	0.30	3.41	2.88	**0.53**	0.30	3.15
	12	3.31	3.43	0.12	0.43	2.81	2.47	0.34	0.43	3.06	2.95	0.11	0.30	3.37	2.64	**0.73**	0.30	3.01
	14	2.87	3.49	**0.62**	0.43	2.56	2.47	0.10	0.43	2.72	2.98	0.26	0.30	3.18	2.51	**0.67**	0.30	2.85
	Mean	3.26	3.47	0.22	0.43	2.94	2.76	0.18	0.43	3.10	3.12	0.11	0.30	3.37	2.85	**0.52**	0.30	3.11
RENDVI	0	0.36	0.38	0.02	0.05	0.36	0.36	0.00	0.05	0.36	0.37	0.01	0.04	0.37	0.36	0.02	0.04	0.36
	3	0.38	0.39	0.00	0.05	0.36	0.36	0.01	0.05	0.37	0.37	0.00	0.04	0.38	0.36	0.03	0.04	0.37
	6	0.40	0.39	0.00	0.05	0.36	0.34	0.01	0.05	0.38	0.37	0.01	0.04	0.39	0.35	0.04	0.04	0.37
	9	0.38	0.39	0.01	0.05	0.36	0.33	0.03	0.05	0.37	0.36	0.01	0.04	0.39	0.34	0.04	0.04	0.36
	12	0.38	0.38	0.01	0.05	0.34	0.29	0.05	0.05	0.36	0.34	0.02	0.04	0.38	0.32	**0.06**	0.04	0.35
	14	0.33	0.39	**0.06**	0.05	0.31	0.30	0.01	0.05	0.32	0.34	0.02	0.04	0.36	0.30	**0.06**	0.04	0.33
	Mean	0.37	0.39	0.02	0.05	0.35	0.33	0.02	0.05	0.36	0.36	0.01	0.04	0.38	0.34	0.04	0.04	0.36
NDRE	0	0.20	0.21	0.01	0.03	0.19	0.18	0.01	0.03	0.19	0.20	0.00	0.02	0.20	0.19	0.01	0.02	0.19
	3	0.21	0.21	0.00	0.03	0.19	0.18	0.01	0.03	0.20	0.20	0.00	0.02	0.21	0.19	0.02	0.02	0.20
	6	0.22	0.22	0.01	0.03	0.19	0.18	0.01	0.03	0.21	0.20	0.01	0.02	0.22	0.19	**0.03**	0.02	0.20
	9	0.21	0.22	0.01	0.03	0.19	0.17	0.02	0.03	0.20	0.19	0.00	0.02	0.22	0.18	**0.04**	0.02	0.20
	12	0.21	0.22	0.00	0.03	0.17	0.15	0.03	0.03	0.19	0.18	0.01	0.02	0.21	0.16	**0.05**	0.02	0.19
	14	0.18	0.21	**0.04**	0.03	0.16	0.14	0.01	0.03	0.17	0.18	0.01	0.02	0.20	0.15	**0.05**	0.02	0.17
	Mean	0.21	0.21	0.01	0.03	0.18	0.17	0.01	0.03	0.19	0.19	0.01	0.02	0.21	0.17	**0.04**	0.02	0.19
CIgreen	0	1.88	1.98	0.10	0.30	1.81	1.77	0.03	0.30	1.84	1.88	0.03	0.21	1.93	1.79	0.14	0.21	1.86
	3	1.97	2.01	0.04	0.30	1.80	1.76	0.04	0.30	1.88	1.88	0.00	0.21	1.99	1.78	**0.22**	0.21	1.88
	6	2.06	2.06	0.00	0.30	1.79	1.68	0.11	0.30	1.93	1.87	0.06	0.21	2.06	1.74	**0.33**	0.21	1.90
	9	1.94	2.03	0.09	0.30	1.76	1.59	0.18	0.30	1.85	1.81	0.04	0.21	1.99	1.67	**0.31**	0.21	1.83
	12	1.81	1.98	0.18	0.30	1.58	1.38	0.20	0.30	1.69	1.68	0.01	0.21	1.90	1.48	**0.42**	0.21	1.69
	14	1.47	2.01	**0.54**	0.30	1.40	1.39	0.01	0.30	1.43	1.70	**0.27**	0.21	1.74	1.40	**0.34**	0.21	1.57
	Mean	1.86	2.01	0.16	0.30	1.69	1.59	0.10	0.30	1.77	1.80	0.07	0.21	1.93	1.64	**0.29**	0.21	1.79
CIrededge	0	0.49	0.52	0.03	0.10	0.47	0.45	0.02	0.10	0.48	0.49	0.01	0.07	0.50	0.46	0.04	0.07	0.48
	3	0.54	0.54	0.01	0.10	0.48	0.46	0.02	0.10	0.51	0.50	0.01	0.07	0.54	0.47	0.07	0.07	0.51
	6	0.58	0.56	0.01	0.10	0.48	0.44	0.04	0.10	0.53	0.50	0.03	0.07	0.57	0.46	**0.11**	0.07	0.51
	9	0.53	0.56	0.03	0.10	0.47	0.40	0.07	0.10	0.50	0.48	0.02	0.07	0.55	0.43	**0.11**	0.07	0.49
	12	0.55	0.55	0.01	0.10	0.42	0.34	0.08	0.10	0.48	0.45	0.03	0.07	0.55	0.38	**0.17**	0.07	0.46
	14	0.44	0.56	**0.11**	0.10	0.37	0.34	0.03	0.10	0.41	0.45	0.04	0.07	0.50	0.36	**0.14**	0.07	0.43
	Mean	0.52	0.55	0.03	0.10	0.45	0.41	0.04	0.10	0.48	0.48	0.02	0.07	0.53	0.43	**0.11**	0.07	0.48

Table C-2 continued

mNDblue_530	0	0.10	0.09	0.01	0.03	0.10	0.11	0.00	0.03	0.10	0.10	0.00	0.02	0.10	0.11	0.01	0.02	0.10
	3	0.09	0.09	0.00	0.03	0.10	0.11	0.01	0.03	0.09	0.10	0.00	0.02	0.09	0.10	0.02	0.02	0.09
	6	0.08	0.08	0.00	0.03	0.10	0.11	0.01	0.03	0.09	0.10	0.00	0.02	0.08	0.11	**0.03**	0.02	0.09
	9	0.10	0.08	0.01	0.03	0.10	0.12	0.02	0.03	0.10	0.10	0.00	0.02	0.09	0.11	0.02	0.02	0.10
	12	0.10	0.09	0.02	0.03	0.13	0.15	0.02	0.03	0.12	0.12	0.00	0.02	0.09	0.14	**0.05**	0.02	0.12
	14	0.12	0.09	**0.04**	0.03	0.15	0.14	0.01	0.03	0.14	0.12	0.02	0.02	0.11	0.15	**0.04**	0.02	0.13
	Mean	0.10	0.09	0.01	0.03	0.11	0.12	0.01	0.03	0.11	0.11	0.01	0.02	0.09	0.12	**0.03**	0.02	0.11
mNDblue_730	0	0.52	0.51	0.01	0.02	0.52	0.53	0.01	0.02	0.52	0.52	0.00	0.01	0.52	0.52	0.01	0.01	0.52
	3	0.50	0.50	0.00	0.02	0.51	0.52	0.01	0.02	0.51	0.51	0.01	0.01	0.50	0.51	0.01	0.01	0.51
	6	0.49	0.50	0.00	0.02	0.52	0.52	0.01	0.02	0.51	0.51	0.01	0.01	0.49	0.52	**0.03**	0.01	0.51
	9	0.51	0.49	0.02	0.02	0.52	0.54	0.02	0.02	0.52	0.52	0.00	0.01	0.50	0.53	**0.02**	0.01	0.52
	12	0.50	0.50	0.00	0.02	0.54	0.55	0.01	0.02	0.52	0.52	0.00	0.01	0.50	0.54	**0.05**	0.01	0.52
	14	0.50	0.50	0.00	0.02	0.55	0.55	0.00	0.02	0.52	0.53	0.00	0.01	0.50	0.55	**0.04**	0.01	0.52
	Mean	0.51	0.50	0.00	0.02	0.53	0.53	0.01	0.02	0.52	0.52	0.00	0.01	0.50	0.53	**0.03**	0.01	0.52
rDVI_790	0	0.419	0.407	0.013	0.018	0.400	0.396	0.004	0.018	0.41	0.40	0.01	0.01	0.41	0.40	0.01	0.01	0.41
	3	0.400	0.404	0.004	0.018	0.407	0.413	0.006	0.018	0.40	0.41	0.00	0.01	0.40	0.41	0.01	0.01	0.41
	6	0.414	0.414	0.000	0.018	0.407	0.425	0.018	0.018	0.41	0.42	0.01	0.01	0.41	0.42	0.00	0.01	0.42
	9	0.417	0.397	**0.019**	0.018	0.420	0.391	**0.029**	0.018	0.42	0.39	**0.02**	0.01	0.41	0.41	0.00	0.01	0.41
	12	0.428	0.395	**0.032**	0.018	0.426	0.406	**0.020**	0.018	0.43	0.40	**0.03**	0.01	0.41	0.42	0.00	0.01	0.41
	14	0.432	0.404	**0.028**	0.018	0.420	0.398	**0.021**	0.018	0.43	0.40	**0.02**	0.01	0.42	0.41	0.01	0.01	0.41
	Mean	0.418	0.404	0.016	0.018	0.413	0.405	0.016	0.018	0.42	0.40	**0.02**	0.01	0.41	0.41	0.01	0.01	0.41
gSRa_790	0	2.87	2.99	0.11	0.30	2.81	2.76	0.05	0.30	2.84	2.87	0.03	0.21	2.93	2.79	0.14	0.21	2.86
	3	2.98	3.01	0.04	0.30	2.79	2.75	0.04	0.30	2.88	2.88	0.00	0.21	2.99	2.77	**0.22**	0.21	2.88
	6	3.07	3.04	0.03	0.30	2.79	2.68	0.11	0.30	2.93	2.86	0.07	0.21	3.06	2.73	**0.32**	0.21	2.89
	9	2.95	3.04	0.09	0.30	2.76	2.60	0.16	0.30	2.85	2.82	0.03	0.21	3.00	2.68	**0.32**	0.21	2.84
	12	2.80	2.97	0.17	0.30	2.59	2.39	0.20	0.30	2.70	2.68	0.01	0.21	2.89	2.49	**0.40**	0.21	2.69
	14	2.46	2.99	**0.53**	0.30	2.40	2.39	0.02	0.30	2.43	2.69	**0.26**	0.21	2.72	2.40	**0.33**	0.21	2.56
	Mean	2.86	3.01	0.16	0.30	2.69	2.60	0.10	0.30	2.77	2.80	0.07	0.21	2.93	2.64	**0.29**	0.21	2.79
SRa_790	0	4.12	4.15	0.03	0.26	4.16	4.09	0.07	0.26	4.14	4.12	0.02	0.21	4.13	4.12	0.01	0.21	4.13
	3	4.08	4.11	0.03	0.26	4.03	4.08	0.05	0.26	4.05	4.09	0.04	0.21	4.09	4.05	0.04	0.21	4.07
	6	4.16	4.11	0.05	0.26	4.06	4.03	0.02	0.26	4.11	4.07	0.04	0.21	4.13	4.05	0.09	0.21	4.09
	9	4.19	4.05	0.14	0.26	4.01	3.95	0.07	0.26	4.10	4.00	0.10	0.21	4.12	3.98	0.14	0.21	4.05
	12	4.09	3.98	0.11	0.26	4.13	3.83	**0.31**	0.26	4.11	3.90	0.21	0.21	4.04	3.98	0.06	0.21	4.01
	14	3.76	4.00	0.24	0.26	3.87	3.80	0.07	0.26	3.81	3.90	0.08	0.21	3.88	3.83	0.04	0.21	3.86
	Mean	4.07	4.07	0.10	0.26	4.04	3.96	0.10	0.26	4.06	4.01	0.08	0.21	4.07	4.00	0.06	0.21	4.03

Table C-3. Full results of the test for main effects of the spectral reflectance indices (SRIs) in response to the combined drought (D) and nitrogen (N) stress. The F-statistics and F-Test probabilities were used to test the effects/responses of the spectral indices to drought and N stresses as well as their interactions. The F-test was done considering all treatment combinations and days after water stress (DAWS). The statistically significant results (p<0.05) indicating differences between means for levels of N or P and their interactions are shown in bold.

Index	D	N	DAWS	D×N	D×DAWS	N×DAWS	D×N×DAWS
NDVI	$F_{1,13.17}$ = 0.86, P = 0.371	$F_{1,13.17}$ =1.79, P = 0.203	$F_{5,65.5}$ = 5.75, P <**0.001**	$F_{1,13.2}$ = 1.72, P = 0.213	$F_{5,65.5}$ = 3.87, P < **0.05**	$F_{5,65.5}$ = 0.55, P = 0.740	$F_{5,65.5}$ = 0.87, P = 0.507
SR	$F_{1,13.0}$ = 1.05, P = 0.325	$F_{1,13.0}$ = 2.08, P = 0.173	$F_{5,66.0}$ = 7.45, P <**0.001**	$F_{1,13.0}$ = 2.50, P = 0.138	$F_{5,66.0}$ = 4.35, P < **0.05**	$F_{5,66.0}$ = 0.68, P = 0.640	$F_{5,66.0}$ = 1.43, P = 0.226
MCARI1	$F_{1,14.0}$ = 9.86, P < **0.05**	$F_{1,14.0}$ = 10.58, P < **0.05**	$F_{5,52.7}$ = 8.34, P <**0.001**	$F_{1,14.0}$ = 4.42, P = 0.054	$F_{5,52.7}$ = 5.61, P <**0.001**	$F_{5,52.7}$ = 3.05, P < **0.05**	$F_{5,52.7}$ = 0.80, P = 0.556
OSAVI	$F_{1,13.8}$ = 1.29, P = 0.276	$F_{1,13.8}$ = 0.40, P = 0.538	$F_{5,52.9}$ = 1.97, P = 0.098	$F_{1,13.8}$ = 0.36, P = 0.559	$F_{5,52.9}$ = 3.03, P < **0.05**	$F_{5,52.9}$ = 0.36, P = 0.871	$F_{5,52.9}$ = 0.90, P = 0.489
G	$F_{1,15.7}$ = 3.67, P = 0.074	$F_{1,15.7}$ = 18.69, P <**0.001**	$F_{5,67.3}$ = 6.10, P <**0.001**	$F_{1,15.7}$ = 3.13, P = 0.096	$F_{5,67.3}$ = 1.71, P = 0.145	$F_{5,67.3}$ = 2.95, P < **0.05**	$F_{5,67.3}$ = 0.77, P = 0.576
MCARI	$F_{1,14.4}$ = 1.22, P = 0.287	$F_{1,14.4}$ = 9.66, P < **0.05**	$F_{5,66.3}$ = 4.76, P <**0.001**	$F_{1,14.4}$ = 1.72, P = 0.210	$F_{5,66.3}$ = 2.04, P = 0.085	$F_{5,66.3}$ = 3.08, P < **0.05**	$F_{5,66.3}$ = 0.54, P = 0.744
TCARI	$F_{1,16.6}$ = 1.91, P = 0.185	$F_{1,16.6}$ = 4.23, P = 0.056	$F_{5,67.5}$ = 5.82, P <**0.001**	$F_{1,16.6}$ = 1.77, P = 0.201	$F_{5,67.5}$ = 3.05, P < **0.05**	$F_{5,67.5}$ = 1.93, P = 0.101	$F_{5,67.5}$ = 0.85, P = 0.521
TVI	$F_{1,14.0}$ = 10.72, P < **0.05**	$F_{1,14.0}$ = 11.09, P < **0.05**	$F_{5,51.9}$ = 7.79, P <**0.001**	$F_{1,14.0}$ = 4.39, P = 0.055	$F_{5,51.9}$ = 6.08, P <**0.001**	$F_{5,51.9}$ = 3.15, P < **0.05**	$F_{5,51.9}$ = 0.72, P = 0.609
ZMI	$F_{1,11.8}$ = 0.93, P = 0.353	$F_{1,11.8}$ = 10.93, P < **0.05**	$F_{5,65.0}$ = 6.72, P <**0.001**	$F_{1,11.8}$ = 3.13, P = 0.103	$F_{5,65.0}$ = 3.05, P < **0.05**	$F_{5,65.0}$ = 2.83, P < **0.05**	$F_{5,65.0}$ = 1.32, P = 0.268
SPRI	$F_{1,23.7}$ = 0.03, P = 0.856	$F_{1,23.7}$ = 1.87, P = 0.184	$F_{5,66.0}$ = 8.52, P <**0.001**	$F_{1,23.7}$ = 0.47, P = 0.500	$F_{5,66.0}$ = 0.72, P = 0.611	$F_{5,66.0}$ = 2.03, P = 0.085	$F_{5,66.0}$ = 0.62, P = 0.687
NPQI	$F_{1,24.1}$ = 0.33, P = 0.572	$F_{1,24.1}$ = 2.91, P = 0.101	$F_{5,63.6}$ = 1.92, P = 0.104	$F_{1,24.1}$ = 0.05, P = 0.818	$F_{5,63.6}$ = 3.70, P < **0.05**	$F_{5,63.6}$ = 0.48, P = 0.792	$F_{5,63.6}$ = 1.12, P = 0.357
PRI	$F_{1,14.9}$ = 1.85, P = 0.194	$F_{1,14.9}$ = 1.09, P = 0.313	$F_{5,62.0}$ = 5.43, P <**0.001**	$F_{1,14.9}$ = 2.06, P = 0.172	$F_{5,62.0}$ = 1.77, P = 0.133	$F_{5,62.0}$ = 0.45, P = 0.814	$F_{5,62.0}$ = 2.42, P < **0.05**
NPCI	$F_{1,23.5}$ = 0.04, P = 0.853	$F_{1,23.5}$ = 2.01, P = 0.170	$F_{5,65.8}$ = 8.62, P <**0.001**	$F_{1,23.5}$ = 0.48, P = 0.495	$F_{5,65.8}$ = 0.71, P = 0.617	$F_{5,65.8}$ = 2.10, P = 0.076	$F_{5,65.8}$ = 0.63, P = 0.674
Ctr1	$F_{1,15.7}$ = 1.17, P = 0.295	$F_{1,15.7}$ = 12.52, P < **0.05**	$F_{5,65.2}$ = 6.66, P <**0.001**	$F_{1,15.7}$ = 3.13, P = 0.096	$F_{5,65.2}$ = 1.53, P = 0.192	$F_{5,65.2}$ = 3.57, P < **0.05**	$F_{5,65.2}$ = 1.43, P = 0.224
Ctr2	$F_{1,13.1}$ = 0.72, P = 0.411	$F_{1,13.1}$ = 4.93, P < **0.05**	$F_{5,65.5}$ = 5.19, P <**0.001**	$F_{1,13.1}$ = 1.30, P = 0.275	$F_{5,65.5}$ = 3.67, P < **0.05**	$F_{5,65.5}$ = 1.11, P = 0.365	$F_{5,65.5}$ = 0.74, P = 0.598
Lic1	$F_{1,13.9}$ = 0.02, P = 0.878	$F_{1,13.9}$ = 1.02, P = 0.330	$F_{5,54.3}$ = 4.65, P < **0.05**	$F_{1,13.9}$ = 0.79, P = 0.388	$F_{5,54.3}$ = 2.66, P < **0.05**	$F_{5,54.3}$ = 0.23, P = 0.947	$F_{5,54.3}$ = 0.73, P = 0.603
Lic2	$F_{1,16.4}$ = 1.22, P = 0.285	$F_{1,16.4}$ = 14.98, P < **0.05**	$F_{5,64.8}$ = 10.11, P < **0.001**	$F_{1,16.4}$ = 2.30, P = 0.148	$F_{5,64.8}$ = 1.95, P = 0.098	$F_{5,64.8}$ = 3.29, P <**0.05**	$F_{5,64.8}$ = 2.08, P = 0.079
SIPI	$F_{1,13.8}$ = 0.34, P = 0.567	$F_{1,13.8}$ = 0.41, P = 0.534	$F_{5,54.1}$ = 3.86, P < **0.05**	$F_{1,13.8}$ = 1.02, P = 0.330	$F_{5,54.1}$ = 3.41, P < **0.05**	$F_{5,54.1}$ = 0.54, P = 0.746	$F_{5,54.1}$ = 1.46, P = 0.217
GM1	$F_{1,12.0}$ = 3.00, P = 0.109	$F_{1,12.0}$ = 8.66, P < **0.05**	$F_{5,65.6}$ = 11.44, P <**0.001**	$F_{1,12.0}$ = 3.79, P = 0.075	$F_{5,65.6}$ = 5.16, P <**0.001**	$F_{5,65.6}$ = 2.22, P = 0.063	$F_{5,65.6}$ = 1.82, P = 0.121
GM2	$F_{1,11.4}$ = 1.23, P = 0.291	$F_{1,11.4}$ = 8.54, P < **0.05**	$F_{5,64.5}$ = 7.72, P <**0.001**	$F_{1,11.4}$ = 3.08, P = 0.106	$F_{5,64.5}$ = 3.68, P < **0.05**	$F_{5,64.5}$ = 2.19, P = 0.066	$F_{5,64.5}$ = 1.20, P = 0.318
ARI1	$F_{1,14.0}$ = 16.59, P < **0.05**	$F_{1,8.2}$ = 8.98, P < **0.05**	$F_{5,54.8}$ = 26.89, P < **0.001**	$F_{1,10.0}$ = 3.98, P = 0.074	$F_{5,54.8}$ = 22.25, P < **0.001**	$F_{5,54.8}$ = 3.20, P < **0.05**	$F_{5,54.8}$ = 4.42, P < **0.05**
ARI2	$F_{1,13.8}$ = 15.16, P < **0.05**	$F_{1,8.7}$ = 8.90, P < **0.05**	$F_{5,55.4}$ = 24.41, P < **0.001**	$F_{1,10.6}$ = 3.71, P = 0.081	$F_{5,55.4}$ = 20.10, P < **0.001**	$F_{5,55.4}$ = 2.32, P = 0.055	$F_{5,55.4}$ = 4.41, P < **0.05**
CRI1	$F_{1,11.8}$ = 0.09, P = 0.775	$F_{1,10.5}$ = 8.13, P < **0.05**	$F_{5,52.6}$ = 5.18, P < **0.001**	$F_{1,12.7}$ = 0.01, P = 0.916	$F_{5,52.6}$ = 2.49, P < **0.05**	$F_{5,52.6}$ = 1.09, P = 0.378	$F_{5,52.6}$ = 3.16, P < **0.05**
CRI2	$F_{1,12.4}$ = 1.38, P = 0.262	$F_{1,10.3}$ = 2.77, P = 0.126	$F_{5,52.2}$ = 10.11, P < **0.001**	$F_{1,12.4}$ = 0.31, P = 0.590	$F_{5,52.2}$ = 6.16, P < **0.001**	$F_{5,52.2}$ = 1.98, P = 0.097	$F_{5,52.2}$ = 3.95, P < **0.05**
RDVI	$F_{1,24.9}$ = 10.31, P < **0.05**	$F_{1,24.9}$ = 0.51, P = 0.482	$F_{5,62.4}$ = 1.05, P = 0.398	$F_{1,24.9}$ = 0.06, P = 0.802	$F_{5,62.4}$ = 4.38, P < **0.05**	$F_{5,62.4}$ = 0.91, P = 0.484	$F_{5,62.4}$ = 0.81, P = 0.544
PRI_550	$F_{1,13.8}$ = 0.33, P = 0.573	$F_{1,9.9}$ = 43.50, P <**0.001**	$F_{5,52.2}$ = 2.29, P = 0.059	$F_{1,11.5}$ = 3.00, P = 0.110	$F_{5,52.2}$ = 0.94, P = 0.462	$F_{5,52.2}$ = 1.05, P = 0.399	$F_{5,52.2}$ = 1.95, P = 0.102
PRI_norm	$F_{1,13.8}$ = 0.99, P = 0.338	$F_{1,10.7}$ = 2.31, P = 0.157	$F_{5,52.1}$ = 0.90, P = 0.487	$F_{1,12.2}$ = 0.00, P = 0.969	$F_{5,52.1}$ = 0.46, P = 0.807	$F_{5,52.1}$ = 0.85, P = 0.522	$F_{5,52.1}$ = 2.23, P = 0.065

PRI/NDVI	$F_{1,16.1} = 2.18$, $P = 0.160$	$F_{1,16.1} = 4.29$, $P = 0.055$	$F_{5, 60.7} = 4.64$, $P <$ **0.05**	$F_{1,16.1} = 1.40$, $P = 0.253$	$F_{5, 60.7} = 1.23$, $P = 0.304$	$F_{5, 60.7} = 0.76$, $P = 0.582$	$F_{5, 60.7} = 2.57$, $P <$ **0.05**
GNDVI_780	$F_{1,12.4} = 1.88$, $P = 0.194$	$F_{1,12.4} = 7.13$, $P <$ **0.05**	$F_{5, 65.6} = 8.15$, $P <$ **0.001**	$F_{1,12.4} = 2.50$, $P = 0.139$	$F_{5, 65.6} = 4.30$, $P <$ **0.05**	$F_{5, 65.6} = 1.65$, $P = 0.159$	$F_{5, 65.6} = 0.91$, $P = 0.480$
MRESR	$F_{1,12.2} = 2.05$, $P = 0.178$	$F_{1,12.2} = 18.10$, $P <$ **0.05**	$F_{5, 64.7} = 7.64$, $P <$ **0.001**	$F_{1,12.2} = 4.15$, $P = 0.064$	$F_{5, 64.7} = 3.69$, $P <$ **0.05**	$F_{5, 64.7} = 3.50$, $P <$ **0.05**	$F_{5, 64.7} = 1.85$, $P = 0.115$
RENDVI	$F_{1,11.7} = 0.97$, $P = 0.345$	$F_{1,11.7} = 8.06$, $P <$ **0.05**	$F_{5, 64.8} = 5.53$, $P <$ **0.001**	$F_{1,11.7} = 2.26$, $P = 0.159$	$F_{5, 64.8} = 4.08$, $P <$ **0.05**	$F_{5, 64.8} = 2.06$, $P = 0.082$	$F_{5, 64.8} = 0.85$, $P = 0.517$
NDRE	$F_{1,11.9} = 0.49$, $P = 0.499$	$F_{1,11.9} = 12.45$, $P <$ **0.05**	$F_{5, 64.8} = 6.14$, $P <$ **0.001**	$F_{1,11.9} = 2.59$, $P = 0.134$	$F_{5, 64.8} = 2.96$, $P <$ **0.05**	$F_{5, 64.8} = 2.85$, $P <$ **0.05**	$F_{5, 64.8} = 1.05$, $P = 0.398$
CIgreen	$F_{1,12.1} = 2.79$, $P = 0.121$	$F_{1,12.1} = 9.91$, $P <$ **0.05**	$F_{5, 65.9} = 12.03$, $P <$ **0.001**	$F_{1,12.1} = 3.59$, $P = 0.082$	$F_{5, 65.9} = 5.38$, $P <$ **0.001**	$F_{5, 65.9} = 2.56$, $P <$ **0.05**	$F_{5, 65.9} = 1.40$, $P = 0.237$
CIrededge	$F_{1,12.5} = 0.75$, $P = 0.403$	$F_{1,12.5} = 14.92$, $P <$ **0.05**	$F_{5, 65.7} = 6.48$, $P <$ **0.001**	$F_{1,12.5} = 2.84$, $P = 0.117$	$F_{5, 65.7} = 3.03$, $P <$ **0.05**	$F_{5, 65.7} = 4.37$, $P <$ **0.05**	$F_{5, 65.7} = 1.29$, $P = 0.277$
mNDblue_530	$F_{1,13.9} = 1.59$, $P = 0.229$	$F_{1,13.9} = 12.27$, $P <$ **0.05**	$F_{5, 65.7} = 7.75$, $P <$ **0.001**	$F_{1,13.9} = 2.14$, $P = 0.166$	$F_{5, 65.7} = 2.34$, $P = 0.051$	$F_{5, 65.7} = 3.17$, $P <$ **0.05**	$F_{5, 65.7} = 0.78$, $P = 0.568$
mNDblue_730	$F_{1,22.5} = 0.03$, $P = 0.861$	$F_{1,22.5} = 55.64$, $P <$ **0.001**	$F_{5, 66.1} = 4.58$, $P <$ **0.05**	$F_{1, 22.5} = 2.81$, $P = 0.108$	$F_{5, 66.1} = 0.20$, $P = 0.960$	$F_{5, 66.1} = 5.83$, $P <$ **0.001**	$F_{5, 66.1} = 1.42$, $P = 0.227$
rDVI_790	$F_{1,16.4} = 18.86$, $P <$ **0.001**	$F_{1,29.9} = 0.45$, $P = 0.507$	$F_{5, 58.5} = 1.95$, $P = 0.099$	$F_{1, 28.6} = 1.60$, $P = 0.216$	$F_{5, 58.5} = 6.56$, $P <$ **0.001**	$F_{5, 58.5} = 1.99$, $P = 0.093$	$F_{5, 58.5} = 0.58$, $P = 0.718$
gSRa_790	$F_{1,11.8} = 2.59$, $P = 0.134$	$F_{1,11.8} = 9.65$, $P <$ **0.05**	$F_{5, 65.4} = 21.21$, $P <$ **0.001**	$F_{1,11.8} = 3.73$, $P = 0.078$	$F_{5, 65.4} = 5.11$, $P <$ **0.001**	$F_{5, 65.4} = 1.96$, $P = 0.096$	$F_{5, 65.4} = 1.48$, $P = 0.209$
SRa_790	$F_{1,14.0} = 0.15$, $P = 0.702$	$F_{1,14.0} = 1.09$, $P = 0.313$	$F_{5, 54.5} = 5.46$, $P <$ **0.001**	$F_{1,14.0} = 0.90$, $P = 0.358$	$F_{5, 54.5} = 2.47$, $P <$ **0.05**	$F_{5, 54.5} = 0.36$, $P = 0.873$	$F_{5, 54.5} = 0.86$, $P = 0.516$

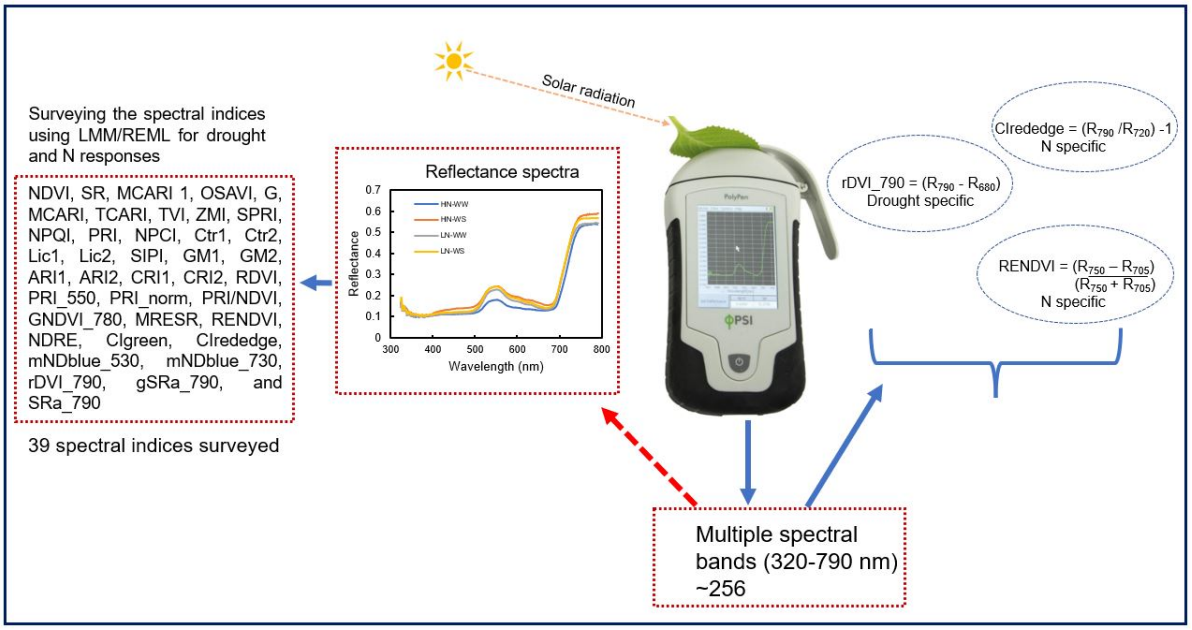

Figure C-3. Schematic measurement of spectral reflectance using the PolyPen RP410 spectrometer to identify responsive spectral reflectance indices (SRIs) by linear mixed models (LMMs) fitted using residual (or restricted) maximum likelihood (REML), LMM/REML for drought and N status in spring wheat.

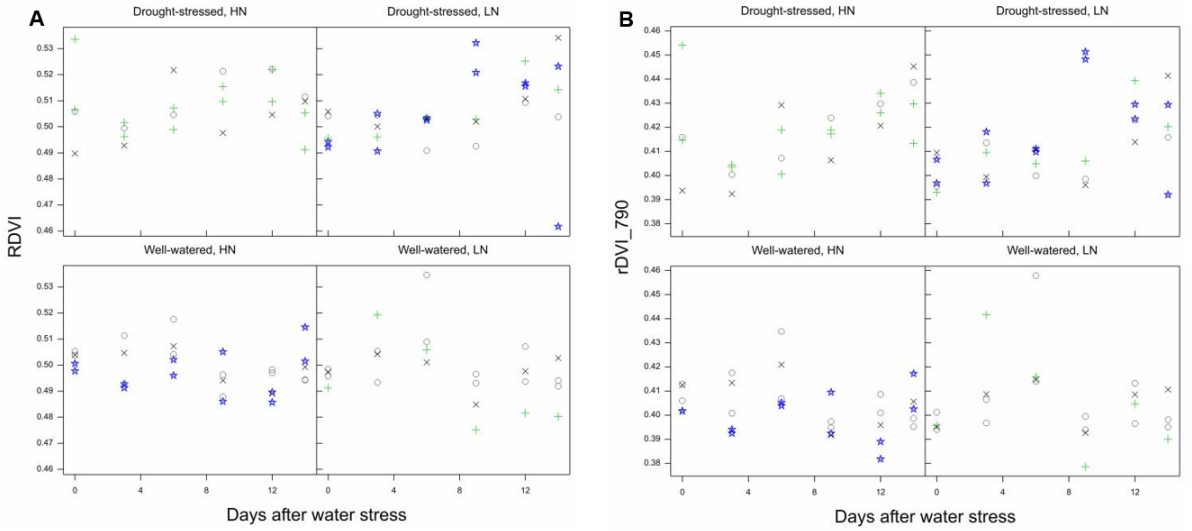

Figure C-4. Raw data distribution of different treatment conditions of drought stress-specific SRIs identified for spring wheat. Raw data distribution of treatments for (A) RDVI and (B) rDVI_790.

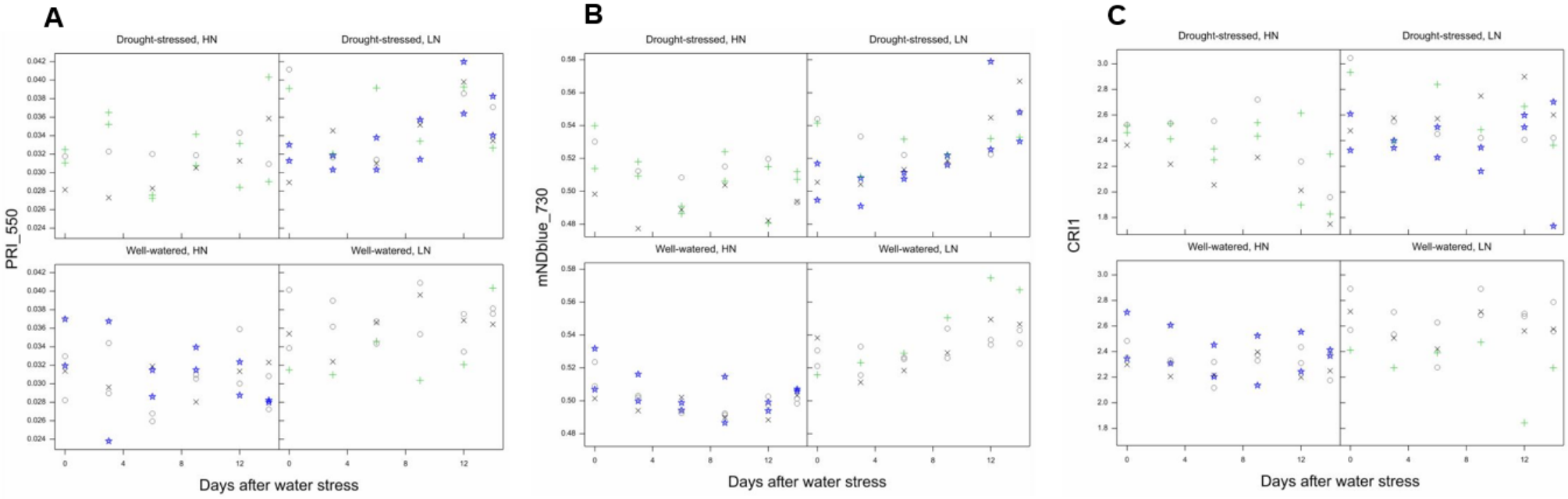

Figure C-5. Raw data distribution of different treatment conditions of some N stress-specific SRIs identified for spring wheat including (A) PRI_550, (B) mNDblue_730 and (C) CRI1.

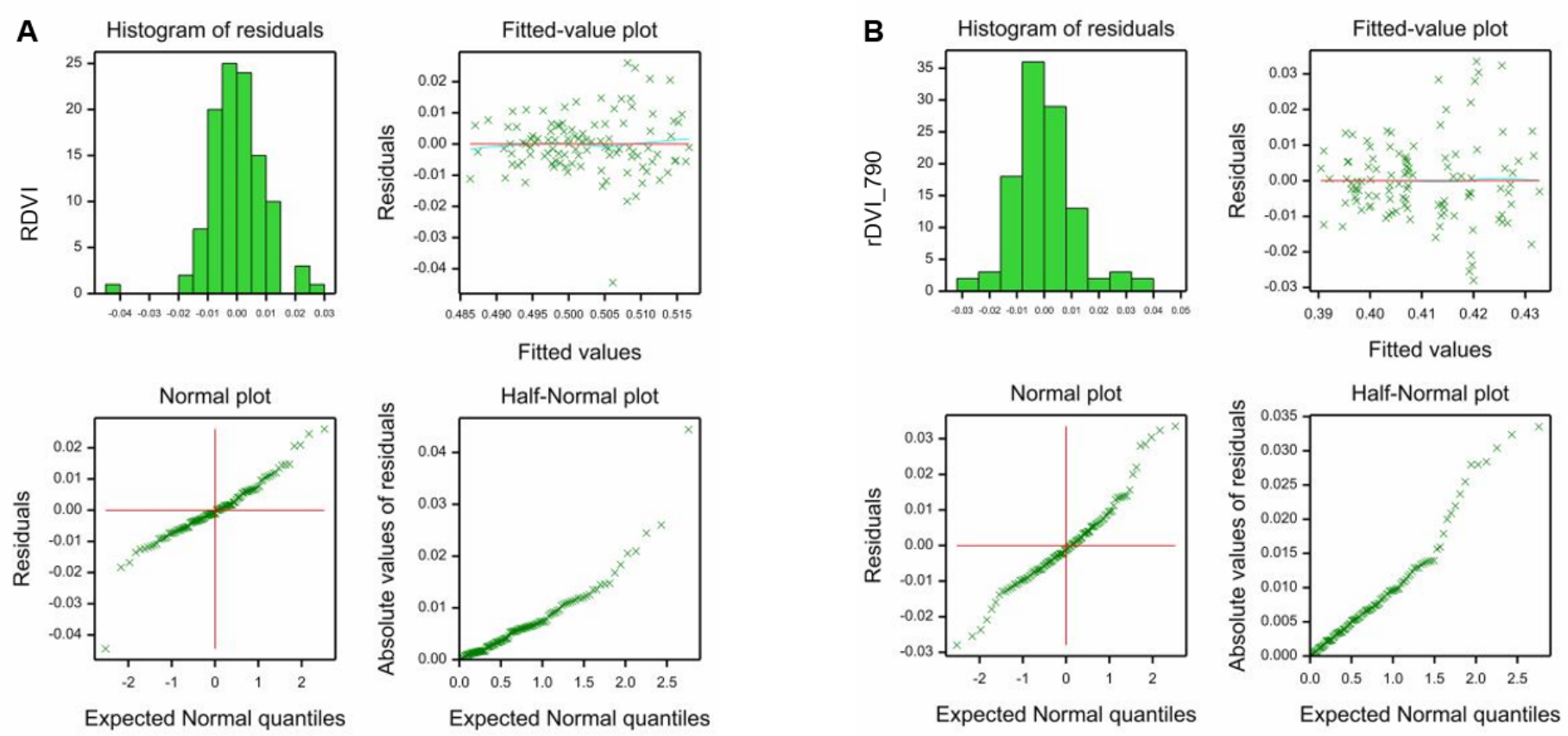

Figure C-6. Residual plots of drought stress-specific SRIs identified for spring wheat including (A) RDVI and (B) rDVI_790. The residuals were inspected to verify the assumptions of normality (using histogram plots) and homogeneity of variance (using plots of fitted values).

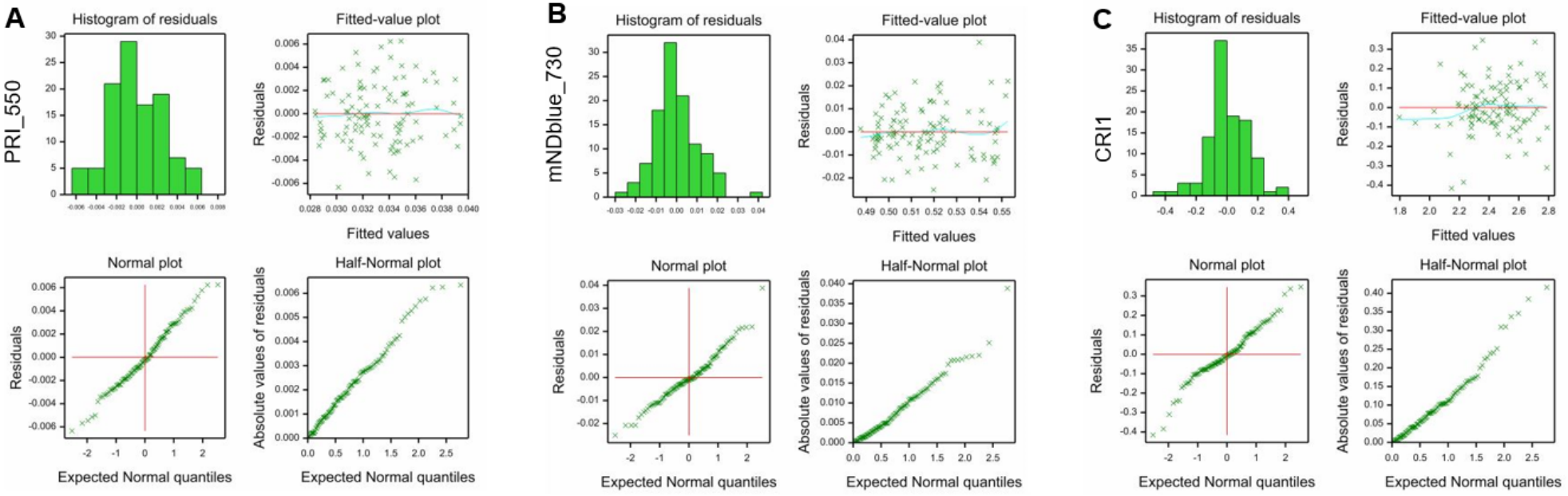

Figure C-7. Residual plots of some N stress-specific SRIs for spring wheat including (A) PRI_550, (B) mNDblue_730 and (C) CRI1. The residuals were examined to verify the assumptions of normality (using histogram plots) and homogeneity of variance (using plots of fitted values).

Appendix D Supplementary material for Chapter 5

Figure D-1. The WGIN diversity N trial plots. The photograph was taken at post-anthesis.